Impact of LRRK2 kinase activation and inhibition *in vivo* and *in vitro*

Jillian H. Kluss

Thesis submitted for the degree of Doctor of Philosophy

June 2022

Supervisors:

Dr Patrick A. Lewis	Dr Mark R. Cookson
Department of Pharmacology	Laboratory of Neurogenetics
School of Pharmacy	National Institute on Aging
University of Reading	National Institutes of Health

Declaration: I confirm that this is my own work and the use of all materials from other sources have been properly and fully acknowledged. Contributions from colleagues and collaborators in the execution of experiments have explicitly been acknowledged in the manuscript. The interpretation and analysis of data resulting from the research conducted in this thesis are entirely my own work.

- Jillian Hanna Kluss

Dedicated to Suzanne B. Strauss

Word count: 50,000

Acknowledgements

The completion of this thesis would not have been possible without the help of the many people I was fortunate to work with during these last four years.

First, I'd like to thank my PhD supervisors. Thank you, Mark for inviting and encouraging me to complete a PhD in your lab. I feel extremely grateful and privileged to be a part of the LNG family and to have had the opportunity to take advantage of all the incredible resources that only the LNG has. It has been wonderful. Thank you, Patrick for supporting my PhD work and walking me through the very unique process of the PhD experience. Meeting and chatting with you throughout the years has been very enriching and stimulating.

A very special thank you goes out to the LNG family, past and present. Adam and Luis, your supervision and support has been invaluable. I've learned so much from you, and believe I am leaving my PhD a better scientist and critical thinker because of you two. Thank you. Natalie, thank you for being my sounding board for new ideas, and allowing me to vent whenever things got particularly difficult and exhausting. Your friendship has been irreplaceable. Sasha, Alice, Melissa, Dorien, Laura, Dave, Rebekah, Nate, Megan, Xylena, Kumaran, George, Cornelis – you are all brilliant. Thank you for creating such a warm, inclusive, and

stimulating environment. This experience wouldn't have been half as rewarding or fun without you all.

Thank you to Dr. Laurie Sanders, my first mentor that introduced me to PD research. Thank you for taking a chance on me and providing such an encouraging and thrilling environment. Thank you to Dr. J. Timothy Greenamyre for graciously welcoming me into your lab that started this journey. To Briana, Megan, Alya, Evan, and Nick – you all are responsible for creating such a positive first look at how incredible wet lab science can be. I am in awe of all of you and so thankful for your continued friendships.

Thank you to my family – Mom, Grandma, Hallie, Gerry, Mark, Dad, and Mia. Your unwavering support and encouragement have been so appreciated and important. This PhD is as much yours as it is mine.

Thank you to my beautiful friends – Julie, Grace, Haley, Cassidy, Jenn, Nicole, Stephen, Becca, and Tess. I am inspired by all of you in so many ways and treasure our friendships deeply. Thank you for being there for me throughout this process.

Declaration of Contributions

The work in this thesis was funded in part by the Intramural Research Program at the National Institute on Aging, National Institutes of Health and the University of Reading. Many colleagues at the Laboratory of Neurogenetics have contributed directly to the work presented in this thesis. Dr. Melissa Conti Mazza performed all oral gavages in mice dosed with acute treatments of MLi-2. Dr. Adamantios Mamais assisted in the collection of mouse tissues in the acute MLi-2 dosing cohorts. Dr. Alexandra Beilina cloned some of the LRRK2 mutant constructs into pCR™8/GW/TOPO™ vectors. Dr. Luis Bonet-Ponce cloned LRRK2 into FBKP-tagged vectors as well as created the LYSO-LRRK2 chimera plasmid. Dr. Luis Bonet-Ponce also arranged Figure 6.4 and carried out experiments and data analyses shown in Figures 7.14, 7.15A-B, and 7.16. Dr. Patrick A. Lewis modeled the LRRK2 molecular structure presented in Figure 3.1B. Lastly, Dr. Mark R. Cookson curated Figure 3.10 from GTEx multi-query.

In addition, collaborations across institutes within the National Institutes of Health have also contributed to the research presented in this thesis. Mass spectrometry experiments were performed by the Proteomics Core, led by Dr. Yan Li (National Institute of Neurological Disorders and Stroke).

Abstract

Parkinson's Disease (PD) is a progressive neurodegenerative disorder that is characterized in part by a loss of dopamine neurons in the Substantia Nigra and affects the nigrostriatal pathway. Mutations in the gene encoding leucine-rich repeat kinase 2 (LRRK2) have been found to cause late onset PD through a gain of function of its kinase domain. Thus, LRRK2 has become an intriguing candidate for therapeutic intervention by kinase inhibition. While preclinical studies have shown that ablating the kinase activity of wildtype LRRK2 is safe with a mild and reversible lung phenotype, the molecular effects of chronic LRRK2 inhibition have not been examined in the context of mutant LRRK2. Using the potent LRRK2 kinase-specific inhibitor, Merck LRRK2 inhibitor 2 (MLi-2), hyperactive G2019S LRRK2 was reduced to wildtype levels chronically in G2019S knock-in (KI) mice and autophosphorylation of LRRK2 and phosphorylation of direct substrates Rab10, Rab12, and Rab29 was assessed. Unbiased total and phospho-proteomics revealed alterations in endolysosomal proteins similar to those found in LRRK2 knockout (KO) animals after 10 weeks of treatment. LRRK2 has been shown to play roles in a number of pathways within the endolysosomal system and studies have reported LRRK2 presence on many organelles from the *trans*-Golgi network (TGN) to the lysosome. Based on the current study's proteomic results, eight different trap plasmids

were generated to evaluate LRRK2 kinase activity at distinct endolysosomal membranes. As a result, LRRK2 kinase activity was found to be enhanced after being trapped to all membranes and downstream Rab10 and Rab12 phosphorylation were increased *in vitro*, but recruitment of these Rabs revealed differential patterns in localization specifically when targeting LRRK2 on lysosomes compared to other membranes. Evaluation of lysosomal position through manipulation of various motor proteins showed phosphorylated Rab10 was preferentially restricted to a subset of perinuclear lysosomes, whereas pRab12 was present at most LRRK2-positive lysosomes regardless of their position.

This is the first study to examine the molecular underpinnings of chronic LRRK2 inhibition in a preclinical *in vivo* PD model and highlights cellular pathways that may be influenced by therapeutic strategies aimed at restoring LRRK2 physiological activity in PD patients. Complementary *in vitro* data provides novel insight into the differences in LRRK2-dependent Rab localization that can help elucidate the role of LRRK2 at the lysosome which may be relevant to PD pathogenesis. The work presented in this thesis additionally contributes to our knowledge on the utility of pS1292 LRRK2 and pS106 Rab12 as robust biomarkers of both kinase hyperactivity and inhibition in G2019S LRRK2 KI mice in brain and peripheral tissues that is worth assessment in patients with PD harboring the G2019S mutation.

Contents

List of Figures

List of Tables

Abbreviations

AA .... *amino acid*

AADC .... *amino acid decarboxylase*

AD .... *Alzheimer's Disease*

ADm .... *Autosomal dominant*

ARc .... *Autosomal recessive*

ARL8B .... *ADP ribosylation factor-like 8B*

ASO .... *antisense oligonucleotide*

BAC .... *bacterial artificial chromosome*

BBB .... *blood-brain barrier*

CHMP4B .... *charged multivesicular body protein 4B*

CNS .... *central nervous system*

COMT .... *Catechol-O-Methyltransferase*

COR .... *C-terminal of Roc*

Cryo-EM .... *cryogenic electron microscopy*

CTSB .... *Cathepsin B*

CTSD .... *Cathepsin D*

Cycs .... Cytochrome C

DAT .... *dopamine transporter*

DBS .... *deep brain stimulation*

DLB .... *dementia with Lewy Bodies*

EEA1 .... *Early endosome antigen 1*

EHD1 .... *EH domain containing 1*

ESCRT .... *endosomal sorting complexes required for transport*

FDA .... *U.S. Food and Drug Administration*

FDR .... *false discovery rate*

FKBP .... *FK506-binding protein*

FRB ………………………………………..………… FKBP-rapamycin-binding

GAP ………………………………………………... GTPase activating protein

GBA …………………………………………………….. glucosylceramidase

GDF ………………………………………………….. GDI displacement factor

GDI ………………………………………………… GDP dissociation inhibitor

GDP ……………………………………………..…… guanosine diphosphate

GEF ……………………………………………..…… guanine exchange factor

GI ……………………………………………………………….. gastrointestinal

GO …………………………………………………………… Gene Ontology

GPi …………………………………………………….. Globus pallidus internus

GTP …………………………………………………….. guanosine triphosphate

GWAS ……………………………………………….. genome wide association study

HRS ……………………………………………………. hepatocyte growth factor

IBD …………………………………………………..… inflammatory bowel disease

iMAC ……………………………………… immobilized metal affinity chromatography

iPSC …………………………………………….. induced pluripotent stem cell

JAK ……………………………………………………………… Janus kinase

JIP4 …………………………………………………….. JNK-interacting protein 4

KI ……………………………………………………………………… knock-in

KO ………………………………………………………………… knockout

L-DOPA ……………………………………………… l-3,4-dihydroxyphenylalanine

LAMP …………………………………………… Lysosomal membrane glycoprotein

LAMTOR ……. Late endosomal/Lysosomal adaptor MAPK and MTOR activator

LB …………………………………………………………………….. Lewy body

LC-MS/MS …….....……… liquid chromatography with tandem mass spectrometry

LLOMe …………………………………………………… L-leucyl-l-leucine methyl ester

LN ………………………………………………………………………… Lewy neurites

LOF .... *loss of function*

LRRK2 .... *Leucine-rich repeat kinase 2*

LYTL .... *lysosomal tubulation driven by LRRK2*

MAO-B .... *monoamine oxidase type B*

MDS-UPDRS … *Movement Disorder Society-Unified Parkinson's Disease Rating*

MEFs .... *Mouse embryonic fibroblasts*

MLi-2 .... *Merck LRRK2 inhibitor 2*

MPP+ *1-methyl-4-phenylpyridinium*

MRP .... *membrane resident protein*

NAC .... *non-A Beta component*

NEM .... *N-ethylmaleimide*

NM .... *neuromelanin*

NTC .... *non-targeting control*

nTPM .... *number of transcripts per million*

OE .... *overexpression*

P0 .... *postnatal day 0*

PBMC .... *peripheral blood mononuclear cells*

PD .... *Parkinson's Disease*

PET .... *Positron emission tomography*

PI(3)-P .... *Phosphatidylinositol 3-phosphate*

PO .... *per os*

PPM1H .... *Protein phosphatase Mg2+/Mn2+ Dependent 1H*

proSP-C .... *Prosurfactant protein C*

PTM .... *post-translational modification*

qPCR .... *quantitative polymerase chain reaction*

REM .... *rapid eye movement*

RILP .... *Rab interacting lysosomal protein*

RILPL1/2 ……………………………... *Rab interacting lysosomal proteins like 1/2*

ROC …………………………………………………….. *Ras-of-complex*

ROS …………………………………………………… reactive oxygen species

scRNA-seq ……………………………………….. *single cell RNA sequencing*

SD …………………………………………………… *standard deviation*

SKIP …………………………………….. *SifA and Kinesin Interacting Protein*

SNpc ………………………………………… *Substantia Nigra pars compacta*

snRNA-seq ……………………………………… *Single nuclei RNA sequencing*

STED ……………………………… *Stimulated emission depletion microscopy*

STN ……………………………………………….. *Subthalamic nucleus*

TCE ……………………………………………… *trichloroethylene*

TGN ………………………………………………. *trans-Golgi network*

TMT ……………………………………………… *tandem mass tag*

Uqcrc1 ………………………. Ubiquinol-cytochrome c reductase core protein 1

Uqcrc2 ………………………. Ubiquinol-cytochrome c reductase core protein 2

Vdac2 …………………………………. voltage dependent anion channel 2

VPS35 …………………………….……… *vacuolar protein sorting ortholog 35*

1   INTRODUCTION

1.1   Parkinson's Disease

1.1.1   History and overview

Depictions of Parkinson-like features were recorded as early as 1000 B.C. in the Ayurveda medical texts of ancient India, in which 'kampavata' (*kampa* meaning temor, and *vata* meaning physiological movement) signs and symptoms included the inability of free movement (akinesia), shaking localized to the head, and a blank stare (Manyam, 1990). The first formal description of PD within the Western world came from British physician James Parkinson in "An Essay on the Shaking Palsy" published in 1817. It was there that he described six cases, all of which possessed a localized tremor to a limb or the head, bent posture, and the inability to control walking speed (Parkinson, 2002). This *paralysis agitans*, or shaking palsy, adopted the name Parkinson's Disease fifty years later by the French physician Jean-Martin Charcot, who identified rigidity and bradykinesia as additional hallmarks, as well as noting a lack of lesions in the brain and spinal cord in autopsies (Charcot, 1879). The latter observation helped to delineate probable causes of disease by segregating the disorder from others such as multiple sclerosis. Interestingly,

both physicians had noted in their reports the difficulty in classifying this

disease, as many presenting symptoms overlapped with other diseases, often

resulting in a misdiagnosis. This is still a hurdle in the accuracy of diagnosis

today as wide-ranging parkinsonian features can present in other neurological

disorders. In the late 1800s, Dr. Sir William Gowers, who having observed

upwards of 80 patients presenting with PD, elaborated on additional details of

age at onset, concluding it to be a disease commencing in late adulthood,

and even noted the slight increase of prevalence in men compared to women

(Gowers, 1888).

1.1.2 Symptomology and Diagnostics

PD is a progressive disorder, characterized by motor and non-motor

symptoms and typically affecting individuals in their later stages of life.

Records from traditional Chinese medicine dating back to 425-221 B.C.

describe symptoms of stiffness and postural disturbances such as the

propensity for the body and limbs to bow forward in addition to an

incontrollable tremor (Zhang et al., 2006). All these symptoms are still used

today in the diagnosis of PD, with the cardinal features being tremor, rigidity,

and bradykinesia.

Additionally, typical PD also features gait changes, asymmetrical reduction in arm swing, and difficulty initiating, terminating, and alternating movement (Hayes, 2019). More subtle features include a decrease in spontaneous swallowing resulting in sialorrhea (Bagheri et al., 1999), urinary constraint (Uchiyama et al., 2011), decrease in blink rate, and a less emotive face due to reduced movement of the facial muscles (Hayes, 2019). The forward lurch of the torso can also lead to postural instability and cause falling in the later stages of the disease.

A slew of non-motor symptoms have also been identified and are becoming more useful in the diagnosis of PD, with constipation being one of the most common that precedes the onset of motor PD symptoms by up to a decade (Abbott et al., 2003; Kaye et al., 2006). Additionally, loss of smell is found in up to 90% of patients and may also precede the onset of motor symptoms as well as disturbances in the rapid eye movement (REM) stage of sleep (Haehner et al., 2009; Poewe, 2008). Depression, anxiety, and fatigue are also common comorbidities, with cognitive impairments becoming more prominent as the disease progresses (Hayes, 2019; Lees et al., 2009; Reijnders et al., 2008).

In addition to symptomatic presentation, usually a clinical diagnosis is made if improvements in tremors, rigidity, and paucity of movements are seen with levodopa treatment (also known as L-DOPA or l-3,4-dihydroxyphenylalanine), a dopamine precursor. Dopamine (DA) and its role in pathogenesis will be introduced in the following section. Although a clinical diagnosis may seem straightforward, because early signs like constipation and muscle stiffness can have ambiguous origin, it is not uncommon for there to be a lag from presentation of the first symptoms to diagnosis of many years (Lees et al., 2009). PD can also include atypical features, such as early cognitive impairment, amyotrophy, gaze palsy, ataxia, and apraxia that may contribute to misdiagnosis (Scholz and Bras, 2015). Conversely, it is not uncommon for patients with other neurological disorders to be given a PD diagnosis, as parkinsonian features like resting tremor and muscle rigidity can have alternative causes such as long-standing essential tremor and multiple system atrophy (Marsili et al., 2018). Thus, accurate clinical diagnosis is challenging due to overlapping clinical features as well as phenotypic variability. It is because of this phenotypic variability that a definite diagnosis of PD cannot be made until autopsy.

1.1.3 Neuropathology

A neuropathological hallmark of PD is a relatively selective loss of DA neurons of the Substantia Nigra *pars compacta* (SNpc) (Lees et al., 2009; Lima et al., 2012). This is visually striking upon autopsy, as these cells contain neuro-melanin, giving them a black appearance in a healthy aging brain that is lost in PD (Figure 1.1).
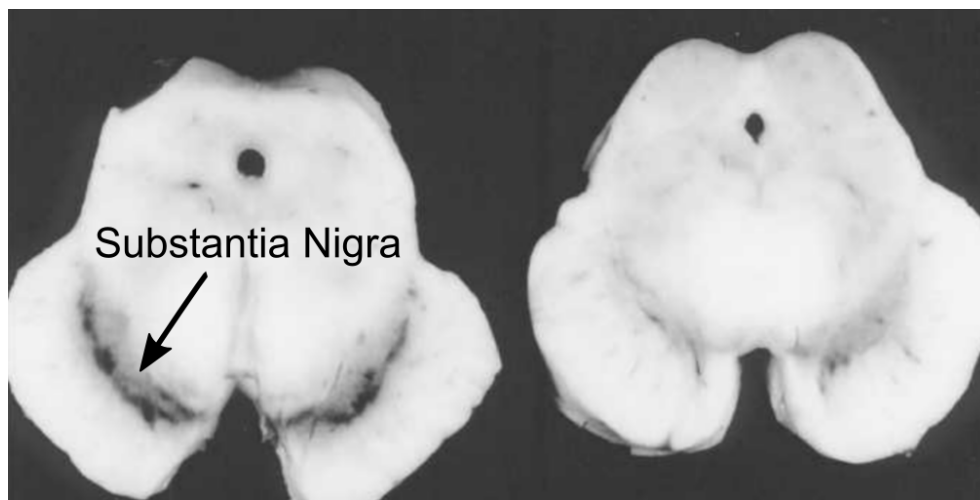
Figure 1.1. **Pathological loss of dopaminergic neuron population of the SNpc in PD.** A healthy aged brain (left) has neuro-melanin pigmented DA neurons in the Substantia Nigra that are lost in a PD affected midbrain (right). Adapted from (Mackenzie, 2001).

These neurons project to the striatum, putamen and caudate nuclei that make up the basal ganglia, and their loss impedes normal motor function. Neuronal loss is also seen in the locus coeruleus, dorsal nuclei of the vagus, raphe nuclei, nucleus basalis of Meynert, and some areas within the brainstem (Damier et al., 1999). It is still unclear why DA neurons are selectively vulnerable to cell death in PD, however, there is evidence that cytosolic DA oxidation leads to the production of damaging free radicals that may compromise the longevity of

these cells (Greenamyre and Hastings, 2004). DA is a neurotransmitter involved

in reward, learning, and voluntary movement systems (Wise, 2004). DA is

synthesized from the hydroxylation of tyrosine at the phenol ring by tyrosine

hydroxylase (TH) to yield dihydroxyphenylalanine (DOPA), the precursor for all

catecholamines such as dopamine, epinephrine, and norepinephrine (Meiser et

al., 2013). DOPA is then decarboxylated into DA by amino acid decarboxylase

(AADC or DOPA decarboxylase) (Meiser et al., 2013). Because of DA's high

volatility, there are a few mechanisms in place to prevent its oxidation in the

cytosol of these neurons. Firstly, once DA is synthesized, it is packaged into

synaptic vesicles via monoamine transporter VMAT2 (Eiden and Weihe, 2011).

Secondly, any DA leaking from these vesicles is quickly degraded through a

process initiated by monoamine oxidase (MAO) via deamination (Meiser et al.,

2013). However, hydrogen peroxidase is a byproduct of this degradation, a

reactive oxygen species (ROS), that can also damage these neurons over time.

Within the synaptic cleft, DA is also taken up by surrounding glial cells that

degrade it via MAO as well as catechol-O-methyl transferase (COMT) (Meiser

et al., 2013) (Figure 1.2).
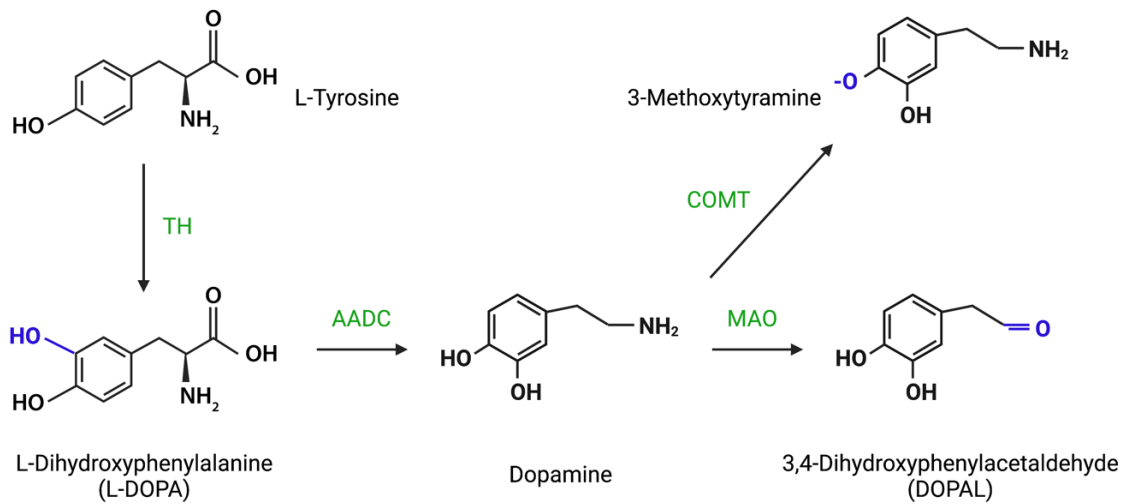
Figure 1.2. **Dopamine synthesis and degradation.** Molecular structures of dopamine precursors and derivatives. Modifications between molecules and enzymes involved in conversions are highlighted in blue and green, respectively.

Although DA oxidation has neurotoxic properties, DA neuron loss is constricted to the SNpc in PD whereas other populations of DA neurons, such as those in the hypothalamus and ventrolateral reticular formation, are left intact (Matzuk and Saper, 1985; Saper et al., 1991). Thus, DA oxidation alone cannot be responsible for the neuronal loss seen in PD. One additional theory is based on the physiology of SNpc DA neurons, as they rely upon L-type calcium channels to govern autonomous pacemaking, while most other neurons use sodium channels, although the direct link between calcium and neuronal vulnerability remains elusive (Chan et al., 2010; Ping and Shepard, 1996).

In addition to observation at autopsy, the development of positron emission tomography (PET) allows for the investigation of dopaminergic neuron loss in living patients using radiotracers such as ^{18}F-DOPA and those used to label the dopamine transporter (DAT), responsible for the reuptake of dopamine after release into the synaptic cleft (Loane and Politis, 2011). PET scans have been infrequently used when diagnosing PD, as they are relatively expensive (Loane and Politis, 2011), however recent approvals for insurance coverage in some countries like the United States have increased their diagnostic potential (American Parkinson Disease Association, 2020).

In addition to cell loss, large proteinaceous neuronal inclusions known as Lewy bodies (LBs) are also found throughout the brain and brainstem (Lewy, 1912). Immunohistochemistry reveals that these inclusions are mostly made up of post-translationally modified (PTM) α-synuclein, a highly expressed presynaptic protein, and also contain neurofilaments and ubiquitin (Figure 1.4A) (Kuzuhara et al., 1988; Lennox et al., 1989; Spillantini et al., 1997). LBs are also found in Dementia with Lewy Bodies (DLB) and in Alzheimer's Disease (AD), making them a common feature of a variety of neurodegenerative diseases classified together as α-synucleinopathies (Kosaka, 1990; Marui et al., 2004; Menšíková et al., 2022). Lewy neurites (LNs), elongated, serpentine or club-like inclusions found in both the soma and axons of neurons, also stain for

α-synuclein (Braak et al., 1999). Using immunohistochemistry on *post-mortem* brain tissue, one study mapped out that the progression of LB deposition is a six-stage process, initiating in the olfactory bulb and the dorsal vagal nucleus and gradually ascending across limbic and cortical areas in later stages (Braak et al., 2003). Based off this model, the SN starts to accumulate these depositions in stage three, although there are criticisms to this model (Burke et al., 2008). Interestingly, one study found that LBs are present in a constant proportion of 3-4% of nigral neurons regardless of disease duration, suggesting that LBs are formed and degraded throughout the course of the disease (Greffard et al., 2010). This is distinct from neurofibrillary tangles found in AD, which accumulate in the brain over time.

α-Synuclein is a very small protein, with only a 140aa sequence and is generally natively unfolded, however, it does form α-helices on negatively charged lipids as well as **β**-sheets (Stefanis, 2012). It is primarily localized in the nucleus and presynaptic terminals of neurons and accounts for an estimated 1% of total soluble cytosolic proteins in whole brain lysates (Iwai et al., 1995; Shibayama-Imazu et al., 1993). The highest expression of α-synuclein is in the brain as well as cerebrospinal fluid (CSF) and red blood cells (Barbour et al., 2008; Borghi et al., 2000). The protein structure is composed of three distinct regions: an N-terminus rich with apolipoprotein binding motifs that allow the

α-helical formation when bound to phospholipids such as membranes

(Davidson et al., 1998), a central hydrophobic region called non-A**β**

component (NAC) which confers the **β**-sheet potential, and a highly negative

C-terminus that is prone to be unstructured and houses most known PTMs

including phosphorylation and nitration (Giasson et al., 2000). Thus, it is

thought that the C-terminal tail acts as its functional core for downstream

signaling. When in the presence of membranes, the N-terminus is highly

structured with two α-helices made up of seven imperfect 11aa repeats from

25-90aa laying close to the phospholipid bilayer (Jao et al., 2008) (Figure 1.3).
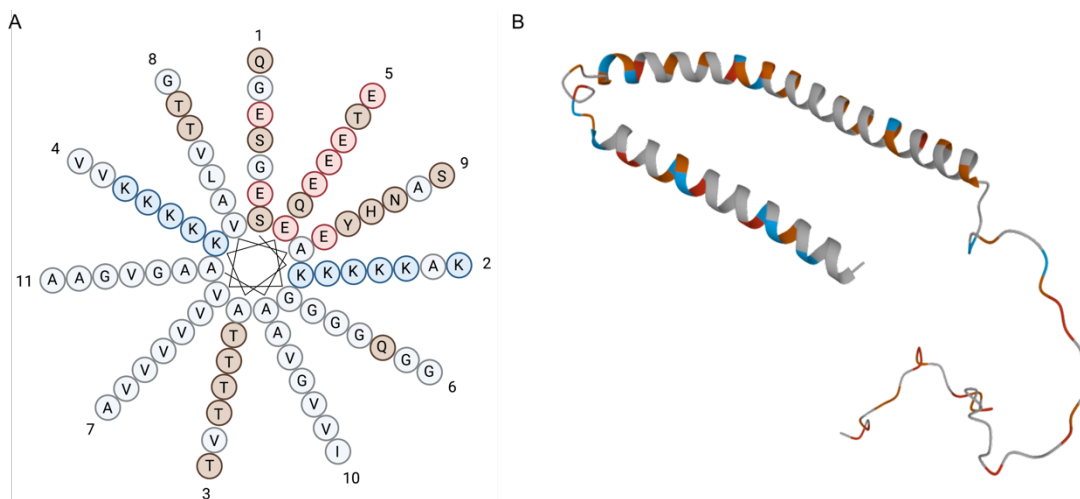
Figure 1.3. **Structure of membrane-bound α-synuclein.** (**A**) Birds-eye-view of the N-terminal α-helical structure of membrane-bound α-synuclein. This structure is comprised of an 11aa right-handed coil. Residues in a single repeat are numbered 1-11 with structural orientation shown in the center starting with aa 1. (**B**) 3D construction of full length α-synuclein. Colors on both A and B denote acidic (red), basic (blue), polar uncharged (brown), and nonpolar (grey) residues. Modeling is based off *Rao et al. 2010* (PDB ID: 2KKW).

Furthermore, the NAC region is believed to play a role in the protein's ability to aggregate, as this fragment was identified in high abundance in purified AD amyloid preparations (Uéda et al., 1993). In addition, one study showed that aggregation of α-synuclein was inhibited with in cells overexpressing a plasmid with a truncated NAC region compared to wildtype, confirming that this region plays a role in the protein's ability to form aggregates (Periquet et al., 2007). In addition, a recent study has found that the constitutively acetylated N-terminal also plays a role in the ability to form aggregates, as loss of this acetylation increases aggregation (Bell et al., 2022). In a healthy state, α-synuclein is soluble and intrinsically disordered, while it is insoluble and highly ordered in disease states. Thus, in a healthy state, its monomeric form adopts a wide range of conformations that are stabilized through long-range electrostatic interactions between N- and C- terminal residues (Dedmon et al., 2005; Breydo et al., 2012) whereby disruptions of these interactions via mutations or PTMs can lead to misfolding of the monomer and propagate aggregation (Villar-Piqué et al., 2016).

Although the mechanism leading to the formation of LBs remains elusive, two recent studies have been able to reveal the structure of LBs using Stimulated Emission Depletion (STED) microscopy (Moors et al., 2021; Shahmoradian et al., 2019). Both identified LBs in the SNpc of *post-mortem*

human brains to have rather smooth edges, with an immunoreactive ring of

phosphorylated α-synuclein at site Ser129 with a dense, unstained core (Figure

1.4B). Phosphorylated Ser129 α-synuclein has previously been shown to be

higher in PD tissue compared to controls (Anderson et al., 2006; Fujiwara et al.,

2002). Ser129 phosphorylation is regulated by Polo-like kinases PLK1, PLK2,

and PLK3, with the strongest affinity for α-synuclein belonging to PLK2 *in vivo*

(Bergeron et al., 2014; Inglis et al., 2009). Shahmoradian and colleagues

additionally found lipid membranes from lysosomes and mitochondria encased

around the LBs, suggesting a protein-lipid compartmentalization

(Shahmoradian et al., 2019).
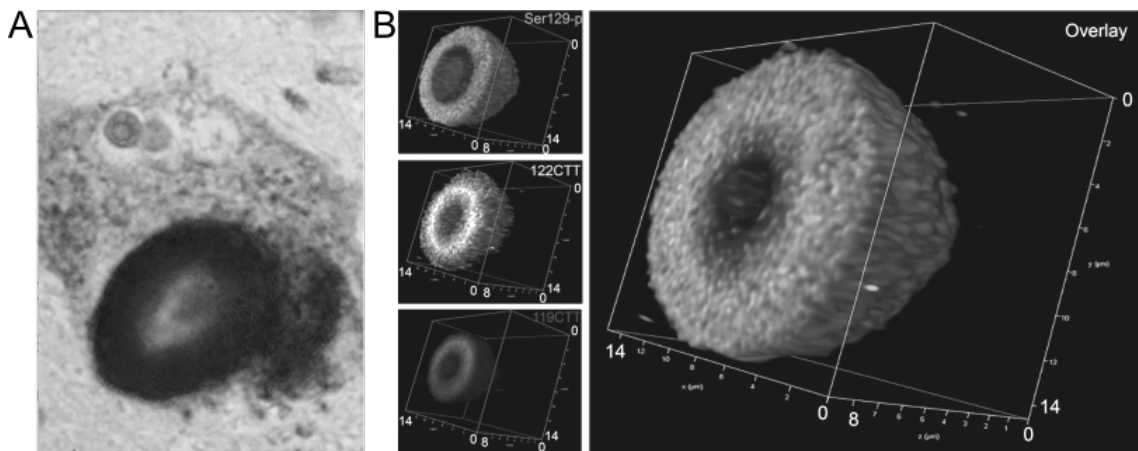
Figure 1.4. **Morphology and structure of Lewy bodies.** (**A**) Large LB inclusion stained for phosphorylated α-synuclein in a pigmented nigral neuron. (**B**) 3D rendering of a STED microscopy image of an LB showing an onion-like organization of α-synuclein PTMs. These images were reproduced from (Wakabayashi et al., 2013; Moors et al., 2021).

1.1.4 Peripheral Pathology and Inflammation

As previously mentioned, one of the most common non-motor symptoms of PD is constipation, which can precede the onset of motor symptoms by decades and continues throughout the disease's progression. In addition to constipation, other gastrointestinal (GI) impairments are commonly observed at all stages of PD, including drooling, dysphagia, and gastroparesis (Pfeiffer, 2003). Although these symptoms are common, the literature on GI pathology in PD are conflicting. Previous studies have observed a loss of vasoactive intestinal peptide neurons as well as DA neurons in the colons of patients with PD, whereas others have reported no difference in neuron count per ganglion nor proportion of DA neurons in the submucosa (Lebouvier et al., 2008; Singaram et al., 1995; Wakabayashi et al., 1993).

Additionally, *post-mortem* pathological examinations identified intraneuronal α-synuclein aggregations in the enteric nervous system, particularly within the myenteric and submucosal plexuses (Braak et al., 2006). Autopsy reports using immunohistochemistry found that α-synuclein aggregates were most abundant in the esophagus and stomach compared to the colon (Annerino et al., 2012; Beach et al., 2010; Gelpi et al., 2014). With the generation of phospho-specific S129 α-synuclein antibodies, several recent studies have also confirmed aggregates containing the phosphorylated protein

in the GI tracts of PD patients in both autopsy and biopsy specimens (Chiang

and Lin, 2019). However, most studies had fewer than 30 participants, some of

which observed α-synuclein accumulation in the GI tracts of control subjects

and some of which observed no difference between patient and control

samples (Chiang and Lin, 2019). Additionally, one study found that the

proportion of α-synuclein positivity did not differ between prodromal and later

stages of PD, suggesting that GI pathology may present itself in prodromal

phases of the disease, but is not progressive (Hilton et al., 2014). Another

study reported a positive correlation with GI pathology and subscores on the

Movement Disorder Society-Unified Parkinson's Disease Rating Scale (MDS-

UPDRS) (Lebouvier et al., 2010), a diagnostic series of tests to categorically

define PD progression. These conflicting data are the result of low sample

numbers, variable GI conditions among individuals, and variable PD subtypes

and disease durations, including different neurodegenerative disease samples

such as Lewy body dementia. Therefore, it is important to design follow-up

studies addressing these variables in order to confirm GI pathology as disease-

specific.

Moreover, alterations in gut microbiota have also been implicated in PD

as well as gut inflammation. Several studies have reported that small intestinal

bacterial overgrowth is more prevalent in patients with PD compared to

healthy controls, with some reporting an improvement in UPDRS scores after treatment for overgrowth (Fasano et al., 2013; Gabrielli et al., 2011; Tan et al., 2014). In addition, a few studies have reported differences the composition of gut microbiota, although results vary widely, making it difficult to conclude which microbiota are increased or decreased in PD (Chiang and Lin, 2019). Interestingly however, a significant decrease in *Faecalibacterium prausnitzii* has been consistently reported across studies, which has also been shown to be depleted in patients with inflammatory bowel diseases (IBDs) (Berry and Reinisch, 2013; Hill-Burns et al., 2017; Petrov et al., 2017; Unger et al., 2016). In both acute and severe colitis mouse models, treatment with *F. prausnitzii* led to a significant decrease in colitis severity as measured by a decrease in neutrophilic infiltration, and down-regulation of pro-inflammatory cytokines and T-cell levels (Martín et al., 2014). This suggests that *F. prausnitzii* acts as an anti-inflammatory agent. In addition, levels of fecal short chain fatty acids are diminished consistently across PD patient cohorts, a main metabolic product of various gut microbiota, supporting a general decrease in some species that could be indicative of alterations in the enteric nervous system (Unger et al., 2016).

Many studies have connected IBD and PD through meta-analyses and found increased co-morbidity in patients across cohorts (Peter et al., 2018;

Vacic et al., 2014; Weimers et al., 2019). Interestingly, one study found that

there was a 78% reduction in the incidence rate of PD among patients with IBD

who were exposed to anti-tumor necrosis factor therapy, a strong anti-

inflammatory treatment, compared to those who were not exposed (Peter et

al., 2018). This finding further supports a role of gut inflammation in the

pathogenesis of PD.

Since GI pathology and symptoms are associated with PD, some have

adopted the 'gut-brain axis' hypothesis of pathogenesis, in which bidirectional

communication between the central and enteric nervous systems (CNS and

ENS) occur via the vagus nerve as well as through an increase in gut

permeability. According to this theory, imbalances in the gut microbiome have

the potential to propagate bacterial infection, inflammation, and α-synuclein

aggregation within the gut that can relay to the CNS (Chiang and Lin, 2019).

Several mouse models have been generated to investigate this hypothesis.

One elegant study tested the ability of exogenous α-synuclein preformed

fibrils injected into the duodenal and pyloric muscle layers of the stomach to

propagate endogenous aggregates in the brains of both wildtype mice with

and without an intact vagus nerve. This resulted in increased endogenous α-

synuclein aggregates in the brains of those with an intact vagus nerve, but not

in the mice in which the vagus nerve was severed (Kim et al., 2019). This data

suggests that propagation of exogenous α-synuclein in the gut can influence

aggregation of endogenous α-synuclein in the brain via the vagus nerve.

Subsequently, Kim and colleagues injected these preformed fibrils into the

duodenal and pyloric layers of the stomach in *Snca* KO mice with intact vagal

nerves and observed no accumulation of α-synuclein aggregates in the brain

(Kim et al., 2019). This result suggests that the exogenous α-synuclein alone

could not accumulate in the brain tissue itself. Another model using mice

overexpressing α-synuclein are significantly slower in removing a nasal

bandage from the bridge of their nose as well as to traverse a beam, and to

descend a pole after they were given fecal transplants from PD patients

compared to fecal transplants from healthy controls (Sampson et al., 2016).

These mice were also shown to have increased aggregation of α-synuclein in

the caudate of the brain as well as microglia activation as measured via IL-6

expression in the frontal cortex, suggesting that dysbiosis of the gut

microbiome instigates α-synuclein aggregation in the brain and

neuroinflammation (Sampson et al., 2016). Remarkably, fecal transplantation of

healthy gut microbiota is a treatment for some patients with PD who have

severe constipation (Huang et al., 2019; Kuai et al., 2021; Xue et al., 2020).

Based off data from animal models, it will be important to evaluate fecal

transplant efficacy as a preventative treatment in prodromal PD patients.

1.2 Therapies for individuals with PD

1.2.1 Conventional therapy

Currently, there are no commercially available disease-modifying medications to slow the progression nor completely halt PD. However, there are a number of drugs used to help ameliorate symptoms to improve quality of life, all of which target the generation or preservation of dopamine or its effects in the brain. Recorded in Ayurvedic texts of ancient India, there is record of a treatment containing the beans of *Mucuna pruriens*, the "cowitch plant", in the treatment of *kampavata* (Manyam, 1990). In 1937, researchers isolated what was thought to be the efficacious ingredient in these beans – l-3,4-dihydroxyphenylalanine (Damodaran and Ramaswamy, 1937). This compound, known as levodopa, was later confirmed in controlled studies to have a positive effect on motor symptoms of PD (Cotzias et al., 1967; Vaidya et al., 1978; Apaydin et al., 2000).

Levodopa, which works to replace the dopamine lost in the SN, continues to be the most used medication for treatment of PD symptoms. A precursor of dopamine, levodopa is taken in oral doses daily and absorbed by the small intestine before crossing the blood-brain barrier where it is converted

into dopamine (Schapira, 2005). This treatment remains relatively efficacious

throughout the course of the disease (Schapira, 2005). However, after ~5 years

of treatment, patients start to develop levodopa-induced dyskinesias,

presumably due to the pulsatile stimulation of dopamine receptors as the drug

peaks and wanes throughout the day in the context of progressive striatal

denervation (Schapira, 2005; Jankovic and Aguilar, 2008). Thus, it is common

in later stages of treatment for levodopa to be paired with other classes of

drugs to help prevent unwanted effects and enhance its therapeutic

properties. Anti-dyskinetic drugs such as amantadine have been reported to

reduce levodopa-induced motor complications without reducing efficacy

(Metman et al., 1999). COMT inhibitors are also used to increase the

absorption of levodopa in the gut and prolong its half-life to increase "on"

times versus "off" and to keep "wearing off" dyskinesias at bay (Nutt et al.,

1994). Lastly, carbidopa, a peripheral dopa decarboxylase inhibitor, is useful in

preventing premature metabolism of levodopa when still in the body,

promoting more efficient absorption and increasing half-life similarly to COMT

inhibitors. Thus, it is common to prescribe cocktail drugs containing levodopa

and carbidopa together such as Sinemet (Jankovic, 2008). However, studies

have reported an alteration in gut microbiota in those taking COMT inhibitors

and, to a lesser extent, carbidopa/levodopa medications which may affect

disease progression based on the correlation between the gut and brain (Hill-Burns et al., 2017).

Eventually, most patients will receive levodopa treatment, however, due to its negative side effects, some physicians may try to delay the start of levodopa treatment in patients with early stages of PD. Dopamine agonists like ropinirole or pramipexole that stimulate D1 and D2 receptors are prescribed as an alternative (Brooks, 2000; Weiner et al., 2001). These drugs are safe and effective alternatives and can circumvent dyskinesia, although it is common for nausea, drowsiness, increased risk-taking behavior, and hypotension to occur, the latter increasing the risk for leg edemas (Claassen et al., 2011; Jankovic, 2008). Some physicians will also use a DA agonist in parallel with levodopa so that the dose of levodopa can be reduced and thus effectively reduce dyskinesia severity (Jankovic, 2008). Similarly, another route is the use of monoamine oxidase type B (MAO-B) inhibitors, effectively inhibiting the metabolism of natural dopamine in the brain to modestly improve motor symptoms in patients with PD in early stages of the disease (Schapira, 2005).

Whether to use DA agonists over levodopa in early stages of PD has caused some debate. Those in favor of early DA agonist use support the idea that the delay in levodopa prolongs years of disease without motor fluctuations

and dyskinesias while still achieving favorable effects on clinical symptoms and potential delaying of disease progression (Parkinson Study Group, 2002; Whone et al., 2003). Conversely, others support the idea that introduction of levodopa in early PD provides longer periods of fine motor control, slower progression of disability, and longer life expectancy (Lees et al., 2001; Rajput et al., 2002). Ultimately, the treatment plan must be tailored to each individual patient and their particular needs and goals.

1.2.2 Deep Brain Stimulation

Deep brain stimulation (DBS) was first approved by the United States Food and Drug Administration (FDA) in 2003 as a treatment for advanced PD. Rather strict inclusion criteria are used to assess candidacy for DBS, including the presence of tremor which fails to improve with conventional levodopa therapy, presence of levodopa-sensitive "off" symptoms or dyskinesia, and an absence of dementia or other cognitive impairments or comorbidities (Hartmann et al., 2019). It is also required that the patient is not older than 70 years old, as this increases the probability of complications during surgery, particularly in bilateral electrode placement. This criterion is based on several studies indicating that older age correlated with less efficacy and a reduced improvement on quality-of-life after DBS surgery compared to younger candidates (Derost et al., 2007; Russmann et al., 2004).

As clarity on basal ganglia circuitry grew, the subthalamic nucleus (STN) has become predominantly favored as the target for electrode placement, although comparative reports on improved motor functions and reduced dependency on levodopa are found on globus pallidum internus (GPi) placement (Hartmann et al., 2019). Thus, the target chosen falls towards patient-specific symptomology, as neurostimulation of the STN typically allows patients to reduce their levodopa intake and thus reduces levodopa-sensitive "off" and "weaning time" motor complications (Deuschl et al., 2006), while GPi stimulation seems to reduce dyskinesias directly (Zhang et al., 2021) as well as improve psychomotor processing speed in the Stroop color-naming test (Elgebaly et al., 2018). DBS is equally effective in both sporadic and monogenic PD patients, making it a viable option for a broad range of genotypically distinct PD cases (Angeli et al., 2013). Interestingly, a large meta-analysis encompassing data from over two thousand PD patients that underwent DBS surgery reported a decrease in long-term memory and verbal fluency compared to control patients that had not undergone the surgery (Bucur and Papagno, 2022). Such negative effects are troublesome; however, it is difficult to distinguish whether the cognitive decline is truly a result of the surgery/stimulation, or due to aging.

1.2.3 Alternative methods: the future of genetically driven individualized therapeutics

For nearly the last six decades, the treatment of PD has been centered on dopamine replacement therapies, as progress in the development of disease-modifying treatments for PD has been limited. Thus, it is a particularly exciting time for PD therapeutics, with multiple clinical trials underway for mechanistically targeted therapies, i.e., LRRK2, GBA and α-synuclein, in the form of small molecules as well as antisense oligonucleotides (ASOs) (McFarthing et al., 2021).

Currently, the most favored target is α-synuclein, with several drugs in clinical trials across phases I, II, and III (McFarthing et al., 2021). The rationale for targeting α-synuclein is based on strong genetic and pathological data, but many of these trials have yet to show efficacy in the treatment of PD. Several of these drugs utilize antibodies raised against α-synuclein with the goal of degrading aggregated protein in the brain such as prasinezumab (Pagano et al., 2021). One trial testing efficacy of treatment of the antibody cinpanemab (BIIB054) generated by Biogen was recently withdrawn after Phase II trials showed no improvement of motor symptoms as evaluated by the MDS-UPDRS (Kuchimanchi et al., 2020). The high failure rate of these trials is not a new

phenomenon, as 99% of the 200 AD trials have also failed, as well as several promising trials for Huntington's Disease (HD) targeting the Huntington protein using ASOs (Kingwell, 2021; Yiannopoulou et al., 2019). This is most probably due to the complexity of neurodegenerative diseases and their aging component that most disease models lack.

Conversely, there are some early-stage α-synuclein trials using active immunotherapy with a short peptide targeting oligomeric forms of the protein that have shown to be responsive in degrading aggregates in preclinical mouse models and have currently passed safety and toxicity in humans (Mandler et al., 2014; Volc et al., 2020). Another trial is investigating the efficacy of venglustat, an allosteric inhibitor of glucosylceramide synthase that may indirectly reduce the opportunity for α-synuclein aggregates to form (Peterschmitt et al., 2021). Taken together, it is expected and realistic to assume the failure of many trials before discovering true disease-modifying treatments, however, the path to effective treatments is now more hopeful than at any other time in the past half century. Additionally, there are some trials in progress that show some promising endpoints in target engagement, mainly in LRRK2-targeting treatments, which will be discussed in detail in Chapter 3.

1.3 Economic and Caregiver Burden

PD is currently the world's fastest growing brain disease (GBD 2016 Neurology Collaborators, 2019). It is estimated that over 6 million individuals are currently living with a PD diagnosis, and that number is expected to double by 2040 (Dorsey and Bloem, 2018). In 2017, it was estimated that the total economic burden of PD in the U.S. was nearly $52 billion, half of which amounted to direct medical costs, the other half indirect from productivity losses, non-medical expenses, and disability income (Yang et al., 2020). Without intervention, total economic burden is projected to increase to $79.1 billion in 2037, without taking natural inflation into consideration (Yang et al., 2020). Overall, the economic and mental burden for patients, caregivers and governments is staggering and it is only a matter of time before this burden causes a national state of emergency. Thus, effective and affordable treatments will be imperative moving forward.

1.4 Etiology

"So slight and nearly imperceptible are the first inroads of this malady, and so extremely slow its progress, that it rarely happens, that the patient can form any recollection of the precise period of its commencement."

James Parkinson – Essay on the Shaking Palsy, 1817.

By the time an individual is diagnosed with PD, up to 80% of striatal dopamine is lost as well as between 30-70% of dopamine neurons in the SNpc (Cheng et al., 2010). Since initial prodromal symptoms of PD can start several decades prior to motor PD, taken together, this makes preventative interventions very difficult.

1.4.1 Age

Aging is the major risk factor for PD. A meta-analysis conducted in 2014 revealed that prevalence is 18 times higher for the disease in people over 80 years of age compared to those that are 50-59 years of age (1,903 vs 107 per 100,000 individuals) (Pringsheim et al., 2014). Studies of have shown dopaminergic neurons in the Substantia Nigra (SN) to be particularly vulnerable to aging, with reports of up to 50% of DA neuron loss even in individuals without neurological disease (Buchman et al., 2012; Reeve et al., 2014; Rudow et al., 2008).

As the human brain ages, its efficiency at handling certain insults of normal cellular function decreases, making it susceptible to prolonged and detrimental damage from oxidative stress, mitochondrial dysfunction, and inflammation (Reeve et al., 2014). Although aging effects the brain globally, DA neurons in the ventral SN may be particularly vulnerable due to the nature of dopamine metabolism which generates several toxic oxidative species including hydrogen peroxide (Meiser et al., 2013). Failure to sequester these species properly results in the accumulation of ubiquitin-positive inclusions and lipofuscin, which may perpetuate intracellular damage and eventual neuron death (Kanaan et al., 2007; Pang et al., 2019). In addition to the oxidation of dopamine, increases in intracellular α-synuclein have been associated with age-related decreases in nigral TH, the rate-limiting enzyme in dopamine synthesis (Chu and Kordower, 2007).

Aging is also associated with neuronal damage due to iron accumulation in the SN and increased microglia activation, an indicator of neuroinflammation (Kanaan et al., 2008; Sugama et al., 2003; Zecca et al., 2004, 2001). Thus, understanding why dopamine neurons are more vulnerable to aging compared to other neuronal cell types in other regions may give insight into the neuronal loss found in PD.

1.4.2 Environmental Risk

Historically, PD was considered to be purely sporadic in nature until 1979, when a case of parkinsonism that persisted for 18 months was reported in a 23-year-old male after injection of a meperidine congener (Davis et al., 1979). Then, in 1983, Dr. J. William Langston identified six patients that rapidly developed PD overnight after using a new synthetic form of heroin, 1-methyl-4-phenyl-1,2,3,6-tetrahydropyridine (MPTP) (Langston, 2017; Langston et al., 1983). The lipophilic MPTP was able to cross the blood-brain barrier (BBB) where it is was quickly converted into the toxic 1-methyl-4-phenylpyridinium (MPP+) (Langston et al., 1984). MPP+ was found to be a high-affinity substrate for the dopamine uptake system, causing selective accumulation in DA neurons and inevitable cell death through the disruption of mitochondrial Complex I (Ramsay et al., 1986; Shen et al., 1985).

This phenomenon of drug-induced parkinsonism led to the hypothesis that neurotoxins are a risk factor for PD. Scientists have since identified over a dozen environmental toxicants associated with PD, particularly found in some herbicides and pesticides like paraquat and rotenone (Ascherio et al., 2006; Elbaz et al., 2009; Tanner et al., 2011; Pezzoli and Cereda, 2013) as well as industrial organic solvents such as trichloroethylene (TCE) (Guehl et al., 1999; Bove et al., 2014; De Miranda and Greenamyre, 2020). Thus, PD prevalence

52

has been shown to be concentrated among people working or living near industrial factories and large-scale agricultural farms where use of these products is prevalent. In fact, some studies have shown those who have lived and consumed private well-water contaminated with pesticides in agricultural regions of California have an increased risk of developing PD (Gatto et al., 2009). These epidemiological and case study findings were partially recapitulated in animal models to further solidify the link between toxicant exposure and DA neuron loss, α-synuclein accumulation, and neuroinflammation (Betarbet et al., 2000; Sherer et al., 2003; Hatcher et al., 2007; Cannon et al., 2009). Exposures to heavy metals such as iron, copper, lead, and mercury have also been proposed to increase risk for PD, although evidence is sparse and difficult to interpret (Ball et al., 2019).

Traumatic brain injury (TBI) has also been linked to PD risk (Gardner et al., 2015; Andrew et al., 2021). One study found that veterans who experienced mild or moderate/severe TBI were 56% and 83% more likely to develop PD, respectively (Gardner et al., 2018). One argument made against TBI incident in older adulthood as a risk factor for PD is that, as most TBI incidents are due to falls, it is difficult to distinguish whether the fall occurred because of undiagnosed, early symptoms of PD already and natural, accidental falls that cause PD (Coronado et al., 2005; Gardner et al., 2015, 2018). One

study of a Danish cohort that evaluated over 1,700 patients with PD reported

no association between any head injury prior to the first cardinal symptom and

PD (Kenborg et al., 2015). Overall, environmental risk is still definitively

ambiguous as a cause of PD given the nature of the disease and its decades-

long prodromal phase. It is difficult to provide direct links of cause when time

between exposure and onset of identifiable symptoms of disease range is in

years. It is also difficult to quantify exposure accurately in retrospect, thus

estimating their effects is challenging.

1.4.3 Genetic Risk

The first monogenetic cause of PD was identified in 1997 where several

family members of an Italian kindred were found to have a single point

mutation in the *SNCA* gene that encodes for α-synuclein (Polymeropoulos et

al., 1997). The mutation discovered changed an alanine to a threonine at the

53rd amino acid (aa) in the 140aa sequence (p.A53T). This was discovered to

effect conformational change of the protein by shifting the balance between α-

helices and β-sheets, promoting protein aggregation (Meade et al., 2019;

Guzzo et al., 2021). This genetic mutation was discovered in the same year that

α-synuclein was identified as a main component of Lewy bodies, and as the

main non-Aβ component of amyloid plaques in AD two years prior (Iwai et al.,

1995), linking familial and sporadic cases for the first time.

It is now believed that monogenetic mutations account for up to 10% of all PD cases (Lesage and Brice, 2009), with identification of multiple autosomal dominant and autosomal recessive genetic mutations (Table 1.1). These mutations span 19 loci, denoted as the *PARK* loci, of which 11 of the genes have been identified. The other 8 loci range in their progress towards confirmed gene identification. *PARK3* and *PARK11* are still unconfirmed disease risk loci since their first descriptions in 1998 and 2002, respectively (Klein and Westenberger, 2012). Three loci have primary gene candidates: UCHL1 (PARK5), HTRA2 (PARK13), and EIF4G1 (PARK18), however all are unconfirmed with only one description each, although efforts have recently been initiated to investigate these candidates further (Chartier-Harlin et al., 2011; Krüger et al., 2011; Leroy et al., 1998). Finally, *PARK10*, *PARK12*, and *PARK16* have been confirmed as PD risk loci via linkage analysis but no candidate genes have been described as of yet (Klein and Westenberger, 2012). Aside from *PARK* genes, common mutations in *Glucosylcerebrosidase 1* (*GBA1*), originally discovered as a cause of Gaucher's disease, have also shown familial links to PD (Sidransky et al., 2009). Additionally, large genome-wide association studies (GWAS) have since identified 90 loci associated with PD lifetime risk (Nalls et al., 2019). The reasons that these genetic variants may contribute to lifetime risk rather than directly cause PD are twofold: these

variants do not have complete penetrance, and there is still a lot that is

unknown regarding gene-gene interaction and influence.

There is accumulating evidence that PD is caused by a combination of

genetic and environmental factors. The lack of penetrance in the most

common genetic mutations leads to the possibility that environmental and

genetic risk are not mutually exclusive, and that both compounding on one

another initiates pathogenesis (Figure 1.5).
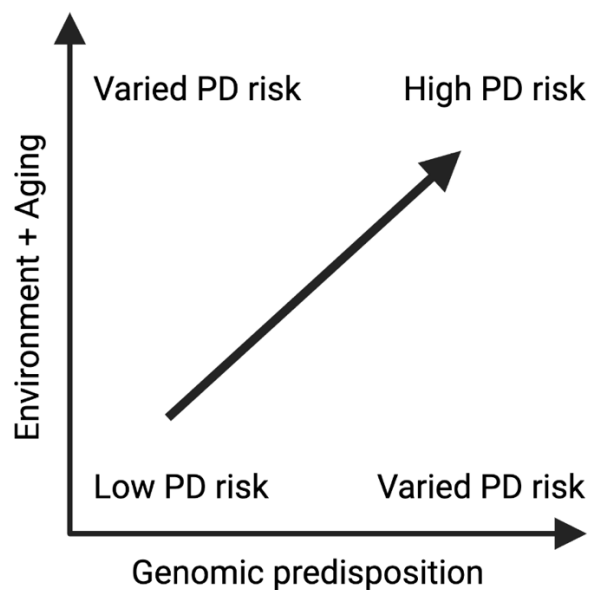
Figure 1.5. **Environment-Genetic relationship hypothesis.** PD risk varies with both genomic predisposition and environmental factors including aging.

For example, an additional and more direct link between genetics and the

environment is currently being investigated through epigenetics, as chemical

pollutants, nutrition, and other environmental stressors can influence gene

expression via epigenetic modifications (Pavlou and Outeiro, 2017). Although

no strong relationships have been identified yet in PD, epigenetic

dysregulation has been thought to play an important role in other

neurodegenerative diseases such as AD (Lu et al., 2014) and HD (Zuccato et

al., 2007). To date, some studies have found abnormal hypo- and hyper- DNA

methylation in over 20 genes in patients with PD compared to healthy controls,

some of which were found in the promoter region of the *SNCA* gene. These

changes in *SNCA* have also been identified in those with alcoholism or

anorexia, hypothesizing that metabolic alterations can trigger these DNA-

methylation events (Bönsch et al., 2005; Frieling et al., 2007; Masliah et al.,

2013; Moore et al., 2014). Some studies have also reported variations in

histone acetylation. One study in particular found increases in acetylation in

the SNpc of post-mortem brains of PD patients (Park et al., 2016). Additionally,

Park et al. found that treatment with rotenone, paraquat, or MPP[+] also

increases histone acetylation in cultured mouse DA neurons (Park et al., 2016).

Thus, it will be imperative to look at combinations of genetic and

environmental risk factors in order to grasp the full picture of PD penetrance.

Locus	Gene	Mutation(s)	Heritability	Frequency	Clinical Presentation	References
PARK1	SNCA	p.A53T, p.A30P, p.E46K, p.G51D, p.A53E	ADm	Rare	Early onset PD	(Polymeropoulos et al., 1997; Krüger et al., 1998; Zarranz et al., 2004; Lesage et al., 2013; Pasanen et al., 2014)
PARK2	PRKN	p.T240R, p.Q311Stop truncation, deletions	ARc	Rare	Juvenile and Early onset PD	(Hattori et al., 1998a, 1998b; Kitada et al., 1998; Leroy et al., 1998; Lucking et al., 1998)
PARK4	SNCA	Triplication, duplication	ADm	Rare	Early onset PD	(Singleton, 2003; Chartier-Harlin et al., 2004; Ibáñez et al., 2004)
PARK6	PINK1	>5 point mutations, truncations	ARc	Rare	Early onset PD	(Valente et al., 2004; Hatano et al., 2004)
PARK7	DJ-1	p.L166P, deletions	ARc	Rare	Early onset PD	(Bonifati et al., 2003)
PARK8	LRRK2	p.R1441C/G/H, p.Y1699C, p.G2019S, p.I2020T, p.N1437H	ADm	Common	Late onset PD	(Paisán-Ruíz et al., 2004; Zimprich et al., 2004; Di Fonzo et al., 2005; Kachergus et al., 2005; Aasly et al., 2010)
PARK9	ATP13A2	Frameshift truncations	ARc	Rare	Juvenile atypical PD	(Ramirez et al., 2006)
PARK14	PLA2G6	>15 point mutations	ARc	Rare	Juvenile and Early onset PD, atypical	(Paisan-Ruiz et al., 2009; Sina et al., 2009; Yoshino et al., 2010; Shi et al., 2011; Lu et al., 2012; Karkheiran et al., 2015)
PARK15	FBXO7	p.T22M, p.R498Stop truncation	ARc	Rare	Juvenile atypical PD	(Di Fonzo et al., 2009)
PARK17	VPS35	p.D260N, p.P316S, p.R524W	ADm	Rare	Late onset PD	(Vilariño-Güell et al., 2011; Zimprich et al., 2011)
PARK19	DNAJC6	p.Q791X, p.Q846X, p.R927G, p.T741=	ARc	Rare	Juvenile and early onset PD, atypical	(Edvardson et al., 2012; Elsayed et al., 2016; Koroğlu et al., 2013; Olgiati et al., 2016)
PARK20	SYNJ1	p.R258Q	ARc	Rare	Juvenile atypical PD	(Krebs et al., 2013; Olgiati et al., 2014; Quadri et al., 2013)

Table 1.1. **Genes harboring causal mutations for monogenic PD.** ADm (autosomal dominant), ARc (autosomal recessive).

1.5 LRRK2 as a genetic and sporadic risk factor

Since its discovery as a PD gene in 2004 by two independent groups, research on *Leucine-Rich Repeat Kinase 2* (*LRRK2*) has gained an overwhelming amount of attention recently, with over 300 original papers and reviews on LRRK2 published annually since 2020 (Figure 1.6). As one of the most common causes of PD worldwide, understanding the normal and pathogenic functions of LRRK2 has grown in importance.
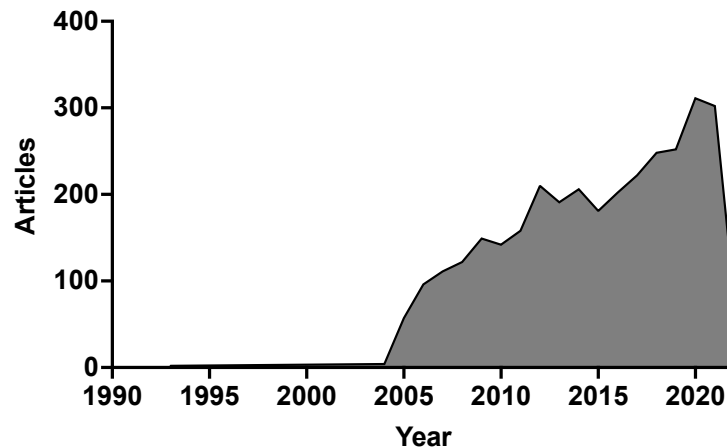
Figure 1.6. **PubMed search of the number of articles containing "LRRK2" from 1990-2022.**

1.5.1 Discovery of LRRK2 mutations and penetrance

The *PARK8* locus was identified in a large Japanese family exhibiting autosomal dominant parkinsonism (Funayama et al., 2002). Linkage analysis identified 116 genes within the locus located on chromosome 12, and the specific gene responsible was discovered independently in two separate studies (Paisán-Ruíz et al., 2004; Zimprich et al., 2004). The original family was

then shown to have a mutation in the same gene, *LRRK2* (Funayama et al.,

2005). Mutations in *LRRK2* were subsequently shown to be a relatively

common genetic cause of PD worldwide (Di Fonzo et al., 2006). To date, out of

approximately 100 putative mutations identified within this gene (Cruts et al.,

2012; Nuytemans et al., 2010; Paisán-Ruíz et al., 2008), eight of these have

been convincingly segregated as disease-causing: G2019S, R1441C/G/H,

Y1699C, I2020T, and N1437H/D (Gasser, 2009; Aasly et al., 2010; Zhao et al.,

2020). The two most common mutations, G2019S and R1441C, are each

responsible for up to around 30% of inherited PD cases in Ashkenazi Jewish

and North African Berber populations, and up to 10 and 2.5% of apparently

sporadic PD cases, respectively (Deng et al., 2006; Hulihan et al., 2008; Correia

Guedes et al., 2010; Bardien et al., 2011; Paisán-Ruiz et al., 2013). The

presence of mutations in what appears to be sporadic cases is likely due to

incomplete but age-dependent penetrance. For example, the penetrance of

G2019S increases from 17% at 50 years old to 85% at 70 years old.

Additionally, there are some carriers who never develop PD (Kachergus et al.,

2005; Hulihan et al., 2008; San Luciano et al., 2010; Lee et al., 2017). Similarly,

R1441C has also been shown to have age-dependent but incomplete

penetrance, suggesting that although these monogenic mutations significantly

increase disease risk, they do not always lead to disease (Trinh et al., 2014;

Kluss et al., 2019; Reed et al., 2019). Interestingly, cohort studies have found

no difference in clinical features between those that are heterozygous and homozygous for these mutations, suggesting no gene dosage effect (Ishihara et al., 2006; Takanashi et al., 2018).

Interestingly, these mutations are population-specific, as G2019S and R1441C are not found in certain Asian populations (Tan et al., 2005; Zabetian et al., 2009), although recent reports on a few Chinese case studies may indicate otherwise (Peng et al., 2017; Lim et al., 2020). Conversely, the most common risk factor found in patients of Asian descent is G2385R, which is not found in Caucasian populations (Funayama et al., 2007; An et al., 2008; Kim et al., 2010; Gopalai et al., 2014). A second common risk variant, R1628P, has also been identified with a more modest effect in certain Asian populations such as the Chinese, Taiwanese, Malaysian, and Singaporean (Ross et al., 2008; Gopalai et al., 2019), with studies reporting no significance in Korean cohorts (Kim et al., 2010), though it is possible that increased cohort size would reveal its significance.

Furthermore, a protective haplotype has been identified encompassing two variants, R1398H and N551K (Tan et al., 2010; Chen et al., 2011; Ross et al., 2011; Gopalai et al., 2019). In one such study on the Han Chinese population, Tan and colleagues estimated that those carrying the haplotype

have around a 20% reduction in PD risk, while those carrying the R1628H risk

variant in addition to the protective haplotype had negligible risk for

developing PD (Tan et al., 2010). This finding suggests that there may be

functional interactions between protective and risk variants whereby the effect

of these variants, and subsequent disease penetrance, requires the presence

of each other.

Lastly, an additional mutation, N1437H was identified in a large

Norwegian family, in which 18 affected carriers presented with typical PD

features (Aasly et al., 2010). Within this family, disease manifested with an early

age at onset (AAO), atypical of other PD LRRK2 mutations, suggesting

penetrance of this mutation may be higher, although a larger sample size will

need to be included in order to accurately predict such penetrance (Aasly et

al., 2010).

1.5.2 Protein structure

The *LRRK2* gene is made up of 51 exons and encodes a 2,527 amino-

acid protein with a predicted molecular mass of ~280 kDa. LRRK2 is a

multidomain protein where the Ras of complex proteins (ROC), C-

terminal of ROC (COR) and kinase domains constitute a catalytic core that is

flanked by protein-protein interaction and scaffolding domains: N-terminal

armadillo, ankyrin, leucine-rich repeats and a C-terminal WD40 domain (Figure

1.7). Interestingly, most disease-linked LRRK2 mutations are found within the

core enzymatic domains and alter enzyme activity *in vitro* (Rudenko and

Cookson, 2014). The G2019S and I2020T mutations are located within the

kinase domain and increase V_{max} for kinase activity while R1441C/G/H, Y1699C,

and N1437H mutations decrease the GTPase activity of the Roc domain and/or

increases GTP binding affinity (Guo et al., 2007; Lewis et al., 2007; Aasly et al.,

2010; Daniëls et al., 2011; Liao et al., 2014; Cookson, 2015). Conversely, the

R1398H protective variant has been shown to increase GTP hydrolysis and

decrease GTP binding *in vitro* (Nixon-Abell et al., 2016). It is thought that as

kinase and GTPase activities are encoded on the same protein, the two

activities may regulate each other.
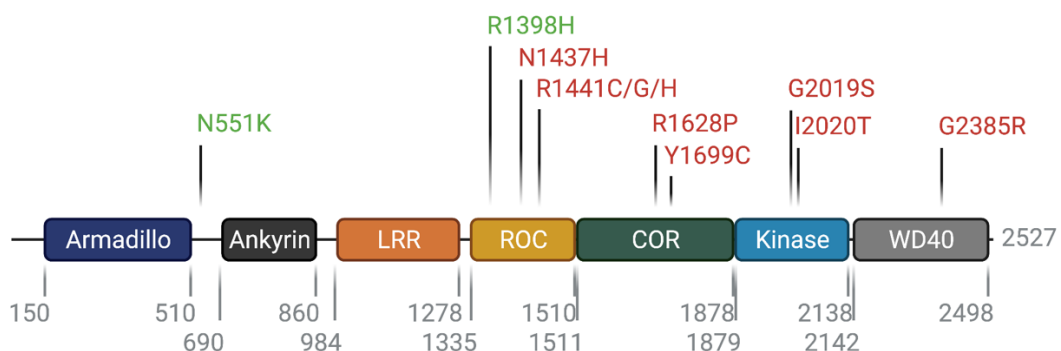
Figure 1.7. **Ideogram of LRRK2 domains and known pathogenic and protective mutations.** Amino acid numbers are shown in grey, protective variants are shown in green, and pathogenic mutations/risk variants are shown in red.

Additionally, LRRK2 is found to exist in both monomeric and

homodimeric forms, and that its kinase activity is increased in the latter form

(Greggio et al., 2008). Many studies have attempted to uncover the quaternary

structure of the protein using different biophysical techniques of various

truncated versions of LRRK2. The ROC domain was first resolved at 2.0 Å and

found to form homodimers that were partially disrupted by pathogenic

mutation R1441C (Deng et al., 2008). It is through this disruption that it is

believed GTP hydrolysis is weakened by the disruptive effect of this mutation,

thus prolonging the GTP-bound form that enhances kinase activity of the

protein. A 2.6 Å resolution of the C-terminal WD40 domain showed canonical

seven-bladed architecture that readily dimerized in solution (Zhang et al.,

2019). This dimerization was obstructed when observing the G2385R mutant,

suggesting that WD40 dimerization inhibits LRRK2 kinase activity (Zhang et al.,

2019).

More recently, utilizing cryo-electron microscopy (cryo-EM), full-length,

monomeric LRRK2 was shown to form a J shape at a 3.5 Å resolution, bringing

ROC and kinase domains in close proximity to one another, which is in

agreement with a cryo-EM experiment on a catalytic core-only truncated form

of the protein (Deniston et al., 2020; Myasnikov et al., 2021) (Figure 1.8). This

confirms the evidence of crosstalk between these domains that was theorized

previously through biochemical assays (West et al., 2005; Smith et al., 2006; Ito

et al., 2007; Lewis et al., 2007; Deng et al., 2008).
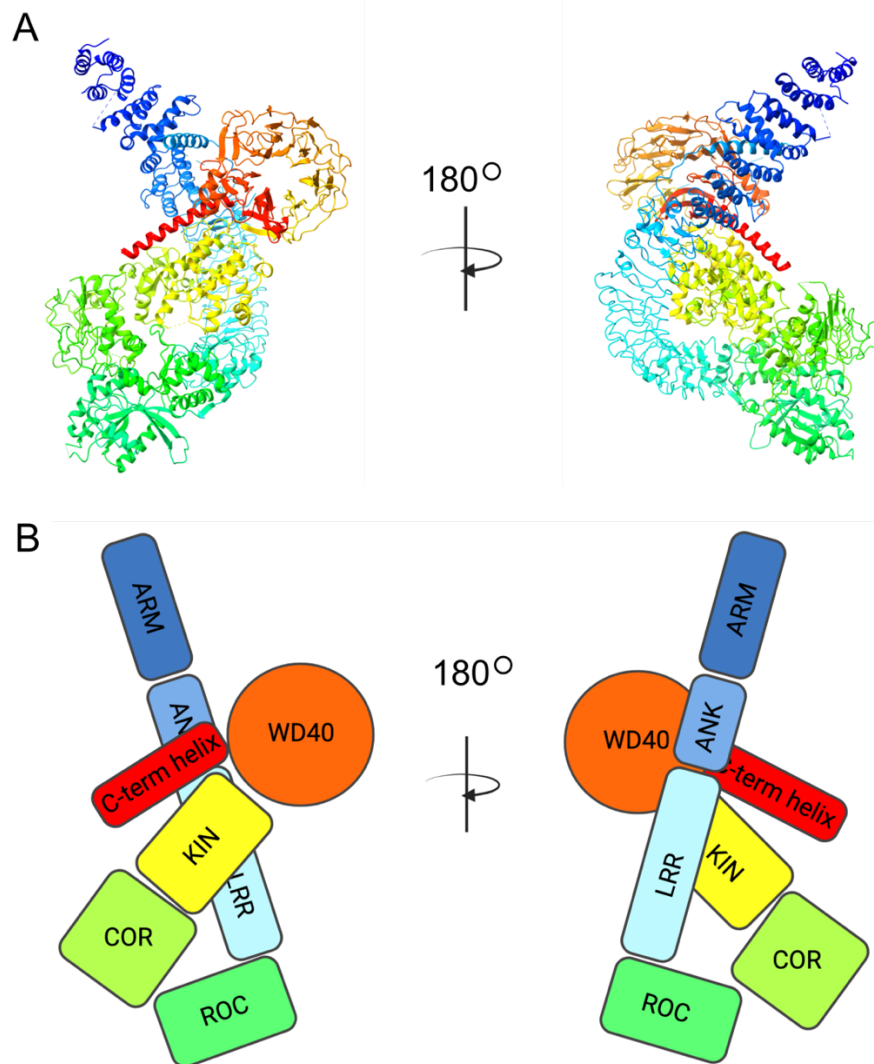
Figure 1.8. **Monomeric structure of LRRK2.** (**A**) "J" shape structure of monomeric LRRK2 at two different angles resolved by cryo-EM. (**B**) Matching cartoon depiction of the structure shown in (A). ARM=armadillo, ANK=ankyrin, LRR=leucine-rich repeat, ROC=Ras of complex, COR=C-terminus of Roc, KIN=kinase. Model was created based on the coordinates from *Myasnikov et al. 2021* (PDB ID: 7LHW) using ChimeraX software.

The full-length structure resolved by Myasnikov et al. revealed many other

interdomain interactions such as those found between the leucine-rich repeat

and the kinase domains through three sites: two on the C-lobe and one on the

N-lobe of the kinase domain (Myasnikov et al., 2021) (Figure 1.9). Interestingly,

one of the C-lobe interactions with the LRR domain involves N2081 whose

mutation to aspartic acid (N2081D) confers risk for Cohn's disease (Figure 1.9)

(Hui et al., 2018). Thus, the N2081D mutation, which shows increased kinase

activity, is expected to destabilize this interaction. Of note, the structure

captured was predicted to be in an ATP-bound, GDP-bound, inactive state,

thus conformational differences, or lack thereof between activity states is not

yet confirmed at this resolution.
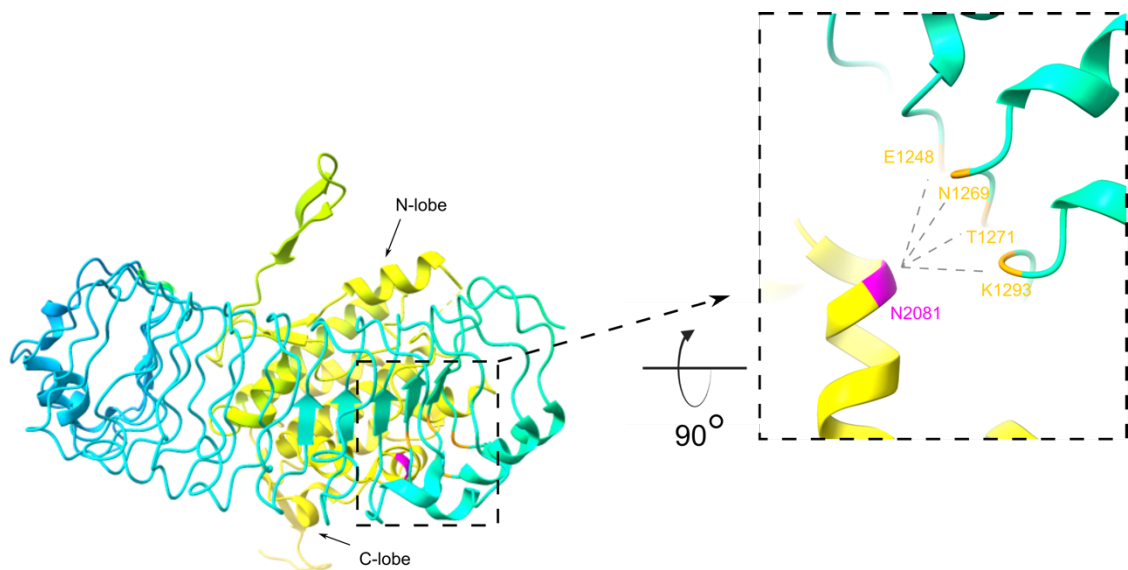
Figure 1.9. **LRR and KIN domains structure and interactions.** Kinase (yellow) and LRR (blue) structure allows for hydrophilic interactions with one another. The N-lobe and C-lobe of the kinase domain are indicated for orientation. Inset illustrates one interaction with the Crohn's disease-associated mutation site N2081 (magenta) on the kinase domain and its possible interactions with four sites on the LRR domain (orange). Model was created based on the coordinates from *Myasnikov et al. 2021* (PDB ID: 7LHW) using ChimeraX software.

The resolved monomeric conformation also depicts an extended N-terminus,

with the armadillo domain showing flexibility compared to the rest of the

protein (Myasnikov et al., 2021). This is perhaps governed by the fact that

homodimerized LRRK2 is the result of interactions between the N-terminals as

well as both COR domains at R1728 (Kalogeropulou et al., 2022) (Figure 1.10).
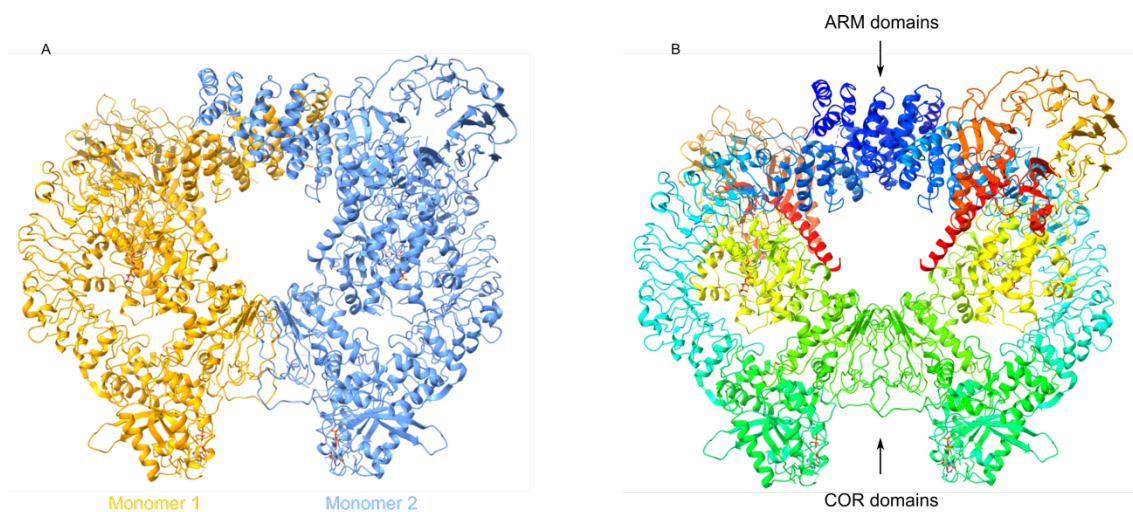
Figure 1.10. **LRRK2 dimer.** (A) Dimer of LRRK2. Each monomer is highlighted in orange and blue to show their separation. (B) Structure of the dimer shows main interactions between both ARM and COR domains. Colors represent each domain similarly to Figure 1.8. Model was created based on the coordinates from *Myasnikov et al. 2021* (PDB ID: 7LHT) using ChimeraX software.

1.5.3 Cellular function

Through Western blot and quantitative-PCR, LRRK2 expression was

found to vary across tissues in humans and animal models (Giasson et al.,

2006; Taymans et al., 2006; Higashi et al., 2007). More recently, with the

establishment of single-cell technology, Human Protein Atlas (proteinatlas.org)

has curated various single-cell RNA sequencing (scRNAseq) datasets, revealing

low LRRK2 expression in most brain cells, with oligodendrocyte precursors, microglia, and certain groups of excitatory neurons having the highest number of transcripts per million (nTPM) (Thul et al., 2017; Karlsson et al., 2021).

At the cellular level, *in vitro* studies using over expressed LRRK2 show a mostly cytosolic distribution, although many studies have identified membrane-bound and microtubule-bound pools of LRRK2, particularly in pathogenic mutations R1441C/G, Y1699C, G2019S, and I2020T (Greggio et al., 2006; Kett et al., 2012). While sequestered in the cytosol, phosphorylation of sites S910 and S935 allow LRRK2 to bind 14-3-3 proteins *in vitro* and *in vivo* (Nichols et al., 2010). Interestingly, pathogenic LRRK2 mutations show decreased association with 14-3-3 (Lavalley et al., 2016; Li et al., 2011), which provides evidence for differences in localization between wildtype and mutant protein. Additionally, neurite shortening has been characterized in neuronal cultures from bacterially artificial chromosome (BAC) transgenic G2019S and R1441C mice compared to wildtype, while overexpression (OE) of the 14-3-3s isoform improved neurite outgrowth (Lavalley et al., 2016). Additionally, LRRK2 kinase hyperactivity observed in G2019S neurons was reduced with OE of 14-3-3s, thus suggesting that 14-3-3 binding may play a role in regulating LRRK2 kinase activity and can ameliorate its mutant-induced toxicity (Lavalley et al., 2016).

In 2016, Steger and colleagues discovered a subset of small Ras-like, Rab GTPases, Rab3a/b/c, Rab5a/b/c/d, Rab8a/b, Rab10, Rab12, Rab29, Rab35, and Rab43, that are phosphorylated by LRRK2 at a serine/threonine residue within the highly conserved switch II region (Steger et al., 2016). Rab proteins are important mediators in various trafficking pathways within cells. They are largely compact and globular, with a GTP-binding and hydrolysis domain and a C-terminal region consisting of one or two cysteines that are prenylated by geranylgeranyl transferases for membrane insertion (Pfeffer, 2013; Bonet-Ponce and Cookson, 2019). The C-terminus of Rabs are highly varied and are believed to be the defining sequences that give certain Rabs specific membrane preference. Once at the membrane, Rabs can recruit effector proteins that carryout various functions. For example, motor adaptor proteins JNK-interacting proteins 3 and 4 (JIP3 and JIP4), and Rab interacting lysosomal proteins like 1 and 2 (RILPL1 and RILPL2) have been shown to be effectors of Rab8a and Rab10, all of which are motor adaptor proteins (Bonet-Ponce et al., 2020; Waschbüsch et al., 2020). Thus, through manipulation of Rab GTPases, LRRK2 may regulate vesicle trafficking. Importantly, all pathogenic variants in LRRK2 that cause disease have been shown to enhance Rab phosphorylation in cells (Steger et al., 2016; Liu et al., 2018). Thus, it is believed that abnormal LRRK2-mediated Rab phosphorylation plays a major role in disease pathogenesis.

Interestingly, a recent study showed that there is an additional binding region located within the armadillo domain of LRRK2 that can bind Rabs 8a, 10, 29, 32, and 38 which are necessary for the stabilization of LRRK2 onto membranes (Vides et al., 2022). This suggests a feed-forward pathway in which LRRK2 is stabilized on membranes by Rabs, allowing LRRK2 to enhance its kinase activity that then can phosphorylate other Rabs to finally recruit downstream effector proteins.

Two Rab substrates of LRRK2 most studied to date are Rab8a and Rab10. Interestingly, both Rabs have been shown to regulate ciliogenesis, possibly through apical transport pathways (Sato et al., 2014; Yoshimura et al., 2007). Rab10 KO mice and A549 cells are reported to have increased ciliogenesis, whereas Rab8a KO cells have less cilia suggesting these Rabs regulate cilia formation in a complementary fashion (Sato et al., 2014; Dhekne et al., 2018). Additionally, when in the presence of a kinase hyperactive LRRK2 mutant such as R1441C or G2019S, impairment of ciliogenesis has been shown as a reduction of cilia formation in serum-starved mouse embryonic fibroblasts (MEFs) that was ameliorated by MLi-2 (Steger et al., 2017). Interestingly, wildtype LRRK2 MEFs were not included for comparison to the mutant variants, thus differences between them cannot be claimed but are implied. Further studies have identified Protein phosphatase Mg2+/Mn2+ Dependent 1H

(PPM1H) as a phosphatase that regulates LRRK2-mediated phosphorylation of

Rab10 and Rab8a and that PPM1H knockdown suppressed ciliogenesis in

MEFs (Berndsen et al., 2019). A recent study has reported that this LRRK2-

mediated ciliogenesis is cell type-specific, in that serum-starved, MLi-2 treated

SH-SY5Y cells as well as rat primary neurons and iPSC derived neurons showed

no differences in ciliogenesis nor were differences found between G2019S

LRRK2 and wildtype variants (Kim et al., 2021). Conversely, a significant

increase in ciliogenesis was observed in heterozygous G2019S patient-derived

fibroblasts and neural stem cells compared to controls (Kim et al., 2021). Taken

together, LRRK2 plays a role in ciliogenesis via the regulation of Rab10 and

Rab8a, although further study needs to investigate how mutants affect

ciliogenesis in different brain cell types.

LRRK2 has also been proposed to play a role in autophagy, as inhibition

of LRRK2 kinase activity has been shown to increase the lipidation of LC3 in

astrocytes (Manzoni et al., 2013). This may be indicative of either induction of

autophagosome formation or inhibition of autophagosome degradation via the

lysosome. Expression of GFP-tagged, PD-causing LRRK2 mutants results in an

increase in lysosome size which is dependent on kinase activity and is

associated with a reduction in lysosomal pH (Henry et al., 2015).

Additionally, loss of LRRK2 leads to accumulation of autophagic markers LC3-II

and p62 *in vivo* (Tong et al., 2010a). Interestingly, comparing these markers in

post-mortem tissue from G2019S LRRK2 PD and idiopathic PD patients

showed decreased LC3-II levels in the basal ganglia compared with controls

(Mamais et al., 2013). This suggests LRRK2 plays a role in trafficking within the

autophagy/lysosomal pathway and is necessary for normal lysosomal function.

In turn, autophagy influences inflammation through the transport of

degradable material to the lysosome via phagophores. Thus, although we have

not yet identified all the intracellular pathways involved in LRRK2-related PD,

one possibility is that inflammatory reactions and intracellular trafficking that

affects the autophagy-lysosome system are mechanistically related to each

other. A more in-depth review on LRRK2 at the lysosome will be provided in

Chapter 7.

Recently, additional investigation into the role of LRRK2 within the

autophagy pathway places its function at the trafficking of these organelles

themselves. Deficits in autophagosome transport and maturation in both

G2019S KI primary neurons and induced pluripotent stem cell (iPSC)-derived

neurons genetically edited to express G2019S LRRK2 have also been shown

(Boecker et al., 2021). Mechanistically, Boecker and colleagues identified the

recruitment of JIP4 by mutant LRRK2 (via phosphorylated Rab10) to

autophagosomes (Boecker et al., 2021). JIP4 is a motor protein that binds to

kinesin for anterograde motility of endosomal organelles (Montagnac et al.,

2009). Thus, recruitment of JIP4 to autophagosomes resulted in an abnormal

tug-of-war between retrograde and anterograde transport in G2019S LRRK2

expressing neurons compared to wildtype, increasing the number of pauses

these organelles made when traveling the length of an axon (Boecker et al.,

2021). Treatment with MLi-2 in the G2019S LRRK2 neurons resulted in the

amelioration of the number of pauses during transport, suggesting that the

defect in retrograde transport is LRRK2 kinase-specific (Boecker et al., 2021).

Previous work has shown that autophagosomal cargo degradation is most

efficient within close proximity to the perinuclear area (Ravikumar et al., 2005)

and that disruption of retrograde axonal transport causes ineffective

autophagosome-lysosome fusion and thus impaired cargo degradation (Wong

and Holzbaur, 2014). Taken together, these works imply that kinase

hyperactive LRRK2 can affect autophagosome positioning within neurons, and

that this creates defects in autophagy.

1.5.4 Posttranslational modifications of LRRK2

Of all the PTMs of LRRK2, phosphorylation is the most extensively

studied and can influence protein localization, stability, and function (Pajarillo

et al., 2019). As mentioned in the previous section, mass spectrometry

experiments on LRRK2 pull-down eluates identified a cluster of serine residues

S860, S910, S935, S955, S973, and S976 situated between ANK and LRR

domains that bind 14-3-3 isoforms (Nichols et al., 2010). Specifically,

phosphorylation of S910 and S935 were found to be necessary for the binding

of LRRK2 to 14-3-3 isoforms that stabilize LRRK2 in the cytosol, as 14-3-3

binding is lost when overexpressing phosphor-null constructs S910A and

S935A *in vitro* (Nichols et al., 2010). Interestingly when inhibiting LRRK2 kinase

activity or in the context of mutant LRRK2, this phosphorylation is dramatically

reduced (Nichols, 2017). Additionally, phosphorylation at S935 was shown to

lower in *post-mortem* brains of PD patients compared to samples from

individuals without neurological disease (Dzamko et al., 2017). These data

suggest that LRRK2 kinase activity regulates the constitutive phosphorylation at

these sites, although the direct mechanism is currently unknown.

Apart from constitutive phosphorylation sites, a number of

autophosphorylation sites have been identified located in and around the ROC

domain, namely S1292, T1343, T1348, T1357, T1368, S1403, T1404, T1410,

T1452, and T1491 (Greggio et al., 2009; Gloeckner et al., 2010; Webber et al.,

2011; Sheng et al., 2012; Liu et al., 2016). Autophosphorylation at all of these

sites was enhanced in R1441C/G/H, Y1699C, G2019S, and I2020T mutations *in*

vitro as well as increased GTPase activity (Liu et al., 2016). In the brain and

peripheral tissues of G2019S KI mice, S1292 autophosphorylation has been

shown to be enhanced compared to wildtype animals (Kluss et al., 2018; Sheng et al., 2012). Interestingly for S1292, one study reported a decrease in neurite shortening when overexpressing a phospho-null variant S1292A in primary rat neurons overexpressing LRRK2 with both R1441G and G2019S mutations, proposing that this autophosphorylation may contribute to the cellular effects of some LRRK2 mutations (Sheng et al., 2012).

In addition to phosphorylation events, LRRK2 can also undergo ubiquitylation at several lysine residues in the N-terminal, K48 and K63, in response to kinase inhibition (Nichols, 2017; Pajarillo et al., 2019). One study used the expression of difopein, a binding partner of 14-3-3 proteins, to reduce 14-3-3 binding to LRRK2 at S935, causing its subsequent dephosphorylation. Cells expressing difopein were observed to have increased ubiquitylation of LRRK2, suggesting that dephosphorylation is a signal for LRRK2 ubiquitylation (Zhao et al., 2015). Constructs expressing R1441C and G2019S LRRK2 mutants also showed exaggerated ubiquitylation, suggesting premature degradation of the protein may contribute to disease pathogenesis (Ding and Goldberg, 2009).

1.5.5 *In vivo* models of LRRK2

A diverse range of animal models has been developed including OE, KI, and KO variations of LRRK2 in order to characterize protein function *in vivo*. Rodents in particular have been widely used, as all residues affected by pathogenic mutations in humans are conserved in rodents, and the rodent homolog of LRRK2 shares approximately 87% identity to that of the human form (Seegobin et al., 2020). In OE models, both rats and mice have been made to express human forms of wildtype, R1441C, and G2019S LRRK2, with reports on phenotypes in the mutant forms including L-DOPA-responsive locomotor defects and pathological accumulations of tau and α-synuclein (Chen et al., 2012; Ramonet et al., 2011; Sloan et al., 2016; Weng et al., 2016; West et al., 2014; Xiong et al., 2018; Zhou et al., 2011). *Drosophila* models of OE human G2019S LRRK2 also show these same phenotypes (Lin et al., 2010; Liu et al., 2008; Ng et al., 2009). Interestingly, rat OE models do not show any DA neuron loss, whereas some mouse OE models do depending on the neuronal promoter used. For example, loss of DA neurons was observed in the SNpc of R1441C and G2019S LRRK2 OE mice using human TH and CMVE/PDGF-beta promoters but not murine Thy1 and ROSA26 nor human PITX3 and CaMKII promoters (Chen et al., 2012; Chou et al., 2014; Herzig et al., 2011; Lin et al., 2009; Liu et al., 2015; Ramonet et al., 2011; Tsika et al., 2014; Weng et al., 2016; Xiong et al., 2018). Overall, a clear advantage of OE

models is that they have enabled the study of neurodegenerative mechanisms, particularly in neuronal circuits of the midbrain. However, the main caveats in any of these OE models are the risk of artificial phenotypes propagated by the OE itself, as well as the interspecies differences that come with introducing human genes into another species. One reassuring observation is that of the models that do produce DA neuron loss, all have reported aging as a necessary factor before loss is observed (between 12-20 months old) (Chen et al., 2012; Chou et al., 2014; Ramonet et al., 2011; Xiong et al., 2018). This gives some confidence in the translatability of the model to the human disease.

Additionally, disease mutations of LRRK2 KI models have been generated in mice in order to avoid unwanted artificiality of the OE model, with R1441C and G2019S variants being the most studied to date. Interestingly, these KI models fail to produce any DA neuron loss and do not exhibit any α-synuclein pathology, thus making them subservient to their OE counterparts for studying brain pathology (Dächsel et al., 2010; Giesert et al., 2017; Herzig et al., 2011; Matikainen-Ankney et al., 2016; Tong et al., 2009; Volta et al., 2017). However, KI mutant models do produce LRRK2 kinase hyperactivity at the endogenous level that has been useful in studying various cellular mechanisms in trafficking and mitochondrial function, as well as are

great models for assessing LRRK2 as a therapeutic target *in vivo* (Kelly et al.,

2021; Kluss et al., 2018; Sheng et al., 2012; Singh et al., 2021; Steger et al.,

2016; Yue et al., 2015). LRRK2 *in vivo* inhibition studies will be introduced in

depth in Chapter 3. Additionally, two groups have reported that the G2019S

LRRK2 KI mice exhibit increased frequency of excitatory post-synaptic

potentials in spiny projection neurons of the striatum (Matikainen-Ankney et

al., 2016; Volta et al., 2017). Much more modest behavioral changes have

been reported compared to OE models, with the most consistent finding

being an increase in latency to fall using a rotarod apparatus (Giesert et al.,

2017; Yue et al., 2015).

LRRK2 deficiency models have been generated in mice, rats, *drosophila*,

and *C. Elegans* to investigate the physiological role of LRRK2. All of them have

shown that those born without LRRK2 do not result in PD-associated

phenotypes such as DA neuron loss nor any neuropathology (Daher et al.,

2014; Herzig et al., 2011; Hinkle et al., 2012; Lin et al., 2009; Tong et al.,

2010a). This is in line with genetic data showing that people with *LRRK2*

haploinsufficiency to not have an increased PD risk (Blauwendraat et al., 2018).

Interestingly, the most striking phenotypes found have been characterized in

the kidney and lung tissues of rodent models. The kidneys of *LRRK2* KO

rodents become enlarged and hyperpigmented in an age-dependent manner

(after approximately 3 months of age) and have an increase in the number and size of lysosomes in the renal cortex (Baptista et al., 2013; Herzig et al., 2011; Hinkle et al., 2012; Tong et al., 2010a, 2012). Other cellular phenotypes include increases in lipid droplets, autophagic markers LC3 and p62, and lysosomal markers LAMP-1 and Cathepsin D, which are all consistent with the suggestion that physiological LRRK2 plays a role in the autophagy-lysosomal pathway (Hinkle et al., 2012; Kluss et al., 2021; Pellegrini et al., 2018; Tong et al., 2010b). Homeostatic parameters of the kidney have also been reported, including increased diastolic blood pressure and decreased specific gravity of urine (Ness et al., 2013). Additionally, the lungs of LRRK2 KO rats exhibit an increased number and size of type II alveolar cell lamellar bodies which are lysosome-derived vesicles that store surfactant (Baptista et al., 2013; Herzig et al., 2011; Miklavc et al., 2014). As of yet, kidney and lung profile studies have not been explored fully in patients with PD nor in those with haploinsufficiency of *LRRK2*, therefore it is difficult determine whether these alterations are translatable. However, in both rodents and humans, LRRK2 is highly expressed in these tissues, one could hypothesize that an absence of LRRK2 may result in some phenotypes in humans similar to those found in rodents.

1.5.6 LRRK2 in sporadic Parkinson's disease

It is increasingly appreciated that microglia can contribute to PD pathogenesis as they mediate the immune responses in the CNS and inflammation is a key factor in neurodegeneration (Kluss et al., 2019). Many studies have nominated LRRK2 as an integral part of the inflammatory response downstream of various proinflammatory signals (Wallings and Tansey, 2019). Markers of LRRK2 kinase activity, both autophosphorylation and phosphorylation of downstream Rab substrates, were found to be increased in microglia in sporadic PD *post-mortem* tissue (Di Maio et al., 2018) suggesting that inflammation may be a trigger of LRRK2 activity in PD patients. Microglial activation in PD could be triggered by an interaction of extracellular forms of the α-synuclein with TLR2 and TLR4 receptors (Kim et al., 2013; Hoenen et al., 2016). A recent report has shown that expression of G2019S LRRK2 causes the mis-trafficking of transferrin to lysosomes proximal to the nucleus in proinflammatory conditions, most probably through Rab8a phosphorylation, in iPSC-derived microglia (Mamais et al., 2021). Therefore, LRRK2 kinase-hyperactive mutants may also disrupt normal trafficking in microglia to promote neuroinflammation.

Additionally, non-coding *LRRK2* variants identified by GWAS affect risk of disease through modulation of LRRK2 protein expression. For example, it

has been shown that a common risk variant, rs76904798, at the LRRK2 locus is associated with higher LRRK2 expression in microglia-like cells derived from human monocytes (Ryan et al., 2017). The minor allele, T, was associated with increased *LRRK2* expression, which was only observed in the microglia-like cells and not in monocytes (Ryan et al., 2017). This finding suggests that *LRRK2* gene expression can be altered by specific alleles or haplotypes across the locus and suggests that *LRRK2* may have a specific role within microglia. A recent study confirmed this expression increase in patients harboring the minor allele in both iPSC-derived microglia at the RNA and protein levels, as well as *post-mortem* human frontal cortex tissue via single nuclei RNA sequencing (snRNAseq) (Langston et al., 2021). As microglia are influenced by myriad of conditions (inflammation, neuronal apoptosis, etc.) this suggests that the role of LRRK2 function may be more prominent under situations where microglia are stimulated.

2 OVERVIEW AND AIMS OF THE THESIS

The multi-faceted functionality of LRRK2 is a direct result of its many interactive domains as well as the versatile roles of its Rab substrates. Thus, its exact involvement in PD pathogenesis has remained rather elusive. However, the hyperactive nature of its kinase in the most common pathologic mutant forms of the protein make LRRK2 an attractive target for kinase inhibition therapies. The goal of this PhD thesis is thus threefold: 1) to establish a preclinical model of acute and chronic administration of a small molecule LRRK2 kinase inhibitor, MLi-2, in G2019S LRRK2 KI mice and use it to establish robust readouts of LRRK2 kinase activity, 2) to evaluate changes in the proteome of animals chronically treated with MLi-2 in both brain and peripheral tissues where LRRK2 is highly expressed, and 3) to investigate the mechanism/s of LRRK2 kinase activation and characterize its influence on downstream substrates Rab10 and Rab12. This can be broken down into the following aims:

Aim 1: Interrogate the pharmacodynamic response of LRRK2 kinase inhibition in G2019S KI mice. This will be achieved by evaluating both dose response and time course paradigms of acute MLi-2 treatment via oral gavage and testing pS935 LRRK2, pS1292 LRRK2, pT73 Rab10, and pS106 Rab12 as

readouts of kinase inhibition in brain, kidney, and lung. These phosphorylation sites will be measured using Western blot.

Aim 2: Achieve chronic inhibition of LRRK2 in G2019S LRRK2 KI mice such that the hyperactive kinase is reduced to activity levels seen in wildtype mice. G2019S LRRK2 KI mice will be given an in-diet dose of MLi-2 for 10 days or 10 weeks and pLRRK2, pRab10, and pRab12 levels assessed in brain, kidney, and lung via Western blot. The target dose achieved each day will be determined in a dose response experiment where a range of in-diet doses of MLi-2 will be tested and pS1292 LRRK2 levels measured in comparison to autophosphorylation observed in wildtype animals at baseline.

Aim 3: Evaluate downstream effects of chronic LRRK2 kinase inhibition in brain, kidney, and lung biomatrices. Tandem mass tag proteomics will be used to assess both total and phospho-proteomes in treated versus untreated G2019S LRRK2 KI mice, where wildtype and LRRK2 KO proteomes will be used for reference.

Aim 4: Investigate LRRK2 kinase activity at different endolysosomal membranes and its effects on downstream Rab10 and Rab12 phosphorylation. LRRK2 will be trapped to early endosomes, late endosomes, recycling endosomes, Golgi,

lysosomes, and plasma membrane using a rapamycin-induced system that forms heterodimers between FKBP and FRB domains. A LRRK2-FKBP construct will be made along with constructs for membrane resident proteins fused with the FRB domain for each membrane of interest. Immunocytochemistry experiments will be done to confirm LRRK2 translocation from the cytosol to each targeted membrane, and kinase activity will be assessed via pS1292 LRRK2 levels as measured by Western blot. Phosphorylation of Rab10 and Rab12 will be assessed for each membrane by Western blot. Additionally, LRRK2-FKBP mutant clones (R1441C, Y1699C, G2019S, and K1906M) will be made via mutagenesis to determine their influence on Rab phosphorylation once trapped to the lysosomal and Golgi membranes. Influence of endogenous Rab29 on LRRK2 activation and downstream Rab phosphorylation will be assessed through Rab29 siRNA knockdown experiments at the Golgi membrane.

Aim 5: Characterize pRab10 and pRab12 localization at LRRK2-positive lysosomes. A lysosome-LRRK2 chimera construct will be made to translocate LRRK2 to the lysosomal membrane and pRab10 and pRab12 will be visualized in immunocytochemistry experiments. Co-localization of LRRK2 to each Rab will be assessed using JACoP plugin in ImageJ.

3 INVESTIGATION OF ACUTE DOSING PARADIGMS USING THE LRRK2-SPECIFIC KINASE INHIBITOR MLI-2 IN G2019S LRRK2 KNOCK-IN MICE

3.1 Introduction

Several *in vitro* studies have shown the hyperactive nature of LRRK2 kinase in pathogenic mutants to be neuronally toxic (Greggio et al., 2006; MacLeod et al., 2006; Smith et al., 2006). Therefore, LRRK2 kinase inhibitors have been proposed as a potential treatment for PD, and currently a few early- and mid-stage clinical trials are assessing LRRK2 as a therapeutic target. One ongoing clinical trial is using an orally administered, type I small molecule LRRK2 kinase inhibitor developed by Denali Therapeutics (clinicaltrials.gov ID: NCT04056689). This compound, denoted as DNL151, and later BIIB122/DNL151 after a partnership between Denali and Biogen was announced mid-2020, was reported to have met all goals in phase 1 of the trial, in which 184 healthy individuals received a range of doses for up to 28 days. These goals included on-target engagement utilizing phosphorylation sites S935 LRRK2 (greater than or equal to 80% dephosphorylation) and T73 Rab10 (up to 50% dephosphorylation) as readouts in whole blood and PBMCs, respectively (Denali Therapeutics Inc., 2021). In addition, this trial reported a

dose-dependent reduction in 22:6-bis[monoacylglycerol] phosphate (BMP) in urine, a lysosomal lipid and marker of lysosomal function. Phase 1b completed in late 2020 reported similar results and included 36 patients with PD (Denali Therapeutics Inc., 2021). So far, BIIB122/DNL151 has been well tolerated with minimal adverse events, namely nausea and headaches, which were quickly reversed after cessation of the drug (Denali Therapeutics Inc., 2021). The development of late-stage clinical trials using BIIB122/DNL151 are currently ongoing, with the goal to enroll 640 early-stage PD patients in phase 2 (Denali Therapeutics Inc., 2022).

In addition, commercially available LRRK2 kinase inhibitors continue to be a vital tool in basic biology research (Vancraenenbroeck et al., 2011; Taymans and Greggio, 2016). Currently, the most widely used LRRK2 kinase inhibitors belong to the type I class of inhibitors that bind to the ATP-binding pocket of LRRK2 with an "in" orientation of the DYG activation loop (Figure 3.1A-B), a conserved motif that activates kinases via phosphorylation (Vijayan et al., 2015). These inhibitors range widely in structure and potency (Table 3.1). Additionally, a number of type II inhibitors have been found to inhibit LRRK2, binding to the ATP pocket with an "out" orientation of the DYG activation loop (Figure 3.1A) (Tasegian et al., 2021). However, no LRRK2-specific type II inhibitors with strong selectivity and potency have been developed to date.

The first generation of type I LRRK2 kinase inhibitors reported had multiple off-target effects from a wide array of kinases, limiting their use in identifying LRRK2-specific function (Covy and Giasson, 2009; Nichols et al., 2009; Dzamko et al., 2010; Lee et al., 2010; Ramsden et al., 2011; Zhang et al., 2012). The next round of molecules possessed greater selectivity for LRRK2, such as LRRK2-IN-1, but ultimately were unable to cross the BBB (Deng et al., 2011; Reith et al., 2012; Choi et al., 2012).
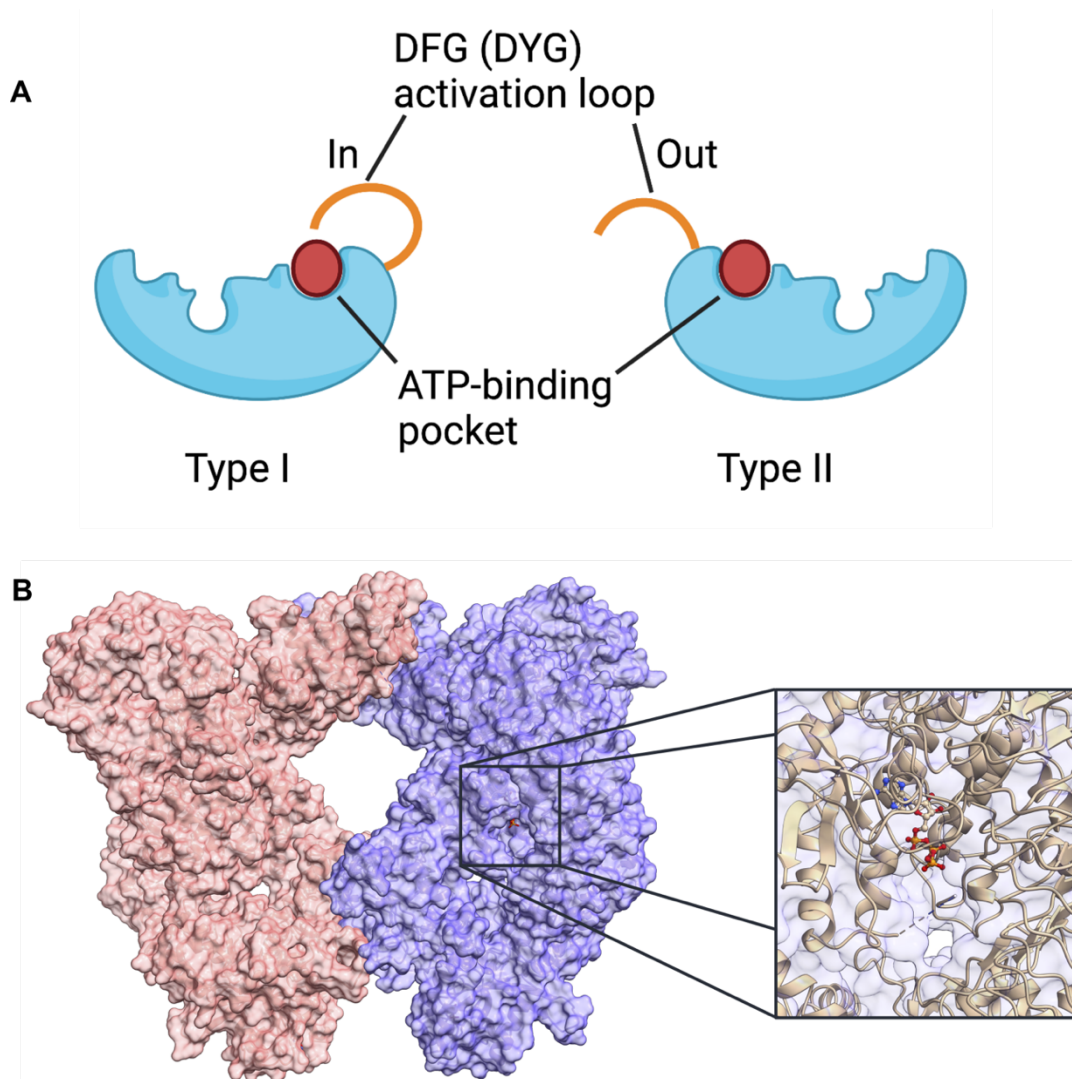
Figure 3.1. **Models of Type I and II kinase inhibitors.** A generic enzyme (blue) is shown depicting the difference in structural conformation of the DFG/DYG motif (orange) when bound to type I and II class kinase inhibitors (red), respectively (**A**). The dimeric structure for the LRRK2 complex, showing the active site of the kinase domain with ATP bound (**B**). Structure from panel B was derived from PDB 7LHT (Myasnikov et al., 2021) using UCSF chimera (Pettersen et al., 2004), created by Dr. Patrick A. Lewis. Figure adapted from (Kluss et al., 2022b).

Currently, the most used LRRK2 inhibitors are the third generation, structurally distinct, and brain penetrant molecules MLi-2 (Fell et al., 2015), PF-06685360 (PFE-360) (Andersen et al., 2018), and GNE-7915 (Estrada et al., 2012) (Table 3.1). Each has been observed to potently inhibit LRRK2 kinase

activity as significant decreases in autophosphorylation at S1292 LRRK2 as well as dephosphorylation of S910, S935, S955, and S975 LRRK2 residues and downstream Rab substrates are found in varying models *in vitro* and *in vivo* (Estrada et al., 2012; Fell et al., 2015; Ito et al., 2016; Kelly et al., 2018; Kluss et al., 2018; Wang et al., 2020). Another molecule, PF-06447475 (Henderson et al., 2015), has been shown to mitigate dopaminergic loss and neuroinflammation associated with α-synuclein OE after a 4-week treatment in human transgenic G2019S LRRK2 rats (Daher et al., 2015). This suggests that LRRK2 kinase inhibition may be useful in curbing α-synuclein-induced inflammation and therefore have neuroprotective effects.
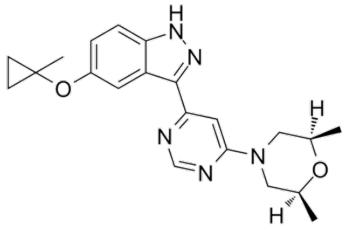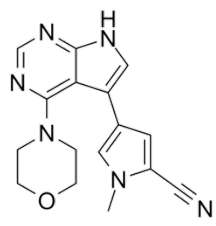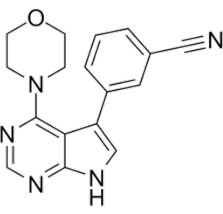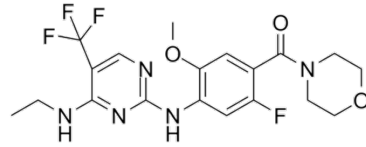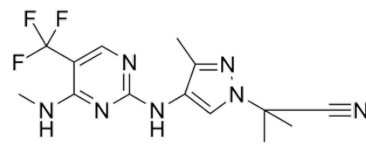
Compound Name	Chemical Structure	WT LRRK2 IC50 [nM]	Reference
MLi-2		0.8	*Fell et al. 2015* *Scott et al. 2017*
PF-06685360 (PFE-360)		2.3	*Andersen et al. 2018*
PF-06447475		3	*Henderson et al. 2015*
GNE-7915		9	*Estrada et al. 2012*
GNE-0877		3	*Estrada et al. 2014*

Table 3.1. **Chemical structures of third generation type I LRRK2-specific kinase inhibitors.** Chemical structures, IC50 of wildtype (WT) LRRK2 *in vitro*, and references are provided.

Of these compounds, MLi-2 (*cis*-2,6-dimethyl-4-(6-(5-(1-

methylcyclopropoxy)-1*H*-indazol-3-yl)pyrimidin-4-yl)morpholine)

was identified in a small-molecule screen in which all other kinases tested

required 100 times the drug concentration necessary to reach IC_{50} compared to

G2019S LRRK2 (0.76nM) (Fell et al., 2015). Using the phosphorylation of S935

LRRK2 as a readout in wildtype mice, Fell et al. observed that a 10mg/kg acute

dose of MLi-2 via oral gavage achieved >90% dephosphorylation after 1 hour

(Fell et al., 2015). Although the phosphorylation of S935 is not mediated by

LRRK2 itself, it can be used as a robust readout of LRRK2 kinase inhibition, as

exposure to type I inhibitors indirectly results in loss of pS935. In contrast,

direct autophosphorylation readouts can be challenging to detect robustly in

wildtype animals, CSF, and blood due to low stoichiometry. However, when

considering mutant LRRK2, much of the information on kinase activity is lost

when only using S935, as hyperactivity of the kinase does not affect

phosphorylation at S935 across models (Delbroek et al., 2013; Ito et al., 2014).

Furthermore, mutations in the ROC-COR bidomain decrease S935

phosphorylation in different models (Nichols et al., 2010). Therefore, there is a

clear need in the field to establish robust biomarkers that can inform on the

effects of both hyperactivity and inhibition of LRRK2.

In this chapter, I evaluated the utility of measuring autophosphorylation

of S1292 LRRK2 and downstream phosphorylation of substrate Rab proteins

Rab10, Rab12, and Rab29 as readouts of LRRK2 kinase activity *in vivo* using

newly developed commercially available antibodies (Michael J. Fox Foundation/Abcam) in G2019S LRRK2 homozygous KI mice. To do this, the LRRK2-specific inhibitor MLi-2 was used in a series of acute dosing paradigms and kinase readouts were assessed in brain, kidney, and lung tissues. As PD mainly affects the brain, brain tissue was utilized to investigate the effects of LRRK2 kinase inhibition. Kidney and lung were used as peripheral indicators of systemic LRRK2 inhibition, as LRRK2 is highly expressed in these tissues. In the context of kinase hyperactive LRRK2, these paradigms revealed that the effects of LRRK2 inhibition on pS1292 and pS935 were very similar in dose response and washout recovery time across all tissues tested. Interestingly, effects of kinase inhibition on pRab substrates varied between tissues, which may be particularly relevant to selection of biomarkers for clinical trials where brain target engagement is inferred from peripheral tissue events. Rab10 phosphorylation was the least affected by LRRK2 inhibition in the brain, specifically. When testing for cell-specific effects on Rab10 in brain tissue, pT73 Rab10 levels were most affected by LRRK2 inhibition in glial cultures versus neuronal culture. Furthermore, although pS1292 and pS935 were decreased in animals dosed with MLi-2 across multiple brain regions, there was no significant LRRK2-dependent dephosphorylation of Rab10. In contrast Rab12 mimicked the strong LRRK2-dependent dephosphorylation seen in pS1292

and pS935 across all experiments and tissues, suggesting that pRab12 may be

a useful biomarker to monitor LRRK2 kinase inhibition.

3.2 Results

3.2.1 Dose dependent sensitivity of LRRK2 autophosphorylation and downstream Rab GTPase phosphorylation to MLi-2 treatment

To identify reliable biomarkers of LRRK2 kinase activity in the context of hyperactive mutant LRRK2, G2019S LRRK2 KI mice were given one dose of MLi-2 at 1, 3, 10, 30, 60, or 90mg/kg via oral gavage and sacrificed 1 hour post dose. This range of dosing was chosen based on previous published data on wildtype mice, in which maximum dephosphorylation of pS935 LRRK2 was observed after an acute dose of 10mg/kg via oral gavage (Fell et al., 2015). Animals used to measure baseline levels of phosphorylation were given a single dose of vehicle. Brain, kidney, and lung tissues were removed for biochemical assays.

An approximate 40% reduction in pS1292 was observed in kidney and lung starting at the lowest dose of 1 mg/kg of MLi-2 (Figure 3.2A-B). Maximal dephosphorylation was achieved in the brain, kidney, and lung at 10 mg/kg for both pS1292 and pS935, followed by a plateau at higher doses (Figure 3.2A-C). Maximal S1292 dephosphorylation in the brain did not exceed 60% with increasing MLi-2 concentrations, suggesting that maximal inhibition was

achieved. The IC_{50} of phospho-site S935 was less than half of the IC_{50} of

pS1292 in the brain (5.02mg/kg versus 10.43mg/kg), suggesting that this

marker is more sensitive to LRRK2 inhibition in the brain compared to lung and

kidney tissue, of which IC_{50} for both sites were comparable (Figure 3.2B-C).

However, the signal to background ratio was much smaller for S1292 staining

in the brain than other tissues, which may have impeded the accuracy of

measurement of this site in Western blot.
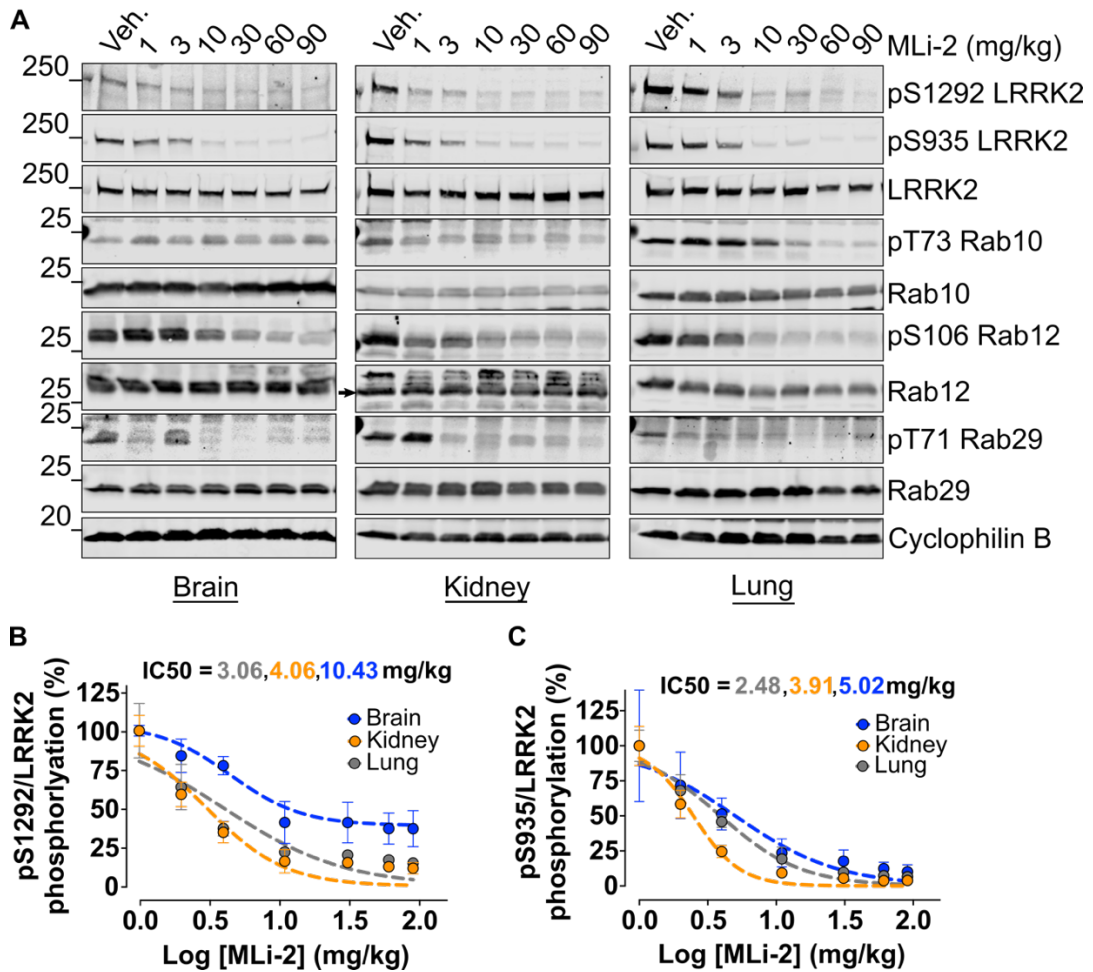
Figure 3.2. **Dose response of acute MLi-2 administration in brain, kidney, and lung tissue of G2019S LRRK2 KI mice.** Representative Western blots probed for pLRRK2, pRabs, and total proteins from animals given a single dose of MLi-2 or vehicle (**A**). Graphs for pLRRK2 sites S1292 (**B**) and S935 (**C**) are shown. A single dose of vehicle is indicated as 0 log [MLi-2] concentration on the x-axis and represents baseline phosphorylation (100%). IC_{50} values are shown for each tissue corresponding to color. N=6 mice; error bars indicate SD.

Phosphorylated Rab GTPases showed more variable responses to MLi-2 across tissues. The T73 Rab10 phospho-site responded significantly to MLi-2 treatment in peripheral tissues but not in the brain, achieving an IC_{50} of 12.22mg/kg and 16.89mg/kg in kidney and lung tissue, respectively (Figure 3.3A; corresponding Western blot in Figure 3.2A). In brain tissue, MLi-2

response was highly varied across animals and did not achieve a 50%

reduction of pT73 Rab10 levels at any dose. Phosphorylation of S106 Rab12

showed a robust response to MLi-2 in both brain and peripheral tissues with

maximal dephosphorylation between 30 and 60 mg/kg MLi-2 (Figure 3.3B;

corresponding Western blot in Figure 3.2A). Phosphorylation levels of T71

Rab29 responded with treatment in all tissues but with higher variability

compared to Rab12, especially at lower doses (Figure 3.3C; corresponding

Western blot in Figure 3.2A). At 10 mg/kg, an approximately 50% decrease in

Rab10, Rab12 and Rab29 phosphorylation was observed in the periphery while

higher doses retained ~ 30% residual phosphorylation signal.
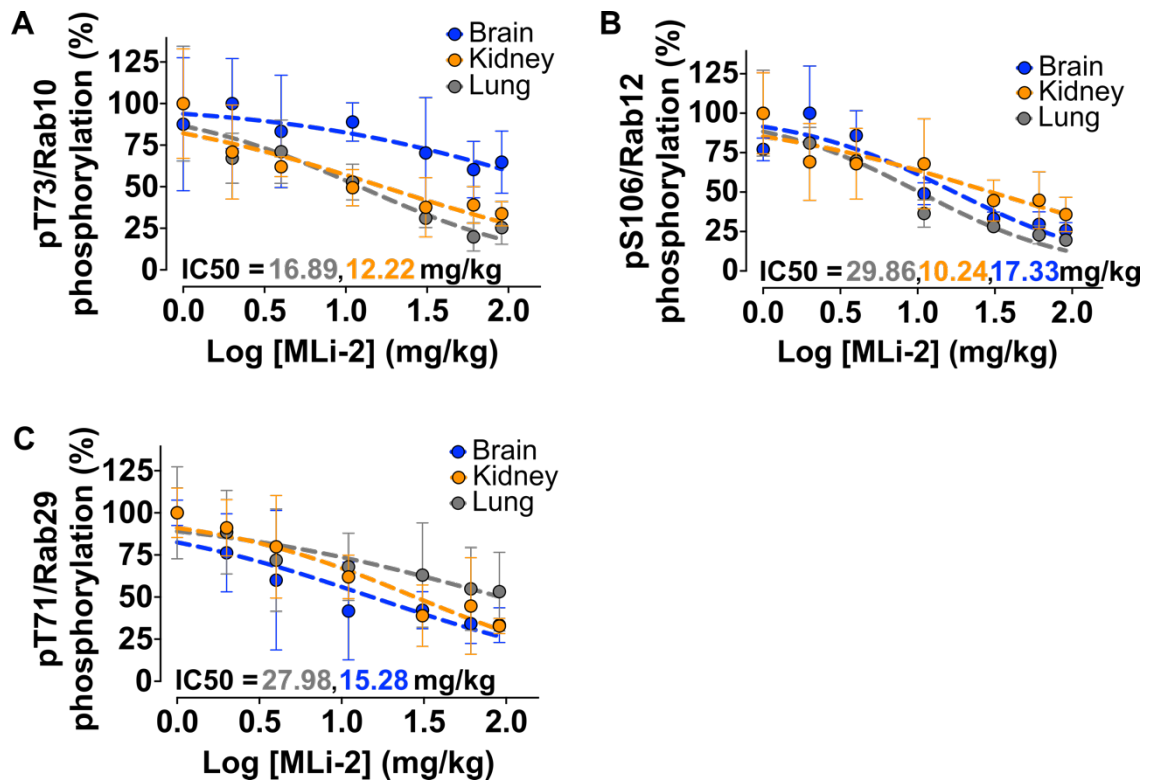
Figure 3.3. **Dose-response curves of LRRK2 Rab substrates Rab10, Rab12, and Rab29.** Graphs of all three pRabs show % dephosphorylation at the indicated log [MLi-2] concentrations. A single dose of vehicle is shown as 0 on the x-axis and represents baseline phosphorylation (100%) (**A-B**). IC_{50} values are shown for each tissue. N=6 mice; SD error bars are shown.

3.2.2 Time course of phosphorylation readouts in G2019S LRRK2 KI mice after acute MLi-2 treatment

To determine the time dependency on phosphorylation changes after acute LRRK2 kinase inhibition, G2019S LRRK2 KI adult mice were given a single 10mg/kg dose of MLi-2 via oral gavage and sacrificed 0.5, 1, 3, 12, 24, or 72 hours post-dose. The dose of 10mg/kg was chosen as it was the lowest dose needed to achieve maximal reduction of S1292 autophosphorylation in the dose response data shown in the previous section. A time point of 0 hours

was included where animals were given an equivalent dose of vehicle and

euthanized immediately thereafter to measure baseline phosphorylation. Brain,

kidney, and lung tissues were removed and processed for Western blot

analyses.

Both pS1292 and pS935 LRRK2 showed rapid dephosphorylation at

0.5 hours, with maximal dephosphorylation achieved at 1 hour post dose

across all tissues (Figure 3.4A-C). This dephosphorylation was sustained for 3

hours post-dose, after which re-phosphorylation was observed, with 50% re-

phosphorylation achieved at 12 hours for both S1292 and S935 LRRK2. Both

phosphorylation sites were fully recovered to baseline levels after 24 hours

post-dose. The dephosphorylation patterns of both phospho-sites tightly

correlated between brain, kidney, and lung tissues.
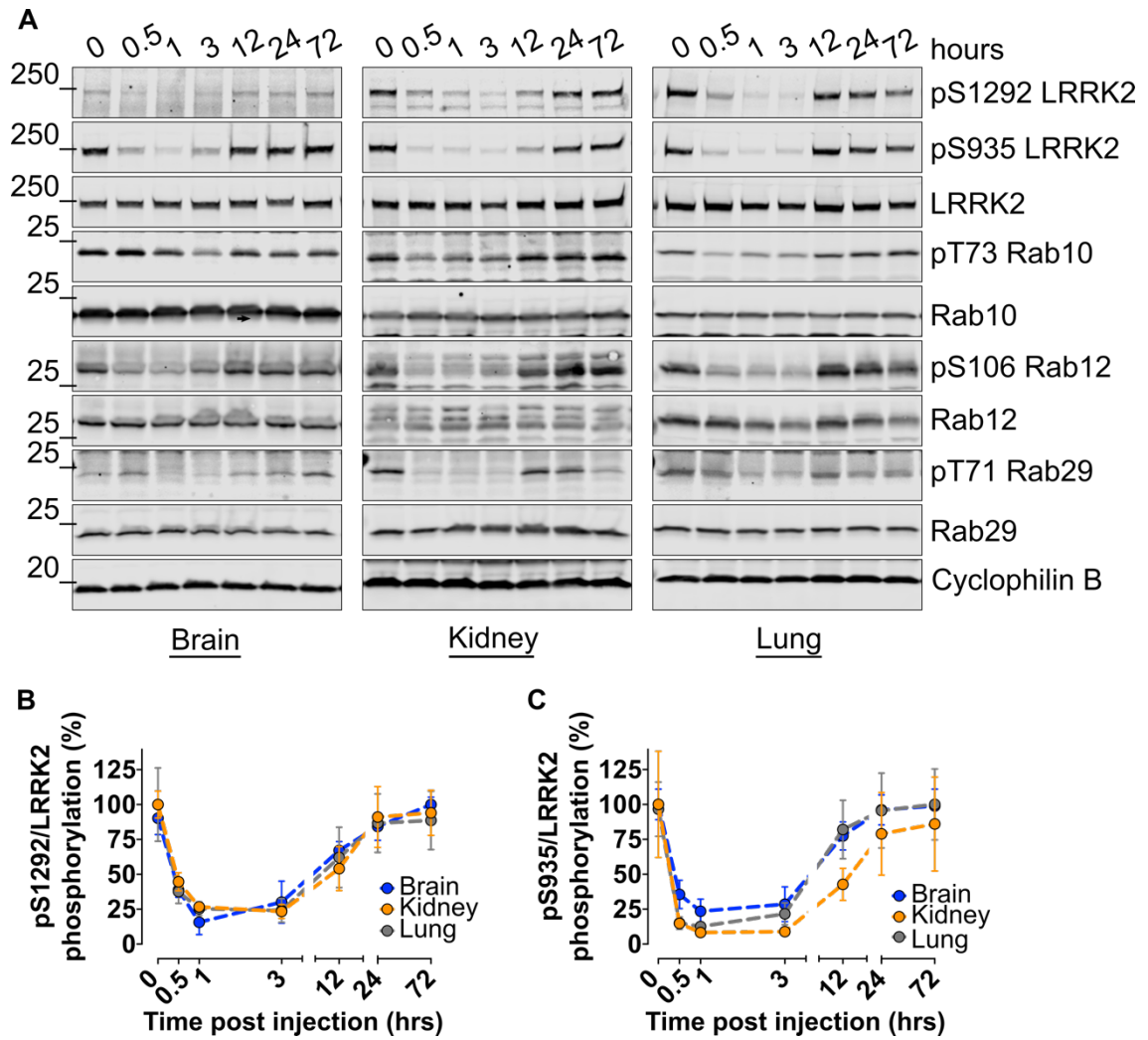
Figure 3.4. **Time course of phosphorylation readouts following acute dose of MLi-2 in G2019S LRRK2 KI mice.** Representative Western blots probed for pLRRK2, pRabs, and total proteins (**A**). Graphs for pS1292 and pS935 are shown with timepoint 0 indicating baseline phosphorylation levels (100%) for brain, kidney, and lung tissues (**B-C**). N=6 mice; error bars indicate SD.

Similarly, maximal dephosphorylation for all pRabs was seen at 1 hour in all tissues. Interestingly however, pRabs recovered more rapidly than pLRRK2, with a full recovery seen by 12 hours compared to 24 hours for pLRRK2 (Figure 3.5A-C). Measures of pT73 Rab10 signal in brain tissue did not show MLi-2-dependent dephosphorylation compared to peripheral tissues at any time

point (Figure 3.5A; corresponding Western blot is shown in Figure 3.4A). S106

Rab12 phosphorylation mimicked pLRRK2 most closely in that all tissues

showed similar dephosphorylation patterns over time (Figure 3.5B;

corresponding Western blot is shown in Figure 3.4A). Additionally, a maximum

of 60% pRab12 dephosphorylation was achieved and sustained for 3 hours

post-dose across all tissues. Of note, Rab12 phosphorylation showed the least

variability across mice relative to Rab10 and Rab29. Dephosphorylation of T71

Rab29 was achieved in all three tissues to varying degrees, with kidneys

showing the strongest response to MLi-2, reaching approximately 75%

dephosphorylation compared to 20–30% seen in brain and lung tissue (Figure

3.5C; corresponding Western blot is shown in Figure 3.4A).
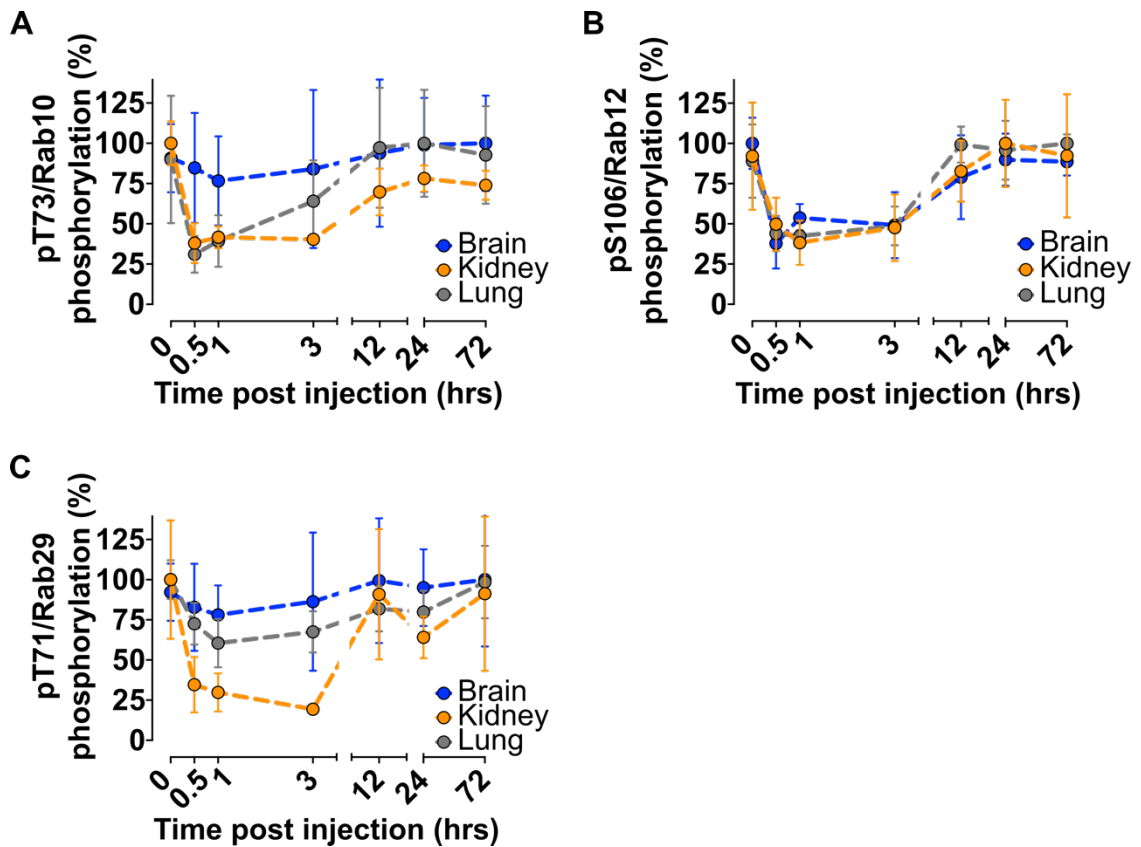
Figure 3.5. **Time course curves for pRab substrates after acute MLi-2 dosing.** G2019S LRRK2 KI mice were given a single dose of MLi-2 at 10mg/kg and sacrificed at the indicated timepoints. Graphs for all three pRabs are shown with timepoint 0 indicating baseline phosphorylation levels (100%) **(A-C)**. N=6 mice; error bars show SD.

Taken together, these data suggest that Rab GTPases are dephosphorylated within the first hour after LRRK2 inhibition in a similar fashion to LRRK2 dephosphorylation, with Rab12 dephosphorylation coinciding most closely with pLRRK2 in the brain and periphery. In contrast, the kinetics of Rab GTPase re-phosphorylation show a quicker recovery at 12 hours compared to 24 hours for LRRK2 phosphorylation sites.

3.2.3 Effect of acute MLi-2 treatment on pRabs across brain regions

Results from the dose response and time course of acute MLi-2 experiments revealed a parallel response pattern between LRRK2 kinase activity, and each individual Rab, with pRab12 being most responsive to MLi-2 across all tissues. Conversely, pRab10 did not show any significant response to MLi-2 treatment in the brain, whereas a reduction in pRab10 was observed in kidney and lung tissues of treated animals. Interestingly, when comparing total levels of Rab10 across tissues, total Rab10 was highest in brain followed by lung and kidney (Figure 3.6).
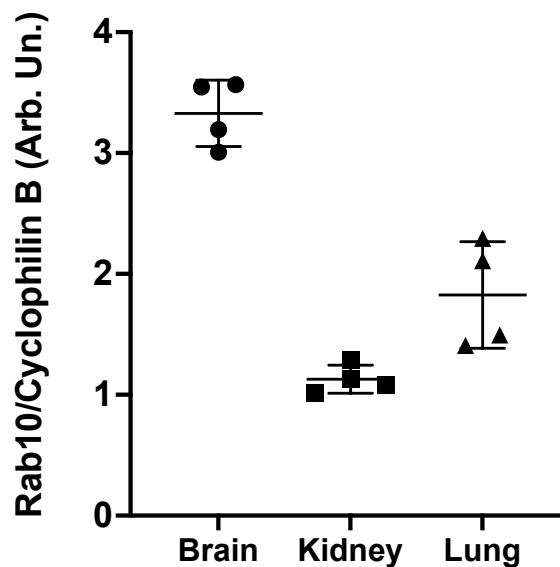
Figure 3.6. **Total Rab10 levels in brain, kidney, and lung tissue homogenates.** Total Rab10 levels measured from the dose response experiment (Figure 3.3). Cyclophilin B was used as a housekeeping protein and values were normalized to an additional sample that was loaded into every gel. N=4 mice; error bars show mean with SD.

These results may suggest that Rab10 may be tightly regulated in the brain compared to other tissues and/or is regulated by other kinases or

phosphatases more abundant than LRRK2. This led me to hypothesize that pools of LRRK2 may not colocalize with pools of Rab10 in brain tissue, and that these differing spatial pools could be determined by brain region or cell type. Since LRRK2 is expressed at variable levels in the brain, whole tissue homogenization may mask region-specific or cell-specific effects of LRRK2 kinase activity on Rab10. Therefore, to test whether there are differential effects of LRRK2 kinase on Rab10 in brain regions, G2019S LRRK2 mice were given a single dose of 10mg/kg MLi-2 via oral gavage and sacrificed 1 hour post-dose. The brains were then removed, and five different regions were dissected: motor cortex, olfactory bulb, hippocampus, striatum, and ventral midbrain. These regions were selected based on where the RNA expression was highest for Rab10 (isocortex, olfactory bulb, hippocampus) and LRRK2 (striatum) (Allen Brain Institute; Lau et al., 2008).

Across brain regions, LRRK2 protein expression was highest in striatum followed by motor cortex (Figure 3.7A-B). Both total Rab10 and Rab12 proteins were highest in ventral midbrain, whereas the other regions showed relatively consistent expression (Figure 3.7A, C-D). Total Rab29 levels were similar across brain regions, with ventral midbrain being the highest and striatum the lowest (Figure 3.7A, E).
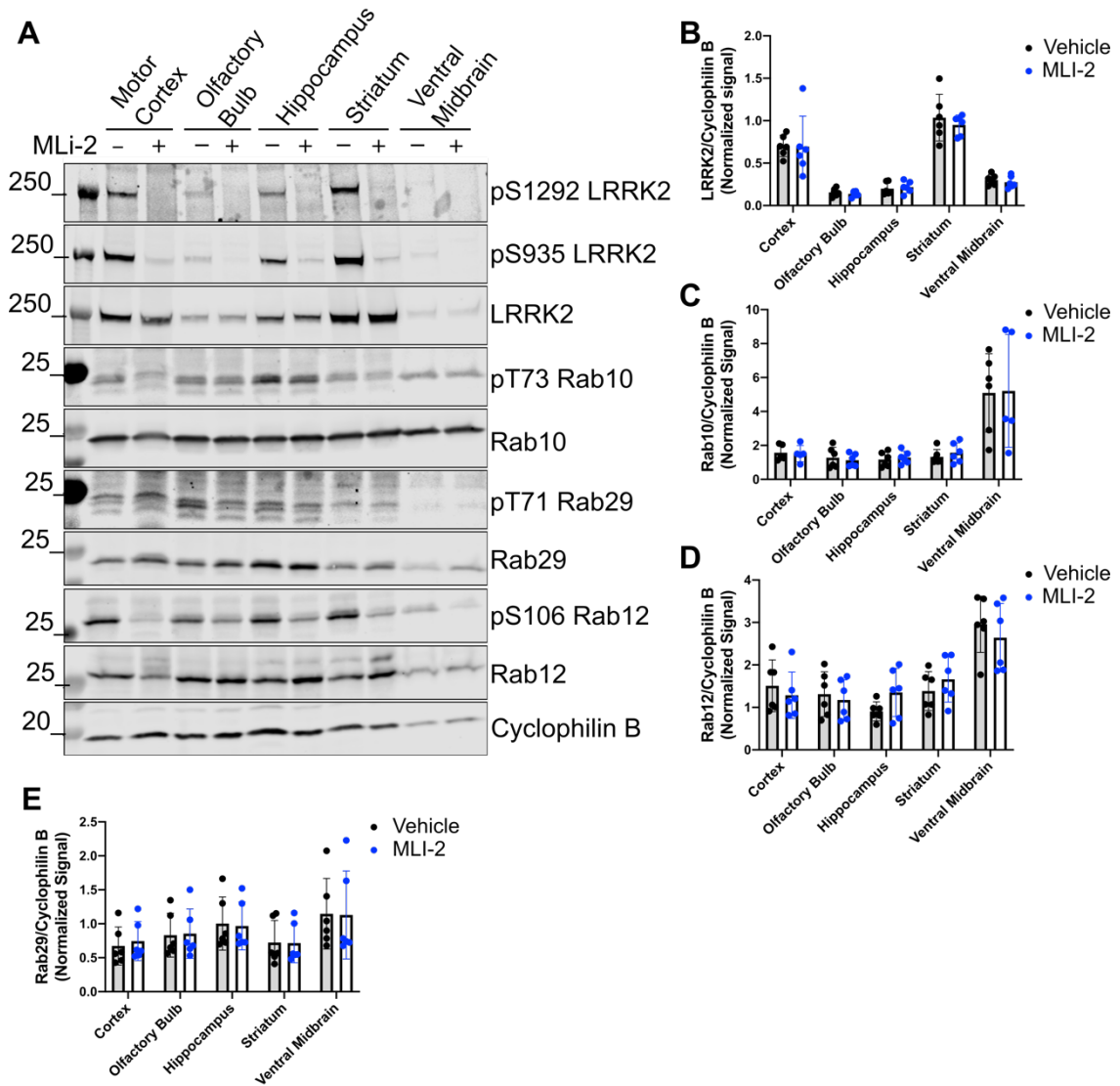
Figure 3.7. **Total levels of LRRK2 and three Rab GTPase substrates across five brain regions in G2019S LRRK2 KI mice.** Representative Western blots probed for pLRRK2, pRab, and total proteins in mice treated with a single dose of MLi-2 (10mg/kg) or DMSO (**A**). Cyclophilin B is used as a housekeeping protein. Bar graphs of total protein levels are shown for cortex, olfactory bulb, hippocampus, striatum, and ventral midbrain regions (**B-E**). N=6 mice; SD error bars are shown.

Interestingly, when comparing MLi-2 versus vehicle treated animals, pRab10 and pRab29 did not show any differences within any of the five brain regions probed, although there was a non-significant decrease in pT71 Rab29 signal in MLi-2 treated animals compared to vehicle treated in the olfactory

bulb (p=0.3982) (Figure 3.8A, C; corresponding Western blots are shown in

Figure 3.7A). Only pS106 Rab12 showed MLi-2 dependent dephosphorylation,

particularly in the hippocampus and striatum (p=0.0147 and p<0.0001,

respectively) with non-significant reductions in all three of the other regions

(Figure 3.8B; corresponding Western blots are shown in Figure 3.7A).
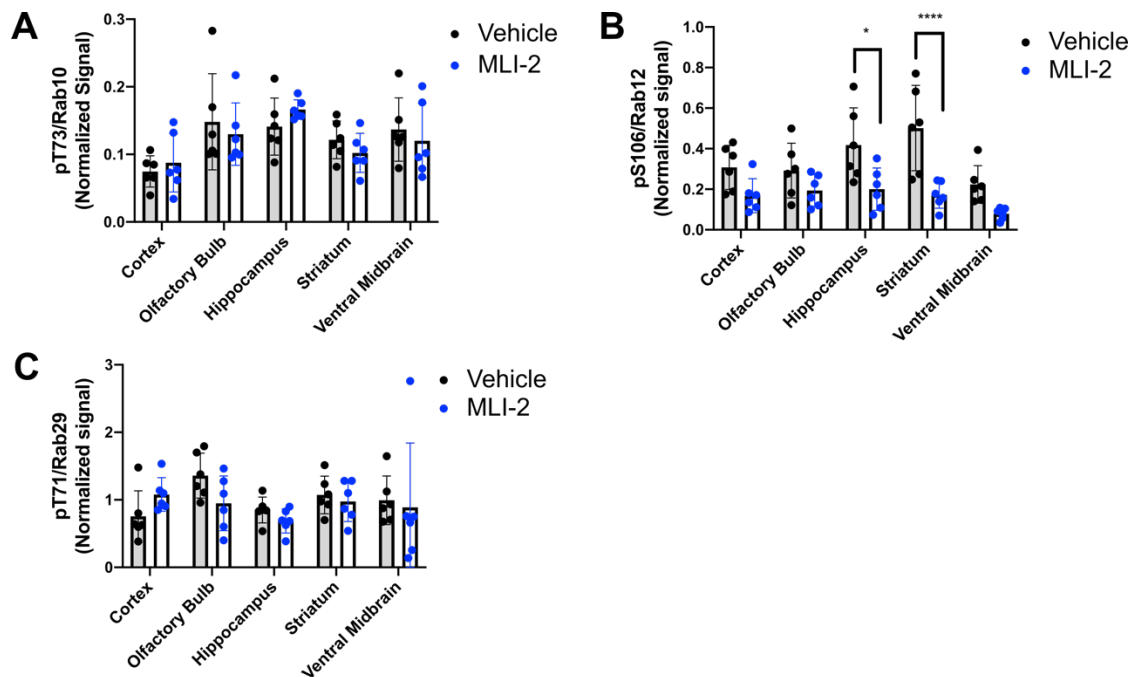
Figure 3.8. **Evaluation of region-specific LRRK2 kinase-dependent phosphorylation of Rab10, Rab12, and Rab29.** Two-way ANOVA with Šidak's multiple comparison tests were performed for each pRab and p-values indicated when significant, *p-value <0.05, ****p-value <0.0001 (**A-C**). N=6 G2019S LRRK2 KI mice; SD error bars are shown.

These data are consistent with the whole brain homogenate

experiments in that pRab12 is the most responsive to LRRK2 kinase inhibition

compared to pRab10 and pRab29, and this is not affected by region-specific

differences.

3.2.4 Cell type differences between neurons and glia in response to

LRRK2 kinase inhibition

To test whether differential patterns of LRRK2-mediated Rab phosphorylation were dependent on cell type, primary astrocyte, microglia, and neuronal cultures were made from P0-P2 G2019S LRRK2 KI pups. Cells were treated with either MLi-2 at 1µM concentration or DMSO for 90 minutes prior to lysis. Western blot analyses showed reduction in T73 Rab10 phosphorylation in glia, with the largest difference observed in astrocytes and a significant effect in microglia (Figure 3.9A-D). In contrast, MLi-2 treated neurons showed a non-significant reduction in pT73 Rab10 levels (p=0.1669) (Figure 3.9E-F). This suggests that the influence of LRRK2 kinase on Rab10 may differ across brain cell types, with glial cells showing a stronger effect.
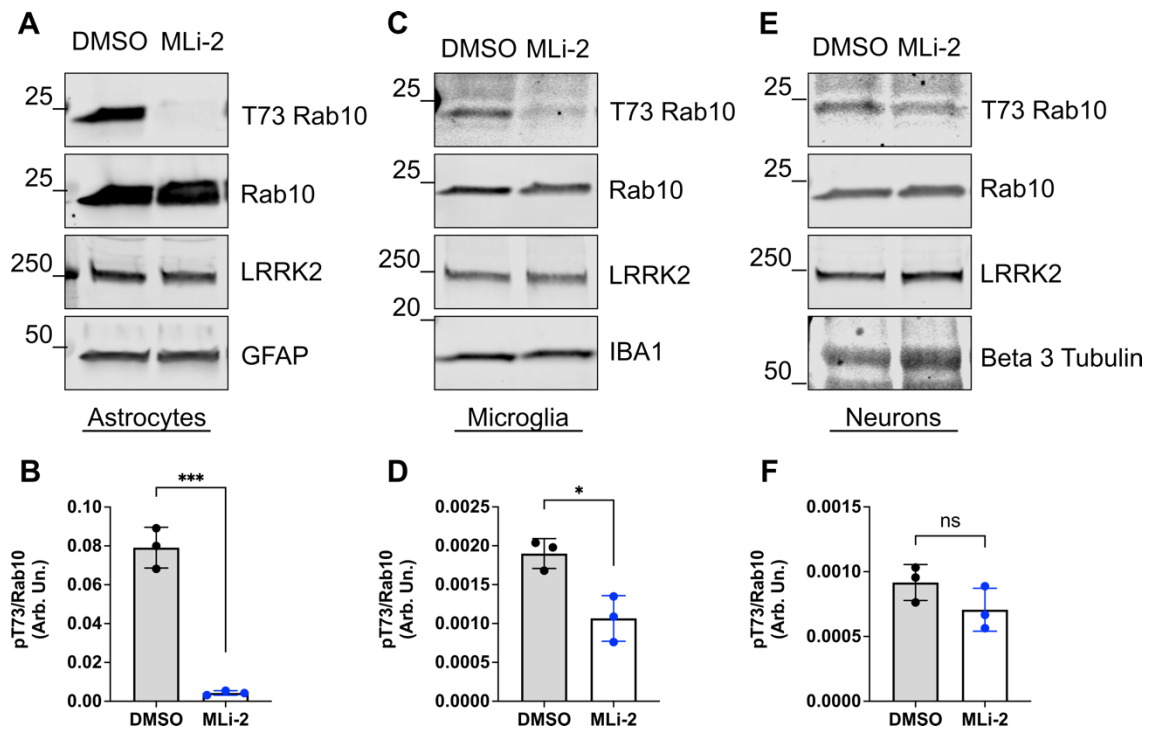
Figure 3.9 **Effect of MLi-2 on T73 Rab10 phosphorylation in mouse brain cells *in vitro*.** Astrocytes, microglia, and neuron cultures from G2019S KI mice were treated with DMSO or MLi-2 for 90 minutes prior to lysis. Representative Western blots probed for pT73 Rab10, total Rab10, LRRK2, and GFAP, IBA1, or Beta 3 Tubulin, respectively (**A,C,E**). Unpaired t-tests were performed, ***p-value <0.001, *p-value <0.05, ns p-value =0.1669 (**B,D,F**). n= 3 independent experiments, 20μg of protein were loaded per sample across cell types; SD error bars are shown.

3.3 Discussion

To test the reliability of phosphorylation markers of LRRK2 kinase activity in a LRRK2 mutant background, I utilized a series of acute dosing paradigms in G2019S LRRK2 KI adult mice. In a dose response experiment, 10mg/kg of MLi-2 was sufficient to maximally reduce pS1292 and pS935 LRRK2 levels in brain, kidney, and lung tissues. Rab12 phosphorylation at S106 showed the strongest response to MLi-2 in all three tissues compared to Rab10 and Rab29, suggesting that pRab12 may be the most reliable biomarker of

LRRK2 kinase inhibition in G2019S LRRK2 animals. Maximal dephosphorylation was achieved after 60 minutes post dose and remained so for three hours post dose for pS1292 and pS935 markers. Full recovery of these phosphorylation sites was observed after 24 hours post dose. Again, S106 Rab12 phosphorylation patterns were most similar to the pLRRK2 sites across all tissues, whereas pT73 Rab10 and pT71 Rab29 showed minimal dependency on MLi-2 in brain. Overall, Rab phosphorylation recovered faster than pLRRK2. This suggests that LRRK2 kinase recovers and can re-phosphorylate Rabs quicker than its autophosphorylation site. To test translatability, future studies should explore Rab12 phosphorylation as a readout of LRRK2 inhibitors in patient blood.

In both dose-response and time-course experiments, the effect of MLi-2 was varied between individual pRabs. Although Rab functions can be highly compensatory for one another (Homma et al., 2019), the three Rabs in question have not been shown to occupy overlapping cellular territories or functions thus far, with Rab10 reported in ciliogenesis and centrosome dynamics pathways (Steger et al., 2017; Dhekne et al., 2018; Lara Ordónez et al., 2019) and lysosomal tubulation under conditions of lysosomal damage (Bonet-Ponce et al., 2020), Rab29 reported as a Golgi resident protein (Beilina et al., 2014; Wang et al., 2014; Purlyte et al., 2019), and Rab12 reported to

play a role in autophagy processes and transmembrane protein degradation

(Matsui et al., 2011; Matsui and Fukuda, 2013). Thus, this may explain part of

the differential effects of LRRK2 kinase inhibition, although both Rab10 and

Rab12 have been shown to interact with RILPL1 and thus share some functional

overlap (Eguchi et al., 2018; Omar et al., 2021).

Additionally, evaluation of the effects of LRRK2 kinase inhibition on

pRabs were consistent across brain regions. Taken together, these experiments

suggest a few possibilities that support the idea that LRRK2 poses a more

regulated relationship with Rab10 compared to other Rabs. Recently, Berndsen

and colleagues identified phosphatase PPM1H that acts to dephosphorylate

Rab10 along with Rab8a and Rab35 at the T73, T72, and T72 sites,

respectively, thereby preventing LRRK2-dependent signaling (Berndsen et al.,

2019). However, PPM1H did not affect Rab12 phosphorylation, suggesting that

the dephosphorylation of Rab12 following LRRK2 inhibition is governed by

distinct pathways separate from those identified for Rab10 and Rab29,

consistent with the data presented in this chapter. When exploring RNA

expression of PPM1H in human brain, kidney, and lung tissue, PPM1H

expression is consistently higher than LRRK2 expression across brain regions

(Figure 3.10). In kidney tissue, PPM1H and LRRK2 expressions are similar

whereas low PPM1H expression is complemented with relatively high LRRK2

expression in lung (Figure 3.10). Of note, RNA expression does not always positively correlate with protein expression nor its activity, thus further experiments would be needed to evaluate phosphatase activity in these tissues. However, if RNA expression does correlate with PPM1H activity, it may explain the difference between the LRRK2-dependent effect on pRab10 in brain versus peripheral tissues, with the lung showing the most influence on MLi-2 treatment in both dosing and time course experiments and suggests a plausible mechanism that is translatable from mice models to human patients.
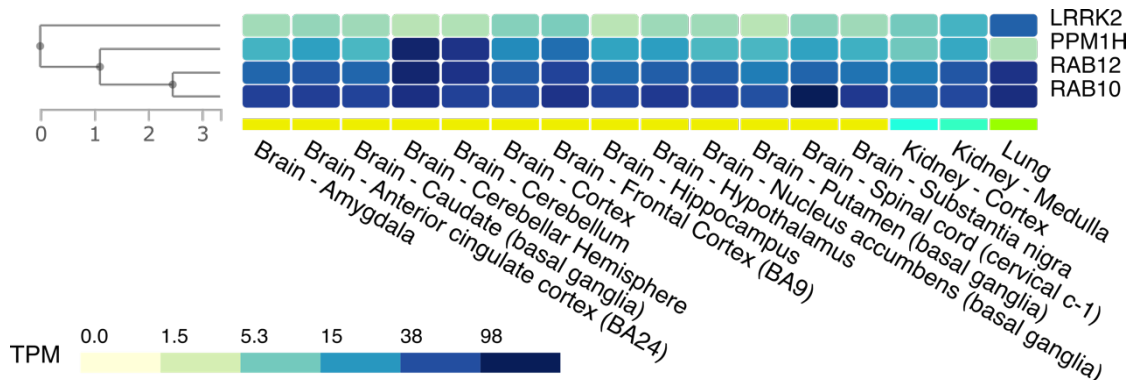
Figure 3.10. **RNA expression of LRRK2, PPM1H, Rab12, and Rab10 in human tissues.** GTEx Multi Gene Query was used and curated by Dr. Mark R. Cookson.

Furthermore, Vieweg et al. reported a PINK1-dependent S111 phospho-site conserved across multiple Rab substrates that can negatively regulate subsequent LRRK2-dependent phosphorylation by preventing Switch-II binding with its guanine nucleotide exchange factors (GEFs), as demonstrated with pT72 Rab8a *in vitro* (Vieweg et al., 2020). It is possible that LRRK2-dependent phosphorylation of Rab10 could be regulated through a similar

unknown mechanism and thus no change to basal levels of phosphorylation is observed with LRRK2 inhibition. Additionally, other as-of-yet-unidentified kinases that phosphorylate these Rabs on the same residue as LRRK2 and normally compete with LRRK2 for binding may be able to phosphorylate these proteins more readily under conditions of LRRK2 inhibition and contributing to the variability observed across animals. Future experimental investigation will be needed to determine other kinases and phosphatases that influence subsets of Rabs and counteract LRRK2 kinase dependence.

Utilizing primary mouse cultures from G2019S LRRK2 KI mice, phosphorylation of T73 Rab10 was evaluated after acute MLi-2 treatments in astrocytes, microglia, and neurons *in vitro*. Interestingly, significant dephosphorylation was observed at T73 Rab10 in astrocyte and microglial cells compared to cortical neurons. A similar effect was observed by Wang et al. in wildtype mouse primary cells (Wang et al., 2021) and suggests that there may be a cell-specific influence on the relationship between Rab10 and LRRK2 in the brain, although further studies will need to be done in order to understand the mechanism/s behind this observation.

4 BIOMARKER EFFICACY IN CHRONIC DOSING OF MLI-2 IN G2019S LRRK2 KI MICE

4.1 Introduction

Some of the most widely used kinase inhibitors in current clinical practice are those that target peripherally rather than within the CNS. For example, Janus kinase inhibitors (JAKs) in the treatment for rheumatoid arthritis (Ferguson and Gray, 2018) acts on lymphocytes in the body and do not cross the BBB. What can be particularly challenging for any drug delivered systemically (i.e. oral, intravenous, or intramuscular administration) for neurodegenerative diseases and nervous system disorders is to design a molecule that can cross the BBB, as well as have limited peripheral side effects with chronic use.

Since the development of third generation LRRK2 inhibitor molecules, several preclinical studies have been conducted in animal models to gain insight into the efficacy and safety of chronically targeting LRRK2 kinase activity. First, several studies in mice and cynomolgus monkeys have shown that total LRRK2 levels in lung and kidney tissues diminish with type I inhibitors GNE-7915, GNE-0877, PFE-360, and MLi-2 within seven days of daily *per os* (PO) dosing (Fuji et al., 2015; Baptista et al., 2020; Bryce et al., 2021), as had

been previously suggested by *in vitro* and kinase-dead KI mice studies (Herzig et al., 2011; Zhao et al., 2015; Lobbestael et al., 2016). However, one of these studies suggests that decreased levels are readily restored in peripheral tissues with cessation of treatment, as was observed in wildtype mice after a seven-day washout period from a 120mg/kg of MLi-2 PO dosing regimen, the dose needed to achieve maximal dephosphorylation of S935 (Bryce et al., 2021). This loss of total LRRK2 was not observed in rats in the same peripheral tissues, however total levels in brain tissue showed a dose-dependent decrease using in-diet dosing of PFE-360 (Kelly et al., 2018). These differences in tissue sensitivity in various animal models suggest either kinase inhibitor-specific effects or species-specific effects. Taken together, these data suggest that kinase activity may play a role in the stability of the protein, and thus dosing may need to be carefully monitored when considering LRRK2 kinase inhibitor use in PD patients.

Moreover, wildtype mice given a 60mg/kg daily in-diet dose of MLi-2 for 6 months showed increased levels of prosurfactant protein C (proSP-C) in lungs, with an observed peak at 28 days, followed by a gradual decrease back to baseline levels (Bryce et al., 2021). This suggests that surfactant trafficking can adapt to chronic high levels of LRRK2 inhibition over time. Further investigation showed that surfactant secretion was not affected by LRRK2

kinase inhibition across species as measured by surfactant D and A levels in

bronchoalveolar lavage fluid (Fuji et al., 2015; Baptista et al., 2020; Bryce et al.,

2021). These studies, executed in wildtype animals, show relatively modest

effects on lung tissue after high doses of MLi-2.

In addition to these molecular changes, reports of morphological

changes have also been documented *in vivo*. This includes enlargement of

type II pneumocytes attributed to abnormal accumulation of lamellar bodies in

the lungs of both wildtype non-human primates and mice, dosed with GNE-

7915, GNE-0877 (Estrada et al., 2014), or MLi-2 for 7 days (Fuji et al., 2015;

Baptista et al., 2020; Bryce et al., 2021). The fact that multiple LRRK2 inhibitor

compounds produced the same results across studies and species

demonstrates that this morphological change is a result of on-target effects

rather than from the inhibition of off-target kinases. Importantly, these changes

were reversible after cessation of treatment and pulmonary function of these

animals was also shown to be unaffected after receiving a 50mg/kg PO MLi-2

daily dose for 28 days (Baptista et al., 2020). One potential concern here is that

vacuolation has not been reported to normalize with continued treatment use,

only after cessation of treatment. Thus, if translatable to humans, this

phenotype may have the potential to harbor long-term adverse effects in PD

patients using a LRRK2 inhibitor treatment chronically. Another concern is that

any negative effects in lungs have the potential to be life threatening, as LRRK2 inhibitors will be primarily targeted towards older adults who may be prone to pneumonia and other related events.

In addition to non-human primates, potentially detrimental events in kidney tissue from rats treated with PFE-360 were also recorded, such as hyperpigmentation of the tissue and accumulation of hyaline droplets within the proximal tubular epithelium (Andersen et al., 2018). As some of these effects overlap with those seen in LRRK2 KO mice (Pellegrini et al., 2018), they are likely to be a result of on target effects of LRRK2 inhibition.

All of these studies used pS935 LRRK2 as the main readout of LRRK2 kinase inhibition in wildtype animals. While pS935 has utility across a range of applications, when considering a mutant LRRK2 background in which LRRK2 kinase is hyperactive, it would be beneficial to gain additional information using a phospho-site that is sensitive to this hyperactivity. In addition, these previous studies set out to test the safety of complete LRRK2 kinase inhibition in the wildtype protein. However, the outcome of maximal inhibition of wildtype LRRK2 may not be equivalent to amelioration of a hyperactive protein back to wildtype activity. Thus, the goal of the current study was threefold: 1) to test the utility of commercially available antibodies raised against

autophosphorylation site S1292 LRRK2, pT73 Rab10, pS106 Rab12, and pT71

Rab29, 2) to mimic a likely clinical use of a LRRK2 inhibitor in which the goal is

to ameliorate hyperactivity in a G2019S LRRK2 background, and 3) to

understand the relationship between level of inhibition and effects on

biochemistry of target tissues including brain and peripheral organs that

express high levels of LRRK2 after chronic treatment.

4.2 Results

4.2.1 Testing MLi-2 in-diet dosing in G2019S LRRK2 mice to ameliorate hyperactive kinase back to wildtype levels of activity

Custom chow was formulated with MLi-2 such that G2019S LRRK2 KI

mice would achieve a dose of approximately 10, 30, or 60mg/kg/day for 10

days. Mice and their chow were weighted daily in order to calculate the

estimated dose of MLi-2 achieved per day (Figure 4.1A-C). All animals were

given chow and water *ad libitum*. Both male and female mice were used in

each dosing group, however, more male mice were randomly assigned to the

60mg/kg/day MLi-2 group based on mice availability, thus this group weighed

an average of 5-8g more than other dosing groups (Figure 4.1A). On average,

all animals ate 3.7g of chow per day (Figure 4.1B), with the 10mg/kg/day and

30mg/kg/day achieving their target dose for the majority of the 10-day dosing period (Figure 4.1C). Since the 60mg/kg/day group weighed more with similar food intake to other groups, these mice only achieved around 51mg/kg/day at the end of the 10-day period (Figure 4.1C). Thus, the 60mg/kg/day group more accurately represents an MLi-2 dose of 48mg/kg/day.
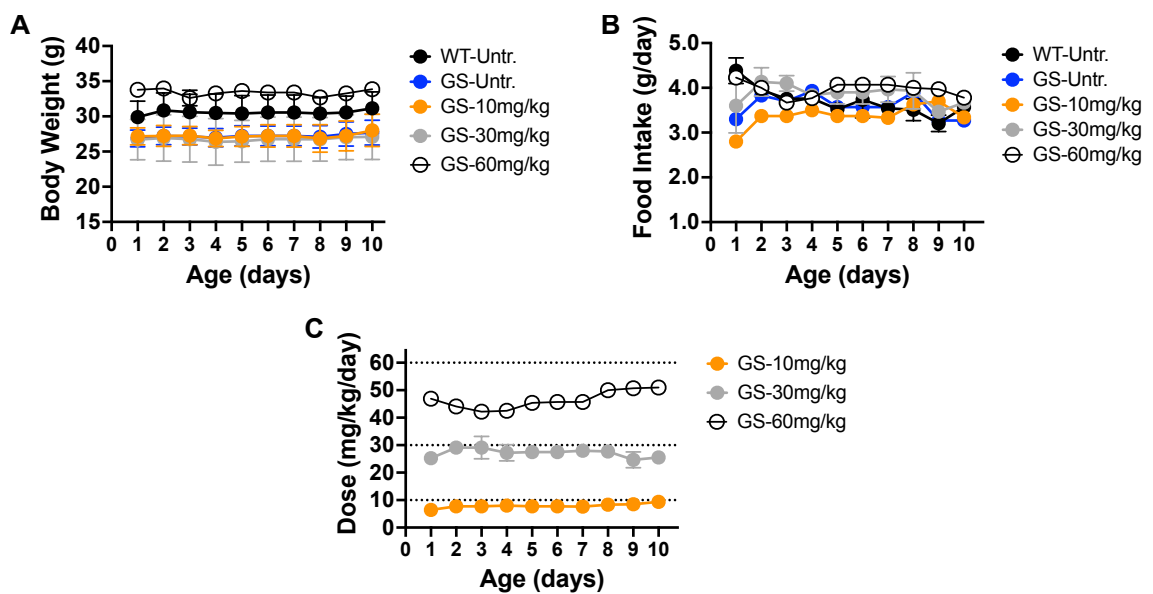
Figure 4.1. **Weight and food tracking in G2019S LRRK2 KI and wildtype mice.** G2019S LRRK2 KI and wildtype mice were given customized chow supplemented with or without MLi-2 to achieve 0, 10, 30, or 60mg/kg/day (N=3). Body weights (**A**) and chow (**B**) were weighed each day for 10 days in order to estimate dose of MLi-2 achieved (**C**).

After 10 days of dosing, mice were sacrificed and brains, kidneys, and lungs, were collected and processed for Western blot. S1292 and S935 phosphorylation sites were probed to evaluate their utility as readouts of both LRRK2 kinase activity and inhibition. Groups of wildtype and G2019S LRRK2 KI mice were also given untreated chow for reference of baseline levels of LRRK2

kinase activity in each background. In the untreated G2019S LRRK2 KI mice,

pS1292 signal was significantly increased across all tissues compared to

wildtype animals which is not reflected in pS935 signals as expected (Figure

4.2A-C). Interestingly, pS935 levels were decreased in G2019S LRRK2

untreated brain tissue compared to wildtype. This observation has been

reported previously in peripheral blood mononuclear cells (PBMCs) of G2019S-

positive PD patients (Padmanabhan et al., 2020; Wang et al., 2021), making

this consistent across species, and most likely biospecimen-specific, as pS935

levels in mouse kidney and lung tissues showed no difference compared to

wildtype (Figure 4.2A, C).
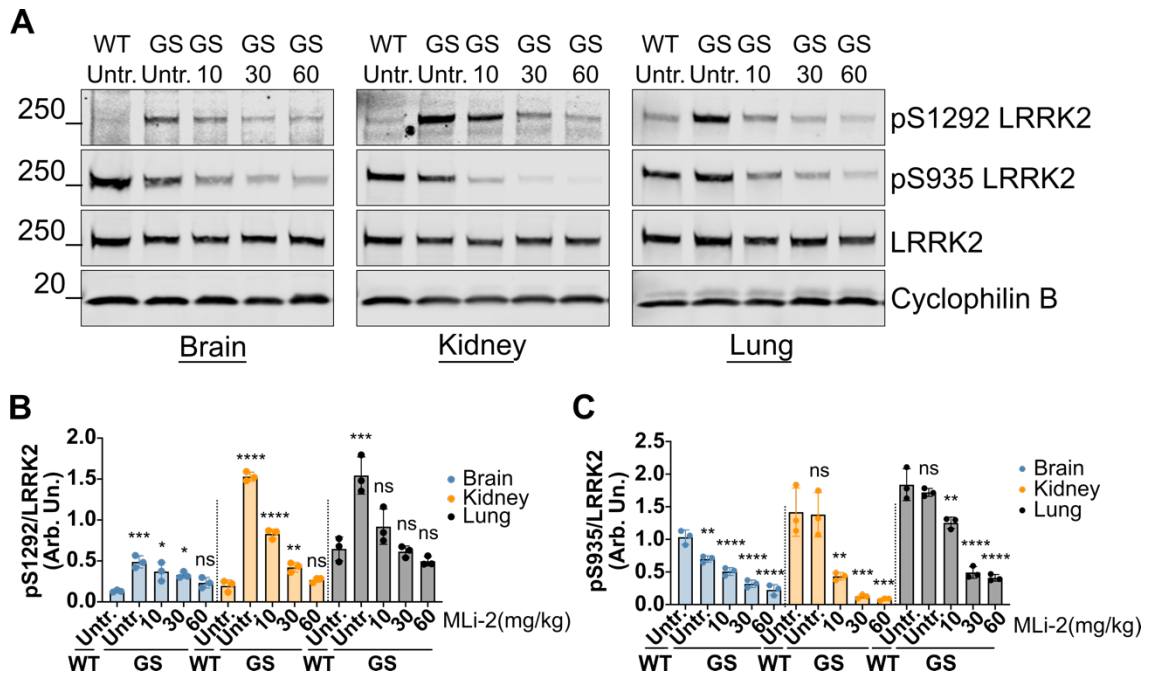
Figure 4.2. **Assessment of MLi-2 in-diet dosing and LRRK2 inhibition in G2019S LRRK2 KI mice.** Wildtype and G2019S LRRK2 KI mice were fed customized chow with and without MLi-2 supplementation to achieve the estimated daily doses indicated. Western blot analyses of S1292 autophosphorylation and S935 phosphorylation were probed, and levels calculated over total LRRK2 protein levels in brain, kidney, and lung tissues. One-way ANOVAs with Tukey's post hoc were performed, ****p-value <0.0001, ***p-value <0.001, **p-value <0.01, *p-value <0.05. N=3; SD error bars are shown.

In the treated animals, 60 mg/kg/day dosing was required to diminish S1292 phosphorylation to wildtype levels in brain and kidney, whereas a 10 mg/kg/day dose was sufficient to decrease phosphorylation to wildtype levels in lung tissue (Figure 4.2A-B). This result suggests that some peripheral tissues with higher expression of LRRK2 may be more sensitive to drug-induced inhibition. Conversely, it could reflect an imbalanced systemic distribution of MLi-2 in the body, with greater accumulation in lungs compared to the brain. Increasing doses of MLi-2 also showed a dose response of pS935

LRRK2 reduction (Figure 4.2A, C). These results indicate that a dose of

60 mg/kg/day is needed in order to inhibit G2019S LRRK2 to wildtype levels *in vivo* across all tissues.

4.2.2 Assessment of pLRRK2 and pRab biomarkers after chronic 60mg/kg/day MLi-2 in-diet dosing in G2019S LRRK2 KI mice

To investigate LRRK2 and Rab phosphorylation as readouts for LRRK2 kinase activity and inhibition over time, G2019S LRRK2 KI mice were given an in-diet MLi-2 treatment regimen of 60mg/kg/day for either 10 days or 10 weeks based on the previous experiment in which 60mg/kg/day was sufficient to reduce S1292 autophosphorylation levels back to wildtype levels in brains, kidneys, and lungs of G2019S LRRK2 KI mice. Both short-term, 10-day and long-term, 10-week chronic treatment periods were chosen to evaluate rapid and progressive changes to phosphorylation sites, respectively. As previously shown, pRab10 and pRab29 signals showed varying degrees of LRRK2 kinase-dependence across tissues, presumably based on the presence of more abundant phosphatases, in acute dosing paradigms. A conjecture arising from this is whether chronic LRRK2 inhibition would affect these signals differently with prolonged exposure to an inhibitor treatment. Additionally, changes at

the proteome level were explored, the results of which will be discussed in Chapter 5.

In both cohorts, G2019S LRRK2 KI mice given a diet of chow supplemented with MLi-2, along with wildtype, G2019S LRRK2 KI, and LRRK2 KO mice given an untreated chow were weighed daily. The untreated animals were used to assess baseline levels of phosphorylation of readout sites for comparison to the treated group after 10 days or 10 weeks. Food intake was measured based on the weight of chow in each cage in order to estimate the daily dose of MLi-2 achieved per mouse. In the 10-day cohort, body weights of all mice remained consistent across the days, with males weighing 5-8g more than females (Figure 4.3A). Across 10-days of treatment, an average of 3.9g of chow was consumed per mouse (Figure 4.3B). When only considering the treated group, an average of 3.6g of chow was consumed, and an estimated 67mg/kg/day dose of MLi-2 was achieved from day 3 through day 10 (Figure 4.3C). In the first two days where animals were acclimating to the food change, an average of 44.5mg/kg/day and 61mg/kg/day MLi-2 was achieved, respectively (Figure 4.3C).

Figure 4.3. **Weight and food intake measurements in the 10-day MLi-2 dosing cohort.** G2019S LRRK2 KI mice were given customized chow supplemented with MLi-2, and untreated chow was given to wildtype, G2019S LRRK2 KI, and LRRK2 KO mice. Body weights were recorded every day and plotted in (**A**), where square data points represent male mice and circle data points represent female mice. Food intake was measured by weighing left over food from all cages each day and subtracting the value from the food weight of the previous day (**B**). These values were used to estimate daily dose of MLi-2 achieved in the G2019S LRRK2 KI mice (**C**).

After 10 days, animals were euthanized and brain, kidney, and lung tissues were extracted, flash frozen and stored at -80 degrees Celsius. Tissues were then homogenized and processed for Western blot, in which pS1292 LRRK2, pS935 LRRK2, pT73 Rab10, pS106 Rab12, pT71 Rab29, and respective total proteins were probed using commercially available antibodies (Figure 4.4A). As expected, pS1292 LRRK2 was significantly increased in G2019S LRRK2 KI animals compared to wildtype, which was decreased to wildtype levels with MLi-2 treatment across all three tissues (Figure 4.4A-B). As expected, S935 phosphorylation showed significant decrease in signal after MLi-2 treatment in G2019S LRRK2 KI animals compared to G2019S LRRK2 KI

animals receiving untreated chow, demonstrating this site's robust readout capacity for LRRK2 inhibition (Figure 4.4A, C). Interestingly, total LRRK2 levels remained stable in the brain, but were reduced in the MLi-2 group in kidney and lung tissues compared to untreated wildtype and G2019S KI animals (Figure 4.4A, D).

When evaluating pRab substrate sites, different patterns were observed between all three Rabs. In brain tissue, T73 Rab10 phosphorylation showed no difference between all genotypes or treated versus untreated G2019S LRRK2 KI mice, whereas in kidney and lung tissue, a significant reduction in phosphorylation was observed in the LRRK2 KO animals compared to wildtype (Figure 4.4A, E). This suggests that there is a LRRK2-dependent effect on pRab10 in peripheral tissues where LRRK2 is highly expressed, when total protein is completely absent. LRRK2 inhibition in G2019S KI animals that were fed MLi-2 showed no difference in T73 phosphorylation in kidney compared to its untreated counterpart, while lung tissue showed a treatment-dependent reduction in signal (Figure 4.4A, E). Hyperactivity of G2019S LRRK2 did not affect pT73 Rab10 levels compared to wildtype across any tissue.

Rab12 phosphorylation at S106 showed a similar pattern to that of S1292 autophosphorylation, in that the effects of both LRRK2 hyperactivity and

inhibition could be observed across brain and peripheral tissues (Figure 4.4A, F). Specifically, pS106 was significantly increased in G2019S KI mice fed untreated chow but comparable to wildtype in MLi-2 treated G2019S KI mice (Figure 4.4A, F). In brain, pT71 Rab29 levels were significantly increased in a G2019S KI background and MLi-2 treatment reduced this phosphorylation, whereas no LRRK2-dependent phosphorylation was observed in the kidney or lung of these animals (Figure 4.4A, G).

Figure 4.4. **LRRK2 and Rab substrate phosphorylation in G2019S LRRK2 KI mice after in-diet MLi-2 dosing for 10 days.** Wildtype, G2019S LRRK2 KI, and LRRK2 KO mice were fed vehicle or MLi-2-containing chow over the course of 10 days following brain, kidney, and lung tissue collection. Western blot analyses were done for all three tissues in which pLRRK2, total LRRK2, and pRab protein signals were evaluated (**A-G**). One-way ANOVAs were performed with Tukey's post-hoc analyses, ****p-value <0.0001, ***p-value <0.001, **p-value <0.01, *p-value <0.05. N=6; SD error bars are shown.

In the 10-week cohort, body weights of all mice increased an average of 4-5g regardless of genotype or gender, with the exception of the LRRK2 KO males that increased 10g on average, from week 1 to week 10 (Figure 4.5A). Increased body weight in LRRK2 KO animals has previously been noted in both mice and rats (Baptista et al., 2013; Mazza et al., 2021; Ness et al., 2013). In general, an increase in body weight across 2.5 months in animals aged from 3 to 5.5 months is expected. Similar to the 10-day cohort, the average food intake of all mice was 3.8g while the average food intake of the G2019S KI group given MLi-2 supplemented chow was 3.6g (Figure 4.5B). Thus, the calculated average daily dose of MLi-2 per mouse was 61.2mg/kg (Figure 4.5C).
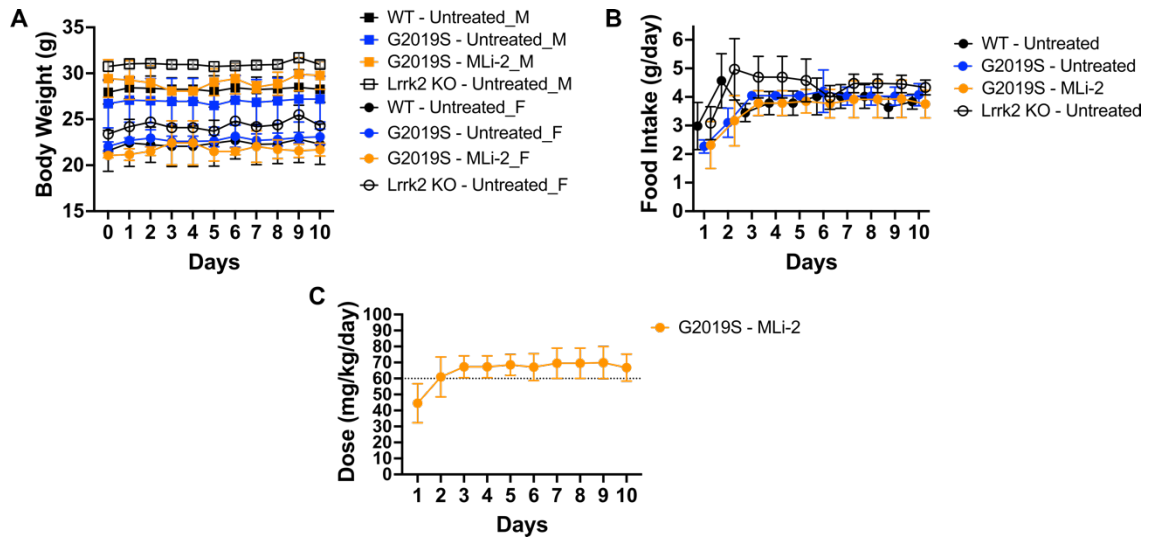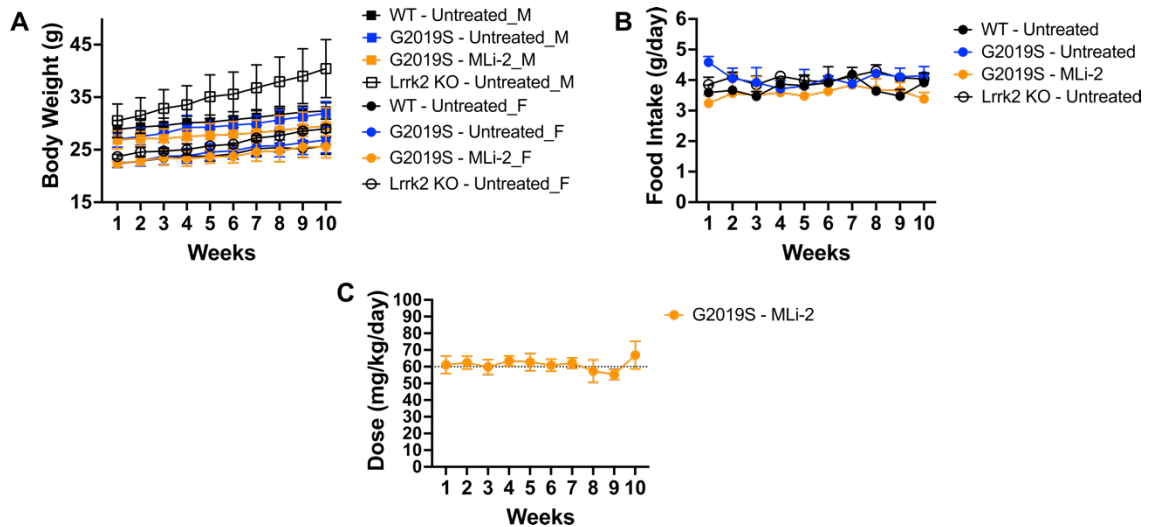
Figure 4.5. **Weight and food intake measurements in the 10-week MLi-2 dosing cohort.** G2019S LRRK2 KI mice were given customized chow supplemented with MLi-2, and untreated chow was given to wildtype, G2019S LRRK2 KI, and LRRK2 KO mice. Body weights were recorded every day, averaged per week and plotted in (**A**), where square data points represent male mice and circle data points represent female mice. Food intake was measured by weighing left over food from all cages each day and subtracting the value from the food weight of the previous day (**B**). These values were used to estimate daily dose of MLi-2 achieved in the G2019S LRRK2 KI mice (**C**).

After the 10-week period, all mice were euthanized and brains, kidneys, and lungs were collected and flash frozen in dry ice and stored at -80 degrees Celsius until processed for Western blot. After 10-weeks of continuous MLi-2 in-diet dosing, Western blot analyses showed the same patterns for pS1292, pS935, and pS106 Rab12 as observed in the 10-day cohort (Figure 4.6A-C, F). Both pS1292 and pS106 levels were increased in G2019S KI mice and an MLi-2 in-diet dose of 60mg/kg/day returned these levels back to wildtype across brain and peripheral tissues, and S935 phosphorylation was still significantly decreased in treated animals after 10-weeks (Figure 4.6A-C, F). Total LRRK2 levels were only decreased in the kidneys of G2019S KI mice treated with MLi-

2 compared to untreated G2019S KI mice, suggesting that degradation of total levels may normalize over time with continued treatment in certain tissues (Figure 4.6A, D). T73 Rab10 phosphorylation was also similar to the 10-day cohort, in that no significant differences were observed in the brains and kidneys of treated animals versus their untreated counterparts (Figure 4.6A, E). Interestingly, the decrease in pT73 Rab10 observed in lungs of the 10-day cohort was not observed in the 10-week cohort, although levels were especially variable in the G2019S KI animals (Figure 4.6A, E). However, a significant reduction in pT73 signal was seen in the peripheral tissues of LRRK2 KO animals compared to wildtype, as was seen in the 10-day cohort (Figure 4.6A, E). Lastly, T71 Rab29 phosphorylation showed no difference across genotype and treatment in brain nor kidney, whereas phosphorylation was reduced in G2019S KI and LRRK2 KO untreated groups in lung (Figure 4.6A, F).
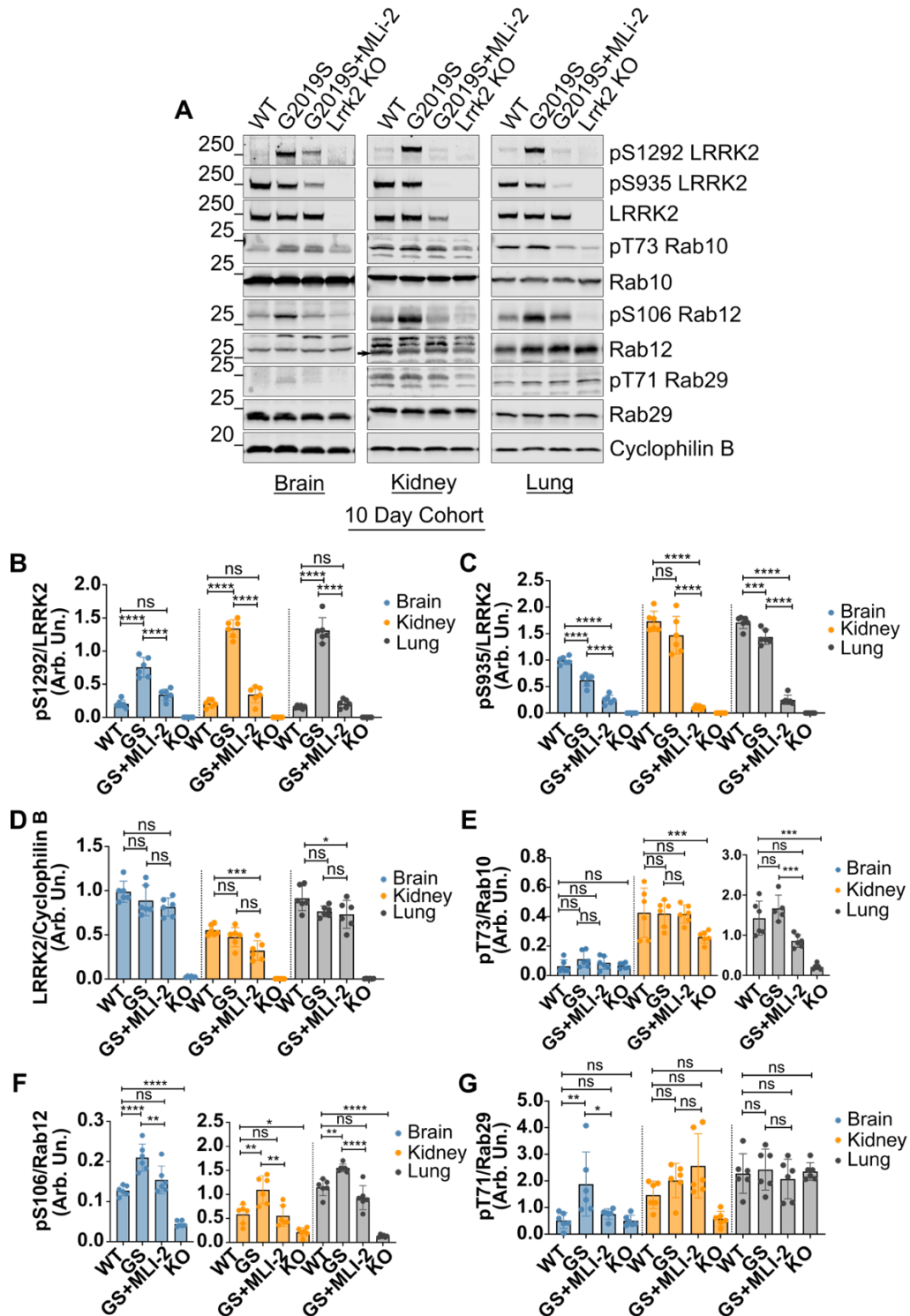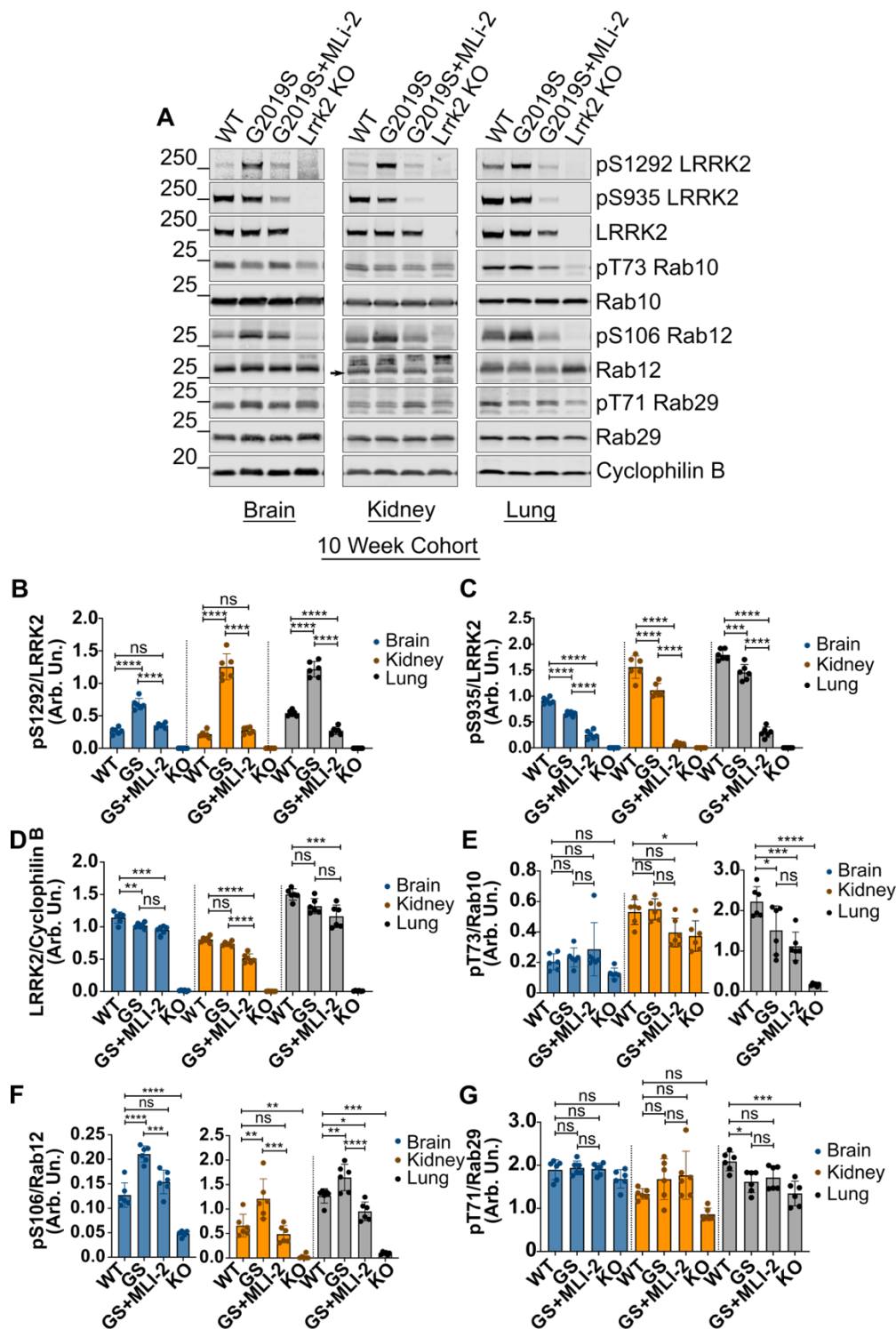
Figure 4.6. **LRRK2 and Rab substrate phosphorylation in G2019S LRRK2 KI mice after in-diet MLi-2 dosing for 10 weeks.** Wildtype, G2019S LRRK2 KI, and LRRK2 KO mice were fed vehicle or MLi-2-containing chow over the course of 10 weeks following brain, kidney, and lung tissue collection. Western blot analyses were done for all three tissues in which pLRRK2, total LRRK2, and pRab protein signals were evaluated (**A-G**). One-way ANOVAs were performed with Tukey's post-hoc analyses, ****p-value <0.0001, ***p-value <0.001, **p-value <0.01, *p-value <0.05. N=6; SD error bars are shown.

Since levels of proSP-C were found to be altered in the lungs of

wildtype mice receiving a 60mg/kg daily dose of MLi-2 for 7 days (Bryce et al.,

2021), proSP-C protein was probed in both 10-day and 10-week cohorts to

determine whether LRRK2 inhibition in G2019S LRRK2 KI mice would differ

from wildtype animals. Interestingly, no differences were observed in either 10-

day nor 10-week cohorts when comparing treated G2019S KI lung tissue and

untreated wildtype or G2019S KI lung tissue, suggesting at amelioration of

LRRK2 kinase hyperactivity to wildtype activity does not affect proSP-C levels

(Figure 4.7A-D). An increase in proSP-C was observed in the lungs of LRRK2

KO animals compared to wildtype, showing that the loss of total LRRK2 protein

can also affect proSP-C levels (Figure 4.7A-D).
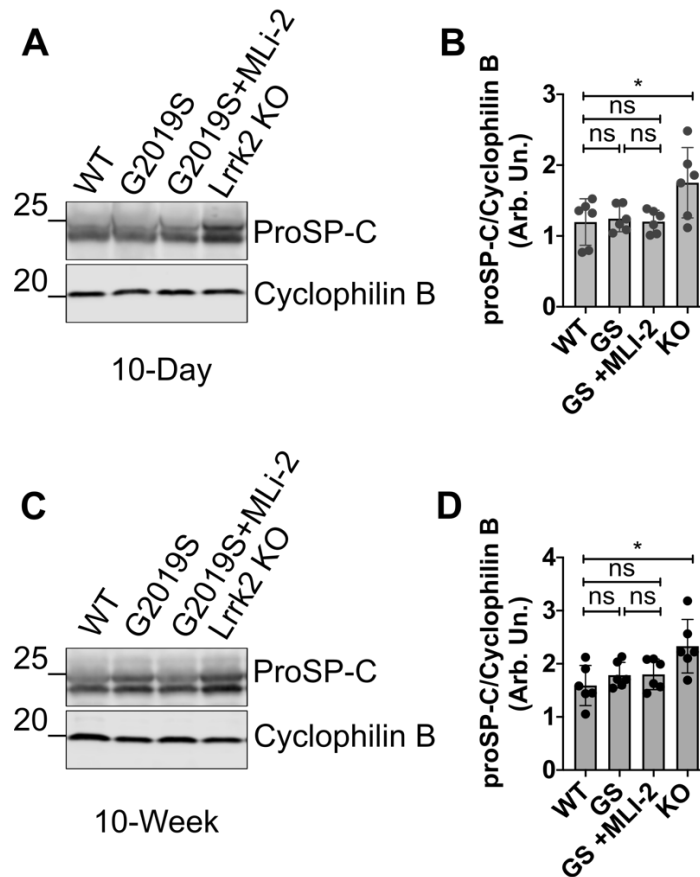
Figure 4.7. **Evaluation of proSP-C levels in the lung tissue of 10-day and 10-week in-diet dosing cohorts.** Wildtype, G2019S LRRK2 KI, and LRRK2 KO mice were fed vehicle or MLi-2-containing chow over the course of 10 days (**A**) or 10 weeks (**C**). Lung tissue analyses were performed via Western blot and proSP-C levels were measured (**B, D**). One-way ANOVAs were performed where *p-value <0.05. n=6; error bars indicate SD.

4.3 Discussion

To evaluate various markers of LRRK2 kinase activity and inhibition *in vivo*, both 10-day and 10-week treatment regimens were carried out, with focus on designing a treatment paradigm that might reasonably mimic clinical applications. Specifically, MLi-2 was utilized to chronically ameliorate the hyperactivity of G2019S mutant LRRK2 to that of wildtype animals. When measuring LRRK2 phosphorylation, the pS1292 autophosphorylation site

provided the most reliable marker of both G2019S-induced hyperactivity and MLi-2 dependent inhibition. Whether this can be extrapolated to human clinical samples is unclear as current tools have not yet allowed for robust detection of pS1292 LRRK2 in peripheral blood, although some studies have demonstrated its efficacy in patient urinary and CSF exosomes (Fraser et al., 2016; Wang and West, 2019).

Using the commercially available pRab antibodies, the S106 Rab12 phosphorylation pattern resembled that of pS1292 LRRK2 most closely across experiments, in that G2019S KI mice displayed hyperphosphorylation of Rab12 that was ameliorated with MLi-2 treatment. Thus, if translatable to humans, for G2019S-carriers and potentially other PD cases, detection of pRab12 has potential as a biomarker for both LRRK2 activity and inhibition. In contrast, the hyperphosphorylation pattern of substrates Rab10 and Rab8a have been demonstrated in mutations within the GTPase domain with a much more subtle increase for G2019S compared to wildtype both *in vitro* as well as in the kidney and lung tissues of R1441C LRRK2 KI mice (Steger et al., 2016; Iannotta et al., 2020). Therefore, Rab10 phosphorylation may be more useful as a readout in patients carrying LRRK2 GTPase domain mutations, although further investigation of this *in vivo* needs to be done.

Furthermore, many studies have demonstrated the dephosphorylation of Rab8a/10/12/29/35 after acute LRRK2 inhibitor treatment in various human and mouse cell types expressing pathogenic mutant LRRK2 *in vitro* (Ito et al., 2016; Thirstrup et al., 2017; Lis et al., 2018; Di Maio et al., 2018; Gomez et al., 2019; Purlyte et al., 2019; Bonet-Ponce et al., 2020). Here, the observation that pRab10 and pRab29 do not show consistent dephosphorylation in MLi-2 treated G2019S KI mice across acute and chronic paradigms highlights a discrepancy between *in vitro* and *in vivo* models. However, one study performed in Long Evans rats with G2019S LRRK2 mutations showed that acute LRRK2 inhibition could reliably decrease pT73 Rab10 levels in brain compared to Sprague Dawley rats harboring the same mutation (Kelly et al., 2021). Therefore, it is possible that LRRK2-dependent Rab10 phosphorylation *in vivo* is species-specific. Additionally, as discussed in the previous chapter, phosphatases such as PPM1H are more abundant in brain and kidney tissues compared to LRRK2 (Figure 3.10). The effect of LRRK2 activity and inhibition on Rab10 phosphorylation thus may be diluted as well as is a possibility for Rab29 phosphorylation from other as of yet unidentified enzymes.

Additionally, in G2019S LRRK2 KI mice given a 60mg/kg/day in-diet dose of MLi-2 for 2.5 months showed no difference in proSP-C levels at both 10 days of dosing and at 10 weeks compared to untreated wildtype animals,

suggesting that inhibition of hyperactive LRRK2 kinase does not develop the same molecular effects in lung tissue as wildtype LRRK2 (Bryce et al., 2021; Kluss et al., 2021). This is an important observation, as patients carrying mutant LRRK2 may then have less of a risk in developing secondary lung effects when drugs target hyperactive LRRK2 compared to those without a LRRK2 mutation. Interestingly, after 10 weeks of MLi-2 in-diet dosing, both S1292 LRRK2 and S106 Rab12 phosphorylation levels were significantly lower than wildtype levels in lung. Thus, it is possible that lung tissue is more sensitive to LRRK2 inhibition than other tissues considered here. Indeed, one study investigating LRRK2 expression and lung adenocarcinoma risk in humans reported a significant correlation between lung cancer prevalence and low LRRK2 expression, suggesting that low levels of LRRK2 may promote lung tumorigenesis (Lebovitz et al., 2021).

5 QUANTITATIVE TOTAL AND PHOSPHO- PROTEOMICS IN MLI-2 CHRONICALLY TREATED G2019S LRRK2 KI MICE

5.1 Introduction

Recent advances in proteomic technology using liquid chromatography with tandem mass spectrometry (LC-MS/MS) and high-throughput screening have underpinned some major discoveries in LRRK2 biology. This includes the identification of binding partners like Rab substrates, Clathrin adaptor protein complex 2 (AP2), Flotillin-2 in the Wingless/Integration (WNT) signaling pathway, p21-activated kinase 6 (PAK6), and Syntaxin-6 (STX6) and vesicle-associated membrane protein 4 (VAMP4) of the Golgi-associated retrograde protein (GARP) complex by utilization of various cancer cell lines and primary rodent brain cell cultures (Steger et al., 2016; Salašová et al., 2017; Civiero et al., 2015; Heaton et al., 2020; Beilina et al., 2020). In addition, a number of studies have employed unbiased quantitative proteomics to understand the function of LRRK2 *in vivo*. For example, abundance proteomics of kidney tissue from 9-month-old LRRK2 KO mice revealed changes in cytoskeletal-associated proteins such as Coronin1C, and upregulation of lysosomal proteases such as Cathepsin D (Ctsd) and Legumain (Pellegrini et al., 2018). Collectively, these

studies have provided substantial insights into the roles of LRRK2 in cellular biology.

Proteomic technology has also proven valuable in analyzing clinical cohorts. Recently, proteomic analyses of urine samples from PD patients identified neurotropic factor VGF as a biomarker to distinguish manifesting versus non-manifesting PD cases in those carrying the G2019S mutation (Virreira Winter et al., 2021). Additionally, significant upregulation in lysosomal proteins Transmembrane protein 192 (TMEM192), Cathepsin B (CTSB) and Galactosidase beta 1 (GLB1) in the urinary proteome of G2019S-carriers versus healthy controls was noted (Virreira Winter et al., 2021). This suggests that of all the various trafficking pathways LRRK2 has been nominated to play a role in, the endolysosomal pathway has direct evidence implicating dysregulation in human mutation carriers.

To date, no proteomic analysis had been used to investigate chronic LRRK2 inhibition *in vivo*. Here, isobaric tandem mass tag (TMT) total and phospho-proteomic analyses were employed to understand the relationship between level of inhibition and effects on biochemistry of target tissues including brain and peripheral tissues that have previously been shown to be

affected by LRRK2 kinase inhibition or KO, kidney and lung (Fuji et al., 2015;

Pellegrini et al., 2018; Baptista et al., 2020; Bryce et al., 2021).

5.2 Results

5.2.1 Total and phospho-proteomics of whole brain tissue from MLi-2 treated G2019S KI mice

To evaluate downstream effects of LRRK2 inhibition in kinase

hyperactive G2019S KI mice, total and phospho-proteomics were employed in

brain, kidney, and lung tissues as depicted in Figure 5.1 using TMTpro-16

reagents (Li et al., 2020). G2019S KI mice treated with MLi-2 in-diet for 10

weeks were used in these experiments to investigate the effects induced after

long-term chronic exposure of a LRRK2 kinase inhibitor. Untreated G2019S KI,

wildtype, and LRRK2 KO mice were included for comparison.
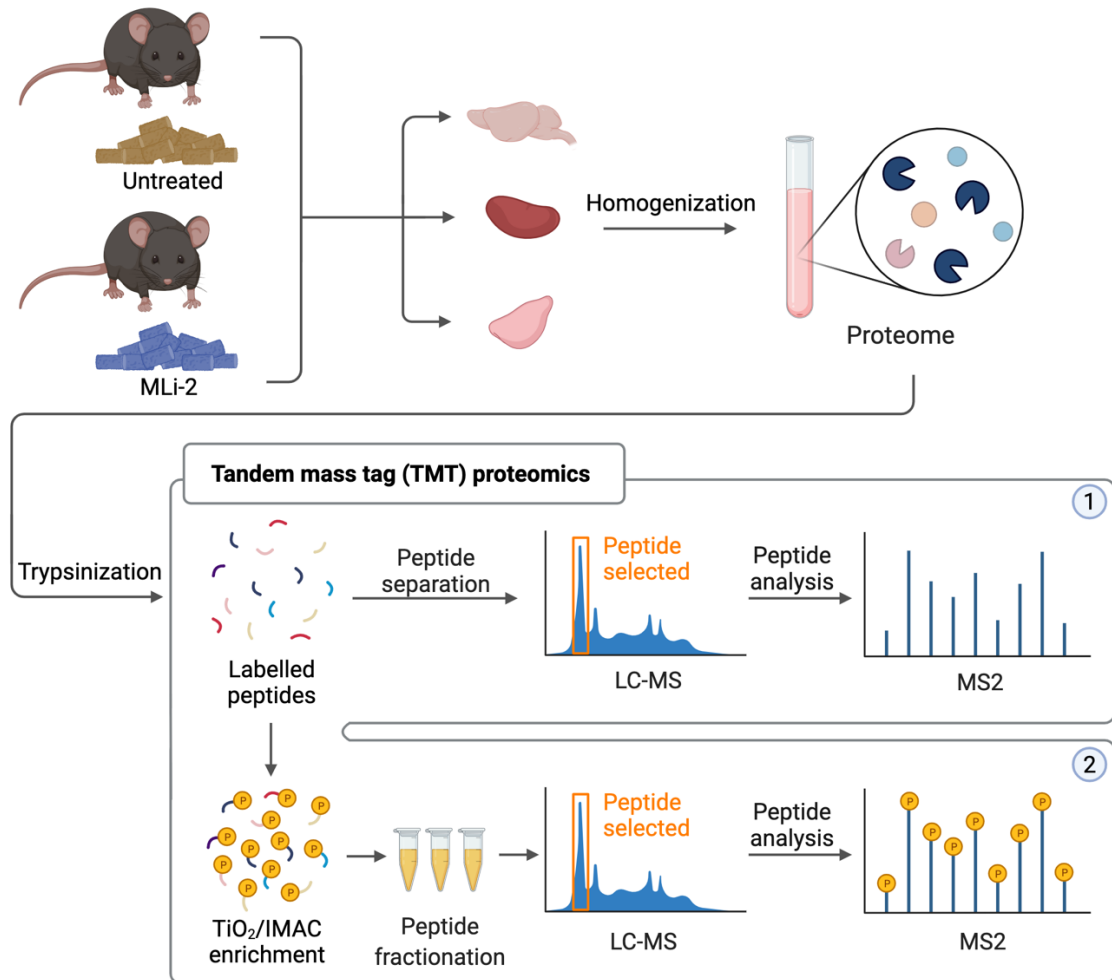
Figure 5.1. **Schematic of tissue processing in TMT proteomics**. Depiction of technical approach for both total (1) and phospho- (2) proteomic data collection in MLi-2 treated and untreated mouse groups.

One hemisphere from each brain was collected and processed for proteomic analyses in which 3,823 total proteins were identified after filtering and merging runs (see 5.4 Materials and Methods). Comparing MLi-2 treated and untreated G2019S KI mice, 319 proteins were significantly different at <0.05 after empirical Bayes analysis followed by false discovery rate (FDR) correction (Figure 5.2A). These included Cytochrome C, NADH:Ubiquinone Oxidoreductase Subunit V3 (Nduvf3), the mitochondrial ATP synthase Atp5g1,

and Voltage Dependent Anion Channel 2 (Vdac2) (Figure 5.2A). Only two hits

passed an arbitrary cutoff of 0.5 $\log_2$ fold change (1.4x), Rab33a and

Cytochrome C (Cycs). Strikingly, Gene Ontology analyses revealed enrichment

for proteins residing in different mitochondrial compartments (Figure 5.2C).

Volcano plots comparing untreated groups of G2019S KI and wildtype mice

showed that a number of mitochondrial proteins had the opposite trend to

that seen in the chronic MLi-2 cohort (Figure 5.2B). For example, Vdac2 and

Cycs showed modest but significant downregulation in brains of G2019S KI

mice compared to wildtype mice, which were reversed in the chronic MLi-2

G2019S KI cohort (Figure 5.2A-B). Although modest changes were observed

overall, these results suggest that MLi-2 treatment can significantly alter the

expression of mitochondrial proteins in G2019S KI mice in a direction

potentially consistent with therapeutic potential.
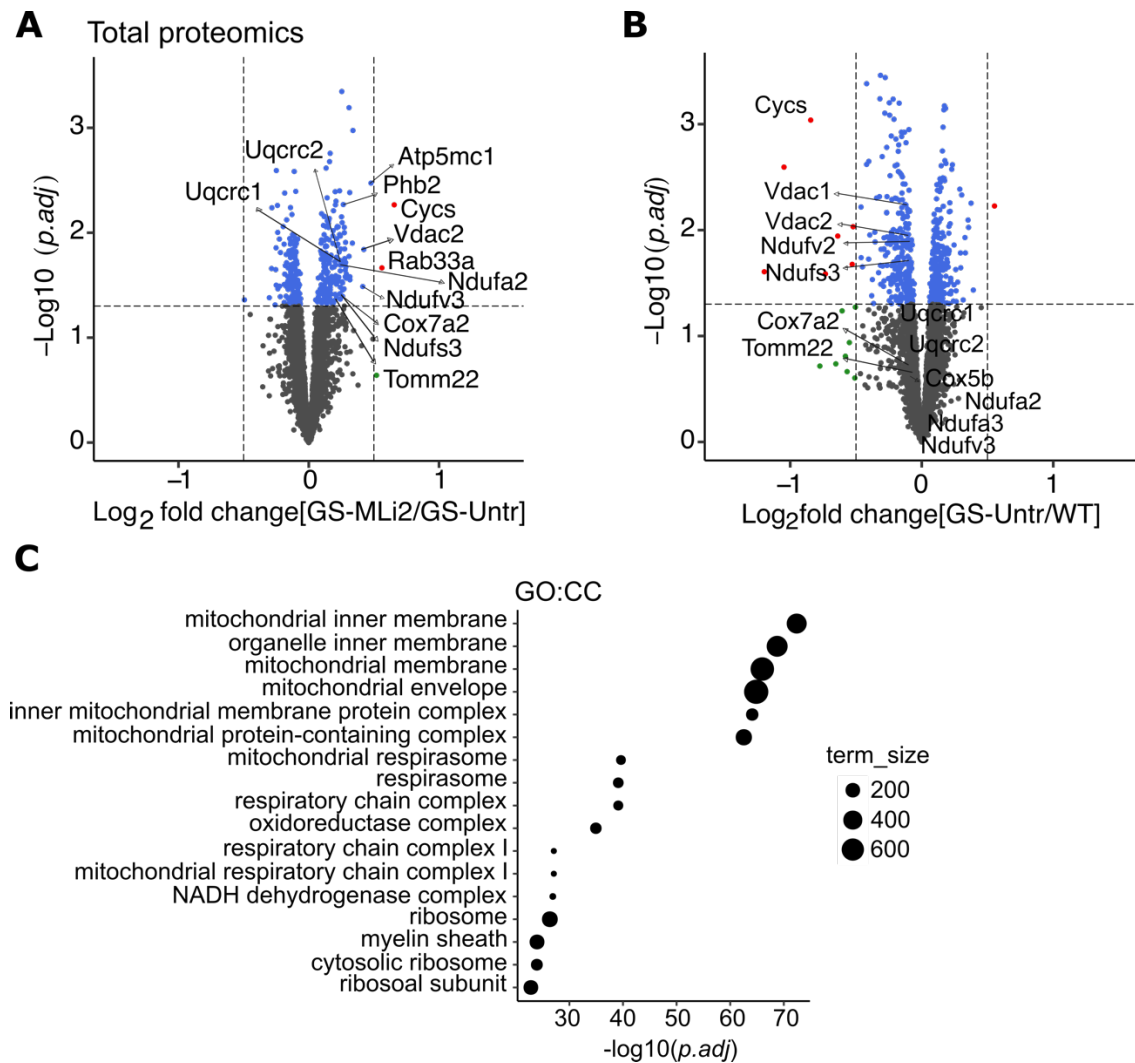
Figure 5.2. **Total brain proteomics.** Volcano plots illustrate differential expression of proteins between MLi-2 treated and untreated G2019S KI mice (**A**) and between untreated G2019S KI and wildtype mice (**B**). A bubble plot shows enrichment of cellular compartments found using the Gene Ontology cellular component database (GO:CC) (**C**). The -log10 cutoff used for the bubble plot was <1e-20 and term size cutoff was <1000. Volcano plot key: grey = non-significant, blue = < 0.05 p-value, green = >1.4x fold change, red = < 0.05 p-value and >1.4x fold change.

Additionally, 2,792 phospho-peptides were identified in the phospho-proteomic analysis, of which 180 were differentially expressed (adjusted p-value <0.05) in MLi-2 treated versus untreated G2019S KI mice (Figure 5.3A). Among these, a decrease in S58 phosphorylation of the ion transporter Fxyd7

and increase in S109 phosphorylation of the protein phosphatase 2A (PP2A)

inhibitor Ensa were observed (Figure 5.3A). Gene Ontology cellular

component analyses identified that there was significant enrichment of

phospho-peptides associated with synaptic, dendritic, and vesicle

compartments including Transmembrane protein 230 (pS24 TMEM230),

sorting nexin 17 (pS336 Snx17), Proline Rich Transmembrane protein 2 (pS244

Prrt2), and transmembrane protein Kiaa1109 (pS3835) (Figure 5.3A-B). Of

interest, no mitochondrial enrichment was found among the phospho-peptide

hits, suggesting that total and phospho- protein alterations identify different

cellular pathways.
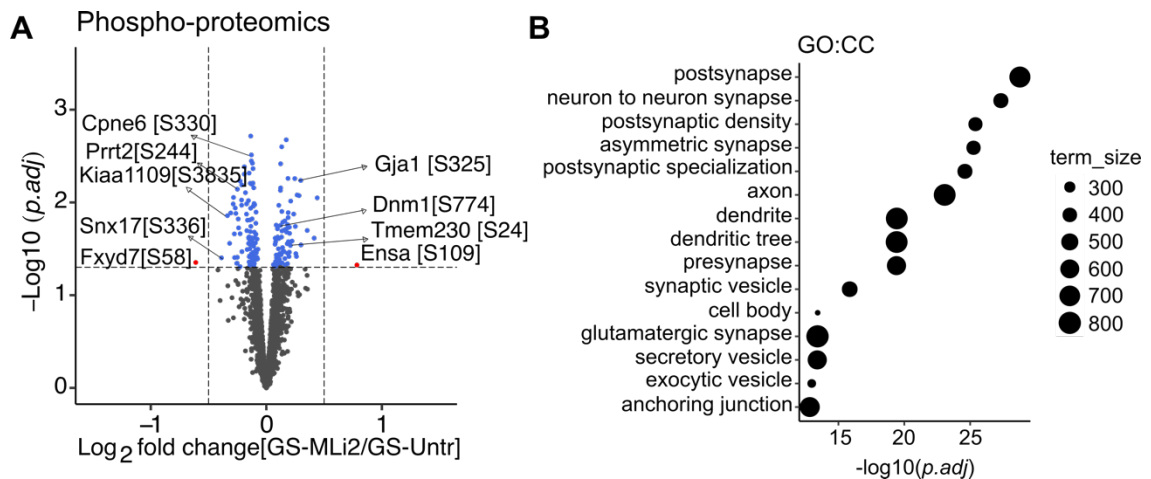
Figure 5.3. **Phospho-proteomics of whole brain homogenates.** Volcano plot showing the differential pattern of phospho-peptide hits between MLi-2-treated vs untreated G2019S KI brains (**A**). The bubble plot showed enrichment terms within these hits using the Gene Ontology cellular component database (**B**). The -log10 cutoff used for the bubble plot was <1e-10 and term size cutoff was <1000. Volcano plot key: grey = non-significant, blue = < 0.05 *p*-value, red = < 0.05 *p*-value and >1.4x fold change.

5.2.2 Kidney total and phospho-proteomic analyses from MLi-2 treated G2019S KI mice

In kidney tissue, 2,455 total proteins were detected after filtration and merged runs, of which 115 were differentially expressed between chronic MLi-2-treated and untreated G2019S KI mice (FDR adjusted $p < 0.05$ and fold change (FC) > 1.4) (Figure 5.4A). Among the differentially abundant proteins, there was an enrichment for endolysosomal, trafficking and mitochondrial proteins (Figure 5.4C). Multiple lysosomal proteins showed significant increases, including in Ctsb, legumain (Lgmn), Glb1, Lysosomal-associated membrane protein 1 (Lamp1), and N-acetylglucosamine-6-sulfatase (Gns). In addition, a number of proteins involved in vesicular trafficking, lipid metabolism, iron uptake and mitochondrial function were also significantly altered in kidneys of MLi-2 treated animals such as Intersectin 1 and 2 (Itsn1 and Itsn2), sorting nexins 5, 9, and 12 (Snx5, Snx9, and Snx12), Cycs, and mitochondrial serine/threonine protein phosphatase 5 (Pgam5) (Figure 5.4A). Interestingly, most of these proteins were not found to be significantly changed when comparing untreated G2019S KI and wildtype animals (Figure 5.4B). This suggests that these expression alterations are the result of LRRK2 inhibition itself and are distinct from changes driven by a hyperactive LRRK2 kinase.

Figure 5.4. **Total kidney proteomics.** Volcano plots illustrate differential expression of proteins between MLi-2 treated and untreated G2019S KI mice (**A**) and between untreated G2019S KI and wildtype mice (**B**). A bubble plot shows enrichment of cellular compartments found using the Gene Ontology cellular component database (GO:CC) (**C**). The -log10 cutoff used for the bubble plot was <1e-3 and term size cutoff was <1000. Volcano plot key: grey = non-significant, blue = < 0.05 p-value, green = >1.4x fold change, red = < 0.05 p-value and >1.4x fold change.

In addition, hierarchical clustering of differential proteins in the G2019S MLi-2-treated group showed most similarity to the LRRK2 KO animals (Figure 5.5), suggesting that chronic inhibition of LRRK2 may mimic features of an absence of LRRK2 in the periphery.
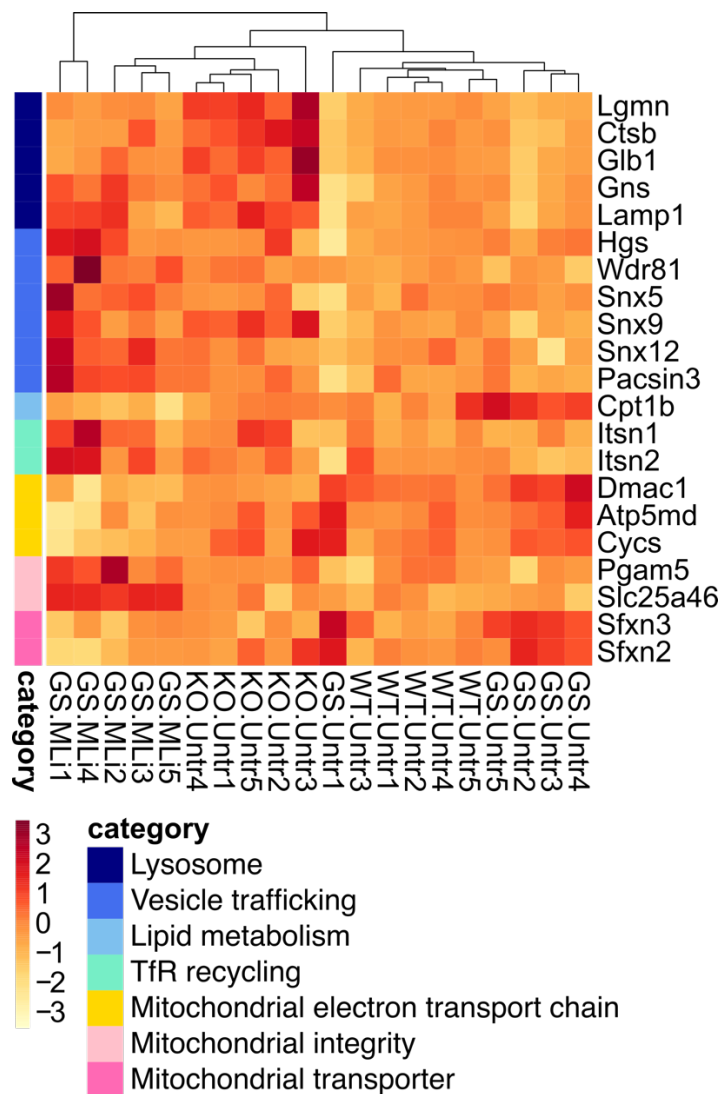
Figure 5.5. **Heatmap of total kidney proteins.** A heatmap with unsupervised hierarchical clustering of selected significant hits across the WT, G2019S KI and LRRK2 KO vehicle cohorts as well as the G2019S KI chronic MLi-2 cohort, highlighting proteins involved in lysosomes, vesicle trafficking, lipid metabolism, transferrin recycling and mitochondrial homeostasis. Z score is used for scaling.

In the phospho-proteomic analysis, 1,099 phospho-peptides were identified after filtering, limiting to proteins that were also identified in the total proteomics dataset. Thirty-four phospho-peptides were significantly altered between MLi-2-treated and untreated G2019S KI mice (FDR adjusted p-value <0.05 and FC >1.4x) (Figure 5.6A). Among these, several trafficking and mitochondrial proteins were identified, including sorting nexin 1 (pS188 Snx1) and vacuolar sorting protein 4b (pS102 Vps4b) (Figure 5.6A, C). In addition, enrichment analysis using the Gene Ontology cell component database revealed an enrichment of the endolysosomal system as well as mitochondrial membrane, reflecting that similar pathways are affected between total proteins and phospho-peptide hits in kidney tissue (Figure 5.6B). Using unsupervised hierarchical clustering of all four mouse groups, MLi-2-treated G2019S KI mice clustered with one another compared to untreated animals which clustered together irrespective of genotype (Figure 5.6C). These results further demonstrate that chronic inhibition of LRRK2 contributes to protein and phospho-protein differences in kidney tissue.
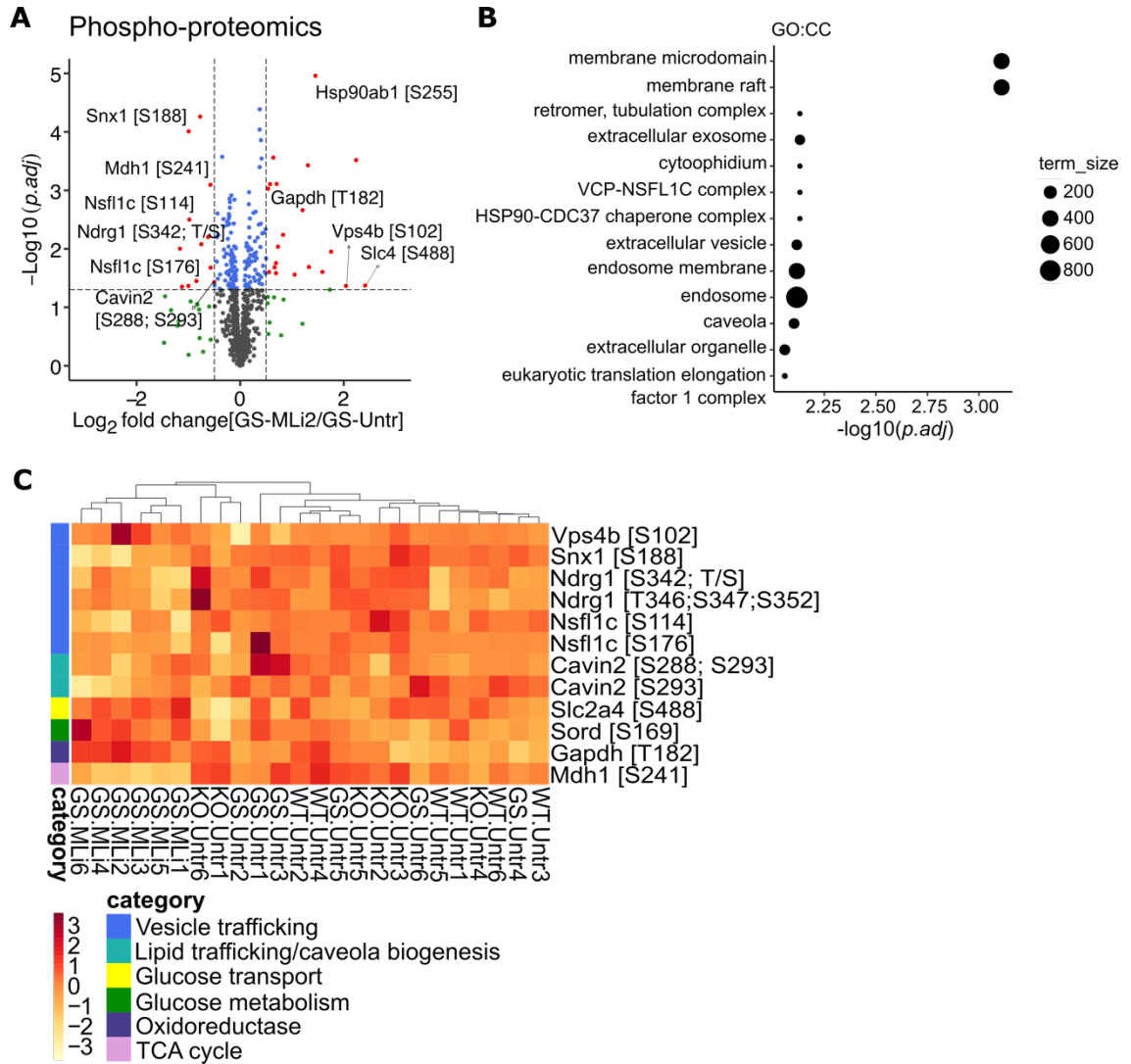
Figure 5.6. **Phospho-proteomics of kidney tissue.** Volcano plots illustrate differential expression of phospho-proteins between MLi-2 treated and untreated G2019S KI mice (**A**). GO:CC enrichment analysis is visualized via bubble plot (**B**). The -log10 cutoff used for the bubble plot was <1e-1 and term size cutoff was <1000. A heatmap with unsupervised hierarchical clustering of selected significant hits across the WT, G2019S KI and LRRK2 KO vehicle cohorts as well as the G2019S KI chronic MLi-2 cohort, highlighting proteins involved vesicle trafficking, lipid metabolism, glucose regulation, and mitochondrial homeostasis (**C**). Z score is used for scaling. Volcano plot key: grey = non-significant, blue = < 0.05 p-value, green = >1.4x fold change, red = < 0.05 p-value and >1.4x fold change.

5.2.3 Lung total and phospho-proteomic analyses from MLi-2

treated G2019S KI mice

In the lung proteomics, 2,702 total proteins were identified after filtering

and merging of consecutive LC-MS/MS runs, 6 proteins were differentially

expressed in MLi-2-treated compared to untreated G2019S KI mice (Figure

5.7A). Among these were the drug metabolism proteins Cyp1a1/Cyp1a2,

Transcription Elongation Factor A1 (Tcea1), angiogenesis protein Tymosin

beta-4x (Tmsb4x) (Figure 5.7A). No differences in total protein expression

changes were observed between untreated G2019S KI and wildtype animals

(Figure 5.7B). In addition, a total of 911 phospho-proteins were recovered, of

which 11 were considered significantly different between MLi-2-treated

G2019S KI mice and their untreated counterpart (Figure 5.7C). Since so few

hits were found for both total and phospho-proteins, enrichment analyses were
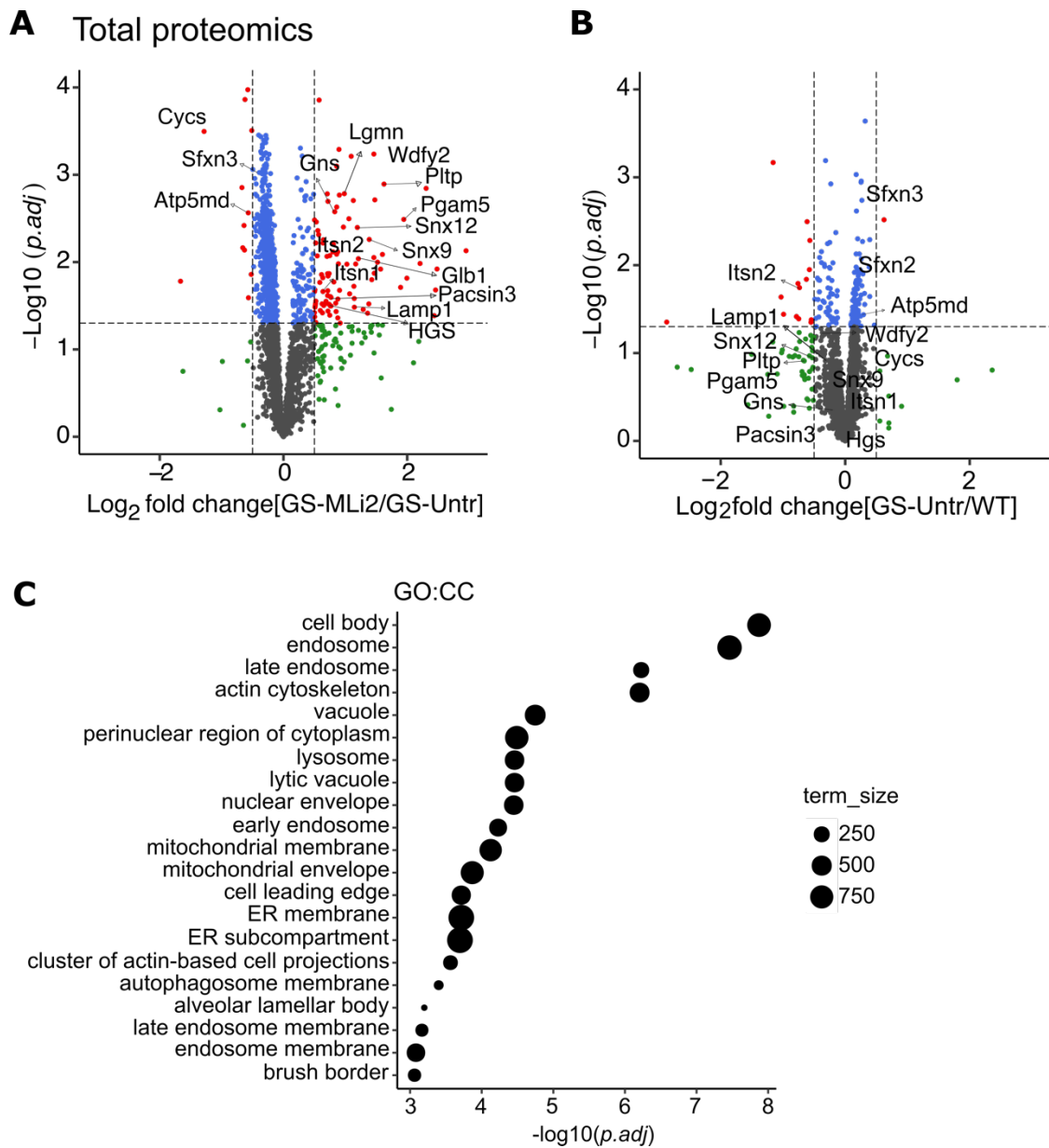
not performed.
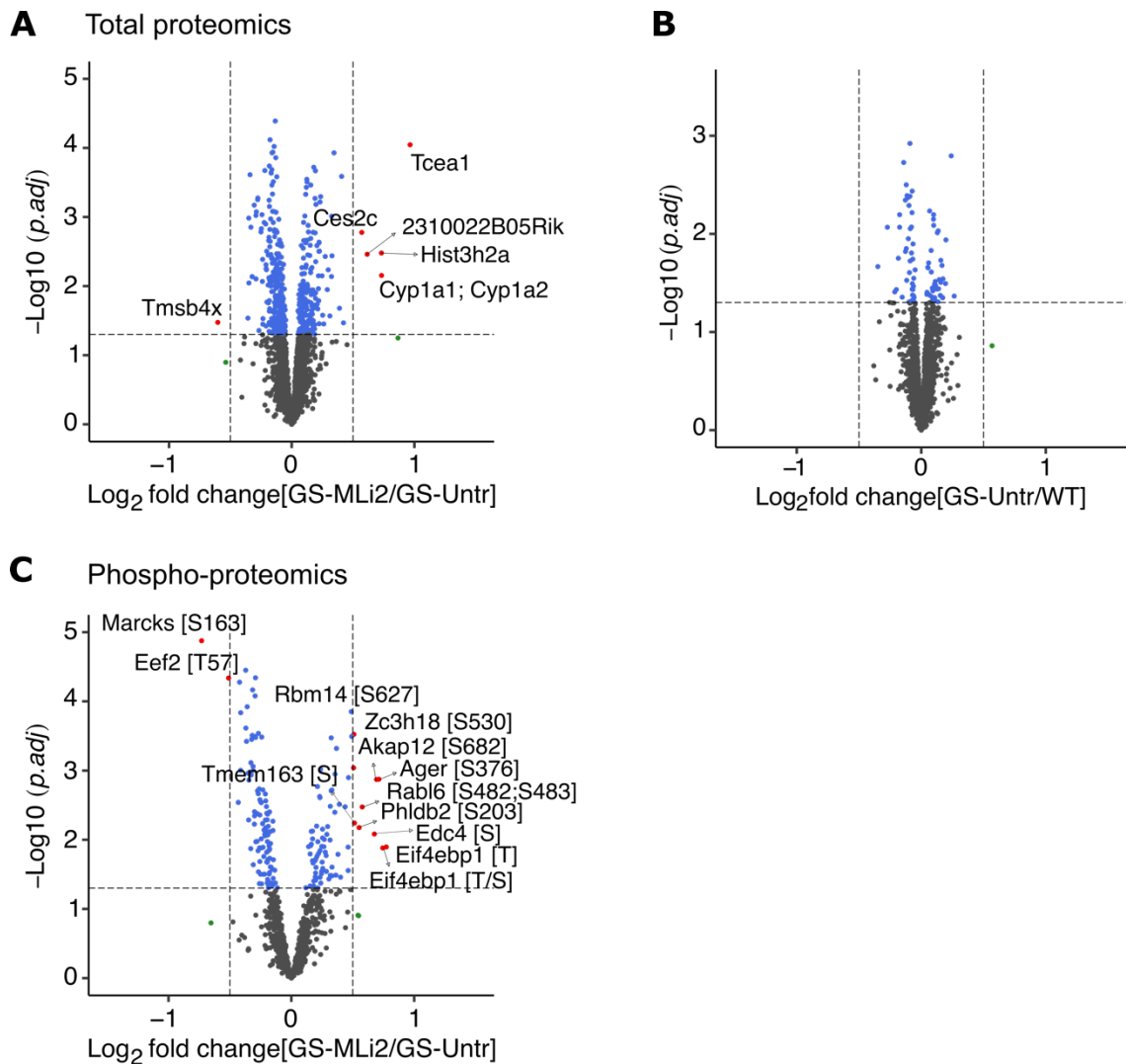
Figure 5.7. **Lung total and phospho- proteomics.** Volcano plots illustrate differential expression of total proteins between MLi-2 treated and untreated G2019S KI mice (**A**) and between untreated G2019S KI and wildtype mice (**B**), and phospho-proteins between MLi-2 treated and untreated G2019S KI mice (**C**). Volcano plot key: grey = non-significant, blue = < 0.05 p-value, green = >1.4x fold change, red = < 0.05 p-value and >1.4x fold change.

5.2.4 Validation of proteomic hits across brain, kidney, and lung tissues

Proteomic analyses in brain, kidney, and lung tissue revealed several significant differences in protein expression and phosphorylation between

G2019S KI mice given MLi-2 customized chow for 10 weeks and their untreated counterparts. To validate these data, Western blots were run and probed for hits where a commercial antibody was available. As the kidney had the largest number of hits, I first started with this tissue. Non-glycosylated Lamp1, Hgs, and Sfxn3 were all significantly increased in G2019S KI mice compared to wildtype mice which was reversed following chronic MLi-2 treatment (Figure 5.8A-D). Additionally, glycosylated Lamp1 and Legumain were both significantly increased in the LRRK2 KO kidneys compared to wildtype, confirming the lysosomal dysregulation previously observed by Pellegrini et al. (Pellegrini et al., 2018) (Figure 5.8A, E-F). Interestingly, MLi-2-treated G2019S KI mice also had increased levels of these proteins, showing a pattern most similar to LRRK2 KO compared to other untreated genotypes (Figure 5.8A, E-F), suggesting that some effects of LRRK2 inhibition mimic LRRK2 KO in kidneys.
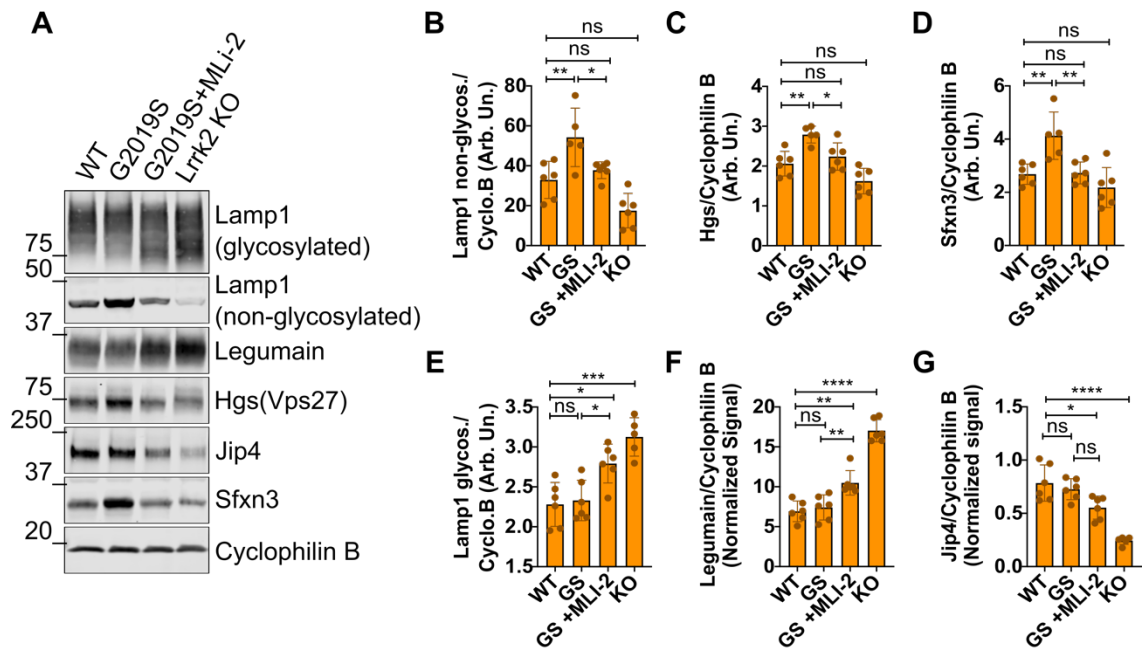
Figure 5.8. **Validation of significant hits in kidney tissue.** Western blots were performed on kidney samples from the 10-week treatment cohort to validate proteomic hits along with Cyclophilin B as the designated housekeeping protein (**A-G**). One-way ANOVAs with Tukey's post-hoc analyses were performed, *p-value <0.05, **p-value <0.01, ***p-value <0.001, ****p-value <0.0001. N=6; SD error bars are shown.

Recent data from our lab has indicated that LRRK2 recruits the scaffold adapter protein Jip4 to damaged lysosomes mediating vesicle sorting and tubulation through phosphorylation of Rab35 and Rab10 (Bonet-Ponce et al., 2020). I therefore tested whether Jip4 levels were altered in the context of chronic LRRK2 inhibition *in vivo*. Surprisingly, LRRK2 KO mice showed a significant decrease in Jip4 levels in kidney compared to wildtype, while the chronic MLi-2 cohort showed a decrease that was also significant compared to wildtype (Figure 5.8A, G). This suggests that in the absence of active LRRK2, Jip4 is downregulated in this tissue.

To determine whether the expression changes observed in the 10-week cohort were present at earlier timepoints, I performed Western blots for these six proteins in the 10-day cohort. Unlike the 10-week cohort, neither non-glycosylated Lamp1, Hgs, nor Sfxn3 showed any differences between MLi-2-treated and untreated G2019S KI kidneys (Figure 5.9A-D). In addition, glycosylated Lamp1 and Legumain were not increased in the G2019S KI mice treated with MLi-2, as observed after 10-weeks of treatment, suggesting these effects only occur after long-term LRRK2 inhibition (Figure 5.9A, E-F). Decreased levels of Jip4 were also not observed in these kidneys, though a significant decrease was still found in the LRRK2 KO samples (Figure 5.9A, G).
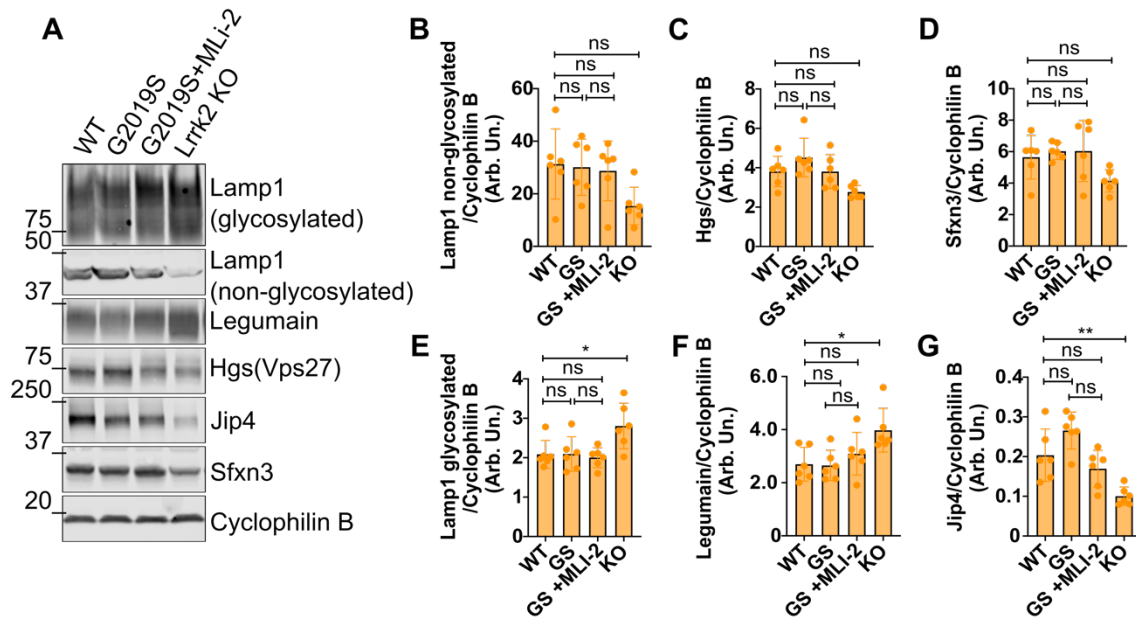
Figure 5.9. **Validation of significant hits in kidney tissue from the 10-day cohort.** Western blots were performed on kidney samples from the 10-day treatment cohort to determine short-term effects of LRRK2 inhibition on downstream hits identified in the proteomics experiments along with Cyclophilin B as the designated housekeeping protein (**A-G**). One-way ANOVAs with Tukey's post-hoc analyses were performed, *p-value <0.05, **p-value <0.01. N=6; SD error bars are shown.

Considering the mitochondrial hits that were found in the brains of the 10-week cohort, only Atp5mc1 and Cytochrome C had antibodies that were previously validated and commercially available. No changes were observed in these tissues via Western blot across any treatment nor genotype in the 10-week cohort (Figure 5.10A-C). Additionally, no differences were found among the six validated proteins from the kidney proteomics, suggesting that the brain is more resilient in terms of endolysosomal therapeutic effects and dysregulations that may be associated with LRRK2 inhibition (Figure 5.10A, D-H).
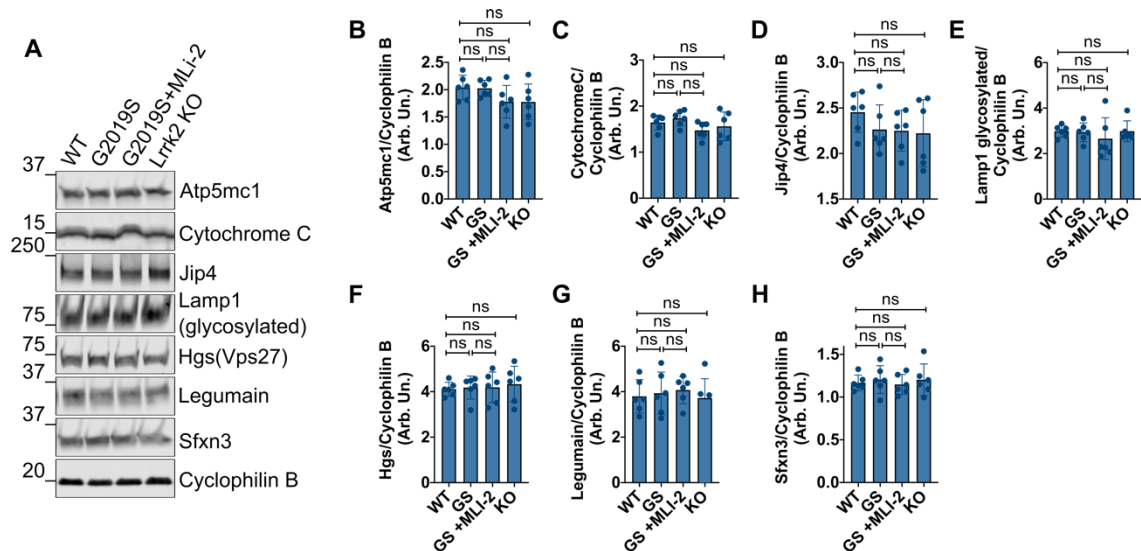
Figure 5.10. **Validation of proteomic hits in brain tissue.** Western blots were performed on brain samples from the 10-week treatment cohort to validate proteomic hits along with Cyclophilin B as the designated housekeeping protein (**A-G**). One-way ANOVAs with Tukey's post-hoc analyses were performed. N=6; SD error bars are shown.

Very few total and phospho-proteins were identified in lung tissue. Among these, Myristoylated alanine-rich C-kinase substrate (Marcks) was shown to be significantly dephosphorylated at S163 in MLi-2-treated compared to untreated G2019S KI animals (Figure 5.7C), which I was able to confirm via Western blot (Figure 5.11A-B). Phosphorylated S163 Marcks was also dephosphorylated in LRRK2 KO tissue, suggesting that this effect is due to a loss of LRRK2 kinase activity. Additionally, Cyp1a1 was validated in Western blot, with a significant increase found in MLi-2-treated animals compared to all untreated groups (Figure 5.11A, C). Kidney proteomic hits were not shown to be altered in lung tissue, confirming that these expression changes are kidney-specific (Figure 5.11A, D-G).
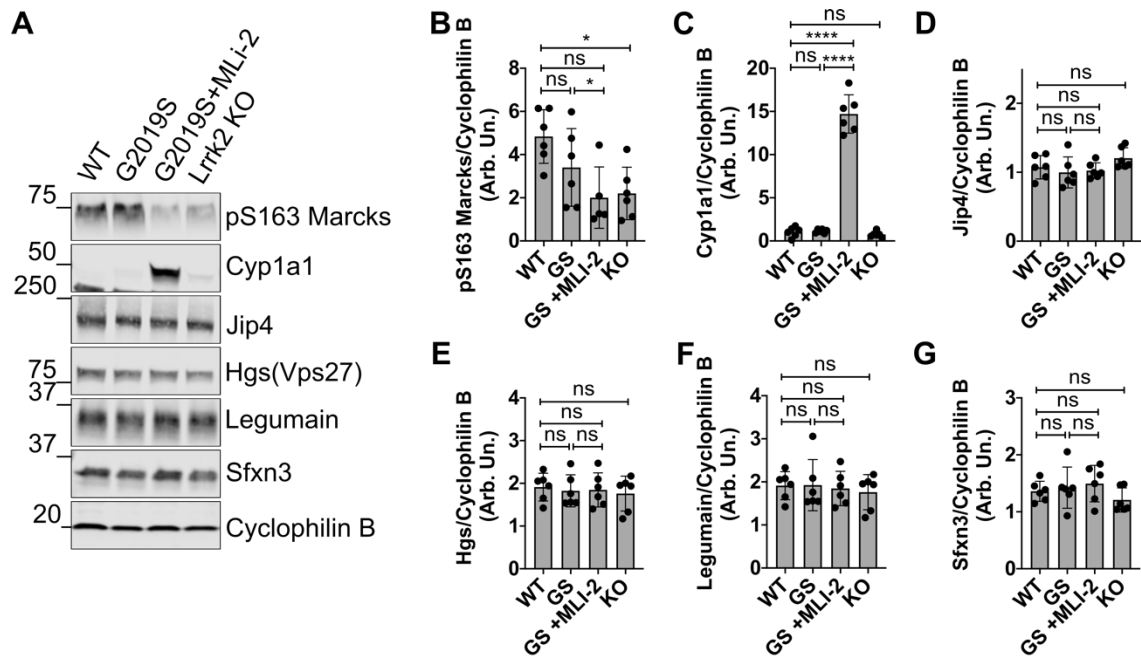
Figure 5.11. **Validation of proteomic hits in lung tissue.** Western blots were performed on lung samples from the 10-week treatment cohort to validate proteomic hits along with Cyclophilin B as the designated housekeeping protein (**A-G**). One-way ANOVAs with Tukey's post-hoc analyses were performed, *p-value <0.05, ****p-value <0.0001. N=6; SD error bars are shown.

5.3 Discussion

To investigate downstream effects of chronic LRRK2 kinase inhibition, unbiased quantitative total and phospho-proteomics analyses were conducted in the brains, kidneys, and lungs of the 10-week MLi-2 in-diet dosing cohort described in Chapter 4. This revealed significant differences in endolysosomal proteins in the kidneys of treated compared to untreated G2019S KI animals. A subset of these proteins, including Legumain and Glb1, have been identified previously by unbiased proteomics in kidney tissue of 9-month-old LRRK2 KO mice (Pellegrini et al., 2018). Of these proteins, we validated the accumulation

of Legumain in 10 weeks, but not 10 days, of MLi-2 treatment in G2019S KI

mice. Legumain, also known as asparaginyl endopeptidase (AEP), is a

lysosomal enzyme with a diverse function of roles reported. Interestingly,

Legumain translocation from the lysosome to the cytosol has been associated

with neurodegenerative states, and conformational changes have been shown

to stabilize the enzyme even in neutral pH (Dall and Brandstetter, 2016).

Recent studies have demonstrated that accumulation of cytosolic Legumain

correlated to significant dephosphorylation at T322 in AD human brains

(Basurto-Islas et al., 2013; Wang et al., 2019; S.-S. Wang et al., 2021). In

addition, a study has shown that Legumain can cleave APP, Tau, and α-

synuclein in an age-dependent manner in both mouse and human neuronal

cultures and brains and that depletion of Legumain can be restorative to

synaptic activity and cognitive function in the 5XFAD mouse model (Wang et

al., 2018). Thus, it would be worth investigating Legumain localization and

phosphorylation in models where LRRK2 kinase is inhibited.

Additionally, data from our previous study investigating the role of

LRRK2 at the lysosomal membrane identified that LRRK2-mediated pT73

Rab10 can recruit Jip4 to the membrane of damaged lysosomes, which then

initiates lysosomal tubulation in primary astrocytes (Bonet-Ponce et al., 2020).

In the present study, LRRK2 KO animals had significantly less Jip4 protein in

kidneys compared to wildtype animals, and prolonged LRRK2 inhibition led to a significant loss of total Jip4 protein in G2019S KI mice. These data suggest that lysosomal dysfunction observed in the context of LRRK2 deficiency can also be recapitulated with long-term chronic MLi-2 treatment *in vivo*.

In both brain and kidney tissues, upregulation of sorting nexin proteins (Snx5, Snx9, and Snx12), as well as dephosphorylation of S488 Snx1 and S336 Snx17 were identified. Snx1 and Snx5 make up part of the Snx-BAR-retromer pentamer complex that is associated with recycling manose-6-phosphate receptor (M6PR) and other receptors back to the TGN from endosomes (Cullen and Korswagen, 2011; Cunningham and Moore, 2020). Additionally, S188 Snx1 phosphorylation has been reported to disrupt membrane binding and restrict Snx1 to the cytosol (Lenoir et al., 2018). VPS35 is a necessary component of the retromer complex, and mutations in this protein cause an autosomal dominant form of PD (Zimprich et al., 2011). Recently, a study showed that the D620N VPS35 mutation enhanced LRRK2-mediated Rab phosphorylation *in vitro* (Mir et al., 2018). Taken together, these data suggest that LRRK2 mediates effects on retrograde trafficking to the TGN that can lead to pathology. However, the precise mechanism(s) at play, and their relationship to more general endolysosomal damage, is unclear and worthy of future inquiry.

In brain tissue, chronic MLi-2 treatment in G2019S KI mice showed a modest but significant upregulation of mitochondrial proteins compared to their untreated counterparts. PD-causing mutations in PINK1, Parkin, and DJ1 have established mitochondrial pathway dysfunction in disease pathogenesis (Bose and Beal, 2016). Production of ROS, mitochondrial elongation, decreased ATP production and mitochondrial DNA damage have been reported in G2019S-PD patient-derived skin biopsies and G2019S-LRRK2 *in vitro* models (Mortiboys et al., 2010; Mamais et al., 2014; Pereira et al., 2014; Sanders et al., 2014; Howlett et al., 2017). In brain tissue, most mitochondrial proteins found in our screens were associated with the respiratory chain Complex I and Complex III, namely, Ndufa2, Nufs3, Ndufv3, Cytochrome C, Uqcrc2, and Uqcrc1. Mutations in PD-genes PINK1 and VPS35 have been reported to cause dysregulation of the respiratory chain system, strengthening the case for mitochondrial dysfunction being a causal factor in PD pathogenesis (Grünewald et al., 2019). Further studies are needed to elucidate the effects of LRRK2 on the respiratory chain system.

In the current study, any effects of chronic LRRK2 kinase inhibition in G2019S KI mice could be interpreted as a) reversal of a KI phenotype, or b) novel pathway dysfunction resulting from loss of active LRRK2. Proteomic analysis of the untreated G2019S KI and wildtype mice revealed a number of

proteins involved in iron transport. The transmembrane ion transporters Sfxn2 and Sfxn3, showed modest upregulation in kidneys of G2019S KI compared to wildtype mice and this was reversed by MLi-2 treatment. Interestingly, the increase in Sfxn3 in untreated G2019S KI animals was validated via Western blot in the 10-week cohort but was not observed in the 10-day group. The difference here may be that the 10-day cohort was collected at 3 months old, whereas the endpoint of the 10-week cohort was almost doubled to 5.5 months old. Thus, the increase in expression of these proteins may be age dependent in G2019S KI mice, although more investigation will need to be done in order to confirm this. Of the mitochondrial proteins identified in the brain proteomics screen, Cytochrome C, Vdac1, Ndufs3, and Ndufv2 were downregulated in untreated G2019S KI brain compared to wildtype and this was reversed in the chronic MLi-2 G2019S KI cohort. These results suggest that alterations in G2019S KI mice may be corrected with LRRK2 inhibition.

Moreover, it was noted that after 10 weeks of MLi-2 in-diet dosing, S1292 LRRK2 and S106 Rab12 phosphorylation were significantly lower than wildtype levels in lung. It is possible that lung tissue is more sensitive to LRRK2 inhibition than other tissues considered here as it has been suggested in a recent study investigating the toxicological and morphological effects of LRRK2 inhibition on nonhuman primate lung, although no pulmonary deficits

were observed (Baptista et al., 2020). The present data supports this, as proteomics analyses showed very little changes in response to chronic LRRK2 inhibition in lung. Further exploration will be necessary to determine whether there is a lung-specific LRRK2-dependent mechanism that is affected by chronic LRRK2 inhibition.

Overall, these proteomic data reveal that chronic LRRK2 inhibition may lead to both dysfunction as well as reversal of kinase hyperactivity within the endolysosomal system over time in the kidneys of G2019S KI mice. Based on the relatively modest protein changes in the brain, the brain may be more resilient to LRRK2 inhibition than peripheral tissues. This further implies that LRRK2 inhibition would be safe for chronic use in PD patients, but careful monitoring of peripheral tissues and dosage may be necessary and the potential effects on mitochondrial function should further be considered.

What remains to be shown is whether any of these molecular effects are translatable to humans. For example, studies have shown that people with LRRK2 haploinsufficiency have reduced levels of total LRRK2 protein (Blauwendraat et al., 2018; Whiffin et al., 2020), however, there have been conflicting reports on whether reduced levels are associated with phenotypes or disease states in these individuals (Blauwendraat et al., 2018), with one

claiming an increased risk for lung adenocarcinoma (Lebovitz et al., 2021). A key caveat is that chronic LRRK2 inhibition is not the same as LOF variants. In the former, the body must alter its normal mechanisms to account for reduced LRRK2 kinase activity, whereas the latter already developed mechanisms to cope with lower LRRK2 levels *in utero*. Lower LRRK2 protein levels may also not produce the same effects as lower kinase activity. In addition, kinase inhibition presumably has the majority of its effect on the kinase domain, whereas LOF would reduce all aspects of LRRK2 function. Thus, it will be imperative to monitor the effects of LRRK2 kinase inhibitors as it relates to normal protein function.

6 LRRK2 KINASE ACTIVITY AND LOCALIZATION OF pRAB10 AND pRAB12 AT ENDOLYSOSOMAL MEMBRANES

6.1 Introduction

The data presented in chapters 3 and 4 illustrated that LRRK2-dependent phosphorylation of Rab10 and Rab12 differed in tissues of G2019S KI mice. Specifically, it was noted that phosphorylation of Rab10 was less responsive than Rab12 to kinase inhibition by MLi-2 in the brain. Additionally, Rab10 phosphorylation was not increased by the G2019S mutation *in vivo*, consistent with some previous reports, whereas Rab12 phosphorylation did respond to the mutation in the same animals. These observations are difficult to reconcile with the proposal that G2019S increases Vmax by ~2 fold and that both Rab10 and Rab12 are direct substrates of LRRK2. It is likely, therefore, that there are additional mechanisms which regulate Rab phosphorylation, and these may be particularly active in the brain.

As previously mentioned, Rab GTPases function as regulatory switches in trafficking pathways along various intracellular membranes (Stenmark, 2009). Briefly, GDP dissociation inhibitors (GDI) bind to prenylated Rabs while in the

cytosol and delivers them to membranes (Pfeffer, 2013). The regulation of the

delivery of Rabs to a specific membrane is thought to be controlled by

membrane-specific resident GDI displacement factors (GDFs) as well as the

hypervariable C-terminals of different Rabs (Pfeffer, 2013; Sivars et al., 2003).

Once at the membrane, GDP is exchanged for GTP via guanine nucleotide

exchange factors (GEFs), causing a conformational change that allows Rabs to

recruit various effector proteins that initiate trafficking events (Stenmark, 2009;

Pfeffer, 2013). Rabs are then inactivated by swapping GTP for GDP via GTPase

activated proteins (GAPs) where it can be extracted from the membrane by

GDI and recycled back to the cytosol (Figure 6.1A).

Through immunoprecipitation assays, LRRK2-dependent

phosphorylation of T73 Rab10 and S106 Rab12 was shown to interfere with the

Rab-GDI interaction *in vitro* (Steger et al., 2016). GDI binds to the switch II

domain of Rabs where these phosphorylation residues are located, suggesting

that LRRK2 functions in the stabilization of Rabs onto target membranes by

preventing GDI from extracting Rabs too soon. Interestingly, this interference

positively correlated with increasing phosphorylation at these residues when

overexpressing various pathogenic mutations of LRRK2 (Steger et al., 2016),

thus suggesting that LRRK2 kinase hyperactivity has the potential to affect the

balance of this pathway at various membranes by blocking the recycling of

Rabs back to the cytosol (Figure 6.1B). Additionally, one study found that

LRRK2-mediated Rab phosphorylation requires nucleotide binding on Rabs,

possibly favoring GTP-bound states (Liu et al., 2018).
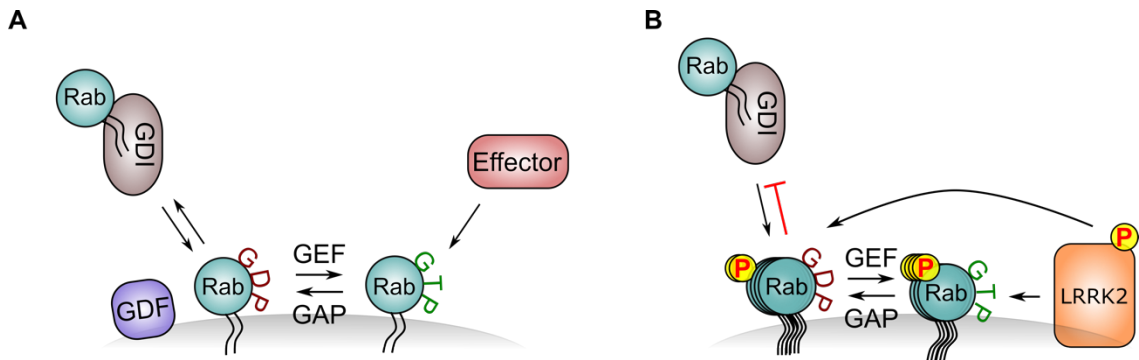
Figure 6.1. **Rab GTPase cycling and recycling.** Prenylated GDP-bound Rabs bind to GDI in the cytosol to be translocated to membranes where GEFs mediate GTP-binding. Effectors carryout downstream trafficking once recruited to the membrane via active GTP-bound Rabs. GAPs inactivate Rabs by swapping GTP to GDP where GDIs can then extract the Rab and recycle it to the cytosol (**A**). The presence of hyperactive LRRK2 may shift the balance between membrane-bound Rabs and cytosolic Rabs (**B**).

Literature on Rab GTPases have categorized some Rabs as resident

proteins for specific membranes, such as Rab5 and Rab7 as early and late

endosomal proteins, respectively (Chavrier et al., 1990; Bucci et al., 1992; Feng

et al., 1995). Rab8a has been found to localize to recycling endosomes to

traffic proteins from the TGN to the plasma membrane (Ang et al., 2003; Rowe

et al., 2008) and centrosomes to promote ciliary formation through a LRRK2-

dependent mechanism (Yoshimura et al., 2007; Waschbüsch et al., 2020).

LRRK2-dependent phosphorylated Rab10 is also found to co-localize to

centrosomes (Dhekne et al., 2018) as well as distressed lysosomes (Eguchi et

al., 2018; Bonet-Ponce et al., 2020; Kuwahara et al., 2020). Fewer studies have investigated Rab12 localization, although it has been shown to play a role in trafficking proteins such as transferrin receptor from recycling endosomes to lysosomes (Matsui and Fukuda, 2011).

These data mapping Rab localization led to the hypothesis that LRRK2-dependent recruitment and subsequent phosphorylation of Rab substrates will also be dependent on which membrane LRRK2 is present at. Since the *in vivo* proteomics data presented in chapter 5 showed the largest differences within the endolysosomal pathway between chronic LRRK2 kinase inhibited and control G2019S KI groups in the kidneys of mice, six different membrane-targeting traps were designed to translocate LRRK2 to early, late, and recycling endosomes as well as Golgi, lysosomes, and the plasma membrane to investigate whether membrane identity influences Rab10 and Rab12 phosphorylation by LRRK2.

6.2 Results

6.2.1 Establishing tools to interrogate the influence of LRRK2 kinase activity on pRabs at various endolysosomal membranes *in vitro*

To evaluate LRRK2 activation patterns and its ability to phosphorylate downstream Rabs at membranes, the rapamycin-binding domain from the 12kDa FK506 binding protein (FKBP), was fused to the N-terminus of LRRK2, and the FKBP-rapamycin-binding (FRB) domain of mTOR was fused to six different membrane resident proteins. Thus, in the presence of rapamycin, the FKBP and FRB domains will form a heterodimer, translocating LRRK2 to a specific membrane (Figure 6.2) (Liberles et al., 1997; Robinson et al., 2010).
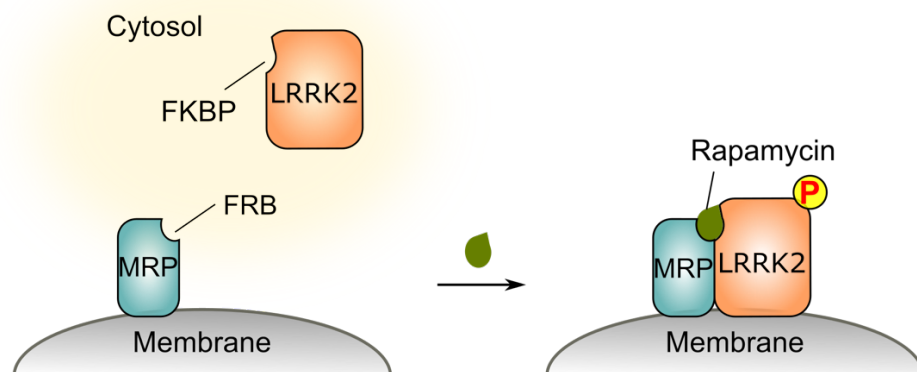
Figure 6.2. **FKBP-FRB rapamycin-binding schematic.** FKBP-LRRK2 and FRB-membrane resident protein (MRP) can form a heterodimer in the presence of rapamycin.

To investigate specific compartments within the endolysosomal pathway, the following membrane resident proteins were tagged with an FRB domain: Rab5 for early endosomes (EE-trap), Rab7 for late endosomes (LE-trap), LAMP1 for lysosomes (Lyso-trap), Giantin for Golgi (Golgi-trap), a plasma membrane-targeting sequence from GAP43 (MLCCMRRTKQVEKNDDQKI) (PM-trap), and EHD1 for recycling endosomes (RE-trap) (Figure 6.3).
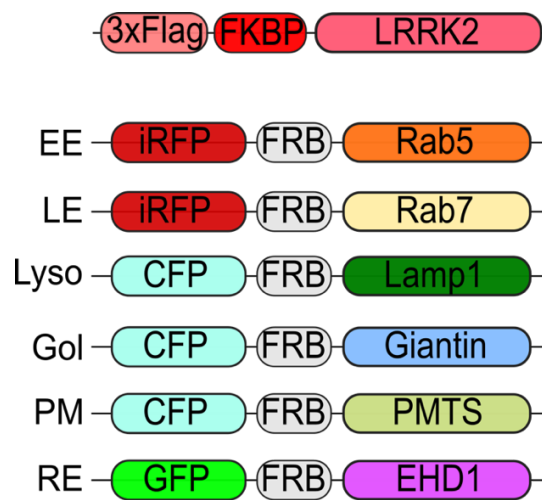
Figure 6.3. **cDNA structures of FKBP-LRRK2 and FRB-membrane traps.** All cDNA plasmids had a CMV promoter and a fluorescent tag or 3xFlag tag as indicated. Key: EE= early endosome, LE= late endosome, Lyso= lysosome, Gol= Golgi, PM= plasma membrane, RE= recycling endosome.

Live imaging of HEK293FT cells overexpressing FKBP-LRRK2 and RE-trap or Lyso-trap showed rapid colocalization of both proteins within seconds after addition of rapamycin at a final concentration of 200nM, demonstrating the utility of the FKBP-FRB system (Figure 6.4A-B). Additionally, OE of FKBP-LRRK2 translated a uniformly cytosolic protein before rapamycin treatment, as

expected, confirming that the FKBP domain did not impede translation of the

protein (Figure 6.4A-B).
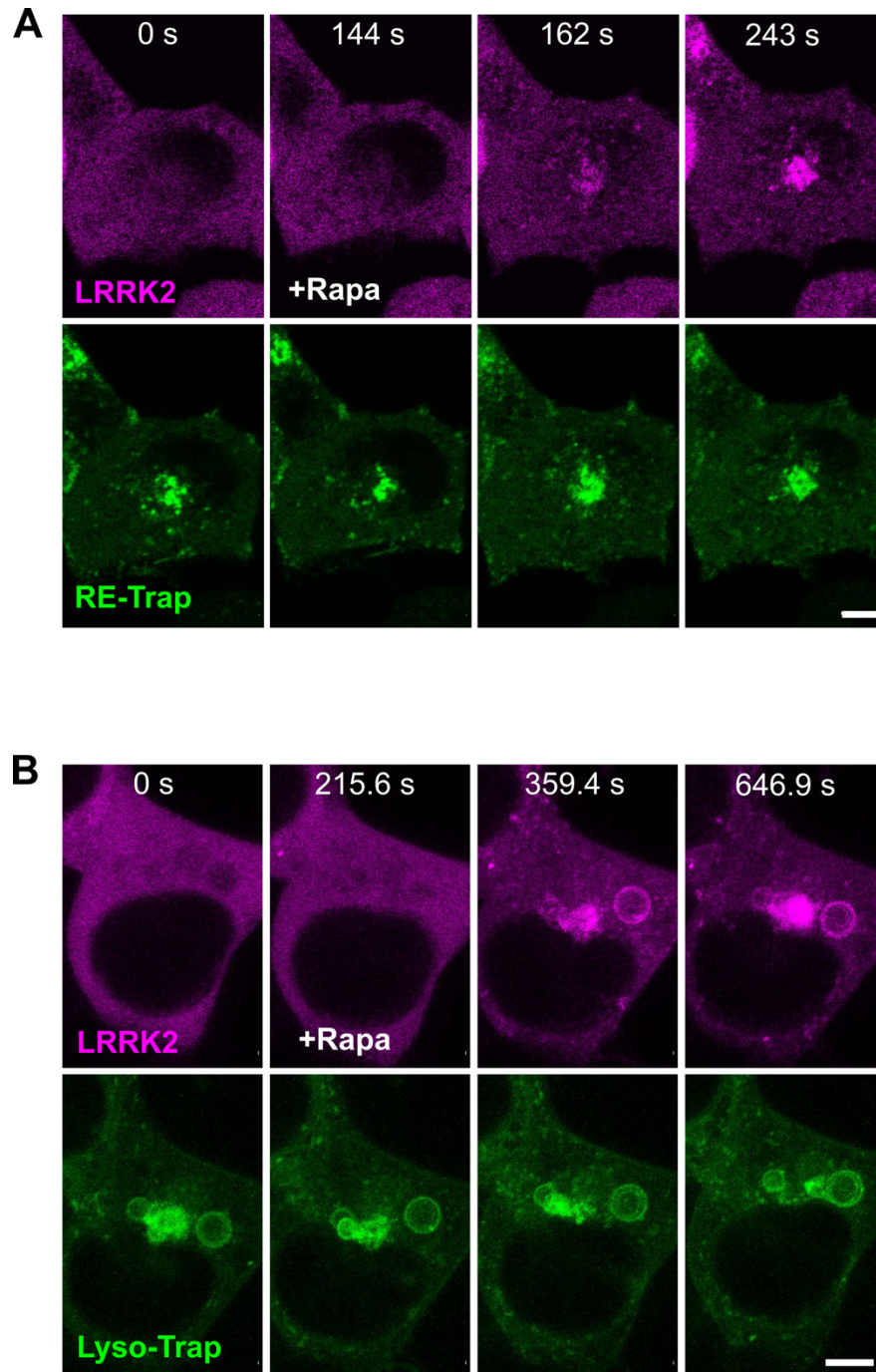
Figure 6.4. **Live imaging of RE-trap and Lyso-trap systems.** FKBP-LRRK2 (magenta) was overexpressed with either RE-trap (green) (**A**) or lyso-trap (green) (**B**) in HEK293FT cells. Time lapse was taken using an inverted confocal microscope at 9 seconds/ frame (video is played at 6 frames/ second). Scale bar= 10μm. Rapamycin was added to the media of cells at the time points indicated. Panels arranged by Dr. Luis Bonet-Ponce.

Since rapamycin can induce autophagy in some models (Lin et al., 2018), control experiments were done to ensure that 200nM rapamycin treatment for 15 minutes would not affect the health of the cells. To do this, cells were co-transfected with FKBP-LRRK2 and Golgi-trap. After 24 hours, cells were either treated with 200nM rapamycin or left untreated followed by a 15-minute incubation prior to lysis with 1% triton for Western blot analysis. Neither p62 nor LC3-II levels were altered in the rapamycin treated cells compared to untreated, suggesting that treatment with 200nM rapamycin for 15 minutes is not enough time to induce autophagy (Figure 6.5A-C).
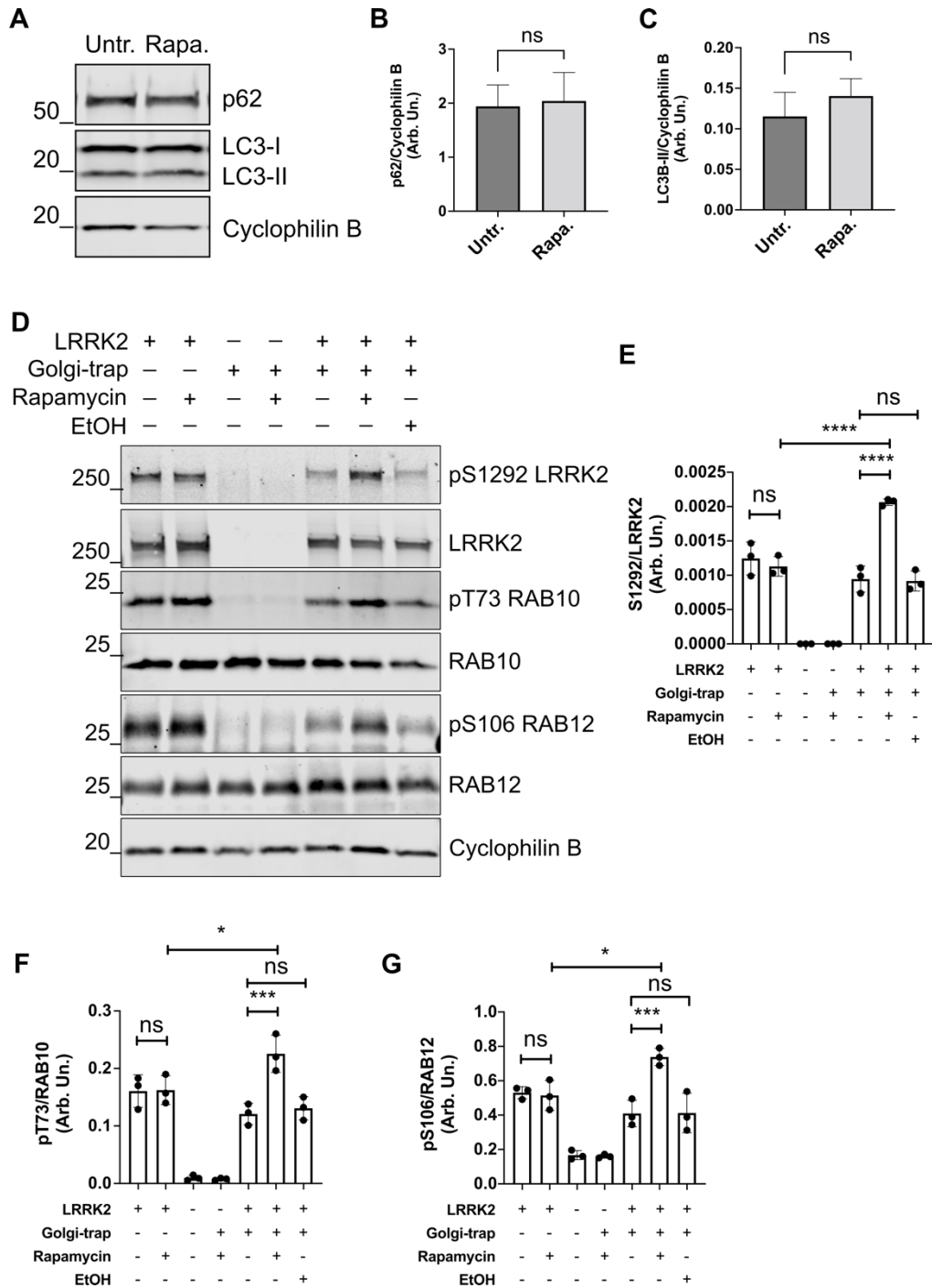
Figure 6.5. **Rapamycin control experiments.** For QC purposes, LRRK2 and the Golgi-trap were transfected 24 hours prior to treating cells with rapamycin for 15 minutes and autophagy markers p62 and LC3-II were probed via Western blot (**A**) and quantified (**B-C**). LRRK2 and the Golgi-trap were transfected together and separately in control, rapamycin, and ethanol (the rapamycin carrier solvent) -treated conditions (**D**). S1292 LRRK2, pT73 RAB10, and pS106 RAB12 were probed via Western blot and quantified (**D-G**). Unpaired, two-tailed student t tests were performed in B-C; One-way ANOVA with Tukey's multiple comparisons tests were performed in E-G, ****$p<0.0001$, ***$p<0.001$, **$p<0.01$, *$p<0.05$, $n = 3$; SD bars shown.

Moreover, to test whether rapamycin itself could activate LRRK2, a combination of conditions were tested in which cells were transfected with LRRK2 on its own or with the Golgi-trap and treated with rapamycin. Previous studies have shown that LRRK2 can be localized to the TGN via Rab29 OE where it is subsequently activated (Beilina et al., 2014; Purlyte et al., 2019), thus the Golgi-trap was chosen for these experiments to test LRRK2 activity. In cells expressing LRRK2 alone, S1292 LRRK2 autophosphorylation, pT73 Rab10, and pS106 Rab12 levels were not altered by rapamycin treatment compared to untreated cells (Figure 6.5D-G). This was also true when testing ethanol treatment alone, the solvent carrier of the rapamycin used. Phosphorylation in all three of these readouts were significantly increased when rapamycin was used on cells expressing both LRRK2 and Golgi-trap together (Figure 6.5D-G). These data demonstrate that rapamycin treatment itself does not activate LRRK2 kinase nor subsequent Rab substrate phosphorylation. Secondly, these data show that LRRK2 kinase activity is increased when at the Golgi membrane compared to a cytosolic localization.

To further evaluate whether the membrane is required for LRRK2 activation, cells were transfected with LRRK2 and an EGFP-FRB plasmid without any membrane resident protein such that, in the presence of

rapamycin, the FKBP-FRB complex is formed within the cytosol. In rapamycin treated cells, no significant differences in phosphorylation were observed compared to untreated cells, suggesting that membrane recruitment enhances LRRK2 kinase activity rather than the FKBP-FRB heterodimer formation itself (Figure 6.6A-D).
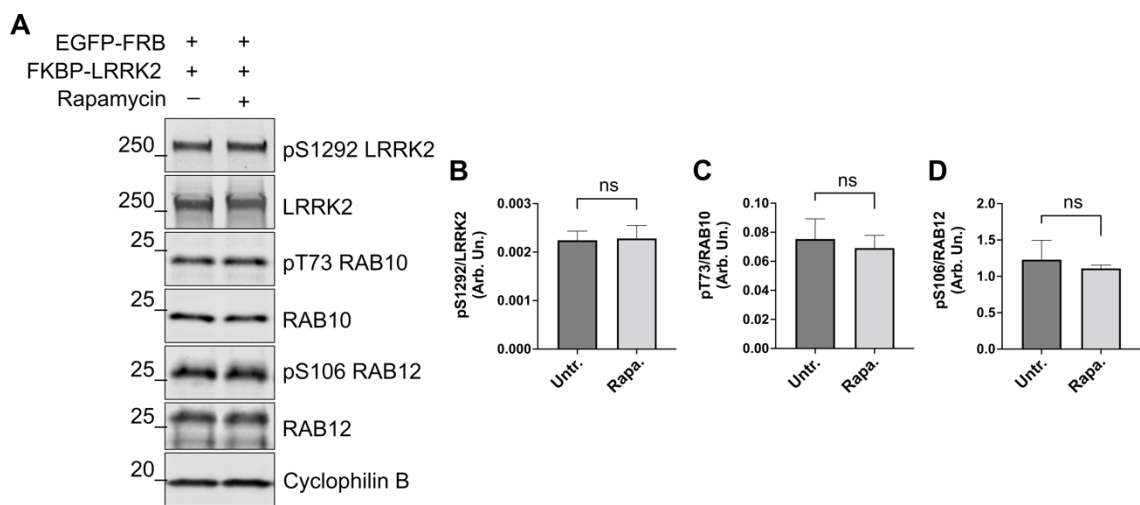
Figure 6.6. **FRB control experiment.** HEK293FT cells were transfected with FKBP-LRRK2 and EGFP-FRB plasmids. Conditions with and without rapamycin treatment were analyzed via Western blot (**A**) and pS1292 LRRK2, pT73 Rab10, and pS106 Rab12 levels were measured (**B-D**). n=3 replicates; SD error bars are shown.

6.2.2 LRRK2 activation at endolysosomal membranes

After performing the above control experiments, LRRK2 was transfected with each of the six membrane-targeting traps in HEK293FT cells and treated with or without rapamycin. Both immunocytochemistry and Western blots were done in parallel in order to visualize LRRK2 and trap localization as well as measure LRRK2 kinase activity via pS1292, pRab10, and pRab12 readouts,

respectively. The following endogenous proteins were also stained to confirm

each trap localized to the correct membrane: LAMTOR4 for lysosomes, TGN46

for Golgi, EEA1 for early endosomes, LAMP1 for late endosomes, Rab8a for

recycling endosomes, and F-actin for the plasma membrane (Figure 6.7A, F,

Figure 6.8A, F, Figure 6.9A, F).
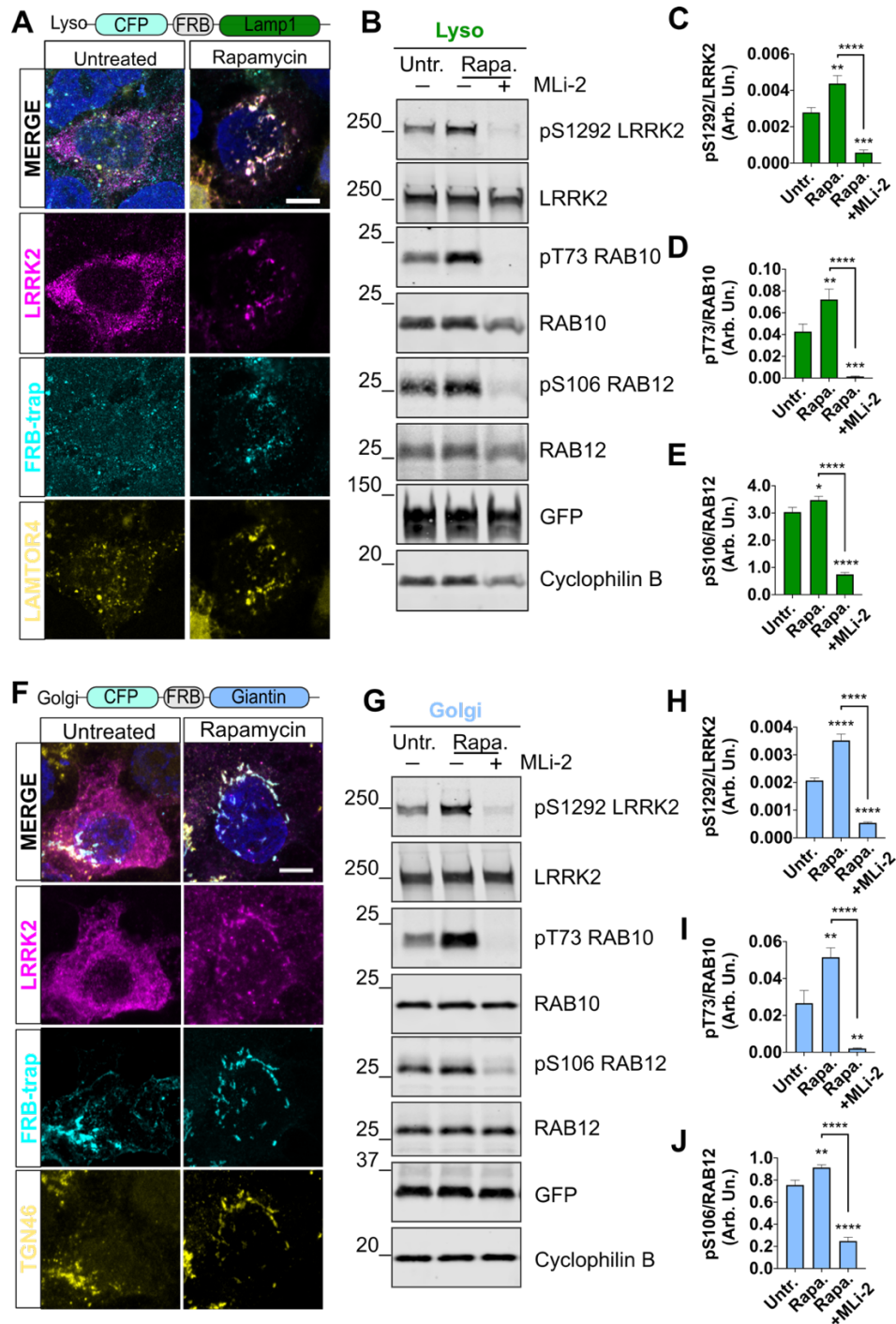
Figure 6.7. **Lyso- and Golgi- traps.** Cells were transfected with lysosome (**A-E**) or Golgi (**F-J**) traps (cyan) along with FKBP-tagged LRRK2 (magenta). All trap construct designs are illustrated above each ICC panel respectively. Endogenous markers for each targeted membrane are shown in yellow. Scale bar= 10μm. Untreated cells were used as negative controls while rapamycin treatment in the absence or presence of MLi-2 were used for recruitment and kinase inhibition of LRRK2 respectively. S1292 LRRK2, Rab10, and Rab12 phosphorylation are probed and measured via Western blot (**B-E**, **G-J**). One-way ANOVAs were performed where *p-value <0.05, **p-value <0.01, ***p-value <0.001, ****p-value <0.0001. n=3 replicates; SD error bars are shown.

All traps co-localized with the endogenous marker used and the addition of

rapamycin successfully relocalized LRRK2 to each membrane investigated

(Figure 6.7A, F, Figure 6.8A, F, Figure 6.9A, F). Surprisingly, when measuring

phosphorylation events at S1292, Rab10, and Rab12, all three readouts were

significantly increased at each membrane and these effects and were

significantly diminished with the addition of MLi-2 treatment (Figure 6.7B-E, G-

J, Figure 6.8B-E, G-J, Figure 6.9B-E, G-J). These data show that, first, LRRK2

kinase activity can be enhanced through proximity to any membrane along the

endolysosomal system and, second, that once activated, LRRK2 is able to

phosphorylate both Rab10 and Rab12 regardless of membrane specificity.
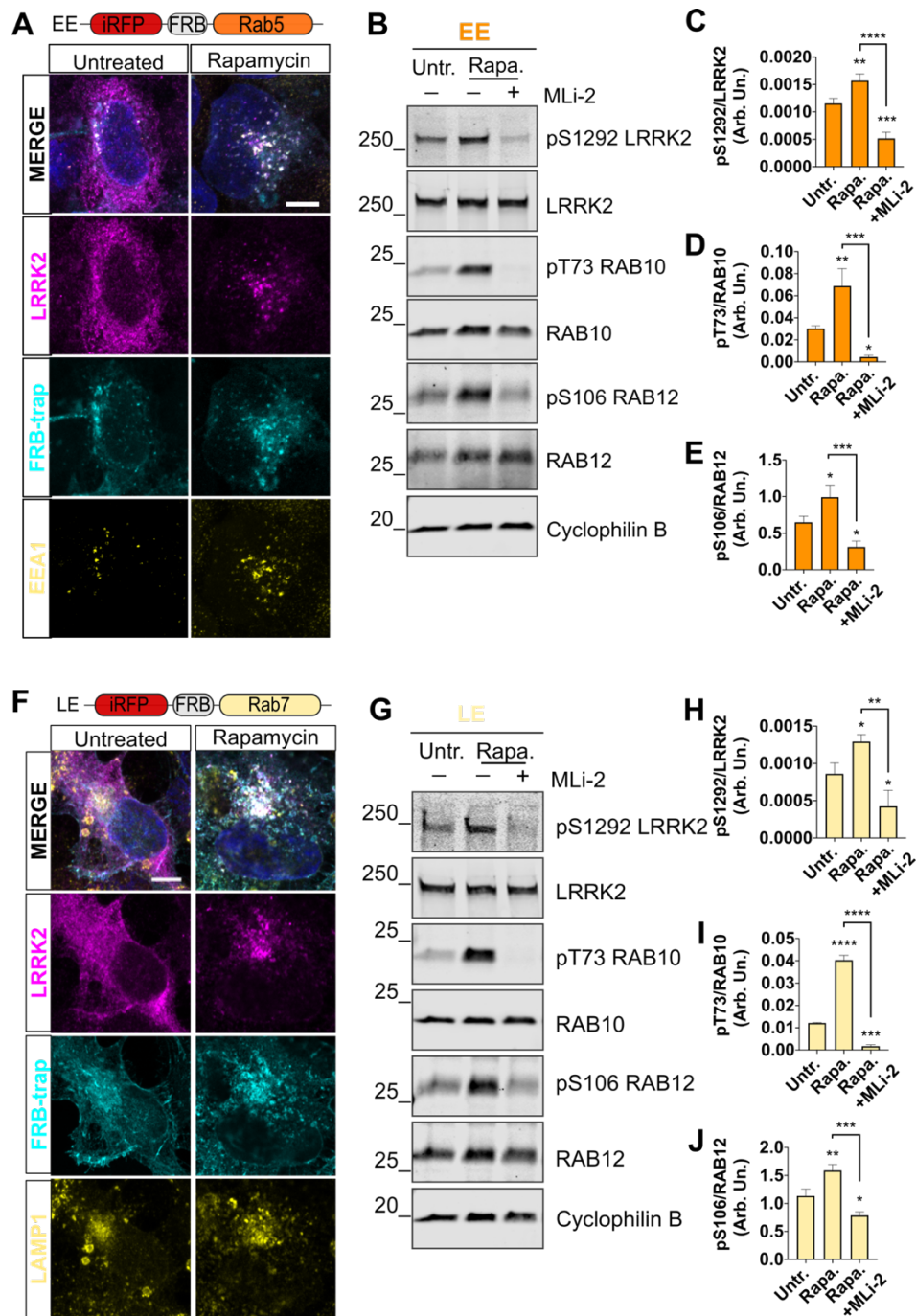
Figure 6.8. **EE- and LE- traps.** Cells were transfected with early endosome (**A-E**) or late endosome (**F-J**) traps (cyan) along with FKBP-tagged LRRK2 (magenta). All trap construct designs are illustrated above each ICC panel respectively. Endogenous markers for each targeted membrane are shown in yellow. Scale bar= 10μm. Untreated cells were used as negative controls while rapamycin treatment in the absence or presence of MLi-2 were used for recruitment and kinase inhibition of LRRK2 respectively. S1292 LRRK2, Rab10, and Rab12 phosphorylation are probed and measured via Western blot (**B-E**, **G-J**). One-way ANOVAs were performed where *p-value <0.05, **p-value <0.01, ***p-value <0.001, ****p-value <0.0001. n=3 replicates; SD error bars are shown.

Taken together, these results show that recruitment to the membrane enhances LRRK2 kinase activity and subsequent Rab phosphorylation within the endolysosomal pathway. Additionally, the reduction of these Rab phosphorylation levels after cells are treated with MLi-2 confirm that these events are LRRK2 dependent.
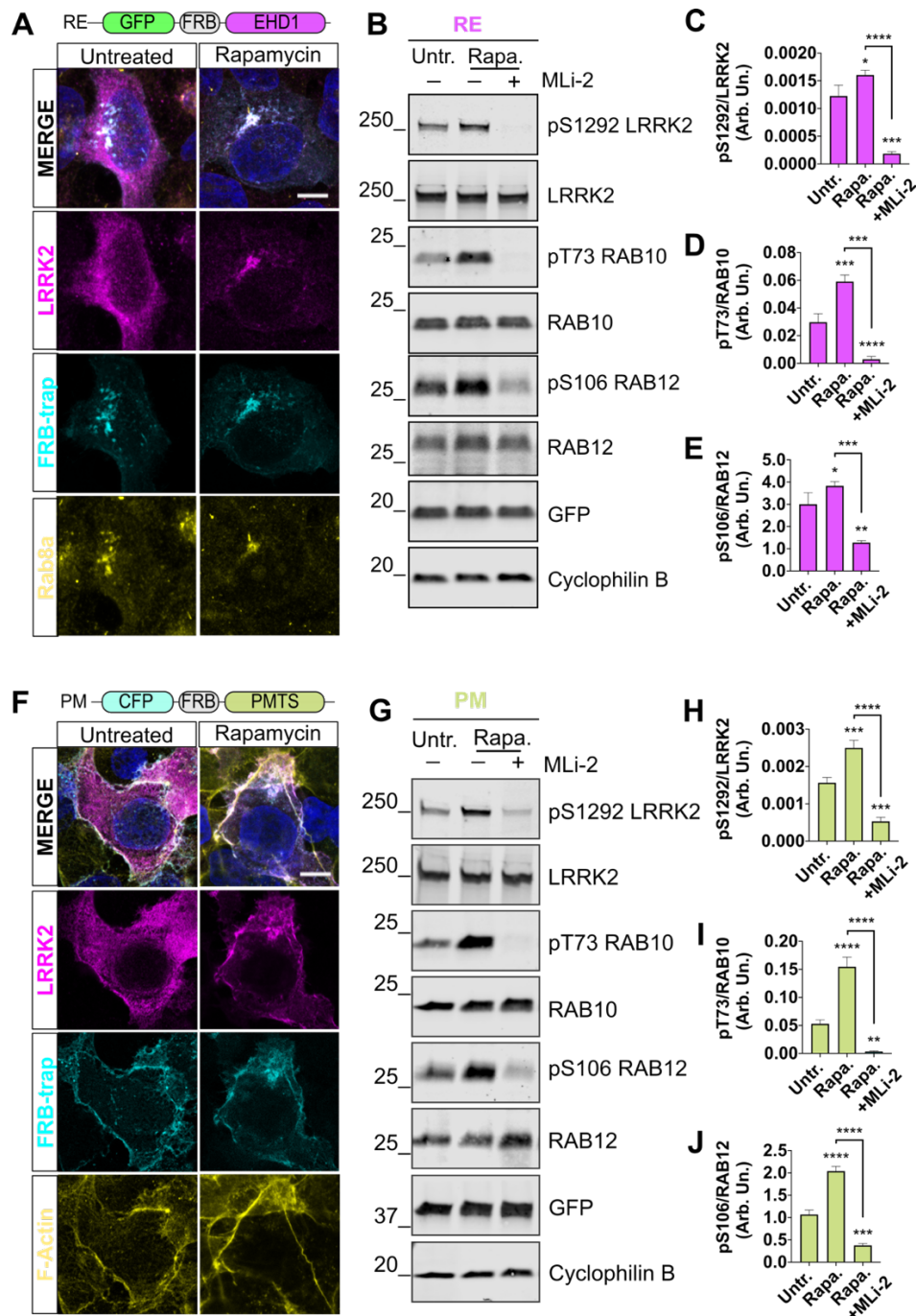
Figure 6.9. **RE- and PM- traps.** Cells were transfected with recycling endosome (**A-E**) or plasma membrane (**F-J**) traps (cyan) along with FKBP-tagged LRRK2 (magenta). All trap construct designs are illustrated above each ICC panel respectively. Endogenous markers for each targeted membrane are shown in yellow. Scale bar= 10µm. Untreated cells were used as negative controls while rapamycin treatment in the absence or presence of MLi-2 were used for recruitment and kinase inhibition of LRRK2 respectively. S1292 LRRK2, Rab10, and Rab12 phosphorylation are probed and measured via Western blot (**B-E**, **G-J**). One-way ANOVAs were performed where *p-value <0.05, **p-value <0.01, ***p-value <0.001, ****p-value <0.0001. n=3 replicates; SD error bars are shown.

6.2.3 Rab phosphorylation patterns in the context of pathogenic LRRK2

Since membrane specificity is unimportant for Rab phosphorylation by LRRK2, I next investigated the effect of pathogenic LRRK2 mutations R1441C, Y1669C, and G2019S on Rab10 and Rab12 phosphorylation when brought to a membrane using the FKBP-FRB system. To do this, mutant LRRK2 plasmids within pCR™8/GW/TOPO™ vectors were swapped into mScarlet-FKBP-pDEST plasmids using Gateway technology. A K1906M LRRK2 kinase-dead mutant was also included as a control for kinase-dependence on the phosphorylation sites under investigation. Each mutant was transfected into HEK293FT cells along with the lyso-trap plasmid and treated with rapamycin. Western blot analyses showed that the G2019S LRRK2 mutation increased S1292 LRRK2 autophosphorylation to a greater extent than R1441C and Y1669C, as expected (Figure 6.10A-B) (Kluss et al., 2018). For each pathogenic mutation, pS1292 LRRK2 significantly increased once LRRK2 was translocated to the lysosomal membrane with rapamycin treatment compared to untreated cells and MLi-2 treatment ablated this signal (Figure 6.10A-B). The K1906M LRRK2 mutant displayed no pS1292 signal.
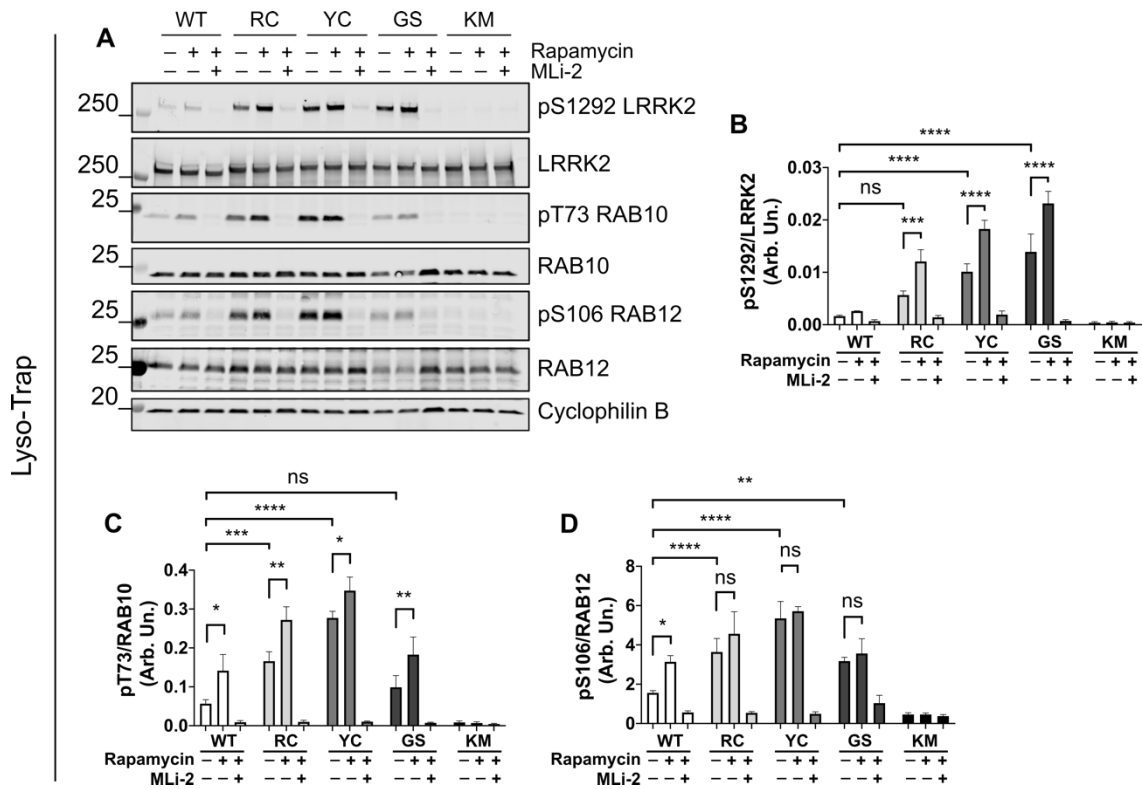
Figure 6.10. **LRRK2 pathogenic mutants at the lysosomal membrane.** The lyso-trap was co-transfected with either Wildtype, R1441C, Y1669C, G2019S, or K1906M LRRK2(-FKBP-mScarlet) varieties and Western blots were run, probing for pS1292 LRRK2, pT73 RAB10, and pS106 RAB12 (**A-D**). Two-way ANOVAs were performed in which *p-value <0.05, **p-value <0.01, ***p-value <0.001, ****p-value <0.0001. n=3 replicates; SD error bars are shown.

Rab10 and Rab12 phosphorylation patterns showed the largest increase in the presence of R1441C and Y1669C LRRK2 mutants at baseline, with minimal phosphorylation measured in K1906M LRRK2 expressing cells (Figure 6.10A, C-D). Once at the membrane, LRRK2 significantly increased Rab10 phosphorylation regardless of wildtype or mutant LRRK2 expression (Figure 6.10A, C). Interestingly, no significant increase in Rab12 phosphorylation at site S106 was observed in rapamycin treated cells compared to untreated cells for any of the pathogenic mutations, with an increase observed in only wildtype

expressing cells (Figure 6.10A, D). LRRK2 inhibition using MLi-2 treatment

significantly reduced pRab10 and pRab12 (Figure 6.10A, C-D).
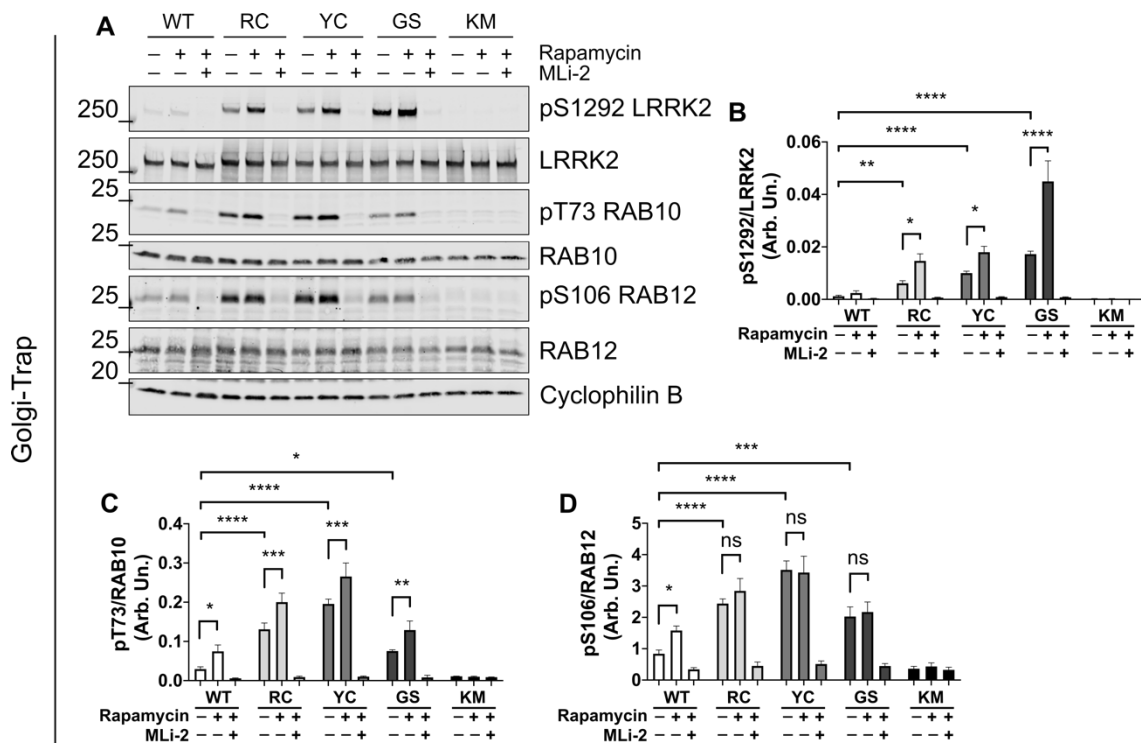
Figure 6.11. **LRRK2 pathogenic mutants at the Golgi membrane.** The Golgi-trap was co-transfected with either Wildtype, R1441C, Y1669C, G2019S, or K1906M LRRK2(-FKBP-mScarlet) varieties and Western blots were run, probing for pS1292 LRRK2, pT73 RAB10, and pS106 RAB12 (**A-D**). Two-way ANOVAs were performed in which *p-value <0.05, **p-value <0.01, ***p-value <0.001, ****p-value <0.0001. n=3 replicates; SD error bars are shown.

Using the Golgi-trap, the same patterns were observed for each

phosphorylation site as was seen in the lyso-trap (Figure 6.11A-D).

Interestingly, when comparing baseline phosphorylation between Rabs, Rab12

phosphorylation was significantly increased in cells expressing G2019S LRRK2

compared to wildtype to a larger degree than Rab10 in both traps (Figure

6.10A, C-D, Figure 6.11A, C-D). This suggests that although both Rab10 and

Rab12 can be phosphorylated on any membrane in the context of wildtype LRRK2, pathogenic mutants may influence divergent phosphorylation patterns between these two Rabs.

6.2.4 The role of Rab29 on LRRK2 activity at the Golgi

Several *in vitro* studies have confirmed that Rab29 OE can be used to translocate LRRK2 from the cytosol to the TGN and thus was thought to be an upstream regulator of LRRK2 activity (Beilina et al., 2014; Wang et al., 2014; Purlyte et al., 2019). Additionally, a mitochondrial-targeting sequence fused to the N-terminus of Rab29 is sufficient to bring LRRK2 to the mitochondrial membrane (Gomez et al., 2019). However, recent studies have found that neither Rab29 KO nor transgenic OE animal models have any effect on LRRK2 kinase activity *in vivo* (Kalogeropulou et al., 2020; Mazza et al., 2021). To examine the role of endogenous Rab29 on LRRK2 activity at the TGN in the context of the FKBP-FRB trap system, siRNA Rab29 knockdown versus non-targeting control (NTC) RNA conditions were employed in cells expressing LRRK2 and Golgi-trap. Rab29 knockdown did not affect S1292 autophosphorylation nor phosphorylation of Rab10 or Rab12 (Figure 6.12A-E). In the presence of rapamycin, phosphorylation levels significantly increased in all three readouts, demonstrating that Rab29 is not important for the enhancement of LRRK2 kinase activity at the Golgi membrane.
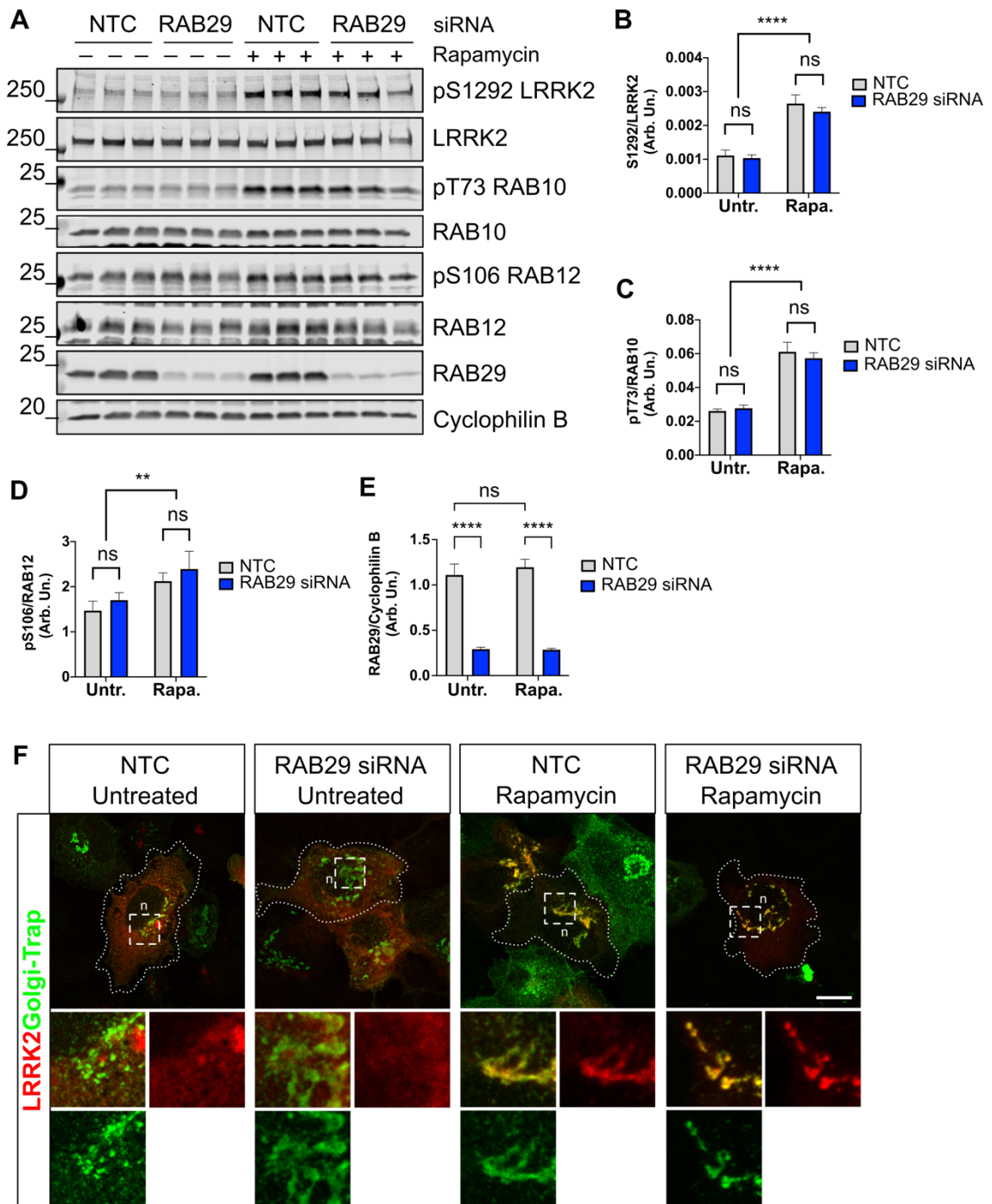
Figure 6.12. **Interrogating LRRK2 kinase activity in Rab29 knockdown cells using Gol-tap.** Following a 24-hour incubation of siRNA Rab29 or non-targeting control, HEK293FT cells were transfected with 3xFlag-FKBP-LRRK2 and Golgi-trap. Cells were then treated with rapamycin for 15 minutes before lysing and pS1292 LRRK2, pT73 RAB10, and pS106 RAB12 levels were evaluated via Western blot (**A-D**). RAB29 knockdown efficiency was measured via total levels of endogenous protein (**E**). Two-way ANOVAs were performed where **p-value <0.01, ****p-value <0.0001. n=3 replicates; SD error bars shown. LRRK2 (red) and Golgi-trap (green) were visualized in NTC or Rab29 siRNA conditions (**F**). Scale bar= 10μm.

Additionally, as a previous study demonstrated that Rab29 may play a role in Golgi membrane integrity (Wang et al., 2014), LRRK2 and Golgi-trap were visualized in these cells to address whether morphological changes could be affecting LRRK2 activity in the absence of Rab29. At baseline, both NTC and Rab29 siRNA conditions showed similar Golgi morphology with diffuse cytosolic LRRK2 that colocalizes to the Golgi in rapamycin-treated cells (Figure 6.12F).

6.3 Discussion

To understand how LRRK2 can phosphorylate Rab10 and Rab12 at various endolysosomal membranes, the FKBP-FRB trap system was used to target LRRK2 to six different intracellular membranes. Surprisingly, LRRK2 localization to any membrane was sufficient to enhance kinase activity, as reflected by S1292 autophosphorylation, and had the ability to phosphorylate both Rab10 and Rab12. This suggests that, although it is likely that certain Rabs function naturally at specific membranes, the machinery necessary to recruit Rab10 and Rab12 and subsequently be phosphorylated by LRRK2 is not membrane specific. One unresolved question is whether Rab10 and Rab12 are already present at these membranes prior to LRRK2 recruitment. If not, LRRK2 may be important in the recruitment of these Rabs in addition to their

subsequent phosphorylation. Further investigation of total Rab proteins and their localization to these membranes will be necessary to answer this question.

Previous studies have demonstrated LRRK2 recruitment and enhanced activity to damaged lysosomes using various reagents as well as bacterial infection (Eguchi et al., 2018; Herbst et al., 2020; Bonet-Ponce et al., 2020). Here, use of the FKBP-FRB trap allowed for the evaluation of LRRK2 activation at the lysosome without membrane damage. Once LRRK2 was trapped to the lysosomal membrane, its kinase activity was significantly enhanced, suggesting that membrane damage may be a trigger to initiate LRRK2 recruitment to a membrane but not necessary for LRRK2 kinase activation. Along the same line, Rab29 deficient cells showed the same magnitude of LRRK2 activation as control siRNA knockdown cells treated with rapamycin using LRRK2, Rab10, and Rab12 phosphorylation readouts, demonstrating that Rab29 is also not required for LRRK2 kinase activation.

When LRRK2 mutants were paired with either lyso-trap or Golgi-trap, Rab12 phosphorylation was not further enhanced once LRRK2 was present at either membrane. This was not observed in cells expressing wildtype LRRK2, and Rab10 phosphorylation increases were observed in both wildtype and

LRRK2 mutants, suggesting a divergence in phosphorylation patterns between Rab10 and Rab12 when GTPase and kinase domain mutants are expressed. Many studies have shown that a larger percentage of membrane-associated LRRK2 is found when overexpressing LRRK2 mutants compared to wildtype (Nichols et al., 2010; Blanca Ramírez et al., 2017; Mamais et al., 2021). Therefore, it is likely that more mutant LRRK2 is present on various membranes already at baseline prior to rapamycin treatment. The absence of a strong difference in Rab12 phosphorylation between baseline and rapamycin-treated cells may be due to stronger presence of Rab12 already at membranes where LRRK2 is present at baseline compared to Rab10. In turn, these results suggest that there is a more complex regulatory mechanism for Rab10 membrane recruitment than Rab12. Of note, there are strong differences in the response of pRabs to LRRK2 *in vivo*. In G2019S KI animals fed MLi-2 via oral gavage as well as in-diet, LRRK2-dependent Rab phosphorylation patterns also differed between Rab10 and Rab12, with Rab12 showing a strong association with both LRRK2 hyperactivity and inhibition in brain and peripheral tissues, whereas Rab10 phosphorylation did not consistently correlate with LRRK2 activity, particularly in the brain. Many more experiments are required in order to elucidate a fuller understanding of Rab recruitment and phosphorylation.

7 INVESTIGATING RAB PHOSPHORYLATION AT LRRK2-POSITIVE LYSOSOMES

7.1 Introduction

Lysosomal degradative capacity progressively declines with aging, and several mutations in genes encoding for lysosomal proteins have been nominated as causes and risk factors for many neurodegenerative diseases including PD (Nalls et al., 2014; Dagan et al., 2015; Kaushik and Cuervo, 2015; Chang et al., 2017; Nalls et al., 2019; Peng et al., 2019; Navarro-Romero et al., 2020). For example, rare mutations in ATP13A2, which encodes for a lysosomal ATPase, cause juvenile-onset PD (Ramirez et al., 2006). Risk factors for PD identified in GWAS that encode lysosomal proteins include GBA1, TMEM175, CTSB, SCARB2, SMPD1, ATP6V0A1, and GALC, all of which are either lysosomal enzymes or lysosomal transmembrane pumps (Nalls et al., 2014; Chang et al., 2017; Nalls et al., 2019). Taken together, these results indicate that lysosome dysfunction may increase PD susceptibility.

Interestingly, recent cellular biological studies have identified specific roles for LRRK2 at the lysosome. Cells harboring LRRK2 pathogenic mutations such as G2019S have enlarged lysosomes with reduced degradative capacity compared to wildtype cells, including fibroblasts taken from PD patients

harboring a G2019S mutation (Henry et al., 2015; Hockey et al., 2015).

Additionally, as stated earlier, LRRK2 KO mice have shown lysosome

abnormalities in kidney tissue, including significant age-dependent

accumulation of lysosomal hydrolases and an increase in the autophagy marker

LC3II (Tong et al., 2010a; Kuwahara et al., 2016; Pellegrini et al., 2018).

Several studies have reported LRRK2 localization at the lysosomal

membrane, particularly in the presence of pathogens or agents that cause

lysosomal stress. Herbst and colleagues found that, when cells were infected

with *Mycobacterium tuberculosis*, *C. albicans*, or *L. monocytogenes,* LRRK2

was recruited to the lysosomal membrane in murine macrophages (Herbst et

al., 2020). Additionally, LRRK2 presence at the lysosome led to the recruitment

and phosphorylation of Rab8a and Rab10, suggesting lysosomal membrane-

associated LRRK2 enhances its kinase activity (Herbst et al., 2020). When

LRRK2 inhibitors were applied, recruitment of pRab8a was lost as well as

subsequent recruitment of CHMP4B, a member of the endosomal sorting

complex required for transport (ESCRT-III) (Herbst et al., 2020). ESCRT-III

machinery act as first responders to limited membrane damage at

endolysosomes in order to repair the damage and prevent lysophagy and

subsequent cell death (Radulovic et al., 2018; Skowyra et al., 2018). Although

this study could not determine the direct mechanism leading to recruitment of

ESCRT machinery, these data suggest that LRRK2 kinase activity is necessary for membrane repair at the lysosome under specific conditions.

Following this report, another study, using L-Leucyl-L-Leucine methyl ester (LLOMe), was able to recapitulate LRRK2 recruitment to the lysosomal membrane in primary murine astrocytes (Bonet-Ponce et al., 2020). LLOMe is a lysosomotropic agent causing lysosomal membrane permeabilization (LMP), activating the recruitment of ESCRT complex proteins CHMP4B and ALIX (Eriksson et al., 2020). With prolonged LLOMe exposure, we discovered increased LRRK2, Rab10, and Rab35 recruitment to the lysosomal membrane, while LRRK2 inhibition via MLi-2 treatment blocked Rab recruitment and phosphorylation (Bonet-Ponce et al., 2020). Using the proximity-based biotinylation-dependent ascorbate peroxidase (APEX2) screen followed by mass spectrometry, JIP4, a motor scaffolding protein, was identified as a novel effector of pRab10. Further interrogation mapped out a mechanism of LYsosomal Tubulation/sorting driven by LRRK2 (LYTL), in which JIP4 recruitment initiated tubular extensions from the membrane of damaged lysosomes (Bonet-Ponce et al., 2020). Taken together, these studies have identified a mechanism of membrane repair that is LRRK2 kinase-dependent at damaged lysosomes following lysosomal stress (Figure 7.1A-B).
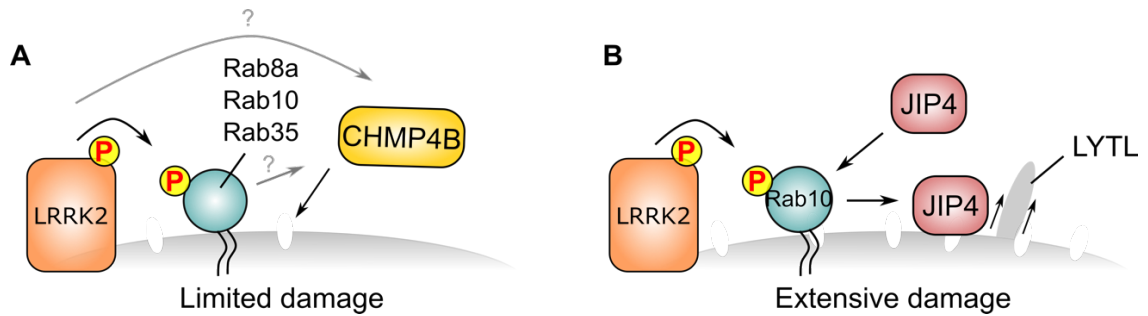
Figure 7.1. **Schematic of LRRK2-dependent mechanisms of recruitment at damaged lysosomes.** With acute damage to the lysosomal membrane, CHMP4 recruitment that is LRRK2-dependent followed by downstream ESCRT-III proteins allow membrane repair (**A**). If extensive damage occurs, LRRK2 recruitment of pRab10 followed by JIP4 initiates tubulation of the lysosomal membrane (LYTL) (**B**).

     In prior chapters of this thesis, I found that when trapping LRRK2 to the lysosomal membrane, LRRK2 activity was significantly enhanced, as estimated by increases in S1292 autophosphorylation as well as T73 Rab10 and S106 Rab12 phosphorylation (Figure 6.7). These results suggest that membrane damage is not required for kinase activation, but rather its proximity to LRRK2. Data from the previous chapters have also highlighted discrepancies between Rab10 and Rab12 LRRK2-dependent phosphorylation *in vitro* and *in vivo*. Therefore, I next examined the phosphorylation patterns of these Rabs at the lysosomal membrane under both undamaged and damaged conditions.

7.2 Results

7.2.1 Evaluating the utility of chimera-LRRK2 plasmids as tools to interrogate membrane-associated LRRK2 kinase activity

To characterize Rab10 and Rab12 phosphorylation further in the context of membrane-bound LRRK2, additional chimera constructs were made to localize LRRK2 to either lysosomal or early endosomal membranes. Chimera constructs consisted of specific transmembrane or membrane-association sequences fused to the N-terminal of LRRK2 such that, upon expression, LRRK2 is directed to the target membrane of interest without addition of co-expressed proteins or treatments like that of the FKBP-FRB system with trap-proteins and rapamycin. Two membrane-specific LRRK2-chimeras were designed taking the first 39aa from regulator complex subunit lysosomal adaptor, MAPK and MTOR activator 1 (LAMTOR1) to direct LRRK2 to lysosomes and double zinc finger and coiled-coil (FYVE-CC2) domains from hepatocyte growth factor (HRS) protein to direct LRRK2 to early endosomes (Komada and Soriano, 1999; Raiborg et al., 2001; Mu et al., 2017). An early endosome chimera was made in order to compare the activation pattern of LRRK2 and subsequent Rab phosphorylation at two distinct membranes that are spatially and functionally distant within the endolysosomal pathway. These

chimeras will be referred to as LYSO-LRRK2 and EE-LRRK2 to denote lysosomal chimera and early endosome chimera, respectively.

To validate the lysosomal chimera, HEK293FT cells were transfected with LYSO-LRRK2 and incubated for 24 hours prior to fixation or lysis. Cells were then stained for LYSO-LRRK2 and endogenous LAMP1, LAMTOR4, and Cathepsin D (Figure 7.2A-C). Using Mander's coefficient, co-localization of LRRK2 to all endogenous lysosomal markers was over 60%, with the strongest colocalization shown with LAMP1 at 78% overlap (Figure 7.2D). Having established correct localization of LRRK2, LYSO-LRRK2 was then compared to the FKBP-FRB targeting scheme in order to compare relative effectiveness of the two approaches to activate LRRK2. Cells transfected with the FKBP-LRRK2 and Lyso-trap constructs and treated with rapamycin showed enhanced LRRK2 activity compared to untreated control cells, as measured by a significant increase in the autophosphorylation of LRRK2 at site S1292 as well as phosphorylation of T73 Rab10 and S106 Rab12 (Figure 7.2E-H). A similar magnitude of LRRK2 activation was observed with the LYSO-LRRK2 construct, as pRab10 and pRab12 levels were significantly increased in rapamycin-treated FKBP-FRB expressing cells and LYSO-LRRK2 expressing cells compared to untreated cells where LRRK2 is localized to the cytosol (Figure 7.2E-H). Thus,

the LYSO-LRRK2 construct is sufficient in directing LRRK2 to lysosomes and

increases its kinase activity similarly to the previous trap model.
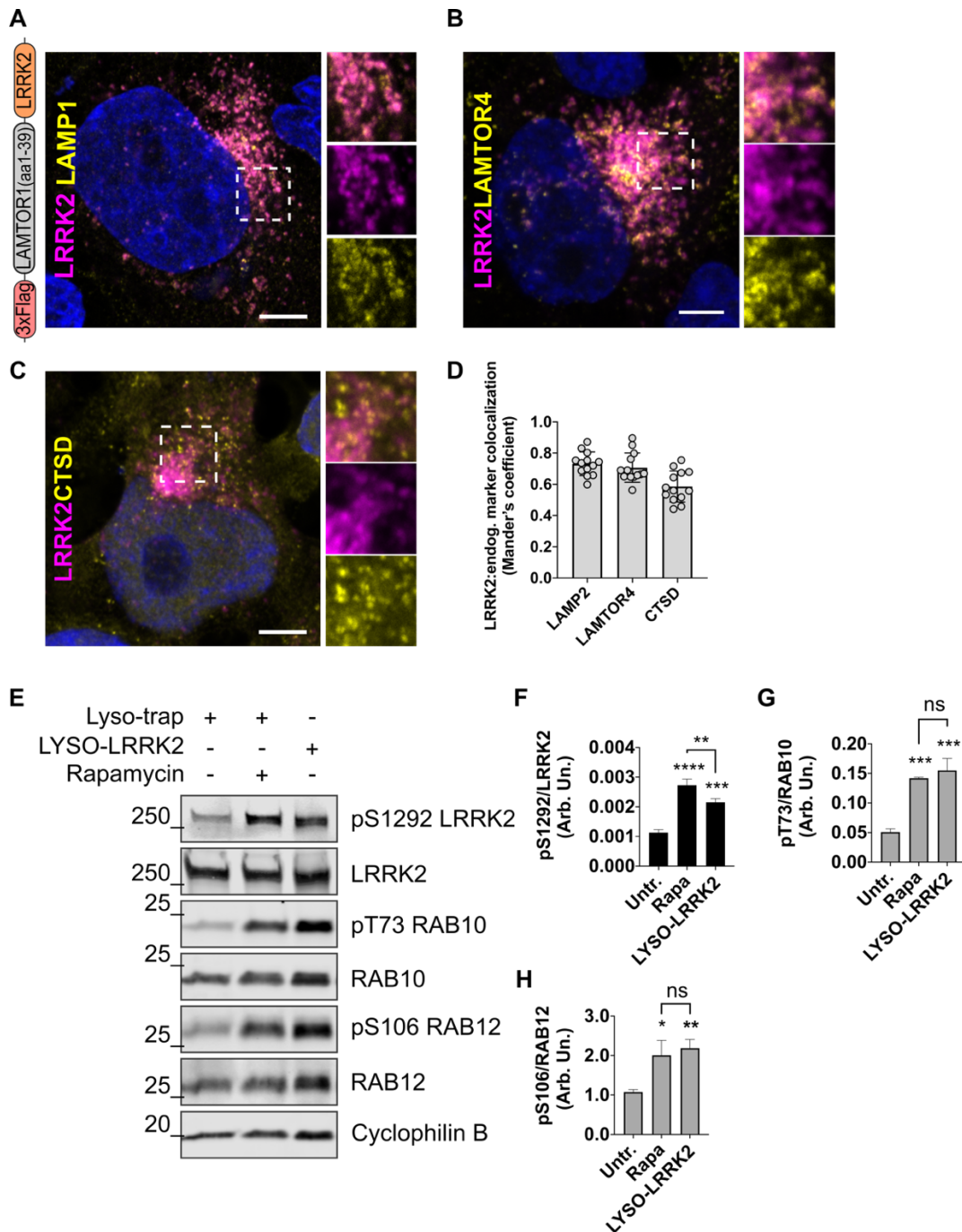
Figure 7.2. **LYSO-LRRK2 chimera characterization.** HEK293FT cells were transfected with LYSO-LRRK2 plasmid (magenta) and stained for endogenous LAMP1 (**A**), LAMTOR4 (**B**), and CTSD (**C**) lysosomal proteins (yellow). The schematic for the LYSO-LRRK2 plasmid design is illustrated on the left. Scale bars= 10μm. LRRK2 colocalization was measured using JACOP package in ImageJ (Mander's coefficient) (**D**). Western blots comparing FKBP-FRB lysosome trap and the LYSO-LRRK2 chimera were probed

and pS1292 LRRK2, pT73 Rab10, pS106 Rab12 levels were measured (**E-H**). One-way ANOVAs were performed where *p-value <0.05, **p-value <0.01, ***p-value <0.001, ****p-value <0.0001. n=3 replicates; SD error bars shown.

To investigate the effects of endosomal localization of LRRK2, HEK293FT cells were transfected with the EE-LRRK2 construct and incubated for 24 hours for expression to take place. Cells were stained for EE-LRRK2 as well as endogenous markers for early endosomes, EEA1 and VPS35 (Figure 7.3A-B). Co-localization measurements showed equal colocalization between LRRK2 and the endogenous markers with 58% overlap (Figure 7.3C). The FYVE-CC2 domains of HRS are membrane-association domains which bind to phosphatidylinositol(3)-phosphate (PI(3)-P) on the surface of a subset of early endosomes (Komada and Soriano, 1999). Therefore, lower co-localization between this construct and EEA1, a general early endosome marker, and VPS35, marking a retromer-specific population of early endosomes, was expected.
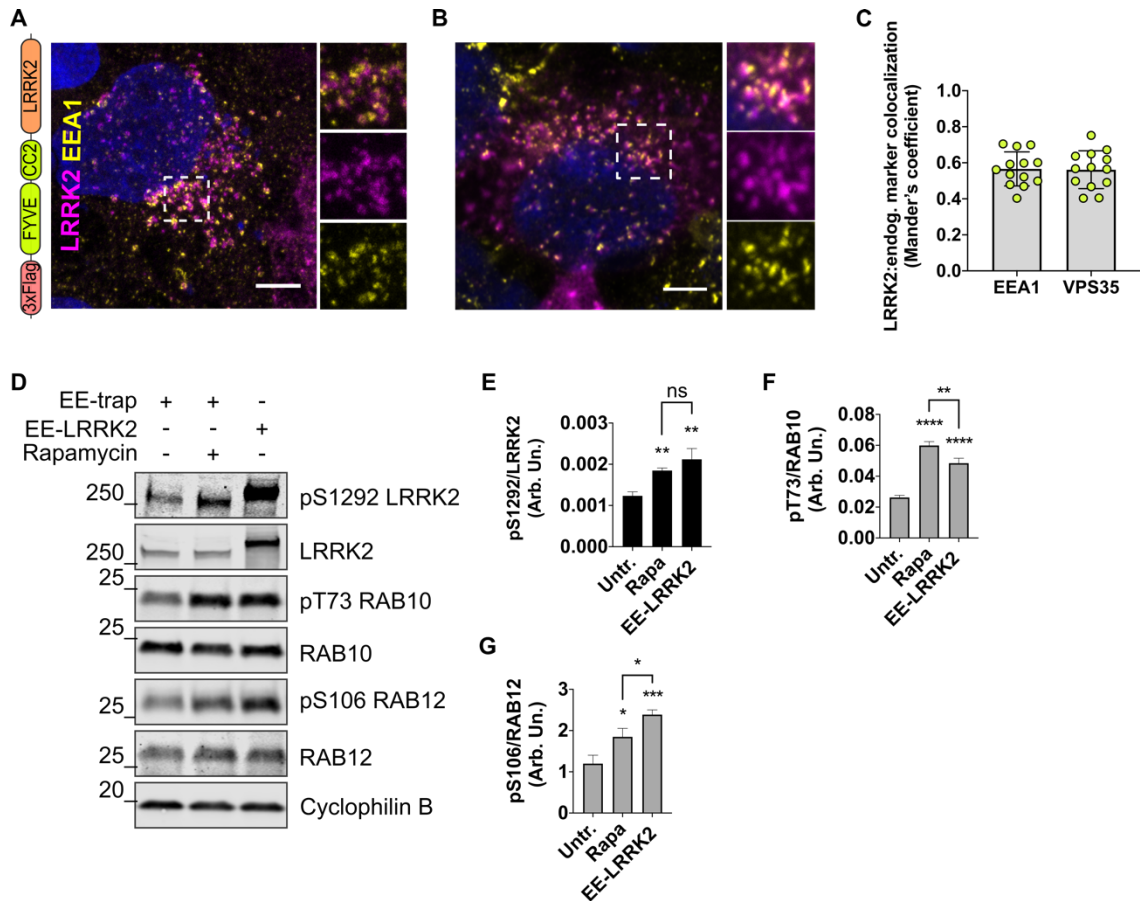
Figure 7.3. **EE-LRRK2 chimera characterization.** HEK293FT cells were transfected with EE-LRRK2 plasmid (magenta) and stained for endogenous EEA1 (**A**) and VPS35 (yellow) (**B**). The schematic for the EE-LRRK2 plasmid design is illustrated on the left. Scale bars= 10µm. LRRK2 colocalization was measured using JACOP package in ImageJ (Mander's coefficient) (**C**). Western blots comparing FKBP-FRB early endosome trap and the EE-LRRK2 chimera were probed and pS1292 LRRK2, pT73 Rab10, pS106 Rab12 levels were measured (**D-G**). One-way ANOVAs were performed where *p-value <0.05, **p-value <0.01, ***p-value <0.001, ****p-value <0.0001. n=3 replicates; SD error bars shown.

Comparison of EE-LRRK2 expressing cells and FKBP-LRRK2 and EE-trap expressing cells treated with rapamycin showed similar increases in S1292 LRRK2 autophosphorylation and Rab10 and Rab12 phosphorylation compared to untreated control cells, thus confirming that EE-LRRK2 was sufficient to direct LRRK2 to early endosomal membranes and enhance kinase activity (Figure 7.3D-G). Collectively, using two orthogonal targeting methods, these

results further support that directing LRRK2 to a given membrane results in

activation and phosphorylation of multiple Rab proteins, irrespective of

membrane identity.

7.2.2 Visualization of pRab10 and pRab12 on LRRK2-positive lysosomes and early endosomes

To confirm that pRabs were present at these membranes, endogenous

pRab10 and pRab12 were visualized in LYSO-LRRK2 expressing HEK293FT

cells. Significant increases in both pT73 Rab10 and pS106 Rab12 that

colocalized with endogenous LAMP2 were observed in cells expressing LYSO-

LRRK2 compared to cells transfected with LRRK2 without lysosomal targeting

(referred to as NT-LRRK2 for "non-targeted") (Figure 7.4A-D). Additionally,

when treated with MLi-2, these signals were completely abolished (Figure

7.4A-D), confirming that both Rab phosphorylation was LRRK2-dependent.
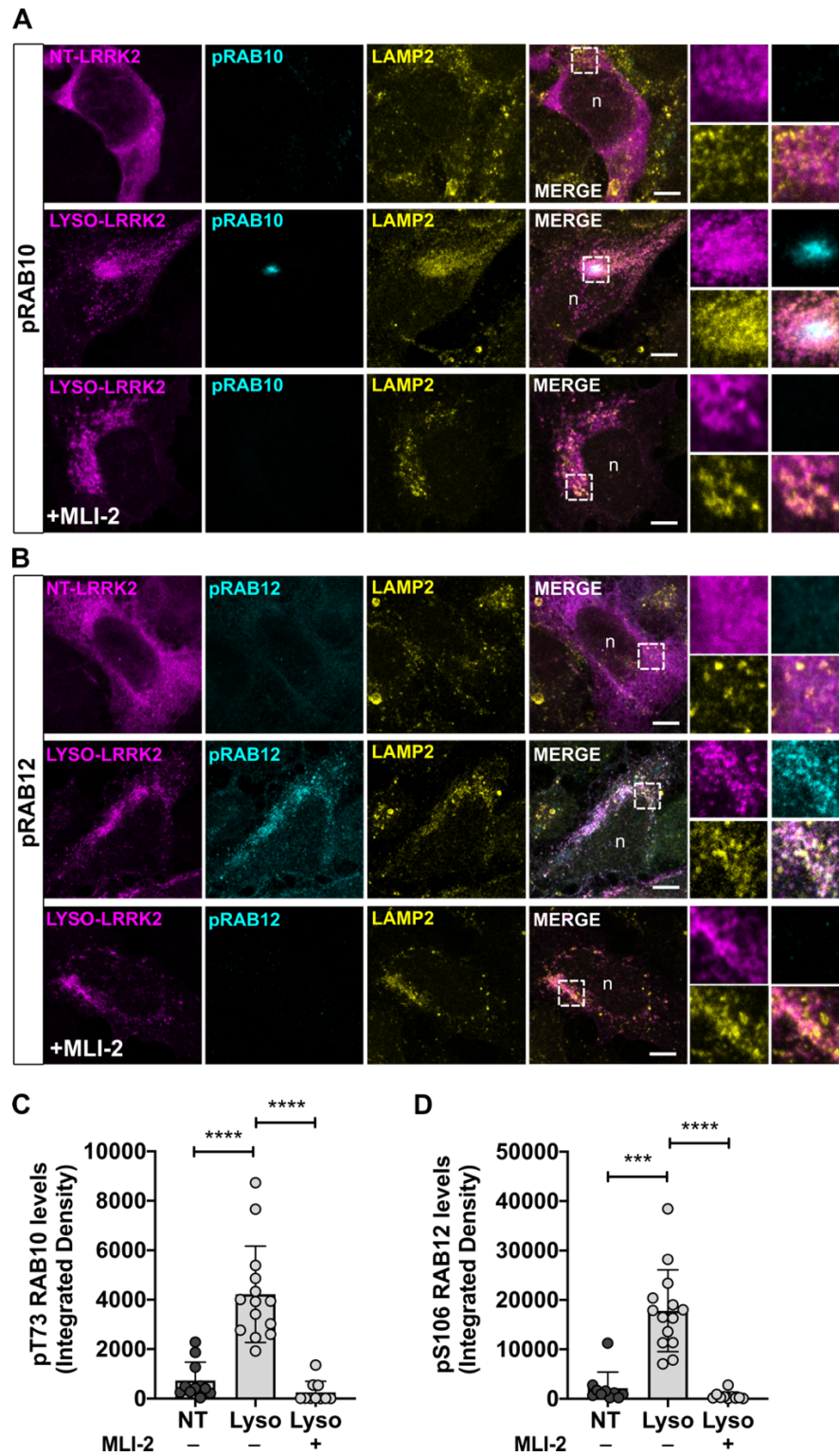
Figure 7.4. **Visualizing pRab10 and pRab12 at LRRK2-positive lysosomes.** Cells expressing either NT-LRRK2 or LYSO-LRRK2 (magenta), with untreated and MLi-2 treated conditions, were stained for pRab10 and pRab12 (cyan) and LAMP2 (yellow) (**A-B**). Scale bars= 10μm and 'n' denotes the cell's nucleus. Integrated densities were measured, and groups compared for both pRab10 and pRab12 signals (**C-D**). One-way

ANOVAs were performed, where ***p-value <0.001, ****p-value <0.0001. n=12-15 cells across 3 technical replicates; SD error bars are shown.

When cells were transfected with the EE-LRRK2 construct, both phosphorylation of Rab10 and Rab12 were significantly increased and colocalized with endogenous EEA1 compared to cells transfected with the NT-LRRK2 construct, and the addition of MLi-2 caused a significant reduction in signals for both pRabs (Figure 7.5A-D). These data show that Rab10 and Rab12 are phosphorylated by LRRK2 and can be recruited to any membrane where LRRK2 kinase is present, likely due to a lack of removal by GDI as previously suggested (Gomez et al., 2019).
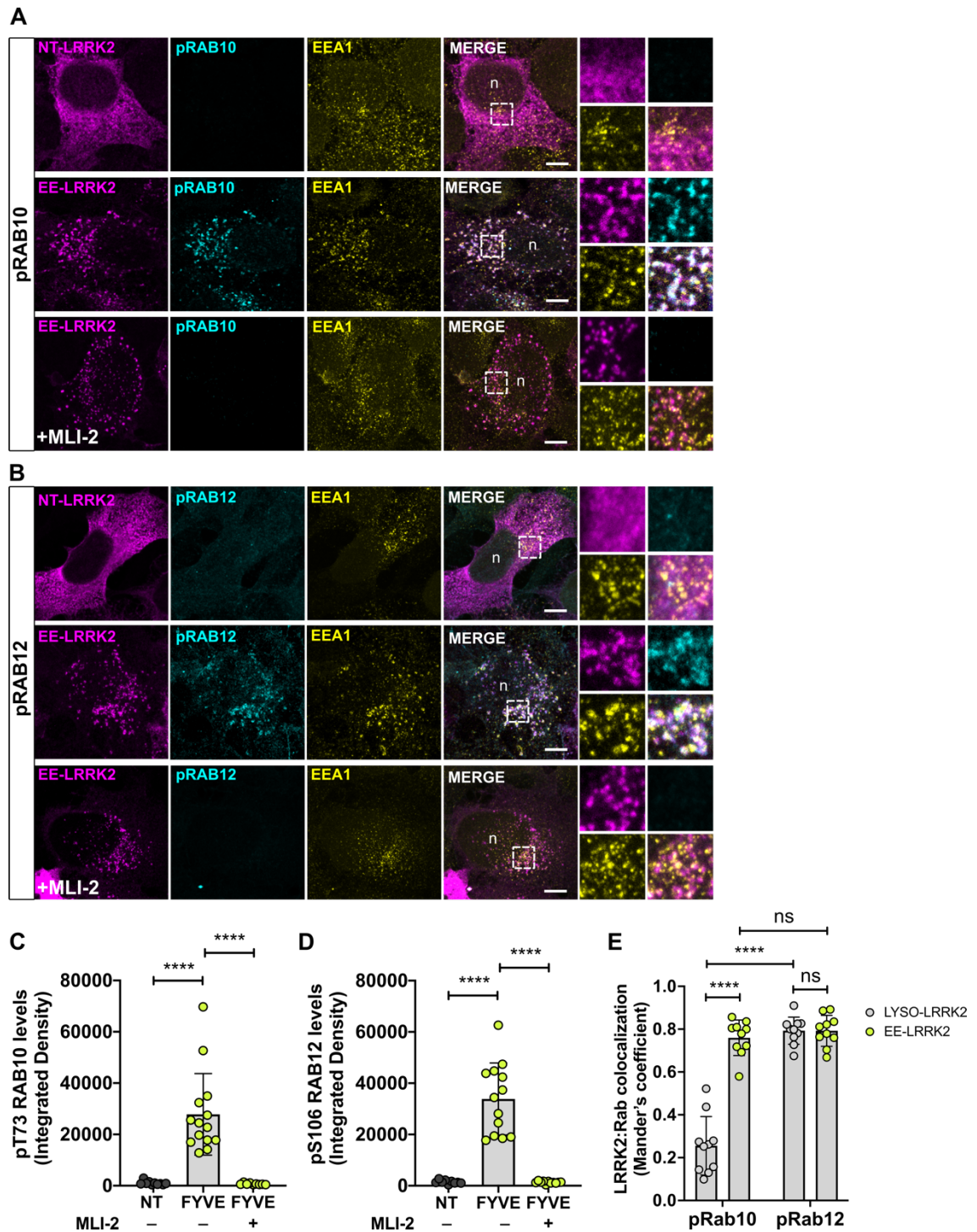
Figure 7.5. **Visualizing pRab10 and pRab12 at LRRK2-positive early endosomes.** Cells expressing either NT-LRRK2 or EE-LRRK2 (magenta), with untreated and MLi-2 treated conditions, were stained for pRab10 and pRab12 (cyan) and EEA1 (yellow) (**A-B**). Scale bars= 10μm and 'n' denotes the nucleus. Integrated densities were measured and groups compared for both pRab10 and pRab12 signals (**C-D**). LRRK2:pRab colocalization was measured using JACOP package in ImageJ (Mander's coefficient) (**E**). One-way ANOVAs were performed, where ****p-value <0.0001. n=12-15 cells across 3 technical replicates; SD error bars are shown.

Inspection of the same images showed that not all LRRK2-positive lysosomes were also pRab10 positive (Figure 7.4A). Therefore, LRRK2:pRab colocalization was measured at LRRK2-positive lysosomes and LRRK2-positive early endosomes using Mander's coefficient. Quantitatively, only a small portion of LRRK2-positive lysosomes colocalized with pT73 Rab10, whereas the majority of LRRK2-positive lysosomes showed colocalization with pS106 Rab12 (Figure 7.5E). Additionally, nearly all LRRK2-positive early endosomes colocalized with both pRab10 and pRab12 (Figure 7.5E). The pRab10 signal was co-localized to a cluster of lysosomes situated in the perinuclear region and was never observed distally. Staining for total Rab10 on cells transfected with LYSO-LRRK2 revealed a similar pattern to pRab10, in that the total protein colocalized only to a subset of perinuclear LRRK2-positive lysosomes (Figure 7.6A). In cells expressing NT-LRRK2, no total Rab10 staining was visible, suggesting that recruitment of Rab10 is stabilized on perinuclear lysosomes when LRRK2 is present at the membrane (Figure 7.6B).
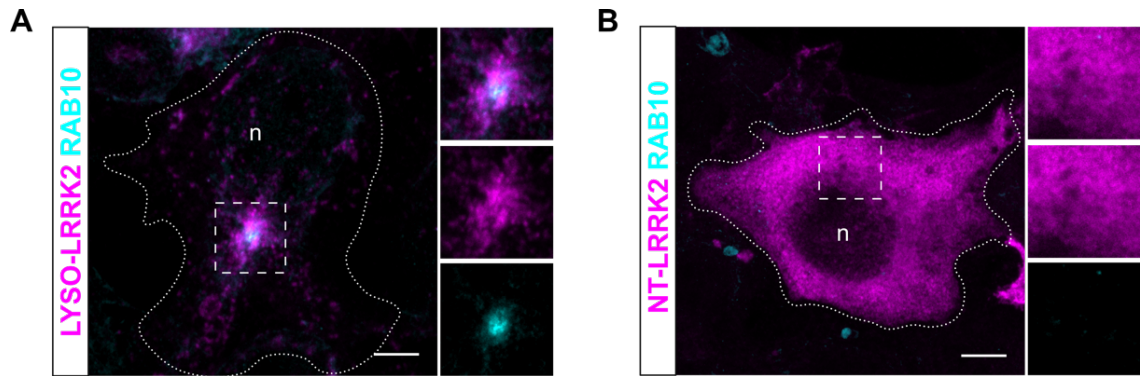
Figure 7.6. **Total Rab10 staining in LYSO-LRRK2 and NT-LRRK2 expressing cells**. LYSO-LRRK2 or NT-LRRK2 (magenta) were transfected into HEK293FT cells and total Rab10 was visualized (cyan) (**A-B**). Scale bars= 10μm. Cell edges are outlined and 'n' denotes the nucleus.

7.2.3 Lysosomal positioning regulates Rab10 phosphorylation on LRRK2-positive lysosomes

Since pRab10 was only present on a subset of LRRK2-positive lysosomes that were proximal to the nucleus, I hypothesized that lysosomal position may play a role in its recruitment. The small Arf-like GTPase ARL8B and kinesin-1 adaptor protein SKIP have been previously shown to direct lysosomes to the cell periphery when overexpressed (Keren-Kaplan and Bonifacino, 2021; Rosa-Ferreira and Munro, 2011). Briefly, ARL8B binds to both the lysosomal membrane and SKIP, which contains two light chain kinesin-binding domains, to promote anterograde movement along microtubules (Figure 7.7A). Interestingly, in cells co-transfected with ARL8B and SKIP proteins (mCherry-ARL8B and 2xMyc-SKIP constructs), considerable morphological changes were observed in which cells formed long processes with a large accumulation of

lysosomes situated at the tips (Figure 7.7B-C). When measuring the number of LRRK2-positive lysosomes at the periphery versus total lysosome count, a significant increase was observed in the number of LRRK2-positive lysosomes situated at the periphery when expressing ARL8B and SKIP together compared to cells expressing LYSO-LRRK2 alone (Figure 7.7C-D).
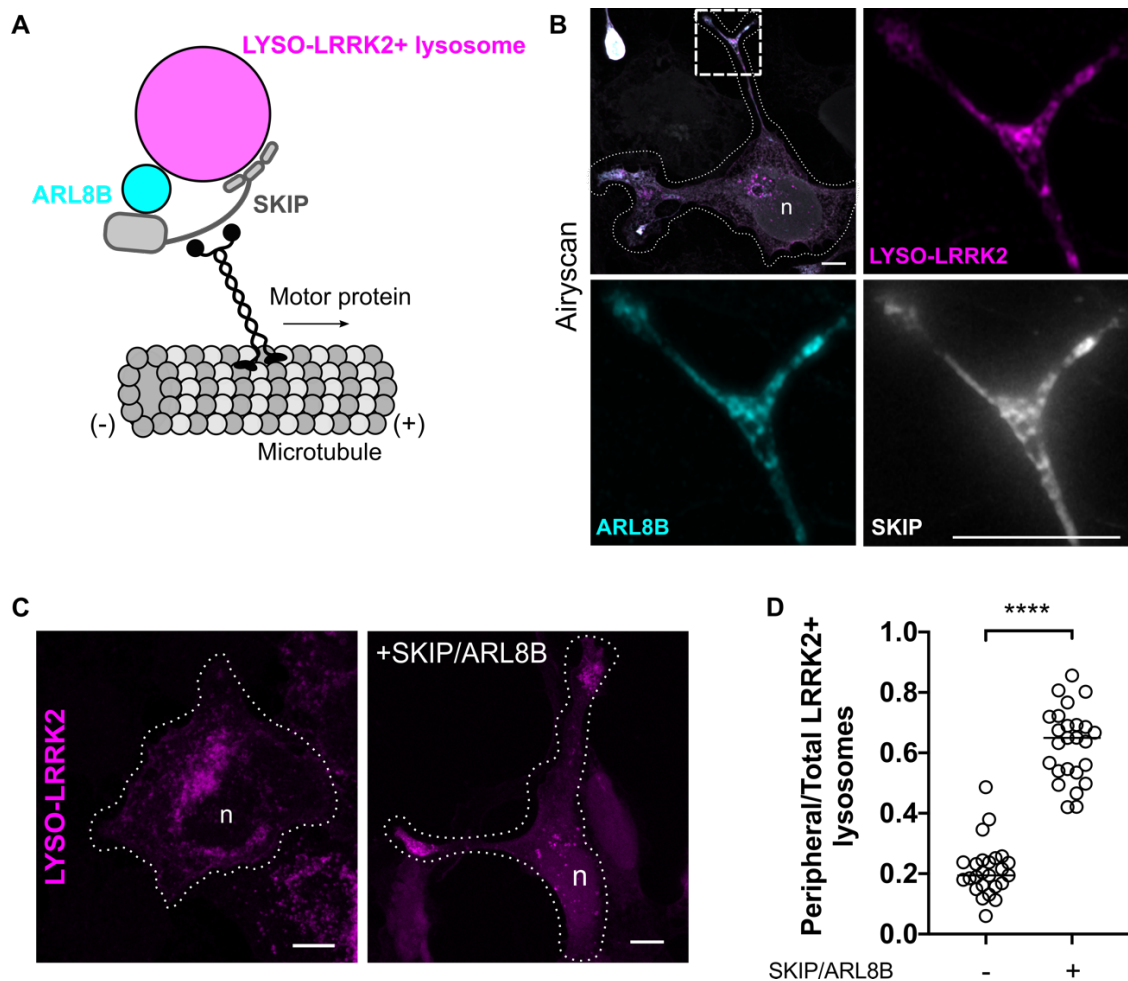
Figure 7.7. **Lysosomal manipulation with ARL8B and SKIP.** Schematic of the mechanism that moves lysosomes to the periphery along microtubules (**A**). Airyscan image of a cell process overexpressing ARL8B (cyan), SKIP (grey), and LYSO-LRRK2 (magenta) (**B**). Scale bar of whole cell= 10μm; scale bar of boxed close up= 2μm. Comparison of cells expressing LYSO-LRRK2 (magenta) alone or with ARL8B/SKIP (**C**). Cell edges are outlined and 'n' denotes the nucleus. Quantification of the ratio of peripheral to total LRRK2-positive lysosomes such as those represented in panel C are shown in (**D**). Peripheral fluorescence refers to the presence of LRRK2 within 2 μm from the cell vertices. Horizontal lines indicate the mean SD from 3 independent experiments.

Interestingly, when investigating pRab10 levels in the presence of ARL8B and SKIP OE, both signal intensity of pRab10 and its colocalization to LRRK2 were significantly decreased compared to cells transfected with LYSO-LRRK2 alone (Figure 7.8A-C). These data demonstrate that lysosomes situated within the perinuclear region have specific properties that allow recruitment and phosphorylation of Rab10 by LRRK2 that are not shared with peripheral lysosomes.
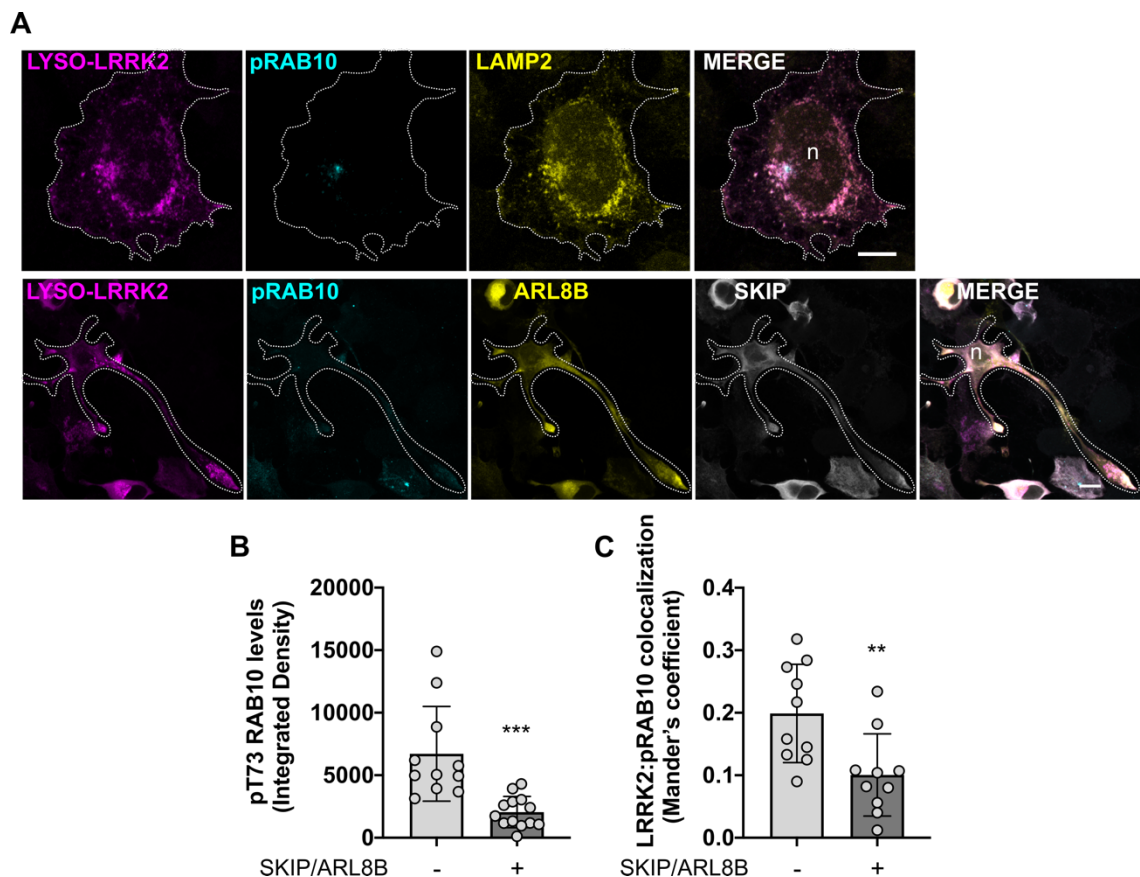
Figure 7.8. **Rab10 phosphorylation in spatially distinct LRRK2-positive lysosomes.** HEK293FT cells expressing LYSO-LRRK2 (magenta) alone or with ARL8B (yellow) and SKIP (grey) were stained for pRab10 (cyan) and LAMP2 (yellow) (**A**). Scale bars= 10µm. Cell edges are outlined and 'n' denotes the nucleus. Integrated density of pRab10 was measured (**B**) as well as colocalization to LRRK2 (**C**). Unpaired student t tests were performed, where **p-value <0.01, ***p-value <0.001. SD error bars are shown; n=12-15 cells across 3 technical replicates.

In order to determine whether lysosomal membrane damage could override this mechanism and force Rab10 to LRRK2-positive lysosomes despite their location, cells were treated with LLOMe for 2 hours prior to fixation. Interestingly, LLOMe-treated cells expressing LYSO-LRRK2 alone showed a significant increase in phosphorylated Rab10 that co-localized to LRRK2 and endogenous LAMP2 staining, while LLOMe did not affect the phosphorylation of Rab10 in cells transfected additionally with SKIP and ARL8B (Figure 7.9A-C).
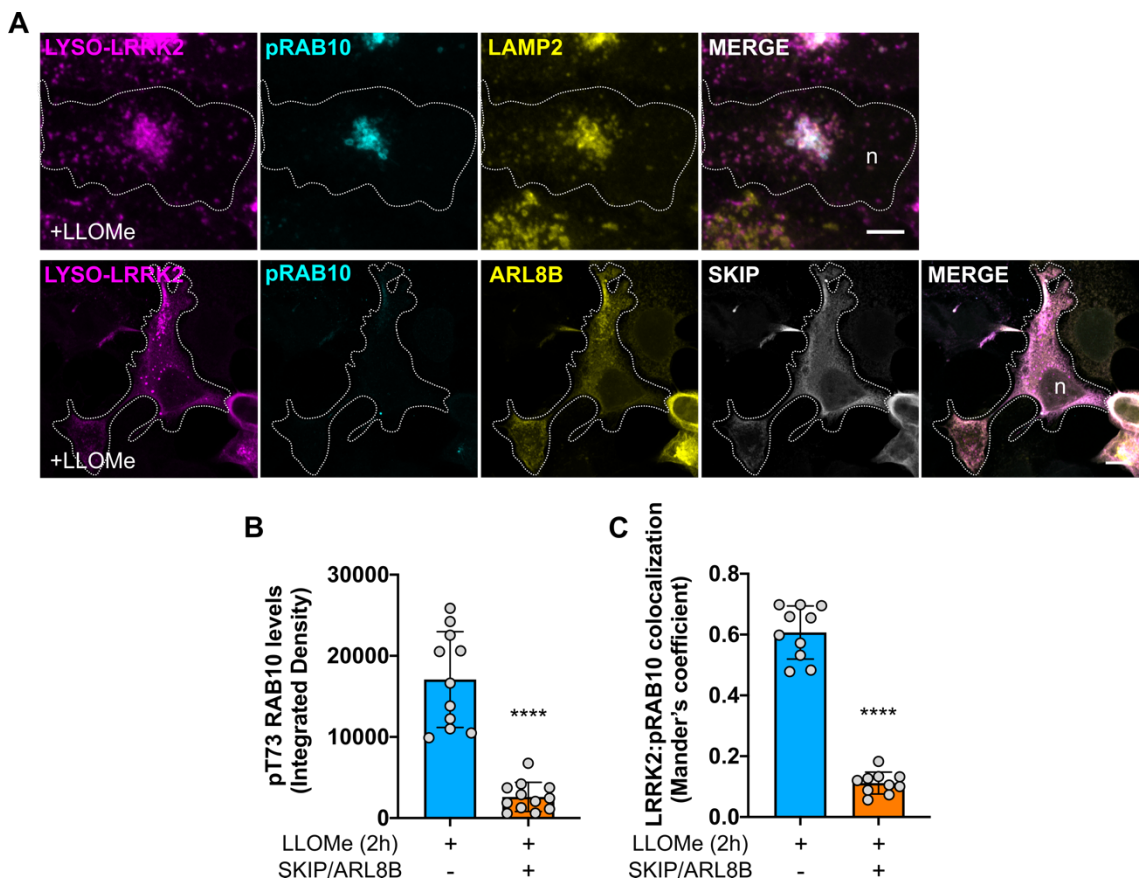
Figure 7.9. **Rab10 phosphorylation in spatially distinct LRRK2-positive lysosomes treated with LLOMe.** HEK293FT cells expressing LYSO-LRRK2 (magenta) alone or with ARL8B (yellow) and SKIP (grey) were treated with LLOMe for 4 hours and stained for pRab10 (cyan) and LAMP2 (yellow) (**A**). Scale bars= 10μm. Cell edges are outlined and 'n' denotes the nucleus. Integrated density of pRab10 was measured (**B**) as well as colocalization to LRRK2 (**C**). Unpaired student t tests were performed, where ****p-value <0.0001. SD error bars are shown; n=12-15 cells across 3 technical replicates.

Western blot analysis further supported these results, showing that LLOMe treatment significantly increased phosphorylation of Rab10 in cells transfected with LYSO-LRRK2 alone which was counteracted by co-transfection with ARL8B and SKIP (Figure 7.10A-B). Interestingly, LLOMe did not have any impact on LRRK2 autophosphorylation at S1292 upon treatment regardless of transfection condition (Figure 7.10A, C), suggesting that LLOMe induces LRRK2 kinase activity in a manner that is distinct from LRRK2 mutations that all increase pS1292, or that LLOMe increases the proximity between LRRK2 and Rabs to provide more opportunity for LRRK2-dependent Rab phosphorylation without increasing LRRK2 kinase activity itself. Additionally, it should be noted that LRRK2 transfection efficiency was decreased when co-transfected with SKIP and ARL8B plasmids (Figure 7.10A, D).
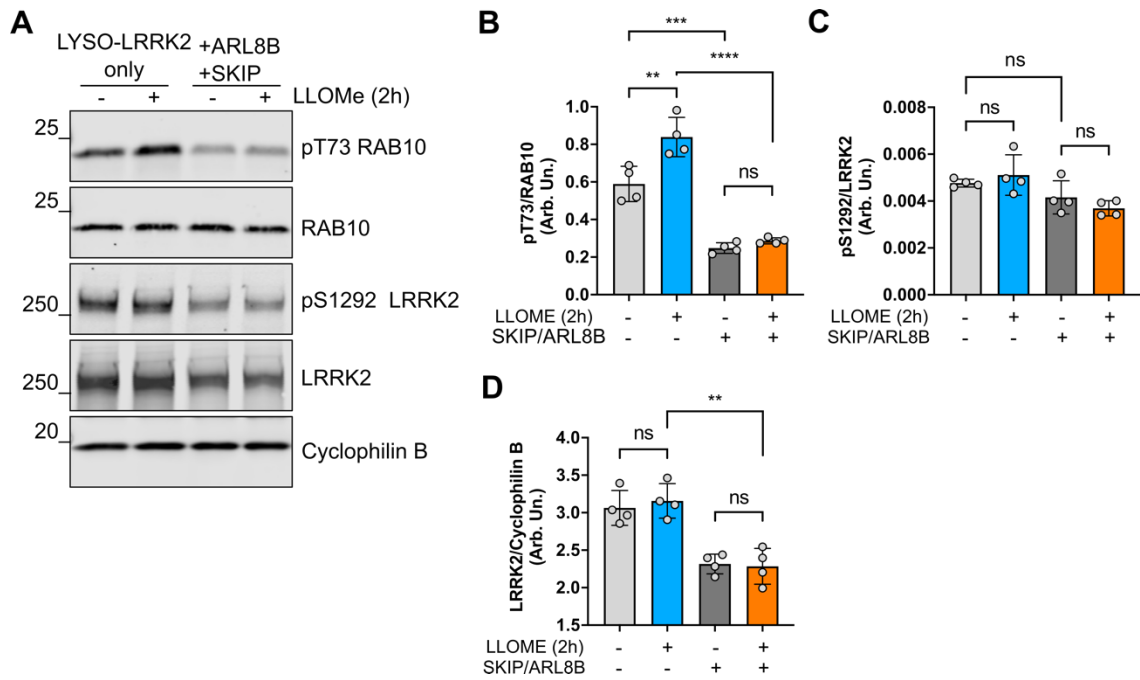
Figure 7.10. **Western blot analyses of pRab10 levels across expression and treatment conditions.** Representative Western blots shown for cells expressing LYSO-LRRK2 alone or with ARL8B/SKIP in untreated and LLOMe-treated conditions (A). Rab10 phosphorylation, pS1292 LRRK2, and total LRRK2 levels were measured (**B-D**). One-way ANOVAs were performed, where **p-value <0.01, ***p-value <0.001, ****p-value <0.0001. SD error bars are shown; n=4 technical replicates.

When staining for pRab12 in cells transiently expressing ARL8B and SKIP, strong colocalization between pRab12 and LRRK2-positive lysosomes was observed regardless of lysosomal position, and acute treatment with LLOMe equally increased pRab12 in cells transfected with LYSO-LRRK2 alone or with ARL8B and SKIP (Figure 7.11A-D). This suggests that there are differing mechanisms at play for LRRK2-dependent phosphorylation of Rab10 and Rab12 at lysosomes. Out of curiosity, pT71 Rab29 levels were also measured for conditions under LLOMe treatment at peripheral and perinuclear lysosomes via Western blot. Interestingly, Rab29 has been shown to act both upstream

and downstream of LRRK2 as a substrate that is phosphorylated within the switch II domain similarly to other LRRK2 Rab substrates (Steger et al., 2016; Purlyte et al., 2019). In cells co-expressing LYSO-LRRK2, ARL8B, and SKIP, Rab29 phosphorylation levels were similar to cells expressing only LYSO-LRRK2 at baseline (Figure 7.11F-G). When treated with LLOMe, a significant increase in pRab29 was measured in cells expressing LYSO-LRRK2 only compared to untreated cells. However, this increase was lost in cells where lysosomes were directed to the periphery with ARL8B and SKIP (Figure 7.11F-G). Thus, Rab10 and Rab29 may share the same or similar mechanism that prevents their phosphorylation on LRRK2-positive lysosomes that are distal to the nucleus, whereas Rab12 is governed by a distinct and separate mechanism.
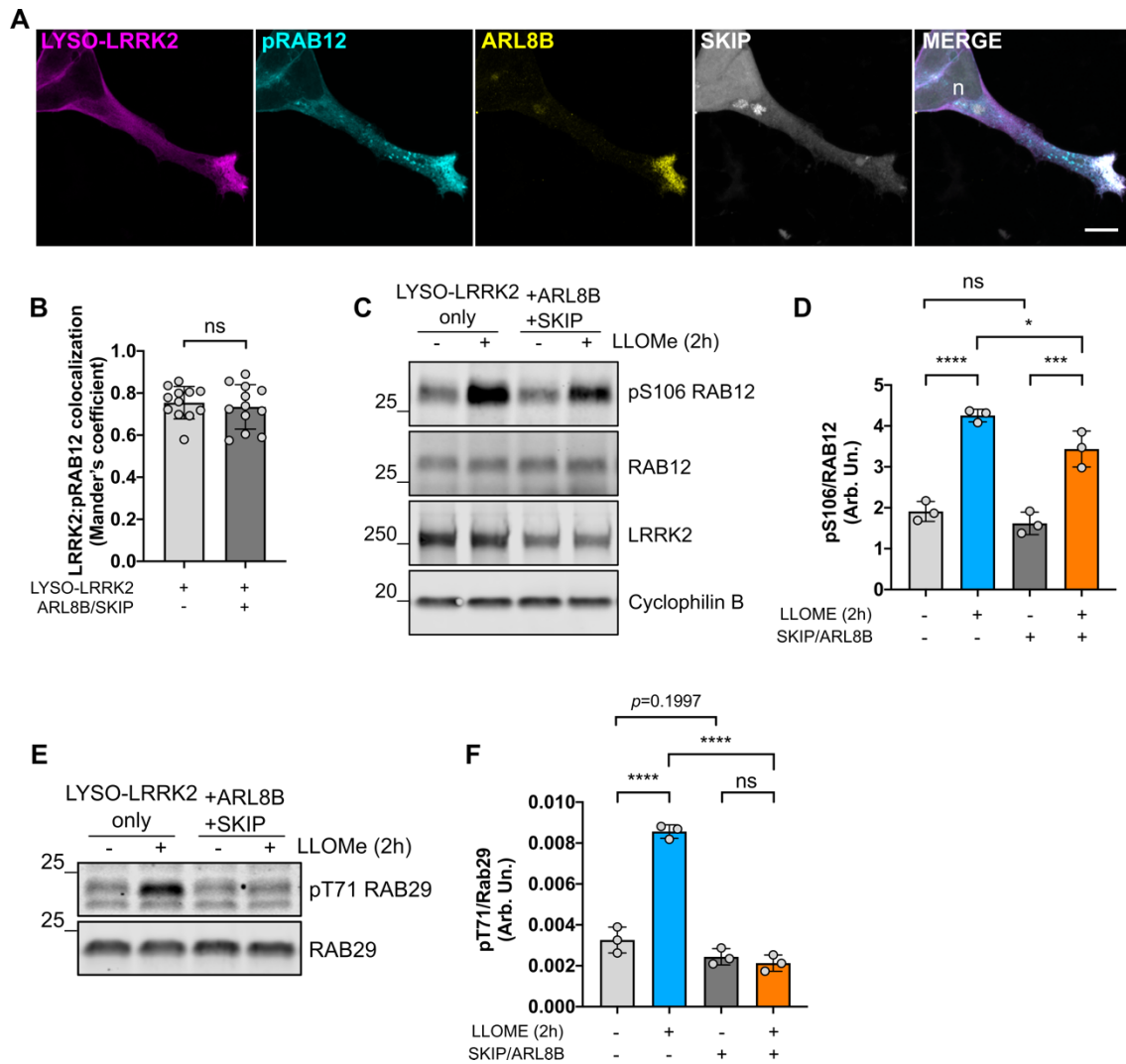
Figure 7.11. **Phosphorylated Rab12 is found at peripheral lysosomes in cells transiently transfected with ARL8B and SKIP plasmids.** A super-resolution confocal microscopy image shows pS106 Rab12 staining (cyan) at LRRK2-positive lysosomes (magenta) when ARL8B (yellow) and SKIP (grey) are co-expressed (**A**). Scale bar= 10μm. Mander's coefficient was used to measure LRRK2:pRab12 colocalization in conditions where ARL8B and SKIP are co-expressed with LYSO-LRRK2 as well as when only LYSO-LRRK2 is expressed alone (**B**). Western blot analyses of Rab12 and Rab29 phosphorylation are shown (**C-F**). Unpaired student t test and one-way ANOVAs were performed where *p-value <0.05, ***p-value <0.001, ****p-value <0.0001. SD error bars are shown; for panel B n=12-14 cells across 3 technical replicates, for panels D and F n=3 technical replicates.

Thus far, experiments manipulating lysosomal redirection to the cell periphery have relied on OE of ARL8B and SKIP. Therefore, to confirm the

present findings without the use of OE, siRNA knockdown of JIP4 was employed. One known function of JIP4 is as a motor adaptor protein that binds to the dynein/dynactin complex to promote transport of lysosomes towards the minus end of microtubules (Willett et al., 2017) (Figure 7.12A). Thus, knocking down JIP4 can prevent lysosomal retrograde transport to the perinuclear area, thereby achieving peripheral sequestration. This was then followed by transient transfection of LYSO-LRRK2 and pRab10 and pRab12 levels were measured via immunocytochemistry. Successful knockdown of JIP4 resulted in a buildup of LRRK2-positive lysosomes situated at the periphery and decreased Rab10 phosphorylation levels were observed compared to cells transfected with non-targeting siRNA control (Figure 7.12B-C). This confirms that JIP4 influences lysosomal positioning and, indirectly, LRRK2-dependent phosphorylation of Rab10. Similar to patterns seen in cells overexpressing ARL8B and SKIP, pRab12-positive lysosomes were visualized across the cell cytoplasm after JIP4 knockdown, further confirming that Rab12 phosphorylation on LRRK2-positive lysosomes is unaffected by position of the lysosome (Figure 7.12B, D). Western blot analyses confirmed sufficient JIP4 knockdown, as well as a reduction of pRab10 compared to NTC conditions (Figure 7.12E-F). Interestingly, JIP4 knockdown markedly reduced total Rab12 protein levels, making the effect on its phosphorylation difficult to interpret via Western blot (Figure 7.12E, G).
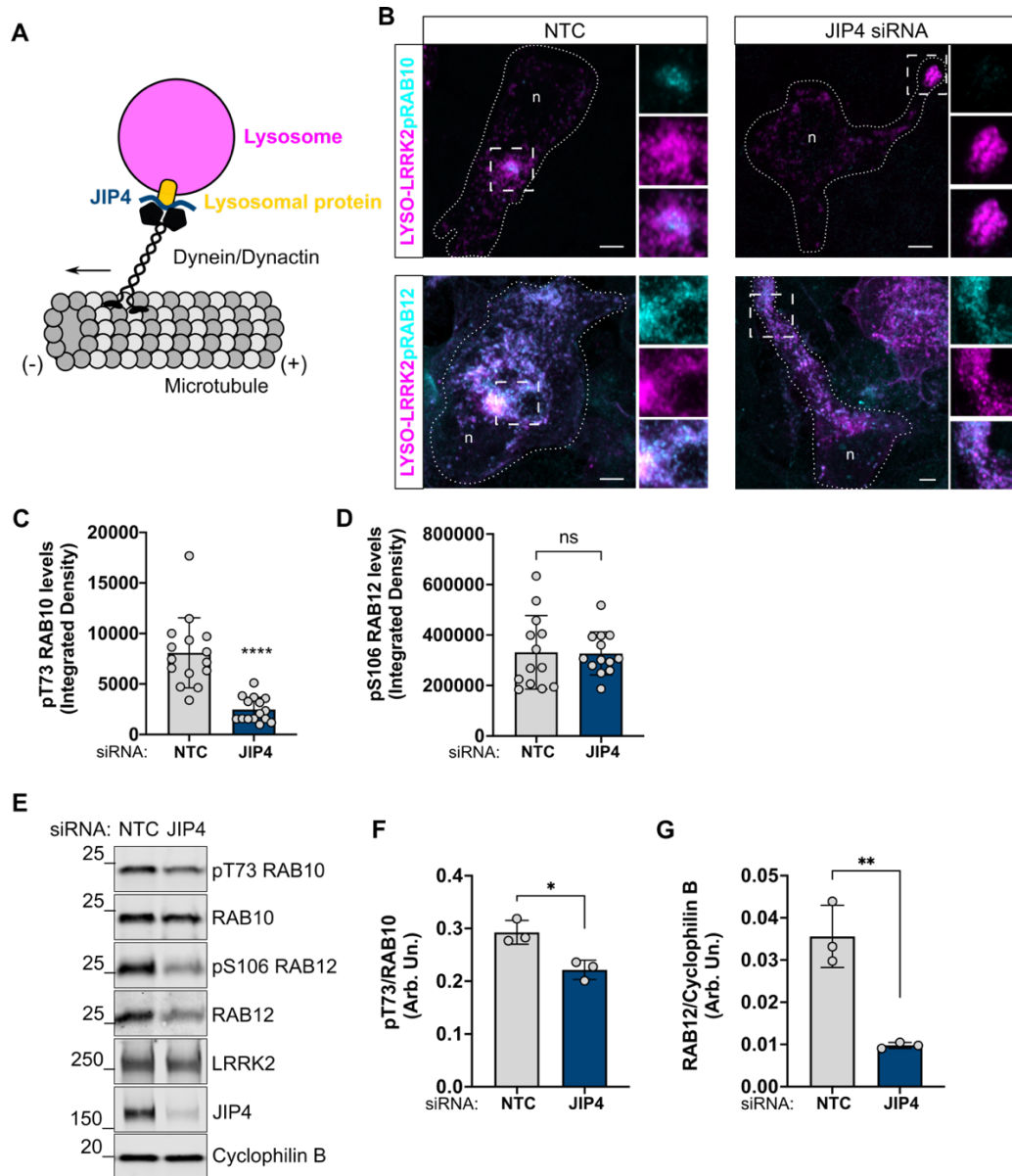
Figure 7.12. **Effect of JIP4 siRNA knockdown on pRab10 at LRRK2-positive lysosomes.** Schematic illustrates JIP4-associated lysosomal trafficking via dynein/dynactin complex on microtubules (**A**). Representative images from NTC or JIP4 siRNA knockdown in cells expressing LYSO-LRRK2 (magenta) and stained for pRab10 or pRab12 (cyan) (**B**). Scale bars= 10μm. Cell edges are outlined and 'n' denotes the nucleus. Integrated densities were measured for pRab10 (**C**) and pRab12 (**D**). Complementary Western blot analyses were performed (**E**) and pRab10 (**F**) and pRab12 (**G**) levels were measured. Unpaired student t tests were performed where *p-value <0.05, **p-value <0.01, ****p-value <0.0001. SD error bars are shown; for panels C-D n=12-15 cells across 3 technical replicates; for panels F-G n=3 technical replicates.

Furthermore, since translocating lysosomes to the periphery of cells reduces Rab10 phosphorylation, I hypothesized that pushing lysosomes into the perinuclear area would have the opposite effect and increase Rab10 phosphorylation using Rab-interacting lysosomal protein (RILP) OE. To achieve this, I used RILP OE. RILP is a Rab7A effector that affects lysosomal positioning within the cell via recruitment of dynein and dynactin proteins (Cantalupo et al., 2001). Overexpressing RILP arrests Rab7A in its GTP-bound active form and sequesters the protein to late endosomal and lysosomal membranes and induces recruitment of the dynein-dynactin complex which promotes vesicle translocation along the minus end of microtubules towards the perinuclear region (Jordens et al., 2001).

Therefore, HEK293FT cells were co-transfected with LYSO-LRRK2 and RILP-GFP and stained for pT73 Rab10 and pS106 Rab12. Excitingly, RILP OE clustered LRRK2-positive lysosomes into the perinuclear region, resulting in the recruitment and phosphorylation of Rab10, as demonstrated by LRRK2:pRab10 colocalization (Figure 7.13A, C). Measurement of signal intensity of pRab10 were also significantly increased compared to cells that were transfected with LYSO-LRRK2 alone (Figure 7.13D). These results further demonstrate that lysosomes situated in the perinuclear area possess favorable characteristics for the recruitment and phosphorylation of Rab10 by LRRK2. Additionally, OE of

RILP also clustered pRab12-positive lysosomes, however we observed no

difference in colocalization with LRRK2 nor levels of phosphorylated Rab12,

suggesting again, that pRab12 is unaffected by lysosomal position (Figure

7.13B, E-F).
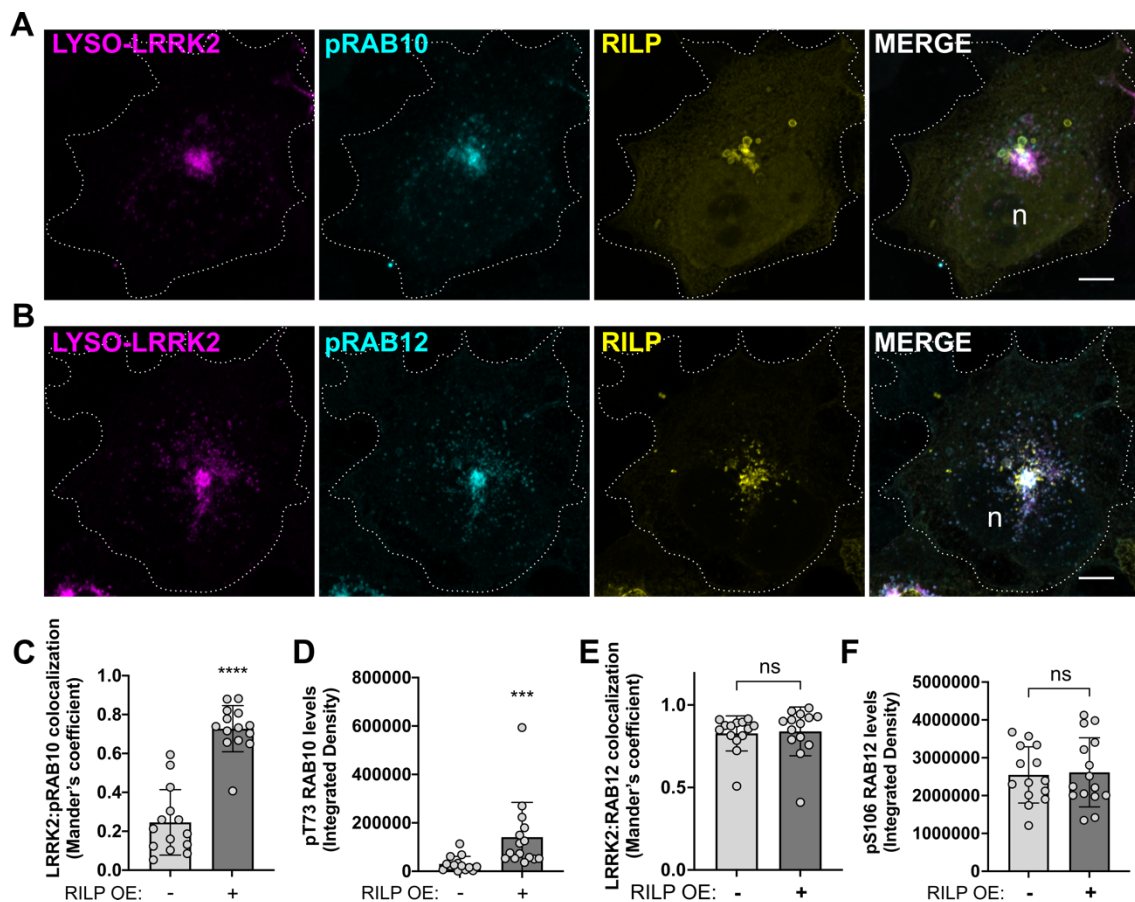
Figure 7.13. **RILP OE increases pRab10 signal at LRRK2-positive perinuclear lysosomes.** LYSO-LRRK2 (magenta) was co-transfected together with RILP (yellow) and endogenous pRab10 (**A**) and pRab12 (**B**) were stained (cyan). Scale bars= 10μm. Cell edges are outlined and 'n' denotes the nucleus. Both integrated densities as well as colocalization of LRRK2 with pRabs were measured for pRab10 (**C-D**) and pRab12 (**E-F**) comparing conditions with and without RILP OE. Unpaired student t tests were performed where ***p-value <0.001 and ****p-value <0.0001. SD error bars are shown; n=12-15 cells across 3 technical replicates.

Taken together, both methods of ARL8B/SKIP OE and JIP4 siRNA knockdown were sufficient in sequestering LRRK2-positive lysosomes to the periphery of cells where pRab10 signal is lost, whereas clustering cells into the perinuclear region via RILP OE increased pRab10. These data suggest that there is an unidentified mechanism in which LRRK2-dependent pRab10 accumulation on lysosomes is favored when arranged proximal to the cell's nucleus, that is not required for pRab12 accumulation.

7.2.4 Lysosomal positioning influences pRab10 using lysosomal damage to drive non-tagged LRRK2 to lysosomes

To make sure that the phenomenon of peripheral lysosomes being recalcitrant to pRab10 formation could be recapitulated in cells without the LYSO-LRRK2 chimera, LLOMe treatment was used in non-targeted, wildtype LRRK2 expressing cells (NT-LRRK2). NT-LRRK2 is primarily cytosolic, and treatment with LLOMe promotes colocalization to the lysosomal membrane (Bonet-Ponce et al., 2020; Herbst et al., 2020). Therefore, cells were transfected with NT-LRRK2 followed by LLOMe treatment for 2 hours. This resulted in LRRK2 localization to the lysosomal membrane with or without the addition of ARL8B and SKIP OE as assessed by colocalization with endogenous LAMP2 (Figure 7.14A-B).
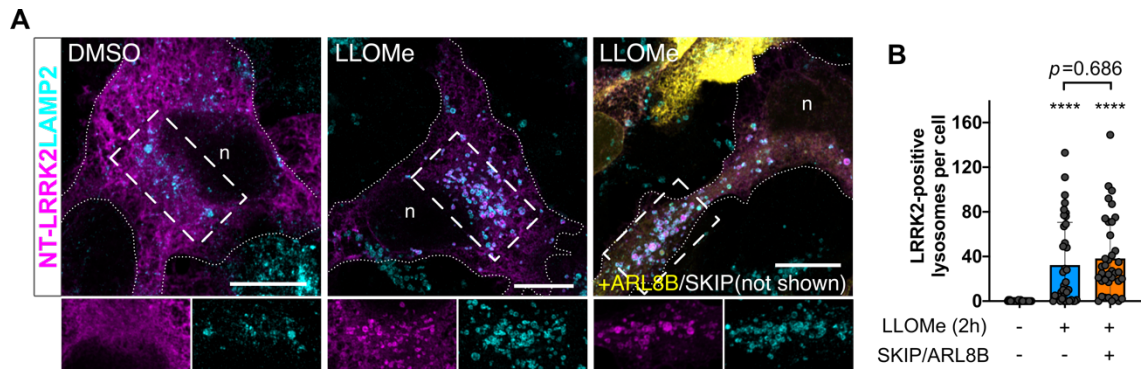
Figure 7.14. **LRRK2 is recruited to lysosomes following acute LLOMe treatment.** NT-LRRK2 (magenta) was transfect with or without ARL8B (yellow) and SKIP and treated with DMSO or LLOMe for 2 hours (**A**). Scale bars= 10μm. Cell edges are outlined and 'n' denotes the nucleus. LRRK2-positive lysosomes were counted as LAMP2-positive structures (cyan) (**B**). One-way ANOVAs were performed where ****p-value <0.0001. SD error bars are shown; n=40 cells across 3 technical replicates.

Interestingly, when cells were treated with LLOMe, colocalization of LRRK2 and pRab10 was found only in a subset of lysosomes within the perinuclear region and this was blocked when lysosomes were pushed to the periphery upon ARL8B and SKIP OE (Figure 7.15A-B). Additionally, pRab12 was recruited to LRRK2-positive lysosomes after LLOMe treatment with and without co-transfection of ARL8B and SKIP proteins (Figure 7.15C-D). This suggests that regardless of lysosomal position, LLOMe treatment is sufficient to bring cytosolic LRRK2 to the lysosomal membrane to recruit pRab12.
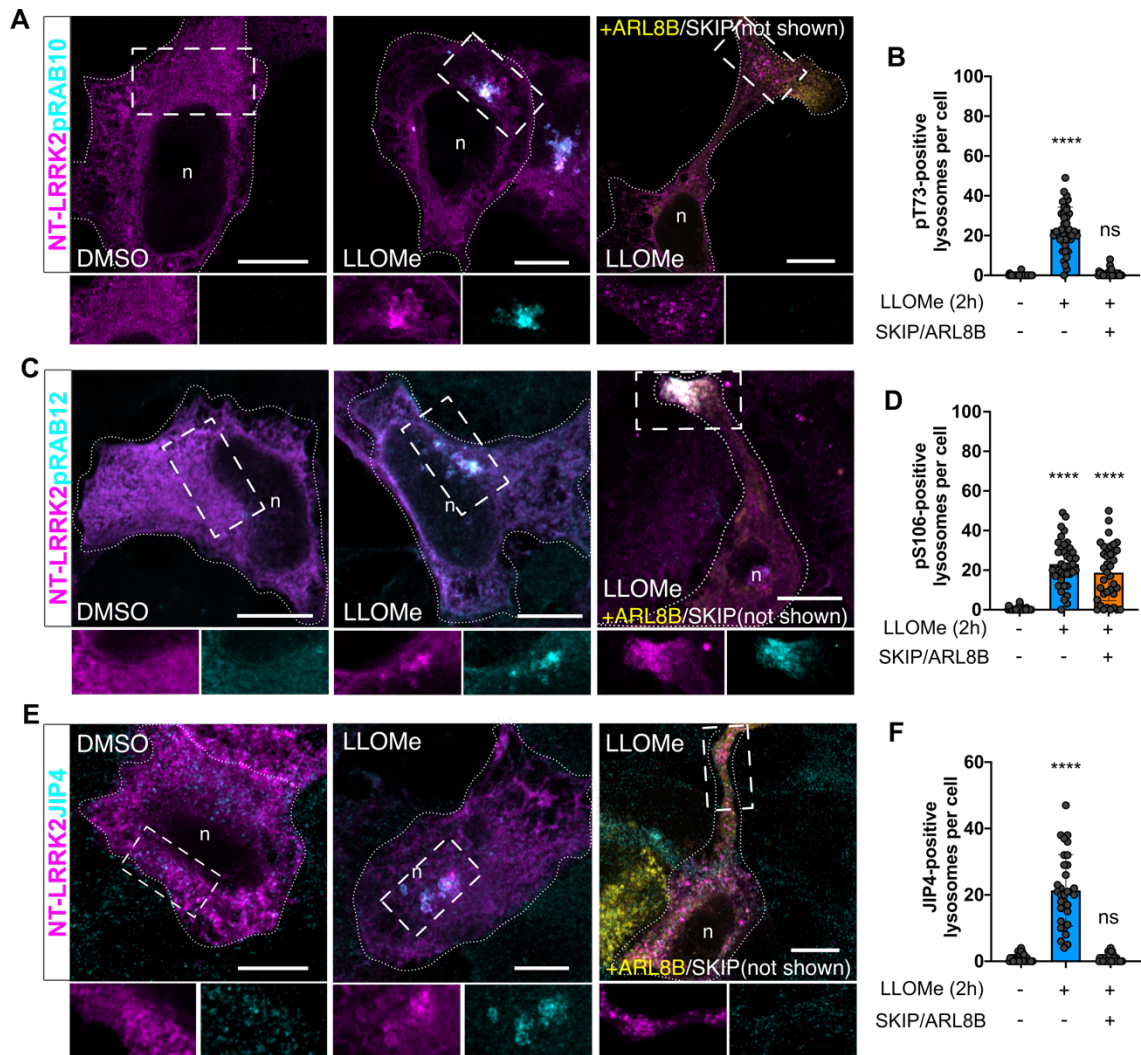
Figure 7.15. **Rabs phosphorylation and JIP4 recruitment to LRRK2-positive lysosomes via LLOMe.** Representative images of NT-LRRK2 (magenta) expressing HEK293FT cells with or without ARL8B (yellow) and SKIP (unstained) co-transfection (A, C, E). Cell outlines are drawn and 'n' denotes the nucleus. Scale bars= 10µm. Cells were treated with DMSO or LLOMe and stained for endogenous pRab10, pRab12, or JIP4 (cyan), of which lysosomal colocalization was counted (B, D, F). One-way ANOVAs were performed where ****p-value <0.0001. SD error bars are shown; n=40 cells across 3 technical replicates.

Furthermore, JIP4 recruitment to LLOMe-treated lysosomes was also

prevented by ARL8B and SKIP OE (Figure 7.15E-F), suggesting that JIP4

recruitment is limited to only pRab10-positive lysosomes, confirming that JIP4

is an effector of Rab10 but not Rab12. This observation also suggests that LYTL

cannot be activated at peripheral lysosomes (Bonet-Ponce et al., 2020). The use of NT-LRRK2 further confirms that pRab10-positive lysosome preference is not an artifact induced by the LYSO-LRRK2 chimera.

7.2.5 Lysosomal positioning influences pRab10 at endogenous LRRK2 levels in primary astrocytes

To evaluate whether the same effects can be seen with LRRK2 at endogenous levels, mouse primary astrocytes, of which contain high levels of LRRK2 expression (Bonet-Ponce et al 2020, Beilina et al 2020), were cultured and investigated. Acute LLOMe treatment for 4 hours significantly increased phosphorylated Rab10 at lysosomes compared to those treated with DMSO as counted by the number of pRab10-positive lysosomes per cell (Figure 7.16A-B), whereas ARL8B and SKIP OE resulted in a significant reduction in the number of pRab10-positive lysosomes, and minimal recruitment to peripheral lysosomes was observed (Figure 7.16A-B). The pRab12 antibody could not be validated in mouse cells, thus, pRab12 could not be interrogated using these cells.
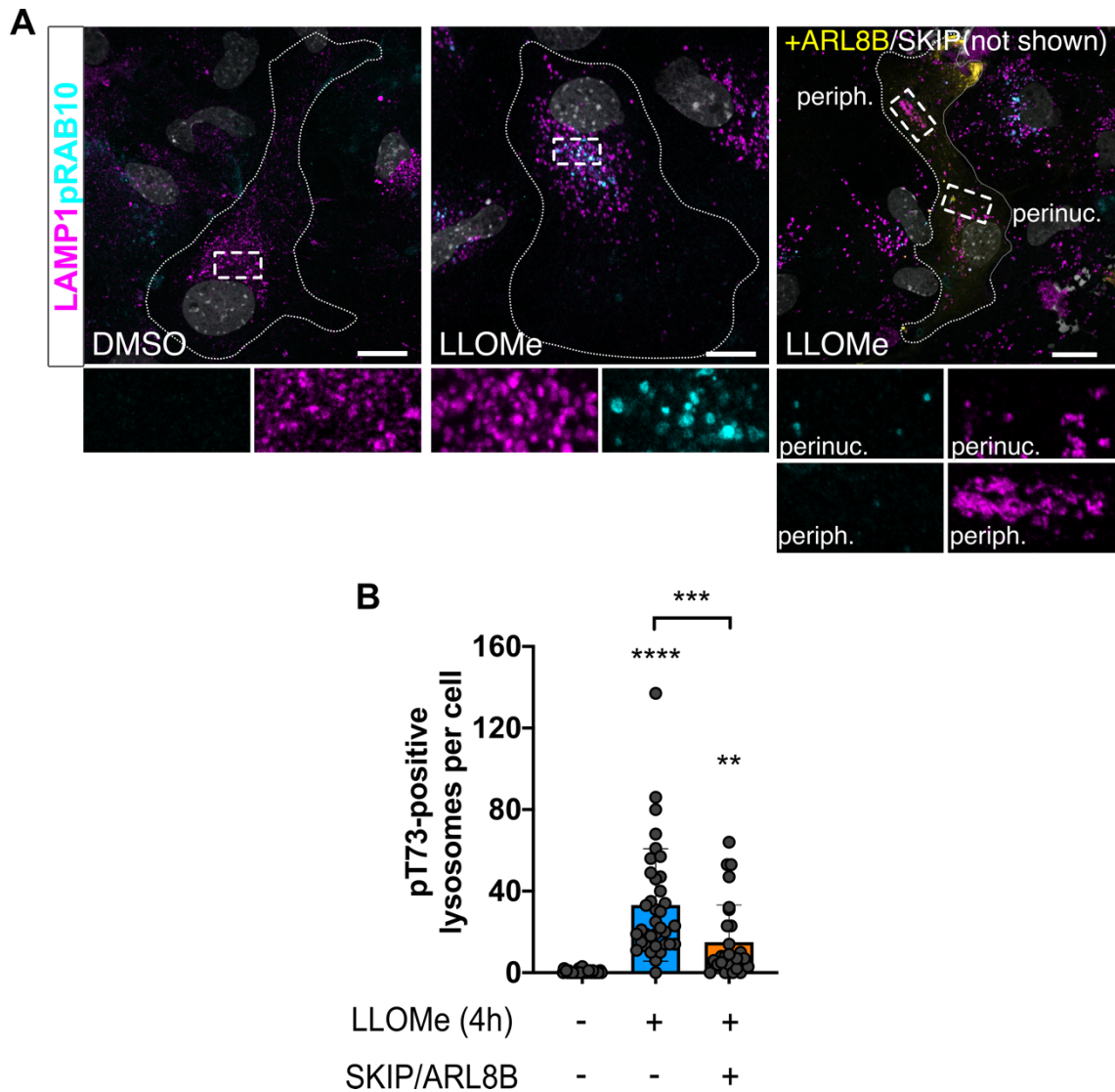
Figure 7.16. **Rab10 phosphorylation in primary murine astrocytes treated with LLOMe.** Cells were treated with DMSO or LLOMe and stained for LAMP1 (magenta) and pRab10 (cyan) (A) and number of pRab10-positive lysosomes were counted (B). Cell outlines are drawn and DAPI staining is shown in grey. 'periph' = periphery and 'perinuc' = perinuclear spatial locations. Scale bars= 10µm. One-way ANOVA was performed, where **p-value <0.01, ***p-value <0.001, ****p-value <0.0001. SD error bars are shown; n=40 cells across 3 technical replicates.

Taken together, these results indicate that LRRK2-dependent Rab10

recruitment to the lysosomal membrane is position-specific and is

recapitulated across multiple models including at endogenous levels of LRRK2.

7.2.6 Investigation of the role of PPM1H on LRRK2-dependent Rab10 phosphorylation

A recent siRNA screen identified the phosphatase PPM1H dephosphorylates T72 Rab8A and T73 Rab10, thus mitigating LRRK2 signaling (Berndsen et al., 2019). Of interest, exogenously expressed PPM1H is reported to be located at the Golgi (Berndsen et al., 2019), thus potentially having spatially restricted effects on cellular phosphorylation. Since only a subset of perinuclear LRRK2-positive lysosomes contained pRab10, I hypothesized that PPM1H might counteract LRRK2-dependent Rab10 phosphorylation on lysosomes in the perinuclear area. Knockdown of PPM1H using siRNA resulted in a significant increase in pRab10 signal on LYSO-LRRK2 lysosomes within the perinuclear region (Figure 7.17A-B). This was verified by Western blot, in which levels of pRab10 significantly increased in cells transfected with PPM1H siRNA compared to NTC control cells (Figure 7.17C-D). In constrast, Rab12 phosphorylation levels remained unchanged, confirming that PPM1H is not a Rab12 phosphatase (Figure 7.17C, E).
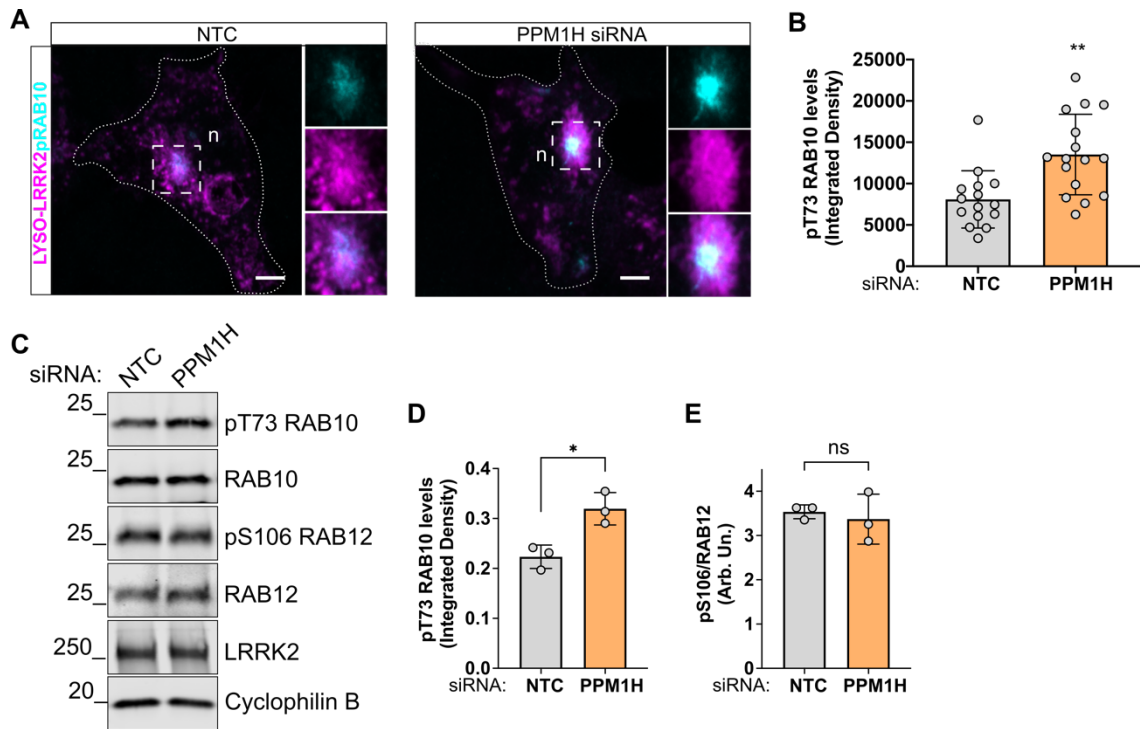
Figure 7.17. **PPM1H siRNA knockdown in HEK293FT cells.** Cells were subjected to NTC or PPM1H siRNA knockdown followed by transfection of LYSO-LRRK2 (magenta) (A). Cells were stained for pRab10 (cyan) (**A**) and integrated density was measured (**B**). Cell outlines are drawn, and 'n' denotes the nucleus. Scale bars= 10µm. Western blot analyses were done and pRab10 and pRab12 levels were measured (**C-E**). Unpaired student t tests were performed *p-value <0.05, **p-value <0.01. SD error bars are shown; in panel B n=15 cells across 3 technical replicates, in panels D-E n=3 technical replicates.

Strikingly, upon PPM1H knockdown, significant increases in the frequency of pRab10-positive lysosomal tubules were visualized (Figure 7.18A, C). Since LYTL is shown to be JIP4-dependent, endogenous levels of JIP4 were also stained in these cells, of which an increase of JIP4-positive tubules was noted (Figure 7.18B, D). This finding demonstrates that PPM1H limits pRab10 phosphorylation at the perinuclear lysosomes and thereby counteracts LYTL.
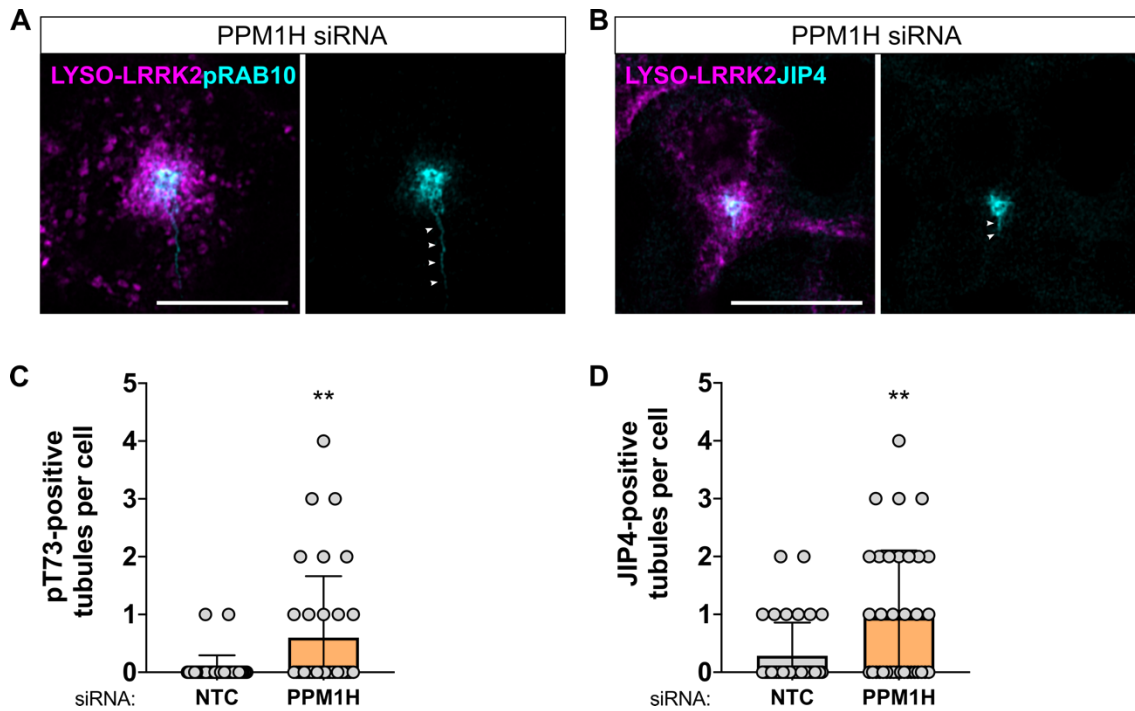
Figure 7.18. **Tubulation rates in PPM1H siRNA knockdown cells.** Representative images of PPM1H siRNA knockdown cells expressing LYSO-LRRK2 (magenta) and endogenous pRab10 (**A**) or JIP4 (**B**) (cyan). Number of pT73 Rab10- (**C**) and JIP4- (**D**) positive tubules were counted in NTC and PPM1H siRNA cells. Unpaired student t tests were performed where **p-value <0.01. SD error bars are shown; n=35 cells across 3 technical replicates.

7.3 Discussion

To understand the dynamics underlying LRRK2 membrane recruitment, activation, and Rab phosphorylation patterns, LRRK2, pRab10, and pRab12 were further investigated at two spatially and functionally distinct membrane organelles, lysosomes and early endosomes. Using newly cloned LRRK2-chimera plasmids, phosphorylated Rab localization patterns were visualized after LRRK2 was translocated to the lysosomal and early endosomal membranes. A striking difference in colocalization pattern between Rabs was observed, with pT73 Rab10 showing strict perinuclear localization in a subset

of lysosomes whereas pS106 Rab12 was found in LRRK2-positive lysosomes throughout the cell, whereas both pRabs were shown to colocalize with LRRK2 at nearly all LRRK2-positive early endosomes. Thus, the current work identifies a spatially dependent, lysosomal-specific mechanism through which LRRK2 recruits and phosphorylates Rab10. When LRRK2-positive lysosomes are pushed to the periphery via ARL8B and SKIP OE, Rab10 can no longer be recruited, in contrast to Rab12. In contrast, pRab10 colocalization to LRRK2 was significantly increased when lysosomes were clustered into the perinuclear region using LLOMe treatment or RILP OE. This phenomenon was also seen with knockdown of endogenous JIP4, revealing a novel role of JIP4 in LRRK2-dependent phosphorylation of Rab10 at lysosomes positioned near the nucleus in addition to its downstream role as a Rab10 effector for the initiation of lysosomal tubulation. Thus, there may be a possible feedforward signaling pathway where lysosomal positioning can be promoted by JIP4 to the perinuclear region that would then localize JIP4 for initiation of LYTL after phosphorylation of Rab10.

What has not been addressed here are the key conditions that determine spatial specificity of phosphorylated Rabs at lysosomes. Lysosomes are highly dynamic and transient organelles responsible for wide ranging cellular functions such as autophagy, nutrient response, cell growth and

migration (Cabukusta and Neefjes, 2018), and clustering lysosomes into the organelle-dense perinuclear cloud has been observed under various conditions of cellular stress and compromisation (de Martín Garrido and Aylett, 2020; Korolchuk et al., 2011). Cells are thought to relocalize lysosomes to the perinuclear area to provide optimal conditions for handling membrane damage, including transfer of undegraded materials to newly synthesized lysosomes, as well as to promote catalytic activity and induce lysophagy of damaged lysosomes. LYTL, exacerbated by LLOMe treatment, requires the recruitment and phosphorylation of Rab10 and its subsequent recruitment of JIP4 to induce tubulation (Bonet-Ponce et al., 2020). This may be beneficial to sort undegraded cargo to other active lysosomes for proper disposal. The current data collectively suggest that at least two conditions are required for pRab10/JIP4 presence on lysosomes: (1) LRRK2 must be active and recruited to lysosomes, and (2) LRRK2-positive lysosomes must be located near the nucleus. This suggests a complex regulation of signaling downstream of LRRK2 that involves multiple conditions and varies depending on which Rab is phosphorylated by LRRK2.

Recent work by Berndsen et al. identified T73 Rab10 as a substrate for PPM1H phosphatase, thus counteracting LRRK2-signaling (Berndsen et al., 2019). Here, knockdown of PPM1H significantly increased pRab10 signal as

well as pRab10- and JIP4-positive tubules on perinuclear lysosomes, while LRRK2-positive peripheral lysosomes were unaffected. PPM1H has been suggested to be resident to the Golgi, thus PPM1H can influence Rab10 phosphorylation events on nearby lysosomes. By extension, this suggests that as of yet unidentified phosphatases may influence Rab10 phosphorylation at peripheral lysosomes and that these phosphatases are likely to be highly active. Of note, Berndsen et al. reported that pS106 Rab12 was not influenced by PPM1H. If different phosphatases act on selected pRabs, the dissociation between the effects of lysosomal positioning between Rab10 and Rab12 may arise from the differential actions of these, again unidentified, phosphatases.

Overall, these results suggest that the presence of LRRK2 at a membrane is sufficient to trigger its activation, Rab phosphorylation and retention at membranes, and that Rab10-specific recruitment to lysosomes is, in part, controlled by lysosomal positioning. Further studies will be needed to identify the key proteins involved in determining optimal conditions for LRRK2-dependent Rab10 recruitment at the lysosomal membrane, including the description of novel phosphatases that can act on Rab12 as well as Rab10 at peripheral lysosomes.

8 GENERAL DISCUSSION

The ongoing clinical trials for LRRK2 kinase inhibitors and ASOs will, over the coming years, clarify whether targeting LRRK2 will be therapeutically advantageous in PD, opening up the possibility for treatment to be patient stratified based on mutations carried, risk status, and/or drug tolerance (Bandres-Ciga et al., 2020). In addition to those with specific LRRK2 mutations, studies have shown that enhanced LRRK2 kinase activity can also be found in patients with idiopathic PD and therefore suggest that LRRK2-modifying treatments may be useful to a broader scope of PD patients rather than mutation carriers only (Di Maio et al., 2018). We are now within the liminal space determining whether targeting LRRK2 has efficacy to either revert, halt, or slow disease progression. In conjunction, LRRK2 is a large, multidomain protein with the potential to affect multiple cellular pathways. Thus, identifying which pathway(s) lead to PD pathogenesis when this kinase is hyperactive will be critical for the efficacy of LRRK2-targeted therapies.

In this thesis, I attempted to address both LRRK2 therapeutic efficacy using a preclinical animal model, and downstream effects of LRRK2 kinase activity via Rab phosphorylation at membranes *in vitro*. Here, I will highlight key findings from this work as well as its limitations. Additionally, I will present

some open questions that remain from my findings and propose additional

experiments that will be useful in future investigations of LRRK2 function.

Finally, I will propose a potential mechanism of LRRK2-dependent cellular

dysfunction that could lead to PD pathogenesis.

8.1 Key findings and limitations

8.1.1 Rab10 phosphorylation does not correspond to LRRK2 kinase activity *in vivo* in G2019S KI mice

When assessing readouts for LRRK2 kinase activity and inhibition *in vivo*

via acute and chronic paradigms of MLi-2 treatment, S1292 LRRK2

autophosphorylation and S106 Rab12 phosphorylation were robust and

consistent readouts of both kinase hyperactivity and inhibition in G2019S KI

mice across brain and peripheral homogenates (Figures 3.3, 3.5, 4.4, 4.6).

Interestingly, T73 Rab10 phosphorylation did not correlate with either

hyperactivity of G2019S KI mouse nor kinase inhibition with MLi-2 treatment

(Figures 3.3, 3.5, 4.4, 4.6). This was particularly pronounced in the brain

compared to kidney and lung in acute dosing paradigms (Figures 3.3, 3.5). This

may be due to high expression, and thus inferring more activity, of PPM1H, a

Rab10 phosphatase, and low expression of LRRK2 in brain compared to other

peripheral tissues such as the lung (Figure 3.10). However, chronic in-diet

treatment for 10 weeks showed no correlation between LRRK2 kinase inhibition and Rab10 phosphorylation in any of the tissues examined (Figures 4.4, 4.6). These data suggest that there are complex regulatory mechanisms of LRRK2-dependent Rab10 phosphorylation that are distinct from Rab12 phosphorylation *in vivo*. Thus, pRab10 is not a reliable readout of neither kinase activity nor inhibition in G2019S KI mice.

The limitations here are particular to the preclinical model; mice do not get PD. Thus, whether these findings can be translated to human G2019S patients is uncertain, however, data from previous work using PD patient urinary exosomes and PBMCs have shown no effect on Rab10 phosphorylation in G2019S carriers (Wang et al., 2021; Wang et al., 2022). Conversely, T73 Rab10 phosphorylation is being used as a biomarker in clinical trials for BIIB122/DNL151, in which a press release informed of an "up to 50% reduction" of pRab10 in PBMCs, suggesting that perhaps this phosphorylation site can be utilized as a readout of kinase inhibition, although carrier status of the patients participating has yet to be disclosed (Denali Therapeutics Inc., 2021).

8.1.2 LRRK2-dependent Rab10 phosphorylation may be cell type-specific in brain

To further investigate brain-specific LRRK2-dependent Rab10 phosphorylation in G2019S KI mice, both region specificity and cell type specificity were tested. No differences in pRab10 signal were observed in the olfactory bulb, hippocampus, motor cortex, striatum, nor ventral midbrain tissues of animals treated with an acute dose of MLi-2 compared to untreated G2019S KI mice (Figure 3.8), suggesting that, regardless of Rab10 and LRRK2 pools in specific regions, LRRK2-dependent Rab10 phosphorylation is highly regulated in the brain, or alternatively, that Rab10 phosphorylation is not specifically LRRK2 dependent. When comparing primary astrocytes, microglia, and neuron cultures *in vitro*, pRab10 was significantly decreased with MLi-2 treatment in glial cultures whereas only a slight non-significant reduction was observed for neuronal cultures (Figure 3.9). This suggests that perhaps LRRK2 kinase is more influential on Rab10 phosphorylation in glia compared to neurons. A limitation here is that *in vitro* mechanisms may not translate *in vivo*, making it difficult to interpret these findings as truly physiological within the complexity of an *in vivo* system. However, as pRab10 levels are not enhanced in either PBMCs or urinary exosomes of PD patients harboring the G2019S mutation (Wang et al., 2021; Wang et al., 2022), the data reported in this thesis

gives some support to the idea that pRab10 is not a strong readout of LRRK2 kinase activity in a G2019S LRRK2 background across species. It would be of interest to assess pRab10 levels in human *post-mortem* brain tissue from G2019S carriers as well as peripheral tissues where LRRK2 expression is high to make a comparison between mouse models and humans. Regardless of the outcome of such experiments, pRab10 does not seem a useful biomarker in human of LRRK2 hyperactivity in a variety of matrices, including biofluids that would be the most straightforward to obtain from human subjects in clinical trials of LRRK2 kinase inhibitors.

8.1.3 Proteomics analyses reflect both therapeutic effects and dysfunction after chronic MLi-2 treatment in G2019S KI mice

Proteomics analyses of G2019S KI animals treated with MLi-2 for 10 weeks showed differences in multiple pathways and organelles across tissues. An enrichment for mitochondrial proteins were increased in the brains of G2019S mice compared to wildtype, which was reduced when G2019S mice were given MLi-2 treatment for 10 weeks (Figure 5.2). This suggests that subtle differences in G2019S KI animals may be ameliorated back to levels seen in wildtype animals. Of the proteins identified, increases in many proteins in the oxidative phosphorylation pathway as well as mitophagy signaling proteins like

cytochrome C (Cycs), ubiquinol-cytochrome c reductase core protein 1 and 2 (Uqcrc1/2), and voltage-dependent anion-selective channel protein 2 (VDAC2) were found in G2019S KI brains (Figure 5.2). This result complements a number of studies that have characterized mitochondrial dysfunction in G2019S LRRK2 cell models, including accumulation of ROS, increased mitochondrial DNA damage, and increased mitochondrial fragmentation and mitophagy (Wang et al., 2012; Niu et al., 2012; Angeles et al., 2014; Sanders et al., 2014; Pereira et al., 2014; Howlett et al., 2017). Interestingly, MLi-2 fed G2019S KI mice showed that alterations in these proteins were reversed back to levels resembling wildtype levels, suggesting LRRK2 kinase inhibitor can reduce mitochondrial dysfunction in hyperactivate kinase mutants *in vivo*. However, changes observed in the brains of G2019S KI mice given untreated chow were so mild that none were able to be validated via Western blot. Therefore, it is difficult to determine whether these subtle changes are strong enough to give rise to phenotypic differences in the brain. It is known that a decline in respiratory function is found in aged mammals (Trifunovic and Larsson, 2008). Thus, it would be interesting to determine how these proteins change in older G2019S mice, if at all. A follow up hypothesis would be that these mitochondrial pathways acquire more stress/damage with age, creating more pronounced mitochondrial defects in older mice. Additionally, since the brain is so complex with highly specific functionalized regions and cell types,

using whole brain homogenates for the proteomics analyses more than likely masked alterations affected by both the G2019S KI genotype as well as LRRK2 inhibition, as implied by some of the presented data in cultured primary cells. The inclusion of scRNA-seq would have been a valuable addition to the experimental design in order to obtain cellular resolution in brain. A caveat to applying scRNA-seq here is that there is little direct evidence to date that LRRK2 has measurable effects on transcriptional programs, thus alterations observed may be indirect. However, pathway analyses could still be identified in separate cell types and later validations could be followed up at the protein level.

Total proteins within endolysosomal trafficking pathways and lysosomal hydrolases were significantly altered in G2019S KI kidneys treated with MLi-2 for 10 weeks and these changes overlapped with those seen in LRRK2 KO kidneys (Figure 5.4). Increases in lysosomal enzymes Legumain, beta-galactosidase (Glb1), and glucosamine (N-acetyl)-6-sulfatase (Gns) have been identified in the kidneys of LRRK2 KO mice (Pellegrini et al., 2018), suggesting that LRRK2 kinase inhibition recapitulates some phenotypes found in LRRK2 KO mice. Interestingly, these proteins were not significantly altered between G2019S KI and wildtype mice fed untreated chow, thus they appear to be sensitive only to kinase inhibition. This study was limited by the amount of MLi-

2 compound available and some appropriate controls were left out. It would have been useful to have MLi-2 treated groups in wildtype and LRRK2 KO mice as well to distinguish effects from the hyperactive mutation and drug treatment itself.

Furthermore, the age of mice chosen for the in-diet dosing experiments started at 3 months old and extended to 5.5-6 months old. This age range covers the start of adulthood in mice. It may have been more informative to start MLi-2 treatment in an aged cohort such as 9 months old, with endpoint then being 11.5-12 months old. As aging is a risk factor for PD, studying G2019S hyperactivity and inhibition in an older cohort may have revealed stronger phenotypes across all tissues examined.

8.1.4 Membrane proximity and not membrane identity is required for LRRK2 kinase activation and Rab phosphorylation

Since the largest effects of kinase inhibition were identified within the endolysosomal organelles in the kidneys of G2019S KI mice, FRB-tagged resident proteins targeting membranes within the endolysosomal pathway were generated along with FKBP-LRRK2 in order to interrogate how LRRK2 kinase activity affects phosphorylation of Rab10 and Rab12 at endolysosomal

membranes. Direction of LRRK2 to membranes resulted in activation of LRRK2 kinase as well as accumulation of both Rab10 and Rab12 at every membrane as determined by S1292 autophosphorylation and Rab phosphorylation, respectively. These results suggest that LRRK2 redirection to any membrane is sufficient to enhance its kinase activity and phosphorylation of Rabs regardless of membrane identity. A limitation of these experiments is that quantitative comparisons of these phosphorylation readouts between each trap are difficult to make. Since so many different traps were used, transfection efficiencies between them will vary by chance and by size of each construct. Additionally, some of the traps produced more artifacts than others which may also affect comparison of phosphorylation between conditions. Therefore, no conclusion could be made on whether some membranes enhanced LRRK2 activity more than others.

8.1.5 Differential patterns of phosphorylation are seen between Rab10 and Rab12 in the context of mutant LRRK2

Within the context of R1441C, Y1699C, and G2019S LRRK2 mutants, Rab10 phosphorylation was further enhanced once LRRK2 was directed to either lysosomal or Golgi membranes compared to the cytosol using the FKBP-FRB trap system. Surprisingly, Rab12 phosphorylation was not enhanced with

LRRK2 translocation suggesting separate mechanisms for LRRK2-dependent phosphorylation of Rab10 and Rab12 or differences in Rab stabilization at the membrane. Immunocytochemistry experiments could have been performed alongside the Western blots to confirm membrane localization of these pRabs for each mutant condition.

8.1.6 Rab10 is present at a subset of LRRK2-positive lysosomes that is position dependent, whereas Rab12 is present at most LRRK2-positive lysosomes

Further interrogation of LRRK2 at the lysosome using the lysosomal targeting sequence of LAMTOR1 resulted in differing pRab localization patterns, where pRab10 was present in only a subset of lysosomes located within the perinuclear cloud, whereas pRab12 was found in most LRRK2-positive lysosomes. This suggests that Rab10 may have a specialized function at certain lysosomes that are clustered around other lysosomes and organelles and that there are optimal conditions present at these lysosomes that allow Rab10 accumulation compared to lysosomes at the periphery. In experiments overexpressing ARL8B and SKIP or following JIP4 knockdown, most lysosomes were sequestered to the periphery of the cell in long processes. Under these conditions, pRab12 was shown to still accumulate on LRRK2-positive

lysosomes, whereas pRab10 did not. This suggests that lysosomal positioning

is important for LRRK2-dependent Rab10 accumulation and phosphorylation.

This phenomenon appeared to be preferential to lysosomes, as pRab10

was found at most LRRK2-positive early endosomes when using the EE-LRRK2

chimera. However, whether this is a lysosomal specific event cannot be

inferred without investigation with other chimera constructs. In particular, I

attempted to make Golgi chimeras but was unsuccessful, as four of these

constructs were not functional, such that the plasmid was degraded within the

cell after translation or was never translated to begin with. In addition, using a

different cell type, such as U2OS cells, could have yielded greater insights from

these imaging experiments in place of HEK293FT cells, as they are much larger

and flatter with larger lysosomes. This would give more clarity, especially within

the perinuclear area where multiple organelles are overlayed.

8.1.7 PPM1H activity regulates LYTL

PPM1H has recently been identified as a phosphatase that counteracts

LRRK2-dependent phosphorylation of Rab10 (Berndsen et al., 2019). In my

thesis work, I found that PPM1H knockdown resulted in a significant increase in

pRab10- and JIP4-positive lysosomes in cells expressing the LYSO-LRRK2

chimera. This suggests that PPM1H can regulate LYTL via counteracting

LRRK2-mediated Rab10 phosphorylation. However, this can only be inferred, as the enzymatic activity of PPM1H has not been measured in HEK293FT cells. An additional experiment in which a PPM1H inhibitor is used prior to staining the cells for pRab10 and JIP4 would be useful in confirming the effects of PPM1H activity in LRRK2-mediated Rab10 phosphorylation.

8.2 Open questions and future work

The data presented in this thesis raise several important questions, namely, in both LRRK2-targeting therapeutics as well as LRRK2 biology in the context of PD pathogenesis. I will attempt to address these questions here and propose future experiments that could be useful in the pursuit of answering these questions.

How does Rab10 and Rab12 phosphorylation respond to LRRK2 inhibition in the context of a GTPase LRRK2 mutation, such as R1441C KI mice?

One recent study showed that Rab10 phosphorylation was robustly increased in the kidneys and lungs of R1441C KI mice compared to wildtype and G2019S KI mice tissues (Iannotta et al., 2020). This suggests that preferential Rab phosphorylation profiles may exist following different LRRK2 mutations. It would then be interesting to test whether LRRK2 inhibition has a

strong effect on Rab10 phosphorylation in R1441C KI animals in both acute and chronic paradigms. If this is true, we could clinically consider different Rabs as readouts of LRRK2 kinase activity and inhibition in patients carrying different LRRK2 mutations.

How is LRRK2 physiologically signaled to the lysosomal membrane?

Based on previous work that introduced lysosomal stressors to the cell, LRRK2 has been shown to be recruited to damaged lysosomal membranes (Eguchi et al., 2018; Herbst et al., 2020; Bonet-Ponce et al., 2020). The exact mechanism for how LRRK2 is recruited to lysosomes and, more generally, to any membrane is still unknown. One hypothesis is that perhaps a change in membrane curvature signals LRRK2 recruitment. Under lysosomal stress many studies have shown morphological changes such as swelling of the lysosome (Hasan et al., 2008). Some elegant studies using vertical nanostructures such as nanopillars of varying diameters to manipulate membrane curvature have shown that clathrin and dynamin-2 accumulated around the nanostructure-induced membrane deformation and increased clathrin-mediated endocytosis (Dalby et al., 2004; Lou et al., 2018). Additionally, other curvature sensing proteins have been found to play roles in autophagy (Nguyen et al., 2017). Although LRRK2 does not contain a canonical curvature-sensing domain, it may interact with a protein that does contain a curvature-sensing domain that

is already present at the membrane or work in a non-canonical way that is yet to be determined. Thus, experiments using lysosomal stressors followed by Focused Ion Beam Scanning Electron Microscopy (FIB-SEM) could be examined for lysosomal membrane bulging which can be correlated with LRRK2 presence.

What prevents Rab10 accumulation and phosphorylation at peripheral lysosomes?

As OE work has characterized PPM1H as a Golgi resident protein (Berndsen et al., 2019), regulation of LRRK2-mediated Rab10 phosphorylation by this protein is restricted to the perinuclear region. Thus, it will be important to uncover the mechanism that counteracts Rab10 phosphorylation specifically at peripheral lysosomes. One possibility is that additional, more active phosphatases located in the periphery are allowing the quick removal of Rab10 from these lysosomes and preventing its accumulation. Thus, additional screens might be helpful in order to identify these phosphatases. Secondly, it is possible that perinuclear lysosomes are labeled with a GDF that Rab10-bound GDI recognizes that peripheral lysosomes lack. To identify perinuclear-specific lysosomal surface proteins, a proteomic screen could be done in which APEX2-Rab10 construct could be co-expressed with the LYSO-LRRK2 chimera and proteins within 10nm from APEX2-Rab10 would be labeled upon

treatment with biotin. Hits could then be validated and peripheral versus

perinuclear distribution could be assessed through immunocytochemistry.

How do mutant lyso-chimeras affect Rab spatial recruitment and

phosphorylation?

Utilizing lyso-trap constructs, phosphorylation of Rab10 and Rab12

levels were increased in LRRK2 mutants compared to wildtype in Western blot.

It would be useful to visualize these pRabs at the lysosomal membrane to

determine how LRRK2 mutants effect pRab localization. To do this, mutant

LYSO-LRRK2 constructs can be made through mutagenesis of the wildtype

construct. This set of experiments would be useful in evaluating differences in

pRab accumulation on lysosomes when in the presence of a hyperactive LRRK2

kinase, and may give additional insight into LRRK2 function at lysosomes.

Are LYTL tubules Rab12-positive?

The work presented in Chapter 7 suggests that LRRK2 presence on

some lysosomes is enough to recruit Rab10 and subsequent JIP4 to initiate

tubulation. Our previous study characterizing this pathway also determined

that these tubules are pRab10 and JIP4-positive, but LRRK2-negative (Bonet-

Ponce et al., 2020). Bonet-Ponce et al. demonstrated with a T73A phospho-

null Rab10 construct that JIP4 presence and tubulation are dramatically

reduced in the presence of LLOMe treatment. The phospho-null version of Rab35 gave the same results, suggesting that other Rabs can interact with JIP4 to initiate tubulation (Bonet-Ponce et al., 2020). It will be interesting to determine which Rab substrates can interact with JIP4 by creating other phospho-null constructs and testing JIP4 recruitment at the lysosome. Additionally, Rab presence on these tubules differed, as endogenous Rab35 staining was restricted to the lysosomal membrane but was not found on the tubules (Bonet-Ponce et al., 2020). This suggests a specific function of Rab10 on tubules that succeeds JIP4 recruitment. Currently, no other Rab substrates have been tested for tubule presence. Thus, it would be interesting to stain for other Rabs such as Rab8a and Rab12 in LYSO-LRRK2 expressing cells to determine whether these proteins are also on tubules or if they are restricted to the mother lysosomal membrane like that of Rab35. Separating these pools of Rabs would be important to delineate additional roles in the tubulation process after formation.

What phosphatases recognize Rab12 as a substrate?

Visualization of pS106 Rab12 showed colocalization with most LRRK2-positive lysosomes in LYSO-LRRK2 expressing cells. Previous work has already shown that Rab12 is not a substrate for PPM1H (Berndsen et al., 2019), thus, it would be important to determine which phosphatase de-phosphorylates

Rab12 via siRNA screen of known phosphatases. Based on the data presented in this thesis, I would hypothesize that a Rab12-recognizing phosphatase is not very active *in vivo* and *in vitro*, thus giving LRRK2 kinase more control over the phosphorylation status of Rab12 compared to Rab10.

Is JIP4 able to induce tubulation at other membranes besides lysosomes?

Using the FKBP-FRB traps, we have recently shown that JIP4 can also be recruited to membranes other than lysosomes, including early and recycling endosomes (Kluss et al., 2022a). Thus, it would be interesting to determine if JIP4 can initiate tubulation at these membranes as well. These traps can be used prior to PPM1H siRNA knockdown to increase the amount of tubulation as seen in Chapter 7. This would determine whether LRRK2-driven tubulation can be generalized to other membranes, or if LYTL is indeed specific to lysosomes only.

Are pRab patterns cell type specific in the human brain?

As shown in Figure 3.9 of this thesis, LRRK2 inhibitor treatment affected Rab10 phosphorylation most in G2019S KI glial primary murine cells compared to neurons. This suggests that LRRK2 influence on Rab10 phosphorylation may vary across cell types in the mouse brain. It will be interesting to repeat this experiment to include R1441C and wildtype primary cells to distinguish

differences in LRRK2-mediated Rab phosphorylation within each genotype, as well as to probe for pT71 Rab29 and pS106 Rab12. Furthermore, our lab has recently created a series of isogenic IPSC lines with the most common mutations and risk variants of LRRK2 (Beylina et al., 2021). Thus, it would be useful to confirm whether LRRK2-dependent Rab phosphorylation differs across human brain cell types by differentiating these iPSC lines into microglia, astrocytes, and neurons. These results will help clarify LRRK2 function through Rabs in different brain cells.

8.3 Hypothetical model leading to PD pathogenesis

Based on the key findings presented in this thesis, I would propose the following model for LRRK2-driven PD pathogenesis (Figure 8.1):
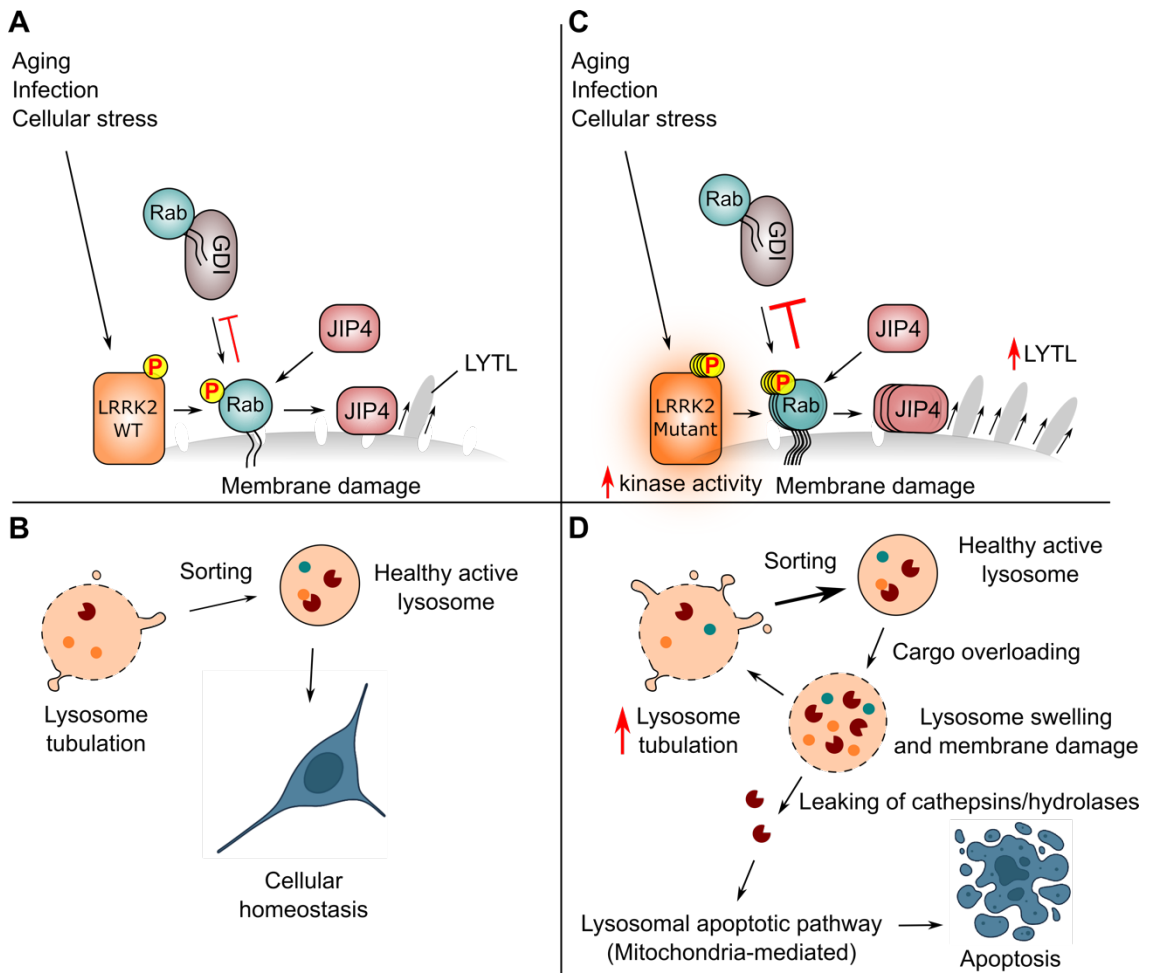
Figure 8.1. **Hypothetical model of LRRK2-mediated cell death via lysosomal stress.** Signaling of wildtype LRRK2 to damaged lysosomes via cellular stress, aging, or infection leads to recruitment and phosphorylation of Rabs that recruit JIP4 to initiate lysosomal tubulation (LYTL) (**A**). This mechanism allows compromised lysosomes to sort undegraded materials to healthy lysosomes to maintain cellular homeostasis (**B**). Under conditions of where mutant LRRK2 is present, overactive LYTL causes overburdening of healthy lysosomes and induces additional stress (**C**). Over time, this may cause cell death through the lysosomal apoptotic pathway mediated by mitochondria (**D**).

In this thesis, inducible models of membrane-bound LRRK2 were created which revealed that LRRK2 kinase activity is enhanced merely by membrane presence, and most likely without any influence of specific membrane proteins. Directing LRRK2 to membranes along the endolysosomal pathway resulted in increased Rab10 and Rab12 phosphorylation revealing a potentially broad mechanism of trafficking mediated by Rab phosphorylation. When using a non-targeting LRRK2 construct, the addition of LLOMe resulted in LRRK2 translocation from the cytosol to the lysosomal membrane suggesting that lysosomal stress signals LRRK2 recruitment and LRRK2-mediated downstream events for initiation of tubulation. These results lead me to propose that LYTL is a stress response (Figure 8.1A).

Live imaging experiments published previously revealed that JIP4-positive lysosomal tubules form vesicles via scission events that make contact with other, CTSB-positive lysosomes (Bonet-Ponce et al., 2020). This finding suggests that the LRRK2-dependent stress response works to redistribute either lipids and/or proteins of damaged lysosomes to active ones that can then perform degradative turnover of these cargo. When ARL8B and SKIP are overexpressed and lysosomes are sequestered to the cell periphery, pRab10 does not accumulate at LRRK2-positive lysosomal membranes, affecting JIP4 recruitment and LYTL (Chapter 7). Thus, perinuclear lysosomal positioning is

necessary for LYTL to take place efficiently. Studies characterizing lysosomal dynamics have demonstrated that lysosomes are the most hydrolase- and enzyme-rich when within the perinuclear cloud, as trafficking of new enzymes takes place here. Alternatively, lysosomes shuttled into the periphery are believed to be pooled as a reserve when needed in situations of cellular stress to maintain homeostasis (Pu et al., 2016; Cabukusta and Neefjes, 2018). Therefore, the data presented in Chapter 7 of this thesis reveals a LRRK2-dependent mechanism that requires lysosomal repositioning to the perinuclear area as a stress response. The proposed hypothesis is that LYTL is constricted to the perinuclear area where tubules containing undegraded proteins and lipids from damaged lysosomes can be sorted to healthier, active lysosomes efficiently (Figure 8.1B).

Under conditions of hyperactive LRRK2 kinase mutants, this pathway is exaggerated (Figure 8.1C). Data from Chapter 6 showed increases in Rab phosphorylation in the presence of mutant LRRK2 where kinase activity is enhanced. Biochemical studies have deduced that wildtype and G2019S LRRK2 show similar rates of membrane localization compared to the cytosol, whereas ROC/COR domain mutants are accumulated at membranes to a greater extent¸ (Berger et al., 2010; Nichols et al., 2010). This is in line with the observation that LRRK2-dependent Rab phosphorylation is greatest with

ROC/COR domain mutants (Figures 7.4, 7.5) (Steger et al., 2016). Thus, with more LRRK2 accumulation, one would expect more pRab accumulation as well. The mechanism stabilizing pRabs on the lysosomal membrane is therefore increased in both kinase and ROC/COR mutations and promotes increased recruitment of JIP4. This recruitment would result in a shift toward earlier tubulation and sorting, perhaps even prematurely, although time course experiments would need to be performed in order to test this. Increased sorting of undegraded materials may then cause stress in otherwise healthy lysosomes, perpetuating lysosomal damage that the cell cannot maintain. It has been established that cellular stress causes lysosomes to swell and leak their contents into the cytosol (Amaral et al., 2018; Hämälistö et al., 2020). Once in the cytosol, proteins such as cathepsins set off a signaling cascade, cleaving BH3-interacting domain death agonist (BID) to promote an oligomorphic complex that is transferred to the outer mitochondrial membrane (Zhu et al., 2017). This causes Cytochrome C release into the cytosol that initiates caspase-dependent apoptosis (Zhu et al., 2020) (Figure 8.1D). In the proteomic data presented in Chapter 5, non-glycosylated LAMP1 was significantly increased in G2019S KI mice compared to wildtype. This may suggest an upregulation in LAMP1 translation to synthesize more healthy lysosomes, as glycosylation of LAMP1 occurs in the rough endoplasmic reticulum before reaching the lysosome. Bulk RNA sequencing will be useful in

determining whether there is an upregulation of translation of lysosomal

integrity proteins in G2019S KI mice.

The most recent PD GWA study identified many risk loci with an

enrichment of lysosomal genes nominated as the most likely hit, including

TMEM175, GALC, and CTSB (Nalls et al., 2019). Other lysosomal genes have

already been confirmed as the risk factor or causal gene such as GBA1 and

ATP13A2, respectively. Thus, it would be reasonable to hypothesize that the

impact of LRRK2 on PD pathogenesis is also mediated through lysosomal

dysfunction. Since PD is characterized by a selective loss of dopaminergic

neurons, it will be critical to evaluate LYTL within striatal and SN regions in

animals harboring kinase hyperactive mutants to discern how this leads to PD

pathogenesis. Although the current literature provides conflicting data on

whether LRRK2 is expressed in dopaminergic neurons, the data presented in

this thesis showed that LRRK2-dependent Rab10 phosphorylation was

strongest in glial cultures. Thus, it is possible that the glia cells within the locus

coeruleus, striatum and SN regions are more effected by a LRRK2 mutation

and that this contributes to dopaminergic cell loss. Previous studies have

shown that glial cells play critical roles in maintaining homeostasis in neurons

(Rasband, 2016; Mederos et al., 2018). One of these ways is by providing

waste removal from neurons. Thus, I would hypothesize that mutant LRRK2

perpetuates lysosomal stress within glia, which can be compounded by external neuronal stress from dopaminergic neurons. Dopaminergic neurons are already more prone to apoptosis due to the nature of dopamine metabolism in aging, thus glia within regions where these neurons are enriched may already have a higher load of stress to maintain. Overstressed glial cells then would provide less support for the already compromised dopaminergic neuron population, lending to the selectivity of these neurons in PD pathogenesis.

CONCLUDING REMARKS

Taken together, the work presented in this thesis underscores the downstream effects of both LRRK2 kinase hyperactivity and inhibition *in vivo* and *in vitro*, and the differential effects of LRRK2-mediated Rab phosphorylation at lysosomes. I additionally identified a novel role of lysosomal positioning in the regulation of LRRK2-dependent Rab10 phosphorylation. As proteomics analysis revealed that kinase inhibition made the largest alterations in endolysosomal proteins, it is worth exploring this pathway in greater detail both generally and in the context of PD.

9 MATERIALS AND METHODS

Animals: All animal procedures were performed in accordance with a protocol

approved by the Institutional Animal Care and Use Committee of the National

Institute on Aging, NIH. Wildtype, G2019S LRRK2 KI, and Lrrk2 KO male and

female mice raised on a C57Bl/6 background were bred in-house on a 12-

hour day/night cycle for the following experiments. All mice were supplied with

Rodent NIH-07 diet and water _ad libitum_. Based on our previous data on

S1292 dephosphorylation in G2019S LRRK2 brain following acute MLi-2

treatment (Kluss et al., 2018), $N = 4$ mice was used in this study for dose

response and time course of acute MLi-2 experiments, as it was estimated at

90% power to detect a difference of effect size 6 at alpha = 0.05. $N = 6$ mice

was used for evaluating the effect of acute LRRK2 kinase inhibition on pRabs

across brain regions as well as for in-diet MLi-2 chronic treatments. All oral

gavages needed in the acute treatment experiments were performed by Dr.

Melissa Conti Mazza.

Dose-response: 28 homozygous G2019S KI C57BL/6 J mice (5–8 months old)

were randomized for treatment using the sample function in R, followed by

matching for sex across groups. Mice were given an acute dose of vehicle

[40% (w/v) Hydroxypropyl-ß-Cyclodextran] or MLi-2 (at 1, 3, 10, 30, 60, or 90 mg/kg dissolved in vehicle) via oral gavage and euthanized 1 hour after treatment. All tissues removed were flash frozen and stored at -80 degrees Celsius prior to homogenization for Western blot.

Time-course: 28 homozygous G2019S KI C57BL/6 J mice (4–7 months old) were randomized for treatment using the sample function in R, followed by matching for sex across groups. Mice were given an acute dose of vehicle [40% (w/v) Hydroxypropyl-ß-Cyclodextran] at time point zero, or MLi-2 (10 mg/kg dissolved in vehicle) via oral gavage and euthanized after time point 0.5, 1, 3, 12, 24, or 72 hours post dose. All tissues removed were flash frozen and stored at -80 degrees Celsius prior to homogenization for Western blot.

10-day dose-response: Three-month old homozygous G2019S LRRK2 KI mice were given customized Rodent NIH-07 chow from Research Diets, either untreated or supplemented with various doses of MLi-2 at 10, 30, or 60 mg/kg/day for 10 days. Untreated wildtype mice were also included to determine the appropriate concentration of MLi-2 necessary to reduce the hyper kinase activity of G2019S LRRK2 back to wildtype levels, using S1292 autophosphorylation as a readout of kinase activity. N=3 mice were used per treatment group. Mice and chow were weighed daily to assess estimated

doses of MLi-2 received each day. No difference was observed in food intake between mice receiving MLi-2 treated chow and mice receiving untreated chow. All mice were given chow and water *ad libitum*. After 10 days, mice were euthanized 2-3 hours post start of their light cycle.

Ten day (short-term) and 10 week (long-term) chronic cohorts: Three-month old littermates from wildtype, homozygous G2019S LRRK2 KI, and homozygous LRRK2 KO litters were randomized into short-term (10 days) and long-term (10 weeks) chronic treatment groups. Wildtype, G2019S LRRK2 KI, and LRRK2 KO groups received untreated chow, and an additional G2019S LRRK2 KI group received chow supplemented to achieve an approximate dose of 60 mg/kg of MLi-2 per day. Both male and female mice were represented equally in all treatment groups. *N*=6 mice were used per treatment group. All mice were given chow and water *ad libitum*. After 10 days, or 10 weeks, mice were euthanized 2-3 hours post start of their light cycle.

Primary cultures: P0-P2 litters from G2019S KI C57BL/6 J mice were euthanized via head decapitation. Brains were extracted and meninges removed. For astrocyte and microglia cultures, cortices were triturated in cold DMEM/F12 (Gibco) with a 5mL pipette. 10μL per brain of trypsin at 2.5mg/ml working concentration was added and incubated for 5 minutes at 37 degrees Celsius.

4μL per brain of DNase at 0.3mg/ml working concentration was then added, mixed, and incubated for 2 minutes at room temperature (RT) prior to additional trituration. Brain homogenates were then spun down at 500 x g for 5 minutes. The supernatants were aspirated and fresh DMEM/F12 supplemented with 10% Fetal Bovine Serum (Gemini) and 1% penicillin/streptomycin (Gibco) was used to resuspend the cell pellets and three brains per T175cm^2 flask were plated. Media was changed every three days. Around 12-14 days, flasks were shaken to separate microglia from astrocytes and microglia were replated for experiments into 6-well plates at 200,000 cells per well. Astrocytes were trypsinized from the remaining T175cm^3 flasks and plated into 6-well plates at 100,000 cells per well. For neuronal cultures, cortices were placed in ice cold HBSS and digested with papain for 30 minutes with mixing every 10 minutes. The brain slurry was then spun down at 200g for 3 minutes and the supernatant aspirated. 10mL of fresh media was added (Basal Medium Eagle (Gibco), 1% glucose (Gibco), 1% Glutamax (Gibco), 1% penicillin/streptomycin (Gibco), 1% N-2 (Gibco), 5% B-27 (Gibco) and pelleted tissue resuspended. DNase was then added and the mixture is triturated ~40x with a 5mL pipette and spun down at 200g for 6 minutes. The supernatant was then aspirated and fresh media added that was additionally supplemented with 5% FBS. Cells were counted and plated at 1.5×10^6 per well of a 24-well plate. Cycloarabinoside was added the next day

(0.005% working concentration). Media was changed once per week for 10 days until used for biochemical assays.

Cell culture: HEK293FT cells and primary astrocytes were maintained in DMEM, or DMEM/F12, respectively, containing 4.5 g/l glucose, 2mM l-glutamine, 1% Pen/Strep and 10% FBS at 37°C in 5% CO_2. For immunocytochemistry experiments, cells were seeded on 12mm coverslips pre-coated with Matrigel. For Western blot experiments, cells were seeded on 24-well plastic plates pre-coated with Matrigel.

Cloning: FKBP sequence was cloned into 3xFLAG-pDEST and mScarlet-pDEST vectors using IN-FUSION HD cloning technology (Clontech, Takara, cat #638920) by Dr. David Hauser and Dr. Luis Bonet-Ponce. LRRK2-Wildtype, LRRK2-R1441C, LRRK2-Y1669C, LRRK2-K1906M and LRRK2-G2019S, previously cloned into pCR™8/GW/TOPO™ vectors (ThermoFisher, cat #250020) by Dr. Elisa Greggio and Dr. Alexandra Beilina, were transferred into the 3xFLAG-FKBP-pDEST and mScarlet-FKBP-pDEST plasmids using Gateway technology (ThermoFisher, cat #11791043). CFP-FRB-LAMP1 vector (Willett et al., 2017) was a gift from Rosa Puertollano (NIH). EHD1-FRB-GFP was kindly provided by Tsukasa Okiyoneda (Kwansei Gakuin University). PM-FRB-CFP (Addgene plasmid #67517) (Varnai et al., 2006), iRFP-FRB-RAB7 (Addgene

plasmid #51613) and iRFP-FRB-RAB5 plasmids (Addgene plasmid #51612) (Hammond et al., 2014) were gifts from Tamas Balla (NIH). FRB-ECFP-Giantin was a provided by Dorus Gadella (Addgene plasmid #67903) (van Unen et al., 2015). LYSO-LRRK2 was created by Dr. Luis Bonet-Ponce by adding the N-terminal domain of the LAMTOR1 sequence (1-39 amino acids) onto the N-terminus of the 3xFLAG-LRRK2 plasmid using IN-FUSION HD cloning technology (LAMTOR1(1-39)-3xFLAG-LRRK2). FYVE-LRRK2 was created by cloning the FYVE-CC2 targeting sequence of HRS into a 3xFLAG pDEST using IN-FUSION HD cloning technology. NT-LRRK2, previously cloned into a pCR™8/GW/TOPO™ vector (ThermoFisher, cat #250020) by Dr. Elisa Greggio and Dr. Alexandra Beilina, was then transferred into the new 3xFLAG-FYVE-CC2-pDEST using Gateway technology (ThermoFisher, cat #11791043). The mCherry-ARL8B and 2xMyc-SKIP plasmids were a generous gift from Juan S. Bonifacino (Keren-Kaplan and Bonifacino, 2021). The EGFP-RILP plasmid (Addgene plasmid #110498) (Mainou and Dermody, 2012) was a gift from Terence Dermody.

Transfection and siRNA knockdown: Transient transfections of HEK293FT cells were performed using Lipofectamine 2000 in Gibco's Opti-MEM (ThermoFisher, cat #31985088) and incubated for 24 hours prior to fixation or lysis. For siRNA knockdown experiments, Rab29, JIP4, PPM1H, or non-

targeting control siRNA (Dharmacon) were transfected using Lipofectamine RNAiMAX (ThermoFisher, cat #13778075) and cells were incubated for 48 hours prior to fixation or lysis. Transfection of primary astrocytes was performed using Lipofectamine Stem Reagent (ThermoFisher, cat #STEM00015) and incubated for 48 hours before fixation. The siRNA sequences are provided below.

SMARTpool siRNA sequences:

RAB29 – UCCCAGGACAGCUUCAGCA, ACACUACAAGUCCACGGUG, UGCUCUGAAGGUUCUCCAG, GUCUGACUACGAGAUAGUG

JIP4 – CCAGGAAACUAGAAAUGUA, GCAAACACAUUGAAGUACA, GUACAAACAGGUAACCAAU, GGAUAUAAAGGUUCAAGCA

PPM1H – CGAGAGAGGAGUUCAUAUA, CAGAUGAUCCUCACAGGUA, GGAAGAGCACACACAAUGA, GAGGAUGGCGGAUAUCUAA

In vitro reagents and treatments: For comparison between de-phosphorylation of pT73 Rab10 across primary brain cells, cultures were treated with MLi-2 (Tocris, cat #5756) or DMSO for 90 minutes at 1μM concentration prior to lysis. For all experiments utilizing the FKBP-FRB complex, rapamycin (Cayman Chemicals, cat #13346) was added at 200nM for 15 minutes prior to fixation in 4% PFA. MLi-2 (Tocris, cat #5756) was used at 1μM in DMSO for 90 min, or LLOMe (Sigma-Aldrich, cat #L7393) was added at 1mM in DMSO for 2 hours in

HEK293FT cells or 4 hours in astrocytes prior to fixation or lysing cells for

downstream analyses.

Western blot: Tissues or cells were homogenized at 20% w/v in 1x Cell

Signaling Lysis Buffer (20mM Tris-HCl (pH 7.5), 150mM NaCl, 1mM Na_2EDTA,

1mM EGTA, 1% Triton, 2.5mM sodium pyrophosphate, 1mM beta-

glycerophosphate, 1mM Na_3VO_4, 1μg/ml leupeptin) (#9803S) with 1x protease

and phosphatase inhibitors (Thermofisher; #1861279 and #78427, respectively)

and left on ice for 30 minutes to lyse. Homogenates were spun at 20,000 g for

10 minutes at 4 degrees Celsius and pelleted debris was removed. Samples

were supplemented with NuPage LDS sample buffer 4x (#NP0008), boiled for

5 minutes at 95 degrees Celsius and 60μg (for tissue) or 20 μg (for cells) was

loaded per sample and run on a Bio-Rad Criterion™ TGX™ polyacrylamide gel

(#5671095) at 200 V for 37 minutes. Gels were transferred to nitrocellulose

(#1704159) on a Bio-Rad Trans-Blot Turbo™ transfer system at 20 V for

10 minutes. A normalizer sample was added to the end of each blot to account

for day-to-day variability in protein transfer and antibody incubation. This stock

was prepared prior to beginning this study and single-use aliquots were

prepared in loading buffer and stored at -80 degrees Celsius until use to

ensure no loss of phosphorylation nor protein degradation. The nitrocellulose

was blocked for 40 minutes in 50% TBS (20 mM Tris, 0.5 M NaCl, pH 7.5), 50%

Odyssey blocking buffer (Li-Cor; 927–40,000) and incubated overnight with primary antibodies in 50% TBS-T (20 mM Tris, 0.5 M NaCl, pH 7.5, 0.1% Tween 20), 50% Odyssey blocking buffer at 4 degrees Celsius. All blots were probed for Cyclophilin B, used as a housekeeping protein to ensure equal loading of samples. All primary antibody concentrations used are provided in Table 9.1. Following 3 × 5 minutes washes with TBS-T, the nitrocellulose was incubated at RT with secondary antibodies for 1 hour, washed 3 × 5 minutes and scanned at the Li-Cor platform.

Immunostaining: HEK293FT cells were fixed with 4% PFA for 10 minutes, permeabilized with 0.1% triton in PBS for 10 minutes and blocked with 5% Donkey Serum (Sigma, cat #D9663) for 1 hour at RT. Primary antibodies were diluted in PBS containing 1% Donkey Serum and 0.1% triton and incubated overnight at 4°C. All primary antibody concentrations used are provided in Table 9.1. After three 5-minute washes with PBS, secondary fluorescently labeled antibodies were diluted in PBS containing 1% Donkey Serum and incubated for 1 hour at RT. Coverslips were washed two times with 1x PBS followed by an additional wash with dH_2O and mounted with ProLong® Gold antifade reagent (ThermoFisher, cat #P10144).

Table 9.1. **Primary antibody information for all chapters.**

Antibody	Host Species	Catalog #	Working dilution [stock conc.]
pS1292 LRRK2 [MJF-19-7-8]	Rabbit; monoclonal	Ab203181 (abcam)	1:2000 (WB) [1.15mg/ml]
pS935 LRRK2 [UDD2 10(12)]	Rabbit; monoclonal	Ab133450 (abcam)	1:2000 (WB) [1.019mg/ml]
LRRK2 [MJFF2]	Rabbit; monoclonal	Ab133474 (abcam)	1:2000 (WB) [0.66mg/ml]
Cyclophilin B	Rabbit; monoclonal	Ab16045 (abcam)	1:2000 (WB) [1mg/ml]
pT73 Rab10 [MJF-R21]	Rabbit; monoclonal	Ab230261 (abcam)	1:2000 (WB) 1:100 (ICC) [0.54mg/ml]
Rab10 [MJF-R23]	Rabbit; monoclonal	Ab237703 (abcam)	1:2000 (WB) 1:100 (ICC) [0.56mg/ml]
pS106 Rab12 [MJF-R25-9]	Rabbit; monoclonal	Ab256487 (abcam)	1:2000 (WB) 1:100 (ICC) [0.62mg/ml]
Rab12	Rabbit; polyclonal	18843-1-AP (Proteintech)	1:1000 (WB) [51μg/150μl]
pT71 Rab29 [MJF-R24-17-1]	Rabbit; monoclonal	Ab241062 (abcam)	1:1000 (WB) [0.54mg/ml]
Rab29 [MJF-R30-124]	Rabbit; monoclonal	Ab256526 (abcam)	0.5 μg/ml (WB) [0.68mg/ml]
GFAP	Rabbit; polyclonal	Ab7260 (abcam)	1:5000 (WB)
IBA1	Rabbit; polyclonal	4987481429246 (Wako)	1:2000 (WB) [0.5mg/ml]
Beta 3 Tubulin	Rabbit; monoclonal	5568S (Cell Signaling]	1:2000 (WB)
ProSP-C	Rabbit; polyclonal	Ab90716 (abcam)	1:1000 (WB) [0.9mg/ml]
Legumain	Rabbit; monoclonal	93627S (Cell Signaling)	1:1000 (WB)
JIP4	Rabbit; monoclonal	5519S (Cell Signaling)	1:1000 (WB) 1:500 (ICC) [45μg/150μl]
Hgs	Rabbit; polyclonal	10390-1-AP (Proteintech)	1:1000 (WB) [45μg/150μl]
Sfxn3	Rabbit; polyclonal	15156-1-AP (Proteintech)	1:1000 (WB) [105μg/150μl]
LAMP1	Rabbit; monoclonal	3243S (Cell Signaling)	1:1000 (WB)

Atp5mc1	Mouse; monoclonal	Ab119686 (abcam)	1:1000 (WB) [1mg/ml]
Cytochrome C	Mouse; monoclonal	Ab13575 (abcam)	1:1000 (WB) [1mg/ml]
pS163 MARCKS	Rabbit; monoclonal	11992S (Cell Signaling)	1:1000 (WB)
Cyp1a1	Rabbit; polyclonal	13241-1-AP (Thermofisher)	1:1000 (WB) [500µg/ml]
FLAG M2	Mouse; monoclonal	F3165 (Sigma-Aldrich)	1:500 (ICC)
FLAG	Rat; monoclonal	637302 (Biolegend)	1:300 (ICC)
LAMP1	Mouse; monoclonal	H4A3 (DSHB)	1:100 (ICC)
GFP	Chicken; polyclonal	GFP-1020 (AvesLab)	1:1000 (ICC)
GFP	Mouse; monoclonal	11814460001 (Millipore Sigma)	1:10000 (WB)
EEA1	Rabbit; monoclonal	3288S (Cell Signaling)	1:100 (ICC)
TGN46	Sheep; polyclonal	AHP500GT (BioRad)	1:500 (ICC)
Rab8a	Rabbit; monoclonal	6975S (Cell Signaling)	1:500 (ICC)
LAMTOR4	Rabbit; monoclonal	12284S (Cell Signaling)	1:200 (ICC)
Alexa Fluor™ 647 Phalloidin (F-actin)	NA	A30107 (ThermoFisher)	1:20 (ICC)
LAMP2	Rat; monoclonal	H4B4 (DSHB)	1:100 (ICC)
LAMP1	Rat; monoclonal	1D4B (DSHB)	1:100 (ICC)
EEA1	Mouse; monoclonal	610457 (BD Laboratories)	1:100 (ICC)
JIP4	Rabbit; monoclonal	AHP500GT (BioRad)	1:500 (ICC)
VPS35	Mouse; monoclonal	856402 (BioLegend)	1:500 (ICC)
Myc	Mouse; monoclonal	13-2500 (ThermoFisher)	1:500 (ICC)
Pericentrin	Mouse; monoclonal	Ab28144 (abcam)	1:300 (ICC)

Secondary antibodies: For Western blot, secondary antibodies were used at 1:10,000 dilution: IRDyes 800CW Goat anti-Rabbit IgG (LiCor; #926–32,211) and 680RD Goat anti-Mouse IgG (LiCor; 926–68,070). All blots presented in each figure panel were derived from the same experiment and were processed in parallel. Raw densitometric signal was normalized to a common normalizer sample that was run on every blot.

For ICC, all secondary antibodies were purchased from ThermoFisher unless indicated otherwise: donkey anti-mouse Alexa-Fluor 568 (cat #A10037, 1:500), donkey anti-rabbit Alexa-Fluor 488 (cat #A-21206, 1:500), donkey anti-mouse Alexa-Fluor 488 (cat #A-21202, 1:500), donkey anti-rat Alexa-Fluor 488 (cat #A-21208, 1:500), donkey anti-goat Alexa-Fluor 488 (cat #A-11055, 1:500), donkey anti-rabbit Alexa-Fluor 568 (cat #A10042, 1:500), donkey anti-mouse Alexa-Fluor 647 (cat #A-31571, 1:500), goat anti-rat Alexa-Fluor 647 (cat #A-21247, 1:250-1:500). Donkey anti-chicken Alexa-Fluor 405 (cat #703-475-155, 1:300) and donkey anti-sheep Alexa-Fluor 647 (cat #713-605-147) were obtained from Jackson ImmunoResearch.

Statistics: Data were plotted and statistical tests were performed using Prism 8 (GraphPad). Statistical analyses of experiments comparing two groups were performed using unpaired student's t test. Statistical analyses of experiments with more than two groups were performed using one-way ANOVAs. Two-way

ANOVAs were used where there were two factors in the model. Tukey's *post-hoc* test was used to determine statistical significance for individual comparisons in those cases where the underlying ANOVA was statistically significant and where all groups' means were compared to every other mean. Unless otherwise stated, error bars represent standard deviation (SD) and points indicate distribution of individual values. Comparisons were considered statistically significant where *p*< 0.05. **p-value* < 0.05; ***p-value* < 0.01; ****p-value* < 0.001; *****p-value* < 0.0001. The statistical test results are displayed in the following tables per chapter.

Table 9.2. **Results of statistical tests for Chapter 3.**

Figure	Variable	Statistical test	Test result	P-value
3.8 B	MLi-2 treatment and brain region	2-way ANOVA with Šidak's multiple comparison	F=4.289	0.0147, <0.0001
3.9 B	MLi-2 treatment	Unpaired t-test	t=12.28	0.0003
3.9 D	MLi-2 treatment	Unpaired t-test	t=4.114	0.0147
3.9 F	MLi-2 treatment	Unpaired t-test	t=1.687	p=0.1669

In chapter 4, one-way ANOVAs were used per individual tissue type in each graph where brain, kidney, and lung tissues are plotted together. F values are thus recorded per tissue (brain first, kidney second, and lung third) and p-values are shown between variables from left to right for each graph.

Table 9.3. **Results of statistical tests for Chapter 4.**

Figure	Variable	Statistical test	Test result	P-value
4.2 B	Genotype ± treatment	1-way ANOVA with Tukey's post hoc	F=11.45, F=290.0, F=20.79	Brain: 0.0007, 0.0122, 0.0379, Kidney: <0.0001, <0.0001, 0.0041, Lung: 0.0003

4.2 C	Genotype ± treatment	1-way ANOVA with Tukey's post hoc	F=56.58 F=25.75 F=82.11	Brain: 0.0018, <0.0001, <0.0001, Kidney: 0.0024, 0.0003, 0.0002, Lung: 0.0016, <0.0001, <0.0001
4.4 B	Genotype ± treatment	1-way ANOVA with Tukey's post hoc	F=74.52 F=232.2 F=207.3	Brain: <0.0001, <0.0001, Kidney: <0.0001, <0.0001, Lung: <0.0001, <0.0001
4.4 C	Genotype ± treatment	1-way ANOVA with Tukey's post hoc	F=178.0 F=119.2 F=427.8	Brain: <0.0001, <0.0001, <0.0001, Kidney: <0.0001, <0.0001, Lung: 0.0007, <0.0001, <0.0001
4.4 D	Genotype ± treatment	1-way ANOVA with Tukey's post hoc	F=85.52 F=50.76 F=83.6	Kidney: 0.0006, Lung: 0.0424
4.4 E	Genotype ± treatment	1-way ANOVA with Tukey's post hoc	F=1.596 F=3.678 F=14.20	Kidney: 0.0006, Lung: 0.0001, 0.0004
4.4 F	Genotype ± treatment	1-way ANOVA with Tukey's post hoc	F=44.72 F=17.99 F=86.21	Brain: <0.0001, <0.0001, 0.0055, Kidney: 0.0023, 0.0278, 0.0012, Lung: 0.0013, <0.0001, <0.0001
4.4 G	Genotype ± treatment	1-way ANOVA with Tukey's post hoc	F=6.353 F=7.798 F=12.47	Brain: 0.0068, 0.0287
4.6 B	Genotype ± treatment	1-way ANOVA with Tukey's post hoc	F=169.4 F=166.8 F=338.4	Brain: <0.0001, <0.0001, Kidney: <0.0001, <0.0001, Lung: <0.0001, <0.0001, <0.0001
4.6 C	Genotype ± treatment	1-way ANOVA with Tukey's post hoc	F=342.3 F=216.3 F=416.7	Brain: <0.0001, <0.0001, <0.0001, Kidney: <0.0001, <0.0001, <0.0001, Lung: 0.0001, <0.0001, <0.0001

4.6 D	Genotype ± treatment	1-way ANOVA with Tukey's post hoc	F=408.4 F=377.8 F=212.0	Brain: 0.0037, 0.0002, Kidney: <0.0001, <0.0001, Lung: 0.0002
4.6 E	Genotype ± treatment	1-way ANOVA with Tukey's post hoc	F=2.722 F=6.523 F=27.88	Kidney: 0.0109, Lung: 0.0271, 0.0006, <0.0001
4.6 F	Genotype ± treatment	1-way ANOVA with Tukey's post hoc	F=72.43 F=22.94 F=79.46	Brain: <0.0001, <0.0001, 0.0003, Kidney: 0.0056, 0.0015, 0.0004, Lung: 0.009, 0.0321, <0.0001, 0.0001
4.6 G	Genotype ± treatment	1-way ANOVA with Tukey's post hoc	F=2.292 F=7.090 F=8.453	Lung: 0.0235, 0.0004
4.7 B	Genotype ± treatment	1-way ANOVA with Tukey's post hoc	F=4.185	0.0344
4.7 D	Genotype ± treatment	1-way ANOVA with Tukey's post hoc	F=4.027	0.0112

In chapter 5, where proteomic analyses are shown, Fisher's exact test (hypergeometric) with FDR correction was used when gene was the variable, and Empirical Bayes test with FDR correction was used when protein was the variable (Figures 5.2-5.7). Refer to appendix 1 for detailed statistics.

Table 9.4. **Results of statistical tests for Chapter 5.**

Figure	Variable	Statistical test	Test result	P-value
5.8 B	Genotype ± treatment	1-way ANOVA with Tukey's post hoc	F=13.58	WTvGS: 0.0081, GSvGS+MLi: 0.0481
5.8 C	Genotype ± treatment	1-way ANOVA with Tukey's post hoc	F=13.72	WTvGS: 0.0042, GSvGS+MLi:0.0348
5.8 D	Genotype ± treatment	1-way ANOVA with Tukey's post hoc	F=9.323	WTvGS: 0.0062, GSvGS+MLi:0.0081
5.8 E	Genotype ± treatment	1-way ANOVA with Tukey's post hoc	F=13.70	GSvGS+MLi:0.0247, WTvGS+MLi:0.0120, WTvKO: 0.0001

5.8 F	Genotype ± treatment	1-way ANOVA with Tukey's post hoc	F=61.36	GSvGS+MLi:0.0077, WTvGS+MLi:0.0021, WTvKO: <0.0001
5.8 G	Genotype ± treatment	1-way ANOVA with Tukey's post hoc	F=27.39	WTvGS+MLi:0.0107, WTvKO: <0.0001
5.9 E	Genotype ± treatment	1-way ANOVA with Tukey's post hoc	F=4.702	0.0367
5.9 F	Genotype ± treatment	1-way ANOVA with Tukey's post hoc	F=4.409	0.0271
5.9 G	Genotype ± treatment	1-way ANOVA with Tukey's post hoc	F=12.35	0.0069
5.11 B	Genotype ± treatment	1-way ANOVA with Tukey's post hoc	F=4.739	GSvGS+MLi:0.0201, WTvKO: 0.0136
5.11 C	Genotype ± treatment	1-way ANOVA with Tukey's post hoc	F=208.2	GSvGS+MLi:<0.0001, WTvGS+MLi:<0.0001

Table 9.5. **Results of statistical tests for Chapter 6.**

Figure	Variable	Statistical test	Test result	P-value
6.5 B	Treatment	Unpaired student t test	t=0.2570	0.8099
6.5 C	Treatment	Unpaired student t test	t=1.193	0.2987
6.5 E	Treatment	1-way ANOVA with Tukey's post hoc	F=79.98	LRRK2+rapvTrap+rap: <0.0001, Trap untr v rap: <0.0001
6.5 F	Treatment	1-way ANOVA with Tukey's post hoc	F=42.18	LRRK2+rapvTrap+rap: 0.0372, Trap untr v rap: 0.0006
6.5 G	Treatment	1-way ANOVA with Tukey's post hoc	F=28.27	LRRK2+rapvTrap+rap: 0.0148, Trap untr v rap: 0.0005
6.6 B	Treatment	Unpaired student t test	t=0.2076	0.8457
6.6 C	Treatment	Unpaired student t test	t=0.7702	0.4842
6.6 D	Treatment	Unpaired student t test	t=0.6531	0.5493
6.7 C	Treatment	1-way ANOVA with Tukey's post hoc	F=116.4	Untr v Rapa: 0.0017, Untr v Rapa+MLi: 0.0003, Rapa v Rapa+MLi: <0.0001
6.7 D	Treatment	1-way ANOVA with Tukey's post hoc	F=81.12	Untr v Rapa: 0.0045, Untr v Rapa+MLi: 0.0008, Rapa+MLi: <0.0001

6.7 E	Treatment	1-way ANOVA with Tukey's post hoc	F=376.3	Untr v Rapa: 0.0145, Untr v Rapa+MLi: <0.0001, Rapa+MLi: <0.0001
6.7 H	Treatment	1-way ANOVA with Tukey's post hoc	F=323.0	Untr v Rapa: <0.0001, Untr v Rapa+MLi: <0.0001, Rapa+MLi: <0.0001
6.7 I	Treatment	1-way ANOVA with Tukey's post hoc	F=75.25	Untr v Rapa: 0.0020, Untr v Rapa+MLi: 0.0022, Rapa+MLi: <0.0001
6.7 J	Treatment	1-way ANOVA with Tukey's post hoc	F=306.8	Untr v Rapa: 0.0032, Untr v Rapa+MLi: <0.0001, Rapa+MLi: <0.0001
6.8 C	Treatment	1-way ANOVA with Tukey's post hoc	F=69.67	Untr v Rapa: 0.0087, Untr v Rapa+MLi: 0.0010, Rapa+MLi: <0.0001
6.8 D	Treatment	1-way ANOVA with Tukey's post hoc	F=36.89	Untr v Rapa:0.0053, Untr v Rapa+MLi: 0.0320, Rapa+MLi: 0.0003
6.8 E	Treatment	1-way ANOVA with Tukey's post hoc	F=26.02	Untr v Rapa: 0.0250, Untr v Rapa+MLi: 0.0275, Rapa+MLi: 0.0009
6.8 H	Treatment	1-way ANOVA with Tukey's post hoc	F=22.40	Untr v Rapa: 0.0361, Untr v Rapa+MLi: 0.0352, Rapa+MLi: 0.0013
6.8 I	Treatment	1-way ANOVA with Tukey's post hoc	F=691.5	Untr v Rapa: <0.0001, Untr v Rapa+MLi: 0.0002, Rapa+MLi: <0.0001
6.8 J	Treatment	1-way ANOVA with Tukey's post hoc	F=48.89	Untr v Rapa: 0.0034, Untr v Rapa+MLi: 0.0125, Rapa+MLi: 0.0002
6.9 C	Treatment	1-way ANOVA with Tukey's post hoc	F=104.6	Untr v Rapa: 0.0228, Untr v Rapa+MLi: 0.0001, Rapa+MLi: <0.0001

6.9 D	Treatment	1-way ANOVA with Tukey's post hoc	F=110.5	Untr v Rapa: 0.0006, Untr v Rapa+MLi: 0.0010, Rapa+MLi: <0.0001
6.9 E	Treatment	1-way ANOVA with Tukey's post hoc	F=48.55	Untr v Rapa: 0.0471, Untr v Rapa+MLi: 0.0015, Rapa+MLi: 0.0002
6.9 H	Treatment	1-way ANOVA with Tukey's post hoc	F=119.8	Untr v Rapa: 0.0008, Untr v Rapa+MLi: 0.0005, Rapa+MLi: <0.0001
6.9 I	Treatment	1-way ANOVA with Tukey's post hoc	F=154.4	Untr v Rapa: <0.0001, Untr v Rapa+MLi: 0.0032, Rapa+MLi: <0.0001
6.9 J	Treatment	1-way ANOVA with Tukey's post hoc	F=277.7	Untr v Rapa: <0.0001, Untr v Rapa+MLi: 0.0002, Rapa+MLi: <0.0001
6.10 B	Genotype ± treatment	2-way ANOVA with Tukey's post hoc	Genotype F=130.8 Treatment F=208.2	RC_Rapa v MLi: 0.0003, YC_Rapa v MLi: <0.0001, GS_Rapa v MLi: <0.0001, WTvYC: <0.0001, WTvGS: <0.0001
6.10 C	Genotype ± treatment	2-way ANOVA with Tukey's post hoc	Genotype F=101.6 Treatment F=234.4	WT_Rapa v MLi: 0.0257, RC_ Rapa v MLi: 0.004, YC_Rapa v MLi: 0.0395, GS_Rapa v MLi: 0.0081, WTvRC: 0.0002, WTvYC: <0.0001
6.10 D	Genotype ± treatment	2-way ANOVA with Tukey's post hoc	Genotype F=65.56 Treatment F=150.5	WT_Rapa v MLi: 0.0213, WTvRC: <0.0001, WTvYC: <0.0001, WTvGS: 0.0013
6.11 B	Genotype ± treatment	2-way ANOVA with Tukey's post hoc	Genotype F=81.40 Treatment F=57.26	RC_Rapa v MLi: 0.0485, YC_Rapa v MLi: 0.0199, GS_Rapa v MLi: <0.0001, WTvRC: 0.0034,

Figure	Variable	Statistical test	Test result	P-value
				WTvYC: <0.0001, WTvGS: <0.0001
6.11 C	Genotype ± treatment	2-way ANOVA with Tukey's post hoc	Genotype F=156.0 Treatment F=310.7	WT_Rapa v MLi: 0.0296, RC_Rapa v MLi: 0.0001, YC_Rapa v MLi: 0.0001, GS_Rapa v MLi: 0.0046, WTvRC: <0.0001, WTvYC: <0.0001, WTvGS: 0.0256
6.11 D	Genotype ± treatment	2-way ANOVA with Tukey's post hoc	Genotype F=112.3 Treatment F=223.4	WT_Rapa v MLi: 0.0315, WTvRC: <0.0001, WTvYC: <0.0001, WTvGS: 0.0001
6.12 B	siRNA ± treatment	2-way ANOVA with Tukey's post hoc	siRNA F=2.485 Treatment F=214.9	<0.0001
6.12 C	siRNA ± treatment	2-way ANOVA with Tukey's post hoc	siRNA F=0.2967 Treatment F=267.3	<0.0001
6.12 D	siRNA ± treatment	2-way ANOVA with Tukey's post hoc	siRNA F=2.901 Treatment F=20.69	0.0019
6.12 E	siRNA ± treatment	2-way ANOVA with Tukey's post hoc	siRNA F=381.9 Treatment F=0.8127	Untr_NTCvRAB29: <0.0001, Rapa_NTCvRAB29: <0.0001

Table 9.6. **Results of statistical tests for Chapter 7.**

Figure	Variable	Statistical test	Test result	P-value
7.2 F	Treatment or plasmid	1-way ANOVA with Tukey's post hoc	F=87.10	Untr v Rapa: <0.0001, Untr v LYSO: 0.0004, Rapa v LYSO: 0.0080
7.2 G	Treatment or plasmid	1-way ANOVA with Tukey's post hoc	F=65.83	Untr v Rapa: 0.0002, Untr v LYSO: 0.0001
7.2 H	Treatment or plasmid	1-way ANOVA with Tukey's post hoc	F=16.40	Untr v Rapa: 0.0101, Untr v LYSO: 0.0042

7.3 E	Treatment or plasmid	1-way ANOVA with Tukey's post hoc	F=22.48	Untr v Rapa: 0.0094, Untr v EE-LRRK2: 0.0015
7.3 F	Treatment or plasmid	1-way ANOVA with Tukey's post hoc	F=142.6	Untr v Rapa: <0.0001, Untr v EE-LRRK2: <0.0001, Rapa v EE-LRRK2: 0.0032
7.3 G	Treatment or plasmid	1-way ANOVA with Tukey's post hoc	F=32.76	Untr v Rapa: 0.0106, Untr v EE-LRRK2: 0.0005, Rapa v EE-LRRK2: 0.0245
7.4 C	Plasmid and treatment	1-way ANOVA with Tukey's post hoc	F=33.11	NTvLYSO: <0.0001, LYSO_+/-MLi: <0.0001
7.4 D	Plasmid and treatment	1-way ANOVA with Tukey's post hoc	F=34.92	NTvLYSO: 0.0001, LYSO_+/-MLi: <0.0001
7.5 C	Plasmid and treatment	1-way ANOVA with Tukey's post hoc	F=26.67	NTvFYVE: <0.0001, FYVE_+/-MLi: <0.0001
7.5 D	Plasmid and treatment	1-way ANOVA with Tukey's post hoc	F=52.73	NTvFYVE: <0.0001, FYVE_+/-MLi: <0.0001
7.5 E	pRab	2-way ANOVA with Tukey's post hoc	pRab: F=31.73 Chimera: F=24.90	pRab10_LYSO v FYVE: <0.0001, LYSO_pRab10 v pRab12: <0.0001
7.7 D	Lysosome position	Unpaired student t test	t=13.88	<0.0001
7.8 B	Lysosome position	Unpaired student t test	t=4.186	0.0004
7.8 C	Lysosome position	Unpaired student t test	t=3.036	0.0071
7.9 B	Lysosome position	Unpaired student t test	t=8.109	<0.0001
7.9 C	Lysosome position	Unpaired student t test	t=16.62	<0.0001
7.10 B	Treatment or lysosome position	1-way ANOVA with Tukey's post hoc	F=59.39	Untr v LLOMe: 0.0018, Untr_+/- SKIP/ARL8B: 0.0001, LLOMe_+/- SKIP/ARL8B:<0.0001

7.10 D	Treatment or lysosome position	1-way ANOVA with Tukey's post hoc	F=19.42	0.0016
7.11 D	Treatment or lysosome position	1-way ANOVA with Tukey's post hoc	F=53.61	Untr v LLOMe: <0.0001, LLOMe_+/- SKIP/ARL8B: 0.0384, SKIP/ARL8B_+/- LLOMe: 0.0003
7.11 F	Treatment or lysosome position	1-way ANOVA with Tukey's post hoc	F=131.7	Untr v LLOMe: <0.0001, LLOMe_+/- SKIP/ARL8B: <0.0001
7.12 F	siRNA	Unpaired student t test	t=4.249	0.0132
7.12 G	siRNA	Unpaired student t test	t=6.046	0.0038
7.12 C	siRNA	Unpaired student t test	t=5.929	<0.0001
7.13 C	RILP OE	Unpaired student t test	t=8.761	<0.0001
7.13 D	RILP OE	Unpaired student t test	t=5.829	0.001
7.14 B	Treatment and plasmid	1-way ANOVA with Tukey's post hoc	F=15.91	DMSOvLLOMe: <0.0001, DMSOvLLOMe +SKIP/ARL8B: <0.0001
7.15 B	Treatment and plasmid	1-way ANOVA with Tukey's post hoc	F=141.1	<0.0001
7.15 D	Treatment and plasmid	1-way ANOVA with Tukey's post hoc	F=49.76	DMSOvLLOMe: <0.0001, DMSOvLLOMe +SKIP/ARL8B: <0.0001
7.15 F	Treatment and plasmid	1-way ANOVA with Tukey's post hoc	F=116.4	<0.0001
7.16 B	Treatment and plasmid	1-way ANOVA with Tukey's post hoc	F=27.14	DMSOvLLOMe: <0.0001, DMSOvLLOMe +SKIP/ARL8B: 0.0076, LLOMe_+/- SKIP/ARL8B: 0.0006

7.17 B	siRNA	Unpaired student t test	t=3.557	0.0013
7.17 D	siRNA	Unpaired student t test	t=4.161	0.0141
7.18 C	siRNA	Unpaired student t test	t=2.950	0.0055
7.18 D	siRNA	Unpaired student t test	t=3.002	0.0038

Confocal microscopy and analyses: Confocal images were taken using a Zeiss LSM 880 microscope equipped with a 63X 1.4 NA objective. Super-resolution imaging was performed using the Airyscan mode. Raw data were processed using Airycan processing in 'auto strength' mode with Zen Black software version 2.3. Only low plasmid expression cells without obvious OE artifacts were imaged. For measuring colocalization, Fiji plugin JACoP was used in which Mander's correlation corrected for threshold was used to quantify LRRK2:pRab colocalization (Bolte and Cordelières, 2006). All analyses of colocalization were performed on super-resolution confocal microscopy images. For measuring signal intensity, integrated density of each cell was measured using Fiji with thresholding (ImageJ, NIH). For measuring peripheral vs total lysosomal count, the Spot Counter plugin was used in Fiji in which all lysosomes within 2μm from the plasma membrane were counted as peripheral. For measuring the distance between lysosomes and the nucleus, the surface and spot rendering tools were used on the Imaris software version 9.7.2.

Tissue preparation for proteomics and phospho-proteomics: One brain hemisphere, one half of a kidney, and one whole lung from each mouse from the 10-week chronic MLi-2 in-diet dosing experiment were processed and submitted for proteomics and phospho-proteomics analysis using TMT quantitation without and with TiO_2/iMAC enrichment, respectively. Briefly, tissues were homogenized in 15% w/v lysis buffer (0.5 mM HEPES, pH 7.4, 225 mM mannitol, 50 mM sucrose, 1 mM EDTA, 1x protease and phosphatase inhibitors (Thermofisher; #1861279 and #78427, respectively), and 2% CHAPS) followed by incubation on ice for 30 min, with periodic vortexing, to lyse. The homogenates were then spun down at 20,000 g at 4 degrees Celsius for 10 min to pellet cellular debris. A protein assay was performed on supernatants to determine protein concentration, and 270 µg of each sample was submitted for mass spectrometry. Additionally, 30 µg of each sample was pooled together to allow for normalization between runs during analysis.

Phosphoproteomics and bioinformatics analysis: Proteins were alkylated with N-ethylmaleimide (NEM), digested with trypsin and labeled with TMTpro reagents. All tissue samples were treated with the same method. Processing was done based on tissue type, where 24 brain, kidney, or lung samples and 2 pooled samples were separated into 2 sets of TMT experiments. Each set contained 12 samples and one pooled sample. The pooled sample in each set

was labeled with TMTpro-126 reagent, while the distribution and labeling of 12 experimental samples were randomized (Table 9.7). After the labeling and quenching, samples were combined. 95% of the combined sample was used for phospho-peptide enrichment using a titanium dioxide method followed by immobilized metal affinity chromatography (iMAC) method. 5% of the combined sample was fractionated using Pierce high pH reverse phase cartridge, and 8 fractions were collected for each set. LC-MS/MS data acquisition were performed on a Thermo Scientific Orbitrap Lumos mass spectrometer which was coupled to a Thermo Scientific Ultimate 3000 HPLC. Peptides were separated on a ES802 nano-column over 136 minutes at a flow rate of 300 n/minute. Both MS1 and MS2 scans were performed in orbitrap. The resolution for MS1 and MS2 scans was 120 K and 50 K, respectively. Peptides were fragmented using the HCD method with collision energy fixed at 32%. The precursor isolation window was 1.5 Da. Proteome Discoverer 2.4 was used for database search and TMT quantitation.

Table 9.7. **Labeling of samples for TMTpro-16 LC-MS/MS.**

TMT Run1		TMT Run2	
126	Pool-1	126	Pool-2
~~127N~~	-	127N	10W-WT4
~~127C~~	-	127C	10W-GS4
~~128N~~	-	128N	10W-GS+4
128C	10W-WT1	~~128C~~	-
129N	10W-GS1	~~129N~~	-
129C	10W-GS+1	~~129C~~	-
130N	10W-KO1	130N	10W-KO4
130C	10W-WT2	130C	10W-WT5
131N	10W-GS2	131N	10W-GS5
131C	10W-GS+2	131C	10W-GS+5
132N	10W-KO2	132N	10W-KO5
132C	10W-WT3	132C	10W-WT6
133N	10W-GS3	133N	10W-GS6
133C	10W-GS+3	133C	10W-GS+6
134N	10W-KO3	134N	10W-KO6

Samples with four conditions were given arbitrary number identifications 1-6 representing the N=6 mice per genotype/treatment. Each run contained 3 samples of each genotype/treatment for a total of 12 samples per run. Three probes were thus unused per run which were chosen at random. The "GS+" group refers to the MLi-2-treated G2019S KI group, "WT" = wildtype, "GS" = G2019S KI untreated, and "KO" = LRRK2 KO samples.

Proteomic data handling and analyses: Ratios of raw abundance values of each sample over the pooled sample were generated and analyzed in R using the limma package (version 4.0, empirical Bayes method) (Ritchie et al., 2015). Briefly, the proteomics datasets from two MS runs were combined and only hits that were detected in at least 4 out of 6 mice were kept, while the missing 1–2 values were imputed. These phospho-peptide and total protein datasets were merged and matched for accession number and the ratio of phospho/total abundance was generated for phospho-peptide significant hit detection. Principal component analysis was conducted for these datasets

which revealed a modest batch effect that was corrected computationally.

Statistical analyses were conducted, namely moderated t-tests between pairs

were visualized as volcano plots (Blighe et al., 2020), and z scores were

calculated for heatmaps. Heatmaps were curated from statistically significant

hits selected based on relevance to neurodegeneration and reported functions

on cellular pathways affected in PD. Proteins were considered significant hits

with an adjusted *p*-value < 0.05, and for kidneys a fold change > 1.4.

Functional enrichment analysis of the significant hits was performed using the

R package gProfiler2 (precision cutoffs of adjusted *p*-values were < 1e-6

and < 1e-20 for kidney and brain hits, respectively, and term size < 1000 was

kept (Reimand et al., 2007). All hits from the lungs did not return any significant

terms within these parameters. Enrichment term networks were visualized

using Cytoscape 3.7 (Shannon et al., 2003).

REFERENCES

Aasly, J.O., Vilariño-Güell, C., Dachsel, J.C., Webber, P.J., West, A.B., Haugarvoll, K., Johansen, K.K., Toft, M., Nutt, J.G., Payami, H., Kachergus, J.M., Lincoln, S.J., Felic, A., Wider, C., Soto-Ortolaza, A.I., Cobb, S.A., White, L.R., Ross, O.A., Farrer, M.J., 2010. Novel pathogenic LRRK2 p.Asn1437His substitution in familial Parkinson's disease. Mov. Disord. Off. J. Mov. Disord. Soc. 25, 2156–2163. https://doi.org/10.1002/mds.23265

Abbott, R.D., Webster Ross, G., White, L.R., Sanderson, W.T., Burchfiel, C.M., Kashon, M., Sharp, D.S., Masaki, K.H., Curb, J.D., Petrovitch, H., 2003. Environmental, life-style, andphysical precursors of clinical Parkinson's disease: recentfindings from the Honolulu-Asia Aging Study. J. Neurol. 250, iii30–iii39. https://doi.org/10.1007/s00415-003-1306-7

Amaral, E.P., Riteau, N., Moayeri, M., Maier, N., Mayer-Barber, K.D., Pereira, R.M., Lage, S.L., Kubler, A., Bishai, W.R., D'Império-Lima, M.R., Sher, A., Andrade, B.B., 2018. Lysosomal Cathepsin Release Is Required for NLRP3-Inflammasome Activation by Mycobacterium tuberculosis in Infected Macrophages. Front. Immunol. 9.

American Parkinson Disease Association, 2020. The FDA approves F-Dopa PET imaging to aid in early diagnosis of Parkinson's disease. Am. Park. Dis. Assoc. URL https://www.apdaparkinson.org/article/the-fda-approves-f-dopa-pet-imaging-to-aid-in-early-diagnosis-of-parkinsons-disease/ (accessed 5.31.22).

An, X.-K., Peng, R., Li, T., Burgunder, J.-M., Wu, Y., Chen, W.-J., Zhang, J.-H., Wang, Y.-C., Xu, Y.-M., Gou, Y.-R., Yuan, G.-G., Zhang, Z.-J., 2008. LRRK2 Gly2385Arg variant is a risk factor of Parkinson's disease among Han-Chinese from mainland China. Eur. J. Neurol. 15, 301–305. https://doi.org/10.1111/j.1468-1331.2007.02052.x

Andersen, M.A., Wegener, K.M., Larsen, S., Badolo, L., Smith, G.P., Jeggo, R., Jensen, P.H., Sotty, F., Christensen, K.V., Thougaard, A., 2018. PFE-360-induced LRRK2 inhibition induces reversible, non-adverse renal changes in rats. Toxicology 395, 15–22. https://doi.org/10.1016/j.tox.2018.01.003

Anderson, J.P., Walker, D.E., Goldstein, J.M., de Laat, R., Banducci, K., Caccavello, R.J., Barbour, R., Huang, J., Kling, K., Lee, M., Diep, L., Keim, P.S., Shen, X., Chataway, T., Schlossmacher, M.G., Seubert, P., Schenk, D., Sinha, S., Gai, W.P., Chilcote, T.J., 2006. Phosphorylation of Ser-129 is the dominant pathological modification of alpha-synuclein in familial and sporadic Lewy body disease. J. Biol. Chem. 281, 29739–29752. https://doi.org/10.1074/jbc.M600933200

Andrew, A.S., Anderson, F.L., Lee, S.L., Von Herrmann, K.M., Havrda, M.C., 2021. Lifestyle Factors and Parkinson's Disease Risk in a Rural New England Case-Control Study. Park. Dis. 2021, e5541760. https://doi.org/10.1155/2021/5541760

Ang, A.L., Fölsch, H., Koivisto, U.-M., Pypaert, M., Mellman, I., 2003. The Rab8 GTPase selectively regulates AP-1B–dependent basolateral transport in polarized Madin-Darby canine kidney cells. J. Cell Biol. 163, 339–350. https://doi.org/10.1083/jcb.200307046

Angeles, D.C., Ho, P., Chua, L.L., Wang, C., Yap, Y.W., Ng, C., Zhou, Z. dong, Lim, K.-L., Wszolek, Z.K., Wang, H.Y., Tan, E.K., 2014. Thiol peroxidases ameliorate LRRK2 mutant-induced mitochondrial and dopaminergic neuronal degeneration in Drosophila. Hum. Mol. Genet. 23, 3157–3165. https://doi.org/10.1093/hmg/ddu026

Angeli, A., Mencacci, N.E., Duran, R., Aviles-Olmos, I., Kefalopoulou, Z., Candelario, J., Rusbridge, S., Foley, J., Pradhan, P., Jahanshahi, M., Zrinzo, L., Hariz, M., Wood, N.W., Hardy, J., Limousin, P., Foltynie, T., MRCP, MD, 2013. Genotype and phenotype in Parkinson's disease: Lessons in heterogeneity from deep brain stimulation. Mov. Disord. 28, 1370–1375. https://doi.org/10.1002/mds.25535

Annerino, D.M., Arshad, S., Taylor, G.M., Adler, C.H., Beach, T.G., Greene, J.G., 2012. Parkinson's disease is not associated with gastrointestinal myenteric ganglion neuron loss. Acta Neuropathol. (Berl.) 124, 665–680. https://doi.org/10.1007/s00401-012-1040-2

Apaydin, H., Ertan, S., Özekmekçi, S., 2000. Broad bean (Vicia faba)—A natural source of L-dopa—Prolongs "on" periods in patients with Parkinson's disease who have "on–off" fluctuations. Mov. Disord. 15, 164–166. https://doi.org/10.1002/1531-8257(200001)15:1<164::AID-MDS1028>3.0.CO;2-E

Ascherio, A., Chen, H., Weisskopf, M.G., O'Reilly, E., McCullough, M.L., Calle, E.E., Schwarzschild, M.A., Thun, M.J., 2006. Pesticide exposure and risk for Parkinson's disease. Ann. Neurol. 60, 197–203. https://doi.org/10.1002/ana.20904

Bagheri, H., Damase-Michel, C., Lapeyre-Mestre, M., Cismondo, S., O'Connell, D., Senard, J.M., Rascol, O., Montastruc, J.L., 1999. A study of salivary secretion in Parkinson's disease. Clin. Neuropharmacol. 22, 213–215.

Ball, N., Teo, W.-P., Chandra, S., Chapman, J., 2019. Parkinson's Disease and the Environment. Front. Neurol. 10.

Bandres-Ciga, S., Diez-Fairen, M., Kim, J.J., Singleton, A.B., 2020. Genetics of Parkinson disease: an introspection of its journey towards precision medicine. Neurobiol. Dis. 137, 104782. https://doi.org/10.1016/j.nbd.2020.104782

Baptista, M.A.S., Dave, K.D., Frasier, M.A., Sherer, T.B., Greeley, M., Beck, M.J., Varsho, J.S., Parker, G.A., Moore, C., Churchill, M.J., Meshul, C.K., Fiske, B.K., 2013. Loss of Leucine-Rich Repeat Kinase 2 (LRRK2) in Rats Leads to Progressive Abnormal Phenotypes in Peripheral Organs. PLoS ONE 8, e80705. https://doi.org/10.1371/journal.pone.0080705

Baptista, M.A.S., Merchant, K., Barrett, T., Bhargava, S., Bryce, D.K., Ellis, J.M., Estrada, A.A., Fell, M.J., Fiske, B.K., Fuji, R.N., Galatsis, P., Henry, A.G., Hill, S., Hirst, W., Houle, C., Kennedy, M.E., Liu, X., Maddess, M.L., Markgraf, C., Mei, H., Meier, W.A., Needle, E., Ploch, S., Royer, C., Rudolph, K., Sharma, A.K., Stepan, A., Steyn, S., Trost, C., Yin, Z., Yu, H., Wang, X., Sherer, T.B., 2020. LRRK2 inhibitors induce reversible changes in nonhuman primate lungs without measurable pulmonary deficits. Sci. Transl. Med. 12. https://doi.org/10.1126/scitranslmed.aav0820

Barbour, R., Kling, K., Anderson, J.P., Banducci, K., Cole, T., Diep, L., Fox, M., Goldstein, J.M., Soriano, F., Seubert, P., Chilcote, T.J., 2008. Red blood cells

are the major source of alpha-synuclein in blood. Neurodegener. Dis. 5, 55–59. https://doi.org/10.1159/000112832

Bardien, S., Lesage, S., Brice, A., Carr, J., 2011. Genetic characteristics of leucine-rich repeat kinase 2 (LRRK2) associated Parkinson's disease. Parkinsonism Relat. Disord. 17, 501–508. https://doi.org/10.1016/j.parkreldis.2010.11.008

Basurto-Islas, G., Grundke-Iqbal, I., Tung, Y.C., Liu, F., Iqbal, K., 2013. Activation of Asparaginyl Endopeptidase Leads to Tau Hyperphosphorylation in Alzheimer Disease. J. Biol. Chem. 288, 17495–17507. https://doi.org/10.1074/jbc.M112.446070

Beach, T.G., Adler, C.H., Sue, L.I., Vedders, L., Lue, L., White, C.L., Akiyama, H., Caviness, J.N., Shill, H.A., Sabbagh, M.N., Walker, D.G., 2010. Multi-organ distribution of phosphorylated **α**-synuclein histopathology in subjects with Lewy body disorders. Acta Neuropathol. (Berl.) 119, 689–702. https://doi.org/10.1007/s00401-010-0664-3

Beilina, A., Bonet-Ponce, L., Kumaran, R., Kordich, J.J., Ishida, M., Mamais, A., Kaganovich, A., Saez-Atienzar, S., Gershlick, D.C., Roosen, D.A., Pellegrini, L., Malkov, V., Fell, M.J., Harvey, K., Bonifacino, J.S., Moore, D.J., Cookson, M.R., 2020. The Parkinson's Disease Protein LRRK2 Interacts with the GARP Complex to Promote Retrograde Transport to the trans-Golgi Network. Cell Rep. 31, 107614. https://doi.org/10.1016/j.celrep.2020.107614

Beilina, A., Rudenko, I.N., Kaganovich, A., Civiero, L., Chau, H., Kalia, S.K., Kalia, L.V., Lobbestael, E., Chia, R., Ndukwe, K., Ding, J., Nalls, M.A., International Parkinson's Disease Genomics Consortium, North American Brain Expression Consortium, Olszewski, M., Hauser, D.N., Kumaran, R., Lozano, A.M., Baekelandt, V., Greene, L.E., Taymans, J.-M., Greggio, E., Cookson, M.R., 2014. Unbiased screen for interactors of leucine-rich repeat kinase 2 supports a common pathway for sporadic and familial Parkinson disease. Proc. Natl. Acad. Sci. U. S. A. 111, 2626–2631. https://doi.org/10.1073/pnas.1318306111

Bell, R., Thrush, R.J., Castellana-Cruz, M., Oeller, M., Staats, R., Nene, A., Flagmeier, P., Xu, C.K., Satapathy, S., Galvagnion, C., Wilson, M.R., Dobson, C.M., Kumita, J.R., Vendruscolo, M., 2022. N-Terminal Acetylation of **α**-Synuclein Slows down Its Aggregation Process and Alters the Morphology of the Resulting Aggregates. Biochemistry. https://doi.org/10.1021/acs.biochem.2c00104

Berger, Z., Smith, K.A., LaVoie, M.J., 2010. Membrane Localization of LRRK2 Is Associated with Increased Formation of the Highly Active LRRK2 Dimer and Changes in Its Phosphorylation. Biochemistry 49, 5511–5523. https://doi.org/10.1021/bi100157u

Bergeron, M., Motter, R., Tanaka, P., Fauss, D., Babcock, M., Chiou, S.-S., Nelson, S., San Pablo, F., Anderson, J.P., 2014. In vivo modulation of polo-like kinases supports a key role for PLK2 in Ser129 **α**-synuclein phosphorylation in mouse brain. Neuroscience 256, 72–82. https://doi.org/10.1016/j.neuroscience.2013.09.061

Berndsen, K., Lis, P., Yeshaw, W.M., Wawro, P.S., Nirujogi, R.S., Wightman, M., Macartney, T., Dorward, M., Knebel, A., Tonelli, F., Pfeffer, S.R., Alessi, D.R., 2019. PPM1H phosphatase counteracts LRRK2 signaling by selectively

dephosphorylating Rab proteins. eLife 8, e50416.
https://doi.org/10.7554/eLife.50416

Berry, D., Reinisch, W., 2013. Intestinal microbiota: a source of novel biomarkers in inflammatory bowel diseases? Best Pract. Res. Clin. Gastroenterol. 27, 47–58. https://doi.org/10.1016/j.bpg.2013.03.005

Betarbet, R., Sherer, T.B., MacKenzie, G., Garcia-Osuna, M., Panov, A.V., Greenamyre, J.T., 2000. Chronic systemic pesticide exposure reproduces features of Parkinson's disease. Nat. Neurosci. 3, 1301–1306. https://doi.org/10.1038/81834

Beylina, A., Langston, R.G., Rosen, D., Reed, X., Cookson, M.R., 2021. Generation of fourteen isogenic cell lines for Parkinson's disease-associated leucine-rich repeat kinase (LRRK2). Stem Cell Res. 53, 102354. https://doi.org/10.1016/j.scr.2021.102354

Blanca Ramírez, M., Ordóñez, A.J.L., Fdez, E., Madero-Pérez, J., Gonnelli, A., Drouyer, M., Chartier-Harlin, M.-C., Taymans, J.-M., Bubacco, L., Greggio, E., Hilfiker, S., 2017. GTP binding regulates cellular localization of Parkinson's disease-associated LRRK2. Hum. Mol. Genet. 26, 2747–2767. https://doi.org/10.1093/hmg/ddx161

Blauwendraat, C., Reed, X., Kia, D.A., Gan-Or, Z., Lesage, S., Pihlstrøm, L., Guerreiro, R., Gibbs, J.R., Sabir, M., Ahmed, S., Ding, J., Alcalay, R.N., Hassin-Baer, S., Pittman, A.M., Brooks, J., Edsall, C., Hernandez, D.G., Chung, S.J., Goldwurm, S., Toft, M., Schulte, C., Bras, J., Wood, N.W., Brice, A., Morris, H.R., Scholz, S.W., Nalls, M.A., Singleton, A.B., Cookson, M.R., COURAGE-PD (Comprehensive Unbiased Risk Factor Assessment for Genetics and Environment in Parkinson's Disease) Consortium, the French Parkinson's Disease Consortium, and the International Parkinson's Disease Genomics Consortium (IPDGC), 2018. Frequency of Loss of Function Variants in LRRK2 in Parkinson Disease. JAMA Neurol. 75, 1416–1422. https://doi.org/10.1001/jamaneurol.2018.1885

Blighe, K., Rana, S., Lewis, M., 2020. EnhancedVolcano: Publication-ready volcano plots with enhanced colouring and labeling. Bioconductor version: Release (3.11). https://doi.org/10.18129/B9.bioc.EnhancedVolcano

Boecker, C.A., Goldsmith, J., Dou, D., Cajka, G.G., Holzbaur, E.L.F., 2021. Increased LRRK2 kinase activity alters neuronal autophagy by disrupting the axonal transport of autophagosomes. Curr. Biol. CB 31, 2140-2154.e6. https://doi.org/10.1016/j.cub.2021.02.061

Bolte, S., Cordelières, F.P., 2006. A guided tour into subcellular colocalization analysis in light microscopy. J. Microsc. 224, 213–232. https://doi.org/10.1111/j.1365-2818.2006.01706.x

Bonet-Ponce, L., Beilina, A., Williamson, C.D., Lindberg, E., Kluss, J.H., Saez-Atienzar, S., Landeck, N., Kumaran, R., Mamais, A., Bleck, C.K.E., Li, Y., Cookson, M.R., 2020. LRRK2 mediates tubulation and vesicle sorting from lysosomes. Sci. Adv. 6, eabb2454. https://doi.org/10.1126/sciadv.abb2454

Bonet-Ponce, L., Cookson, M.R., 2019. The role of Rab GTPases in the pathobiology of Parkinson' disease. Curr. Opin. Cell Biol., Membrane Trafficking 59, 73–80. https://doi.org/10.1016/j.ceb.2019.03.009

Bonifati, V., Rizzu, P., van Baren, M.J., Schaap, O., Breedveld, G.J., Krieger, E., Dekker, M.C.J., Squitieri, F., Ibanez, P., Joosse, M., van Dongen, J.W., Vanacore, N., van Swieten, J.C., Brice, A., Meco, G., van Duijn, C.M., Oostra, B.A., Heutink, P., 2003. Mutations in the DJ-1 gene associated with autosomal recessive early-onset parkinsonism. Science 299, 256–259. https://doi.org/10.1126/science.1077209

Bönsch, D., Lenz, B., Kornhuber, J., Bleich, S., 2005. DNA hypermethylation of the alpha synuclein promoter in patients with alcoholism. NeuroReport 16, 167–170.

Borghi, R., Marchese, R., Negro, A., Marinelli, L., Forloni, G., Zaccheo, D., Abbruzzese, G., Tabaton, M., 2000. Full length alpha-synuclein is present in cerebrospinal fluid from Parkinson's disease and normal subjects. Neurosci. Lett. 287, 65–67. https://doi.org/10.1016/s0304-3940(00)01153-8

Bose, A., Beal, M.F., 2016. Mitochondrial dysfunction in Parkinson's disease. J. Neurochem. 139 Suppl 1, 216–231. https://doi.org/10.1111/jnc.13731

Bove, F.J., Ruckart, P.Z., Maslia, M., Larson, T.C., 2014. Mortality study of civilian employees exposed to contaminated drinking water at USMC Base Camp Lejeune: a retrospective cohort study. Environ. Health 13, 68. https://doi.org/10.1186/1476-069X-13-68

Braak, H., Del Tredici, K., Rüb, U., de Vos, R.A.I., Jansen Steur, E.N.H., Braak, E., 2003. Staging of brain pathology related to sporadic Parkinson's disease. Neurobiol. Aging 24, 197–211. https://doi.org/10.1016/s0197-4580(02)00065-9

Braak, H., Müller, C.M., Rüb, U., Ackermann, H., Bratzke, H., de Vos, R.A.I., Del Tredici, K., 2006. Pathology associated with sporadic Parkinson's disease — where does it end?, in: Riederer, P., Reichmann, H., Youdim, M.B.H., Gerlach, M. (Eds.), Parkinson's Disease and Related Disorders, Journal of Neural Transmission. Supplementa. Springer, Vienna, pp. 89–97. https://doi.org/10.1007/978-3-211-45295-0_15

Braak, H., Sandmann-Keil, D., Gai, W., Braak, E., 1999. Extensive axonal Lewy neurites in Parkinson's disease: a novel pathological feature revealed by **α**-synuclein immunocytochemistry. Neurosci. Lett. 265, 67–69. https://doi.org/10.1016/S0304-3940(99)00208-6

Breydo, L., Wu, J.W., Uversky, V.N., 2012. **A**-synuclein misfolding and Parkinson's disease. Biochim. Biophys. Acta 1822, 261–285. https://doi.org/10.1016/j.bbadis.2011.10.002

Brooks, D.J., 2000. Dopamine agonists: their role in the treatment of Parkinson's disease. J. Neurol. Neurosurg. Psychiatry 68, 685–689. https://doi.org/10.1136/jnnp.68.6.685

Bryce, D., Ware, C.M., Woodhouse, J.D., Ciaccio, P.J., Ellis, J.M., Hegde, L.G., Kuruvilla, S., Maddess, M.L., Markgraf, C.G., Otte, K.M., Poulet, F.M., Timmins, L.M., Kennedy, M., Fell, M.J., 2021. Characterization of the onset, progression, and reversibility of morphological changes in mouse lung following pharmacological inhibition of LRRK2 kinase activity. J. Pharmacol. Exp. Ther. https://doi.org/10.1124/jpet.120.000217

Bucci, C., Parton, R.G., Mather, I.H., Stunnenberg, H., Simons, K., Hoflack, B., Zerial, M., 1992. The small GTPase rab5 functions as a regulatory factor in the early endocytic pathway. Cell 70, 715–728. https://doi.org/10.1016/0092-8674(92)90306-w

Buchman, A.S., Shulman, J.M., Nag, S., Leurgans, S.E., Arnold, S.E., Morris, M.C., Schneider, J.A., Bennett, D.A., 2012. Nigral pathology and parkinsonian signs in elders without Parkinson disease. Ann. Neurol. 71, 258–266. https://doi.org/10.1002/ana.22588

Bucur, M., Papagno, C., 2022. Deep Brain Stimulation in Parkinson Disease: A Meta-analysis of the Long-term Neuropsychological Outcomes. Neuropsychol. Rev. https://doi.org/10.1007/s11065-022-09540-9

Burke, R.E., Dauer, W.T., Vonsattel, J.P.G., 2008. A Critical Evaluation of The Braak Staging Scheme for Parkinson's Disease. Ann. Neurol. 64, 485–491. https://doi.org/10.1002/ana.21541

Cabukusta, B., Neefjes, J., 2018. Mechanisms of lysosomal positioning and movement. Traffic Cph. Den. 19, 761–769. https://doi.org/10.1111/tra.12587

Cannon, J.R., Tapias, V.M., Na, H.M., Honick, A.S., Drolet, R.E., Greenamyre, J.T., 2009. A highly reproducible rotenone model of Parkinson's disease. Neurobiol. Dis. 34, 279–290. https://doi.org/10.1016/j.nbd.2009.01.016

Cantalupo, G., Alifano, P., Roberti, V., Bruni, C.B., Bucci, C., 2001. Rab-interacting lysosomal protein (RILP): the Rab7 effector required for transport to lysosomes. EMBO J. 20, 683–693. https://doi.org/10.1093/emboj/20.4.683

Chan, C.S., Gertler, T.S., Surmeier, D.J., 2010. A molecular basis for the increased vulnerability of substantia nigra dopamine neurons in aging and Parkinson's disease. Mov. Disord. 25, S63–S70. https://doi.org/10.1002/mds.22801

Chang, D., Nalls, M.A., Hallgrímsdóttir, I.B., Hunkapiller, J., van der Brug, M., Cai, F., International Parkinson's Disease Genomics Consortium, 23andMe Research Team, Kerchner, G.A., Ayalon, G., Bingol, B., Sheng, M., Hinds, D., Behrens, T.W., Singleton, A.B., Bhangale, T.R., Graham, R.R., 2017. A meta-analysis of genome-wide association studies identifies 17 new Parkinson's disease risk loci. Nat. Genet. 49, 1511–1516. https://doi.org/10.1038/ng.3955

Charcot, J.M., 1879. Lectures on the Diseases of the Nervous System: Delivered at La Salpêtrière. H. C. Lea.

Chartier-Harlin, M.-C., Dachsel, J.C., Vilariño-Güell, C., Lincoln, S.J., Leprêtre, F., Hulihan, M.M., Kachergus, J., Milnerwood, A.J., Tapia, L., Song, M.-S., Le Rhun, E., Mutez, E., Larvor, L., Duflot, A., Vanbesien-Mailliot, C., Kreisler, A., Ross, O.A., Nishioka, K., Soto-Ortolaza, A.I., Cobb, S.A., Melrose, H.L., Behrouz, B., Keeling, B.H., Bacon, J.A., Hentati, E., Williams, L., Yanagiya, A., Sonenberg, N., Lockhart, P.J., Zubair, A.C., Uitti, R.J., Aasly, J.O., Krygowska-Wajs, A., Opala, G., Wszolek, Z.K., Frigerio, R., Maraganore, D.M., Gosal, D., Lynch, T., Hutchinson, M., Bentivoglio, A.R., Valente, E.M., Nichols, W.C., Pankratz, N., Foroud, T., Gibson, R.A., Hentati, F., Dickson, D.W., Destée, A., Farrer, M.J., 2011. Translation initiator EIF4G1 mutations in familial Parkinson disease. Am. J. Hum. Genet. 89, 398–406. https://doi.org/10.1016/j.ajhg.2011.08.009

Chartier-Harlin, M.-C., Kachergus, J., Roumier, C., Mouroux, V., Douay, X., Lincoln, S., Levecque, C., Larvor, L., Andrieux, J., Hulihan, M., Waucquier, N., Defebvre, L., Amouyel, P., Farrer, M., Destée, A., 2004. α-synuclein locus duplication as a cause of familial Parkinson's disease. The Lancet 364, 1167–1169. https://doi.org/10.1016/S0140-6736(04)17103-1

Chavrier, P., Parton, R.G., Hauri, H.P., Simons, K., Zerial, M., 1990. Localization of low molecular weight GTP binding proteins to exocytic and endocytic compartments. Cell 62, 317–329. https://doi.org/10.1016/0092-8674(90)90369-P

Chen, C.-Y., Weng, Y.-H., Chien, K.-Y., Lin, K.-J., Yeh, T.-H., Cheng, Y.-P., Lu, C.-S., Wang, H.-L., 2012. (G2019S) LRRK2 activates MKK4-JNK pathway and causes degeneration of SN dopaminergic neurons in a transgenic mouse model of PD. Cell Death Differ. 19, 1623–1633. https://doi.org/10.1038/cdd.2012.42

Chen, L., Zhang, S., Liu, Y., Hong, H., Wang, H., Zheng, Y., Zhou, H., Chen, J., Xian, W., He, Y., Li, J., Liu, Z., Pei, Z., Zeng, J., 2011. LRRK2 R1398H polymorphism is associated with decreased risk of Parkinson's disease in a Han Chinese population. Parkinsonism Relat. Disord. 17, 291–292. https://doi.org/10.1016/j.parkreldis.2010.11.012

Cheng, H.-C., Ulane, C.M., Burke, R.E., 2010. Clinical Progression in Parkinson's Disease and the Neurobiology of Axons. Ann. Neurol. 67, 715–725. https://doi.org/10.1002/ana.21995

Chiang, H.-L., Lin, C.-H., 2019. Altered Gut Microbiome and Intestinal Pathology in Parkinson's Disease. J. Mov. Disord. 12, 67–83. https://doi.org/10.14802/jmd.18067

Choi, H.G., Zhang, J., Deng, X., Hatcher, J.M., Patricelli, M.P., Zhao, Z., Alessi, D.R., Gray, N.S., 2012. Brain Penetrant LRRK2 Inhibitor. ACS Med. Chem. Lett. 3, 658–662. https://doi.org/10.1021/ml300123a

Chou, J.-S., Chen, C.-Y., Chen, Y.-L., Weng, Y.-H., Yeh, T.-H., Lu, C.-S., Chang, Y.-M., Wang, H.-L., 2014. (G2019S) LRRK2 causes early-phase dysfunction of SNpc dopaminergic neurons and impairment of corticostriatal long-term depression in the PD transgenic mouse. Neurobiol. Dis. 68, 190–199. https://doi.org/10.1016/j.nbd.2014.04.021

Chu, Y., Kordower, J.H., 2007. Age-associated increases of α-synuclein in monkeys and humans are associated with nigrostriatal dopamine depletion: Is this the target for Parkinson's disease? Neurobiol. Dis. 25, 134–149. https://doi.org/10.1016/j.nbd.2006.08.021

Civiero, L., Cirnaru, M.D., Beilina, A., Rodella, U., Russo, I., Belluzzi, E., Lobbestael, E., Reyniers, L., Hondhamuni, G., Lewis, P.A., Van den Haute, C., Baekelandt, V., Bandopadhyay, R., Bubacco, L., Piccoli, G., Cookson, M.R., Taymans, J., Greggio, E., 2015. Leucine-rich repeat kinase 2 interacts with p21-activated kinase 6 to control neurite complexity in mammalian brain. J. Neurochem. 135, 1242–1256. https://doi.org/10.1111/jnc.13369

Claassen, D.O., van den Wildenberg, W.P.M., Ridderinkhof, K.R., Jessup, C.K., Harrison, M.B., Wooten, G.F., Wylie, S.A., 2011. The Risky Business of Dopamine Agonists in Parkinson Disease and Impulse Control Disorders. Behav. Neurosci. 125, 492–500. https://doi.org/10.1037/a0023795

Cookson, M.R., 2015. LRRK2 Pathways Leading to Neurodegeneration. Curr. Neurol. Neurosci. Rep. 15, 42. https://doi.org/10.1007/s11910-015-0564-y

Coronado, V.G., Thomas, K.E., Sattin, R.W., Johnson, R.L., 2005. The CDC traumatic brain injury surveillance system: characteristics of persons aged 65 years and older hospitalized with a TBI. J. Head Trauma Rehabil. 20, 215–228. https://doi.org/10.1097/00001199-200505000-00005

Correia Guedes, L., Ferreira, J.J., Rosa, M.M., Coelho, M., Bonifati, V., Sampaio, C., 2010. Worldwide frequency of G2019S LRRK2 mutation in Parkinson's disease: a systematic review. Parkinsonism Relat. Disord. 16, 237–242. https://doi.org/10.1016/j.parkreldis.2009.11.004

Cotzias, G.C., Van Woert, M.H., Schiffer, L.M., 1967. Aromatic Amino Acids and Modification of Parkinsonism. N. Engl. J. Med. 276, 374–379. https://doi.org/10.1056/NEJM196702162760703

Covy, J.P., Giasson, B.I., 2009. Identification of compounds that inhibit the kinase activity of leucine-rich repeat kinase 2. Biochem. Biophys. Res. Commun. 378, 473–477. https://doi.org/10.1016/j.bbrc.2008.11.048

Cruts, M., Theuns, J., Van Broeckhoven, C., 2012. Locus-specific mutation databases for neurodegenerative brain diseases. Hum. Mutat. 33, 1340–1344. https://doi.org/10.1002/humu.22117

Cullen, P.J., Korswagen, H.C., 2011. Sorting nexins provide diversity for retromer-dependent trafficking events. Nat. Cell Biol. 14, 29–37. https://doi.org/10.1038/ncb2374

Cunningham, L.A., Moore, D.J., 2020. Chapter 8 - Endosomal sorting pathways in the pathogenesis of Parkinson's disease, in: Björklund, A., Cenci, M.A. (Eds.), Progress in Brain Research, Recent Advances in Parkinson's Disease. Elsevier, pp. 271–306. https://doi.org/10.1016/bs.pbr.2020.02.001

Dächsel, J.C., Behrouz, B., Yue, M., Beevers, J.E., Melrose, H.L., Farrer, M.J., 2010. A comparative study of Lrrk2 function in primary neuronal cultures. Parkinsonism Relat. Disord. 16, 650–655. https://doi.org/10.1016/j.parkreldis.2010.08.018

Dagan, E., Schlesinger, I., Ayoub, M., Mory, A., Nassar, M., Kurolap, A., Peretz-Aharon, J., Gershoni-Baruch, R., 2015. The contribution of Niemann-Pick SMPD1 mutations to Parkinson disease in Ashkenazi Jews. Parkinsonism Relat. Disord. 21, 1067–1071. https://doi.org/10.1016/j.parkreldis.2015.06.016

Daher, J.P.L., Abdelmotilib, H.A., Hu, X., Volpicelli-Daley, L.A., Moehle, M.S., Faser, K.B., Needle, E., Chen, Y., Steyn, S.J., Galatsis, P., Hirst, W.D., West, A.B., 2015. LRRK2 Pharmacological Inhibition Abates α-Synuclein Induced Neurodegeneration. J. Biol. Chem. jbc.M115.660001. https://doi.org/10.1074/jbc.M115.660001

Daher, J.P.L., Volpicelli-Daley, L.A., Blackburn, J.P., Moehle, M.S., West, A.B., 2014. Abrogation of α-synuclein–mediated dopaminergic neurodegeneration in LRRK2-deficient rats. Proc. Natl. Acad. Sci. 111, 9289–9294. https://doi.org/10.1073/pnas.1403215111

Dalby, M.J., Berry, C.C., Riehle, M.O., Sutherland, D.S., Agheli, H., Curtis, A.S.G., 2004. Attempted endocytosis of nano-environment produced by colloidal lithography

by human fibroblasts. Exp. Cell Res. 295, 387–394.
https://doi.org/10.1016/j.yexcr.2004.02.004

Dall, E., Brandstetter, H., 2016. Structure and function of legumain in health and disease. Biochimie, A potpourri of proteases and inhibitors: from molecular toolboxes to signaling scissors 122, 126–150.
https://doi.org/10.1016/j.biochi.2015.09.022

Damier, P., Hirsch, E.C., Agid, Y., Graybiel, A.M., 1999. The substantia nigra of the human brain: II. Patterns of loss of dopamine-containing neurons in Parkinson's disease. Brain 122, 1437–1448. https://doi.org/10.1093/brain/122.8.1437

Damodaran, M., Ramaswamy, R., 1937. Isolation of l-3:4-dihydroxyphenylalanine from the seeds of Mucuna pruriens. Biochem. J. 31, 2149–2152.

Daniëls, V., Vancraenenbroeck, R., Law, B.M.H., Greggio, E., Lobbestael, E., Gao, F., De Maeyer, M., Cookson, M.R., Harvey, K., Baekelandt, V., Taymans, J.-M., 2011. Insight into the mode of action of the LRRK2 Y1699C pathogenic mutant. J. Neurochem. 116, 304–315. https://doi.org/10.1111/j.1471-4159.2010.07105.x

Davidson, W.S., Jonas, A., Clayton, D.F., George, J.M., 1998. Stabilization of α-Synuclein Secondary Structure upon Binding to Synthetic Membranes*. J. Biol. Chem. 273, 9443–9449. https://doi.org/10.1074/jbc.273.16.9443

Davis, G.C., Williams, A.C., Markey, S.P., Ebert, M.H., Caine, E.D., Reichert, C.M., Kopin, I.J., 1979. Chronic parkinsonism secondary to intravenous injection of meperidine analogues. Psychiatry Res. 1, 249–254.
https://doi.org/10.1016/0165-1781(79)90006-4

de Martín Garrido, N., Aylett, C.H.S., 2020. Nutrient Signaling and Lysosome Positioning Crosstalk Through a Multifunctional Protein, Folliculin. Front. Cell Dev. Biol. 8, 108. https://doi.org/10.3389/fcell.2020.00108

De Miranda, B.R., Greenamyre, J.T., 2020. Trichloroethylene, a ubiquitous environmental contaminant in the risk for Parkinson's disease. Environ. Sci. Process. Impacts 22, 543–554. https://doi.org/10.1039/C9EM00578A

Dedmon, M.M., Lindorff-Larsen, K., Christodoulou, J., Vendruscolo, M., Dobson, C.M., 2005. Mapping long-range interactions in alpha-synuclein using spin-label NMR and ensemble molecular dynamics simulations. J. Am. Chem. Soc. 127, 476–477. https://doi.org/10.1021/ja044834j

Delbroek, L., Van Kolen, K., Steegmans, L., da Cunha, R., Mandemakers, W., Daneels, G., De Bock, P.-J., Zhang, J., Gevaert, K., De Strooper, B., Alessi, D.R., Verstreken, P., Moechars, D.W., 2013. Development of an enzyme-linked immunosorbent assay for detection of cellular and in vivo LRRK2 S935 phosphorylation. J. Pharm. Biomed. Anal. 76, 49–58.
https://doi.org/10.1016/j.jpba.2012.12.002

Denali Therapeutics Inc., 2022. Denali Therapeutics and Biogen Announce Initiation of Phase 2b Study of LRRK2 Inhibitor in Parkinson's Disease [WWW Document]. Denali. URL https://www.denalitherapeutics.com/investors/press-release (accessed 6.9.22).

Denali Therapeutics Inc., 2021. Denali Therapeutics Presents Positive Results from Phase 1 and Phase 1b Studies of Its LRRK2 Inhibitor, BIIB122/DNL151, Supporting Late-Stage Development Plans in Parkinson's Disease [WWW

Document]. Denali. URL https://www.denalitherapeutics.com/investors/press-release (accessed 5.31.22).

Deng, H., Le, W., Guo, Y., Hunter, C.B., Xie, W., Huang, M., Jankovic, J., 2006. Genetic analysis of LRRK2 mutations in patients with Parkinson disease. J. Neurol. Sci. 251, 102–106. https://doi.org/10.1016/j.jns.2006.09.017

Deng, J., Lewis, P.A., Greggio, E., Sluch, E., Beilina, A., Cookson, M.R., 2008. Structure of the ROC domain from the Parkinson's disease-associated leucine-rich repeat kinase 2 reveals a dimeric GTPase. Proc. Natl. Acad. Sci. 105, 1499–1504. https://doi.org/10.1073/pnas.0709098105

Deng, X., Dzamko, N., Prescott, A., Davies, P., Liu, Q., Yang, Q., Lee, J.-D., Patricelli, M.P., Nomanbhoy, T.K., Alessi, D.R., Gray, N.S., 2011. Characterization of a selective inhibitor of the Parkinson's disease kinase LRRK2. Nat. Chem. Biol. 7, 203–205. https://doi.org/10.1038/nchembio.538

Deniston, C.K., Salogiannis, J., Mathea, S., Snead, D.M., Lahiri, I., Matyszewski, M., Donosa, O., Watanabe, R., Böhning, J., Shiau, A.K., Knapp, S., Villa, E., Reck-Peterson, S.L., Leschziner, A.E., 2020. Structure of LRRK2 in Parkinson's disease and model for microtubule interaction. Nature 588, 344–349. https://doi.org/10.1038/s41586-020-2673-2

Derost, P.-P., Ouchchane, L., Morand, D., Ulla, M., Llorca, P.-M., Barget, M., Debilly, B., Lemaire, J.-J., Durif, F., 2007. Is DBS-STN appropriate to treat severe Parkinson disease in an elderly population? Neurology 68, 1345–1355. https://doi.org/10.1212/01.wnl.0000260059.77107.c2

Deuschl, G., Schade-Brittinger, C., Krack, P., Volkmann, J., Schäfer, H., Bötzel, K., Daniels, C., Deutschländer, A., Dillmann, U., Eisner, W., Gruber, D., Hamel, W., Herzog, J., Hilker, R., Klebe, S., Kloß, M., Koy, J., Krause, M., Kupsch, A., Lorenz, D., Lorenzl, S., Mehdorn, H.M., Moringlane, J.R., Oertel, W., Pinsker, M.O., Reichmann, H., Reuß, A., Schneider, G.-H., Schnitzler, A., Steude, U., Sturm, V., Timmermann, L., Tronnier, V., Trottenberg, T., Wojtecki, L., Wolf, E., Poewe, W., Voges, J., 2006. A Randomized Trial of Deep-Brain Stimulation for Parkinson's Disease. N. Engl. J. Med. 355, 896–908. https://doi.org/10.1056/NEJMoa060281

Dhekne, H.S., Yanatori, I., Gomez, R.C., Tonelli, F., Diez, F., Schüle, B., Steger, M., Alessi, D.R., Pfeffer, S.R., 2018. A pathway for Parkinson's Disease LRRK2 kinase to block primary cilia and Sonic hedgehog signaling in the brain. eLife 7, e40202. https://doi.org/10.7554/eLife.40202

Di Fonzo, A., Dekker, M.C.J., Montagna, P., Baruzzi, A., Yonova, E.H., Correia Guedes, L., Szczerbinska, A., Zhao, T., Dubbel-Hulsman, L.O.M., Wouters, C.H., de Graaff, E., Oyen, W.J.G., Simons, E.J., Breedveld, G.J., Oostra, B.A., Horstink, M.W., Bonifati, V., 2009. FBXO7 mutations cause autosomal recessive, early-onset parkinsonian-pyramidal syndrome. Neurology 72, 240–245. https://doi.org/10.1212/01.wnl.0000338144.10967.2b

Di Fonzo, A., Rohé, C.F., Ferreira, J., Chien, H.F., Vacca, L., Stocchi, F., Guedes, L., Fabrizio, E., Manfredi, M., Vanacore, N., Goldwurm, S., Breedveld, G., Sampaio, C., Meco, G., Barbosa, E., Oostra, B.A., Bonifati, V., Italian Parkinson Genetics Network, 2005. A frequent LRRK2 gene mutation associated with autosomal

dominant Parkinson's disease. Lancet Lond. Engl. 365, 412–415.
https://doi.org/10.1016/S0140-6736(05)17829-5

Di Fonzo, A., Tassorelli, C., De Mari, M., Chien, H.F., Ferreira, J., Rohé, C.F., Riboldazzi, G., Antonini, A., Albani, G., Mauro, A., Marconi, R., Abbruzzese, G., Lopiano, L., Fincati, E., Guidi, M., Marini, P., Stocchi, F., Onofrj, M., Toni, V., Tinazzi, M., Fabbrini, G., Lamberti, P., Vanacore, N., Meco, G., Leitner, P., Uitti, R.J., Wszolek, Z.K., Gasser, T., Simons, E.J., Breedveld, G.J., Goldwurm, S., Pezzoli, G., Sampaio, C., Barbosa, E., Martignoni, E., Oostra, B.A., Bonifati, V., Italian Parkinson's Genetics Network, 2006. Comprehensive analysis of the LRRK2 gene in sixty families with Parkinson's disease. Eur. J. Hum. Genet. EJHG 14, 322–331. https://doi.org/10.1038/sj.ejhg.5201539

Di Maio, R., Hoffman, E.K., Rocha, E.M., Keeney, M.T., Sanders, L.H., De Miranda, B.R., Zharikov, A., Van Laar, A., Stepan, A.F., Lanz, T.A., Kofler, J.K., Burton, E.A., Alessi, D.R., Hastings, T.G., Greenamyre, J.T., 2018. LRRK2 activation in idiopathic Parkinson's disease. Sci. Transl. Med. 10, eaar5429. https://doi.org/10.1126/scitranslmed.aar5429

Ding, X., Goldberg, M.S., 2009. Regulation of LRRK2 Stability by the E3 Ubiquitin Ligase CHIP. PLoS ONE 4, e5949. https://doi.org/10.1371/journal.pone.0005949

Dorsey, E.R., Bloem, B.R., 2018. The Parkinson Pandemic—A Call to Action. JAMA Neurol. 75, 9–10. https://doi.org/10.1001/jamaneurol.2017.3299

Dzamko, N., Deak, M., Hentati, F., Reith, A.D., Prescott, A.R., Alessi, D.R., Nichols, R.J., 2010. Inhibition of LRRK2 kinase activity leads to dephosphorylation of Ser910/Ser935, disruption of 14-3-3 binding and altered cytoplasmic localization. Biochem. J. 430, 405–413. https://doi.org/10.1042/BJ20100784

Dzamko, N., Gysbers, A.M., Bandopadhyay, R., Bolliger, M.F., Uchino, A., Zhao, Y., Takao, M., Wauters, S., van de Berg, W.D.J., Takahashi-Fujigasaki, J., Nichols, R.J., Holton, J.L., Murayama, S., Halliday, G.M., 2017. LRRK2 levels and phosphorylation in Parkinson's disease brain and cases with restricted Lewy bodies. Mov. Disord. Off. J. Mov. Disord. Soc. 32, 423–432. https://doi.org/10.1002/mds.26892

Edvardson, S., Cinnamon, Y., Ta-Shma, A., Shaag, A., Yim, Y.-I., Zenvirt, S., Jalas, C., Lesage, S., Brice, A., Taraboulos, A., Kaestner, K.H., Greene, L.E., Elpeleg, O., 2012. A Deleterious Mutation in DNAJC6 Encoding the Neuronal-Specific Clathrin-Uncoating Co-Chaperone Auxilin, Is Associated with Juvenile Parkinsonism. PLOS ONE 7, e36458. https://doi.org/10.1371/journal.pone.0036458

Eguchi, T., Kuwahara, T., Sakurai, M., Komori, T., Fujimoto, T., Ito, G., Yoshimura, S.-I., Harada, A., Fukuda, M., Koike, M., Iwatsubo, T., 2018. LRRK2 and its substrate Rab GTPases are sequentially targeted onto stressed lysosomes and maintain their homeostasis. Proc. Natl. Acad. Sci. U. S. A. 115, E9115–E9124. https://doi.org/10.1073/pnas.1812196115

Eiden, L.E., Weihe, E., 2011. VMAT2: a dynamic regulator of brain monoaminergic neuronal function interacting with drugs of abuse. Ann. N. Y. Acad. Sci. 1216, 86–98. https://doi.org/10.1111/j.1749-6632.2010.05906.x

Elbaz, A., Clavel, J., Rathouz, P.J., Moisan, F., Galanaud, J.-P., Delemotte, B., Alpérovitch, A., Tzourio, C., 2009. Professional exposure to pesticides and Parkinson disease. Ann. Neurol. 66, 494–504. https://doi.org/10.1002/ana.21717

Elgebaly, A., Elfil, M., Attia, A., Magdy, M., Negida, A., 2018. Neuropsychological performance changes following subthalamic versus pallidal deep brain stimulation in Parkinson's disease: a systematic review and metaanalysis. CNS Spectr. 23, 10–23. https://doi.org/10.1017/S1092852917000062

Elsayed, L.E.O., Drouet, V., Usenko, T., Mohammed, I.N., Hamed, A.A.A., Elseed, M.A., Salih, M.A.M., Koko, M.E., Mohamed, A.Y.O., Siddig, R.A., Elbashir, M.I., Ibrahim, M.E., Durr, A., Stevanin, G., Lesage, S., Ahmed, A.E., Brice, A., 2016. A Novel Nonsense Mutation in DNAJC6 Expands the Phenotype of Autosomal-Recessive Juvenile-Onset Parkinson's Disease. Ann. Neurol. 79, 335–337. https://doi.org/10.1002/ana.24591

Eriksson, I., Wäster, P., Öllinger, K., 2020. Restoration of lysosomal function after damage is accompanied by recycling of lysosomal membrane proteins. Cell Death Dis. 11, 1–16. https://doi.org/10.1038/s41419-020-2527-8

Estrada, A.A., Chan, B.K., Baker-Glenn, C., Beresford, A., Burdick, D.J., Chambers, M., Chen, H., Dominguez, S.L., Dotson, J., Drummond, J., Flagella, M., Fuji, R., Gill, A., Halladay, J., Harris, S.F., Heffron, T.P., Kleinheinz, T., Lee, D.W., Pichon, C.E.L., Liu, X., Lyssikatos, J.P., Medhurst, A.D., Moffat, J.G., Nash, K., Scearce-Levie, K., Sheng, Z., Shore, D.G., Wong, S., Zhang, S., Zhang, X., Zhu, H., Sweeney, Z.K., 2014. Discovery of Highly Potent, Selective, and Brain-Penetrant Aminopyrazole Leucine-Rich Repeat Kinase 2 (LRRK2) Small Molecule Inhibitors. J. Med. Chem. 57, 921–936. https://doi.org/10.1021/jm401654j

Estrada, A.A., Liu, X., Baker-Glenn, C., Beresford, A., Burdick, D.J., Chambers, M., Chan, B.K., Chen, H., Ding, X., DiPasquale, A.G., Dominguez, S.L., Dotson, J., Drummond, J., Flagella, M., Flynn, S., Fuji, R., Gill, A., Gunzner-Toste, J., Harris, S.F., Heffron, T.P., Kleinheinz, T., Lee, D.W., Le Pichon, C.E., Lyssikatos, J.P., Medhurst, A.D., Moffat, J.G., Mukund, S., Nash, K., Scearce-Levie, K., Sheng, Z., Shore, D.G., Tran, T., Trivedi, N., Wang, S., Zhang, S., Zhang, X., Zhao, G., Zhu, H., Sweeney, Z.K., 2012. Discovery of highly potent, selective, and brain-penetrable leucine-rich repeat kinase 2 (LRRK2) small molecule inhibitors. J. Med. Chem. 55, 9416–9433. https://doi.org/10.1021/jm301020q

Fasano, A., Bove, F., Gabrielli, M., Petracca, M., Zocco, M.A., Ragazzoni, E., Barbaro, F., Piano, C., Fortuna, S., Tortora, A., Di Giacopo, R., Campanale, M., Gigante, G., Lauritano, E.C., Navarra, P., Marconi, S., Gasbarrini, A., Bentivoglio, A.R., 2013. The role of small intestinal bacterial overgrowth in Parkinson's disease. Mov. Disord. Off. J. Mov. Disord. Soc. 28, 1241–1249. https://doi.org/10.1002/mds.25522

Fell, M.J., Mirescu, C., Basu, K., Cheewatrakoolpong, B., DeMong, D.E., Ellis, J.M., Hyde, L.A., Lin, Y., Markgraf, C.G., Mei, H., Miller, M., Poulet, F.M., Scott, J.D., Smith, M.D., Yin, Z., Zhou, X., Parker, E.M., Kennedy, M.E., Morrow, J.A., 2015. MLi-2, a Potent, Selective, and Centrally Active Compound for Exploring the Therapeutic Potential and Safety of LRRK2 Kinase Inhibition. J. Pharmacol. Exp. Ther. 355, 397–409. https://doi.org/10.1124/jpet.115.227587

Feng, Y., Press, B., Wandinger-Ness, A., 1995. Rab 7: an important regulator of late endocytic membrane traffic. J. Cell Biol. 131, 1435–1452. https://doi.org/10.1083/jcb.131.6.1435

Ferguson, F.M., Gray, N.S., 2018. Kinase inhibitors: the road ahead. Nat. Rev. Drug Discov. 17, 353–377. https://doi.org/10.1038/nrd.2018.21

Fraser, K.B., Rawlins, A.B., Clark, R.G., Alcalay, R.N., Standaert, D.G., Liu, N., West, A.B., 2016. Ser(P)-1292 LRRK2 in urinary exosomes is elevated in idiopathic Parkinson's disease. Mov. Disord. 31, 1543–1550. https://doi.org/10.1002/mds.26686

Frieling, H., Gozner, A., Römer, K.D., Lenz, B., Bönsch, D., Wilhelm, J., Hillemacher, T., de Zwaan, M., Kornhuber, J., Bleich, S., 2007. Global DNA hypomethylation and DNA hypermethylation of the alpha synuclein promoter in females with anorexia nervosa. Mol. Psychiatry 12, 229–230. https://doi.org/10.1038/sj.mp.4001931

Fuji, R.N., Flagella, M., Baca, M., Baptista, M.A.S., Brodbeck, J., Chan, B.K., Fiske, B.K., Honigberg, L., Jubb, A.M., Katavolos, P., Lee, D.W., Lewin-Koh, S.-C., Lin, T., Liu, X., Liu, S., Lyssikatos, J.P., O'Mahony, J., Reichelt, M., Roose-Girma, M., Sheng, Z., Sherer, T., Smith, A., Solon, M., Sweeney, Z.K., Tarrant, J., Urkowitz, A., Warming, S., Yaylaoglu, M., Zhang, S., Zhu, H., Estrada, A.A., Watts, R.J., 2015. Effect of selective LRRK2 kinase inhibition on nonhuman primate lung. Sci. Transl. Med. 7, 273ra15. https://doi.org/10.1126/scitranslmed.aaa3634

Fujiwara, H., Hasegawa, M., Dohmae, N., Kawashima, A., Masliah, E., Goldberg, M.S., Shen, J., Takio, K., Iwatsubo, T., 2002. α-Synuclein is phosphorylated in synucleinopathy lesions. Nat. Cell Biol. 4, 160–164. https://doi.org/10.1038/ncb748

Funayama, M., Hasegawa, K., Kowa, H., Saito, M., Tsuji, S., Obata, F., 2002. A new locus for Parkinson's disease (PARK8) maps to chromosome 12p11.2-q13.1. Ann. Neurol. 51, 296–301.

Funayama, M., Hasegawa, K., Ohta, E., Kawashima, N., Komiyama, M., Kowa, H., Tsuji, S., Obata, F., 2005. An LRRK2 mutation as a cause for the parkinsonism in the original PARK8 family. Ann. Neurol. 57, 918–921. https://doi.org/10.1002/ana.20484

Funayama, M., Li, Y., Tomiyama, H., Yoshino, H., Imamichi, Y., Yamamoto, M., Murata, M., Toda, T., Mizuno, Y., Hattori, N., 2007. Leucine-rich repeat kinase 2 G2385R variant is a risk factor for Parkinson disease in Asian population. Neuroreport 18, 273–275. https://doi.org/10.1097/WNR.0b013e32801254b6

Gabrielli, M., Bonazzi, P., Scarpellini, E., Bendia, E., Lauritano, E.C., Fasano, A., Ceravolo, M.G., Capecci, M., Rita Bentivoglio, A., Provinciali, L., Tonali, P.A., Gasbarrini, A., 2011. Prevalence of small intestinal bacterial overgrowth in Parkinson's disease. Mov. Disord. Off. J. Mov. Disord. Soc. 26, 889–892. https://doi.org/10.1002/mds.23566

Gardner, R.C., Burke, J.F., Nettiksimmons, J., Goldman, S., Tanner, C.M., Yaffe, K., 2015. Traumatic brain injury in later life increases risk for Parkinson's disease. Ann. Neurol. 77, 987–995. https://doi.org/10.1002/ana.24396

Gardner, R.C., Byers, A.L., Barnes, D.E., Li, Y., Boscardin, J., Yaffe, K., 2018. Mild TBI and risk of Parkinson disease: A Chronic Effects of Neurotrauma Consortium Study. Neurology 90, e1771–e1779. https://doi.org/10.1212/WNL.0000000000005522

Gasser, T., 2009. Molecular pathogenesis of Parkinson disease: insights from genetic studies. Expert Rev. Mol. Med. 11, e22. https://doi.org/10.1017/S1462399409001148

Gatto, N.M., Cockburn, M., Bronstein, J., Manthripragada, A.D., Ritz, B., 2009. Well-Water Consumption and Parkinson's Disease in Rural California. Environ. Health Perspect. 117, 1912–1918. https://doi.org/10.1289/ehp.0900852

GBD 2016 Neurology Collaborators, 2019. Global, regional, and national burden of neurological disorders, 1990-2016: a systematic analysis for the Global Burden of Disease Study 2016. Lancet Neurol. 18, 459–480. https://doi.org/10.1016/S1474-4422(18)30499-X

Gelpi, E., Navarro-Otano, J., Tolosa, E., Gaig, C., Compta, Y., Rey, M.J., Martí, M.J., Hernández, I., Valldeoriola, F., Reñé, R., Ribalta, T., 2014. Multiple organ involvement by alpha-synuclein pathology in Lewy body disorders. Mov. Disord. Off. J. Mov. Disord. Soc. 29, 1010–1018. https://doi.org/10.1002/mds.25776

Giasson, B.I., Covy, J.P., Bonini, N.M., Hurtig, H.I., Farrer, M.J., Trojanowski, J.Q., Van Deerlin, V.M., 2006. Biochemical and pathological characterization of Lrrk2. Ann. Neurol. 59, 315–322. https://doi.org/10.1002/ana.20791

Giasson, B.I., Duda, J.E., Murray, I.V.J., Chen, Q., Souza, J.M., Hurtig, H.I., Ischiropoulos, H., Trojanowski, J.Q., -Y. Lee, V.M., 2000. Oxidative Damage Linked to Neurodegeneration by Selective α-Synuclein Nitration in Synucleinopathy Lesions. Science 290, 985–989. https://doi.org/10.1126/science.290.5493.985

Giesert, F., Glasl, L., Zimprich, A., Ernst, L., Piccoli, G., Stautner, C., Zerle, J., Hölter, S.M., Vogt Weisenhorn, D.M., Wurst, W., 2017. The pathogenic LRRK2 R1441C mutation induces specific deficits modeling the prodromal phase of Parkinson's disease in the mouse. Neurobiol. Dis. 105, 179–193. https://doi.org/10.1016/j.nbd.2017.05.013

Gloeckner, C.J., Boldt, K., von Zweydorf, F., Helm, S., Wiesent, L., Sarioglu, H., Ueffing, M., 2010. Phosphopeptide analysis reveals two discrete clusters of phosphorylation in the N-terminus and the Roc domain of the Parkinson-disease associated protein kinase LRRK2. J. Proteome Res. 9, 1738–1745. https://doi.org/10.1021/pr9008578

Gomez, R.C., Wawro, P., Lis, P., Alessi, D.R., Pfeffer, S.R., 2019. Membrane association but not identity is required for LRRK2 activation and phosphorylation of Rab GTPases. J. Cell Biol. 218, 4157–4170. https://doi.org/10.1083/jcb.201902184

Gopalai, A.A., Lim, J.L., Li, H.-H., Zhao, Y., Lim, T.T., Eow, G.B., Puvanarajah, S., Viswanathan, S., Norlinah, M.I., Abdul Aziz, Z., Lim, S.K., Tan, C.T., Tan, A.H., Lim, S.-Y., Tan, E.-K., Ahmad Annuar, A., 2019. LRRK2 N551K and R1398H variants are protective in Malays and Chinese in Malaysia: A case-control

association study for Parkinson's disease. Mol. Genet. Genomic Med. 7, e604. https://doi.org/10.1002/mgg3.604

Gopalai, A.A., Lim, S.-Y., Chua, J.Y., Tey, S., Lim, T.T., Mohamed Ibrahim, N., Tan, A.H., Eow, G.B., Abdul Aziz, Z., Puvanarajah, S.D., Viswanathan, S., Looi, I., Lim, S.K., Tan, L.P., Chong, Y.B., Tan, C.T., Zhao, Y., Tan, E.K., Ahmad-Annuar, A., 2014. LRRK2 G2385R and R1628P Mutations Are Associated with an Increased Risk of Parkinson's Disease in the Malaysian Population. BioMed Res. Int. 2014, e867321. https://doi.org/10.1155/2014/867321

Gowers, 1888. A MANUAL OF DISEASES OF THE NERVOUS SYSTEM. J. Nerv. Ment. Dis. 13, 325–327.

Greenamyre, J.T., Hastings, T.G., 2004. Parkinson's--Divergent Causes, Convergent Mechanisms. Science 304, 1120–1122. https://doi.org/10.1126/science.1098966

Greffard, S., Verny, M., Bonnet, A.-M., Seilhean, D., Hauw, J.-J., Duyckaerts, C., 2010. A stable proportion of Lewy body bearing neurons in the substantia nigra suggests a model in which the Lewy body causes neuronal death. Neurobiol. Aging 31, 99–103. https://doi.org/10.1016/j.neurobiolaging.2008.03.015

Greggio, E., Jain, S., Kingsbury, A., Bandopadhyay, R., Lewis, P., Kaganovich, A., van der Brug, M.P., Beilina, A., Blackinton, J., Thomas, K.J., Ahmad, R., Miller, D.W., Kesavapany, S., Singleton, A., Lees, A., Harvey, R.J., Harvey, K., Cookson, M.R., 2006. Kinase activity is required for the toxic effects of mutant LRRK2/dardarin. Neurobiol. Dis. 23, 329–341. https://doi.org/10.1016/j.nbd.2006.04.001

Greggio, E., Taymans, J.-M., Zhen, E.Y., Ryder, J., Vancraenenbroeck, R., Beilina, A., Sun, P., Deng, J., Jaffe, H., Baekelandt, V., Merchant, K., Cookson, M.R., 2009. The Parkinson's disease kinase LRRK2 autophosphorylates its GTPase domain at multiple sites. Biochem. Biophys. Res. Commun. 389, 449–454. https://doi.org/10.1016/j.bbrc.2009.08.163

Greggio, E., Zambrano, I., Kaganovich, A., Beilina, A., Taymans, J.-M., Daniëls, V., Lewis, P., Jain, S., Ding, J., Syed, A., Thomas, K.J., Baekelandt, V., Cookson, M.R., 2008. The Parkinson Disease-associated Leucine-rich Repeat Kinase 2 (LRRK2) Is a Dimer That Undergoes Intramolecular Autophosphorylation. J. Biol. Chem. 283, 16906–16914. https://doi.org/10.1074/jbc.M708718200

Grünewald, A., Kumar, K.R., Sue, C.M., 2019. New insights into the complex role of mitochondria in Parkinson's disease. Prog. Neurobiol. 177, 73–93. https://doi.org/10.1016/j.pneurobio.2018.09.003

Guehl, D., Bezard, E., Dovero, S., Boraud, T., Bioulac, B., Gross, C., 1999. Trichloroethylene and parkinsonism: a human and experimental observation. Eur. J. Neurol. 6, 609–611. https://doi.org/10.1046/j.1468-1331.1999.650609.x

Guo, L., Gandhi, P.N., Wang, W., Petersen, R.B., Wilson-Delfosse, A.L., Chen, S.G., 2007. The Parkinson's disease-associated protein, leucine-rich repeat kinase 2 (LRRK2), is an authentic GTPase that stimulates kinase activity. Exp. Cell Res. 313, 3658–3670. https://doi.org/10.1016/j.yexcr.2007.07.007

Guzzo, A., Delarue, P., Rojas, A., Nicolaï, A., Maisuradze, G.G., Senet, P., 2021. Missense Mutations Modify the Conformational Ensemble of the α-Synuclein Monomer Which Exhibits a Two-Phase Characteristic. Front. Mol. Biosci. 8.

Haehner, A., Boesveldt, S., Berendse, H.W., Mackay-Sim, A., Fleischmann, J., Silburn, P.A., Johnston, A.N., Mellick, G.D., Herting, B., Reichmann, H., Hummel, T., 2009. Prevalence of smell loss in Parkinson's disease – A multicenter study. Parkinsonism Relat. Disord. 15, 490–494. https://doi.org/10.1016/j.parkreldis.2008.12.005

Hämälistö, S., Stahl, J.L., Favaro, E., Yang, Q., Liu, B., Christoffersen, L., Loos, B., Guasch Boldú, C., Joyce, J.A., Reinheckel, T., Barisic, M., Jäättelä, M., 2020. Spatially and temporally defined lysosomal leakage facilitates mitotic chromosome segregation. Nat. Commun. 11, 229. https://doi.org/10.1038/s41467-019-14009-0

Hammond, G.R.V., Machner, M.P., Balla, T., 2014. A novel probe for phosphatidylinositol 4-phosphate reveals multiple pools beyond the Golgi. J. Cell Biol. 205, 113–126. https://doi.org/10.1083/jcb.201312072

Hartmann, C.J., Fliegen, S., Groiss, S.J., Wojtecki, L., Schnitzler, A., 2019. An update on best practice of deep brain stimulation in Parkinson's disease. Ther. Adv. Neurol. Disord. 12, 1756286419838096. https://doi.org/10.1177/1756286419838096

Hasan, N., Greenwood, T., Glunde, K., 2008. Lysosome swelling precedes lysosomal membrane permeabilization in breast cancer cells. Cancer Res. 68, LB-51.

Hatano, Y., Li, Y., Sato, K., Asakawa, S., Yamamura, Y., Tomiyama, H., Yoshino, H., Asahina, M., Kobayashi, S., Hassin-Baer, S., Lu, C.-S., Ng, A.R., Rosales, R.L., Shimizu, N., Toda, T., Mizuno, Y., Hattori, N., 2004. Novel PINK1 mutations in early-onset parkinsonism. Ann. Neurol. 56, 424–427. https://doi.org/10.1002/ana.20251

Hatcher, J.M., Richardson, J.R., Guillot, T.S., McCormack, A.L., Di Monte, D.A., Jones, D.P., Pennell, K.D., Miller, G.W., 2007. Dieldrin exposure induces oxidative damage in the mouse nigrostriatal dopamine system. Exp. Neurol. 204, 619–630. https://doi.org/10.1016/j.expneurol.2006.12.020

Hattori, N., Kitada, T., Matsumine, H., Asakawa, S., Yamamura, Y., Yoshino, H., Kobayashi, T., Yokochi, M., Wang, M., Yoritaka, A., Kondo, T., Kuzuhara, S., Nakamura, S., Shimizu, N., Mizuno, Y., 1998a. Molecular genetic analysis of a novel Parkin gene in Japanese families with autosomal recessive juvenile parkinsonism: evidence for variable homozygous deletions in the Parkin gene in affected individuals. Ann. Neurol. 44, 935–941. https://doi.org/10.1002/ana.410440612

Hattori, N., Matsumine, H., Asakawa, S., Kitada, T., Yoshino, H., Elibol, B., Brookes, A.J., Yamamura, Y., Kobayashi, T., Wang, M., Yoritaka, A., Minoshima, S., Shimizu, N., Mizuno, Y., 1998b. Point mutations (Thr240Arg and Gln311Stop) [correction of Thr240Arg and Ala311Stop] in the Parkin gene. Biochem. Biophys. Res. Commun. 249, 754–758. https://doi.org/10.1006/bbrc.1998.9134

Hayes, M.T., 2019. Parkinson's Disease and Parkinsonism. Am. J. Med. 132, 802–807. https://doi.org/10.1016/j.amjmed.2019.03.001

Heaton, G.R., Landeck, N., Mamais, A., Nalls, M.A., Nixon-Abell, J., Kumaran, R., Beilina, A., Pellegrini, L., Li, Y., Harvey, K., Cookson, M.R., 2020. Sequential screening nominates the Parkinson's disease associated kinase LRRK2 as a

regulator of Clathrin-mediated endocytosis. Neurobiol. Dis. 141, 104948. https://doi.org/10.1016/j.nbd.2020.104948

Henderson, J.L., Kormos, B.L., Hayward, M.M., Coffman, K.J., Jasti, J., Kurumbail, R.G., Wager, T.T., Verhoest, P.R., Noell, G.S., Chen, Y., Needle, E., Berger, Z., Steyn, S.J., Houle, C., Hirst, W.D., Galatsis, P., 2015. Discovery and preclinical profiling of 3-[4-(morpholin-4-yl)-7H-pyrrolo[2,3-d]pyrimidin-5-yl]benzonitrile (PF-06447475), a highly potent, selective, brain penetrant, and in vivo active LRRK2 kinase inhibitor. J. Med. Chem. 58, 419–432. https://doi.org/10.1021/jm5014055

Henry, A.G., Aghamohammadzadeh, S., Samaroo, H., Chen, Y., Mou, K., Needle, E., Hirst, W.D., 2015. Pathogenic LRRK2 mutations, through increased kinase activity, produce enlarged lysosomes with reduced degradative capacity and increase ATP13A2 expression. Hum. Mol. Genet. 24, 6013–6028. https://doi.org/10.1093/hmg/ddv314

Herbst, S., Campbell, P., Harvey, J., Bernard, E.M., Papayannopoulos, V., Wood, N.W., Morris, H.R., Gutierrez, M.G., 2020. LRRK2 activation controls the repair of damaged endomembranes in macrophages. EMBO J. 39, e104494. https://doi.org/10.15252/embj.2020104494

Herzig, M.C., Kolly, C., Persohn, E., Theil, D., Schweizer, T., Hafner, T., Stemmelen, C., Troxler, T.J., Schmid, P., Danner, S., Schnell, C.R., Mueller, M., Kinzel, B., Grevot, A., Bolognani, F., Stirn, M., Kuhn, R.R., Kaupmann, K., van der Putten, P.H., Rovelli, G., Shimshek, D.R., 2011. LRRK2 protein levels are determined by kinase function and are crucial for kidney and lung homeostasis in mice. Hum. Mol. Genet. 20, 4209–4223. https://doi.org/10.1093/hmg/ddr348

Higashi, S., Moore, D.J., Colebrooke, R.E., Biskup, S., Dawson, V.L., Arai, H., Dawson, T.M., Emson, P.C., 2007. Expression and localization of Parkinson's disease-associated leucine-rich repeat kinase 2 in the mouse brain. J. Neurochem. 100, 368–381. https://doi.org/10.1111/j.1471-4159.2006.04246.x

Hill-Burns, E.M., Debelius, J.W., Morton, J.T., Wissemann, W.T., Lewis, M.R., Wallen, Z.D., Peddada, S.D., Factor, S.A., Molho, E., Zabetian, C.P., Knight, R., Payami, H., 2017. Parkinson's Disease and PD Medications Have Distinct Signatures of the Gut Microbiome. Mov. Disord. Off. J. Mov. Disord. Soc. 32, 739–749. https://doi.org/10.1002/mds.26942

Hilton, D., Stephens, M., Kirk, L., Edwards, P., Potter, R., Zajicek, J., Broughton, E., Hagan, H., Carroll, C., 2014. Accumulation of α-synuclein in the bowel of patients in the pre-clinical phase of Parkinson's disease. Acta Neuropathol. (Berl.) 127, 235–241. https://doi.org/10.1007/s00401-013-1214-6

Hinkle, K.M., Yue, M., Behrouz, B., Dächsel, J.C., Lincoln, S.J., Bowles, E.E., Beevers, J.E., Dugger, B., Winner, B., Prots, I., Kent, C.B., Nishioka, K., Lin, W.-L., Dickson, D.W., Janus, C.J., Farrer, M.J., Melrose, H.L., 2012. LRRK2 knockout mice have an intact dopaminergic system but display alterations in exploratory and motor co-ordination behaviors. Mol. Neurodegener. 7, 25. https://doi.org/10.1186/1750-1326-7-25

Hockey, L.N., Kilpatrick, B.S., Eden, E.R., Lin-Moshier, Y., Brailoiu, G.C., Brailoiu, E., Futter, C.E., Schapira, A.H., Marchant, J.S., Patel, S., 2015. Dysregulation of

lysosomal morphology by pathogenic LRRK2 is corrected by TPC2 inhibition. J. Cell Sci. 128, 232–238. https://doi.org/10.1242/jcs.164152

Hoenen, C., Gustin, A., Birck, C., Kirchmeyer, M., Beaume, N., Felten, P., Grandbarbe, L., Heuschling, P., Heurtaux, T., 2016. Alpha-Synuclein Proteins Promote Pro-Inflammatory Cascades in Microglia: Stronger Effects of the A53T Mutant. PloS One 11, e0162717. https://doi.org/10.1371/journal.pone.0162717

Homma, Y., Kinoshita, R., Kuchitsu, Y., Wawro, P.S., Marubashi, S., Oguchi, M.E., Ishida, M., Fujita, N., Fukuda, M., 2019. Comprehensive knockout analysis of the Rab family GTPases in epithelial cells. J. Cell Biol. 218, 2035–2050. https://doi.org/10.1083/jcb.201810134

Howlett, E.H., Jensen, N., Belmonte, F., Zafar, F., Hu, X., Kluss, J., Schüle, B., Kaufman, B.A., Greenamyre, J.T., Sanders, L.H., 2017. LRRK2 G2019S-induced mitochondrial DNA damage is LRRK2 kinase dependent and inhibition restores mtDNA integrity in Parkinson's disease. Hum. Mol. Genet. 26, 4340–4351. https://doi.org/10.1093/hmg/ddx320

Huang, H., Xu, H., Luo, Q., He, J., Li, M., Chen, H., Tang, W., Nie, Y., Zhou, Y., 2019. Fecal microbiota transplantation to treat Parkinson's disease with constipation: A case report. Medicine (Baltimore) 98, e16163. https://doi.org/10.1097/MD.0000000000016163

Hui, K.Y., Fernandez-Hernandez, H., Hu, J., Schaffner, A., Pankratz, N., Hsu, N.-Y., Chuang, L.-S., Carmi, S., Villaverde, N., Li, X., Rivas, M., Levine, A.P., Bao, X., Labrias, P.R., Haritunians, T., Ruane, D., Gettler, K., Chen, E., Li, D., Schiff, E.R., Pontikos, N., Barzilai, N., Brant, S.R., Bressman, S., Cheifetz, A.S., Clark, L.N., Daly, M.J., Desnick, R.J., Duerr, R.H., Katz, S., Lencz, T., Myers, R.H., Ostrer, H., Ozelius, L., Payami, H., Peter, Y., Rioux, J.D., Segal, A.W., Scott, W.K., Silverberg, M.S., Vance, J.M., Ubarretxena-Belandia, I., Foroud, T., Atzmon, G., Pe'er, I., Ioannou, Y., McGovern, D.P.B., Yue, Z., Schadt, E.E., Cho, J.H., Peter, I., 2018. Functional variants in the LRRK2 gene confer shared effects on risk for Crohn's disease and Parkinson's disease. Sci. Transl. Med. 10, eaai7795. https://doi.org/10.1126/scitranslmed.aai7795

Hulihan, M.M., Ishihara-Paul, L., Kachergus, J., Warren, L., Amouri, R., Elango, R., Prinjha, R.K., Upmanyu, R., Kefi, M., Zouari, M., Sassi, S.B., Yahmed, S.B., El Euch-Fayeche, G., Matthews, P.M., Middleton, L.T., Gibson, R.A., Hentati, F., Farrer, M.J., 2008. LRRK2 Gly2019Ser penetrance in Arab-Berber patients from Tunisia: a case-control genetic study. Lancet Neurol. 7, 591–594. https://doi.org/10.1016/S1474-4422(08)70116-9

Iannotta, L., Biosa, A., Kluss, J.H., Tombesi, G., Kaganovich, A., Cogo, S., Plotegher, N., Civiero, L., Lobbestael, E., Baekelandt, V., Cookson, M.R., Greggio, E., 2020. Divergent Effects of G2019S and R1441C LRRK2 Mutations on LRRK2 and Rab10 Phosphorylations in Mouse Tissues. Cells 9, 2344. https://doi.org/10.3390/cells9112344

Ibáñez, P., Bonnet, A.-M., Débarges, B., Lohmann, E., Tison, F., Pollak, P., Agid, Y., Dürr, A., Brice, A., 2004. Causal relation between alpha-synuclein gene duplication and familial Parkinson's disease. Lancet Lond. Engl. 364, 1169–1171. https://doi.org/10.1016/S0140-6736(04)17104-3

Inglis, K.J., Chereau, D., Brigham, E.F., Chiou, S.-S., Schöbel, S., Frigon, N.L., Yu, M., Caccavello, R.J., Nelson, S., Motter, R., Wright, S., Chian, D., Santiago, P., Soriano, F., Ramos, C., Powell, K., Goldstein, J.M., Babcock, M., Yednock, T., Bard, F., Basi, G.S., Sham, H., Chilcote, T.J., McConlogue, L., Griswold-Prenner, I., Anderson, J.P., 2009. Polo-like kinase 2 (PLK2) phosphorylates alpha-synuclein at serine 129 in central nervous system. J. Biol. Chem. 284, 2598–2602. https://doi.org/10.1074/jbc.C800206200

Ishihara, L., Warren, L., Gibson, R., Amouri, R., Lesage, S., Dürr, A., Tazir, M., Wszolek, Z.K., Uitti, R.J., Nichols, W.C., Griffith, A., Hattori, N., Leppert, D., Watts, R., Zabetian, C.P., Foroud, T.M., Farrer, M.J., Brice, A., Middleton, L., Hentati, F., 2006. Clinical features of Parkinson disease patients with homozygous leucine-rich repeat kinase 2 G2019S mutations. Arch. Neurol. 63, 1250–1254. https://doi.org/10.1001/archneur.63.9.1250

Ito, G., Fujimoto, T., Kamikawaji, S., Kuwahara, T., Iwatsubo, T., 2014. Lack of Correlation between the Kinase Activity of LRRK2 Harboring Kinase-Modifying Mutations and Its Phosphorylation at Ser910, 935, and Ser955. PLOS ONE 9, e97988. https://doi.org/10.1371/journal.pone.0097988

Ito, G., Katsemonova, K., Tonelli, F., Lis, P., Baptista, M.A.S., Shpiro, N., Duddy, G., Wilson, S., Ho, P.W.-L., Ho, S.-L., Reith, A.D., Alessi, D.R., 2016. Phos-tag analysis of Rab10 phosphorylation by LRRK2: a powerful assay for assessing kinase function and inhibitors. Biochem. J. 473, 2671–2685. https://doi.org/10.1042/BCJ20160557

Ito, G., Okai, T., Fujino, G., Takeda, K., Ichijo, H., Katada, T., Iwatsubo, T., 2007. GTP binding is essential to the protein kinase activity of LRRK2, a causative gene product for familial Parkinson's disease. Biochemistry 46, 1380–1388. https://doi.org/10.1021/bi061960m

Iwai, A., Masliah, E., Yoshimoto, M., Ge, N., Flanagan, L., de Silva, H.A., Kittel, A., Saitoh, T., 1995. The precursor protein of non-A beta component of Alzheimer's disease amyloid is a presynaptic protein of the central nervous system. Neuron 14, 467–475. https://doi.org/10.1016/0896-6273(95)90302-x

Jankovic, J., 2008. Parkinson's disease: clinical features and diagnosis. J. Neurol. Neurosurg. Psychiatry 79, 368–376. https://doi.org/10.1136/jnnp.2007.131045

Jankovic, J., Aguilar, L.G., 2008. Current approaches to the treatment of Parkinson's disease. Neuropsychiatr. Dis. Treat. 4, 743–757.

Jao, C.C., Hegde, B.G., Chen, J., Haworth, I.S., Langen, R., 2008. Structure of membrane-bound α-synuclein from site-directed spin labeling and computational refinement. Proc. Natl. Acad. Sci. 105, 19666–19671. https://doi.org/10.1073/pnas.0807826105

Jordens, I., Fernandez-Borja, M., Marsman, M., Dusseljee, S., Janssen, L., Calafat, J., Janssen, H., Wubbolts, R., Neefjes, J., 2001. The Rab7 effector protein RILP controls lysosomal transport by inducing the recruitment of dynein-dynactin motors. Curr. Biol. 11, 1680–1685. https://doi.org/10.1016/S0960-9822(01)00531-0

Kachergus, J., Mata, I.F., Hulihan, M., Taylor, J.P., Lincoln, S., Aasly, J., Gibson, J.M., Ross, O.A., Lynch, T., Wiley, J., Payami, H., Nutt, J., Maraganore, D.M.,

Czyzewski, K., Styczynska, M., Wszolek, Z.K., Farrer, M.J., Toft, M., 2005. Identification of a novel LRRK2 mutation linked to autosomal dominant parkinsonism: evidence of a common founder across European populations. Am. J. Hum. Genet. 76, 672–680. https://doi.org/10.1086/429256

Kalogeropulou, A.F., Lis, P., Polinski, N.K., Alessi, D.R., 2020. Rab29 knock-out or transgenic overexpression does not impact basal LRRK2 activity in wildtype and pathogenic mouse and cell line models. bioRxiv 2020.06.08.139675. https://doi.org/10.1101/2020.06.08.139675

Kalogeropulou, A.F., Purlyte, E., Tonelli, F., Lange, S.M., Wightman, M., Prescott, A.R., Padmanabhan, S., Sammler, E., Alessi, D.R., 2022. Impact of 100 LRRK2 variants linked to Parkinson's Disease on kinase activity and microtubule binding. Biochem. J. BCJ20220161. https://doi.org/10.1042/BCJ20220161

Kanaan, N.M., Kordower, J.H., Collier, T.J., 2008. Age and region-specific responses of microglia, but not astrocytes, suggest a role in selective vulnerability of dopamine neurons after 1-methyl-4-phenyl-1,2,3,6-tetrahydropyridine exposure in monkeys. Glia 56, 1199–1214. https://doi.org/10.1002/glia.20690

Kanaan, N.M., Kordower, J.H., Collier, T.J., 2007. Age-related accumulation of Marinesco bodies and lipofuscin in rhesus monkey midbrain dopamine neurons: Relevance to selective neuronal vulnerability. J. Comp. Neurol. 502, 683–700. https://doi.org/10.1002/cne.21333

Karkheiran, S., Shahidi, G.A., Walker, R.H., Paisán-Ruiz, C., 2015. PLA2G6-associated Dystonia–Parkinsonism: Case Report and Literature Review. Tremor Hyperkinetic Mov. 5, 317. https://doi.org/10.7916/D84Q7T4W

Karlsson, M., Zhang, C., Méar, L., Zhong, W., Digre, A., Katona, B., Sjöstedt, E., Butler, L., Odeberg, J., Dusart, P., Edfors, F., Oksvold, P., von Feilitzen, K., Zwahlen, M., Arif, M., Altay, O., Li, X., Ozcan, M., Mardinoglu, A., Fagerberg, L., Mulder, J., Luo, Y., Ponten, F., Uhlén, M., Lindskog, C., 2021. A single–cell type transcriptomics map of human tissues. Sci. Adv. 7, eabh2169. https://doi.org/10.1126/sciadv.abh2169

Kaushik, S., Cuervo, A.M., 2015. Proteostasis and aging. Nat. Med. 21, 1406–1415. https://doi.org/10.1038/nm.4001

Kaye, J., Gage, H., Kimber, A., Storey, L., Trend, P., 2006. Excess burden of constipation in Parkinson's disease: A pilot study. Mov. Disord. 21, 1270–1273. https://doi.org/10.1002/mds.20942

Kelly, K., Chang, A., Hastings, L., Abdelmotilib, H., West, A.B., 2021. Genetic background influences LRRK2-mediated Rab phosphorylation in the rat brain. Brain Res. 1759, 147372. https://doi.org/10.1016/j.brainres.2021.147372

Kelly, K., Wang, S., Boddu, R., Liu, Z., Moukha-Chafiq, O., Augelli-Szafran, C., West, A.B., 2018. The G2019S mutation in LRRK2 imparts resiliency to kinase inhibition. Exp. Neurol. 309, 1–13. https://doi.org/10.1016/j.expneurol.2018.07.012

Kenborg, L., Rugbjerg, K., Lee, P.-C., Ravnskjær, L., Christensen, J., Ritz, B., Lassen, C.F., 2015. Head injury and risk for Parkinson disease: Results from a Danish case-control study. Neurology 84, 1098–1103. https://doi.org/10.1212/WNL.0000000000001362

Keren-Kaplan, T., Bonifacino, J.S., 2021. ARL8 Relieves SKIP Autoinhibition to Enable Coupling of Lysosomes to Kinesin-1. Curr. Biol. 31, 540-554.e5. https://doi.org/10.1016/j.cub.2020.10.071

Kett, L.R., Boassa, D., Ho, C.C.-Y., Rideout, H.J., Hu, J., Terada, M., Ellisman, M., Dauer, W.T., 2012. LRRK2 Parkinson disease mutations enhance its microtubule association. Hum. Mol. Genet. 21, 890–899. https://doi.org/10.1093/hmg/ddr526

Kim, C., Ho, D.-H., Suk, J.-E., You, S., Michael, S., Kang, J., Lee, S.J., Masliah, E., Hwang, D., Lee, H.-J., Lee, S.-J., 2013. Neuron-released oligomeric **α**-synuclein is an endogenous agonist of TLR2 for paracrine activation of microglia. Nat. Commun. 4, 1562. https://doi.org/10.1038/ncomms2534

Kim, H., Sim, H., Lee, J.-E., Seo, M.K., Lim, J., Bang, Y., Nam, D., Lee, S.-Y., Chung, S.-K., Choi, H.J., Park, S.W., Son, I., Kim, J., Seol, W., 2021. Ciliogenesis is Not Directly Regulated by LRRK2 Kinase Activity in Neurons. Exp. Neurobiol. 30, 232–243. https://doi.org/10.5607/en21003

Kim, J.-M., Lee, J.-Y., Kim, H.J., Kim, J.S., Shin, E.-S., Cho, J.-H., Park, S.S., Jeon, B.S., 2010. The LRRK2 G2385R variant is a risk factor for sporadic Parkinson's disease in the Korean population. Parkinsonism Relat. Disord. 16, 85–88. https://doi.org/10.1016/j.parkreldis.2009.10.004

Kim, S., Kwon, S.-H., Kam, T.-I., Panicker, N., Karuppagounder, S.S., Lee, S., Lee, J.H., Kim, W.R., Kook, M., Foss, C.A., Shen, C., Lee, H., Kulkarni, S., Pasricha, P.J., Lee, G., Pomper, M.G., Dawson, V.L., Dawson, T.M., Ko, H.S., 2019. Transneuronal Propagation of Pathologic **α**-Synuclein from the Gut to the Brain Models Parkinson's Disease. Neuron 103, 627-641.e7. https://doi.org/10.1016/j.neuron.2019.05.035

Kingwell, K., 2021. Double setback for ASO trials in Huntington disease. Nat. Rev. Drug Discov. 20, 412–413. https://doi.org/10.1038/d41573-021-00088-6

Kitada, T., Asakawa, S., Hattori, N., Matsumine, H., Yamamura, Y., Minoshima, S., Yokochi, M., Mizuno, Y., Shimizu, N., 1998. Mutations in the parkin gene cause autosomal recessive juvenile parkinsonism. Nature 392, 605–608. https://doi.org/10.1038/33416

Klein, C., Westenberger, A., 2012. Genetics of Parkinson's Disease. Cold Spring Harb. Perspect. Med. 2, a008888. https://doi.org/10.1101/cshperspect.a008888

Kluss, J.H., Bonet-Ponce, L., Lewis, P.A., Cookson, M.R., 2022a. Directing LRRK2 to membranes of the endolysosomal pathway triggers RAB phosphorylation and JIP4 recruitment. Neurobiol. Dis. 170, 105769. https://doi.org/10.1016/j.nbd.2022.105769

Kluss, J.H., Conti, M.M., Kaganovich, A., Beilina, A., Melrose, H.L., Cookson, M.R., Mamais, A., 2018. Detection of endogenous S1292 LRRK2 autophosphorylation in mouse tissue as a readout for kinase activity. Npj Park. Dis. 4, 13. https://doi.org/10.1038/s41531-018-0049-1

Kluss, J.H., Lewis, P.A., Greggio, E., 2022b. Leucine-rich repeat kinase 2 (LRRK2): an update on the potential therapeutic target for Parkinson's disease. Expert Opin. Ther. Targets 0, null. https://doi.org/10.1080/14728222.2022.2082937

Kluss, J.H., Mamais, A., Cookson, M.R., 2019. LRRK2 links genetic and sporadic Parkinson's disease. Biochem. Soc. Trans. BST20180462. https://doi.org/10.1042/BST20180462

Kluss, J.H., Mazza, M.C., Li, Y., Manzoni, C., Lewis, P.A., Cookson, M.R., Mamais, A., 2021. Preclinical modeling of chronic inhibition of the Parkinson's disease associated kinase LRRK2 reveals altered function of the endolysosomal system in vivo. Mol. Neurodegener. 16, 17. https://doi.org/10.1186/s13024-021-00441-8

Komada, M., Soriano, P., 1999. Hrs, a FYVE finger protein localized to early endosomes, is implicated in vesicular traffic and required for ventral folding morphogenesis. Genes Dev. 13, 1475–1485.

Koroğlu, Ç., Baysal, L., Cetinkaya, M., Karasoy, H., Tolun, A., 2013. DNAJC6 is responsible for juvenile parkinsonism with phenotypic variability. Parkinsonism Relat. Disord. 19, 320–324. https://doi.org/10.1016/j.parkreldis.2012.11.006

Korolchuk, V.I., Saiki, S., Lichtenberg, M., Siddiqi, F.H., Roberts, E.A., Imarisio, S., Jahreiss, L., Sarkar, S., Futter, M., Menzies, F.M., O'Kane, C.J., Deretic, V., Rubinsztein, D.C., 2011. Lysosomal positioning coordinates cellular nutrient responses. Nat. Cell Biol. 13, 453–460. https://doi.org/10.1038/ncb2204

Kosaka, K., 1990. Diffuse lewy body disease in Japan. J. Neurol. 237, 197–204. https://doi.org/10.1007/BF00314594

Krebs, C.E., Karkheiran, S., Powell, J.C., Cao, M., Makarov, V., Darvish, H., Di Paolo, G., Walker, R.H., Shahidi, G.A., Buxbaum, J.D., De Camilli, P., Yue, Z., Paisán-Ruiz, C., 2013. The Sac1 domain of SYNJ1 identified mutated in a family with early-onset progressive Parkinsonism with generalized seizures. Hum. Mutat. 34, 1200–1207. https://doi.org/10.1002/humu.22372

Krüger, R., Kuhn, W., Müller, T., Woitalla, D., Graeber, M., Kösel, S., Przuntek, H., Epplen, J.T., Schöls, L., Riess, O., 1998. Ala30Pro mutation in the gene encoding alpha-synuclein in Parkinson's disease. Nat. Genet. 18, 106–108. https://doi.org/10.1038/ng0298-106

Krüger, R., Sharma, M., Riess, O., Gasser, T., Van Broeckhoven, C., Theuns, J., Aasly, J., Annesi, G., Bentivoglio, A.R., Brice, A., Djarmati, A., Elbaz, A., Farrer, M., Ferrarese, C., Gibson, J.M., Hadjigeorgiou, G.M., Hattori, N., Ioannidis, J.P.A., Jasinska-Myga, B., Klein, C., Lambert, J.-C., Lesage, S., Lin, J.-J., Lynch, T., Mellick, G.D., de Nigris, F., Opala, G., Prigione, A., Quattrone, A., Ross, O.A., Satake, W., Silburn, P.A., Tan, E.K., Toda, T., Tomiyama, H., Wirdefeldt, K., Wszolek, Z., Xiromerisiou, G., Maraganore, D.M., Genetic Epidemiology of Parkinson's disease consortium, 2011. A large-scale genetic association study to evaluate the contribution of Omi/HtrA2 (PARK13) to Parkinson's disease. Neurobiol. Aging 32, 548.e9–18. https://doi.org/10.1016/j.neurobiolaging.2009.11.021

Kuai, X., Yao, X., Xu, L., Zhou, Y., Zhang, L., Liu, Y., Pei, S., Zhou, C., 2021. Evaluation of fecal microbiota transplantation in Parkinson's disease patients with constipation. Microb. Cell Factories 20, 98. https://doi.org/10.1186/s12934-021-01589-0

Kuchimanchi, M., Monine, M., Kandadi Muralidharan, K., Woodward, C., Penner, N., 2020. Phase II Dose Selection for Alpha Synuclein-Targeting Antibody

Cinpanemab (BIIB054) Based on Target Protein Binding Levels in the Brain. CPT Pharmacomet. Syst. Pharmacol. 9, 515–522. https://doi.org/10.1002/psp4.12538

Kuwahara, T., Funakawa, K., Komori, T., Sakurai, M., Yoshii, G., Eguchi, T., Fukuda, M., Iwatsubo, T., 2020. Roles of lysosomotropic agents on LRRK2 activation and Rab10 phosphorylation. Neurobiol. Dis. 145, 105081. https://doi.org/10.1016/j.nbd.2020.105081

Kuwahara, T., Inoue, K., D'Agati, V.D., Fujimoto, T., Eguchi, T., Saha, S., Wolozin, B., Iwatsubo, T., Abeliovich, A., 2016. LRRK2 and RAB7L1 coordinately regulate axonal morphology and lysosome integrity in diverse cellular contexts. Sci. Rep. 6, 29945. https://doi.org/10.1038/srep29945

Kuzuhara, S., Mori, H., Izumiyama, N., Yoshimura, M., Ihara, Y., 1988. Lewy bodies are ubiquitinated. A light and electron microscopic immunocytochemical study. Acta Neuropathol. (Berl.) 75, 345–353. https://doi.org/10.1007/BF00687787

Langston, J.W., 2017. The MPTP Story. J. Park. Dis. 7, S11–S19. https://doi.org/10.3233/JPD-179006

Langston, J.W., Ballard, P., Tetrud, J.W., Irwin, I., 1983. Chronic Parkinsonism in Humans Due to a Product of Meperidine-Analog Synthesis. Science 219, 979–980. https://doi.org/10.1126/science.6823561

Langston, J.W., Irwin, I., Langston, E.B., Forno, L.S., 1984. 1-Methyl-4-phenylpyridinium ion (MPP+): Identification of a metabolite of MPTP, a toxin selective to the substantia nigra. Neurosci. Lett. 48, 87–92. https://doi.org/10.1016/0304-3940(84)90293-3

Langston, R.G., Beilina, A., Reed, X., Singleton, A.B., Blauwendraat, C., Gibbs, J.R., Cookson, M.R., 2021. Association of a Common Genetic Variant with Parkinson's Disease is Propagated through Microglia. https://doi.org/10.1101/2021.01.15.426824

Lara Ordónez, A.J., Fernández, B., Fdez, E., Romo-Lozano, M., Madero-Pérez, J., Lobbestael, E., Baekelandt, V., Aiastui, A., López de Munaín, A., Melrose, H.L., Civiero, L., Hilfiker, S., 2019. RAB8, RAB10 and RILPL1 contribute to both LRRK2 kinase–mediated centrosomal cohesion and ciliogenesis deficits. Hum. Mol. Genet. 28, 3552–3568. https://doi.org/10.1093/hmg/ddz201

Lau, C., Ng, L., Thompson, C., Pathak, S., Kuan, L., Jones, A., Hawrylycz, M., 2008. Exploration and visualization of gene expression with neuroanatomy in the adult mouse brain. BMC Bioinformatics 9, 153. https://doi.org/10.1186/1471-2105-9-153

Lavalley, N.J., Slone, S.R., Ding, H., West, A.B., Yacoubian, T.A., 2016. 14-3-3 Proteins regulate mutant LRRK2 kinase activity and neurite shortening. Hum. Mol. Genet. 25, 109–122. https://doi.org/10.1093/hmg/ddv453

Lebouvier, T., Chaumette, T., Damier, P., Coron, E., Touchefeu, Y., Vrignaud, S., Naveilhan, P., Galmiche, J.-P., Varannes, S.B. des, Derkinderen, P., Neunlist, M., 2008. Pathological lesions in colonic biopsies during Parkinson's disease. Gut 57, 1741–1743. https://doi.org/10.1136/gut.2008.162503

Lebouvier, T., Neunlist, M., Bruley des Varannes, S., Coron, E., Drouard, A., N'Guyen, J.-M., Chaumette, T., Tasselli, M., Paillusson, S., Flamand, M., Galmiche, J.-P.,

Damier, P., Derkinderen, P., 2010. Colonic Biopsies to Assess the Neuropathology of Parkinson's Disease and Its Relationship with Symptoms. PLoS ONE 5, e12728. https://doi.org/10.1371/journal.pone.0012728

Lebovitz, C., Wretham, N., Osooly, M., Milne, K., Dash, T., Thornton, S., Tessier-Cloutier, B., Sathiyaseelan, P., Bortnik, S., Go, N.E., Halvorsen, E., Cederberg, R.A., Chow, N., Dos Santos, N., Bennewith, K.L., Nelson, B.H., Bally, M.B., Lam, W.L., Gorski, S.M., 2021. Loss of Parkinson's susceptibility gene LRRK2 promotes carcinogen-induced lung tumorigenesis. Sci. Rep. 11, 2097. https://doi.org/10.1038/s41598-021-81639-0

Lee, A.J., Wang, Y., Alcalay, R.N., Mejia-Santana, H., Saunders-Pullman, R., Bressman, S., Corvol, J.-C., Brice, A., Lesage, S., Mangone, G., Tolosa, E., Pont-Sunyer, C., Vilas, D., Schüle, B., Kausar, F., Foroud, T., Berg, D., Brockmann, K., Goldwurm, S., Siri, C., Asselta, R., Ruiz-Martinez, J., Mondragón, E., Marras, C., Ghate, T., Giladi, N., Mirelman, A., Marder, K., Michael J. Fox LRRK2 Cohort Consortium, 2017. Penetrance estimate of LRRK2 p.G2019S mutation in individuals of non-Ashkenazi Jewish ancestry. Mov. Disord. Off. J. Mov. Disord. Soc. 32, 1432–1438. https://doi.org/10.1002/mds.27059

Lee, B.D., Shin, J.-H., VanKampen, J., Petrucelli, L., West, A.B., Ko, H.S., Lee, Y.-I., Maguire-Zeiss, K.A., Bowers, W.J., Federoff, H.J., Dawson, V.L., Dawson, T.M., 2010. Inhibitors of leucine-rich repeat kinase-2 protect against models of Parkinson's disease. Nat. Med. 16, 998–1000. https://doi.org/10.1038/nm.2199

Lees, A.J., Hardy, J., Revesz, T., 2009. Parkinson's disease. Lancet Lond. Engl. 373, 2055–2066. https://doi.org/10.1016/S0140-6736(09)60492-X

Lees, A.J., Katzenschlager, R., Head, J., Ben-Shlomo, Y., 2001. Ten-year follow-up of three different initial treatments in de-novo PD: a randomized trial. Neurology 57, 1687–1694. https://doi.org/10.1212/wnl.57.9.1687

Lennox, G., Lowe, J., Morrell, K., Landon, M., Mayer, R.J., 1989. Anti-ubiquitin immunocytochemistry is more sensitive than conventional techniques in the detection of diffuse Lewy body disease. J. Neurol. Neurosurg. Psychiatry 52, 67–71. https://doi.org/10.1136/jnnp.52.1.67

Lenoir, M., Ustunel, C., Rajesh, S., Kaur, J., Moreau, D., Gruenberg, J., Overduin, M., 2018. Phosphorylation of conserved phosphoinositide binding pocket regulates sorting nexin membrane targeting. Nat. Commun. 9, 1–12. https://doi.org/10.1038/s41467-018-03370-1

Leroy, E., Anastasopoulos, D., Konitsiotis, S., Lavedan, C., Polymeropoulos, M.H., 1998. Deletions in the Parkin gene and genetic heterogeneity in a Greek family with early onset Parkinson's disease. Hum. Genet. 103, 424–427.

Lesage, S., Anheim, M., Letournel, F., Bousset, L., Honoré, A., Rozas, N., Pieri, L., Madiona, K., Dürr, A., Melki, R., Verny, C., Brice, A., French Parkinson's Disease Genetics Study Group, 2013. G51D α-synuclein mutation causes a novel parkinsonian-pyramidal syndrome. Ann. Neurol. 73, 459–471. https://doi.org/10.1002/ana.23894

Lesage, S., Brice, A., 2009. Parkinson's disease: from monogenic forms to genetic susceptibility factors. Hum. Mol. Genet. 18, R48–R59. https://doi.org/10.1093/hmg/ddp012

Lewis, P.A., Greggio, E., Beilina, A., Jain, S., Baker, A., Cookson, M.R., 2007. The R1441C mutation of LRRK2 disrupts GTP hydrolysis. Biochem. Biophys. Res. Commun. 357, 668–671. https://doi.org/10.1016/j.bbrc.2007.04.006

Lewy, F., 1912. Paralysis agitans. 1. Pathologische Anatomie. Handb. Neurol. Dritter Band Spez. Neurol. I 920–933.

Li, J., Van Vranken, J.G., Pontano Vaites, L., Schweppe, D.K., Huttlin, E.L., Etienne, C., Nandhikonda, P., Viner, R., Robitaille, A.M., Thompson, A.H., Kuhn, K., Pike, I., Bomgarden, R.D., Rogers, J.C., Gygi, S.P., Paulo, J.A., 2020. TMTpro reagents: a set of isobaric labeling mass tags enables simultaneous proteome-wide measurements across 16 samples. Nat. Methods 17, 399–404. https://doi.org/10.1038/s41592-020-0781-4

Li, X., Wang, Q.J., Pan, N., Lee, S., Zhao, Y., Chait, B.T., Yue, Z., 2011. Phosphorylation-Dependent 14-3-3 Binding to LRRK2 Is Impaired by Common Mutations of Familial Parkinson's Disease. PLOS ONE 6, e17153. https://doi.org/10.1371/journal.pone.0017153

Liao, J., Wu, C.-X., Burlak, C., Zhang, S., Sahm, H., Wang, M., Zhang, Z.-Y., Vogel, K.W., Federici, M., Riddle, S.M., Nichols, R.J., Liu, D., Cookson, M.R., Stone, T.A., Hoang, Q.Q., 2014. Parkinson disease-associated mutation R1441H in LRRK2 prolongs the "active state" of its GTPase domain. Proc. Natl. Acad. Sci. U. S. A. 111, 4055–4060. https://doi.org/10.1073/pnas.1323285111

Liberles, S.D., Diver, S.T., Austin, D.J., Schreiber, S.L., 1997. Inducible gene expression and protein translocation using nontoxic ligands identified by a mammalian three-hybrid screen. Proc. Natl. Acad. Sci. U. S. A. 94, 7825–7830.

Lim, S.-Y., Lim, J.L., Ahmad-Annuar, A., Lohmann, K., Tan, A.H., Lim, K.B., Tay, Y.W., Shing, Y.L., Muthusamy, K.A., Bauer, P., Rolfs, A., Klein, C., 2020. Clinical Phenotype of LRRK2 R1441C in 2 Chinese Sisters. Neurodegener. Dis. 20, 39–45. https://doi.org/10.1159/000508131

Lima, M.M.S., Martins, E.F., Delattre, A.M., Proenca, M.B., Mori, M.A., Carabelli, B., Ferraz, A.C., 2012. Motor and Non-Motor Features of Parkinson's Disease – A Review of Clinical and Experimental Studies. CNS Neurol. Disord. - Drug Targets 11, 439–449.

Lin, C.-H., Tsai, P.-I., Wu, R.-M., Chien, C.-T., 2010. LRRK2 G2019S Mutation Induces Dendrite Degeneration through Mislocalization and Phosphorylation of Tau by Recruiting Autoactivated GSK3β. J. Neurosci. 30, 13138–13149. https://doi.org/10.1523/JNEUROSCI.1737-10.2010

Lin, X., Han, L., Weng, J., Wang, K., Chen, T., 2018. Rapamycin inhibits proliferation and induces autophagy in human neuroblastoma cells. Biosci. Rep. 38, BSR20181822. https://doi.org/10.1042/BSR20181822

Lin, X., Parisiadou, L., Gu, X.-L., Wang, L., Shim, H., Sun, L., Xie, C., Long, C.-X., Yang, W.-J., Ding, J., Chen, Z.Z., Gallant, P.E., Tao-Cheng, J.-H., Rudow, G., Troncoso, J.C., Liu, Z., Li, Z., Cai, H., 2009. Leucine-Rich Repeat Kinase 2 Regulates the Progression of Neuropathology Induced by Parkinson's-Disease-Related Mutant α-synuclein. Neuron 64, 807–827. https://doi.org/10.1016/j.neuron.2009.11.006

Lis, P., Burel, S., Steger, M., Mann, M., Brown, F., Diez, F., Tonelli, F., Holton, J.L., Ho, P.W., Ho, S.-L., Chou, M.-Y., Polinski, N.K., Martinez, T.N., Davies, P., Alessi, D.R., 2018. Development of phospho-specific Rab protein antibodies to monitor in vivo activity of the LRRK2 Parkinson's disease kinase. Biochem. J. 475, 1–22. https://doi.org/10.1042/BCJ20170802

Liu, G., Sgobio, C., Gu, X., Sun, L., Lin, X., Yu, J., Parisiadou, L., Xie, C., Sastry, N., Ding, J., Lohr, K.M., Miller, G.W., Mateo, Y., Lovinger, D.M., Cai, H., 2015. Selective expression of Parkinson's disease-related Leucine-rich repeat kinase 2 G2019S missense mutation in midbrain dopaminergic neurons impairs dopamine release and dopaminergic gene expression. Hum. Mol. Genet. 24, 5299–5312. https://doi.org/10.1093/hmg/ddv249

Liu, Z., Bryant, N., Kumaran, R., Beilina, A., Abeliovich, A., Cookson, M.R., West, A.B., 2018. LRRK2 phosphorylates membrane-bound Rabs and is activated by GTP-bound Rab7L1 to promote recruitment to the trans-Golgi network. Hum. Mol. Genet. 27, 385–395. https://doi.org/10.1093/hmg/ddx410

Liu, Z., Mobley, J.A., DeLucas, L.J., Kahn, R.A., West, A.B., 2016. LRRK2 autophosphorylation enhances its GTPase activity. FASEB J. 30, 336–347. https://doi.org/10.1096/fj.15-277095

Liu, Z., Wang, X., Yu, Y., Li, X., Wang, T., Jiang, H., Ren, Q., Jiao, Y., Sawa, A., Moran, T., Ross, C.A., Montell, C., Smith, W.W., 2008. A Drosophila model for LRRK2-linked parkinsonism. Proc. Natl. Acad. Sci. 105, 2693–2698. https://doi.org/10.1073/pnas.0708452105

Loane, C., Politis, M., 2011. Positron emission tomography neuroimaging in Parkinson's disease. Am. J. Transl. Res. 3, 323–341.

Lobbestael, E., Civiero, L., De Wit, T., Taymans, J.-M., Greggio, E., Baekelandt, V., 2016. Pharmacological LRRK2 kinase inhibition induces LRRK2 protein destabilization and proteasomal degradation. Sci. Rep. 6. https://doi.org/10.1038/srep33897

Lou, H.-Y., Zhao, W., Zeng, Y., Cui, B., 2018. The Role of Membrane Curvature in Nanoscale Topography-Induced Intracellular Signaling. Acc. Chem. Res. 51, 1046–1053. https://doi.org/10.1021/acs.accounts.7b00594

Lu, C.-S., Lai, S.-C., Wu, R.-M., Weng, Y.-H., Huang, C.-L., Chen, R.-S., Chang, H.-C., Wu-Chou, Y.-H., Yeh, T.-H., 2012. PLA2G6 mutations in PARK14-linked young-onset parkinsonism and sporadic Parkinson's disease. Am. J. Med. Genet. B Neuropsychiatr. Genet. 159B, 183–191. https://doi.org/10.1002/ajmg.b.32012

Lu, T., Aron, L., Zullo, J., Pan, Y., Kim, H., Chen, Y., Yang, T.-H., Kim, H.-M., Drake, D., Liu, X.S., Bennett, D.A., Colaiácovo, M.P., Yankner, B.A., 2014. REST and Stress Resistance in Aging and Alzheimer's Disease. Nature 507, 448–454. https://doi.org/10.1038/nature13163

Lucking, C.B., Abbas, N., Dürr, A., Bonifati, V., Bonnet, A.M., de Broucker, T., De Michele, G., Wood, N.W., Agid, Y., Brice, A., 1998. Homozygous deletions in parkin gene in European and North African families with autosomal recessive juvenile parkinsonism. The European Consortium on Genetic Susceptibility in Parkinson's Disease and the French Parkinson's Disease Genetics Study Group.

Lancet Lond. Engl. 352, 1355–1356. https://doi.org/10.1016/s0140-6736(05)60746-5

Mackenzie, I.R.A., 2001. The pathology of Parkinson's disease | British Columbia Medical Journal. BCMJ 43, 142–147.

MacLeod, D., Dowman, J., Hammond, R., Leete, T., Inoue, K., Abeliovich, A., 2006. The familial Parkinsonism gene LRRK2 regulates neurite process morphology. Neuron 52, 587–593. https://doi.org/10.1016/j.neuron.2006.10.008

Mainou, B.A., Dermody, T.S., 2012. Transport to late endosomes is required for efficient reovirus infection. J. Virol. 86, 8346–8358. https://doi.org/10.1128/JVI.00100-12

Mamais, A., Chia, R., Beilina, A., Hauser, D.N., Hall, C., Lewis, P.A., Cookson, M.R., Bandopadhyay, R., 2014. Arsenite stress down-regulates phosphorylation and 14-3-3 binding of leucine-rich repeat kinase 2 (LRRK2), promoting self-association and cellular redistribution. J. Biol. Chem. 289, 21386–21400. https://doi.org/10.1074/jbc.M113.528463

Mamais, A., Kluss, J.H., Bonet-Ponce, L., Landeck, N., Langston, R.G., Smith, N., Beilina, A., Kaganovich, A., Ghosh, M.C., Pellegrini, L., Kumaran, R., Papazoglou, I., Heaton, G.R., Bandopadhyay, R., Maio, N., Kim, C., LaVoie, M.J., Gershlick, D.C., Cookson, M.R., 2021. Mutations in LRRK2 linked to Parkinson disease sequester Rab8a to damaged lysosomes and regulate transferrin-mediated iron uptake in microglia. PLOS Biol. 19, e3001480. https://doi.org/10.1371/journal.pbio.3001480

Mamais, A., Raja, M., Manzoni, C., Dihanich, S., Lees, A., Moore, D., Lewis, P.A., Bandopadhyay, R., 2013. Divergent α-synuclein solubility and aggregation properties in G2019S LRRK2 Parkinson's disease brains with Lewy Body pathology compared to idiopathic cases. Neurobiol. Dis. 58, 183–190. https://doi.org/10.1016/j.nbd.2013.05.017

Mandler, M., Valera, E., Rockenstein, E., Weninger, H., Patrick, C., Adame, A., Santic, R., Meindl, S., Vigl, B., Smrzka, O., Schneeberger, A., Mattner, F., Masliah, E., 2014. Next-generation active immunization approach for synucleinopathies: implications for Parkinson's disease clinical trials. Acta Neuropathol. (Berl.) 127, 861–879. https://doi.org/10.1007/s00401-014-1256-4

Manyam, B.V., 1990. Paralysis agitans and levodopa in "Ayurveda": Ancient Indian medical treatise. Mov. Disord. 5, 47–48. https://doi.org/10.1002/mds.870050112

Manzoni, C., Mamais, A., Dihanich, S., Abeti, R., Soutar, M.P.M., Plun-Favreau, H., Giunti, P., Tooze, S.A., Bandopadhyay, R., Lewis, P.A., 2013. Inhibition of LRRK2 kinase activity stimulates macroautophagy. Biochim. Biophys. Acta BBA - Mol. Cell Res. 1833, 2900–2910. https://doi.org/10.1016/j.bbamcr.2013.07.020

Marsili, L., Rizzo, G., Colosimo, C., 2018. Diagnostic Criteria for Parkinson's Disease: From James Parkinson to the Concept of Prodromal Disease. Front. Neurol. 9, 156. https://doi.org/10.3389/fneur.2018.00156

Martín, R., Chain, F., Miquel, S., Lu, J., Gratadoux, J.-J., Sokol, H., Verdu, E.F., Bercik, P., Bermúdez-Humarán, L.G., Langella, P., 2014. The commensal bacterium Faecalibacterium prausnitzii is protective in DNBS-induced chronic moderate

and severe colitis models. Inflamm. Bowel Dis. 20, 417–430. https://doi.org/10.1097/01.MIB.0000440815.76627.64

Marui, W., Iseki, E., Kato, M., Akatsu, H., Kosaka, K., 2004. Pathological entity of dementia with Lewy bodies and its differentiation from Alzheimer's disease. Acta Neuropathol. (Berl.) 108, 121–128. https://doi.org/10.1007/s00401-004-0869-4

Masliah, E., Dumaop, W., Galasko, D., Desplats, P., 2013. Distinctive patterns of DNA methylation associated with Parkinson disease. Epigenetics 8, 1030–1038. https://doi.org/10.4161/epi.25865

Matikainen-Ankney, B.A., Kezunovic, N., Mesias, R.E., Tian, Y., Williams, F.M., Huntley, G.W., Benson, D.L., 2016. Altered Development of Synapse Structure and Function in Striatum Caused by Parkinson's Disease-Linked LRRK2–G2019S Mutation. J. Neurosci. 36, 7128–7141. https://doi.org/10.1523/JNEUROSCI.3314-15.2016

Matsui, T., Fukuda, M., 2013. Rab12 regulates mTORC1 activity and autophagy through controlling the degradation of amino-acid transporter PAT4. EMBO Rep. 14, 450–457. https://doi.org/10.1038/embor.2013.32

Matsui, T., Fukuda, M., 2011. Small GTPase Rab12 regulates transferrin receptor degradation. Cell. Logist. 1, 155–158. https://doi.org/10.4161/cl.1.4.18152

Matsui, T., Itoh, T., Fukuda, M., 2011. Small GTPase Rab12 regulates constitutive degradation of transferrin receptor. Traffic Cph. Den. 12, 1432–1443. https://doi.org/10.1111/j.1600-0854.2011.01240.x

Matzuk, M.M., Saper, C.B., 1985. Preservation of hypothalamic dopaminergic neurons in Parkinson's disease. Ann. Neurol. 18, 552–555. https://doi.org/10.1002/ana.410180507

Mazza, M.C., Nguyen, V., Beilina, A., Karakoleva, E., Coyle, M., Ding, J., Bishop, C., Cookson, M.R., 2021. Combined Knockout of Lrrk2 and Rab29 Does Not Result in Behavioral Abnormalities in vivo. J. Park. Dis. 11, 569–584. https://doi.org/10.3233/JPD-202172

McFarthing, K., Rafaloff, G., Baptista, M.A.S., Wyse, R.K., Stott, S.R.W., 2021. Parkinson's Disease Drug Therapies in the Clinical Trial Pipeline: 2021 Update. J. Park. Dis. 11, 891–903. https://doi.org/10.3233/JPD-219006

Meade, R.M., Fairlie, D.P., Mason, J.M., 2019. Alpha-synuclein structure and Parkinson's disease – lessons and emerging principles. Mol. Neurodegener. 14, 29. https://doi.org/10.1186/s13024-019-0329-1

Mederos, S., González-Arias, C., Perea, G., 2018. Astrocyte–Neuron Networks: A Multilane Highway of Signaling for Homeostatic Brain Function. Front. Synaptic Neurosci. 10.

Meiser, J., Weindl, D., Hiller, K., 2013. Complexity of dopamine metabolism. Cell Commun. Signal. 11, 34. https://doi.org/10.1186/1478-811X-11-34

Menšíková, K., Matěj, R., Colosimo, C., Rosales, R., Tučková, L., Ehrmann, J., Hraboš, D., Kolaříková, K., Vodička, R., Vrtěl, R., Procházka, M., Nevrlý, M., Kaiserová, M., Kurčová, S., Otruba, P., Kaňovský, P., 2022. Lewy body disease or diseases with Lewy bodies? Npj Park. Dis. 8, 1–11. https://doi.org/10.1038/s41531-021-00273-9

Metman, L.V., Del Dotto, P., LePoole, K., Konitsiotis, S., Fang, J., Chase, T.N., 1999. Amantadine for levodopa-induced dyskinesias: a 1-year follow-up study. Arch. Neurol. 56, 1383–1386. https://doi.org/10.1001/archneur.56.11.1383

Miklavc, P., Ehinger, K., Thompson, K.E., Hobi, N., Shimshek, D.R., Frick, M., 2014. Surfactant Secretion in LRRK2 Knock-Out Rats: Changes in Lamellar Body Morphology and Rate of Exocytosis. PLOS ONE 9, e84926. https://doi.org/10.1371/journal.pone.0084926

Mir, R., Tonelli, F., Lis, P., Macartney, T., Polinski, N.K., Martinez, T.N., Chou, M.-Y., Howden, A.J.M., König, T., Hotzy, C., Milenkovic, I., Brücke, T., Zimprich, A., Sammler, E., Alessi, D.R., 2018. The Parkinson's disease VPS35[D620N] mutation enhances LRRK2-mediated Rab protein phosphorylation in mouse and human. Biochem. J. 475, 1861–1883. https://doi.org/10.1042/BCJ20180248

Montagnac, G., Sibarita, J.-B., Loubéry, S., Daviet, L., Romao, M., Raposo, G., Chavrier, P., 2009. ARF6 Interacts with JIP4 to Control a Motor Switch Mechanism Regulating Endosome Traffic in Cytokinesis. Curr. Biol. 19, 184–195. https://doi.org/10.1016/j.cub.2008.12.043

Moore, K., McKnight, A.J., Craig, D., O'Neill, F., 2014. Epigenome-Wide Association Study for Parkinson's Disease. NeuroMolecular Med. 16, 845–855. https://doi.org/10.1007/s12017-014-8332-8

Moors, T.E., Maat, C.A., Niedieker, D., Mona, D., Petersen, D., Timmermans-Huisman, E., Kole, J., El-Mashtoly, S.F., Spycher, L., Zago, W., Barbour, R., Mundigl, O., Kaluza, K., Huber, S., Hug, M.N., Kremer, T., Ritter, M., Dziadek, S., Geurts, J.J.G., Gerwert, K., Britschgi, M., van de Berg, W.D.J., 2021. The subcellular arrangement of alpha-synuclein proteoforms in the Parkinson's disease brain as revealed by multicolor STED microscopy. Acta Neuropathol. (Berl.) 142, 423–448. https://doi.org/10.1007/s00401-021-02329-9

Mortiboys, H., Johansen, K.K., Aasly, J.O., Bandmann, O., 2010. Mitochondrial impairment in patients with Parkinson disease with the G2019S mutation in LRRK2. Neurology 75, 2017–2020. https://doi.org/10.1212/WNL.0b013e3181ff9685

Mu, Z., Wang, L., Deng, W., Wang, J., Wu, G., 2017. Structural insight into the Ragulator complex which anchors mTORC1 to the lysosomal membrane. Cell Discov. 3, 1–10. https://doi.org/10.1038/celldisc.2017.49

Myasnikov, A., Zhu, H., Hixson, P., Xie, B., Yu, K., Pitre, A., Peng, J., Sun, J., 2021. Structural analysis of the full-length human LRRK2. Cell 184, 3519-3527.e10. https://doi.org/10.1016/j.cell.2021.05.004

Nalls, M.A., Blauwendraat, C., Vallerga, C.L., Heilbron, K., Bandres-Ciga, S., Chang, D., Tan, M., Kia, D.A., Noyce, A.J., Xue, A., Bras, J., Young, E., von Coelln, R., Simón-Sánchez, J., Schulte, C., Sharma, M., Krohn, L., Pihlstrøm, L., Siitonen, A., Iwaki, H., Leonard, H., Faghri, F., Gibbs, J.R., Hernandez, D.G., Scholz, S.W., Botia, J.A., Martinez, M., Corvol, J.-C., Lesage, S., Jankovic, J., Shulman, L.M., Sutherland, M., Tienari, P., Majamaa, K., Toft, M., Andreassen, O.A., Bangale, T., Brice, A., Yang, J., Gan-Or, Z., Gasser, T., Heutink, P., Shulman, J.M., Wood, N.W., Hinds, D.A., Hardy, J.A., Morris, H.R., Gratten, J., Visscher, P.M., Graham, R.R., Singleton, A.B., Adarmes-Gómez, A.D., Aguilar, M., Aitkulova, A.,

Akhmetzhanov, V., Alcalay, R.N., Alvarez, I., Alvarez, V., Bandres-Ciga, S., Barrero, F.J., Bergareche Yarza, J.A., Bernal-Bernal, I., Billingsley, K., Blauwendraat, C., Blazquez, M., Bonilla-Toribio, M., Botía, J.A., Boungiorno, M.T., Bras, J., Brice, A., Brockmann, K., Bubb, V., Buiza-Rueda, D., Cámara, A., Carrillo, F., Carrión-Claro, M., Cerdan, D., Chelban, V., Clarimón, J., Clarke, C., Compta, Y., Cookson, M.R., Corvol, J.-C., Craig, D.W., Danjou, F., Diez-Fairen, M., Dols-Icardo, O., Duarte, J., Duran, R., Escamilla-Sevilla, F., Escott-Price, V., Ezquerra, M., Faghri, F., Feliz, C., Fernández, M., Fernández-Santiago, R., Finkbeiner, S., Foltynie, T., Gan-Or, Z., Garcia, C., García-Ruiz, P., Gasser, T., Gibbs, J.R., Gomez Heredia, M.J., Gómez-Garre, P., González, M.M., Gonzalez-Aramburu, I., Guelfi, S., Guerreiro, R., Hardy, J., Hassin-Baer, S., Hernandez, D.G., Heutink, P., Hoenicka, J., Holmans, P., Houlden, H., Infante, J., Iwaki, H., Jesús, S., Jimenez-Escrig, A., Kaishybayeva, G., Kaiyrzhanov, R., Karimova, A., Kia, D.A., Kinghorn, K.J., Koks, S., Krohn, L., Kulisevsky, J., Labrador-Espinosa, M.A., Leonard, H.L., Lesage, S., Lewis, P., Lopez-Sendon, J.L., Lovering, R., Lubbe, S., Lungu, C., Macias, D., Majamaa, K., Manzoni, C., Marín, J., Marinus, J., Marti, M.J., Martinez, M., Martínez Torres, I., Martínez-Castrillo, J.C., Mata, M., Mencacci, N.E., Méndez-del-Barrio, C., Middlehurst, B., Mínguez, A., Mir, P., Mok, K.Y., Morris, H.R., Muñoz, E., Nalls, M.A., Narendra, D., Noyce, A.J., Ojo, O.O., Okubadejo, N.U., Pagola, A.G., Pastor, P., Perez Errazquin, F., Periñán-Tocino, T., Pihlstrom, L., Plun-Favreau, H., Quinn, J., R'Bibo, L., Reed, X., Rezola, E.M., Rizig, M., Rizzu, P., Robak, L., Rodriguez, A.S., Rouleau, G.A., Ruiz-Martínez, J., Ruz, C., Ryten, M., Sadykova, D., Scholz, S.W., Schreglmann, S., Schulte, C., Sharma, M., Shashkin, C., Shulman, J.M., Sierra, M., Siitonen, A., Simón-Sánchez, J., Singleton, A.B., Suarez-Sanmartin, E., Taba, P., Tabernero, C., Tan, M.X., Tartari, J.P., Tejera-Parrado, C., Toft, M., Tolosa, E., Trabzuni, D., Valldeoriola, F., van Hilten, J.J., Van Keuren-Jensen, K., Vargas-González, L., Vela, L., Vives, F., Williams, N., Wood, N.W., Zharkinbekova, N., Zharmukhanov, Z., Zholdybayeva, E., Zimprich, A., Ylikotila, P., Shulman, L.M., von Coelln, R., Reich, S., Savitt, J., Agee, M., Alipanahi, B., Auton, A., Bell, R.K., Bryc, K., Elson, S.L., Fontanillas, P., Furlotte, N.A., Huber, K.E., Hicks, B., Jewett, E.M., Jiang, Y., Kleinman, A., Lin, K.-H., Litterman, N.K., McCreight, J.C., McIntyre, M.H., McManus, K.F., Mountain, J.L., Noblin, E.S., Northover, C.A.M., Pitts, S.J., Poznik, G.D., Sathirapongsasuti, J.F., Shelton, J.F., Shringarpure, S., Tian, C., Tung, J., Vacic, V., Wang, X., Wilson, C.H., Anderson, T., Bentley, S., Dalrymple-Alford, J., Fowdar, J., Gratten, J., Halliday, G., Henders, A.K., Hickie, I., Kassam, I., Kennedy, M., Kwok, J., Lewis, S., Mellick, G., Montgomery, G., Pearson, J., Pitcher, T., Sidorenko, J., Silburn, P.A., Vallerga, C.L., Visscher, P.M., Wallace, L., Wray, N.R., Xue, A., Yang, J., Zhang, F., 2019. Identification of novel risk loci, causal insights, and heritable risk for Parkinson's disease: a meta-analysis of genome-wide association studies. Lancet Neurol. 18, 1091–1102. https://doi.org/10.1016/S1474-4422(19)30320-5

Nalls, M.A., Pankratz, N., Lill, C.M., Do, C.B., Hernandez, D.G., Saad, M., DeStefano, A.L., Kara, E., Bras, J., Sharma, M., Schulte, C., Keller, M.F., Arepalli, S., Letson, C., Edsall, C., Stefansson, H., Liu, X., Pliner, H., Lee, J.H., Cheng, R.,

International Parkinson's Disease Genomics Consortium (IPDGC), Parkinson's Study Group (PSG) Parkinson's Research: The Organized GENetics Initiative (PROGENI), 23andMe, GenePD, NeuroGenetics Research Consortium (NGRC), Hussman Institute of Human Genomics (HIHG), Ashkenazi Jewish Dataset Investigator, Cohorts for Health and Aging Research in Genetic Epidemiology (CHARGE), North American Brain Expression Consortium (NABEC), United Kingdom Brain Expression Consortium (UKBEC), Greek Parkinson's Disease Consortium, Alzheimer Genetic Analysis Group, Ikram, M.A., Ioannidis, J.P.A., Hadjigeorgiou, G.M., Bis, J.C., Martinez, M., Perlmutter, J.S., Goate, A., Marder, K., Fiske, B., Sutherland, M., Xiromerisiou, G., Myers, R.H., Clark, L.N., Stefansson, K., Hardy, J.A., Heutink, P., Chen, H., Wood, N.W., Houlden, H., Payami, H., Brice, A., Scott, W.K., Gasser, T., Bertram, L., Eriksson, N., Foroud, T., Singleton, A.B., 2014. Large-scale meta-analysis of genome-wide association data identifies six new risk loci for Parkinson's disease. Nat. Genet. 46, 989–993. https://doi.org/10.1038/ng.3043

Navarro-Romero, A., Montpeyó, M., Martinez-Vicente, M., 2020. The Emerging Role of the Lysosome in Parkinson's Disease. Cells 9, 2399. https://doi.org/10.3390/cells9112399

Ness, D., Ren, Z., Gardai, S., Sharpnack, D., Johnson, V.J., Brennan, R.J., Brigham, E.F., Olaharski, A.J., 2013. Leucine-Rich Repeat Kinase 2 (LRRK2)-Deficient Rats Exhibit Renal Tubule Injury and Perturbations in Metabolic and Immunological Homeostasis. PLOS ONE 8, e66164. https://doi.org/10.1371/journal.pone.0066164

Ng, C.-H., Mok, S.Z.S., Koh, C., Ouyang, X., Fivaz, M.L., Tan, E.-K., Dawson, V.L., Dawson, T.M., Yu, F., Lim, K.-L., 2009. Parkin Protects against LRRK2 G2019S Mutant-Induced Dopaminergic Neurodegeneration in Drosophila. J. Neurosci. 29, 11257–11262. https://doi.org/10.1523/JNEUROSCI.2375-09.2009

Nguyen, N., Shteyn, V., Melia, T.J., 2017. Sensing Membrane Curvature in Macroautophagy. J. Mol. Biol. 429, 457–472. https://doi.org/10.1016/j.jmb.2017.01.006

Nichols, R.J., 2017. LRRK2 Phosphorylation. Adv. Neurobiol. 14, 51–70. https://doi.org/10.1007/978-3-319-49969-7_3

Nichols, R.J., Dzamko, N., Hutti, J.E., Cantley, L.C., Deak, M., Moran, J., Bamborough, P., Reith, A.D., Alessi, D.R., 2009. Substrate specificity and inhibitors of LRRK2, a protein kinase mutated in Parkinson's disease. Biochem. J. 424, 47–60. https://doi.org/10.1042/BJ20091035

Nichols, R.J., Dzamko, N., Morrice, N.A., Campbell, D.G., Deak, M., Ordureau, A., Macartney, T., Tong, Y., Shen, J., Prescott, A.R., Alessi, D.R., 2010. 14-3-3 binding to LRRK2 is disrupted by multiple Parkinson's disease-associated mutations and regulates cytoplasmic localization. Biochem. J. 430, 393–404. https://doi.org/10.1042/BJ20100483

Niu, J., Yu, M., Wang, C., Xu, Z., 2012. Leucine-rich repeat kinase 2 disturbs mitochondrial dynamics via Dynamin-like protein. J. Neurochem. 122, 650–658. https://doi.org/10.1111/j.1471-4159.2012.07809.x

Nixon-Abell, J., Berwick, D.C., Grannó, S., Spain, V.A., Blackstone, C., Harvey, K., 2016. Protective LRRK2 R1398H Variant Enhances GTPase and Wnt Signaling Activity. Front. Mol. Neurosci. 9. https://doi.org/10.3389/fnmol.2016.00018

Nutt, J.G., Woodward, W.R., Beckner, R.M., Stone, C.K., Berggren, K., Carter, J.H., Gancher, S.T., Hammerstad, J.P., Gordin, A., 1994. Effect of peripheral catechol-O-methyltransferase inhibition on the pharmacokinetics and pharmacodynamics of levodopa in parkinsonian patients. Neurology 44, 913–913. https://doi.org/10.1212/WNL.44.5.913

Nuytemans, K., Theuns, J., Cruts, M., Van Broeckhoven, C., 2010. Genetic etiology of Parkinson disease associated with mutations in the SNCA, PARK2, PINK1, PARK7, and LRRK2 genes: a mutation update. Hum. Mutat. 31, 763–780. https://doi.org/10.1002/humu.21277

Olgiati, S., De Rosa, A., Quadri, M., Criscuolo, C., Breedveld, G.J., Picillo, M., Pappatà, S., Quarantelli, M., Barone, P., De Michele, G., Bonifati, V., 2014. PARK20 caused by SYNJ1 homozygous Arg258Gln mutation in a new Italian family. Neurogenetics 15, 183–188. https://doi.org/10.1007/s10048-014-0406-0

Olgiati, S., Quadri, M., Fang, M., Rood, J.P.M.A., Saute, J.A., Chien, H.F., Bouwkamp, C.G., Graafland, J., Minneboo, M., Breedveld, G.J., Zhang, J., International Parkinsonism Genetics Network, Verheijen, F.W., Boon, A.J.W., Kievit, A.J.A., Jardim, L.B., Mandemakers, W., Barbosa, E.R., Rieder, C.R.M., Leenders, K.L., Wang, J., Bonifati, V., 2016. DNAJC6 Mutations Associated With Early-Onset Parkinson's Disease. Ann. Neurol. 79, 244–256. https://doi.org/10.1002/ana.24553

Omar, J., Rosenbaum, E., Efergan, A., Sneineh, B.A., Yeheskel, A., Maruta, Y., Fukuda, M., Sagi-Eisenberg, R., 2021. Biochemical and structural insights into Rab12 interactions with RILP and its family members. Sci. Rep. 11, 10317. https://doi.org/10.1038/s41598-021-89394-y

Padmanabhan, S., Lanz, T.A., Gorman, D., Wolfe, M., Joyce, A., Cabrera, C., Lawrence-Henderson, R., Levers, N., Joshi, N., Ma, T.C., Liong, C., Narayan, S., Alcalay, R.N., Hutten, S.J., Baptista, M.A.S., Merchant, K., 2020. An Assessment of LRRK2 Serine 935 Phosphorylation in Human Peripheral Blood Mononuclear Cells in Idiopathic Parkinson's Disease and G2019S LRRK2 Cohorts. J. Park. Dis. 10, 623–629. https://doi.org/10.3233/JPD-191786

Pagano, G., Boess, F.G., Taylor, K.I., Ricci, B., Mollenhauer, B., Poewe, W., Boulay, A., Anzures-Cabrera, J., Vogt, A., Marchesi, M., Post, A., Nikolcheva, T., Kinney, G.G., Zago, W.M., Ness, D.K., Svoboda, H., Britschgi, M., Ostrowitzki, S., Simuni, T., Marek, K., Koller, M., Sevigny, J., Doody, R., Fontoura, P., Umbricht, D., Bonni, A., PASADENA Investigators, Prasinezumab Study Group, 2021. A Phase II Study to Evaluate the Safety and Efficacy of Prasinezumab in Early Parkinson's Disease (PASADENA): Rationale, Design, and Baseline Data. Front. Neurol. 12, 705407. https://doi.org/10.3389/fneur.2021.705407

Paisan-Ruiz, C., Bhatia, K.P., Li, A., Hernandez, D., Davis, M., Wood, N.W., Hardy, J., Houlden, H., Singleton, A., Schneider, S.A., 2009. Characterization of PLA2G6 as a locus for dystonia-parkinsonism. Ann. Neurol. 65, 19–23. https://doi.org/10.1002/ana.21415

Paisán-Ruíz, C., Jain, S., Evans, E.W., Gilks, W.P., Simón, J., van der Brug, M., López de Munain, A., Aparicio, S., Gil, A.M., Khan, N., Johnson, J., Martinez, J.R., Nicholl, D., Carrera, I.M., Pena, A.S., de Silva, R., Lees, A., Martí-Massó, J.F., Pérez-Tur, J., Wood, N.W., Singleton, A.B., 2004. Cloning of the gene containing mutations that cause PARK8-linked Parkinson's disease. Neuron 44, 595–600. https://doi.org/10.1016/j.neuron.2004.10.023

Paisán-Ruiz, C., Lewis, P.A., Singleton, A.B., 2013. LRRK2: Cause, Risk, and Mechanism. J. Park. Dis. 3, 85–103. https://doi.org/10.3233/JPD-130192

Paisán-Ruíz, C., Nath, P., Washecka, N., Gibbs, J.R., Singleton, A.B., 2008. Comprehensive analysis of LRRK2 in publicly available Parkinson's disease cases and neurologically normal controls. Hum. Mutat. 29, 485–490. https://doi.org/10.1002/humu.20668

Pajarillo, E., Rizor, A., Lee, J., Aschner, M., Lee, E., 2019. The role of posttranslational modifications of α-synuclein and LRRK2 in Parkinson's disease: Potential contributions of environmental factors. Biochim. Biophys. Acta Mol. Basis Dis. 1865, 1992–2000. https://doi.org/10.1016/j.bbadis.2018.11.017

Pang, S.Y.-Y., Ho, P.W.-L., Liu, H.-F., Leung, C.-T., Li, L., Chang, E.E.S., Ramsden, D.B., Ho, S.-L., 2019. The interplay of aging, genetics and environmental factors in the pathogenesis of Parkinson's disease. Transl. Neurodegener. 8, 23. https://doi.org/10.1186/s40035-019-0165-9

Park, G., Tan, J., Garcia, G., Kang, Y., Salvesen, G., Zhang, Z., 2016. Regulation of Histone Acetylation by Autophagy in Parkinson Disease. J. Biol. Chem. 291, 3531–3540. https://doi.org/10.1074/jbc.M115.675488

Parkinson, J., 2002. An Essay on the Shaking Palsy. J. Neuropsychiatry Clin. Neurosci. 14, 223–236. https://doi.org/10.1176/jnp.14.2.223

Parkinson Study Group, 2002. Dopamine transporter brain imaging to assess the effects of pramipexole vs levodopa on Parkinson disease progression. JAMA 287, 1653–1661. https://doi.org/10.1001/jama.287.13.1653

Pasanen, P., Myllykangas, L., Siitonen, M., Raunio, A., Kaakkola, S., Lyytinen, J., Tienari, P.J., Pöyhönen, M., Paetau, A., 2014. Novel α-synuclein mutation A53E associated with atypical multiple system atrophy and Parkinson's disease-type pathology. Neurobiol. Aging 35, 2180.e1–5. https://doi.org/10.1016/j.neurobiolaging.2014.03.024

Pavlou, M.A.S., Outeiro, T.F., 2017. Epigenetics in Parkinson's Disease, in: Delgado-Morales, R. (Ed.), Neuroepigenomics in Aging and Disease, Advances in Experimental Medicine and Biology. Springer International Publishing, Cham, pp. 363–390. https://doi.org/10.1007/978-3-319-53889-1_19

Pellegrini, L., Hauser, D.N., Li, Y., Mamais, A., Beilina, A., Kumaran, R., Wetzel, A., Nixon-Abell, J., Heaton, G., Rudenko, I., Alkaslasi, M., Ivanina, N., Melrose, H.L., Cookson, M.R., Harvey, K., 2018. Proteomic analysis reveals co-ordinated alterations in protein synthesis and degradation pathways in LRRK2 knockout mice. Hum. Mol. Genet. 27, 3257–3271. https://doi.org/10.1093/hmg/ddy232

Peng, F., Sun, Y.-M., Chen, C., Luo, S.-S., Li, D.-K., Wang, Y.-X., Yang, K., Liu, F.-T., Zuo, C.-T., Ding, Z.-T., An, Y., Wu, J.-J., Wang, J., 2017. The heterozygous R1441C mutation of leucine-rich repeat kinase 2 gene in a Chinese patient with

Parkinson disease: A five-year follow-up and literatures review. J. Neurol. Sci. 373, 23–26. https://doi.org/10.1016/j.jns.2016.12.009

Peng, W., Minakaki, G., Nguyen, M., Krainc, D., 2019. Preserving Lysosomal Function in the Aging Brain: Insights from Neurodegeneration. Neurotherapeutics 16, 611–634. https://doi.org/10.1007/s13311-019-00742-3

Pereira, C., Miguel Martins, L., Saraiva, L., 2014. LRRK2, but not pathogenic mutants, protects against H2O2 stress depending on mitochondrial function and endocytosis in a yeast model. Biochim. Biophys. Acta BBA - Gen. Subj. 1840, 2025–2031. https://doi.org/10.1016/j.bbagen.2014.02.015

Periquet, M., Fulga, T., Myllykangas, L., Schlossmacher, M.G., Feany, M.B., 2007. Aggregated alpha-synuclein mediates dopaminergic neurotoxicity in vivo. J. Neurosci. Off. J. Soc. Neurosci. 27, 3338–3346. https://doi.org/10.1523/JNEUROSCI.0285-07.2007

Peter, I., Dubinsky, M., Bressman, S., Park, A., Lu, C., Chen, N., Wang, A., 2018. Anti–Tumor Necrosis Factor Therapy and Incidence of Parkinson Disease Among Patients With Inflammatory Bowel Disease. JAMA Neurol. 75, 939–946. https://doi.org/10.1001/jamaneurol.2018.0605

Peterschmitt, M.J., Crawford, N.P.S., Gaemers, S.J.M., Ji, A.J., Sharma, J., Pham, T.T., 2021. Pharmacokinetics, Pharmacodynamics, Safety, and Tolerability of Oral Venglustat in Healthy Volunteers. Clin. Pharmacol. Drug Dev. 10, 86–98. https://doi.org/10.1002/cpdd.865

Petrov, V.A., Saltykova, I.V., Zhukova, I.A., Alifirova, V.M., Zhukova, N.G., Dorofeeva, Y.B., Tyakht, A.V., Kovarsky, B.A., Alekseev, D.G., Kostryukova, E.S., Mironova, Y.S., Izhboldina, O.P., Nikitina, M.A., Perevozchikova, T.V., Fait, E.A., Babenko, V.V., Vakhitova, M.T., Govorun, V.M., Sazonov, A.E., 2017. Analysis of Gut Microbiota in Patients with Parkinson's Disease. Bull. Exp. Biol. Med. 162, 734–737. https://doi.org/10.1007/s10517-017-3700-7

Pettersen, E.F., Goddard, T.D., Huang, C.C., Couch, G.S., Greenblatt, D.M., Meng, E.C., Ferrin, T.E., 2004. UCSF Chimera--a visualization system for exploratory research and analysis. J. Comput. Chem. 25, 1605–1612. https://doi.org/10.1002/jcc.20084

Pezzoli, G., Cereda, E., 2013. Exposure to pesticides or solvents and risk of Parkinson disease. Neurology 80, 2035–2041. https://doi.org/10.1212/WNL.0b013e318294b3c8

Pfeffer, S.R., 2013. Rab GTPase regulation of membrane identity. Curr. Opin. Cell Biol., Cell organelles 25, 414–419. https://doi.org/10.1016/j.ceb.2013.04.002

Pfeiffer, R.F., 2003. Gastrointestinal dysfunction in Parkinson's disease. Lancet Neurol. 2, 107–116. https://doi.org/10.1016/S1474-4422(03)00307-7

Ping, H.X., Shepard, P.D., 1996. Apamin-sensitive Ca(2+)-activated K+ channels regulate pacemaker activity in nigral dopamine neurons. Neuroreport 7, 809–814. https://doi.org/10.1097/00001756-199602290-00031

Poewe, W., 2008. Non-motor symptoms in Parkinson's disease. Eur. J. Neurol. 15, 14–20. https://doi.org/10.1111/j.1468-1331.2008.02056.x

Polymeropoulos, M.H., Lavedan, C., Leroy, E., Ide, S.E., Dehejia, A., Dutra, A., Pike, B., Root, H., Rubenstein, J., Boyer, R., Stenroos, E.S., Chandrasekharappa, S.,

Athanassiadou, A., Papapetropoulos, T., Johnson, W.G., Lazzarini, A.M., Duvoisin, R.C., Di Iorio, G., Golbe, L.I., Nussbaum, R.L., 1997. Mutation in the alpha-synuclein gene identified in families with Parkinson's disease. Science 276, 2045–2047.

Pringsheim, T., Jette, N., Frolkis, A., Steeves, T.D.L., 2014. The prevalence of Parkinson's disease: A systematic review and meta-analysis. Mov. Disord. 29, 1583–1590. https://doi.org/10.1002/mds.25945

Pu, J., Guardia, C.M., Keren-Kaplan, T., Bonifacino, J.S., 2016. Mechanisms and functions of lysosome positioning. J. Cell Sci. 129, 4329–4339. https://doi.org/10.1242/jcs.196287

Purlyte, E., Dhekne, H.S., Sarhan, A.R., Gomez, R., Lis, P., Wightman, M., Martinez, T.N., Tonelli, F., Pfeffer, S.R., Alessi, D.R., 2019. Rab29 activation of the Parkinson's disease-associated LRRK2 kinase. EMBO J. 38, e101237. https://doi.org/10.15252/embj.2018101237

Quadri, M., Fang, M., Picillo, M., Olgiati, S., Breedveld, G.J., Graafland, J., Wu, B., Xu, F., Erro, R., Amboni, M., Pappatà, S., Quarantelli, M., Annesi, G., Quattrone, A., Chien, H.F., Barbosa, E.R., International Parkinsonism Genetics Network, Oostra, B.A., Barone, P., Wang, J., Bonifati, V., 2013. Mutation in the SYNJ1 gene associated with autosomal recessive, early-onset Parkinsonism. Hum. Mutat. 34, 1208–1215. https://doi.org/10.1002/humu.22373

Radulovic, M., Schink, K.O., Wenzel, E.M., Nähse, V., Bongiovanni, A., Lafont, F., Stenmark, H., 2018. ESCRT-mediated lysosome repair precedes lysophagy and promotes cell survival. EMBO J. 37, e99753. https://doi.org/10.15252/embj.201899753

Raiborg, C., Bremnes, B., Mehlum, A., Gillooly, D.J., D'Arrigo, A., Stang, E., Stenmark, H., 2001. FYVE and coiled-coil domains determine the specific localisation of Hrs to early endosomes. J. Cell Sci. 114, 2255–2263. https://doi.org/10.1242/jcs.114.12.2255

Rajput, A.H., Fenton, M.E., Birdi, S., Macaulay, R., George, D., Rozdilsky, B., Ang, L.C., Senthilselvan, A., Hornykiewicz, O., 2002. Clinical-pathological study of levodopa complications. Mov. Disord. Off. J. Mov. Disord. Soc. 17, 289–296. https://doi.org/10.1002/mds.10031

Ramirez, A., Heimbach, A., Gründemann, J., Stiller, B., Hampshire, D., Cid, L.P., Goebel, I., Mubaidin, A.F., Wriekat, A.-L., Roeper, J., Al-Din, A., Hillmer, A.M., Karsak, M., Liss, B., Woods, C.G., Behrens, M.I., Kubisch, C., 2006. Hereditary parkinsonism with dementia is caused by mutations in ATP13A2, encoding a lysosomal type 5 P-type ATPase. Nat. Genet. 38, 1184–1191. https://doi.org/10.1038/ng1884

Ramonet, D., Daher, J.P.L., Lin, B.M., Stafa, K., Kim, J., Banerjee, R., Westerlund, M., Pletnikova, O., Glauser, L., Yang, L., Liu, Y., Swing, D.A., Beal, M.F., Troncoso, J.C., McCaffery, J.M., Jenkins, N.A., Copeland, N.G., Galter, D., Thomas, B., Lee, M.K., Dawson, T.M., Dawson, V.L., Moore, D.J., 2011. Dopaminergic Neuronal Loss, Reduced Neurite Complexity and Autophagic Abnormalities in Transgenic Mice Expressing G2019S Mutant LRRK2. PLOS ONE 6, e18568. https://doi.org/10.1371/journal.pone.0018568

Ramsay, R.R., Salach, J.I., Singer, T.P., 1986. Uptake of the neurotoxin 1-methyl-4-phenylpyridine (MPP+) by mitochondria and its relation to the inhibition of the mitochondrial oxidation of NAD+-linked substrates by MPP+. Biochem. Biophys. Res. Commun. 134, 743–748. https://doi.org/10.1016/S0006-291X(86)80483-1

Ramsden, N., Perrin, J., Ren, Z., Lee, B.D., Zinn, N., Dawson, V.L., Tam, D., Bova, M., Lang, M., Drewes, G., Bantscheff, M., Bard, F., Dawson, T.M., Hopf, C., 2011. Chemoproteomics-based design of potent LRRK2-selective lead compounds that attenuate Parkinson's disease-related toxicity in human neurons. ACS Chem. Biol. 6, 1021–1028. https://doi.org/10.1021/cb2002413

Rasband, M.N., 2016. Glial Contributions to Neural Function and Disease. Mol. Cell. Proteomics MCP 15, 355–361. https://doi.org/10.1074/mcp.R115.053744

Ravikumar, B., Acevedo-Arozena, A., Imarisio, S., Berger, Z., Vacher, C., O'Kane, C.J., Brown, S.D.M., Rubinsztein, D.C., 2005. Dynein mutations impair autophagic clearance of aggregate-prone proteins. Nat. Genet. 37, 771–776. https://doi.org/10.1038/ng1591

Reed, X., Bandrés-Ciga, S., Blauwendraat, C., Cookson, M.R., 2019. The role of monogenic genes in idiopathic Parkinson's disease. Neurobiol. Dis. 124, 230–239. https://doi.org/10.1016/j.nbd.2018.11.012

Reeve, A., Simcox, E., Turnbull, D., 2014. Ageing and Parkinson's disease: why is advancing age the biggest risk factor? Ageing Res. Rev. 14, 19–30. https://doi.org/10.1016/j.arr.2014.01.004

Reijnders, J.S.A.M., Ehrt, U., Weber, W.E.J., Aarsland, D., Leentjens, A.F.G., 2008. A systematic review of prevalence studies of depression in Parkinson's disease. Mov. Disord. 23, 183–189. https://doi.org/10.1002/mds.21803

Reimand, J., Kull, M., Peterson, H., Hansen, J., Vilo, J., 2007. g:Profiler—a web-based toolset for functional profiling of gene lists from large-scale experiments. Nucleic Acids Res. 35, W193–W200. https://doi.org/10.1093/nar/gkm226

Reith, A.D., Bamborough, P., Jandu, K., Andreotti, D., Mensah, L., Dossang, P., Choi, H.G., Deng, X., Zhang, J., Alessi, D.R., Gray, N.S., 2012. GSK2578215A; a potent and highly selective 2-arylmethyloxy-5-substitutent-N-arylbenzamide LRRK2 kinase inhibitor. Bioorg. Med. Chem. Lett. 22, 5625–5629. https://doi.org/10.1016/j.bmcl.2012.06.104

Ritchie, M.E., Phipson, B., Wu, D., Hu, Y., Law, C.W., Shi, W., Smyth, G.K., 2015. limma powers differential expression analyses for RNA-sequencing and microarray studies. Nucleic Acids Res. 43, e47–e47. https://doi.org/10.1093/nar/gkv007

Robinson, M.S., Sahlender, D.A., Foster, S.D., 2010. Rapid Inactivation of Proteins by Rapamycin-Induced Rerouting to Mitochondria. Dev. Cell 18, 324–331. https://doi.org/10.1016/j.devcel.2009.12.015

Rosa-Ferreira, C., Munro, S., 2011. Arl8 and SKIP Act Together to Link Lysosomes to Kinesin-1. Dev. Cell 21, 1171–1178. https://doi.org/10.1016/j.devcel.2011.10.007

Ross, O.A., Soto-Ortolaza, A.I., Heckman, M.G., Aasly, J.O., Abahuni, N., Annesi, G., Bacon, J.A., Bardien, S., Bozi, M., Brice, A., Brighina, L., Van Broeckhoven, C., Carr, J., Chartier-Harlin, M.-C., Dardiotis, E., Dickson, D.W., Diehl, N.N., Elbaz, A., Ferrarese, C., Ferraris, A., Fiske, B., Gibson, J.M., Gibson, R., Hadjigeorgiou,

G.M., Hattori, N., Ioannidis, J.P., Jasinska-Myga, B., Jeon, B.S., Kim, Y.J., Klein, C., Kruger, R., Kyratzi, E., Lesage, S., Lin, C.-H., Lynch, T., Maraganore, D.M., Mellick, G.D., Mutez, E., Nilsson, C., Opala, G., Park, S.S., Puschmann, A., Quattrone, A., Sharma, M., Silburn, P.A., Sohn, Y.H., Stefanis, L., Tadic, V., Theuns, J., Tomiyama, H., Uitti, R.J., Valente, E.M., van de Loo, S., Vassilatis, D.K., Vilariño-Güell, C., White, L.R., Wirdefeldt, K., Wszolek, Z.K., Wu, R.-M., Farrer, M.J., 2011. Association of LRRK2 exonic variants with susceptibility to Parkinson's disease: a case–control study. Lancet Neurol. 10, 898–908. https://doi.org/10.1016/S1474-4422(11)70175-2

Ross, O.A., Wu, Y.-R., Lee, M.-C., Funayama, M., Chen, M.-L., Soto, A.I., Mata, I.F., Lee-Chen, G.-J., Chen, C.M., Tang, M., Zhao, Y., Hattori, N., Farrer, M.J., Tan, E.-K., Wu, R.-M., 2008. Analysis of Lrrk2 R1628P as a risk factor for Parkinson's disease. Ann. Neurol. 64, 88–92. https://doi.org/10.1002/ana.21405

Rowe, R.K., Suszko, J.W., Pekosz, A., 2008. Roles for the recycling endosome, Rab8, and Rab11 in hantavirus release from epithelial cells. Virology 382, 239–249. https://doi.org/10.1016/j.virol.2008.09.021

Rudenko, I.N., Cookson, M.R., 2014. Heterogeneity of leucine-rich repeat kinase 2 mutations: genetics, mechanisms and therapeutic implications. Neurother. J. Am. Soc. Exp. Neurother. 11, 738–750. https://doi.org/10.1007/s13311-014-0284-z

Rudow, G., O'Brien, R., Savonenko, A.V., Resnick, S.M., Zonderman, A.B., Pletnikova, O., Marsh, L., Dawson, T.M., Crain, B.J., West, M.J., Troncoso, J.C., 2008. Morphometry of the human substantia nigra in ageing and Parkinson's disease. Acta Neuropathol. (Berl.) 115, 461. https://doi.org/10.1007/s00401-008-0352-8

Russmann, H., Ghika, J., Villemure, J.-G., Robert, B., Bogousslavsky, J., Burkhard, P.R., Vingerhoets, F.J.G., 2004. Subthalamic nucleus deep brain stimulation in Parkinson disease patients over age 70 years. Neurology 63, 1952–1954. https://doi.org/10.1212/01.wnl.0000144198.26309.d8

Ryan, K.J., White, C.C., Patel, K., Xu, J., Olah, M., Replogle, J.M., Frangieh, M., Cimpean, M., Winn, P., McHenry, A., Kaskow, B.J., Chan, G., Cuerdon, N., Bennett, D.A., Boyd, J.D., Imitola, J., Elyaman, W., Jager, P.L.D., Bradshaw, E.M., 2017. A human microglia-like cellular model for assessing the effects of neurodegenerative disease gene variants. Sci. Transl. Med. 9, eaai7635. https://doi.org/10.1126/scitranslmed.aai7635

Salašová, A., Yokota, C., Potěšil, D., Zdráhal, Z., Bryja, V., Arenas, E., 2017. A proteomic analysis of LRRK2 binding partners reveals interactions with multiple signaling components of the WNT/PCP pathway. Mol. Neurodegener. 12, 54. https://doi.org/10.1186/s13024-017-0193-9

Sampson, T.R., Debelius, J.W., Thron, T., Janssen, S., Shastri, G.G., Ilhan, Z.E., Challis, C., Schretter, C.E., Rocha, S., Gradinaru, V., Chesselet, M.-F., Keshavarzian, A., Shannon, K.M., Krajmalnik-Brown, R., Wittung-Stafshede, P., Knight, R., Mazmanian, S.K., 2016. Gut Microbiota Regulate Motor Deficits and Neuroinflammation in a Model of Parkinson's Disease. Cell 167, 1469-1480.e12. https://doi.org/10.1016/j.cell.2016.11.018

San Luciano, M., Lipton, R.B., Wang, C., Katz, M., Zimmerman, M.E., Sanders, A.E., Ozelius, L.J., Bressman, S.B., Saunders-Pullman, R., 2010. Clinical expression of LRRK2 G2019S mutations in the elderly. Mov. Disord. Off. J. Mov. Disord. Soc. 25, 2571–2576. https://doi.org/10.1002/mds.23330

Sanders, L.H., Laganière, J., Cooper, O., Mak, S.K., Vu, B.J., Huang, Y.A., Paschon, D.E., Vangipuram, M., Sundararajan, R., Urnov, F.D., Langston, J.W., Gregory, P.D., Zhang, H.S., Greenamyre, J.T., Isacson, O., Schüle, B., 2014. LRRK2 mutations cause mitochondrial DNA damage in iPSC-derived neural cells from Parkinson's disease patients: reversal by gene correction. Neurobiol. Dis. 62, 381–386. https://doi.org/10.1016/j.nbd.2013.10.013

Saper, C.B., Sorrentino, D.M., German, D.C., de Lacalle, S., 1991. Medullary catecholaminergic neurons in the normal human brain and in Parkinson's disease. Ann. Neurol. 29, 577–584. https://doi.org/10.1002/ana.410290602

Sato, T., Iwano, T., Kunii, M., Matsuda, S., Mizuguchi, R., Jung, Y., Hagiwara, H., Yoshihara, Y., Yuzaki, M., Harada, R., Harada, A., 2014. Rab8a and Rab8b are essential for several apical transport pathways but insufficient for ciliogenesis. J. Cell Sci. 127, 422–431. https://doi.org/10.1242/jcs.136903

Schapira, A.H.V., 2005. Present and future drug treatment for Parkinson's disease. J. Neurol. Neurosurg. Psychiatry 76, 1472–1478. https://doi.org/10.1136/jnnp.2004.035980

Scholz, S.W., Bras, J., 2015. Genetics Underlying Atypical Parkinsonism and Related Neurodegenerative Disorders. Int. J. Mol. Sci. 16, 24629–24655. https://doi.org/10.3390/ijms161024629

Seegobin, S.P., Heaton, G.R., Liang, D., Choi, I., Blanca Ramirez, M., Tang, B., Yue, Z., 2020. Progress in LRRK2-Associated Parkinson's Disease Animal Models. Front. Neurosci. 14.

Shahmoradian, S.H., Lewis, A.J., Genoud, C., Hench, J., Moors, T.E., Navarro, P.P., Castaño-Díez, D., Schweighauser, G., Graff-Meyer, A., Goldie, K.N., Sütterlin, R., Huisman, E., Ingrassia, A., Gier, Y. de, Rozemuller, A.J.M., Wang, J., Paepe, A.D., Erny, J., Staempfli, A., Hoernschemeyer, J., Großerüschkamp, F., Niedieker, D., El-Mashtoly, S.F., Quadri, M., Van IJcken, W.F.J., Bonifati, V., Gerwert, K., Bohrmann, B., Frank, S., Britschgi, M., Stahlberg, H., Van de Berg, W.D.J., Lauer, M.E., 2019. Lewy pathology in Parkinson's disease consists of crowded organelles and lipid membranes. Nat. Neurosci. 22, 1099–1109. https://doi.org/10.1038/s41593-019-0423-2

Shannon, P., Markiel, A., Ozier, O., Baliga, N.S., Wang, J.T., Ramage, D., Amin, N., Schwikowski, B., Ideker, T., 2003. Cytoscape: a software environment for integrated models of biomolecular interaction networks. Genome Res. 13, 2498–2504. https://doi.org/10.1101/gr.1239303

Shen, R.-S., Abell, C.W., Gessner, W., Brossi, A., 1985. Serotonergic conversion of MPTP and dopaminergic accumulation of MPP+. FEBS Lett. 189, 225–230. https://doi.org/10.1016/0014-5793(85)81028-0

Sheng, Z., Zhang, S., Bustos, D., Kleinheinz, T., Pichon, C.E.L., Dominguez, S.L., Solanoy, H.O., Drummond, J., Zhang, X., Ding, X., Cai, F., Song, Q., Li, X., Yue, Z., Brug, M.P. van der, Burdick, D.J., Gunzner-Toste, J., Chen, H., Liu, X.,

Estrada, A.A., Sweeney, Z.K., Scearce-Levie, K., Moffat, J.G., Kirkpatrick, D.S., Zhu, H., 2012. Ser1292 Autophosphorylation Is an Indicator of LRRK2 Kinase Activity and Contributes to the Cellular Effects of PD Mutations. Sci. Transl. Med. 4, 164ra161-164ra161. https://doi.org/10.1126/scitranslmed.3004485

Sherer, T.B., Kim, J.-H., Betarbet, R., Greenamyre, J.T., 2003. Subcutaneous Rotenone Exposure Causes Highly Selective Dopaminergic Degeneration and **α**-Synuclein Aggregation. Exp. Neurol. 179, 9–16. https://doi.org/10.1006/exnr.2002.8072

Shi, C. -h, Tang, B. -s, Wang, L., Lv, Z. -y, Wang, J., Luo, L. -z, Shen, L., Jiang, H., Yan, X. -x, Pan, Q., Xia, K., Guo, J. -f, 2011. PLA2G6 gene mutation in autosomal recessive early-onset parkinsonism in a Chinese cohort. Neurology 77, 75–81. https://doi.org/10.1212/WNL.0b013e318221acd3

Shibayama-Imazu, T., Okahashi, I., Omata, K., Nakajo, S., Ochiai, H., Nakai, Y., Hama, T., Nakamura, Y., Nakaya, K., 1993. Cell and tissue distribution and developmental change of neuron specific 14 kDa protein (phosphoneuroprotein 14). Brain Res. 622, 17–25. https://doi.org/10.1016/0006-8993(93)90796-p

Sidransky, E., Nalls, M.A., Aasly, J.O., Aharon-Peretz, J., Annesi, G., Barbosa, E.R., Bar-Shira, A., Berg, D., Bras, J., Brice, A., Chen, C.-M., Clark, L.N., Condroyer, C., De Marco, E.V., Dürr, A., Eblan, M.J., Fahn, S., Farrer, M.J., Fung, H.-C., Gan-Or, Z., Gasser, T., Gershoni-Baruch, R., Giladi, N., Griffith, A., Gurevich, T., Januario, C., Kropp, P., Lang, A.E., Lee-Chen, G.-J., Lesage, S., Marder, K., Mata, I.F., Mirelman, A., Mitsui, J., Mizuta, I., Nicoletti, G., Oliveira, C., Ottman, R., Orr-Urtreger, A., Pereira, L.V., Quattrone, A., Rogaeva, E., Rolfs, A., Rosenbaum, H., Rozenberg, R., Samii, A., Samaddar, T., Schulte, C., Sharma, M., Singleton, A., Spitz, M., Tan, E.-K., Tayebi, N., Toda, T., Troiano, A.R., Tsuji, S., Wittstock, M., Wolfsberg, T.G., Wu, Y.-R., Zabetian, C.P., Zhao, Y., Ziegler, S.G., 2009. Multicenter analysis of glucocerebrosidase mutations in Parkinson's disease. N. Engl. J. Med. 361, 1651–1661. https://doi.org/10.1056/NEJMoa0901281

Sina, F., Shojaee, S., Elahi, E., Paisán-Ruiz, C., 2009. R632W mutation in PLA2G6 segregates with dystonia-parkinsonism in a consanguineous Iranian family. Eur. J. Neurol. 16, 101–104. https://doi.org/10.1111/j.1468-1331.2008.02356.x

Singaram, C., Gaumnitz, E.A., Torbey, C., Ashraf, W., Quigley, E.M.M., Sengupta, A., Pfeiffer, R., 1995. Dopaminergic defect of enteric nervous system in Parkinson's disease patients with chronic constipation. The Lancet 346, 861–864. https://doi.org/10.1016/S0140-6736(95)92707-7

Singh, F., Prescott, A.R., Rosewell, P., Ball, G., Reith, A.D., Ganley, I.G., 2021. Pharmacological rescue of impaired mitophagy in Parkinson's disease-related LRRK2 G2019S knock-in mice. eLife 10, e67604. https://doi.org/10.7554/eLife.67604

Singleton, A.B., 2003. -Synuclein Locus Triplication Causes Parkinson's Disease. Science 302, 841–841. https://doi.org/10.1126/science.1090278

Sivars, U., Aivazian, D., Pfeffer, S.R., 2003. Yip3 catalyses the dissociation of endosomal Rab–GDI complexes. Nature 425, 856–859. https://doi.org/10.1038/nature02057

Skowyra, M.L., Schlesinger, P.H., Naismith, T.V., Hanson, P.I., 2018. Triggered recruitment of ESCRT machinery promotes endolysosomal repair. Science 360, eaar5078. https://doi.org/10.1126/science.aar5078

Sloan, M., Alegre-Abarrategui, J., Potgieter, D., Kaufmann, A.-K., Exley, R., Deltheil, T., Threlfell, S., Connor-Robson, N., Brimblecombe, K., Wallings, R., Cioroch, M., Bannerman, D.M., Bolam, J.P., Magill, P.J., Cragg, S.J., Dodson, P.D., Wade-Martins, R., 2016. LRRK2 BAC transgenic rats develop progressive, L-DOPA-responsive motor impairment, and deficits in dopamine circuit function. Hum. Mol. Genet. 25, 951–963. https://doi.org/10.1093/hmg/ddv628

Smith, W.W., Pei, Z., Jiang, H., Dawson, V.L., Dawson, T.M., Ross, C.A., 2006. Kinase activity of mutant LRRK2 mediates neuronal toxicity. Nat. Neurosci. 9, 1231–1233. https://doi.org/10.1038/nn1776

Spillantini, M.G., Schmidt, M.L., Lee, V.M.-Y., Trojanowski, J.Q., Jakes, R., Goedert, M., 1997. α-Synuclein in Lewy bodies. Nature 388, 839–840. https://doi.org/10.1038/42166

Stefanis, L., 2012. α-Synuclein in Parkinson's Disease. Cold Spring Harb. Perspect. Med. 2, a009399. https://doi.org/10.1101/cshperspect.a009399

Steger, M., Diez, F., Dhekne, H.S., Lis, P., Nirujogi, R.S., Karayel, O., Tonelli, F., Martinez, T.N., Lorentzen, E., Pfeffer, S.R., Alessi, D.R., Mann, M., 2017. Systematic proteomic analysis of LRRK2-mediated Rab GTPase phosphorylation establishes a connection to ciliogenesis. eLife 6. https://doi.org/10.7554/eLife.31012

Steger, M., Tonelli, F., Ito, G., Davies, P., Trost, M., Vetter, M., Wachter, S., Lorentzen, E., Duddy, G., Wilson, S., Baptista, M.A., Fiske, B.K., Fell, M.J., Morrow, J.A., Reith, A.D., Alessi, D.R., Mann, M., 2016. Phosphoproteomics reveals that Parkinson's disease kinase LRRK2 regulates a subset of Rab GTPases. eLife 5. https://doi.org/10.7554/eLife.12813

Stenmark, H., 2009. Rab GTPases as coordinators of vesicle traffic. Nat. Rev. Mol. Cell Biol. 10, 513–525. https://doi.org/10.1038/nrm2728

Sugama, S., Yang, L., Cho, B.P., DeGiorgio, L.A., Lorenzl, S., Albers, D.S., Beal, M.F., Volpe, B.T., Joh, T.H., 2003. Age-related microglial activation in 1-methyl-4-phenyl-1,2,3,6-tetrahydropyridine (MPTP)-induced dopaminergic neurodegeneration in C57BL/6 mice. Brain Res. 964, 288–294. https://doi.org/10.1016/S0006-8993(02)04085-4

Takanashi, M., Funayama, M., Matsuura, E., Yoshino, H., Li, Y., Tsuyama, S., Takashima, H., Nishioka, K., Hattori, N., 2018. Isolated nigral degeneration without pathological protein aggregation in autopsied brains with LRRK2 p.R1441H homozygous and heterozygous mutations. Acta Neuropathol. Commun. 6, 105. https://doi.org/10.1186/s40478-018-0617-y

Tan, A.H., Mahadeva, S., Thalha, A.M., Gibson, P.R., Kiew, C.K., Yeat, C.M., Ng, S.W., Ang, S.P., Chow, S.K., Tan, C.T., Yong, H.S., Marras, C., Fox, S.H., Lim, S.-Y., 2014. Small intestinal bacterial overgrowth in Parkinson's disease. Parkinsonism Relat. Disord. 20, 535–540. https://doi.org/10.1016/j.parkreldis.2014.02.019

Tan, E.-K., Peng, R., Teo, Y.-Y., Tan, L.C., Angeles, D., Ho, P., Chen, M.-L., Lin, C.-H., Mao, X.-Y., Chang, X.-L., Prakash, K.M., Liu, J.-J., Au, W.-L., Le, W.-D., Jankovic,

J., Burgunder, J.-M., Zhao, Y., Wu, R.-M., 2010. Multiple LRRK2 variants modulate risk of Parkinson disease: a Chinese multicenter study. Hum. Mutat. 31, 561–568. https://doi.org/10.1002/humu.21225

Tan, E.K., Shen, H., Tan, L.C.S., Farrer, M., Yew, K., Chua, E., Jamora, R.D., Puvan, K., Puong, K.Y., Zhao, Y., Pavanni, R., Wong, M.C., Yih, Y., Skipper, L., Liu, J.-J., 2005. The G2019S LRRK2 mutation is uncommon in an Asian cohort of Parkinson's disease patients. Neurosci. Lett. 384, 327–329. https://doi.org/10.1016/j.neulet.2005.04.103

Tanner, C.M., Kamel, F., Ross, G.W., Hoppin, J.A., Goldman, S.M., Korell, M., Marras, C., Bhudhikanok, G.S., Kasten, M., Chade, A.R., Comyns, K., Richards, M.B., Meng, C., Priestley, B., Fernandez, H.H., Cambi, F., Umbach, D.M., Blair, A., Sandler, D.P., Langston, J.W., 2011. Rotenone, Paraquat, and Parkinson's Disease. Environ. Health Perspect. 119, 866–872. https://doi.org/10.1289/ehp.1002839

Tasegian, A., Singh, F., Ganley, I.G., Reith, A.D., Alessi, D.R., 2021. Impact of Type II LRRK2 inhibitors on signaling and mitophagy. Biochem. J. 478, 3555–3573. https://doi.org/10.1042/BCJ20210375

Taymans, J.-M., Greggio, E., 2016. LRRK2 Kinase Inhibition as a Therapeutic Strategy for Parkinson's Disease, Where Do We Stand? Curr. Neuropharmacol. 14, 214–225. https://doi.org/10.2174/1570159X13666151030102847

Taymans, J.-M., Van den Haute, C., Baekelandt, V., 2006. Distribution of PINK1 and LRRK2 in rat and mouse brain. J. Neurochem. 98, 951–961. https://doi.org/10.1111/j.1471-4159.2006.03919.x

Thirstrup, K., Dächsel, J.C., Oppermann, F.S., Williamson, D.S., Smith, G.P., Fog, K., Christensen, K.V., 2017. Selective LRRK2 kinase inhibition reduces phosphorylation of endogenous Rab10 and Rab12 in human peripheral mononuclear blood cells. Sci. Rep. 7, 10300. https://doi.org/10.1038/s41598-017-10501-z

Thul, P.J., Åkesson, L., Wiking, M., Mahdessian, D., Geladaki, A., Ait Blal, H., Alm, T., Asplund, A., Björk, L., Breckels, L.M., Bäckström, A., Danielsson, F., Fagerberg, L., Fall, J., Gatto, L., Gnann, C., Hober, S., Hjelmare, M., Johansson, F., Lee, S., Lindskog, C., Mulder, J., Mulvey, C.M., Nilsson, P., Oksvold, P., Rockberg, J., Schutten, R., Schwenk, J.M., Sivertsson, Å., Sjöstedt, E., Skogs, M., Stadler, C., Sullivan, D.P., Tegel, H., Winsnes, C., Zhang, C., Zwahlen, M., Mardinoglu, A., Pontén, F., von Feilitzen, K., Lilley, K.S., Uhlén, M., Lundberg, E., 2017. A subcellular map of the human proteome. Science 356, eaal3321. https://doi.org/10.1126/science.aal3321

Tong, Y., Giaime, E., Yamaguchi, H., Ichimura, T., Liu, Y., Si, H., Cai, H., Bonventre, J.V., Shen, J., 2012. Loss of leucine-rich repeat kinase 2 causes age-dependent bi-phasic alterations of the autophagy pathway. Mol. Neurodegener. 7, 2. https://doi.org/10.1186/1750-1326-7-2

Tong, Y., Pisani, A., Martella, G., Karouani, M., Yamaguchi, H., Pothos, E.N., Shen, J., 2009. R1441C mutation in LRRK2 impairs dopaminergic neurotransmission in mice. Proc. Natl. Acad. Sci. 106, 14622–14627. https://doi.org/10.1073/pnas.0906334106

Tong, Y., Yamaguchi, H., Giaime, E., Boyle, S., Kopan, R., Kelleher, R.J., Shen, J., 2010a. Loss of leucine-rich repeat kinase 2 causes impairment of protein degradation pathways, accumulation of **α**-synuclein, and apoptotic cell death in aged mice. Proc. Natl. Acad. Sci. 107, 9879–9884. https://doi.org/10.1073/pnas.1004676107

Tong, Y., Yamaguchi, H., Giaime, E., Boyle, S., Kopan, R., Kelleher, R.J., Shen, J., 2010b. Loss of leucine-rich repeat kinase 2 causes impairment of protein degradation pathways, accumulation of **α**-synuclein, and apoptotic cell death in aged mice. Proc. Natl. Acad. Sci. 107, 9879–9884. https://doi.org/10.1073/pnas.1004676107

Trifunovic, A., Larsson, N.-G., 2008. Mitochondrial dysfunction as a cause of ageing. J. Intern. Med. 263, 167–178. https://doi.org/10.1111/j.1365-2796.2007.01905.x

Trinh, J., Guella, I., Farrer, M.J., 2014. Disease penetrance of late-onset parkinsonism: a meta-analysis. JAMA Neurol. 71, 1535–1539. https://doi.org/10.1001/jamaneurol.2014.1909

Tsika, E., Kannan, M., Foo, C.S.-Y., Dikeman, D., Glauser, L., Gellhaar, S., Galter, D., Knott, G.W., Dawson, T.M., Dawson, V.L., Moore, D.J., 2014. Conditional expression of Parkinson's disease-related R1441C LRRK2 in midbrain dopaminergic neurons of mice causes nuclear abnormalities without neurodegeneration. Neurobiol. Dis. 71, 345–358. https://doi.org/10.1016/j.nbd.2014.08.027

Uchiyama, T., Sakakibara, R., Yamamoto, T., Ito, T., Yamaguchi, C., Awa, Y., Yanagisawa, M., Higuchi, Y., Sato, Y., Ichikawa, T., Yamanishi, T., Hattori, T., Kuwabara, S., 2011. Urinary dysfunction in early and untreated Parkinson's disease. J. Neurol. Neurosurg. Psychiatry 82, 1382–1386. https://doi.org/10.1136/jnnp.2011.241075

Uéda, K., Fukushima, H., Masliah, E., Xia, Y., Iwai, A., Yoshimoto, M., Otero, D.A., Kondo, J., Ihara, Y., Saitoh, T., 1993. Molecular cloning of cDNA encoding an unrecognized component of amyloid in Alzheimer disease. Proc. Natl. Acad. Sci. 90, 11282–11286. https://doi.org/10.1073/pnas.90.23.11282

Unger, M.M., Spiegel, J., Dillmann, K.-U., Grundmann, D., Philippeit, H., Bürmann, J., Faßbender, K., Schwiertz, A., Schäfer, K.-H., 2016. Short chain fatty acids and gut microbiota differ between patients with Parkinson's disease and age-matched controls. Parkinsonism Relat. Disord. 32, 66–72. https://doi.org/10.1016/j.parkreldis.2016.08.019

Vacic, V., Ozelius, L.J., Clark, L.N., Bar-Shira, A., Gana-Weisz, M., Gurevich, T., Gusev, A., Kedmi, M., Kenny, E.E., Liu, X., Mejia-Santana, H., Mirelman, A., Raymond, D., Saunders-Pullman, R., Desnick, R.J., Atzmon, G., Burns, E.R., Ostrer, H., Hakonarson, H., Bergman, A., Barzilai, N., Darvasi, A., Peter, I., Guha, S., Lencz, T., Giladi, N., Marder, K., Pe'er, I., Bressman, S.B., Orr-Urtreger, A., 2014. Genome-wide mapping of IBD segments in an Ashkenazi PD cohort identifies associated haplotypes. Hum. Mol. Genet. 23, 4693–4702. https://doi.org/10.1093/hmg/ddu158

Vaidya, A.B., Rajagopalan, T.G., Mankodi, N.A., Antarkar, D.S., Tathed, P.S., Purohit, A.V., Wadia, N.H., 1978. Treatment of Parkinson's disease with the cowhage plant-Mucuna pruriens Bak. Neurol. India 26, 171–176.

Valente, E.M., Abou-Sleiman, P.M., Caputo, V., Muqit, M.M.K., Harvey, K., Gispert, S., Ali, Z., Del Turco, D., Bentivoglio, A.R., Healy, D.G., Albanese, A., Nussbaum, R., González-Maldonado, R., Deller, T., Salvi, S., Cortelli, P., Gilks, W.P., Latchman, D.S., Harvey, R.J., Dallapiccola, B., Auburger, G., Wood, N.W., 2004. Hereditary early-onset Parkinson's disease caused by mutations in PINK1. Science 304, 1158–1160. https://doi.org/10.1126/science.1096284

van Unen, J., Reinhard, N.R., Yin, T., Wu, Y.I., Postma, M., Gadella, T.W.J., Goedhart, J., 2015. Plasma membrane restricted RhoGEF activity is sufficient for RhoA-mediated actin polymerization. Sci. Rep. 5, 14693. https://doi.org/10.1038/srep14693

Vancraenenbroeck, R., Lobbestael, E., De Maeyer, M., Baekelandt, V., Taymans, J.-M., 2011. Kinases as Targets for Parkinson's Disease: From Genetics to Therapy. CNS Neurol. Disord. - Drug Targets- CNS Neurol. Disord. 10, 724–740. https://doi.org/10.2174/187152711797247858

Varnai, P., Thyagarajan, B., Rohacs, T., Balla, T., 2006. Rapidly inducible changes in phosphatidylinositol 4,5-bisphosphate levels influence multiple regulatory functions of the lipid in intact living cells. J. Cell Biol. 175, 377–382. https://doi.org/10.1083/jcb.200607116

Vides, E.G., Adhikari, A., Lis, P., Purlyte, E., Shumate, J., Lasso, E.S., Dhekne, H.S., Alessi, D.R., Pfeffer, S.R., 2022. A Feed-forward Pathway Drives LRRK2 kinase Membrane Recruitment and Apparent Activation. bioRxiv 2022.04.25.489459. https://doi.org/10.1101/2022.04.25.489459

Vieweg, S., Mulholland, K., Bräuning, B., Kachariya, N., Lai, Y.-C., Toth, R., Singh, P.K., Volpi, I., Sattler, M., Groll, M., Itzen, A., Muqit, M.M.K., 2020. PINK1-dependent phosphorylation of Serine111 within the SF3 motif of Rab GTPases impairs effector interactions and LRRK2-mediated phosphorylation at Threonine72. Biochem. J. 477, 1651–1668. https://doi.org/10.1042/BCJ20190664

Vijayan, R.S.K., He, P., Modi, V., Duong-Ly, K.C., Ma, H., Peterson, J.R., Dunbrack, R.L., Levy, R.M., 2015. Conformational Analysis of the DFG-Out Kinase Motif and Biochemical Profiling of Structurally Validated Type II Inhibitors. J. Med. Chem. 58, 466–479. https://doi.org/10.1021/jm501603h

Vilariño-Güell, C., Wider, C., Ross, O.A., Dachsel, J.C., Kachergus, J.M., Lincoln, S.J., Soto-Ortolaza, A.I., Cobb, S.A., Wilhoite, G.J., Bacon, J.A., Behrouz, B., Melrose, H.L., Hentati, E., Puschmann, A., Evans, D.M., Conibear, E., Wasserman, W.W., Aasly, J.O., Burkhard, P.R., Djaldetti, R., Ghika, J., Hentati, F., Krygowska-Wajs, A., Lynch, T., Melamed, E., Rajput, A., Rajput, A.H., Solida, A., Wu, R.-M., Uitti, R.J., Wszolek, Z.K., Vingerhoets, F., Farrer, M.J., 2011. VPS35 mutations in Parkinson disease. Am. J. Hum. Genet. 89, 162–167. https://doi.org/10.1016/j.ajhg.2011.06.001

Villar-Piqué, A., Lopes da Fonseca, T., Outeiro, T.F., 2016. Structure, function and toxicity of alpha-synuclein: the Bermuda triangle in synucleinopathies. J. Neurochem. 139 Suppl 1, 240–255. https://doi.org/10.1111/jnc.13249

Virreira Winter, S., Karayel, O., Strauss, M.T., Padmanabhan, S., Surface, M., Merchant, K., Alcalay, R.N., Mann, M., 2021. Urinary proteome profiling for stratifying

patients with familial Parkinson's disease. EMBO Mol. Med. 13, e13257. https://doi.org/10.15252/emmm.202013257

Volc, D., Poewe, W., Kutzelnigg, A., Lührs, P., Thun-Hohenstein, C., Schneeberger, A., Galabova, G., Majbour, N., Vaikath, N., El-Agnaf, O., Winter, D., Mihailovska, E., Mairhofer, A., Schwenke, C., Staffler, G., Medori, R., 2020. Safety and immunogenicity of the **α**-synuclein active immunotherapeutic PD01A in patients with Parkinson's disease: a randomised, single-blinded, phase 1 trial. Lancet Neurol. 19, 591–600. https://doi.org/10.1016/S1474-4422(20)30136-8

Volta, M., Beccano-Kelly, D.A., Paschall, S.A., Cataldi, S., MacIsaac, S.E., Kuhlmann, N., Kadgien, C.A., Tatarnikov, I., Fox, J., Khinda, J., Mitchell, E., Bergeron, S., Melrose, H., Farrer, M.J., Milnerwood, A.J., 2017. Initial elevations in glutamate and dopamine neurotransmission decline with age, as does exploratory behavior, in LRRK2 G2019S knock-in mice. eLife 6, e28377. https://doi.org/10.7554/eLife.28377

Wakabayashi, K., Takahashi, H., Ohama, E., Takeda, S., Ikuta, F., 1993. Lewy bodies in the visceral autonomic nervous system in Parkinson's disease. Adv. Neurol. 60, 609–612.

Wakabayashi, K., Tanji, K., Odagiri, S., Miki, Y., Mori, F., Takahashi, H., 2013. The Lewy Body in Parkinson's Disease and Related Neurodegenerative Disorders. Mol. Neurobiol. 47, 495–508. https://doi.org/10.1007/s12035-012-8280-y

Wallings, R.L., Tansey, M.G., 2019. LRRK2 regulation of immune-pathways and inflammatory disease. Biochem. Soc. Trans. 47, 1581–1595. https://doi.org/10.1042/BST20180463

Wang, S., Kelly, K., Brotchie, J.M., Koprich, J.B., West, A.B., 2020. Exosome markers of LRRK2 kinase inhibition. NPJ Park. Dis. 6, 32. https://doi.org/10.1038/s41531-020-00138-7

Wang, S., Ma, Z., Xu, X., Wang, Z., Sun, L., Zhou, Y., Lin, X., Hong, W., Wang, T., 2014. A Role of Rab29 in the Integrity of the Trans-Golgi Network and Retrograde Trafficking of Mannose-6-Phosphate Receptor. PLoS ONE 9, e96242. https://doi.org/10.1371/journal.pone.0096242

Wang, S., Unnithan, S., Bryant, N., Chang, A., Rosenthal, L.S., Pantelyat, A., Dawson, T.M., Al-Khalidi, H.R., West, A.B., 2022. Elevated Urinary Rab10 Phosphorylation in Idiopathic Parkinson Disease. Mov. Disord. https://doi.org/10.1002/mds.29043

Wang, S., West, A.B., 2019. Caught in the act: LRRK2 in exosomes. Biochem. Soc. Trans. 47, 663–670. https://doi.org/10.1042/BST20180467

Wang, S.-S., Liu, Z.-K., Liu, J.-J., Cheng, Q., Wang, Y.-X., Liu, Y., Ni, W.-W., Chen, H.-Z., Song, M., 2021. Imaging asparaginyl endopeptidase (AEP) in the live brain as a biomarker for Alzheimer's disease. J. Nanobiotechnology 19, 249. https://doi.org/10.1186/s12951-021-00988-0

Wang, X., Negrou, E., Maloney, M.T., Bondar, V.V., Andrews, S.V., Montalban, M., Llapashtica, C., Maciuca, R., Nguyen, H., Solanoy, H., Arguello, A., Przybyla, L., Moerke, N.J., Huntwork-Rodriguez, S., Henry, A.G., 2021. Understanding LRRK2 kinase activity in preclinical models and human subjects through quantitative

analysis of LRRK2 and pT73 Rab10. Sci. Rep. 11, 12900. https://doi.org/10.1038/s41598-021-91943-4

Wang, X., Yan, M.H., Fujioka, H., Liu, J., Wilson-Delfosse, A., Chen, S.G., Perry, G., Casadesus, G., Zhu, X., 2012. LRRK2 regulates mitochondrial dynamics and function through direct interaction with DLP1. Hum. Mol. Genet. 21, 1931–1944. https://doi.org/10.1093/hmg/dds003

Wang, Z.-H., Gong, K., Liu, X., Zhang, Z., Sun, X., Wei, Z.Z., Yu, S.P., Manfredsson, F.P., Sandoval, I.M., Johnson, P.F., Jia, J., Wang, J.-Z., Ye, K., 2018. C/EBPβ regulates delta-secretase expression and mediates pathogenesis in mouse models of Alzheimer's disease. Nat. Commun. 9, 1784. https://doi.org/10.1038/s41467-018-04120-z

Wang, Z.-H., Xiang, J., Liu, X., Yu, S.P., Manfredsson, F.P., Sandoval, I.M., Wu, S., Wang, J.-Z., Ye, K., 2019. Deficiency in BDNF/TrkB Neurotrophic Activity Stimulates δ-Secretase by Upregulating C/EBPβ in Alzheimer's Disease. Cell Rep. 28, 655-669.e5. https://doi.org/10.1016/j.celrep.2019.06.054

Waschbüsch, D., Purlyte, E., Pal, P., McGrath, E., Alessi, D.R., Khan, A.R., 2020. Structural Basis for Rab8a Recruitment of RILPL2 via LRRK2 Phosphorylation of Switch 2. Structure 28, 406-417.e6. https://doi.org/10.1016/j.str.2020.01.005

Webber, P.J., Smith, A.D., Sen, S., Renfrow, M.B., Mobley, J.A., West, A.B., 2011. Autophosphorylation in the Leucine-Rich Repeat Kinase 2 (LRRK2) GTPase Domain Modifies Kinase and GTP-Binding Activities. J. Mol. Biol. 412, 94–110. https://doi.org/10.1016/j.jmb.2011.07.033

Weimers, P., Halfvarson, J., Sachs, M.C., Saunders-Pullman, R., Ludvigsson, J.F., Peter, I., Burisch, J., Olén, O., 2019. Inflammatory Bowel Disease and Parkinson's Disease: A Nationwide Swedish Cohort Study. Inflamm. Bowel Dis. 25, 111–123. https://doi.org/10.1093/ibd/izy190

Weiner, W.J., Factor, S.A., Jankovic, J., Hauser, R.A., Tetrud, J.W., Waters, C.H., Shulman, L.M., Glassman, P.M., Beck, B., Paume, D., Doyle, C., 2001. The long-term safety and efficacy of pramipexole in advanced Parkinson's disease. Parkinsonism Relat. Disord. 7, 115–120. https://doi.org/10.1016/s1353-8020(00)00031-6

Weng, Y.-H., Chen, C.-Y., Lin, K.-J., Chen, Y.-L., Yeh, T.-H., Hsiao, I.-T., Chen, I.-J., Lu, C.-S., Wang, H.-L., 2016. (R1441C) LRRK2 induces the degeneration of SN dopaminergic neurons and alters the expression of genes regulating neuronal survival in a transgenic mouse model. Exp. Neurol. 275, 104–115. https://doi.org/10.1016/j.expneurol.2015.09.001

West, A.B., Cowell, R.M., Daher, J.P.L., Moehle, M.S., Hinkle, K.M., Melrose, H.L., Standaert, D.G., Volpicelli-Daley, L.A., 2014. Differential LRRK2 expression in the cortex, striatum, and substantia nigra in transgenic and nontransgenic rodents. J. Comp. Neurol. 522, 2465–2480. https://doi.org/10.1002/cne.23583

West, A.B., Moore, D.J., Biskup, S., Bugayenko, A., Smith, W.W., Ross, C.A., Dawson, V.L., Dawson, T.M., 2005. Parkinson's disease-associated mutations in leucine-rich repeat kinase 2 augment kinase activity. Proc. Natl. Acad. Sci. U. S. A. 102, 16842–16847. https://doi.org/10.1073/pnas.0507360102

Whiffin, N., Armean, I.M., Kleinman, A., Marshall, J.L., Minikel, E.V., Goodrich, J.K., Quaife, N.M., Cole, J.B., Wang, Q., Karczewski, K.J., Cummings, B.B., Francioli, L., Laricchia, K., Guan, A., Alipanahi, B., Morrison, P., Baptista, M.A.S., Merchant, K.M., Genome Aggregation Database Production Team, Genome Aggregation Database Consortium, Ware, J.S., Havulinna, A.S., Iliadou, B., Lee, J.-J., Nadkarni, G.N., Whiteman, C., 23andMe Research Team, Daly, M., Esko, T., Hultman, C., Loos, R.J.F., Milani, L., Palotie, A., Pato, C., Pato, M., Saleheen, D., Sullivan, P.F., Alföldi, J., Cannon, P., MacArthur, D.G., 2020. The effect of LRRK2 loss-of-function variants in humans. Nat. Med. 26, 869–877. https://doi.org/10.1038/s41591-020-0893-5

Whone, A.L., Watts, R.L., Stoessl, A.J., Davis, M., Reske, S., Nahmias, C., Lang, A.E., Rascol, O., Ribeiro, M.J., Remy, P., Poewe, W.H., Hauser, R.A., Brooks, D.J., REAL-PET Study Group, 2003. Slower progression of Parkinson's disease with ropinirole versus levodopa: The REAL-PET study. Ann. Neurol. 54, 93–101. https://doi.org/10.1002/ana.10609

Willett, R., Martina, J.A., Zewe, J.P., Wills, R., Hammond, G.R.V., Puertollano, R., 2017. TFEB regulates lysosomal positioning by modulating TMEM55B expression and JIP4 recruitment to lysosomes. Nat. Commun. 8, 1580. https://doi.org/10.1038/s41467-017-01871-z

Wise, R.A., 2004. Dopamine, learning and motivation. Nat. Rev. Neurosci. 5, 483–494. https://doi.org/10.1038/nrn1406

Wong, Y.C., Holzbaur, E.L.F., 2014. The Regulation of Autophagosome Dynamics by Huntingtin and HAP1 Is Disrupted by Expression of Mutant Huntingtin, Leading to Defective Cargo Degradation. J. Neurosci. 34, 1293–1305. https://doi.org/10.1523/JNEUROSCI.1870-13.2014

Xiong, Y., Neifert, S., Karuppagounder, S.S., Liu, Q., Stankowski, J.N., Lee, B.D., Ko, H.S., Lee, Y., Grima, J.C., Mao, X., Jiang, H., Kang, S.-U., Swing, D.A., Iacovitti, L., Tessarollo, L., Dawson, T.M., Dawson, V.L., 2018. Robust kinase- and age-dependent dopaminergic and norepinephrine neurodegeneration in LRRK2 G2019S transgenic mice. Proc. Natl. Acad. Sci. 115, 1635–1640. https://doi.org/10.1073/pnas.1712648115

Xue, L.-J., Yang, X.-Z., Tong, Q., Shen, P., Ma, S.-J., Wu, S.-N., Zheng, J.-L., Wang, H.-G., 2020. Fecal microbiota transplantation therapy for Parkinson's disease. Medicine (Baltimore) 99, e22035. https://doi.org/10.1097/MD.0000000000022035

Yang, W., Hamilton, J.L., Kopil, C., Beck, J.C., Tanner, C.M., Albin, R.L., Ray Dorsey, E., Dahodwala, N., Cintina, I., Hogan, P., Thompson, T., 2020. Current and projected future economic burden of Parkinson's disease in the U.S. Npj Park. Dis. 6, 1–9. https://doi.org/10.1038/s41531-020-0117-1

Yiannopoulou, K.G., Anastasiou, A.I., Zachariou, V., Pelidou, S.-H., 2019. Reasons for Failed Trials of Disease-Modifying Treatments for Alzheimer Disease and Their Contribution in Recent Research. Biomedicines 7, 97. https://doi.org/10.3390/biomedicines7040097

Yoshimura, S., Egerer, J., Fuchs, E., Haas, A.K., Barr, F.A., 2007. Functional dissection of Rab GTPases involved in primary cilium formation. J. Cell Biol. 178, 363–369. https://doi.org/10.1083/jcb.200703047

Yoshino, H., Tomiyama, H., Tachibana, N., Ogaki, K., Li, Y., Funayama, M., Hashimoto, T., Takashima, S., Hattori, N., 2010. Phenotypic spectrum of patients with PLA2G6 mutation and PARK14-linked parkinsonism. Neurology 75, 1356–1361. https://doi.org/10.1212/WNL.0b013e3181f73649

Yue, M., Hinkle, K.M., Davies, P., Trushina, E., Fiesel, F.C., Christenson, T.A., Schroeder, A.S., Zhang, L., Bowles, E., Behrouz, B., Lincoln, S.J., Beevers, J.E., Milnerwood, A.J., Kurti, A., McLean, P.J., Fryer, J.D., Springer, W., Dickson, D.W., Farrer, M.J., Melrose, H.L., 2015. Progressive dopaminergic alterations and mitochondrial abnormalities in LRRK2 G2019S knock-in mice. Neurobiol. Dis. 78, 172–195. https://doi.org/10.1016/j.nbd.2015.02.031

Zabetian, C.P., Yamamoto, M., Lopez, A.N., Ujike, H., Mata, I.F., Izumi, Y., Kaji, R., Maruyama, H., Morino, H., Oda, M., Hutter, C.M., Edwards, K.L., Schellenberg, G.D., Tsuang, D.W., Yearout, D., Larson, E.B., Kawakami, H., 2009. LRRK2 mutations and risk variants in Japanese patients with Parkinson's disease. Mov. Disord. Off. J. Mov. Disord. Soc. 24, 1034–1041. https://doi.org/10.1002/mds.22514

Zarranz, J.J., Alegre, J., Gómez-Esteban, J.C., Lezcano, E., Ros, R., Ampuero, I., Vidal, L., Hoenicka, J., Rodriguez, O., Atarés, B., Llorens, V., Gomez Tortosa, E., del Ser, T., Muñoz, D.G., de Yebenes, J.G., 2004. The new mutation, E46K, of alpha-synuclein causes Parkinson and Lewy body dementia. Ann. Neurol. 55, 164–173. https://doi.org/10.1002/ana.10795

Zecca, L., Gallorini, M., Schünemann, V., Trautwein, A.X., Gerlach, M., Riederer, P., Vezzoni, P., Tampellini, D., 2001. Iron, neuromelanin and ferritin content in the substantia nigra of normal subjects at different ages: consequences for iron storage and neurodegenerative processes. J. Neurochem. 76, 1766–1773. https://doi.org/10.1046/j.1471-4159.2001.00186.x

Zecca, L., Stroppolo, A., Gatti, A., Tampellini, D., Toscani, M., Gallorini, M., Giaveri, G., Arosio, P., Santambrogio, P., Fariello, R.G., Karatekin, E., Kleinman, M.H., Turro, N., Hornykiewicz, O., Zucca, F.A., 2004. The role of iron and copper molecules in the neuronal vulnerability of locus coeruleus and substantia nigra during aging. Proc. Natl. Acad. Sci. 101, 9843–9848. https://doi.org/10.1073/pnas.0403495101

Zhang, J., Deng, X., Choi, H.G., Alessi, D.R., Gray, N.S., 2012. Characterization of TAE684 as a potent LRRK2 kinase inhibitor. Bioorg. Med. Chem. Lett. 22, 1864–1869. https://doi.org/10.1016/j.bmcl.2012.01.084

Zhang, J., Li, J., Chen, F., Liu, X., Jiang, C., Hu, X., Ma, L., Xu, Z., 2021. STN versus GPi deep brain stimulation for dyskinesia improvement in advanced Parkinson's disease: A meta-analysis of randomized controlled trials. Clin. Neurol. Neurosurg. 201, 106450. https://doi.org/10.1016/j.clineuro.2020.106450

Zhang, P., Fan, Y., Ru, H., Wang, L., Magupalli, V.G., Taylor, S.S., Alessi, D.R., Wu, H., 2019. Crystal structure of the WD40 domain dimer of LRRK2. Proc. Natl. Acad. Sci. 201817889. https://doi.org/10.1073/pnas.1817889116

Zhang, Z.-X., Dong, Z.-H., Román, G.C., 2006. Early Descriptions of Parkinson Disease in Ancient China. Arch. Neurol. 63, 782–784. https://doi.org/10.1001/archneur.63.5.782

Zhao, J., Molitor, T.P., Langston, J.W., Nichols, R.J., 2015. LRRK2 dephosphorylation increases its ubiquitination. Biochem. J. 469, 107–120. https://doi.org/10.1042/BJ20141305

Zhao, Y., Qin, L., Pan, H., Liu, Z., Jiang, L., He, Y., Zeng, Q., Zhou, Xun, Zhou, Xiaoxia, Zhou, Yangjie, Fang, Z., Wang, Z., Xiang, Y., Yang, H., Wang, Y., Zhang, K., Zhang, R., He, R., Zhou, Xiaoting, Zhou, Z., Yang, N., Liang, D., Chen, J., Zhang, X., Zhou, Yao, Liu, H., Deng, P., Xu, Kun, Xu, Ke, Zhou, C., Zhong, J., Xu, Q., Sun, Q., Li, B., Zhao, G., Wang, T., Chen, L., Shang, H., Liu, W., Chan, P., Xue, Z., Wang, Q., Guo, L., Wang, X., Xu, C., Zhang, Zhentao, Chen, T., Lei, L., Zhang, H., Wang, C., Tan, J., Yan, X., Shen, L., Jiang, H., Zhang, Zhuohua, Hu, Z., Xia, K., Yue, Z., Li, J., Guo, J., Tang, B., 2020. The role of genetics in Parkinson's disease: a large cohort study in Chinese mainland population. Brain 143, 2220–2234. https://doi.org/10.1093/brain/awaa167

Zhou, H., Huang, C., Tong, J., Hong, W.C., Liu, Y.-J., Xia, X.-G., 2011. Temporal Expression of Mutant LRRK2 in Adult Rats Impairs Dopamine Reuptake. Int. J. Biol. Sci. 7, 753–761. https://doi.org/10.7150/ijbs.7.753

Zhu, S., Yao, R., Li, Y., Zhao, P., Ren, C., Du, X., Yao, Y., 2020. Lysosomal quality control of cell fate: a novel therapeutic target for human diseases. Cell Death Dis. 11, 1–13. https://doi.org/10.1038/s41419-020-03032-5

Zhu, X., Sun, Y., Chen, D., Li, J., Dong, X., Wang, J., Chen, H., Wang, Y., Zhang, F., Dai, J., Pirraco, R.P., Guo, S., Marques, A.P., Reis, R.L., Li, W., 2017. Mastocarcinoma therapy synergistically promoted by lysosome dependent apoptosis specifically evoked by 5-Fu@nanogel system with passive targeting and pH activatable dual function. J. Controlled Release 254, 107–118. https://doi.org/10.1016/j.jconrel.2017.03.038

Zimprich, A., Benet-Pagès, A., Struhal, W., Graf, E., Eck, S.H., Offman, M.N., Haubenberger, D., Spielberger, S., Schulte, E.C., Lichtner, P., Rossle, S.C., Klopp, N., Wolf, E., Seppi, K., Pirker, W., Presslauer, S., Mollenhauer, B., Katzenschlager, R., Foki, T., Hotzy, C., Reinthaler, E., Harutyunyan, A., Kralovics, R., Peters, A., Zimprich, F., Brücke, T., Poewe, W., Auff, E., Trenkwalder, C., Rost, B., Ransmayr, G., Winkelmann, J., Meitinger, T., Strom, T.M., 2011. A mutation in VPS35, encoding a subunit of the retromer complex, causes late-onset Parkinson disease. Am. J. Hum. Genet. 89, 168–175. https://doi.org/10.1016/j.ajhg.2011.06.008

Zimprich, A., Müller-Myhsok, B., Farrer, M., Leitner, P., Sharma, M., Hulihan, M., Lockhart, P., Strongosky, A., Kachergus, J., Calne, D.B., Stoessl, J., Uitti, R.J., Pfeiffer, R.F., Trenkwalder, C., Homann, N., Ott, E., Wenzel, K., Asmus, F., Hardy, J., Wszolek, Z., Gasser, T., 2004. The PARK8 Locus in Autosomal Dominant Parkinsonism: Confirmation of Linkage and Further Delineation of the Disease-Containing Interval. Am. J. Hum. Genet. 74, 11–19.

Zuccato, C., Belyaev, N., Conforti, P., Ooi, L., Tartari, M., Papadimou, E., MacDonald, M., Fossale, E., Zeitlin, S., Buckley, N., Cattaneo, E., 2007. Widespread

Disruption of Repressor Element-1 Silencing Transcription Factor/Neuron-Restrictive Silencer Factor Occupancy at Its Target Genes in Huntington's Disease. J. Neurosci. 27, 6972–6983. https://doi.org/10.1523/JNEUROSCI.4278-06.2007

APPENDIX 1

Proteomics statistical analyses for volcano plots and Gene Ontology bubble

plots presented in Chapter 5 can be found in the following link:

https://drive.google.com/drive/folders/1PwPaOYj2aqndLTGsWXM7A9PrwJjFjV

qi?usp=sharing

APPENDIX 2

Manuscripts

The following papers were published, submitted, and/or prepared during the course of this PhD:

Kluss, J. H., Mamais, A., and Cookson, M. R. (2019). LRRK2 links genetic and sporadic Parkinson's disease. *Biochemical Society Transactions* https://doi.org/10.1042/BST20180462

I contributed to the conceptualization and writing of the manuscript.

Iannotta, L., Biosa, A., **Kluss, J. H.**, Tombesi, G., Kaganovich, A., Cogo, S., Plotegher, N., Civiero, L., Lobbestael, E., Baekelandt, V., Cookson, M. R., and Greggio, E. (2020). Divergent effects of G2019S and R1441C LRRK2 mutations on LRRK2 and Rab10 phosphorylations in mouse tissues. *Cells* https://doi.org/10.3390/cells9112344

I contributed to experimental design, carried out experiments, and analyzed data that is presented in this manuscript.

Bonet-Ponce, L., Beilina, A., Williamson, C. D., Lindberg, E., **Kluss, J. H.**, Saez-Atienzar, S., Landeck, N., Kumaran, R., Mamais, A., Bleck, C. K., Li, Y., and Cookson, M. R. (2020). LRRK2 mediated tubulation and vesicle sorting from lysosomes. *Science Advances* https://doi.org/10.1126/sciadv.abb2454

I carried out experiments and analyzed data that is presented in this manuscript.

Kluss, J. H., Mazza Conti, M., Li, Y., Manzoni, C., Lewis, P. A., Cookson, M. R., and Mamais, A. (2021). Preclinical modeling of chronic inhibition of the Parkinson's disease associated kinase LRRK2 reveals altered function of the endolysosomal system in vivo. *Molecular Neurodegeneration* https://doi.org/10.1186/s13024-021-00441-8

I contributed to the conceptualization, experimental design, data acquisition, and interpretation of data and writing of the manuscript.

Mamais, A., **Kluss, J. H.**, Bonet-Ponce, L., Landeck, N., Langston, R. G., Smith, N., Beilina, A., Kaganovich, A., Ghosh, M. C., Pellegrini, L., Kumaran, R., Papazoglou, I., Heaton, G. R., Harvey, K., Bandopadhyay, R., Maio, N., Kim, C., LaVoie, M. J., Gershlick, D. C., and Cookson, M. R. (2021). Mutations in LRRK2 linked to Parkinson disease sequester Rab8a to damaged lysosomes and regulated transferrin-mediated iron uptake in microglia. *PLOS Biology* https://doi.org/10.1371/journal.pbio.3001621

I contributed to the experimental design, carried out experiments, and acquired data that is presented in this manuscript.

Kluss, J. H., Bonet-Ponce, L., Lewis, P. A., and Cookson, M. R. (2022). Directing LRRK2 to membranes of the endolysosomal pathway triggers RAB phosphorylation and JIP4 recruitment. *Neurobiology of Disease* https://doi.org/10.1016/j.nbd.2022.105769

I contributed to the conceptualization, experimental design, data acquisition, and interpretation of data and writing of the manuscript.

Kluss J. H., Lewis, P. A., and Greggio, E. (2022). Leucine-rich repeat kinase 2 (LRRK2): an update on the potential therapeutic target for Parkinson's disease. *Expert Opinion on Therapeutic Targets* https://doi.org/10.1080/14728222.2022.2082937

I contributed to the conceptualization and writing of the manuscript.

Kluss, J. H., Beilina, A., Williamson, C. D., Lewis, P. A., Cookson, M. R., and Bonet-Ponce, L. (2022). Lysosomal positioning regulates Rab10 phosphorylation at LRRK2-positive lysosomes. *Manuscript under review.*

I contributed to the conceptualization, experimental design, data acquisition, and interpretation of data and writing of the manuscript.

PORTLAND PRESS

Review Article

LRRK2 links genetic and sporadic Parkinson's disease

Jillian H. Kluss, Adamantios Mamais and ⬤ Mark R. Cookson

Cell Biology and Gene Expression Section, Laboratory of Neurogenetics, National Institute on Aging, National Institutes of Health, Bldg. 35, 35 Convent Drive, Bethesda, MD 20892-3707, U.S.A.

Correspondence: Mark R. Cookson (cookson@mail.nih.gov)

The past two decades in research has revealed the importance of leucine-rich repeat kinase 2 (LRRK2) in both monogenic and sporadic forms of Parkinson's disease (PD). In families, mutations in LRRK2 can cause PD with age-dependent but variable penetrance and genome-wide association studies have found variants of the gene that are risk factors for sporadic PD. Functional studies have suggested that the common mechanism that links all disease-associated variants is that they increase LRRK2 kinase activity, albeit in different ways. Here, we will discuss the roles of LRRK2 in areas of inflammation and vesicular trafficking in the context of monogenic and sporadic PD. We will also provide a hypothetical model that links inflammation and vesicular trafficking together in an effort to outline how these pathways might interact and eventually lead to neuronal cell death. We will also highlight the translational potential of LRRK2-specific kinase inhibitors for the treatment of PD.

Introduction

Parkinson's disease (PD) is a neurodegenerative disorder affecting over 4 million people over the age of 50 within the world's top 15 most populated countries, a number that is expected to double by 2030 [1]. Historically, PD had been considered a purely sporadic disorder. It is now understood that many forms of PD have a genetic component as well as an environmental component of varying degrees [2–4]. Although ~90% of PD cases are sporadic (sPD), i.e. having no clearly defined single cause, the remaining 10% show a clear family history and are thus considered monogenic PD [5].

A central question in PD research is whether genetic PD is distinguishable mechanistically from the sporadic disease as this has implications for whether treatments for one group of patients might be useful for the other. Many studies have addressed a possible divergence in the clinical and pathological characteristics of patients harboring PD-linked mutations compared with sporadic cases. Patients carrying mutations in the *Leucine-rich repeat kinase 2* (*LRRK2*) gene, one of the most common genetic contributors of PD [6–8], manifest clinical features which are almost indistinguishable from the sporadic form. Similar patterns of motor symptoms between both forms, including the hallmark bradykinesia, tremor, rigidity, and postural instability have been reported. Nonmotor symptoms which include hallucinations, depression, anxiety, cognitive impairment, and pain also appear in both familial and sporadic PD [9,10]. Interestingly, LRRK2-PD has been associated with a spectrum of neuropathological features, including α-synuclein positive Lewy bodies, accumulation of phosphorylated tau as well as TDP-43 aggregates [11]. Nonetheless, neuronal loss and gliosis in the substantia nigra is the common pathological feature amongst all of the LRRK2 mutation cases, with the majority of G2019S LRRK2-PD cases displaying Lewy body pathology comparable with that of sporadic PD [11–13]. This suggests that there are convergent pathways that drive neuropathology in genetic and sporadic disease and close examination of the genes and risk factors involved in the two forms can highlight common cellular pathways of dysfunction.

In this review, we outline evidence from genetics and functional data that support a role for *LRRK2* in the pathogenesis of both familial and sporadic forms of PD. This review aims to serve three purposes: first, to highlight major findings regarding LRRK2 as a common factor between genetic and sporadic PD via genome-wide association studies (GWAS), as well as new *in vitro* and *in vivo* studies that have been published in the last few years supporting this association. Second, to explore potential implications of LRRK2 genetics and function on disease etiology through a comprehensive model of cellular pathways. Finally, to investigate LRRK2 as a druggable target and highlight the current efforts focusing on the development of future therapeutics.

Genetics
LRRK2 mutations cause autosomal dominant PD and can be a risk factor for sPD

Nearly 16 years ago, the *PARK8* locus was identified in a large Japanese family exhibiting autosomal dominant parkinsonism [14]. Linkage analysis identified 116 genes within the locus located on chromosome 12, and the specific gene responsible was discovered independently by two other groups [15,16]. The original family was then shown to have a mutation in the same gene, *LRRK2* [17]. Mutations in *LRRK2* were subsequently shown to be a relatively common genetic cause of PD worldwide [18]. To date, out of the ∼100 mutations identified within this gene [19–21], only six of these have been convincingly segregated as disease-causing: G2019S, R1441C/G/H, Y1699C, and I2020T [22,23]. The two most common mutations, G2019S and R1441C, are each responsible for up to ∼30% of inherited PD cases in certain populations, and up to 10 and 2.5% of sporadic PD cases, respectively [24–27]. The presence of mutations in what appears to be sporadic cases is likely due to incomplete but age-dependent penetrance. For example, G2019S has an age range of penetrance increasing from 17% at 50 years old to 85% at 70 years old; additionally, there are some carriers who never develop PD [28–30]. Similarly, R1441C has been shown to have reduced penetrance, suggesting that although these monogenic mutations significantly increase disease risk, they do not always lead to disease [31,32].

The *LRRK2* gene is made up of 51 exons and encodes a 2527 amino-acid protein with a predicted molecular mass of ∼286 kDa. LRRK2 is a multidomain protein where the Ras of complex proteins (Roc), C-terminal of ROC (COR) and kinase domains constitute a catalytic core that is flanked by protein–protein interaction domains: N-terminal armadillo, ankyrin, leucine-rich repeats and a C-terminal WD40 domain. Interestingly, most disease-linked *LRRK2* mutations are found within the core enzymatic domains and alter enzyme activity *in vitro* [33]. The G2019S mutation is located within the kinase domain and increases V_{max} for kinase activity while R1441C/G/H and Y1699C mutations decrease the GTPase activity of the Roc domain [34–38]. It is thought that these two events are related to each other in that kinase and GTPase activities being encoded on the same protein may regulate each other. Supporting this idea, measurements of Rab substrates in cells show that all mutations support increased phosphorylation [39,40].

In recent years, GWAS have been used to identify risk loci for many disorders, including PD. These genomic surveys have shown that the *LRRK2* locus contains common variation that increases risk of developing sporadic PD [41,42]. The GWAS signal is explained by non-coding variability, which imparts only a moderate risk for disease. Additionally, *LRRK2* contains some protein-coding changes that increase risk for disease. Sequencing *LRRK2* from the Taiwanese population identified G2385R variant as a common variant among healthy controls, present in ∼5% of people. However, the variant was found to be twice as common in patients with PD [18]. The two-fold increase in risk was replicated in many other studies, confirming G2385R as a risk factor in Asian populations [43–49]. Located in the C-terminal WD40 domain, this mutation likely alters the protein structure and modulates LRRK2 binding to interactors associated with vesicular trafficking [50]. Our laboratory has shown that the G2385R variant promotes LRRK2 protein turnover by increasing binding affinity to Hsc70 and CHIP resulting in lower steady-state levels [51,52] and recent data suggest that this variant compromises LRRK2 dimerization [53]. In terms of effects on the kinase activity, purified protein shows decreased autophosphorylation in *in vitro* kinase assays and can rescue the hyperactivation effect of the G2019S mutation [51]. In a cellular context, however, G2385R autophosphorylation at S1292 is retained [54]. This highlights how the context of the assay, *in vitro* purified protein versus cellular context, is important when assaying LRRK2 function. As outlined below, LRRK2 is sequestered to the TGN (*trans*-Golgi network) in co-expression with Rab29 and phosphorylates membrane-bound Rab GTPases, while the R1441C, Y1699C and G2019S mutations enhance this activation [40,55]. In this assay, the G2385R variant is sequestered to the TGN much like the WT protein [56]. In co-expression experiments in cells, however, G2385R shows increased kinase activity towards

Rab10 compared with WT protein similar to what is reported for the other genetic variants [53]. These results suggest that certain molecular mechanisms that mediate G2385R disease risk may be shared with familial mutations, however, the effects of this variant result in G2385R being a risk factor rather than a penetrant mutation.

Similarly, the rarer R1628P variant has also been found to increase risk of PD two-fold in Asian populations [57]. This variant has been found to increase LRRK2 kinase activity indirectly and cause cell death *in vitro* [58]. Intriguingly, R1398H has been identified as protective against PD in several cohorts by lowering activity of the protein [59–61]. Rare coding variants in LRRK2 have been associated with an earlier age of onset of disease [28,62–65].

Collectively, these findings show that both coding and non-coding variants at the *LRRK2* locus have a strong link to PD and influence penetrance, age of onset, and cause both vulnerability towards and protection against developing PD. Importantly, all of these cases are 'sporadic' PD, suggesting that LRRK2 plays a role in this more common form of the disease. Another way to think about the role of LRRK2 in PD is that because the various alleles have differing penetrance, some will occur in a recognizable pattern in families while others will be found in isolated cases without apparent family history.

GWAS suggest modified expression of LRRK2 is associated with sporadic PD

There has been speculation that non-coding *LRRK2* variants affect risk of disease through modulation of LRRK2 protein expression. For example, it has been shown that a common risk variant at the LRRK2 locus is associated with higher LRRK2 expression in microglia-like cells derived from human monocytes [66]. In 94 healthy participants, 94 genes from loci associated with Alzheimer's, Parkinson's, and multiple sclerosis diseases were examined in both monocytes and their monocyte-derived microglia-like counterparts. Comparing these data with a GWAS-derived list of disease-associated single nucleotide polymorphisms (SNPs) [67], results suggest the T allele at rs76904798 *LRRK2* increased in expression. This finding suggests that *LRRK2* gene expression can be altered by specific alleles or haplotypes. It also leads to the hypothesis that *LRRK2* may have a specific role within microglia. As microglia are influenced by myriad of conditions (inflammation, neuronal apoptosis, etc.) this suggests that the role of LRRK2 risk variants may be more prominent under situations where microglia are stimulated. We speculate that this concept might be related to penetrance of variants in LRRK2, if there is a requirement for immune stimulation to express disease processes. This will be discussed in more depth in the next section.

Higher LRRK2 activity is found in both genetic and sporadic PD patients and is reflected in *in vitro* and *in vivo* models

LRRK2 is a large multidomain protein harboring two enzymatic cores that has a large spectrum of interacting factors linking it to diverse cellular pathways. LRRK2 expression is ubiquitous, with varying degrees of expression in peripheral tissues as well as the brain [15,68–70]. At the cellular level, LRRK2 expression has been reported in astrocytes, microglia, neurons, endothelial cells and peripheral immune cells [71–74]. Thus, it is likely that LRRK2 plays distinct signaling roles in different cell types, specifically involving its kinase activity and autophosphorylation (Figure 1). In this section, we will discuss recent findings that support the relationship of LRRK2 in monogenic and sporadic PD to inflammation and vesicular trafficking.

The role of LRRK2 in PD-related inflammation

It is increasingly appreciated that microglia can contribute to disease pathogenesis as they mediate the immune responses in the central nervous system and inflammation is a key factor in neurodegeneration. Many studies have nominated LRRK2 as an integral part of inflammatory response downstream of various proinflammatory signals. Recent studies propose a role of LRRK2 in phagocytosis and highlight how an increase in protein levels or activity may impair an inflammatory response [75,76]. *In vitro* studies using mouse cultures report increased LRRK2 expression in microglia as well as bone marrow-derived macrophages after introducing proinflammatory agents such as lipopolysaccharide. Additionally, LRRK2 knockdown ameliorates this inflammatory signaling, suggesting LRRK2 and inflammation have a complex, modulatory relationship that still needs mechanistic clarification [72,77]. A similar relationship has been found to occur in peripheral immune cells in sPD patients [78]. For example, LRRK2 expression is higher in T cells, B cells, and CD16$^+$ monocytes from sporadic PD patients compared with controls and this is correlated with higher cytokine levels. This supports the idea that
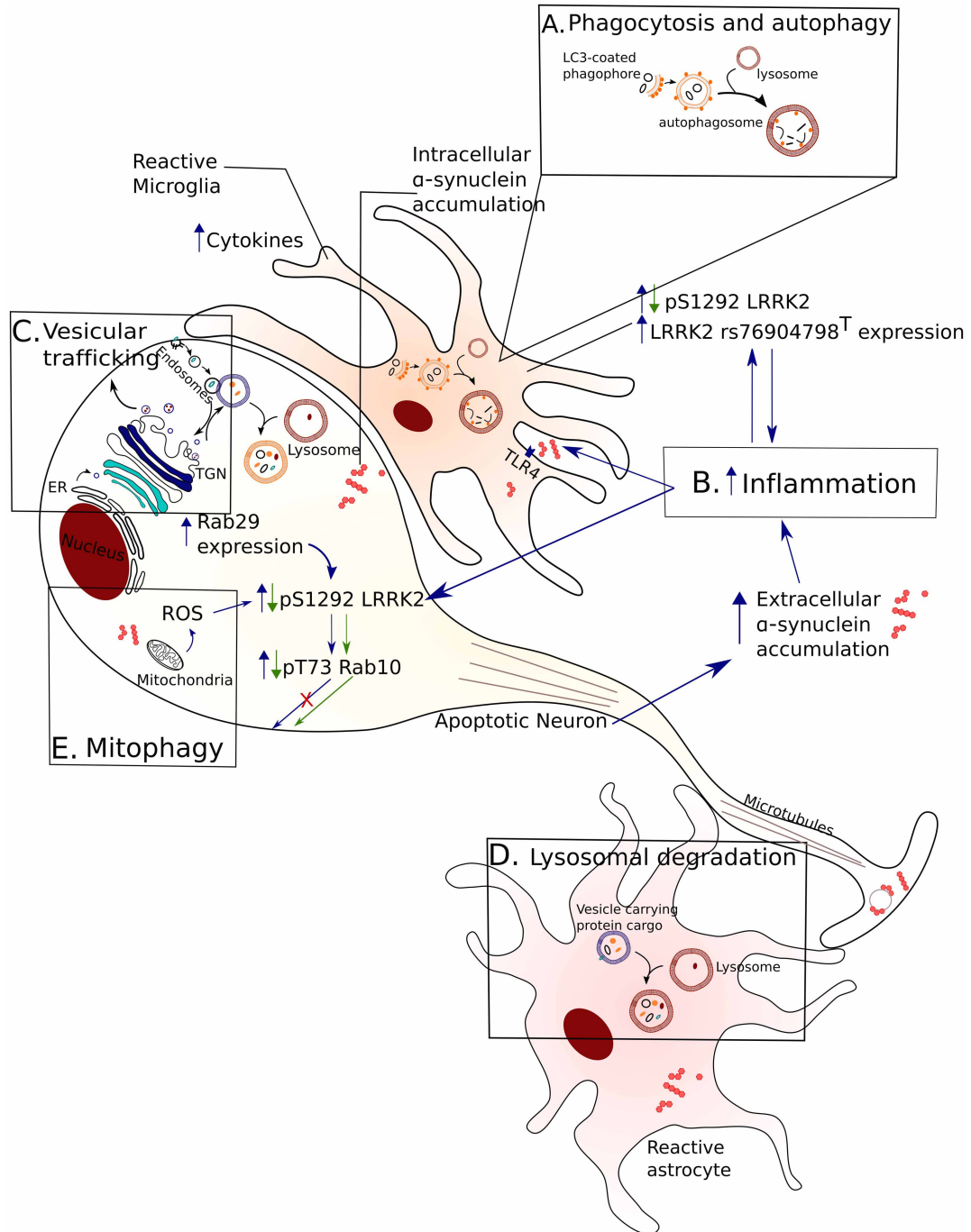
Figure 1. Physiological pathways of LRRK2 activity.

Part 1 of 2

A common function of LRRK2 in genetic and sPD can be modeled on physiological signaling pathways important for neuronal survival. A generic apoptotic neuron (without dendrites for simplicity) and reactive glial cells are depicted and highlighted pathways are shown along with downstream effects of increased LRRK2 activity. Blue arrows indicate a gain-of-function pathway where increased LRRK2 kinase activity may drive dysfunction while green arrows highlight the molecular events of pharmacological LRRK2 inhibition. (A) LRRK2 has been linked to autophagosome maturation and impaired phagocytosis nominating these processes as possible culprits in the clearance of aggregated synuclein. (B) LRRK2 is activated in systems of induced inflammation while higher LRRK2 levels are seen in immune cells from idiopathic PD patients compared with healthy controls. Accumulation of extracellular synuclein can further induce an inflammatory response and this, in turn, can lead to LRRK2 activation. (C) LRRK2 interacts with Rab29 and mediates TGN dynamics while Rab29 expression can drive LRRK2

Figure 1. Physiological pathways of LRRK2 activity.   Part 2 of 2

activation. Active LRRK2 phosphorylates Rab GTPases with downstream effects on vesicular trafficking as well as impaired autophagy/lysosomal pathways (D) that can impair clearance of aggregated proteins. (E) Progressive increase in ROS with ageing can activate LRRK2 that in turn can affect mitochondrial function and impair mitochondrial clearance through mitophagy.

the increase in LRRK2 expression is relevant to sporadic PD pathology and may contribute to inflammation associated with PD.

LRRK2 is autophosphorylated at serine 1292 and this is a robust physiological readout of its kinase activity in different systems [79–81]. In a recent study, a novel approach that allows pS1292 visualization within cells was developed using proximity-ligation amplification to examine endogenous LRRK2 autophosphorylation [82]. The authors used *in vivo* administration of rotenone as a model of reactive oxygen species (ROS)-induction and PD-related pathology, based on previous research that linked ROS and mitochondrial impairment to LRRK2 activation in cells [83–86]. They reported an increase in pS1292 LRRK2 in nigrostriatal neurons of rotenone-treated rats compared with controls, which was ameliorated with LRRK2-specific kinase inhibitors. In the same study, pS1292 LRRK2 autophosphorylation was six-fold higher in surviving nigrostriatal neurons from sporadic PD patients compared with healthy controls. There was also a four-fold increase in phosphorylated Rab10 (pT73), a LRRK2 substrate that is known to play a role in vesicular trafficking. This study supports a concomitant activation of LRRK2 across familial and sporadic PD and links the oxidative stress response to LRRK2-mediated pathways of neurodegeneration.

The kinase activity of LRRK2 was found to be increased in microglia in sporadic PD postmortem tissue, through monitoring its autophosphorylation state and also downstream substrates [82] suggesting that inflammation may be a trigger of LRRK2 activity in PD patients. Microglial inflammation in PD could be triggered by an interaction of extracellular forms of the neuronal protein α-synuclein with TLR4 receptors [87]. Such species of α-synuclein could either be actively secreted from neurons or might accumulate due to neuronal cell death. Such events could then perpetuate neuroinflammation by releasing additional toxic materials such as ROS [88]. Alpha-synuclein accumulation in neurons can also induce mitophagy, a process linked to LRRK2 activity [89,90], resulting in increased ROS production [91]. Taken together, these data highlight how ROS accumulation and inflammation may activate wild type LRRK2 in sporadic PD within nigrostriatal dopamine neurons and microglia, and that amplification of damage by LRRK2 in both glial and neuronal cells is a plausible mechanism by which disease may progress (Figure 1).

The role of LRRK2 mutations in vesicular trafficking

The above considerations suggest that there are multiple cell types that may mediate the involvement of LRRK2 in monogenic and sporadic PD. However, it is important to also discuss the subcellular events that LRRK2 can influence and whether these are relevant to neurodegeneration. LRRK2 has been linked to processes of vesicular trafficking through interactions with multiple proteins associated with cellular membranes [92]. For example, LRRK2 can phosphorylate a subset of Rab GTPases, including Rab8a and Rab10, both of which play roles in vesicular trafficking to the plasma membrane [39,93]. Importantly, all pathogenic variants in LRRK2 that cause disease have been shown to enhance Rab phosphorylation in cells [39,40]. Another Rab upstream of LRRK2 is Rab29 which has been shown to bind LRRK2 at its ankyrin domain and recruits it to the TGN [55]. Interestingly, Rab29 is found in the *PARK16* locus and is reported to be a PD risk factor [94]. Overexpression of Rab29 results in an increase in pS1292 LRRK2 and pT73 Rab10 *in vitro*, which were ameliorated followed by Rab29 knockdown [54]. Similar results were seen in studies that also demonstrated a requirement for Rab29 to be associated with membranes due to prenylation at the C-terminus of the protein [40]. These results are consistent with prior observations that LRRK2 mutants, which are activated by Rab29 to a greater extent that the wild type protein, enhance association of LRRK2 with the TGN [55].

Once activated, LRRK2 can affect multiple aspects of vesicular trafficking, one of which is the autophagy/lysosomal pathway (Figure 1). Autophagy is a maintenance process for degrading damaged organelles and proteins within the cell and is an integral part of the inflammatory response. During the initiation of autophagy, the protein LC3 is lipidated and associates with the membrane of nascent autophagic vesicles. Inhibition of LRRK2 kinase activity has been shown to increase the lipidation of LC3 in astrocytes [95]. This may be indicative of either induction of autophagosome formation or inhibition of autophagosome/autolysosome

degradation. Expression of GFP-tagged, PD-causing LRRK2 mutants results in an increase in lysosome size which is dependent on kinase activity and is associated with a reduction in lysosomal pH [96]. *In vivo*, loss of LRRK2 led to accumulation of autophagic markers LC3-II and p62 [97]. Interestingly, comparing these markers in postmortem tissue from G2019S LRRK2 PD and sPD patients showed decreased LC3-II levels in the basal ganglia of both sporadic and genetic PD forms compared with controls [98]. This suggests LRRK2 plays a crucial role in trafficking within the autophagy/lysosomal pathway and is necessary for normal lysosomal function. In turn, autophagy influences inflammation through the transport of degradable material to the lysosome via phagophores. Thus, although we have not yet identified all the intracellular pathways involved in LRRK2-related PD, one possibility is that inflammatory reactions and intracellular trafficking that affects the autophagy–lysosome system are mechanistically related to each other.

Kinase activity: a push towards new LRRK2-targeting drug therapies

The results discussed above strongly indicate that LRRK2 mutations lead to a gain of function of kinase-dependent activity. Consistent with this idea, rare loss of function LRRK2 alleles can be found within the human population but are not associated with PD [99]. Furthermore, kinase-dead versions of mutant LRRK2 are less toxic than their kinase active counterparts in many cellular and animal models. Therefore, it is reasonable to expect that lowering LRRK2 kinase activity would be therapeutically useful. This hypothesis has led to the development of small molecule LRRK2 kinase inhibitors.

Pharmacological inhibition of LRRK2 has been shown to be neuroprotective in human cell lines and PD-relevant animal models [100,101]. In parallel to the development of these tools, discovery of robust and reliable biomarkers of kinase activity has been critical to be able to monitor the effectiveness of such compounds. A recent study from our laboratory found that pS1292 is a reliable readout of LRRK2 kinase activity *in vivo* [79] while others have shown the same for downstream Rab proteins [102]. A recent study suggested that peripheral blood neutrophils may be useful to monitor LRRK2 activity in the clinic as they are abundant, homogenous and express relatively high levels of LRRK2 and the substrate Rab10 [103].

Therefore, there are potential therapeutic agents and biomarkers of target engagement that would allow the hypothesis that LRRK2 activity is pathogenic in PD to be tested in a clinical setting. However, it remains unclear as to which patients would benefit from such a therapy. Importantly, if monogenic and sporadic PD share not just some clinical features but are also mechanistically linked by LRRK2 kinase activity, then LRRK2 inhibitors may be beneficial not only for mutation carriers but for the broader sporadic PD population. Recently, one small-molecule LRRK2 inhibitor, DNL201, reached clinical testing in 2017 and showed inhibition of LRRK2 kinase activity in a healthy volunteer phase I study [104]. Another LRRK2 inhibitor, DNL151, is currently being assessed in healthy volunteers in the Netherlands in order to select the most promising molecule to be assessed in patients with PD carrying an *LRRK2* mutation.

Although these inhibitors are promising, it is worth mentioning that since normal LRRK2 function is not fully elucidated, the downstream effects of inhibiting this enzymatic activity in humans are currently unknown. Polymorphisms around LRRK2 have been identified as risk variants for Chron's disease and leprosy [105,106] while LRRK2 phosphorylation and protein levels are modulated in response to different proinflammatory stimuli [73,107]. In turn, LRRK2 expression enhances transcriptional activation of inflammatory responses [73] and PD-linked mutations induce cytokine production in activated microglia [108]. Inhibiting LRRK2 pharmacologically can impair microglial inflammatory responses [77] and LRRK2 deficiency impairs pathogen clearance *in vivo* [109].

In the context of vesicular trafficking, LRRK2 has a spectrum of interacting factors and pathways that it is involved in, therefore nominating possible side effects of targeting its activity is challenging. *In vivo* models suggest that *LRRK2* deficiency induces lysosomal defects [110] and compromises the ability of lysosomes to degrade autophagic cargo by impairing trans-Golgi to lysosome trafficking [111]. Compromised lysosomal function can alter the capacity of lysosomes to degrade phagocytosed material and modulate the inflammatory response and cytokine production. These studies highlight a role of LRRK2 in lysosomal processing and inflammatory signaling and suggest that pharmacological inhibition of its kinase activity may compromise activation of inflammatory responses. A decline in immune function is an established hallmark of aging, and, in the setting of chronic LRRK2 kinase inhibition that is relevant to the clinic, it will be important to monitor the integrity of the patients' immune system. Studies on the safety implications of targeting LRRK2 kinase activity have reported macroscopic changes in *in vivo* model organisms. Morphological changes in lung from nonhuman primates, and kidney tissue from rats treated with specific LRRK2 inhibitors have been reported [112–114]. The mechanism by

which the lung and kidney are affected is not completely clear but may be mediated by changes in epithelial integrity, as the lung phenotype is associated with infiltrating type-II pneumocytes into the alveolar space and the kidney phenotype is driven in part by accumulation of hemoglobin in the kidney parenchyma. The key question for drug development aimed at LRRK2 kinase activity is whether such events induce clinically significant problems in persons with PD. Reassuringly, effects are reversible after cessation of dosing in animal models, suggesting that there are unlikely to be long-term adverse events, but human safety data will be critical to whether LRRK2 kinase inhibitors can be tolerated clinically in PD patients.

Perspectives

Convergent results from genetic and functional assays support the idea that LRRK2 is a viable drug target in both monogenic and sporadic PD. While there are important additional mechanistic data that are required for a full understanding of LRRK2-associated pathways, current models suggest that intracellular trafficking may be affected by LRRK2 mutations and that this may be related to events in both neurons and non-neuronal cells that mediate neuroinflammation. With these events in mind, it can be speculated that the complex role of LRRK2 within the cell may be one of a master orchestrator, interacting within various cellular pathways in order to maintain homeostasis. A gain-of-function mutation may shift this delicate balancing act, disrupting normal degradative processes and eventually leading to PD pathogenesis.

Roughly 1 million people are living with PD in the US alone which is predicted to increase [115]. As of yet, there continues to be a significant unmet medical need in the field of neurodegeneration for effective, long-lasting treatments that either halt or slow disease progression. Currently, there are very few options in drug treatment, all of which target symptoms of the disease rather than cause, for many reasons — insufficient drug exposure in the brain, failure to provide evidence of target engagement using biomarkers, lack of a causative candidate that is targetable, etc. — however, this is starting to change. With the improvement of clinically applicable technologies, laboratory explorations of LRRK2 substrates and functions have identified potential biomarkers for clinical use in blood and urinary exosomes [81] providing direct assessments of LRRK2-specific drug inhibitors. These assessments can now provide data that can be used to predict potential areas of concern for on-target side effects of chronic LRRK2 inhibition. Therefore, while the hypothesis that LRRK2 kinase activity can be inhibited to benefit people with PD remains untested, the important tools that would be needed to address this idea are now available.

Abbreviations

COR, C-terminus of Roc; GWAS, genome-wide association studies; LBs, Lewy Bodies; LRRK2, leucine-rich repeat kinase 2; PBMCs, peripheral blood mononuclear cells; PD, Parkinson's disease; Roc, Ras of complex; ROS, reactive oxygen species; SNCA, Alpha-synuclein; SNPs, single nucleotide polymorphisms; sPD, sporadic Parkinson's disease; TGN, *trans*-Golgi network.

Author Contribution

J.H.K., A.M. and M.R.C. wrote the manuscript. All authors read and approved the final manuscript.

Funding

Competing Interests

The Authors declare that there are no competing interests associated with the manuscript.

References

1   Dorsey, E.R., Constantinescu, R., Thompson, J.P., Biglan, K.M., Holloway, R.G., Kieburtz, K. et al. (2007) Projected number of people with Parkinson disease in the most populous nation, 2005 through 2030. *Neurology* **68**, 384–386 https://doi.org/10.1212/01.wnl.0000247740.47667.03

2   Farrer, M.J., Williams, L.N., Algom, A.A., Kachergus, J., Hulihan, M.M., Ross, O.A. et al. (2009) Glucosidase-beta variations and Lewy body disorders. *Parkinsonism Relat. Disord.* **15**, 414–416 https://doi.org/10.1016/j.parkreldis.2008.08.004

3   Singleton, A. and Hardy, J. (2011) A generalizable hypothesis for the genetic architecture of disease: pleomorphic risk loci. *Hum. Mol. Genet.* **20**, R158–R162 https://doi.org/10.1093/hmg/ddr358

4   Singleton, A.B., Farrer, M.J. and Bonifati, V. (2013) The genetics of Parkinson's disease: progress and therapeutic implications. *Mov. Disord.* **28**, 14–23 https://doi.org/10.1002/mds.25249

5   Corti, O., Lesage, S. and Brice, A. (2011) What genetics tells us about the causes and mechanisms of Parkinson's disease. *Physiol. Rev.* **91**, 1161–1218 https://doi.org/10.1152/physrev.00022.2010

6   Brice, A. (2005) Genetics of Parkinson's disease: LRRK2 on the rise. *Brain* **128**, 2760–2762 https://doi.org/10.1093/brain/awh676

7   Lesage, S., Dürr, A., Tazir, M., Lohmann, E., Leutenegger, A.-L., Janin, S. et al. (2006) *LRRK2* g2019s as a cause of Parkinson's disease in North African Arabs. *N. Engl. J. Med.* **354**, 422–423 https://doi.org/10.1056/NEJMc055540

8   Ozelius, L.J., Senthil, G., Saunders-Pullman, R., Ohmann, E., Deligtisch, A., Tagliati, M. et al. (2006) *LRRK2* g2019s as a cause of Parkinson's disease in Ashkenazi Jews. *N. Engl. J. Med.* **354**, 424–425 https://doi.org/10.1056/NEJMc055509

9   Haugarvoll, K., Rademakers, R., Kachergus, J.M., Nuytemans, K., Ross, O.A., Gibson, J.M. et al. (2008) *LRRK2* r1441c parkinsonism is clinically similar to sporadic Parkinson disease. *Neurology* **70**, 1456–1460 https://doi.org/10.1212/01.wnl.0000304044.22253.03

10   Healy, D.G., Wood, N.W. and Schapira, A.H.V. (2008) Test for LRRK2 mutations in patients with Parkinson's disease. *Pract. Neurol.* **8**, 381–385 https://doi.org/10.1136/jnnp.2008.162420

11   Wider, C., Dickson, D.W. and Wszolek, Z.K. (2010) Leucine-rich repeat kinase 2 gene-associated disease: redefining genotype-phenotype correlation. *Neurodegener. Dis.* **7**, 175–179 https://doi.org/10.1159/000289232

12   Poulopoulos, M., Cortes, E., Vonsattel, J.-P.G., Fahn, S., Waters, C., Cote, L.J. et al. (2012) Clinical and pathological characteristics of LRRK2 G2019S patients with PD. *J. Mol. Neurosci.* **47**, 139–143 https://doi.org/10.1007/s12031-011-9696-y

13   Kalia, L.V., Lang, A.E., Hazrati, L.-N., Fujioka, S., Wszolek, Z.K., Dickson, D.W. et al. (2015) Clinical correlations with Lewy body pathology in *LRRK2*-related Parkinson disease. *JAMA Neurol.* **72**, 100–105 https://doi.org/10.1001/jamaneurol.2014.2704

14   Funayama, M., Hasegawa, K., Kowa, H., Saito, M., Tsuji, S. and Obata, F. (2002) A new locus for Parkinson's disease (PARK8) maps to chromosome 12p11.2-q13.1. *Ann. Neurol.* **51**, 296–301 https://doi.org/10.1002/ana.10113

15   Paisán-Ruíz, C., Jain, S., Evans, E.W., Gilks, W.P., Simón, J., van der Brug, M. et al. (2004) Cloning of the gene containing mutations that cause PARK8-linked Parkinson's disease. *Neuron* **44**, 595–600 https://doi.org/10.1016/j.neuron.2004.10.023

16   Zimprich, A., Müller-Myhsok, B., Farrer, M., Leitner, P., Sharma, M., Hulihan, M. et al. (2004) The PARK8 locus in autosomal dominant parkinsonism: confirmation of linkage and further delineation of the disease-containing interval. *Am. J. Hum. Genet.* **74**, 11–19 https://doi.org/10.1086/380647

17   Funayama, M., Hasegawa, K., Ohta, E., Kawashima, N., Komiyama, M., Kowa, H. et al. (2005) An *LRRK2* mutation as a cause for the parkinsonism in the original PARK8 family. *Ann. Neurol.* **57**, 918–921 https://doi.org/10.1002/ana.20484

18   Di Fonzo, A., Tassorelli, C., De Mari, M., Chien, H.F., Ferreira, J., Rohé, C.F. et al. (2006) Comprehensive analysis of the LRRK2 gene in sixty families with Parkinson's disease. *Eur. J. Hum. Genet.* **14**, 322–331 https://doi.org/10.1038/sj.ejhg.5201539

19   Cruts, M., Theuns, J. and Van Broeckhoven, C. (2012) Locus-specific mutation databases for neurodegenerative brain diseases. *Hum. Mutat.* **33**, 1340–1344 https://doi.org/10.1002/humu.22117

20   Nuytemans, K., Theuns, J., Cruts, M. and Van Broeckhoven, C. (2010) Genetic etiology of Parkinson disease associated with mutations in the SNCA, PARK2, PINK1, PARK7, and LRRK2 genes: a mutation update. *Hum. Mutat.* **31**, 763–780 https://doi.org/10.1002/humu.21277

21   Paisán-Ruíz, C., Nath, P., Washecka, N., Gibbs, J.R. and Singleton, A.B. (2008) Comprehensive analysis of *LRRK2* in publicly available Parkinson's disease cases and neurologically normal controls. *Hum. Mutat.* **29**, 485–490 https://doi.org/10.1002/humu.20668

22   Gasser, T. (2009) Molecular pathogenesis of Parkinson disease: insights from genetic studies. *Expert. Rev. Mol. Med.* **11**, e22 https://doi.org/10.1017/S1462399409001148

23   Aasly, J.O., Vilariño-Güell, C., Dachsel, J.C., Webber, P.J., West, A.B., Haugarvoll, K. et al. (2010) Novel pathogenic LRRK2 p.Asn1437His substitution in familial Parkinson's disease. *Mov. Disord.* **25**, 2156–2163 https://doi.org/10.1002/mds.23265

24   Paisán-Ruíz, C., Lewis, P.A. and Singleton, A.B. (2013) *LRRK2*: cause, risk, and mechanism. *J. Parkinsons Dis.* **3**, 85–103 https://doi.org/10.3233/JPD-130192

25   Bardien, S., Lesage, S., Brice, A. and Carr, J. (2011) Genetic characteristics of leucine-rich repeat kinase 2 (LRRK2) associated Parkinson's disease. *Parkinsonism Relat. Disord.* **17**, 501–508 https://doi.org/10.1016/j.parkreldis.2010.11.008

26   Guedes L, C., Ferreira, J.J., Rosa, M.M., Coelho, M., Bonifati, V. and Sampaio, C. (2010) Worldwide frequency of G2019S LRRK2 mutation in Parkinson's disease: a systematic review. *Parkinsonism Relat. Disord.* **16**, 237–242 https://doi.org/10.1016/j.parkreldis.2009.11.004

27   Deng, H., Le, W., Guo, Y., Hunter, C.B., Xie, W., Huang, M. et al. (2006) Genetic analysis of LRRK2 mutations in patients with Parkinson disease. *J. Neurol. Sci.* **251**, 102–106 https://doi.org/10.1016/j.jns.2006.09.017

28   Lee, A.J., Wang, Y., Alcalay, R.N., Mejia-Santana, H., Saunders-Pullman, R., Bressman, S. et al. (2017) Penetrance estimate of *LRRK2* p.G2019S mutation in individuals of non-Ashkenazi Jewish ancestry. *Mov. Disord.* **32**, 1432–1438 https://doi.org/10.1002/mds.27059

29   Kachergus, J., Mata, I.F., Hulihan, M., Taylor, J.P., Lincoln, S., Aasly, J. et al. (2005) Identification of a novel LRRK2 mutation linked to autosomal dominant parkinsonism: evidence of a common founder across European populations. *Am. J. Hum. Genet.* **76**, 672–680 https://doi.org/10.1086/429256

30   San Luciano, M., Lipton, R.B., Wang, C., Katz, M., Zimmerman, M.E., Sanders, A.E. et al. (2010) Clinical expression of *LRRK2* G2019S mutations in the elderly. *Mov. Disord.* **25**, 2571–2576 https://doi.org/10.1002/mds.23330

31   Trinh, J., Guella, I. and Farrer, M.J. (2014) Disease penetrance of late-onset parkinsonism: a meta-analysis. *JAMA Neurol.* **71**, 1535–1539 https://doi.org/10.1001/jamaneurol.2014.1909

32   Reed, X., Bandrés-Ciga, S., Blauwendraat, C. and Cookson, M.R. (2019) The role of monogenic genes in idiopathic Parkinson's disease. *Neurobiol. Dis.* **124**, 230–239 https://doi.org/10.1016/j.nbd.2018.11.012

33   Rudenko, I.N. and Cookson, M.R. (2014) Heterogeneity of leucine-rich repeat kinase 2 mutations: genetics, mechanisms and therapeutic implications. *Neurotherapeutics* **11**, 738–750 https://doi.org/10.1007/s13311-014-0284-z

34   Cookson, M.R. (2015) *LRRK2* pathways leading to neurodegeneration. *Curr. Neurol. Neurosci. Rep.* **15**, 42 https://doi.org/10.1007/s11910-015-0564-y

35   Lewis, P.A., Greggio, E., Beilina, A., Jain, S., Baker, A. and Cookson, M.R. (2007) The R1441C mutation of *LRRK2* disrupts GTP hydrolysis. *Biochem. Biophys. Res. Commun.* **357**, 668–671 https://doi.org/10.1016/j.bbrc.2007.04.006

36   Daniëls, V., Vancraenenbroeck, R., Law, B.M.H., Greggio, E., Lobbestael, E., Gao, F. et al. (2011) Insight into the mode of action of the *LRRK2* Y1699C pathogenic mutant. *J. Neurochem.* **116**, 304–315 https://doi.org/10.1111/j.1471-4159.2010.07105.x

37   Liao, J., Wu, C.-X., Burlak, C., Zhang, S., Sahm, H., Wang, M. et al. (2014) Parkinson disease-associated mutation R1441H in LRRK2 prolongs the 'active state' of its GTPase domain. *Proc. Natl Acad. Sci. U.S.A.* **111**, 4055–4060 https://doi.org/10.1073/pnas.1323285111

658

38 Guo, L., Gandhi, P.N., Wang, W., Petersen, R.B., Wilson-Delfosse, A.L. and Chen, S.G. (2007) The Parkinson's disease-associated protein, leucine-rich repeat kinase 2 (LRRK2), is an authentic GTPase that stimulates kinase activity. *Exp. Cell Res.* **313**, 3658–3670 https://doi.org/10.1016/j.yexcr.2007.07.007

39 Steger, M., Tonelli, F., Ito, G., Davies, P., Trost, M., Vetter, M. et al. (2016) Phosphoproteomics reveals that Parkinson's disease kinase LRRK2 regulates a subset of Rab GTPases. *eLife* **5**, e12813 https://doi.org/10.7554/eLife.12813

40 Liu, Z., Bryant, N., Kumaran, R., Beilina, A., Abeliovich, A., Cookson, M.R. et al. (2018) *LRRK2* phosphorylates membrane-bound Rabs and is activated by GTP-bound Rab7L1 to promote recruitment to the trans-Golgi network. *Hum. Mol. Genet.* **27**, 385–395 https://doi.org/10.1093/hmg/ddx410

41 Chang, D., Nalls, M.A., Hallgrímsdóttir, I.B., Hunkapiller, J., van der Brug, M., Cai, F. et al. (2017) A meta-analysis of genome-wide association studies identifies 17 new Parkinson's disease risk loci. *Nat. Genet.* **49**, 1511–1516 https://doi.org/10.1038/ng.3955

42 International Parkinson Disease Genomics Consortium, Nalls, M.A., Plagnol, V., Hernandez, D.G., Sharma, M., Sheerin, U.-M. et al. (2011) Imputation of sequence variants for identification of genetic risks for Parkinson's disease: a meta-analysis of genome-wide association studies. *Lancet* **377**, 641–649 https://doi.org/10.1016/S0140-6736(10)62345-8

43 Li, C., Ting, Z., Qin, X., Ying, W., Li, B., Guo Qiang, L. et al. (2007) The prevalence of *LRRK2* Gly2385Arg variant in Chinese Han population with Parkinson's disease. *Mov. Disord.* **22**, 2439–2443 https://doi.org/10.1002/mds.21763

44 Tan, E.-K. (2007) The role of common genetic risk variants in Parkinson disease. *Clin. Genet.* **72**, 387–393 https://doi.org/10.1111/j.1399-0004.2007.00890.x

45 Funayama, M., Li, Y., Tomiyama, H., Yoshino, H., Imamichi, Y., Yamamoto, M. et al. (2007) Leucine-rich repeat kinase 2 G2385R variant is a risk factor for Parkinson disease in Asian population. *NeuroReport* **18**, 273–275 https://doi.org/10.1097/WNR.0b013e32801254b6

46 Chan, D.K.Y., Ng, P.W., Mok, V., Yeung, J., Fang, Z.M., Clarke, R. et al. (2008) *LRRK2* gly2385arg mutation and clinical features in a Chinese population with early-onset Parkinson's disease compared to late-onset patients. *J. Neural Transm.* **115**, 1275–1277 https://doi.org/10.1007/s00702-008-0065-0

47 Choi, J.M., Woo, M.S., Ma, H.-I., Kang, S.Y., Sung, Y.-H., Yong, S.W. et al. (2008) Analysis of PARK genes in a Korean cohort of early-onset Parkinson disease. *Neurogenetics* **9**, 263–269 https://doi.org/10.1007/s10048-008-0138-0

48 Zabetian, C.P., Yamamoto, M., Lopez, A.N., Ujike, H., Mata, I.F., Izumi, Y. et al. (2009) *LRRK2* mutations and risk variants in Japanese patients with Parkinson's disease. *Mov. Disord.* **24**, 1034–1041 https://doi.org/10.1002/mds.22514

49 Miyake, Y., Tsuboi, Y., Koyanagi, M., Fujimoto, T., Shirasawa, S., Kiyohara, C. et al. (2010) *LRRK2* gly2385arg polymorphism, cigarette smoking, and risk of sporadic Parkinson's disease: a case–control study in Japan. *J. Neurol. Sci.* **297**, 15–18 https://doi.org/10.1016/j.jns.2010.07.002

50 Carrion, M.D.P., Marsicano, S., Daniele, F., Marte, A., Pischedda, F., Cairano, E.D. et al. (2017) The *LRRK2* G2385R variant is a partial loss-of-function mutation that affects synaptic vesicle trafficking through altered protein interactions. *Sci. Rep.* **7**, 5377 https://doi.org/10.1038/s41598-017-05760-9

51 Rudenko, I.N., Kaganovich, A., Hauser, D.N., Beylina, A., Chia, R., Ding, J. et al. (2012) The G2385R variant of leucine-rich repeat kinase 2 associated with Parkinson's disease is a partial loss-of-function mutation. *Biochem. J.* **446**, 99–111 https://doi.org/10.1042/BJ20120637

52 Rudenko, I.N., Kaganovich, A., Langston, R.G., Beylina, A., Ndukwe, K., Kumaran, R. et al. (2017) The G2385R risk factor for Parkinson's disease enhances CHIP-dependent intracellular degradation of LRRK2. *Biochem J.* **474**, 1547–1558 https://doi.org/10.1042/BCJ20160909

53 Zhang, P., Fan, Y., Ru, H., Wang, L., Magupalli, V.G., Taylor, S.S. et al. (2019) Crystal structure of the WD40 domain dimer of *LRRK2*. *Proc. Natl Acad. Sci. U.S.A.* **116**, 1579–1584 https://doi.org/10.1073/pnas.1817889116

54 Purlyte, E., Dhekne, H.S., Sarhan, A.R., Gomez, R., Lis, P., Wightman, M. et al. (2018) Rab29 activation of the Parkinson's disease-associated *LRRK2* kinase. *EMBO J.* **37**, 1–18 https://doi.org/10.15252/embj.201798099

55 Beilina, A., Rudenko, I.N., Kaganovich, A., Civiero, L., Chau, H., Kalia, S.K. et al. (2014) Unbiased screen for interactors of leucine-rich repeat kinase 2 supports a common pathway for sporadic and familial Parkinson disease. *Proc. Natl Acad. Sci. U.S.A.* **111**, 2626–2631 https://doi.org/10.1073/pnas.1318306111

56 Langston, R.G., Rudenko, I.N., Kumaran, R., Hauser, D.N., Kaganovich, A., Ponce, L.B. et al. (2018) Differences in stability, activity and mutation effects between human and mouse leucine-rich repeat kinase 2. *Neurochem. Res.* https://doi.org/10.1007/s11064-018-2650-4

57 Ross, O.A., Wu, Y.-R., Lee, M.-C., Funayama, M., Chen, M.-L., Soto, A.I. et al. (2008) Analysis of Lrrk2 R1628P as a risk factor for Parkinson's disease. *Ann. Neurol.* **64**, 88–92 https://doi.org/10.1002/ana.21405

58 Shu, Y., Ming, J., Zhang, P., Wang, Q., Jiao, F. and Tian, B. (2016) Parkinson-related LRRK2 mutation R1628P enables Cdk5 phosphorylation of LRRK2 and upregulates its kinase activity. *PLoS ONE* **11**, e0149739 https://doi.org/10.1371/journal.pone.0149739

59 Ross, O.A., Soto-Ortolaza, A.I., Heckman, M.G., Aasly, J.O., Abahuni, N., Annesi, G. et al. (2011) Association of LRRK2 exonic variants with susceptibility to Parkinson's disease: a case–control study. *Lancet Neurol.* **10**, 898–908 https://doi.org/10.1016/S1474-4422(11)70175-2

60 Tan, E.-K., Peng, R., Teo, Y.-Y., Tan, L.C., Angeles, D., Ho, P. et al. (2010) Multiple LRRK2 variants modulate risk of Parkinson disease: a Chinese multicenter study. *Hum. Mutat.* **31**, 561–568 https://doi.org/10.1002/humu.21225

61 Nixon-Abell, J., Berwick, D.C., Grannó, S., Spain, V.A., Blackstone, C. and Harvey, K. (2016) Protective LRRK2 R1398H variant enhances GTPase and Wnt signaling activity. *Front. Mol. Neurosci.* **9**, 18 https://doi.org/10.3389/fnmol.2016.00018

62 Malek, N., Weil, R., Bresner, C., Lawton, M., Grosset, K., Tan, M. et al. (2018) Features of *GBA*-associated Parkinson's disease at presentation in the United Kingdom tracking Parkinson's study. *J. Neurol. Neurosurg. Psychiatry* **89**, 702–709 https://doi.org/10.1136/jnnp-2017-317348

63 Marder, K., Wang, Y., Alcalay, R.N., Mejia-Santana, H., Tang, M.-X., Lee, A. et al. (2015) Age-specific penetrance of *LRRK2* G2019S in the Michael J. Fox Ashkenazi Jewish LRRK2 Consortium. *Neurology* **85**, 89–95 https://doi.org/10.1212/WNL.0000000000001708

64 Xiao, B., Deng, X., Ng, E.Y.-L., Allen, J.C., Lim, S.-Y., Ahmad-Annuar, A. et al. (2018) Association of *LRRK2* haplotype with age at onset in Parkinson disease. *JAMA Neurol.* **75**, 127–128 https://doi.org/10.1001/jamaneurol.2017.3363

65 Blauwendraat, C., Heilbron, K., Vallerga, C.L., Bandres-Ciga, S., von Coelln, R., Pihlstrom, L. et al. (2018) Parkinson disease age of onset GWAS: defining heritability, genetic loci and a-synuclein mechanisms. *bioRxiv* https://doi.org/10.1101/424010

66 Ryan, K.J., White, C.C., Patel, K., Xu, J., Olah, M., Replogle, J.M. et al. (2017) A human microglia-like cellular model for assessing the effects of neurodegenerative disease gene variants. *Sci. Transl. Med.* **9**, eaai7635 https://doi.org/10.1126/scitranslmed.aai7635

67 Nalls, M.A., Pankratz, N., Lill, C.M., Do, C.B., Hernandez, D.G., Saad, M. et al. (2014) Large-scale meta-analysis of genome-wide association data identifies six new risk loci for Parkinson's disease. *Nat. Genet.* **46**, 989–993 https://doi.org/10.1038/ng.3043

68   Zimprich, A., Biskup, S., Leitner, P., Lichtner, P., Farrer, M., Lincoln, S. et al. (2004) Mutations in LRRK2 cause autosomal-dominant parkinsonism with pleomorphic pathology. *Neuron* **44**, 601–607 https://doi.org/10.1016/j.neuron.2004.11.005

69   Miklossy, J., Arai, T., Guo, J.-P., Klegeris, A., Yu, S., McGeer, E.G. et al. (2006) *LRRK2* expression in normal and pathologic human brain and in human cell lines. *J. Neuropathol. Exp. Neurol.* **65**, 953–963 https://doi.org/10.1097/01.jnen.0000235121.98052.54

70   Westerlund, M., Ran, C., Borgkvist, A., Sterky, F.H., Lindqvist, E., Lundströmer, K. et al. (2008) Lrrk2 and α-synuclein are co-regulated in rodent striatum. *Mol. Cell. Neurosci.* **39**, 586–591 https://doi.org/10.1016/j.mcn.2008.08.001

71   Cook, D.A. and Tansey, M.G. (2017) LRRK2. In *Neuroimmune Pharmacology* (Ikezu, T., Gendelman, H.E., eds), pp. 107–116, Springer International Publishing, Cham

72   Hakimi, M., Selvanantham, T., Swinton, E., Padmore, R.F., Tong, Y., Kabbach, G. et al. (2011) Parkinson's disease-linked *LRRK2* is expressed in circulating and tissue immune cells and upregulated following recognition of microbial structures. *J. Neural. Transm.* **118**, 795–808 https://doi.org/10.1007/s00702-011-0653-2

73   Gardet, A., Benita, Y., Li, C., Sands, B.E., Ballester, I., Stevens, C. et al. (2010) LRRK2 is involved in the IFN-γ response and host response to pathogens. *J. Immunol.* **185**, 5577–5585 https://doi.org/10.4049/jimmunol.1000548

74   Hongge, L., Kexin, G., Xiaojie, M., Nian, X. and Jinsha, H. (2015) The role of *LRRK2* in the regulation of monocyte adhesion to endothelial cells. *J. Mol. Neurosci.* **55**, 233–239 https://doi.org/10.1007/s12031-014-0312-9

75   Härtlova, A., Herbst, S., Peltier, J., Rodgers, A., Bilkei-Gorzo, O., Fearns, A. et al. (2018) LRRK2 is a negative regulator of *Mycobacterium tuberculosis* phagosome maturation in macrophages. *EMBO J.* **37**, e98694 https://doi.org/10.15252/embj.201798694

76   Kim, K.S., Marcogliese, P.C., Yang, J., Callaghan, S.M., Resende, V., Abdel-Messih, E. et al. (2018) Regulation of myeloid cell phagocytosis by *LRRK2* via WAVE2 complex stabilization is altered in Parkinson's disease. *Proc. Natl Acad. Sci. U.S.A.* **115**, E5164–E5173 https://doi.org/10.1073/pnas.1718946115

77   Moehle, M.S., Webber, P.J., Tse, T., Sukar, N., Standaert, D.G., DeSilva, T.M. et al. (2012) *LRRK2* inhibition attenuates microglial inflammatory responses. *J. Neurosci.* **32**, 1602–1611 https://doi.org/10.1523/JNEUROSCI.5601-11.2012

78   Cook, D.A., Kannarkat, G.T., Cintron, A.F., Butkovich, L.M., Fraser, K.B., Chang, J. et al. (2017) LRRK2 levels in immune cells are increased in Parkinson's disease. *NPJ Parkinsons Dis.* **3**, 11 https://doi.org/10.1038/s41531-017-0010-8

79   Kluss, J.H., Conti, M.M., Kaganovich, A., Beilina, A., Melrose, H.L., Cookson, M.R. et al. (2018) Detection of endogenous S1292 LRRK2 autophosphorylation in mouse tissue as a readout for kinase activity. *NPJ Parkinsons Dis.* **4**, 13 https://doi.org/10.1038/s41531-018-0049-1

80   Sheng, Z., Zhang, S., Bustos, D., Kleinheinz, T., Pichon, C.E.L., Dominguez, S.L. et al. (2012) Ser1292 autophosphorylation is an indicator of LRRK2 kinase activity and contributes to the cellular effects of PD mutations. *Sci. Transl. Med.* **4**, 164ra161 https://doi.org/10.1126/scitranslmed.3004485

81   Fraser, K.B., Rawlins, A.B., Clark, R.G., Alcalay, R.N., Standaert, D.G., Liu, N. et al. (2016) Ser(P)-1292 LRRK2 in urinary exosomes is elevated in idiopathic Parkinson's disease. *Mov. Disord.* **31**, 1543–1550 https://doi.org/10.1002/mds.26686

82   Maio, R.D., Hoffman, E.K., Rocha, E.M., Keeney, M.T., Sanders, L.H., Miranda, B.R.D. et al. (2018) *LRRK2* activation in idiopathic Parkinson's disease. *Sci. Transl. Med.* **10**, eaar5429 https://doi.org/10.1126/scitranslmed.aar5429

83   Mamais, A., Chia, R., Beilina, A., Hauser, D.N., Hall, C., Lewis, P.A. et al. (2014) Arsenite stress down-regulates phosphorylation and 14-3-3 binding of leucine-rich repeat kinase 2 (LRRK2), promoting self-association and cellular redistribution. *J. Biol. Chem.* **289**, 21386–21400 https://doi.org/10.1074/jbc.M113.528463

84   Mortiboys, H., Johansen, K.K., Aasly, J.O. and Bandmann, O. (2010) Mitochondrial impairment in patients with Parkinson disease with the G2019S mutation in LRRK2. *Neurology* **75**, 2017–2020 https://doi.org/10.1212/WNL.0b013e3181ff9685

85   Sanders, L.H., Laganière, J., Cooper, O., Mak, S.K., Vu, B.J., Huang, Y.A. et al. (2014) LRRK2 mutations cause mitochondrial DNA damage in iPSC-derived neural cells from Parkinson's disease patients: reversal by gene correction. *Neurobiol. Dis.* **62**, 381–386 https://doi.org/10.1016/j.nbd.2013.10.013

86   Papkovskaia, T.D., Chau, K.-Y., Inesta-Vaquera, F., Papkovsky, D.B., Healy, D.G., Nishio, K. et al. (2012) G2019s leucine-rich repeat kinase 2 causes uncoupling protein-mediated mitochondrial depolarization. *Hum. Mol. Genet.* **21**, 4201–4213 https://doi.org/10.1093/hmg/dds244

87   Hoenen, C., Gustin, A., Birck, C., Kirchmeyer, M., Beaume, N., Felten, P. et al. (2016) α-Synuclein proteins promote pro-inflammatory cascades in microglia: stronger effects of the A53T mutant. *PLoS ONE* **11**, e0162717 https://doi.org/10.1371/journal.pone.0162717

88   Lull, M.E. and Block, M.L. (2010) Microglial activation and chronic neurodegeneration. *Neurotherapeutics* **7**, 354–365 https://doi.org/10.1016/j.nurt.2010.05.014

89   Saez-Atienzar, S., Bonet-Ponce, L., Blesa, J.R., Romero, F.J., Murphy, M.P., Jordan, J. et al. (2014) The LRRK2 inhibitor GSK2578215A induces protective autophagy in SH-SY5Y cells: involvement of Drp-1-mediated mitochondrial fission and mitochondrial-derived ROS signaling. *Cell Death Dis.* **5**, e1368 https://doi.org/10.1038/cddis.2014.320

90   Su, Y.-C., Guo, X. and Qi, X. (2015) Threonine 56 phosphorylation of Bcl-2 is required for LRRK2 G2019S-induced mitochondrial depolarization and autophagy. *Biochim. Biophys. Acta, Mol. Basis Dis.* **1852**, 12–21 https://doi.org/10.1016/j.bbadis.2014.11.009

91   Choubey, V., Safiulina, D., Vaarmann, A., Cagalinec, M., Wareski, P., Kuum, M. et al. (2011) Mutant A53T α-synuclein induces neuronal death by increasing mitochondrial autophagy. *J. Biol. Chem.* **286**, 10814–10824 https://doi.org/10.1074/jbc.M110.132514

92   Cookson, M.R. (2016) Cellular functions of LRRK2 implicate vesicular trafficking pathways in Parkinson's disease. *Biochem. Soc. Trans.* **44**, 1603–1610 https://doi.org/10.1042/BST20160228

93   Ito, G., Katsemonova, K., Tonelli, F., Lis, P., Baptista, M.A.S., Shpiro, N. et al. (2016) Phos-tag analysis of Rab10 phosphorylation by LRRK2: a powerful assay for assessing kinase function and inhibitors. *Biochem. J.* **473**, 2671–2685 https://doi.org/10.1042/BCJ20160557

94   Satake, W., Nakabayashi, Y., Mizuta, I., Hirota, Y., Ito, C., Kubo, M. et al. (2009) Genome-wide association study identifies common variants at four loci as genetic risk factors for Parkinson's disease. *Nat. Genet.* **41**, 1303–1307 https://doi.org/10.1038/ng.485

95   Manzoni, C., Mamais, A., Dihanich, S., Abeti, R., Soutar, M.P.M., Plun-Favreau, H. et al. (2013) Inhibition of LRRK2 kinase activity stimulates macroautophagy. *Biochim. Biophys. Acta, Mol. Cell Res.* **1833**, 2900–2910 https://doi.org/10.1016/j.bbamcr.2013.07.020

96   Henry, A.G., Aghamohammadzadeh, S., Samaroo, H., Chen, Y., Mou, K., Needle, E. et al. (2015) Pathogenic LRRK2 mutations, through increased kinase activity, produce enlarged lysosomes with reduced degradative capacity and increase ATP13A2 expression. *Hum. Mol. Genet.* **24**, 6013–6028 https://doi.org/10.1093/hmg/ddv314

97   Tong, Y., Yamaguchi, H., Giaime, E., Boyle, S., Kopan, R., Kelleher, R.J. et al. (2010) Loss of leucine-rich repeat kinase 2 causes impairment of protein degradation pathways, accumulation of α-synuclein, and apoptotic cell death in aged mice. *Proc. Natl Acad. Sci. U.S.A.* **107**, 9879–9884 https://doi.org/10.1073/pnas.1004676107

98   Mamais, A., Raja, M., Manzoni, C., Dihanich, S., Lees, A., Moore, D. et al. (2013) Divergent α-synuclein solubility and aggregation properties in G2019S LRRK2 Parkinson's disease brains with Lewy Body pathology compared to idiopathic cases. *Neurobiol. Dis.* **58**, 183–190 https://doi.org/10.1016/j.nbd.2013.05.017

99   Blauwendraat, C., Reed, X., Kia, D.A., Gan-Or, Z., Lesage, S., Pihlstrøm, L. et al. (2018) Frequency of loss of function variants in *LRRK2* in Parkinson disease. *JAMA Neurol.* **75**, 1416–1422 https://doi.org/10.1001/jamaneurol.2018.1885

100 Daher, J.P.L., Abdelmotilib, H.A., Hu, X., Volpicelli-Daley, L.A., Moehle, M.S., Faser, K.B. et al. (2015) LRRK2 pharmacological inhibition abates α-synuclein induced neurodegeneration. *J. Biol. Chem.* **290**, 19433–19444 https://doi.org/10.1074/jbc.M115.660001

101 Lee, B.D., Shin, J.-H., VanKampen, J., Petrucelli, L., West, A.B., Ko, H.S. et al. (2010) Inhibitors of leucine-rich repeat kinase-2 protect against models of Parkinson's disease. *Nat. Med.* **16**, 998–1000 https://doi.org/10.1038/nm.2199

102 Steger, M., Diez, F., Dhekne, H.S., Lis, P., Nirujogi, R.S., Karayel, O. et al. (2017) Systematic proteomic analysis of LRRK2-mediated Rab GTPase phosphorylation establishes a connection to ciliogenesis. *eLife* **6**, e31012 https://doi.org/10.7554/eLife.31012

103 Fan, Y., Howden, A.J.M., Sarhan, A.R., Lis, P., Ito, G., Martinez, T.N. et al. (2018) Interrogating Parkinson's disease LRRK2 kinase pathway activity by assessing Rab10 phosphorylation in human neutrophils. *Biochem. J.* **475**, 23–44 https://doi.org/10.1042/BCJ20170803

104 Denali Therapeutics Announces First Patient Dosed in Phase 1B Study. [Internet]. Denali. [cited 2019 Jan 8]. Available from: https://denalitherapeutics.com/investors/press-release/denali-therapeutics-announces-first-patient-dosed-in-phase-1b-study-of-dnl201-for-parkinsons-disease-1

105 Barrett, J.C., Hansoul, S., Nicolae, D.L., Cho, J.H., Duerr, R.H., Rioux, J.D. et al. (2008) Genome-wide association defines more than 30 distinct susceptibility loci for Crohn's disease. *Nat. Genet.* **40**, 955–962 https://doi.org/10.1038/ng.175

106 Zhang, F.-R., Huang, W., Chen, S.-M., Sun, L.-D., Liu, H., Li, Y. et al. (2009) Genomewide association study of leprosy. *N. Engl. J. Med.* **361**, 2609–2618 https://doi.org/10.1056/NEJMoa0903753

107 Dzamko, N., Inesta-Vaquera, F., Zhang, J., Xie, C., Cai, H., Arthur, S. et al. (2012) The IkappaB kinase family phosphorylates the Parkinson's disease kinase LRRK2 at Ser935 and Ser910 during Toll-like receptor signaling. *PLoS ONE* **7**, e39132 https://doi.org/10.1371/journal.pone.0039132

108 Gillardon, F., Schmid, R. and Draheim, H. (2012) Parkinson's disease-linked leucine-rich repeat kinase 2(R1441G) mutation increases proinflammatory cytokine release from activated primary microglial cells and resultant neurotoxicity. *Neuroscience* **208**, 41–48 https://doi.org/10.1016/j.neuroscience.2012.02.001

109 Liu, W., Liu, X., Li, Y., Zhao, J., Liu, Z., Hu, Z. et al. (2017) LRRK2 promotes the activation of NLRC4 inflammasome during *Salmonella Typhimurium* infection. *J. Exp. Med.* **214**, 3051–3066 https://doi.org/10.1084/jem.20170014

110 Pellegrini, L., Hauser, D.N., Li, Y., Mamais, A., Beilina, A., Kumaran, R. et al. (2018) Proteomic analysis reveals co-ordinated alterations in protein synthesis and degradation pathways in *LRRK2* knockout mice. *Hum. Mol. Genet.* **27**, 3257–3271 https://doi.org/10.1093/hmg/ddy232

111 Lanning, N.J., VanOpstall, C., Goodall, M.L., MacKeigan, J.P. and Looyenga, B.D. (2018) LRRK2 deficiency impairs *trans*-golgi to lysosome trafficking and endocytic cargo degradation in human renal proximal tubule epithelial cells. *Am. J. Physiol. Renal. Physiol.* **315**, F1465–F1477 https://doi.org/10.1152/ajprenal.00009.2018

112 Fuji, R.N., Flagella, M., Baca, M., Baptista, M.A.S., Brodbeck, J., Chan, B.K. et al. (2015) Effect of selective *LRRK2* kinase inhibition on nonhuman primate lung. *Sci. Transl. Med.* **7**, 273ra15 https://doi.org/10.1126/scitranslmed.aaa3634

113 Andersen, M.A., Wegener, K.M., Larsen, S., Badolo, L., Smith, G.P., Jeggo, R. et al. (2018) PFE-360-induced LRRK2 inhibition induces reversible, non-adverse renal changes in rats. *Toxicology* **395**, 15–22 https://doi.org/10.1016/j.tox.2018.01.003

114 Baptista, M., Merchant, K., Barrett, T., Bryce, D., Ellis, M., Estrada, A. et al. (2018) LRRK2 kinase inhibitors induce a reversible effect in the lungs of non-human primates with no measurable pulmonary deficits. *bioRxiv* https://doi.org/10.1101/390815

115 Marras, C., Beck, J.C., Bower, J.H., Roberts, E., Ritz, B., Ross, G.W. et al. (2018) Prevalence of Parkinson's disease across North America. *NPJ Parkinsons Dis.* **4**, 21 https://doi.org/10.1038/s41531-018-0058-0

Divergent Effects of G2019S and R1441C LRRK2 Mutations on LRRK2 and Rab10 Phosphorylations in Mouse Tissues

Lucia Iannotta [1,†], **Alice Biosa** [1,†,‡], **Jillian H. Kluss** [2], **Giulia Tombesi** [1], **Alice Kaganovich** [1,2], **Susanna Cogo** [1], **Nicoletta Plotegher** [1], **Laura Civiero** [1,3], **Evy Lobbestael** [4], **Veerle Baekelandt** [4], **Mark R. Cookson** [2] and **Elisa Greggio** [1,*]

[1] Department of Biology, University of Padova, 35131 Padova, Italy; lucia.iannotta@unipd.it (L.I.); alice.biosa@autifony.com (A.B.); giulia.tombesi@phd.unipd.it (G.T.); kaganovichal@grc.nia.nih.gov (A.K.); susanna.cogo@unipd.it (S.C.); nicoletta.plotegher@unipd.it (N.P.); laura.civiero@unipd.it (L.C.)

[2] Cell Biology and Gene Expression Section, National Institute on Aging, National Institutes of Health, Bethesda, MD 20892, USA; jillian.kluss@nih.gov (J.H.K.); cookson@mail.nih.gov (M.R.C.)

[3] IRCCS San Camillo Hospital, 30126 Venice, Italy

[4] Laboratory for Neurobiology and Gene Therapy, KU Leuven, 3000 Leuven, Belgium; evy.lobbestael@kuleuven.be (E.L.); veerle.baekelandt@kuleuven.be (V.B.)

[*] Correspondence: elisa.greggio@unipd.it; Tel.: +39-0498276244

[†] These authors contributed equally.

[‡] Present address: Autifony SRL, 37135, Verona, Italy.

Abstract: Mutations in LRRK2 cause familial Parkinson's disease and common variants increase disease risk. LRRK2 kinase activity and cellular localization are tightly regulated by phosphorylation of key residues, primarily Ser1292 and Ser935, which impacts downstream phosphorylation of its substrates, among which Rab10. A comprehensive characterization of LRRK2 activity and phosphorylation in brain as a function of age and mutations is missing. Here, we monitored Ser935 and Ser1292 phosphorylation in midbrain, striatum, and cortex of 1, 6, and 12 months-old mice carrying G2019S and R1441C mutations or murine bacterial artificial chromosome (BAC)-Lrrk2-G2019S. We observed that G2019S and, at a greater extent, R1441C brains display decreased phospho-Ser935, while Ser1292 autophosphorylation increased in G2019S but not in R1441C brain, lung, and kidney compared to wild-type. Further, Rab10 phosphorylation, is elevated in R1441C carrying mice, indicating that the effect of LRRK2 mutations on substrate phosphorylation is not generalizable. In BAC-Lrrk2-G2019S striatum and midbrain, Rab10 phosphorylation, but not Ser1292 autophosphorylation, decreases at 12-months, pointing to autophosphorylation and substrate phosphorylation as uncoupled events. Taken together, our study provides novel evidence that LRRK2 phosphorylation in mouse brain is differentially impacted by mutations, brain area, and age, with important implications as diagnostic markers of disease progression and stratification.

Keywords: LRRK2; phosphorylation; Rab10; mutant mice; striatum; cortex; midbrain; lung; kidney; age-dependent changes

---

1. Introduction

Mutations in the gene encoding leucine-rich repeat kinase 2 (LRRK2) cause autosomal dominant Parkinson's disease (PD), while common variants in the LRRK2 locus increase the lifetime risk of disease [1]. LRRK2 is a large signaling protein comprising serine-threonine kinase and ROC-COR GTPase catalytic domains as well as scaffolding modules [2]. PD-causing mutations are gain of

function through a direct activating effect on kinase activity (G2019S) or by decreasing GTP hydrolysis (R1441C/G/H and Y1699C), which affects LRRK2 subcellular access to its substrates, the most validated being a subset of Rab GTPases [3]. LRRK2 controls its own phosphorylation through a yet unclear mechanism, likely involving heterologous kinases (CK1α, IKKs, PKA) and phosphatases (PP1) within a cluster of N-terminus residues, the two major ones being Ser910 and Ser935 (reviewed in [4]). Phosphorylation of these residues provides the docking sites for the binding of 14-3-3 proteins, which regulate LRRK2 activity and subcellular localization [5,6]. LRRK2 kinase inhibition results in LRRK2 dephosphorylation at Ser910/Ser935 and consequent dissociation from 14-3-3 proteins [4–6]. These residues are dephosphorylated also in several LRRK2 PD mutants with hyperactive kinase activity, raising a question as to whether dephosphorylated LRRK2 is pathogenic, protective or both, depending on the upstream mechanism that governs the dephosphorylation event.

Autophosphorylation of Ser1292 is a robust readout of LRRK2 kinase activity in cells [7], which was shown to positively correlate with Thr73 phosphorylation of Rab10, a well-established LRRK2 substrate [3]. As predicted, Ser1292-LRRK2 and Thr73-Rab10 are hyperphosphorylated in the presence of gain of function LRRK2 mutants in cells and mouse and human peripheral tissues [3,7–9], as well as in the substantia nigra (SN) dopaminergic neurons of postmortem brain tissue from idiopathic PD patients [10]. Despite being well-established in cells, Rab10 phosphorylation in the brain has proven difficult to detect, possibly due to the high levels of PPM1H, a phosphatase selectively dephosphorylating Rab GTPases [11], or to a lower basal activity of LRRK2 in neuronal cells compared to peripheral tissues.

To gain insights into the effects of LRRK2 mutations on protein activity and phosphorylation ex-vivo, we performed a comprehensive survey of LRRK2 and Rab10 phosphorylation in midbrain, striatum, and cortex, as well as in peripheral tissues of three LRRK2 mutant mice, namely knockin (KI) Lrrk2-G2019S, KI Lrrk2-R1441C, and BAC overexpressing murine Lrrk2-G2019S. We observed that KI G2019S animals exhibit elevated pSer1292 in brain and lung/kidney but no increased pThr73-Rab10 in lung/kidney as compared to wild-type (WT), whilst KI mice carrying the ROC R1441C mutation display pSer1292 levels surprisingly similar to WT brain/lung/kidney but increased pT73-Rab10. Phospho-Ser935 is barely detectable in KI R1441C brains, and halved in KI G2019S compared to WT. In mice overexpressing the murine Lrrk2 locus (BAC-Lrrk2-G2019S), total and phospho-LRRK2 levels increase in the aging striatum, while phospho-Thr73 Rab10 is decreased at 12 months, indicating that LRRK2 and Rab10 phosphorylations are uncoupled, at least in this model. Finally, histological evaluation of BAC-G2019S brains confirmed that Lrrk2 expression is considerably higher in the striatum compared to the cortex and further revealed that aged mice display elevated GFAP levels, suggestive of enhanced gliosis.

Taken together, our comprehensive ex-vivo study provides evidence that LRRK2 phosphorylation in murine brain is differentially impacted by mutations and that pSer1292/pSer935-LRRK2 and pThr73-Rab10 may be diagnostic of G2019S and R1441C-linked diseases, respectively.

2. Materials and Methods

2.1. Animals

C57BL/6 LRRK2 wild-type and mouse LRRK2 G2019S BAC (GS BAC) mice were obtained from Jackson Laboratory [B6.Cg-Tg(Lrrk2*G2019S)2Yue/J]. Non-transgenic wild-type (WT) mice were littermates obtained from the heterozygous breeding. Housing and handling of mice were done in compliance with national guidelines. All animal procedures were approved by the Ethical Committee of the University of Padova and the Italian Ministry of Health (#200/2019-PR and 1041/2016-PR).

Homozygous LRRK2 G2019S knock-in (GSKI), R1441C knock-in (RCKI), knockout (KO) and parental WT mice were housed at the National Institute on Aging, NIH, [12,13] according to a protocol approved by the Institutional Animal Care and Use Committee of the National Institute on Aging, NIH (463-LNG-2019).

Dissections of cortex, midbrain, and striatal regions were performed in 1, 6, and 12 months-old mice of all genotypes. 4–5 mice/genotype/age were used in all experiments.

2.2. Antibodies

For western blotting the following antibodies were used: total LRRK2 [MJFF2 (c41-2)] (Abcam, Cambridge, UK, Cat# ab133474, 1:300), phospho-S935 LRRK2 (Abcam, Cambridge, UK, Cat# ab133450, 1:500), phospho-S1292 LRRK2 (Abcam, Cambridge, UK, Cat# ab203181, 1:300), total Rab10 (Abcam, Cambridge, UK, Cat# ab104859, 1:500), phospho-T73 Rab10 (Abcam, Cambridge, UK, Cat# ab230261, 1:400), tyrosine hydroxylase (Millipore, Burlington, MA, USA Cat# AB152, 1:10000), DARPP32 (Millipore, Burlington, MA, USA Cat# AB10518, 1:10000) and β-actin (Sigma-Aldrich, St. Louis, MO, USA Cat# A2066, 1:10000). For immunofluorescence: β-tubulin-III (Sigma-Aldrich, St. Louis, MO, USA, Cat# T8578, 1:1000); total LRRK2 [MJFF2 (c41-2)] (Abcam, Cambridge, UK, Cat# ab133474, 1:200), phospho-S935 LRRK2 [UDD2 10(12)] (Abcam, Cambridge, UK, Cat# ab172382, 1:200), GLT1 (EMD Millipore, Burlington, MA, USA Cat# AB1783, 1:400), GFAP (Dako-Agilent, Santa Clara, CA, USA, Cat# Z0334, 1:400) CD11b [M1/70] (eBioscience™ from Thermo Fisher Scientific, Waltham, MA, USA, Cat# 14-0112-82, 1:200).

2.3. Brain Lysis and Western Blotting

Brain regions were mechanically lysed in 25 mM pH = 7.5 Tris-HCl, 150 mM NaCl, 1% (*v/v*) NP40, 1% (*w/v*) sodium deoxycholate, 0.1% (*w/v*) SDS, 2 mM EGTA, 20 mM sodium fluoride, 50 mM beta glycerophosphate, 50 mM sodium pyrophosphate, 20 mM sodium orthovanadate. 70 μg of protein samples were resolved on pre-casted 4–20% Tris-glycine polyacrylamide gels (Biorad, Hercules, CA, USA).

Resolved proteins were transferred to polyvinylidenedifluoride (PVDF) membranes using semidry Biorad transfer machine (Trans-Blot Turbo Transfer System, Biorad, Hercules, CA, USA). After 1h of saturation in 0.1% Tween-20 (TBS-T) plus 5% non-fat dry milk, PVDF membranes were incubated overnight at 4 °C with specific primary antibodies. The PVDF sheets were washed in TBS-T (3 × 10 min) at room temperature (RT) followed by incubation for 1 h at RT with horseradish peroxidase-conjugated IgG. Immunoreactive proteins were visualized using chemiluminescence (Immobilon ECL western HRP substrate, Millipore, Burlington, MA, USA). Densitometric analysis was carried out using Image J software (U. S. National Institutes of Health, Bethesda, MD, USA). Levels of phospho-LRRK2/total LRRK2, phospho-RAB10/total RAB10 ratios were compared between control and mutant mice at different ages.

2.4. Immunofluorescence

Animals were terminally anesthetized with xylazine (Rompun®) and ketamine (Zoletil®) and transcardially perfused with 0.9% saline followed by ice cold 4% paraformaldehyde (PFA). Brains were dissected and post-fixed in 4% PFA at 4 °C overnight, then transferred to a sucrose gradient in phosphate-buffered saline (PBS) (20% and 30%) at 4 °C for cryopreservation. Once saturated in sucrose, 40 μm thick coronal slices were obtained by sectioning the brains with a vibratome. Sections were rinsed three times with PBS and then the sample autofluorescence was quenched in 50 nM NH$_4$Cl in PBS. After three more washings, tissue sections were immersed in a solution made of 0.1% Sudan Black B (SBB) and 70% ethanol for 15 min at RT. To remove the excess of SBB the slices were rinsed three times with PBS and then they were permeabilized and saturated for 2 h in blocking solution (15% vol/vol goat serum, 2% wt/vol BSA, 0.25% wt/vol gelatin, 0.2% wt/vol glycine in PBS) containing 0.5% Triton X-100. Incubation with the primary antibodies was carried out overnight at 4 °C in blocking solution. Samples were washed three times with PBS and then sections were incubated with appropriate secondary antibodies diluted 1:200 in blocking solution. Images were acquired with Zeiss LSM700 confocal microscope, using 20×/0.8 M27 objective.

2.5. Statistical Analysis

All quantitative data are expressed as mean ± SEM (standard error of the mean) from at least 4 different mice/genotype/age. Significance of differences between two groups was verified by Student t-test while comparisons between 3 or more groups were performed by one-way analysis of variance (ANOVA) with Dunnett's Multiple comparison test/Bonferroni's post-hoc test.

3. Results

3.1. LRRK2 Expression in Midbrain, Striatum, and Cortex

To explore LRRK2 phosphorylation in mouse brain, we dissected three brain regions, namely striatum, cortex, and midbrain (Figure 1a). These areas are relevant in PD pathology [14] and LRRK2 was previously shown to be highly expressed in striatum and cortex [15,16]. Here we confirmed that Lrrk2 steady state levels are higher in the cortex and striatum compared to midbrain (Figure 1b), while the levels of phosphorylated Ser935 are higher in striatum compared to the other regions (Figure 1c). In addition, the lower Lrrk2 expression in the midbrain appears age-independent (Figure 1c).
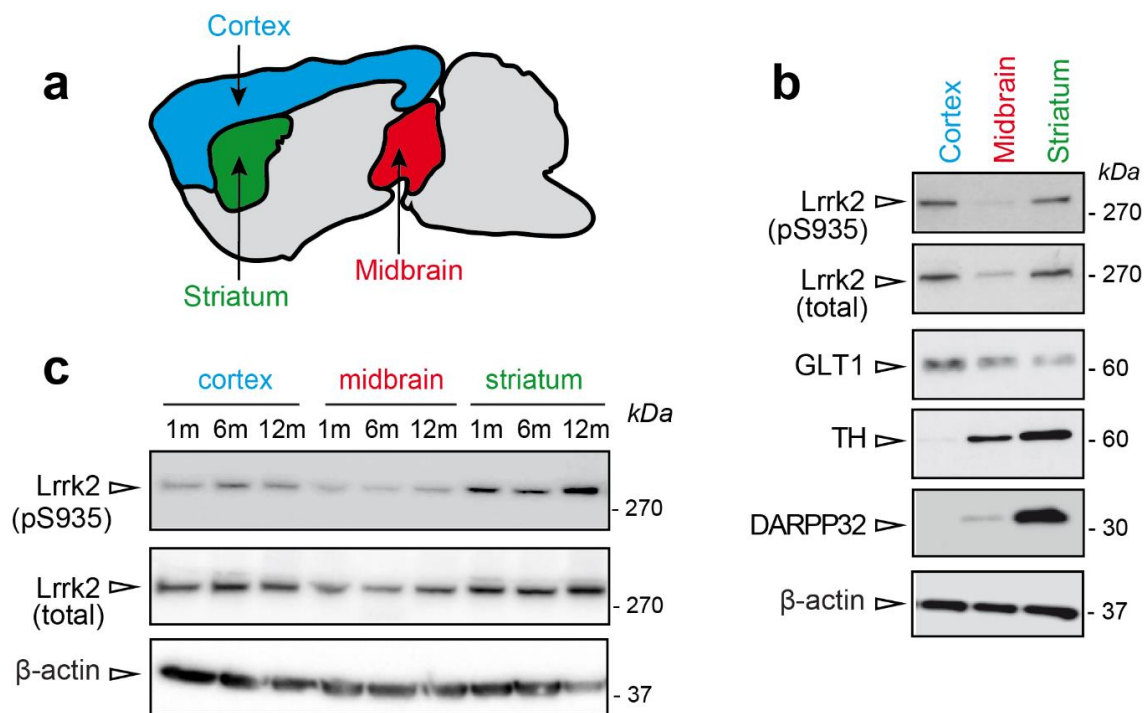
Figure 1. Lrrk2 steady state levels in Parkinson's disease (PD)-relevant areas. (**a**) Schematic representation of cortex (blue), midbrain (red), and striatum (green) localization in mouse brain. (**b**) Representative western blot showing Lrrk2 steady state and phosphorylation levels in PD-relevant areas striatum, cortex, and midbrain of 24 months-old wild-type mice. (**c**) Lrrk2 steady state and phosphorylation levels in striatum, midbrain, and cortex of wild-type mice at different ages (1, 6 and 12 months-old).

3.2. Changes in Ser935 and Ser1292 Phosphorylation in G2019S and R1441C Knockin Brains at Different Ages

Phosphorylation levels of Ser935 and Ser1292 are a readout of LRRK2 activity, and pSer935 is widely used to assess on-target LRRK2 inhibitor engagement [17]. While pSer935 and pSer1292 have been detected in mouse brains [7,18], a systematic comparison across different LRRK2 mutations, brain regions and ages has not been performed. To this aim, we dissected the striatum, cortex, and midbrain of 9 groups of animals (4–5 mice per group) carrying three genotypes (wild-type (WT), KI Lrrk2-G2019S (GSKI), and KI Lrrk2-R1441C (RCKI)) at three different ages (1, 6, and 12 months). To highlight possible differences across genotypes, age-matched WT, GSKI, and RCKI lysates were

loaded on the same gel. After western blotting analysis with phospho-Ser1292, phospho-Ser935, and total LRRK2 antibodies (Figure 2a) and subsequent quantification of western blot signals (Figure 2b–d), we made several interesting observations.

First, the levels of phospho-Ser935 in RCKI brains are ~5 times lower than in the WT in all brain areas, in 1 and 6 month-old animals (Figure 2b–d). Instead, at 12 months, the effect is blunted in the cortex, halved in the midbrain but still persistent in the striatum (Figure 2b–d). Second, the levels of phospho-Ser935 in GSKI striatum, midbrain, and cortex are ~50% lower than in WT, in 1 month-old animals and in striatum and midbrain of 6 months-old mice (Figure 2b–d). This result was unexpected given that LRRK2 G2019S from cells display similar Ser935 phosphorylation than LRRK2 WT [9]. At 12 months, Ser935 phosphorylation in the striatum is dramatically reduced to ~10% of the WT, reduced in the cortex but stable in the midbrain. Third, we detected autophosphorylation of Ser1292 only in GSKI, but, quite surprisingly, not in RCKI brains, which behaved as the WT (Figure 2a). This result is in apparent contrast with what has been reported in different cell models where LRRK2 R1441C display increased phospho-Ser1292 (Figure 2a) [3,7]. Of note, in 1-month-old animals phospho-S1292 is detectable only in the striatum, where Lrrk2 expression is higher (Figure 2a).

Last, we observed some differences in Lrrk2 steady state levels across genotypes, but without a consistent trend in one specific region or at a specific age, with the exception of 6 months mice were total Lrrk2 levels are lower in GSKI cortex and midbrain (Figure 2a–d).

3.3. Changes in Ser935-Lrrk2, Ser1292-Lrrk2, and Thr73-Rab10 Phosphorylation in G2019S and R1441C Knockin Lungs and Kidneys

Based on the unexpected finding that R1441C KI brains display undetectable Ser1292 autophosphorylation, we next asked whether this phenotype is restricted to the brain or whether it also applies to other tissues. Because lungs and kidneys have been previously shown to express high levels of LRRK2 [19–21] and LRRK2 inhibitors cause morphological changes in type II pneumocytes [22], we evaluated LRRK2 phosphorylation in these tissues isolated from 12 months-old WT, RCKI, GSKI, and Lrrk2 KO mice. After western blot analysis, we observed that pSer1292 is ~4 times higher in GSKI compared to WT, while RCKI lungs and kidneys exhibit similar phospho-Ser1292 levels as the WT (Figure 3a–c), confirming the previous results in brains (Figure 2).

To understand whether the lack of phospho-Ser1292 activation in RCKI mice reflects a general inability of this mutation to manifest a similar gain of kinase function observed in cell models [7], we evaluated Rab10 phosphorylation at Thr73 [3,9,23,24]. Strikingly, Rab10 phosphorylation is significantly higher in RCKI lungs and kidneys compared to WT (Figure 3a,b). Instead, lung and kidney from GSKI mice display levels of Rab10 phosphorylation similar to WT, overall suggesting that autophosphorylation and Rab10 phosphorylation are uncoupled events and may constitute independent readouts of LRRK2 activation. Of note, we could not convincingly detect Rab10 phosphorylation in any brain regions under endogenous (WT and KI) Lrrk2 expression. Finally, the degree of Ser935 phosphorylation in GSKI kidneys, and to a lesser extent in lungs, is in between the level of WT and RCKI conditions, confirming the trend observed in brain (Figure 3a–c).
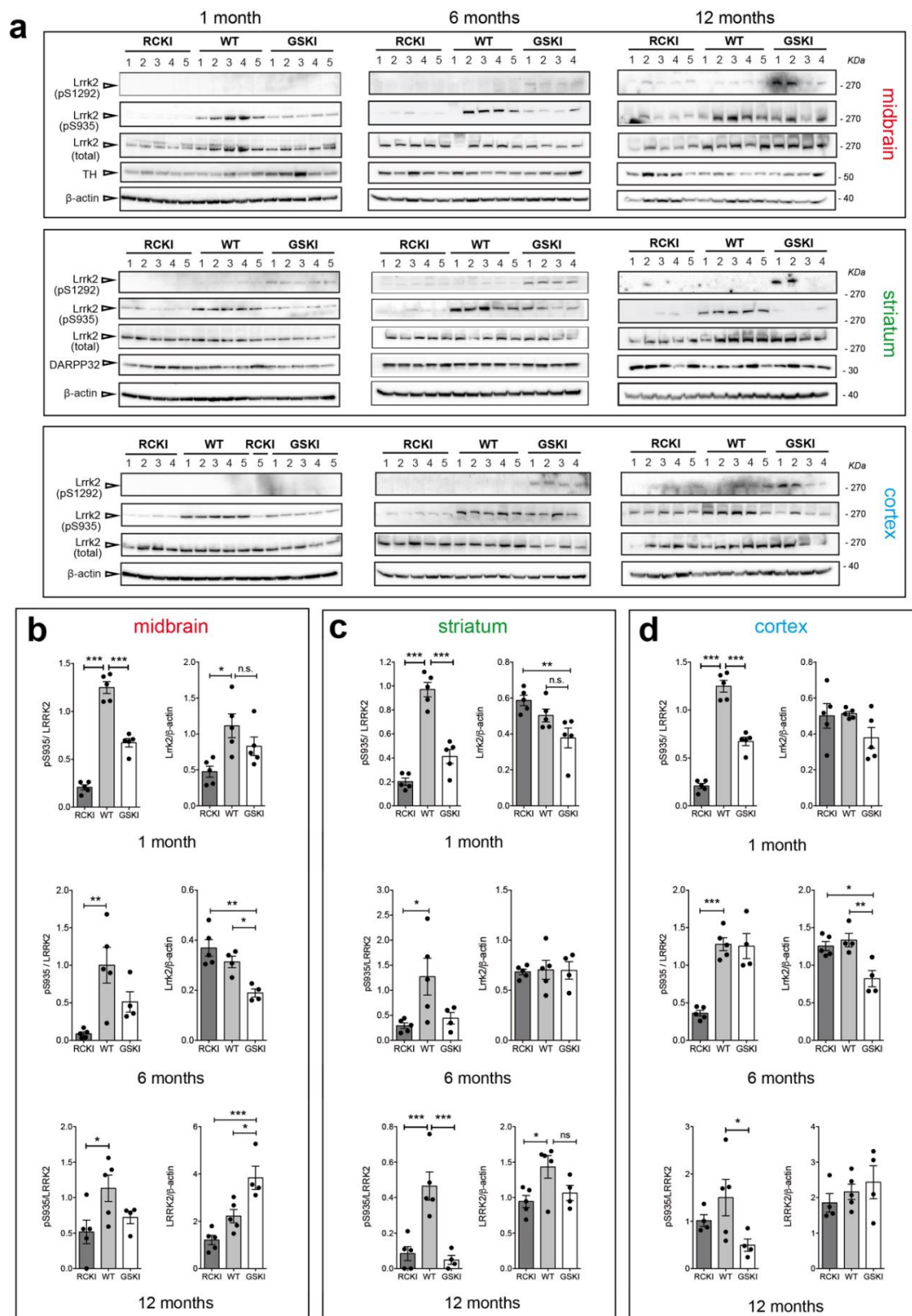
Figure 2. Age-related changes in Ser935 and Ser1292 phosphorylation levels in G2019S and R1441C knockin brain areas. (**a**) Representative western blots of R1441C knockin (RCKI), wild-type (WT) and G2019S knockin (GSKI) lysates from midbrain, striatum, and cortex of 1, 6, and 12-month-old animals (**b-d**). Quantifications of Ser935 phosphorylation (phospho/total LRRK2) and total Lrrk2 levels (Lrrk2/β-actin) in midbrain (**b**), striatum (**c**), and cortex (**d**) at 1, 6, and 12-month-old mice. Each dot in the bar graph represents one animal. Data are shown as mean ± SEM; One-way ANOVA with Dunnett post-hoc test (ns: not significant; * $p < 0.05$; ** $p < 0.01$; *** $p < 0.001$).
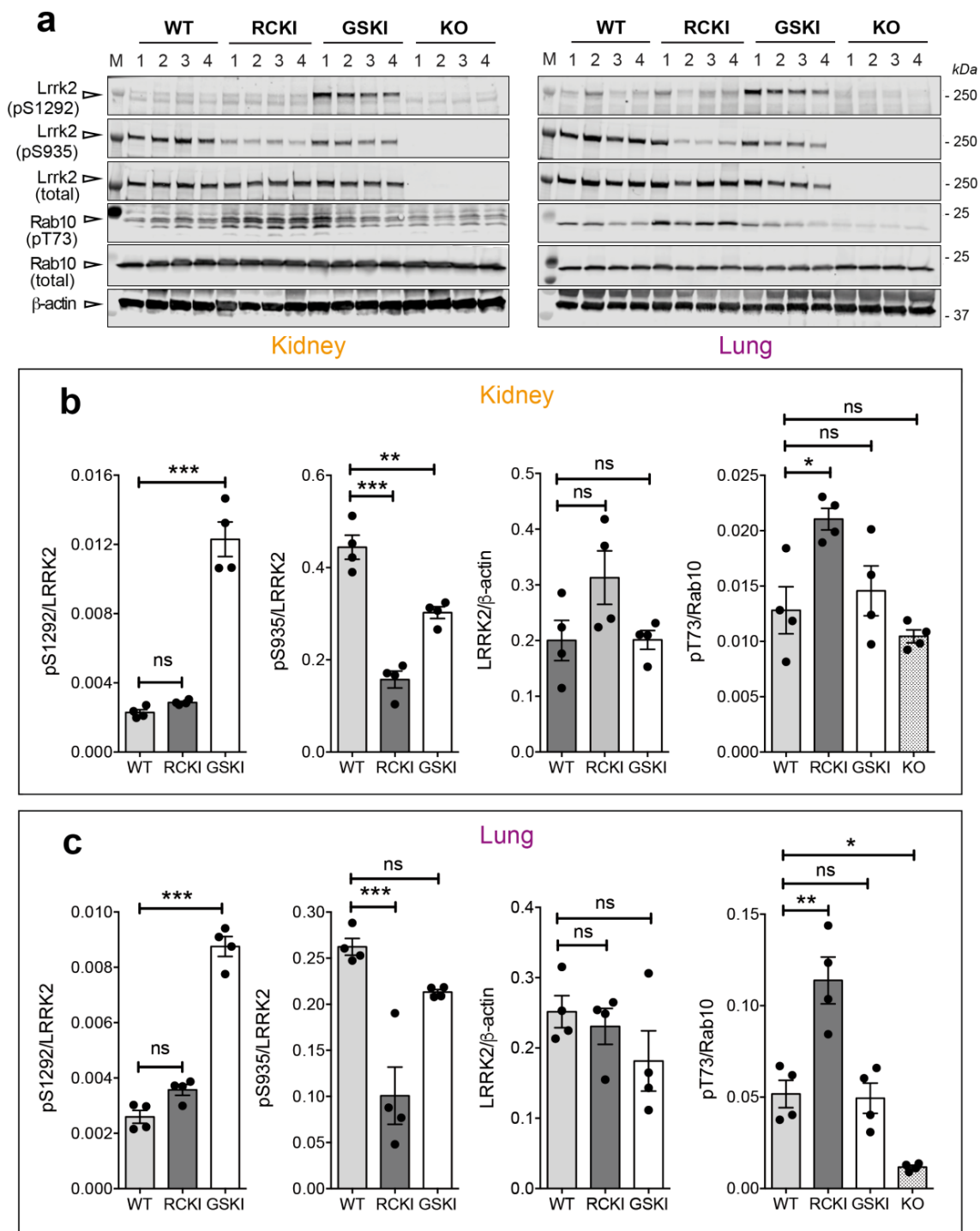
Figure 3. Differences in Ser935-Lrrk2, Ser1292-Lrrk2 and Thr73-Rab10 phosphorylations and total Lrrk2 between G2019S and R1441C knockin lungs and kidneys. (**a**) Representative western blots of WT, RCKI, GSKI, and knockout (KO) lysates from kidney and lung of 12-months-old animals showing Lrrk2 and Rab10 phosphorylation levels. (**b**,**c**) Quantifications of Ser935, Ser1292 phosphorylations (phospho/total Lrrk2), total Lrrk2 (Lrrk2/β-actin), and Thr73-Rab10 phosphorylation (phospho/total Rab10) in kidneys and lungs respectively of WT, RCKI, GSKI mice. Each dot in the bar graph represents one animal. Data are shown as mean ± SEM; One-way ANOVA with Dunnett post-hoc test (ns: not significant; * $p < 0.05$; ** $p < 0.01$; *** $p < 0.001$).

3.4. Age-Dependent Increase of Lrrk2 Phosphorylation and Steady State Levels in BAC-Lrrk2 G2019S Brains

We next examined the effect of the G2019S mutation in a different mouse model, namely the hemizygous BAC murine Lrrk2 G2019S (mBAC G2019S) mouse. This model, which was developed by Zhenyu Yue and collaborators (Mount Sinai, US), displays ~six-fold higher Lrrk2 expression compared to the endogenous locus [25] and it was shown to develop an age-related decline in striatal dopamine content [25] and 20% loss of TH neurons at 20 months of age [26]. Due to the large differences in Lrrk2 expression between WT and mBAC G2019S mice, we did not compare the genotypes but rather examined Lrrk2 and Rab10 phosphorylation in mBAC G2019S comparing striatum, cortex and midbrain at different ages (5 mice per age). Of note, while phospho-Thr73 Rab10 could not be robustly detected in brains with endogenous Lrrk2 expression (data not shown), it is clearly detectable in mBAC G2019S brains (Figure 4a–c).

In this dataset, we observed that: (i) LRRK2 expression increases upon aging in striatum and cortex; (ii) pSer935 and pSer1292 increase with aging in the striatum; (iii) Rab10 phosphorylation decreases at 12 months when Lrrk2 expression peaks, further supporting the notion that autophosphorylation and Rab10 phosphorylation are uncoupled events, at least in this context (Figure 4a–c). The observed differences in endogenous Lrrk2 levels across brain regions (Figure 1) are not as pronounced in the BAC G2019S mouse model (Figure S1), suggesting that Lrrk2 overexpression may blunt these tissue-specific variations. Finally, we prepared coronal brain slices from 1 and 12-month-old mBAC G2019S mice to evaluate Lrrk2 expression and phosphorylation at the cellular level with MJFF2(c41-2) and UDD210(12) antibodies, respectively. As shown in Figure 5a–f and Figure S3, total and phospho-Lrrk2 antibodies give high and specific signals (Figure S2) in the striatum, while the labeling in the cortex is much weaker (Figure S4).

We also observed that Lrrk2 (MJFF2) partially colocalizes with *β*-III-tubulin, a neuronal marker (Figure 5a,b) and to a lesser extent with GLT-1, a major glutamate transporter mainly expressed by astrocytes (Figure 5c–d). Instead, no co-localization with the microglial marker CD11b was observed (Figure 5e,f). Quite interestingly, we further noticed that phospho-Lrrk2 (phospho-Ser935) colocalizes with *β*-III-tubulin but no (or very faint) co-localization with GLT1 could be observed (Figure S3), suggesting that LRRK2 Ser935 phosphorylation is higher in neurons than in astrocytes. Given the age-dependent increase in expression of Lrrk2 in BAC-G2019S mice (Figure 4), we wondered whether this is paralleled to an increase in gliosis, a pathological feature reported in mutant LRRK2-associated PD [27]. To this end, coronal slices from 1 and 12-months-old BAC-G2019S mice were stained for GFAP, an intermediate cytoskeletal protein whose expression increases during astrogliosis [28]. As shown in Figure 5g,h, striatal astrocytes from 12-months-old mice exhibit a more ramified morphology as compared to 1-month-old animals, overall pointing to enhanced gliosis in aging BAC-G2019S brains. In addition, we observed a more intense CD11b signal as well as the presence of ramified microglial cells in cortico-striatal slices from 12 month-old BAC-G2019S mice, overall pointing at an increased inflammatory state in aged BAC-G2019S brains (Figure 5i,j).
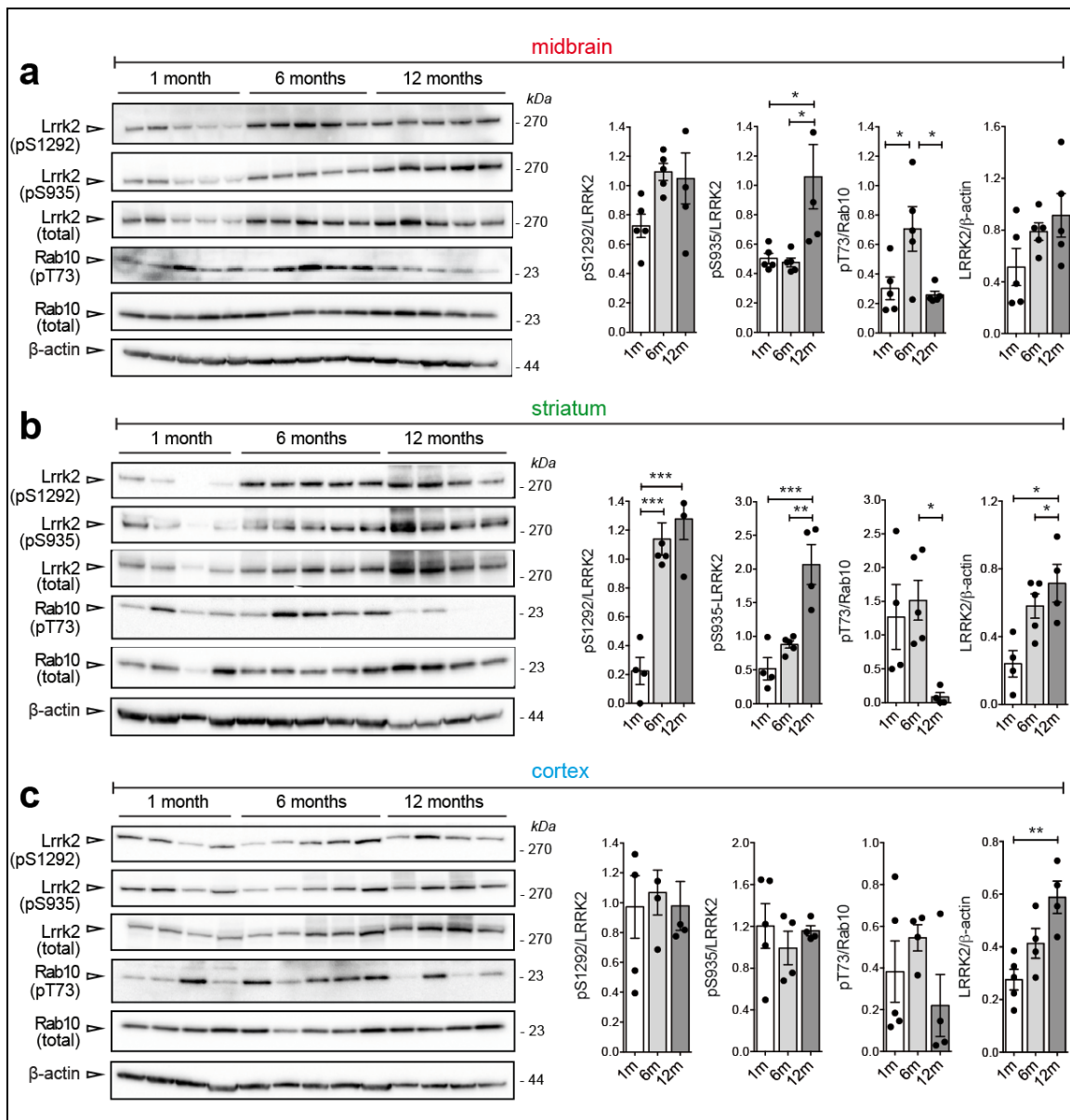
Figure 4. Age-dependent increase of Lrrk2 phosphorylation and steady state levels in BAC-Lrrk2 G2019S brains. (**a**) Representative western blots and relative quantifications of Ser935, Ser1292 phosphorylations (phospho/total Lrrk2), total Lrrk2 (total Lrrk2/β-actin), and Thr73-Rab10 phosphorylation (phospho/total Rab10) in midbrain, (**b**) striatum, and (**c**) cortex of murine BAC-G2019S mice at different ages (1, 6, and 12-months). Each dot in the bar graph represents one animal. Data are shown as mean ± SEM; One-way ANOVA with Dunnett post-hoc test (* $p < 0.05$; ** $p < 0.01$; *** $p < 0.001$).
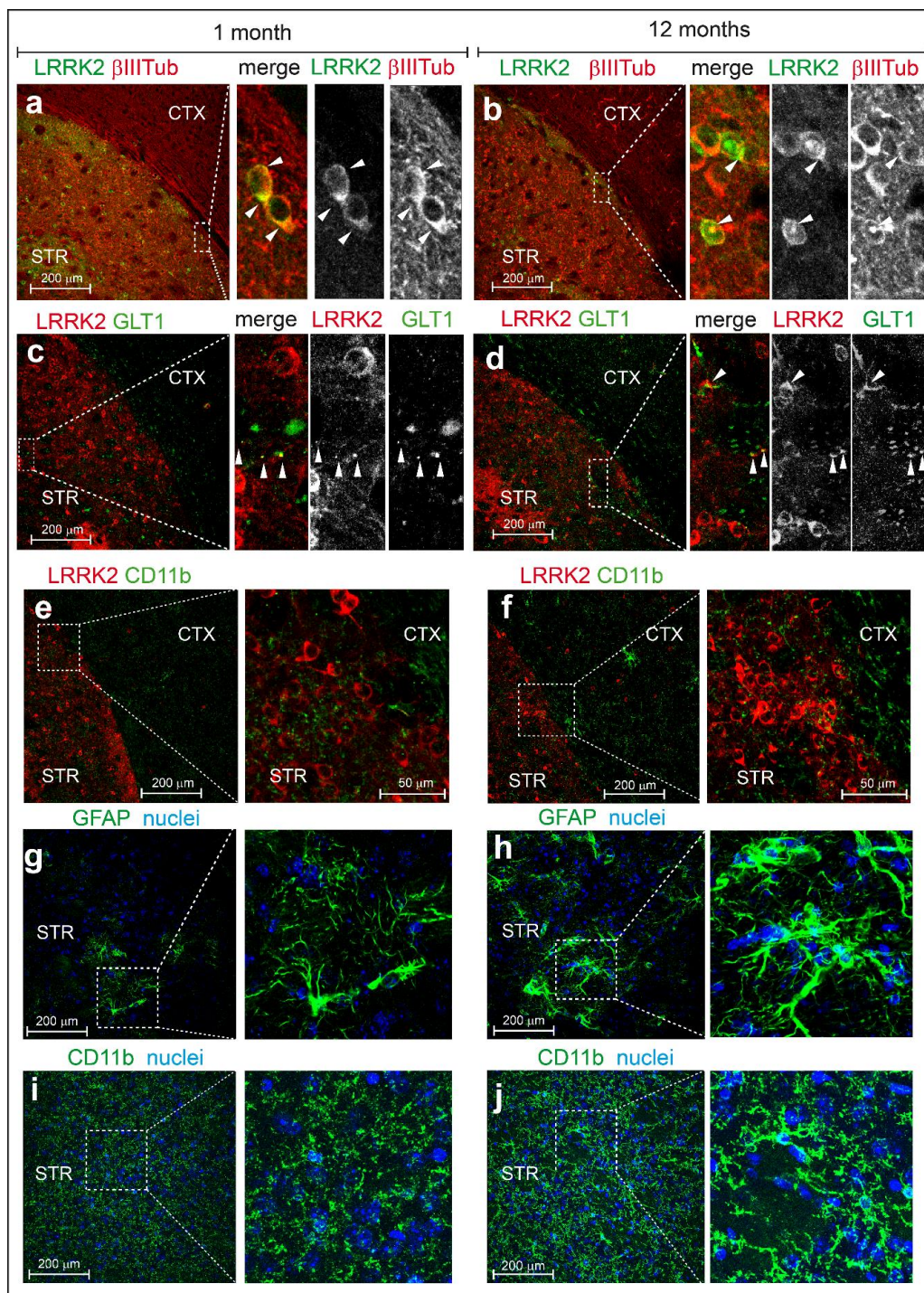
Figure 5. Immunofluorescent analysis of Lrrk2 distribution and subcellular localization in mBAC-Lrrk2-G2019S brain. Representative co-immunofluorescent staining of brain slices from hemizygous transgenic mice overexpressing murine BAC-Lrrk2-G2019S. In detail: (**a**,**b**) tot-Lrrk2 (green) distribution in cortex and striatum and subcellular localization in β-III-tubulin positive neurons (red) of 1-month-old and 12-months-old mice; (**c**,**d**) tot-Lrrk2 (red) distribution in cortex and striatum and subcellular localization in GLT-1 positive astrocytes (green) of 1-month-old and 12-months-old mice; (**e**,**f**) tot-Lrrk2 (red) distribution in cortex and striatum and subcellular localization in CD11b positive microglia (green) of 1-month-old and 12-months-old mice. Representative immunofluorescent staining of (**g**,**h**) GFAP and (**i**,**j**) CD11b-positive cells highlighting the different shape and activation level of striatal astrocytes and microglia respectively, at 1 and 12 months of age. *n* = 3 animals each staining. Scale bars 200 μm, and 50 μm.

4. Discussion

Understanding the effects of pathogenic mutations on LRRK2 phosphorylation and cellular activity is critical to clarify their impact on LRRK2 signaling and to identify mutation-specific effects important for disease diagnosis. There is general consensus that both kinase and non-kinase mutations increase LRRK2 activity towards its major substrates, namely LRRK2 itself and a subset of RAB GTPases [3,7]. However, most of these studies use cell models with protein overexpression or primary cells isolated from KI mice [3,7]. In contrast, the impact of mutations in a complex environment such as the brain where different cell types constantly exchange information, is poorly known. Here, by comparing LRRK2 mouse-models brains and peripheral tissues carrying two major mutations, namely G2019S in the kinase domain and R1441C in the ROC/GTPase domain, we found that heterologous phosphorylation (Ser935), autophosphorylation (Ser1292), and substrate phosphorylation (Rab10) have patterns not strictly predicted by cellular studies. First, we observed that Lrrk2 is highly expressed in the mouse striatum, while the protein shows significantly lower levels in the midbrain (Figure 6a).

High levels of LRRK2 in the striatum were previously reported [15,16], as well as specific functions in striatal medium spiny neurons [29,30]. Of interest, in all the models analyzed we found the clearest effects in the striatum. GSKI mice exhibit an age-dependent decline in Ser935 phospho-levels (Figure 6b), while increased levels and phosphorylation of Lrrk2 with aging are found in BAC-G2019S mice overexpressing the endogenous murine Lrrk2 locus (Figure 6c). In BAC-G2019S mice, the kinase is expressed in neurons and in some GLT1-positive structures, consistent with the previously reported expression in astroglia [31,32]. Not all LRRK2 positive cell bodies co-localize with the neuronal specific marker β-III-tubulin, supporting LRRK2 expression also in non-neuronal cells [31,32].

By comparing LRRK2 and Rab10 phosphorylation in KI G2019S and R1441C brains and lung/kidney, we made two major observations. First, the G2019S mutation increases autophosphorylation at Ser1292 while the R1441C mutation does not (Figure 6b). Second, R1441C but not G2019S results in increased phospho-Rab10, at least in kidneys and lungs where detection of phospho-Rab10 was possible (Figure 6b). The lack of phospho-Rab10 detection in the brain may be explained by the high expression levels in this tissue of PPM1H, a phosphatase selectively dephosphorylating Rab GTPases [11]. Furthermore, the R1441C mutation dramatically reduces Ser935 phosphorylation (Figure 6b), in line with cellular studies [5,6], instead the phosphorylation tone of Ser935 in GSKI is in between WT and RCKI (Figure 6b). The R1441 residue is located in the GTPase/ROC domain and substitution of the arginine with a cysteine decreases GTP hydrolysis [33] by locking the GTPase in its GTP-bound monomeric conformation, thereby trapping LRRK2 in an "on" conformation [34,35]. From our analysis, Ser935 phosphorylation is dramatically reduced in brain, lung, and kidney of RCKI mice, consistent with cellular studies [5,6]. Phosphorylation of Ser935 and Ser910 is necessary for the binding of 14-3-3 proteins, which results in LRRK2 diffuse cytoplasmic localization, at least under overexpression conditions [5]. In contrast, dephosphorylation of these residues by the action of LRRK2 phosphatases or via PAK6 phosphorylation of 14-3-3s, causes LRRK2 to compartmentalize [36,37]. In agreement, the basal dephosphorylated state of LRRK2 R1441C in Ser935 is coupled to a compartmentalized phenotype in cells, possibly indicating that the kinase is constitutively localized in its signaling domains [6,38]. Recent studies showed that membrane-bound RAB29 recruits and activates LRRK2 via its ankyrin (ANK) region which is near the cluster of serins that contains Ser935 [39–41]. Purlyte et al. further observed that pathogenic LRRK2 mutants with increased GTP binding (e.g., R1441G and Y1699C) display higher levels of Ser1292 autophosphorylation than wild-type LRRK2, but that the already higher levels of basal phospho-RAB10 are not further increased upon RAB29 expression [39], overall suggesting that ROC mutants may be constitutively recruited at RAB10-positive membranes domains independently on RAB29. This model would also explain why low Ser935 phosphorylation in LRRK2 R1441C still guarantees RAB10 phosphorylation, given that phospho-Ser935 is normally required for RAB29 recruitment of LRRK2 [39]. Further supporting these conclusions, a recent study also from Alessi's group [42] reported that Rab29 KO in R1441C KI mice does not reduce the elevated

Rab10 phosphorylation in MEFs or tissues, again suggesting that endogenous Rab29 is not sufficient to explain the elevated activity of the R1441C pathogenic mutant. This model fits with another observation by the same authors showing that RAB29-deficient binding mutants in the ANK domain are devoid of Ser935 phosphorylation but can still promote LRRK2-mediated RAB10 phosphorylation [39]. It remains to be explained why the R1441C mutation results in increased Ser1292 autophosphorylation in cells overexpressing this mutant form of LRRK2 but not in brain and peripheral tissues isolated from mice (Figure 6b). One obvious difference is that we are comparing overexpression versus endogenous expression, which should warn on interpreting overexpression studies with caution. Another possibility is that humans and mice possess different regulatory mechanisms or expression levels of LRRK2 and its interactors/substrates, which would result in different cellular outcomes.
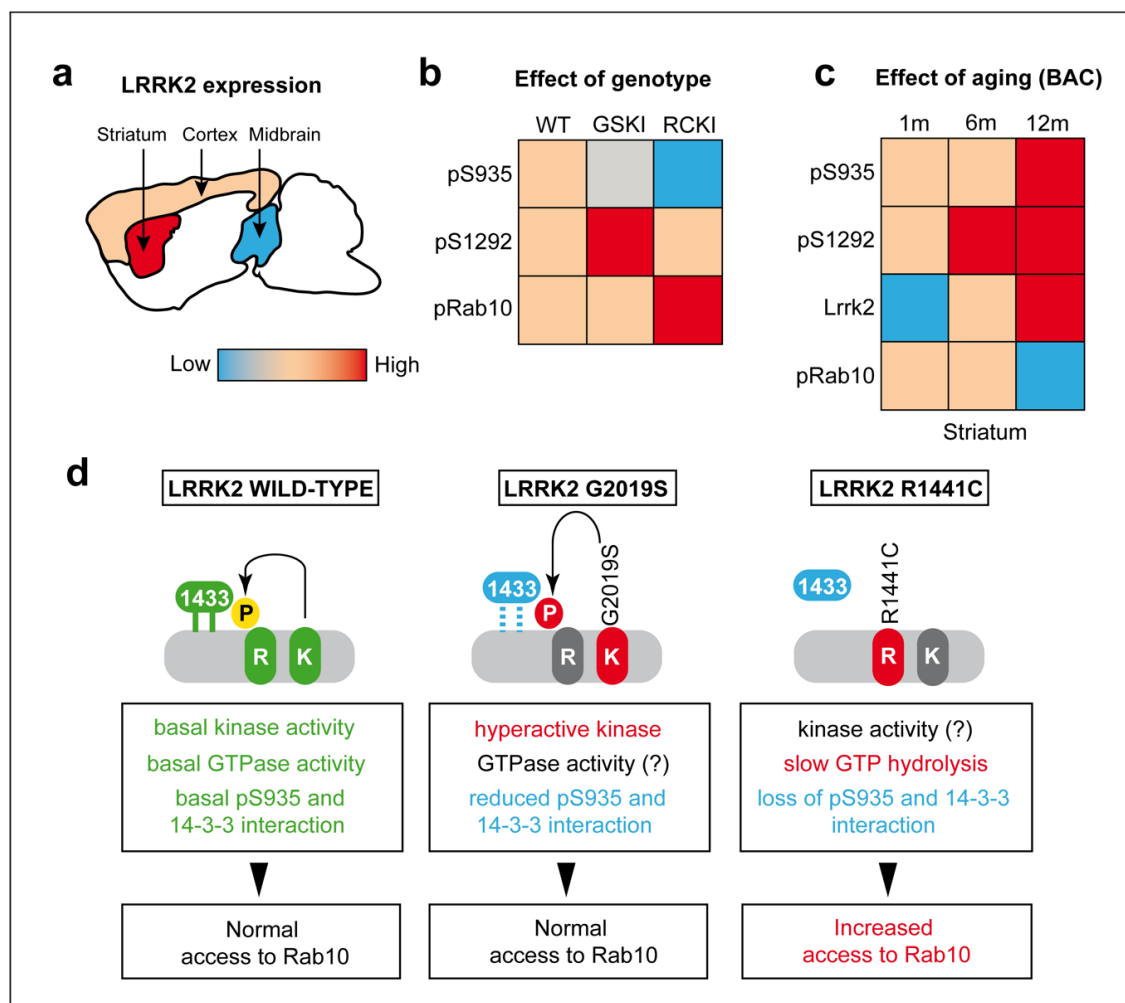
Figure 6. The differential impact of LRRK2 mutations on Rab10 phosphorylation in brain. (**a**) Schematic representation of LRRK2 protein levels in cortex, midbrain, and striatum. (**b**) LRRK2 and Rab10 phosphorylation levels as function of LRRK2 common mutations (G2019S and R1441C) and (**c**) as function of ageing in murine BAC-Lrrk2-G2019S mice. (**d**) Schematic summary of the possible molecular mechanisms underlying the different levels of Rab10 phosphorylation in presence of wild-type or mutated LRRK2. In detail, our data suggest that in the presence of the R1441C-LRRK2 mutation, the reduced phosphorylation at Ser935 may lead to a reduction of LRRK2-14-3-3s binding and thus to an increased access to Rab10.

Taking these and our findings together, we can postulate that GTP-locked LRRK2 R1441C does not need to undergo autophosphorylation in vivo being "constitutively" localized at RAB10-membranes

(or other compartments), bypassing RAB29-mediated recruitment and activation (Figure 6d). The consequence of a chronic RAB10 hyperphosphorylation could result in reduced ciliogenesis, thus impacting on brain functionality as suggested by recent works [43,44]. Future studies addressing the precise consequences of R1441C-dependent RAB10 hyperphosphorylation on ciliogenesis, as well as on lysosomal function [41,45], will better clarify the pathogenic mechanisms of this mutation.

Our study further highlights that LRRK2 mutations located in different domains (i.e., GTPase and kinase) likely operate through different pathogenic mechanisms. Knock-in mice carrying the G2019S mutation at the endogenous locus exhibit increased autophosphorylation at Ser1292 but Rab10 phosphorylation levels are similar to wild-type (Figures 2 and 6b–d). In contrast with the R1441C mutation which does not affect *per se* the catalytic properties of the kinase, the G2019S mutation located in the activation loop of the kinase increases activity by doubling the Vmax [46]. Based on the above considerations, we can predict that the higher autophosphorylation observed is a direct consequence of a kinase intrinsically more active, an outcome that is also observed in cellular models [3,7,47]. The fact that this hyperactive kinase does not hyper-phosphorylate Rab10 can be explained by the fact that LRRK2 G2019S requires RAB29 recruitment to RAB10-containing membranes similarly to wild-type LRRK2, as shown by Purtyle and collaborators [39] (Figure 6d). This implies that hyper-phosphorylation of other autophosphorylation sites located in the ROC domain [4] does not result in a GTP-locked protein but rather provide some fine regulation whose effect is not captured when assessing phospho-Rab10.

Translating these findings into therapeutic implications, kinase inhibitors are predicted to normalize the intrinsically higher kinase activity of LRRK2 G2019S carriers. While R1441C carriers may also benefit from a kinase inhibitor-based therapy through "on site" reduction of substrate hyperphosphorylation (i.e., Rab10), strategies that can correct the lower GTP hydrolysis of RocCOR mutants may represent an alternative, and possibly more effective, therapeutic approach for LRRK2-R1441C carriers. Another implication of the different mode of action for these two mutations is that they may require distinct pharmacodynamic readouts to assess on-target kinase inhibition: dephosphorylation of Ser935/Ser1292 for G2019S carriers and Rab10 dephosphorylation for R1441C carriers.

One intriguing observation from our analysis is that phosphorylation of Ser935 in GSKI brain lung and kidney is reduced by ~half. These results were not observed in cell lines [9] but are in line with two recent papers where pSer935 was reported to be reduced in peripheral blood mononuclear cells (PBMCs) of disease-manifesting G2019S carriers compared to idiopathic PD or controls [48,49], overall supporting the GSKI mouse with endogenous mutant Lrrk2 expression as a valuable pre-symptomatic model of disease. Since overexpression of RAB29 was observed to reduce Ser935 phosphorylation in both WT and G2019S LRRK2 [39], one possibility is that the decreased phospho-Ser935 observed in GSKI tissues is due to increased RAB29-dependent recruitment. If this is true, the lack of increase in phospho-Rab10 may suggest that LRRK2 G2019S is recruited to subcellular membrane compartments that are Rab10 negative (Figure 6d). Further studies comparing in vivo the effect of G2019S and R1441C mutations against different RAB GTPases may reveal how different mutations impact different cellular processes.

In line with a previous study by Mercatelli and collaborators [50], we also observed reduced total Lrrk2 levels in cortex and midbrain of GSKI compared to WT in 6 month-old animals (Figure 2). The reasons for this decline are unclear, although it could be speculated that it represents a neuronal response to downregulate the excessive kinase activity associated with mutant Lrrk2, a compensatory mechanism that is lost in aged mice (12 months), consistent with the late onset of PD pathology. Instead, the R1441C mice show a mild decline in total Lrrk2 levels at 12 months of age (Figure 2), further evidencing how the two mutations manifest with distinct phenotypes.

Finally, by comparing the effect of aging on Lrrk2 and Rab10 phosphorylation in the context of BAC-Lrrk2-G2019S overexpressing mice, we collected further evidence that Ser1292 autophosphorylation and Rab10 phosphorylation are uncoupled phenomena. Specifically, while Lrrk2 levels and phosphorylation increase with aging (up to 12 months), phosphorylation of Rab10 decreases

at 12 months, with the strongest effect observed in the striatum (Figure 6c). The reasons behind this effect are unclear. One possibility could be that the levels of PPM1H increase with aging to counteract the parallel increase in Lrrk2 observed. Intriguingly, a recent study found a genetic association between PPM1H and INFα levels in systemic lupus erythematosus (SLE) patients [51]. As also LRRK2 can modulate the risk of inflammatory diseases such as SLE [52,53] and neuroinflammation is increased in 12-month old BAC G2019S mice (Figure 5), future studies should be directed at exploring the possible link between LRRK2 and PPM1H in PD-related inflammation. While additional investigations are clearly required, these findings together with the previous observations in KI mice support the importance of encoding the effects of different LRRK2 mutations in specific tissues and at specific ages.

PD is a multisystemic disorder for which no cure is available. LRRK2 inhibitors are under clinical development and phase I clinical trials have already proved efficacy and safety [54]. However, LRRK2-PD neuropathology is variable, ranging from typical Lewy bodies pathology, to pure nigral degeneration, Tau pathology, and progressive supranuclear palsy-like pathology [27], which may reflect the different mode of action of different mutations in combination with other genetic and environmental factors. Thus, inhibition of LRRK2 activity with kinase inhibitors may work well with G2019S patients but may be less effective against mutations impairing GTP hydrolysis. A clear understanding of the impact of LRRK2 pathogenic mutations on autologous and heterologous LRRK2 phosphorylation in peripheral tissues from patients not only appears valuable as a predictive biomarker of disease but could also provide the mechanistic knowledge to develop personalized treatments for different LRRK2-PD.

References

1. Kluss, J.H.; Mamais, A.; Cookson, M.R. LRRK2 links genetic and sporadic Parkinson's disease. *Biochem. Soc. Trans.* **2019**, *47*, 651–661. [CrossRef]

2. Cookson, M.R. LRRK2 Pathways Leading to Neurodegeneration. *Curr. Neurol. Neurosci. Rep.* **2015**, *15*, 42. [CrossRef] [PubMed]

3. Steger, M.; Tonelli, F.; Ito, G.; Davies, P.; Trost, M.; Vetter, M.; Wachter, S.; Lorentzen, E.; Duddy, G.; Wilson, S.; et al. Phosphoproteomics reveals that Parkinson's disease kinase LRRK2 regulates a subset of Rab GTPases. *Elife* **2016**, *5*, e12813. [CrossRef]

4. Marchand, A.; Drouyer, M.; Sarchione, A.; Chartier-Harlin, M.-C.; Taymans, J.-M. LRRK2 Phosphorylation, More Than an Epiphenomenon. *Front. Neurosci.* **2020**, *14*, 527. [CrossRef] [PubMed]

5. Nichols, R.J.; Dzamko, N.; Morrice, N.A.; Campbell, D.G.; Deak, M.; Ordureau, A.; Macartney, T.; Tong, Y.; Shen, J.; Prescott, A.R.; et al. 14-3-3 Binding to LRRK2 is disrupted by multiple Parkinson's disease-associated mutations and regulates cytoplasmic localization. *Biochem. J.* **2010**, *430*, 393–404. [CrossRef] [PubMed]

6. Dzamko, N.; Deak, M.; Hentati, F.; Reith, A.D.; Prescott, A.R.; Alessi, D.R.; Nichols, R.J. Inhibition of LRRK2 kinase activity leads to dephosphorylation of Ser910/Ser935, disruption of 14-3-3 binding and altered cytoplasmic localization. *Biochem. J.* **2010**, *430*, 405–413. [CrossRef]

7. Sheng, Z.; Zhang, S.; Bustos, D.; Kleinheinz, T.; Le Pichon, C.E.; Dominguez, S.L.; Solanoy, H.O.; Drummond, J.; Zhang, X.; Ding, X.; et al. Ser1292 autophosphorylation is an indicator of LRRK2 kinase activity and contributes to the cellular effects of PD mutations. *Sci. Transl. Med.* **2012**, *4*, 164ra161. [CrossRef] [PubMed]

8. Karayel, O.; Tonelli, F.; Virreira Winter, S.; Geyer, P.E.; Fan, Y.; Sammler, E.M.; Alessi, D.; Steger, M.; Mann, M. Accurate MS-based Rab10 phosphorylation stoichiometry determination as readout for LRRK2 activity in Parkinson's disease. *Mol. Cell. Proteom.* **2020**, *19*, 1546–1560. [CrossRef]

9. Fan, Y.; Howden, A.J.M.; Sarhan, A.R.; Lis, P.; Ito, G.; Martinez, T.N.; Brockmann, K.; Gasser, T.; Alessi, D.R.; Sammler, E.M. Interrogating Parkinson's disease LRRK2 kinase pathway activity by assessing Rab10 phosphorylation in human neutrophils. *Biochem. J.* **2018**, *475*, 23–44. [CrossRef]

10. Di Maio, R.; Hoffman, E.K.; Rocha, E.M.; Keeney, M.T.; Sanders, L.H.; De Miranda, B.R.; Zharikov, A.; Van Laar, A.; Stepan, A.F.; Lanz, T.A.; et al. LRRK2 activation in idiopathic Parkinson's disease. *Sci. Transl. Med.* **2018**, *10*, eaar5429. [CrossRef]

11. Berndsen, K.; Lis, P.; Yeshaw, W.M.; Wawro, P.S.; Nirujogi, R.S.; Wightman, M.; Macartney, T.; Dorward, M.; Knebel, A.; Tonelli, F.; et al. PPM1H phosphatase counteracts LRRK2 signaling by selectively dephosphorylating rab proteins. *Elife* **2019**, *8*, e50416. [CrossRef] [PubMed]

12. Russo, I.; Di Benedetto, G.; Kaganovich, A.; Ding, J.; Mercatelli, D.; Morari, M.; Cookson, M.R.; Bubacco, L.; Greggio, E. Leucine-rich repeat kinase 2 controls protein kinase A activation state through phosphodiesterase 4. *J. Neuroinflammation* **2018**, *15*, 297. [CrossRef] [PubMed]

13. Pellegrini, L.; Hauser, D.N.; Li, Y.; Mamais, A.; Beilina, A.; Kumaran, R.; Wetzel, A.; Nixon-Abell, J.; Heaton, G.; Rudenko, I.; et al. Proteomic analysis reveals co-ordinated alterations in protein synthesis and degradation pathways in LRRK2 knockout mice. *Hum. Mol. Genet.* **2018**, *27*, 3257–3271. [CrossRef] [PubMed]

14. McGregor, M.M.; Nelson, A.B. Circuit Mechanisms of Parkinson's Disease. *Neuron* **2019**, *101*, 1042–1056. [CrossRef]

15. Mandemakers, W.; Snellinx, A.; Snellinx, A.; O'Neill, M.J.; de Strooper, B. LRRK2 expression is enriched in the striosomal compartment of mouse striatum. *Neurobiol. Dis.* **2012**, *48*, 582–593. [CrossRef]

16. West, A.B.; Cowell, R.M.; Daher, J.P.L.; Moehle, M.S.; Hinkle, K.M.; Melrose, H.L.; Standaert, D.G.; Volpicelli-Daley, L.A. Differential LRRK2 expression in the cortex, striatum, and substantia nigra in transgenic and nontransgenic rodents. *J. Comp. Neurol.* **2014**, *522*, 2465–2480. [CrossRef]

17. Hatcher, J.M.; Zhang, J.; Choi, H.G.; Ito, G.; Alessi, D.R.; Gray, N.S. Discovery of a pyrrolopyrimidine (JH-II-127), a highly potent, selective, and brain penetrant LRRK2 inhibitor. *ACS Med. Chem. Lett.* **2015**, *6*, 584–589. [CrossRef]

18. Zhao, Y.; Keshiya, S.; Atashrazm, F.; Gao, J.; Ittner, L.M.; Alessi, D.R.; Halliday, G.M.; Fu, Y.; Dzamko, N. Nigrostriatal pathology with reduced astrocytes in LRRK2 S910/S935 phosphorylation deficient knockin mice. *Neurobiol. Dis.* **2018**, *120*, 76–87. [CrossRef]

19. Biskup, S.; Moore, D.J.; Rea, A.; Lorenz-Deperieux, B.; Coombes, C.E.; Dawson, V.L.; Dawson, T.M.; West, A.B. Dynamic and redundant regulation of LRRK2 and LRRK1 expression. *BMC Neurosci.* **2007**, *8*, 102. [CrossRef]

20. Maekawa, T.; Kubo, M.; Yokoyama, I.; Ohta, E.; Obata, F. Age-dependent and cell-population-restricted LRRK2 expression in normal mouse spleen. *Biochem. Biophys. Res. Commun.* **2010**, *392*, 431–435. [CrossRef]

21. Biskup, S.; Moore, D.J.; Celsi, F.; Higashi, S.; West, A.B.; Andrabi, S.A.; Kurkinen, K.; Yu, S.W.; Savitt, J.M.; Waldvogel, H.J.; et al. Localization of LRRK2 to membranous and vesicular structures in mammalian brain. *Ann. Neurol.* **2006**, *60*, 557–569. [CrossRef] [PubMed]

22. Fell, M.J.; Mirescu, C.; Basu, K.; Cheewatrakoolpong, B.; DeMong, D.E.; Ellis, J.M.; Hyde, L.A.; Lin, Y.; Markgraf, C.G.; Mei, H.; et al. MLi-2, a potent, selective, and centrally active compound for exploring the therapeutic potential and safety of LRRK2 kinase inhibition. *J. Pharmacol. Exp. Ther.* **2015**, *355*, 397–409. [CrossRef] [PubMed]

23. Thirstrup, K.; Dächsel, J.C.; Oppermann, F.S.; Williamson, D.S.; Smith, G.P.; Fog, K.; Christensen, K.V. Selective LRRK2 kinase inhibition reduces phosphorylation of endogenous Rab10 and Rab12 in human peripheral mononuclear blood cells. *Sci. Rep.* **2017**, *7*, 1–18. [CrossRef] [PubMed]

24. Ito, G.; Katsemonova, K.; Tonelli, F.; Lis, P.; Baptista, M.A.S.; Shpiro, N.; Duddy, G.; Wilson, S.; Ho, P.W.L.; Ho, S.L.; et al. Phos-Tag analysis of Rab10 phosphorylation by LRRK2: A powerful assay for assessing kinase function and inhibitors. *Biochem. J.* **2016**, *473*, 2671–2685. [CrossRef] [PubMed]

25. Li, X.; Patel, J.C.; Wang, J.; Avshalumov, M.V.; Nicholson, C.; Buxbaum, J.D.; Elder, G.A.; Rice, M.E.; Yue, Z. Enhanced striatal dopamine transmission and motor performance with LRRK2 overexpression in mice is eliminated by familial Parkinson's disease mutation G2019S. *J. Neurosci.* **2010**, *30*, 1788–1797. [CrossRef]

26. Chen, Z.C.; Zhang, W.; Chua, L.L.; Chai, C.; Li, R.; Lin, L.; Cao, Z.; Angeles, D.C.; Stanton, L.W.; Peng, J.H.; et al. Phosphorylation of amyloid precursor protein by mutant LRRK2 promotes AICD activity and neurotoxicity in Parkinson's disease. *Sci. Signal.* **2017**, *10*, eaam6790. [CrossRef]

27. Zimprich, A.; Biskup, S.; Leitner, P.; Lichtner, P.; Farrer, M.; Lincoln, S.; Kachergus, J.; Hulihan, M.; Uitti, R.J.; Calne, D.B.; et al. Mutations in LRRK2 cause autosomal-dominant parkinsonism with pleomorphic pathology. *Neuron* **2004**, *44*, 601–607. [CrossRef]

28. Pekny, M.; Pekna, M. Astrocyte reactivity and reactive astrogliosis: Costs and benefits. *Physiol. Rev.* **2014**, *94*, 1077–1098. [CrossRef]

29. Parisiadou, L.; Yu, J.; Sgobio, C.; Xie, C.; Liu, G.; Sun, L.; Gu, X.L.; Lin, X.; Crowley, N.A.; Lovinger, D.M.; et al. LRRK2 regulates synaptogenesis and dopamine receptor activation through modulation of PKA activity. *Nat. Neurosci.* **2014**, *17*, 367–376. [CrossRef]

30. Matikainen-Ankney, B.A.; Kezunovic, N.; Mesias, R.E.; Tian, Y.; Williams, F.M.; Huntley, G.W.; Benson, D.L. Altered development of synapse structure and function in striatum caused by Parkinson's disease-linked LRRK2-G2019S mutation. *J. Neurosci.* **2016**, *36*, 7128–7141. [CrossRef]

31. Zhang, Y.; Sloan, S.A.; Clarke, L.E.; Caneda, C.; Plaza, C.A.; Blumenthal, P.D.; Vogel, H.; Steinberg, G.K.; Edwards, M.S.B.; Li, G.; et al. Purification and Characterization of Progenitor and Mature Human Astrocytes Reveals Transcriptional and Functional Differences with Mouse. *Neuron* **2016**, *89*, 37–53. [CrossRef]

32. Zhang, Y.; Chen, K.; Sloan, S.A.; Bennett, M.L.; Scholze, A.R.; O’Keeffe, S.; Phatnani, H.P.; Guarnieri, P.; Caneda, C.; Ruderisch, N.; et al. An RNA-sequencing transcriptome and splicing database of glia, neurons, and vascular cells of the cerebral cortex. *J. Neurosci.* **2014**, *34*, 11929–11947. [CrossRef]

33. Lewis, P.A.; Greggio, E.; Beilina, A.; Jain, S.; Baker, A.; Cookson, M.R. The R1441C mutation of LRRK2 disrupts GTP hydrolysis. *Biochem. Biophys. Res. Commun.* **2007**, *357*, 668–671. [CrossRef] [PubMed]

34. Wu, C.X.; Liao, J.; Park, Y.; Reed, X.; Engel, V.A.; Hoang, N.C.; Takagi, Y.; Johnson, S.M.; Wang, M.; Federici, M.; et al. Parkinson's disease-associated mutations in the GTPase domain of LRRK2 impair its nucleotide-dependent conformational dynamics. *J. Biol. Chem.* **2019**, *294*, 5907–5913. [CrossRef] [PubMed]

35. Deyaert, E.; Wauters, L.; Guaitoli, G.; Konijnenberg, A.; Leemans, M.; Terheyden, S.; Petrovic, A.; Gallardo, R.; Nederveen-Schippers, L.M.; Athanasopoulos, P.S.; et al. A homologue of the Parkinson's disease-associated protein LRRK2 undergoes a monomer-dimer transition during GTP turnover. *Nat. Commun.* **2017**, *8*, 1–12. [CrossRef]

36. Lobbestael, E.; Zhao, J.; Rudenko, I.N.; Beylina, A.; Gao, F.; Wetter, J.; Beullens, M.; Bollen, M.; Cookson, M.R.; Baekelandt, V.; et al. Identification of protein phosphatase 1 as a regulator of the LRRK2 phosphorylation cycle. *Biochem. J.* **2013**, *456*, 119–128. [CrossRef]

37. Civiero, L.; Cogo, S.; Kiekens, A.; Morganti, C.; Tessari, I.; Lobbestael, E.; Baekelandt, V.; Taymans, J.M.; Chartier-Harlin, M.C.; Franchin, C.; et al. PAK6 phosphorylates 14-3-3γ to regulate steady state phosphorylation of LRRK2. *Front. Mol. Neurosci.* **2017**, *10*, 417. [CrossRef]

38. Ramírez, M.B.; Ordóñez, A.J.L.; Fdez, E.; Madero-Pérez, J.; Gonnelli, A.; Drouyer, M.; Chartier-Harlin, M.C.; Taymans, J.M.; Bubacco, L.; Greggio, E.; et al. GTP binding regulates cellular localization of Parkinson's disease-associated LRRK2. Hum. *Mol. Genet.* **2017**, *26*, 2747–2767.

39. Purlyte, E.; Dhekne, H.S.; Sarhan, A.R.; Gomez, R.; Lis, P.; Wightman, M.; Martinez, T.N.; Tonelli, F.; Pfeffer, S.R.; Alessi, D.R. Rab29 activation of the Parkinson's disease-associated LRRK2 kinase. *EMBO J.* **2018**, *37*, e97479. [CrossRef]

40. Liu, Z.; Bryant, N.; Kumaran, R.; Beilina, A.; Abeliovich, A.; Cookson, M.R.; West, A.B. LRRK2 phosphorylates membrane-bound Rabs and is activated by GTP-bound Rab7L1 to promote recruitment to the trans-Golgi network. *Hum. Mol. Genet.* **2018**, *27*, 385–395. [CrossRef]

41. Eguchi, T.; Kuwahara, T.; Sakurai, M.; Komori, T.; Fujimoto, T.; Ito, G.; Yoshimura, S.I.; Harada, A.; Fukuda, M.; Koike, M.; et al. LRRK2 and its substrate Rab GTPases are sequentially targeted onto stressed lysosomes and maintain their homeostasis. *Proc. Natl. Acad. Sci. USA* **2018**, *115*, E9115–E9124. [CrossRef] [PubMed]

42. Kalogeropulou, A.F.; Lis, P.; Polinski, N.K.; Alessi, D.R. Rab29 knock-out or transgenic overexpression does not impact basal LRRK2 activity in wildtype and pathogenic mouse and cell line models. *bioRxiv* **2020**. [CrossRef]

43. Dhekne, H.S.; Yanatori, I.; Gomez, R.C.; Tonelli, F.; Diez, F.; Schüle, B.; Steger, M.; Alessi, D.R.; Pfeffer, S.R. A pathway for parkinson's disease LRRK2 kinase to block primary cilia and sonic hedgehog signaling in the brain. *Elife* **2018**, *7*, e40202. [CrossRef] [PubMed]

44. Lara Ordónez, A.J.; Fernández, B.; Fdez, E.; Romo-Lozano, M.; Madero-Pérez, J.; Lobbestael, E.; Baekelandt, V.; Aiastui, A.; López De Munaín, A.; Melrose, H.L.; et al. RAB8, RAB10 and RILPL1 contribute to both LRRK2 kinase-mediated centrosomal cohesion and ciliogenesis deficits. *Hum. Mol. Genet.* **2019**, *28*, 3552–3568. [CrossRef] [PubMed]

45. Bonet-Ponce, L.; Beilina, A.; Williamson, C.D.; Lindberg, E.; Kluss, J.H.; Saez-Atienzar, S.; Landeck, N.; Kumaran, R.; Mamais, A.; Bleck, C.K.E.; et al. LRRK2 mediates tubulation and vesicle sorting from membrane damaged lysosomes. *bioRxiv* **2020**. [CrossRef]

46. Covy, J.P.; Giasson, B.I. The G2019S pathogenic mutation disrupts sensitivity of leucine-rich repeat kinase 2 to manganese kinase inhibition. *J. Neurochem.* **2010**, *115*, 36–46. [CrossRef]

47. Greggio, E.; Jain, S.; Kingsbury, A.; Bandopadhyay, R.; Lewis, P.; Kaganovich, A.; van der Brug, M.P.; Beilina, A.; Blackinton, J.; Thomas, K.J.; et al. Kinase activity is required for the toxic effects of mutant LRRK2/dardarin. *Neurobiol. Dis.* **2006**, *23*, 329–341. [CrossRef]

48. Padmanabhan, S.; Lanz, T.A.; Gorman, D.; Wolfe, M.; Joyce, A.; Cabrera, C.; Lawrence-Henderson, R.; Levers, N.; Joshi, N.; Ma, T.C.; et al. An Assessment of LRRK2 Serine 935 Phosphorylation in Human Peripheral Blood Mononuclear Cells in Idiopathic Parkinson's Disease and G2019S LRRK2 Cohorts. *J. Parkinsons. Dis.* **2020**, *10*, 623–629. [CrossRef]

49. Melachroinou, K.; Kang, M.S.; Liong, C.; Narayan, S.; Levers, N.; Joshi, N.; Kopil, K.; Hutten, S.J.; Baptista, M.A.S.; Padmanabhan, S.; et al. Elevated In Vitro Kinase Activity in Peripheral Blood Mononuclear Cells of Leucine-Rich Repeat Kinase 2 G2019S Carriers: A Novel Enzyme-Linked Immunosorbent Assay–Based Method. *Mov. Disord.* **2020**. [CrossRef]

50. Mercatelli, D.; Bolognesi, P.; Frassineti, M.; Pisanò, C.A.; Longo, F.; Shimshek, D.R.; Morari, M. Leucine-rich repeat kinase 2 (LRRK2) inhibitors differentially modulate glutamate release and Serine935 LRRK2 phosphorylation in striatal and cerebrocortical synaptosomes. *Pharmacol. Res. Perspect.* **2019**, 7. [CrossRef]

51. Ghodke-Puranik, Y.; Imgruet, M.; Dorschner, J.M.; Shrestha, P.; McCoy, K.; Kelly, J.A.; Marion, M.; Guthridge, J.M.; Langefeld, C.D.; Harley, J.B.; et al. Novel genetic associations with interferon in systemic lupus erythematosus identified by replication and fine-mapping of trait-stratified genome-wide screen. *Cytokine* **2020**, *132*, 154631. [CrossRef] [PubMed]

52. Zhang, Y.M.; Zhou, X.J.; Cheng, F.J.; Qi, Y.Y.; Hou, P.; Zhao, M.H.; Zhang, H. Autophagy-related gene LRRK2 is likely a susceptibility gene for systemic lupus erythematosus in northern Han Chinese. *Oncotarget* **2017**, *8*, 13754–13761. [CrossRef] [PubMed]

53. Zhang, M.; Yao, C.; Cai, J.; Liu, S.; Liu, X.N.; Chen, Y.; Wang, S.; Ji, P.; Pan, M.; Kang, Z.; et al. LRRK2 is involved in the pathogenesis of system lupus erythematosus through promoting pathogenic antibody production. *J. Transl. Med.* **2019**, *17*, 1–13. [CrossRef] [PubMed]

54. Denali|Pipeline. Available online: https://denalitherapeutics.com/pipeline (accessed on 27 July 2020).

CELL BIOLOGY

LRRK2 mediates tubulation and vesicle sorting from lysosomes

Luis Bonet-Ponce[1], Alexandra Beilina[1], Chad D. Williamson[2], Eric Lindberg[3], Jillian H. Kluss[1], Sara Saez-Atienzar[4], Natalie Landeck[1], Ravindran Kumaran[1], Adamantios Mamais[1], Christopher K. E. Bleck[3], Yan Li[5], Mark R. Cookson[1]*

Genetic variation around the LRRK2 gene affects risk of both familial and sporadic Parkinson's disease (PD). However, the biological functions of LRRK2 remain incompletely understood. Here, we report that LRRK2 is recruited to lysosomes after exposure of cells to the lysosome membrane–rupturing agent LLOME. Using an unbiased proteomic screen, we identified the motor adaptor protein JIP4 as an LRRK2 partner at the lysosomal membrane. LRRK2 can recruit JIP4 to lysosomes in a kinase-dependent manner via the phosphorylation of RAB35 and RAB10. Using super-resolution live-cell imaging microscopy and FIB-SEM, we demonstrate that JIP4 promotes the formation of LAMP1-negative tubules that release membranous content from lysosomes. Thus, we describe a new process orchestrated by LRRK2, which we name LYTL (LYsosomal Tubulation/sorting driven by LRRK2), by which lysosomal tubulation is used to release vesicles from lysosomes. Given the central role of the lysosome in PD, LYTL is likely to be disease relevant.

INTRODUCTION

Mutations in *LRRK2* are a relatively common cause of familial late-onset Parkinson's disease (PD) (*1*, *2*), and variations at the LRRK2 locus have also been linked to the more numerous sporadic PD (*3*, *4*). LRRK2 encodes leucine-rich repeat kinase 2, a large protein with extensive protein scaffolding sequences as well as two enzymatic activities. Most of the proven pathogenic mutations are located in the ROC (Ras of complex proteins)–COR (C terminus of ROC) bidomain or adjacent kinase domain that control guanosine triphosphate (GTP) hydrolysis and kinase activity, respectively. The majority of evidence suggests that mutations lead to a toxic function of the protein (*5*). At the cellular level, evidence suggests that LRRK2 can regulate membrane trafficking events via phosphorylation of a subset of RAB GTPases (*6*–*8*), although the precise relationship(s) between LRRK2 mutations, RAB phosphorylation, and neurodegeneration remains uncertain.

Recent data have pointed to the lysosome as a crucial organelle in PD. Genetically, mutations in genes encoding for lysosomal proteins have been identified in familial cases of PD (*9*) and have been nominated as risk factors for sporadic PD (*3*), leading to the suggestion that PD should be considered a lysosomal disease (*10*). An accumulation of lysosomal damage with age in kidneys, which normally express high levels of LRRK2, has been documented in knockout (KO) mice (*11*). Pathogenic LRRK2 mutations affect lysosomal structure and function in cultured astrocytes (*12*) and other cell types (*13*, *14*). However, the mechanistic basis by which LRRK2 affects lysosome function is unclear. In addition, because LRRK2 can be

localized to a wide range of other membrane-bound structures in cells (*7*, *15*, *16*), whether LRRK2-mediated lysosomal defects are primary events or secondary effects driven by toxicity to other cellular components is uncertain.

Here, we describe that LRRK2 translocates to the lysosomal surface in response to lysosomal membrane permeabilization, leading to the phosphorylation and recruitment of Ras-related in brain 35 (RAB35) and RAB10. As a consequence, both RAB proteins promote the translocation of the motor adaptor protein c-Jun N-terminal kinase (JNK)–interacting protein 4 (JIP4). JIP4 is present in, and helps to form, lysosomal associated membrane protein 1 (LAMP1)–negative tubular structures stemming from lysosomes. Live-cell super-resolution microscopy reveals that these tubules bud, extend, and release small vesicular structures, suggesting a scenario where lysosomes (undergoing membrane permeabilization) sort membranous content that can then interact with other lysosomes. We call this newly described process LYsosomal Tubulation/sorting driven by LRRK2 (LYTL).

RESULTS

LRRK2, along with the motor adaptor protein JIP4, gets recruited to the membrane of a subset of lysosomes

To understand how LRRK2 might affect lysosomal function, we first examined the localization of LRRK2 in cells. For these experiments, we used mouse primary astrocytes as follows: (i) primary astrocytes express LRRK2 endogenously (fig. S1A), (ii) their flattened morphology allows us to monitor membrane trafficking events, and (iii) they have been proposed to play a role in the pathobiology of PD through non–cell-autonomous effects on microglia and neurons (*17*).

Exogenously expressed LRRK2 has been widely reported in the literature to have a diffuse cytosolic distribution (*7*, *18*, *19*). However, when expressed in mouse primary astrocytes, LRRK2 colocalized with a subset of structures positive for the late-endosomal/lysosome (LE/LYS) membrane marker LAMP1 in about half of the cells examined. Specifically, LRRK2 is present at a subset of LE/LYS (2.72 ± 0.41 LRRK2-positive LE/LYS structures per cell) (Fig. 1A)

[1]Cell Biology and Gene Expression Section, National Institute on Aging, National Institutes of Health, Bethesda, MD 20892, USA. [2]Cell Biology and Neurobiology Branch, National Institute of Child Health and Human Development, National Institutes of Health, Bethesda, MD 20892, USA. [3]Electron Microscopy Core, National Heart, Lung, and Blood Institute, National Institutes of Health, Bethesda, MD 20892, USA. [4]Neuromuscular Diseases Research Section, National Institute on Aging, National Institutes of Health, Bethesda, MD 20892, USA. [5]Proteomics Core Facility, National Institute of Neurological Disorders and Stroke, National Institutes of Health, Bethesda, MD 20892, USA.
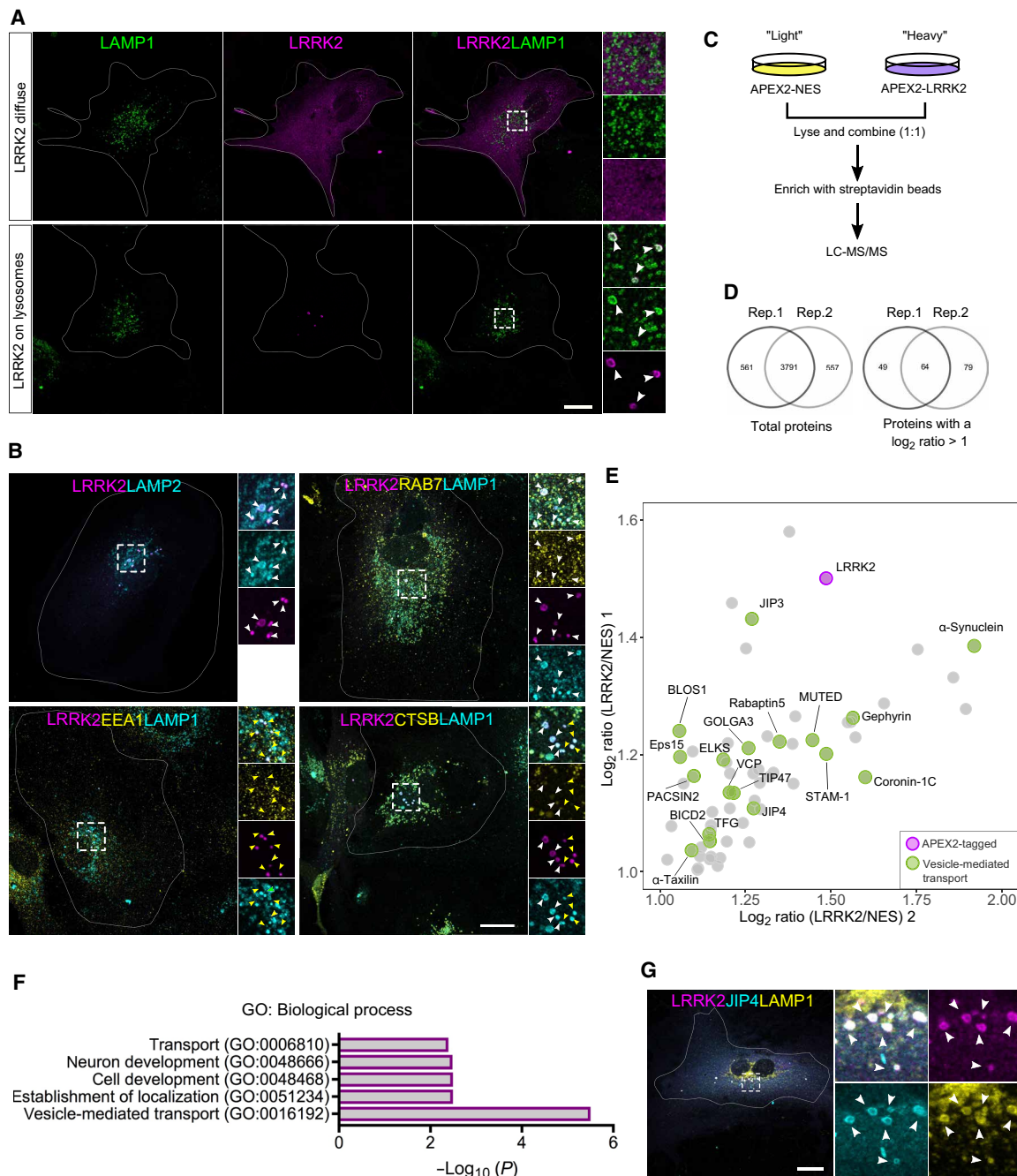*Corresponding author: Email: cookson@mail.nih.gov

Fig. 1. LRRK2 and JIP4 are localized at the membrane of a subset of lysosomes in primary astrocytes. (**A**) Representative confocal images of 3xflag-LRRK2 and LAMP1 expression in mouse primary astrocytes. (**B**) Representative confocal images of astrocytes expressing 3xflag-LRRK2 costained with LAMP2, RAB7, EEA1, and CTSB. (**C**) Outline of the APEX2 proteomic approach to detect LRRK2-membrane interactors. (**D**) Venn diagrams showing the number of common proteins detected in both replicates (left) and the number of proteins selected as candidates due to having a twofold enrichment in LRRK2 versus negative control in both replicates (right). (**E**) Scatter plot depicting the 64 LRRK2-interacting candidates from the APEX2 screening. LRRK2 is marked in red, and proteins involved in vesicle-mediated transport are marked in green. (**F**) Gene Ontology (GO) search of the top 5 enriched terms for biological process of the 64 LRRK2 potential interacting partners, with P values adjusted using a Bonferroni correction indicated on the horizontal axis. (**G**) Representative confocal image of an astrocyte expressing 3xflag-LRRK2 and GFP-JIP4 and stained for LAMP1. White arrowheads show colocalization, and yellow arrowheads show structures without localization. Scale bar, 20 μm.

that is also positive for the LE/LYS marker RAB7 and the lysosomal marker LAMP2. These structures only occasionally contain the lysosomal enzyme cathepsin B (CTSB) and were negative for the early endosomal marker EEA1 (Fig. 1B). The combination of the presence of multiple LE/LYS markers with variable levels of CTSB suggests that LRRK2 is recruited to LYS with a low degradative capacity (20).

We next asked whether LRRK2 enzymatic activity could play a role in its recruitment to LYS by expressing the hyperactive and

pathogenic mutations G2019S (kinase domain) and R1441C (GTPase domain), along with the artificial inactive mutations K1906M (kinase dead) and T1348N (GTP-binding null) (fig. S1B). An increase in the recruitment of LRRK2 to LYS was observed in both hyperactive mutations compared to the wild-type (WT) form, whereas a decrease was seen with either inactive mutations (fig. S1, C to E). Domain-specific LRRK2 constructs (ΔHEAT, ΔWD40, HEAT, ROC-COR-Kinase, and ROC-COR) (fig. S1F) showed much less recruitment to LYS compared to the full-length construct (fig. S1, G to I). However, comparing the domains to each other, we detected a higher amount of cells with lysosomal LRRK2 for the HEAT and ΔWD40 domains compared to the other three domains (fig. S1, G and J), suggesting that although every domain seems to be important to maintain LRRK2 at the lysosomal membrane, recruitment likely happens through its N-terminal region.

These results suggest that while not all LRRK2 is lysosomal, it is likely to play a role in a small subset of these organelles. To identify lysosome-specific functional interactors of LRRK2, we used the unbiased proximity-based biotinylation protein-protein interaction method ascorbate peroxidase 2 (APEX2) (21), followed by quantitative proteomics in human embryonic kidney (HEK) 293FT cells with stable isotope–labeled amino acids. As a cytosolic control to exclude nonspecific interactions, APEX2 was tagged to a nuclear export signal (NES) (Fig. 1C). Both vectors (APEX2-3xflag-LRRK2 and APEX2-3xflag-NES) were successfully validated using immunostaining and Western blot (fig. S2, A and B). From the mass spectrometry hits found in two independent replicates with the LRRK2 vector but not APEX-NES (table S1), 64 proteins were selected as possible candidates for LRRK2 interaction (Fig. 1, D and E; fig. S2C; and table S2). Among these candidates, six have already been linked to LRRK2 in previous studies (α-synuclein, JIP3, JIP4, coronin-1C, gephyrin, and PACSIN2) (22–24), suggesting that this method can detect authentic LRRK2 interactors. Fifteen of the candidate proteins have a role in vesicle-mediated transport (Fig. 1F), and six (BLOS1, Muted, JIP3, JIP4, BICD2, and STAM1) have been linked to lysosome biogenesis or dynamics in previous studies. To further prioritize the lysosomal-related hits, we tested whether they were recruited to LRRK2-positive LYS in astrocytes. JIP4 was the only candidate that colocalized with LRRK2-positive LYS (Fig. 1G and fig. S2D). We were able to validate that there was a physical interaction between these two proteins by overexpressing LRRK2 and blotting for endogenous JIP4 in cells (fig. S2E). We therefore considered JIP4, previously nominated by several independent laboratories using different techniques (8, 23), to be a reliable LRRK2 interacting protein and a candidate for mediating any functional effects of LRRK2 on the lysosome.

LRRK2 recruitment to lysosomes occurs as a response to lysosomal membrane rupture, independent of lysophagy

JIP4 is a cytosolic scaffolding protein, associated with multiple aspects of vesicle-mediated transport by acting as an adaptor for both dynein and kinesin motor proteins (25). JIP4 has also been linked to stress response (26), leading us to speculate that the LRRK2:JIP4 complex might respond to lysosomal damage. Such a role would be consistent with the data above showing that LRRK2-positive LYS has low levels of CTSB (Fig. 1B), which is seen when the lysosomal membrane is ruptured and the organellar contents leak into the cytosol (27). To test the hypothesis that lysosomal membrane damage might trigger LRRK2:JIP4 recruitment to LYS, we treated primary

astrocytes with the lysosomotropic reagent L-leucyl-L-leucine methyl ester (LLOME). LLOME enters the cell via endocytosis and is transported to the lysosomes where it undergoes condensation by cathepsin C, leading to lysosomal membrane rupture (28). Exposure of cells to 1 mM LLOME triggered a notable and time-dependent increase in LRRK2 recruitment to the lysosomal membrane (Fig. 2A and fig. S3A). We confirmed that LRRK2 is recruited to inactive putative lysosomes by showing that these structures are negative for both LysoTracker and Magic Red CTSB (Fig. 2, B and C), fluorescent probes that measure lysosomal pH and activity, respectively.

One widely reported effect of lysosome membrane disruption is the induction of lysophagy, a mechanism to clear ruptured lysosomes from cells via selective autophagy. Galectin-3 (Gal3) is diffusely distributed in the cell under normal conditions but is recruited to the ruptured membrane and initiates lysophagy after a high degree of lysosomal membrane damage (29). In our experimental paradigm, Gal3 was recruited to a subset of lysosomes after LLOME treatment (Fig. 2, D and E). However, LRRK2-positive LYS was partially positive for Gal3 (Fig. 2, D and F), suggesting that LRRK2:JIP4 are recruited to a different lysosomal pool than those that will be degraded by lysophagy.

To further determine if LRRK2 modifies lysophagy, we pretreated cells with the potent LRRK2 kinase inhibitor MLi-2 before adding LLOME. MLi-2 was able to completely block endogenous LRRK2 kinase activity in mouse primary astrocytes as documented by inhibition of both the LRRK2 autophosphorylation site pS1292 and pT73 on RAB10, a known substrate of LRRK2 (fig. S2F). In contrast, LRRK2 kinase inhibition did not affect Gal3 recruitment to the LYS in the presence of LLOME (Fig. 2G) and did not modify the autophagic response triggered by LLOME, as measured by LC3 lipidation (Fig. 2H). This was further confirmed in stable HEK293T cells inducibly expressing LRRK2 (fig. S3, F and G). Together, our data suggest that LRRK2 plays a lysophagy-independent role in response to lysosomal membrane permeabilization (Fig. 2I). We therefore considered whether LRRK2 recruitment occurs before the lysosomal membrane is ruptured enough to recruit Gal3 and trigger lysophagy and whether JIP4 might be important in mediating effects of LRRK2 on lysosomal function.

LRRK2 recruits JIP4 to ruptured lysosomes in a kinase-dependent manner

As expected, exogenously expressed JIP4 translocates to the membrane of LRRK2-positive LYS in a time-dependent manner (Fig. 3A and fig. S4D). However, we noted the presence of several LRRK2-positive/JIP4-negative LYS, even after 6 hours of LLOME exposure (Fig. 3A). This result raised the possibility that exogenous tagged JIP4 may be competing with endogenous JIP4 in mouse astrocytes. We were unable to directly address this question in mouse cells as the JIP4 antibody did not produce signal above background in primary astrocytes. However, the same antibody did produce staining in human cells, and we therefore instead used inducible HEK293T lines. Endogenous JIP4 was observed on LRRK2-positive LYS after LLOME treatment in HEK293T cells (fig. S4, B and C), at relatively more rapid time points than with exogenous JIP4, being visible at 2 hours of treatment. We also noted that the addition of LLOME did not alter protein levels of endogenous JIP4 (fig. S4A). MLi-2 treatment numerically decreased the lysosomal localization of LRRK2, but this effect was not statistically significant ($P = 0.09$; fig. S3, C to E), whereas this treatment completely blocked the recruitment of JIP4
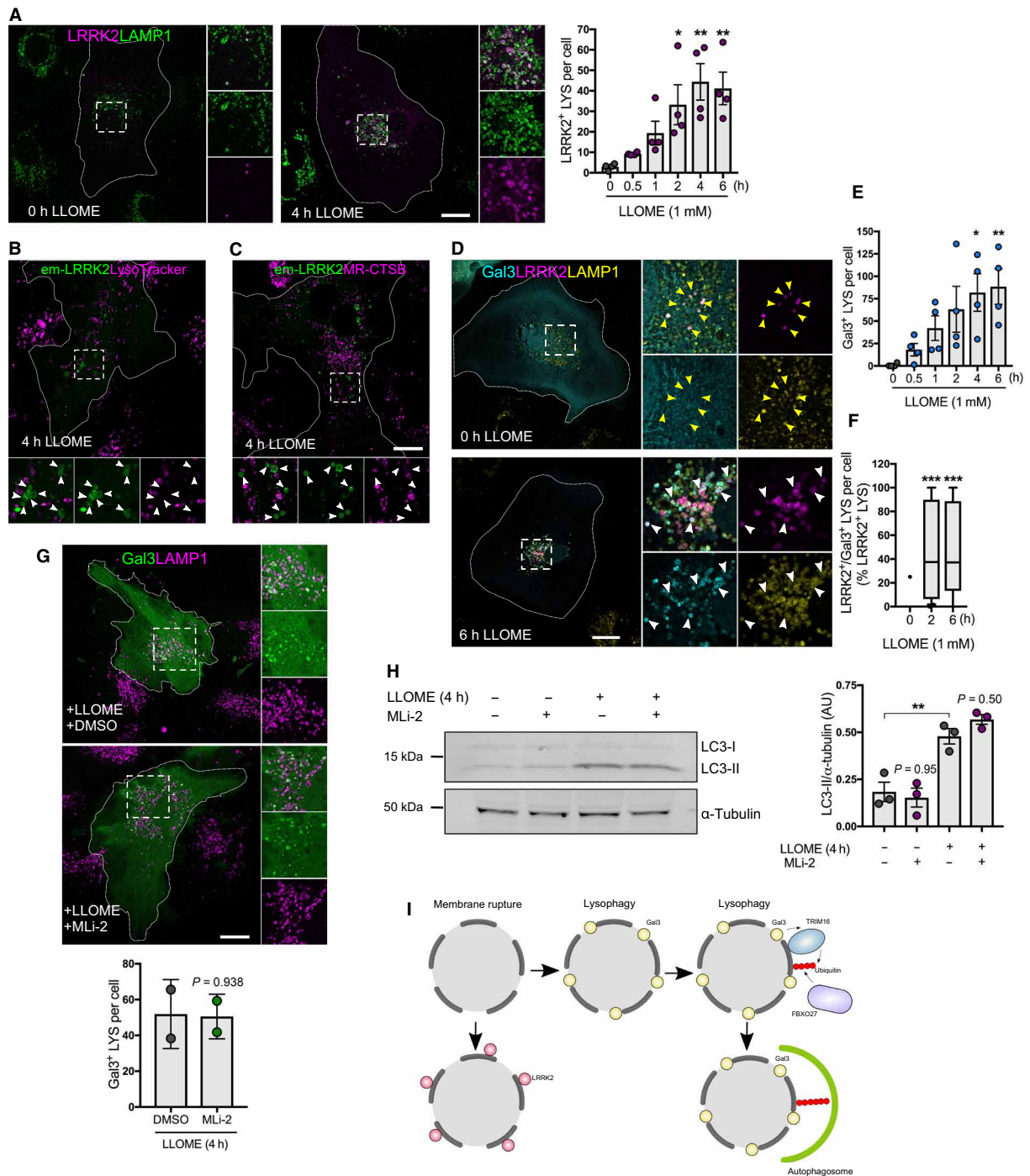
Fig. 2. Lysosomal membrane permeabilization enhances LRRK2 recruitment to the lysosomal membrane. (**A**) Confocal images of astrocytes untreated or treated with LLOME expressing 3xflag-LRRK2 and LAMP1. The histogram shows the number of LRRK2-positive lysosomes per cell. Data are mean ± SEM ($n = 20$ cells per N, $N = 5$). One-way ANOVA with Dunnett's. (**B** and **C**) Live-cell confocal images of astrocytes expressing Emerald-GFP-LRRK2 exposed to LysoTracker Red DND-99 (B) or Magic Red CTSB (C) and treated with LLOME. White arrowheads show absence of colocalization between LRRK2 and the two dyes. (**D** to **F**) Confocal images of astrocytes expressing 3xflag-LRRK2, EGFP-Gal3, and LAMP1, untreated or treated with LLOME (D). Yellow arrowheads indicate absence of colocalization, while white arrowheads show colocalization. (E) Histogram shows the number of Gal3-positive lysosomes per cell in cotransfected cells. Data are means ± SEM. One-way ANOVA with Dunnett's ($n = 10$ to 20 cells per N, $N = 4$). (F) Colocalization analysis using $n = 20$ cells from a single experiment. The percentage of LRRK2-positive/Gal-positive lysosomes normalized by the total number of LRRK2-positive lysosomes was measured in each cell. Box plot shows the median, and the whiskers show the 10th to 90th percentile. One-way ANOVA with Dunnett's. (**G**) Confocal images of astrocytes expressing EGFP-Gal3 and LAMP1, pretreated with DMSO or MLi-2 and incubated with LLOME (4 hours). Data are means ± SD. Unpaired t test ($n = 20$ to 39 cells, $N = 2$). (**H**) Western blot of astrocytes pretreated with MLi-2 before adding LLOME. Histogram shows normalized LC3-II levels using two-way ANOVA with Tukey's. Data are means ± SEM from $n = 3$. AU, arbitrary units. (**I**) Working model suggesting that the function of LRRK2 at ruptured lysosomes is independent of lysophagy. Scale bar, 20 μm. *$P < 0.05$; **$P < 0.01$, ***$P < 0.001$.

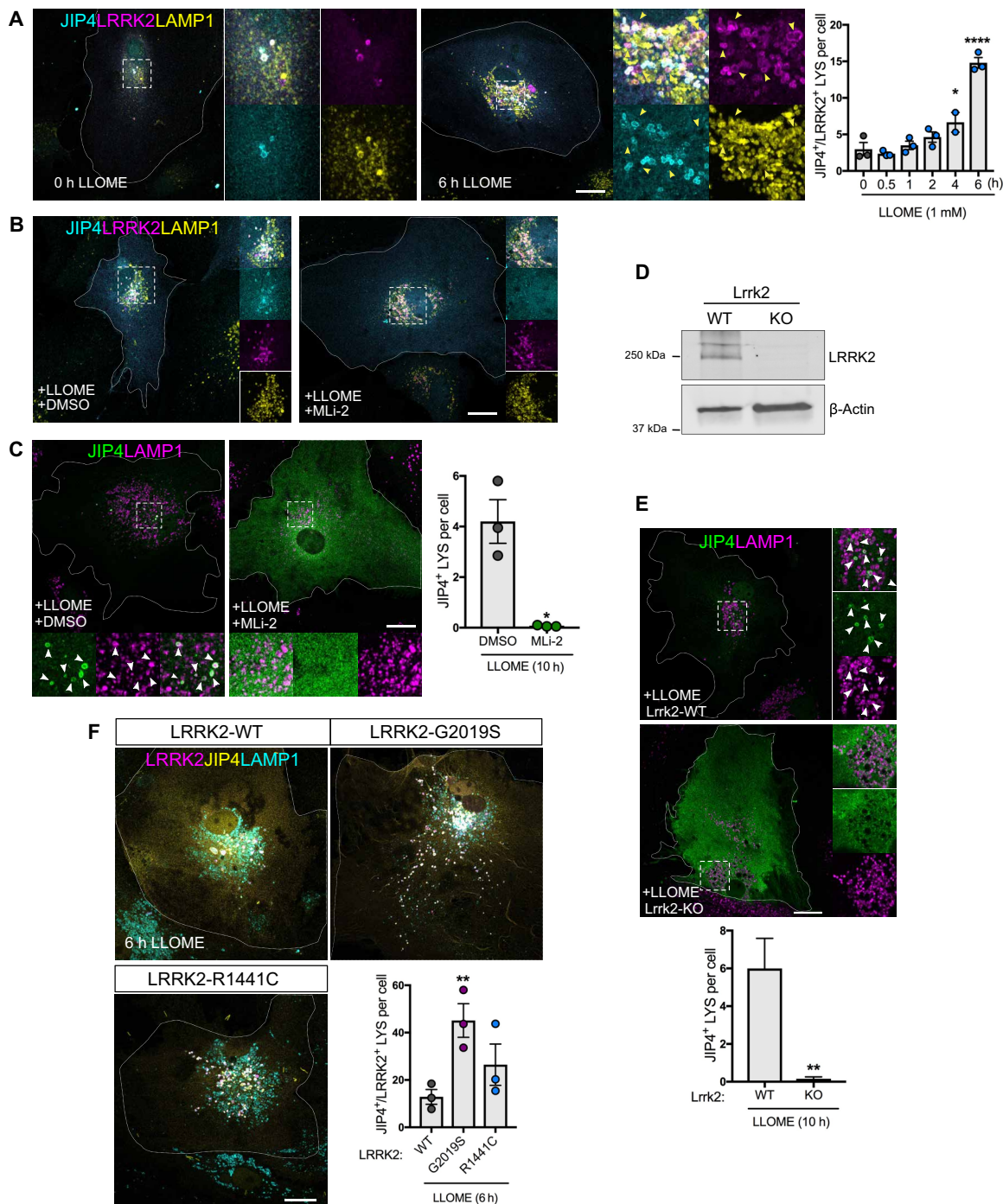**Fig. 3. LRRK2 recruits JIP4 through its kinase activity.** (**A**) Representative confocal images of astrocytes expressing 3xflag-LRRK2, GFP-JIP4, and LAMP1 untreated or treated with LLOME. Histogram depicts the number of JIP4-positive lysosomes per cell after LLOME ($n = 20$ cells per N, $N = 3$). Data are means ± SEM. One-way ANOVA with Dunnett's post hoc test. (**B**) Representative confocal images of astrocytes expressing 3xflag-LRRK2, GFP-JIP4, and LAMP1. Cells were pretreated with DMSO or MLi-2 and incubated with LLOME (6 hours). (**C**) Astrocytes expressing GFP-JIP4 and LAMP1 were pretreated with DMSO or MLi-2 before adding LLOME (10 hours). Histogram shows the number of JIP4-positive lysosomes per cell ($n = 20$ to 30 cells per N, from $N = 3$). Data are means ± SEM using unpaired t test with Welch's correction. (**D**) Western blot confirming lack of LRRK2 expression in KO astrocytes compared to WT. (**E**) Images of Lrrk2-WT or Lrrk2-KO astrocytes transfected with GFP-JIP4 and treated with LLOME (10 hours). Statistical analysis used an unpaired t test with Welch's correction ($n = 13$ cells per condition in a single experiment). (**F**) Astrocytes expressing GFP-JIP4 were cotransfected with 3xflag-LRRK2-WT, 3xflag-LRRK2-G2019S, or 3xflag-LRRK2-R1441C, stained for LAMP1, and treated with LLOME (6 hours). Histogram shows the number of JIP4-positive lysosomes per cell. Data are means ± SEM ($n = 20$ cells per N, from $N = 3$). One-way ANOVA with Dunnett's. Yellow arrowheads indicate LRRK2-positive/JIP4-negative lysosomes. White arrowheads show colocalization. Scale bar, 20 μm. *$P < 0.05$; **$P < 0.01$,****$P < 0.0001$.

to LRRK2-positive LYS (Fig. 3B), demonstrating that LRRK2 kinase activity is required for JIP4 translocation to the lysosomal membrane. JIP4 translocation was also seen in experiments where we did not transfect cells with LRRK2 (Fig. 3C and fig. S4D), thus showing that LRRK2 is able to recruit JIP4 while expressed at endogenous levels. Pharmacological kinase inhibition of endogenous LRRK2 was also able to arrest JIP4 lysosomal membrane localization (Fig. 3C). With endogenous LRRK2, the recruitment of JIP4 to the lysosomal membrane occurs 10 hours after LLOME addition (fig. S4D). These results demonstrate that increasing expression of LRRK2 accelerates JIP4 recruitment to the LYS surface in a kinase-dependent manner.

To confirm that these observations were not due to off-target effects of MLi-2, we compared the amount of lysosomal JIP4 in Lrrk2-WT and Lrrk2-KO astrocytes in the presence of LLOME. Consistent with previous data, cells lacking endogenous LRRK2 did not recruit JIP4 to the LYS membrane (Fig. 3, D and E). Conversely, cells expressing the G2019S mutation (fig. S3H) show a nearly threefold increase in the number of JIP4-positive LYS per cell compared to cells only expressing the WT form of the protein (Fig. 3F). These results further confirm that endogenous LRRK2 recruits JIP4 to damaged lysosomes in a kinase-dependent manner.

LRRK2 phosphorylates RAB10 and RAB35 at the lysosomal membrane

Because JIP4 recruitment to the lysosomal membrane is slower than LRRK2, we speculated that LRRK2 might require intermediate partners to recruit JIP4 after lysosomal membrane damage. LLOME addition was able to trigger LRRK2-lysosomal localization in HEK293FT cells tagged with APEX2 (fig. S5A), so we repeated the APEX2 proteomic analysis in these cells in the presence or absence of LLOME (Fig. 4A). From this screen, we found several endolysosomal markers, including LAMP2, LAMTOR2, PSAP, RAB25, and GABARAPL1/2, confirming by proteomics the enrichment of LRRK2 in the endolysosomal system after LLOME treatment (Fig. 4B and table S3). Two known substrates of LRRK2, RAB35 and RAB10, were also enriched by LLOME treatment (Fig. 4B). By staining for endogenous RAB35 in primary astrocytes, we observed a LLOME-driven recruitment of RAB35 to LRRK2-positive LYS (Fig. 4C), with similar results for a GFP-tagged version of RAB10 (Fig. 4D). We therefore asked whether lysosomal membrane permeabilization triggers an LRRK2-dependent phosphorylation of both RAB proteins. LLOME addition induces a strong increase in phospho-RAB10 (pT73) that is not seen in cells expressing the kinase-dead (K1906M) mutant LRRK2 or in cells treated with MLi-2 (Fig. 4E). Because there are no commercially available antibodies for phospho-RAB35, we used Phos-tag gels that allow the recognition of phosphorylated forms of proteins due to altered motility in acrylamide gels. Cells treated with LLOME show a nearly threefold increase in phospho-RAB35 levels (Fig. 4F), which was blocked by coincubation with MLi-2. The LRRK2 autophosphorylation site pS1292 was not sensitive to the addition of LLOME. To ensure that LRRK2-mediated RAB phosphorylation occurs at the lysosomal membrane, we exogenously expressed LRRK2 and RAB10 in the presence of LLOME and stained for phospho-RAB10 using the RAB10-pT73 antibody. As expected, the RAB10-pT73 signal colocalizes with LRRK2 in the lysosomal surface (Fig. 4G and fig. S5B). Collectively, these results show that lysosomal membrane damage triggers increased kinase activity toward RAB substrates.

LRRK2 recruitment of JIP4 occurs through RAB35 and RAB10 phosphorylation

We next asked whether LRRK2 could also recruit RAB35 and RAB10 to the lysosomal membrane in a kinase-dependent manner, similar to JIP4. LRRK2 pharmacological kinase inhibition completely prevented RAB35 and RAB10 recruitment to LRRK2-positive LYS (Fig. 4, H and I). In astrocytes expressing LRRK2 at endogenous levels, both RAB35 and RAB10 were recruited to the lysosomal membrane after LLOME treatment (fig. S5, C and D), and this was also blocked by MLi-2 (fig. S5, E and F). These results show that endogenous LRRK2 is able to relocalize both RAB proteins to LYS in a kinase-dependent manner. As both RAB35 and RAB10 are recruited to the LYS in a similar fashion to LRRK2, we wanted to determine if RAB35 or RAB10 was important to maintain LRRK2 at the lysosomal membrane. However, depletion of RAB35 and RAB10 expression (fig. S5, G and H) did not alter the ability of LRRK2 to translocate to lysosomes (fig. S5I). Together, our data indicate that LRRK2 precedes and mediates the recruitment of RAB35 and RAB10 to LYS in a kinase-dependent fashion.

In astrocytes transiently transfected with tagged versions of LRRK2, JIP4, and RAB35 and stained for endogenous RAB10, all four proteins are present in the same structures (fig. S6A), suggesting a possible link between the two RAB proteins and JIP4. JIP4 has been previously shown to require several RAB GTPases to ensure its presence in the recycling endosomal membrane (30), so we hypothesized that LRRK2 is able to recruit JIP4 to ruptured LYS via phosphorylation of RAB35 and RAB10. First, we examined the response of RAB35/RAB10 mutants that cannot be phosphorylated by LRRK2 (T72/73A) to LLOME compared to their WT counterparts. Both RAB phospho-null mutants had a significantly lower lysosomal localization after LLOME treatment and were instead found diffusely distributed in the cytosol (fig. S6, B and C). Next, we asked whether the phospho-null version of RAB GTPases affects the recruitment of JIP4 to LYS. For both RAB35 and RAB10, cells expressing the phospho-null mutation were unable to recruit JIP4 to the lysosomal membrane, even in those cells where RAB35-T72A and RAB10-T73A had a lysosomal localization (Fig. 4, J and K). Furthermore, cells knocked down for RAB10 showed significantly lower JIP4 presence on lysosomes (fig. S6D) after LLOME addition, while the effect of RAB35 depletion did not reach statistical significance ($P = 0.09$). Using coimmunoprecipitation in cells treated with LLOME, we were able to see endogenous JIP4 physically interacting with RAB10-WT but not RAB10-T73A (Fig. 4L). Under the same conditions, we failed to detect a physical interaction between JIP4 and RAB35. Together, our data show that LRRK2 recruits JIP4 through the phosphorylated form of RAB10, and JIP4 is a RAB downstream interactor in the context of lysosomal membrane damage.

JIP4 enhances the formation of tubular structures emanating from lysosomes

To further investigate the JIP4 in the lysosomal membrane, we imaged primary astrocytes transfected with LRRK2 and JIP4 using an Airyscan detector. The improved resolution of this approach allowed us to observe the presence of JIP4-positive/LRRK2-negative/LAMP1-negative tubular structures that stem from LYS in LLOME-treated astrocytes (Fig. 5, A and B, and movie S1). Consistent with the observation that the G2019S mutation leads to higher recruitment of JIP4 to the LYS, this mutation was also associated with a higher number of tubules in the cell (Fig. 5C). JIP4-positive lysosomal tubules
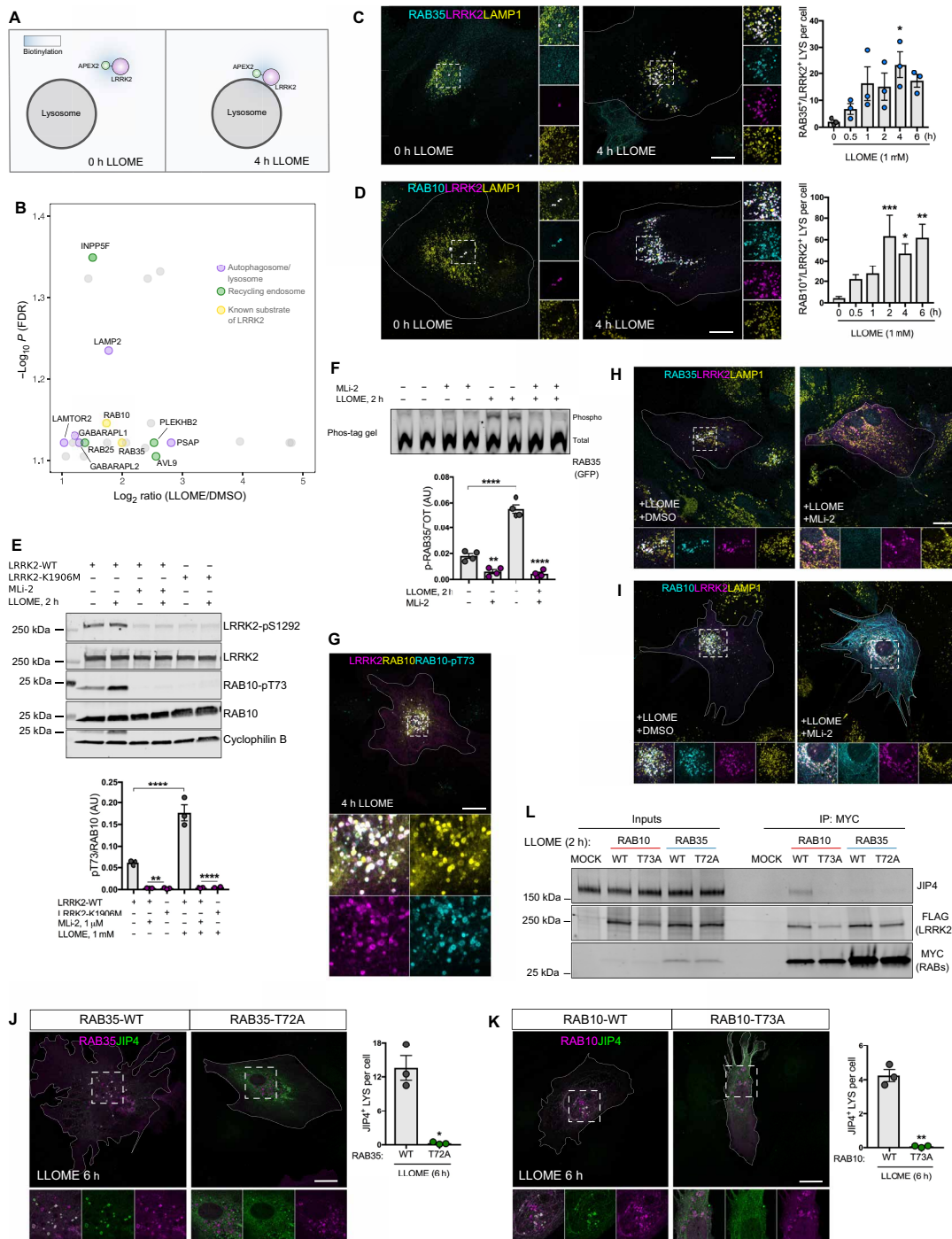
Fig. 4. LRRK2 phosphorylates RAB35 and RAB10 in the membrane of ruptured lysosomes. (**A**) Cartoon of the APEX2 screening in HEK293FT cells in the presence or absence of LLOME. (**B**) Volcano plot showing the subset of proteins with fold change > 2 and false discovery rate (FDR)–corrected $P < 0.08$ ($n = 3$) in proximity with LRRK2 in LLOME-treated cells. (**C** and **D**) Astrocytes expressing 3xflag-LRRK2, RAB35 (C), GFP-RAB10 (D), and LAMP1 treated or not with LLOME. The number of RAB35-positive (C) ($n = 20$ cells per N, $N = 3$) or RAB10-positive (D) ($n = 20$ cells in a single experiment) lysosomes per cell was quantified. Data are means ± SEM. One-way ANOVA with Dunnett's. (**E**) Western blot images of HEK293FT cells transfected with 3xflag-LRRK2 (WT or K1906M) and pretreated with DMSO or MLi-2 before LLOME was added. Data are means ± SEM ($n = 4$). Two-way ANOVA with Tukey's. (**F**) Phos-tag gel image of HEK293FT cells expressing 3xflag-LRRK2 and GFP-RAB35, pretreated with DMSO or MLi-2 and incubated with LLOME. Normalized phospho-RAB35 levels were measured ($n = 4$). Data are means ± SEM. Two-way ANOVA with Tukey's. (**G**) Astrocyte expressing 3xflag-LRRK2, 2xmyc-RAB10, and RAB10-T73. (**H** and **I**) Astrocytes expressing 3xflag-LRRK2, RAB35 (H), GFP-RAB10 (I), and LAMP1 pretreated with DMSO or MLi-2 and incubated with LLOME. (**J** and **K**) Astrocytes were transfected with GFP-JIP4 and 2xmyc-RAB35-(WT/T72A) (J) or 2xmyc-RAB10-(WT/T73A) (K) and treated with LLOME. JIP4-positive lysosomes per cell were quantified ($n = 20$ cells per N, $N = 3$). Unpaired t test with Welch's. Data are means ± SEM. (**L**) HEK293FT cells transfected with 3xflag-LRRK2 along with 2xmyc-RAB10-(WT/T73A) or 2xmyc-RAB35-(WT/T72A) were treated with LLOME, and lysates were subjected to immunoprecipitation with anti-myc antibodies. White arrowheads indicate colocalization. Scale bar, 20 μm. *$P < 0.05$, **$P < 0.01$, ***$P < 0.001$, ****$P < 0.0001$.
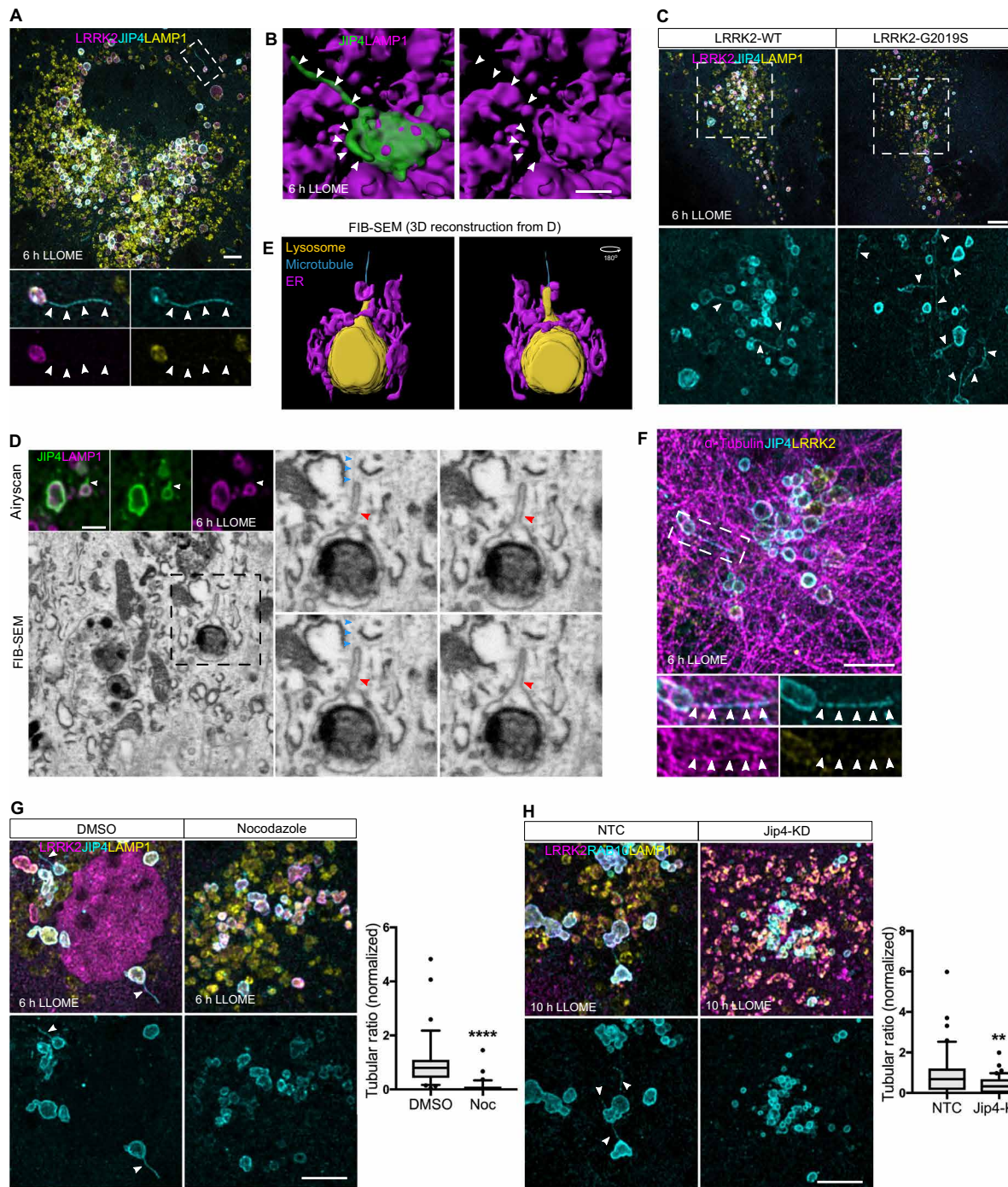
Fig. 5. JIP4 promotes the formation of LAMP1-negative lysosomal tubular structures. (**A**) Representative Airyscan image of a LLOME-treated astrocyte (6 hours) express-ing GFP-JIP4, 3xflag-LRRK2, and LAMP1. (**B**) Three-dimensional (3D) surface reconstruction was done in astrocytes treated with LLOME (6 hours) and previously transfected with 3xflag-LRRK2, mNeonGreen-JIP4, and LAMP1-HaloTag. (**C**) Super-resolution images comparing the number of JIP4-positives tubules in cells expressing LRRK2-WT and G2019S after LLOME treatment (6 hours). (**D**) FIB-SEM image of a tubule stemming from a lysosome in a 3xflag-LRRK2-G2019S–transfected astrocyte. Top panel shows the LAMP1-HaloTag/mNeonGreen-JIP4–labeled lysosomes. Bottom panel shows the correlated EM image, and right panel shows a lysosome with a tubule in different z planes. (**E**) 3D surface reconstruction of (D) showing a microtubule and the endoplasmic reticulum (ER) in contact with the lysosome. (**F**) Super-resolution image of an astrocyte expressing 3xflag-LRRK2-G2019S, GFP-JIP4, and α-tubulin. (**G**) Representative super-resolution images of astrocytes expressing 3xflag-LRRK2-G2019S, GFP-JIP4, and LAMP1 and treated with LLOME (6 hours). Cells were treated with DMSO or nocodazole (Noc). JIP4 tubulation index was measured using an unpaired t test with Welch's correction (n = 36 to 38 cells pooled from three experiments). Box plot shows the median, and the whiskers show the 10th to 90th percentile. (**H**) Confocal super-resolution images of astrocytes expressing 3xflag-LRRK2-G2019S, RAB10, and LAMP1 and incubated with LLOME (10 hours). RAB10 tubulation index was measured using an unpaired t test with Welch's correction (n = 41 cells pooled from two experiments). Box plot shows the median, and the whiskers show the 10th to 90th percentile. White and red (FIB-SEM picture) arrowheads indicate lysosomal tubular structures, and blue arrowheads indicate microtubules. Scale bar, 5 μm or 2 μm (B and D). *P < 0.05, **P < 0.01, ****P < 0.0001.

were also negative for LAMP1 when imaging living cells (fig. S6E). Furthermore, these tubules were negative for LIMP2, another typical lysosomal membrane marker (fig. S6F), and for the lysosomal luminal marker Dextran-555 (fig. S6G).

Next, we analyzed the tubular structures using focused ion beam scanning electron microscopy (FIB-SEM) on astrocytes incubated with LLOME. We first observed that the JIP4/LAMP1-positive compartments contained electron-dense structures (Fig. 5D, fig. S7A, and movie S2), consistent with their lysosomal nature. Typically, the parent lysosomes contained what appear to be partially degraded content, confirming our previous assumption that these are enzymatically inactive lysosomes. By analyzing the JIP4-positive tubules at the structural level, we were able to confirm that the tubular membrane originates from the lysosomal membrane (red arrowheads in Fig. 5D and fig. S7, A and B). We also noted that JIP4-positive lysosomal tubules display variable morphologies, particularly in relation to overall length and thickness (Fig. 5D; fig. S7, A and B; and movie S2), suggesting a dynamic process of their generation and resolution.

We detected microtubules connecting with JIP4-positive tubules (Fig. 5D, blue arrowheads). It has been shown that JIP4, through its interaction with motor proteins and microtubules, is required for the formation of endosomal sorting tubules (31). Consistent with the FIB-SEM observations, we saw JIP4-positive tubules that colocalized with α-tubulin (Fig. 5E) and disruption of microtubules with nocodazole was associated with a prevention of tubule formation (Fig. 5F), indicating that these structures are dependent on microtubules. Endogenous RAB10, but not RAB35, was present in a subset of JIP4-positive tubules (fig. S7, C and D), consistent with the coimmunoprecipitation results obtained in Fig. 4L. This observation allowed us to use RAB10 as a marker protein to determine whether JIP4 was necessary for tubule formation. Overexpression of JIP4 leads to an increase in the number of RAB10-labeled tubules (fig. S7F), and cells knocked down for JIP4 (fig. S7E) showed fewer RAB10-positive tubules (Fig. 5G) in LLOME-exposed astrocytes. Therefore, JIP4 is required for the extension of lysosomal membranes into tubules, likely via an interaction with microtubules.

JIP4-positive tubules release vesicular structures that interact with other lysosomes

We next used super-resolution imaging to observe tubular dynamics in living cells, without fixation after LLOME treatment. JIP4-positive tubules bud, extend, and release from lysosomes to form vesicular structures that were released into the cytosol (Fig. 6, A and E, and movies S3 and S4). JIP4-positive vesicles were observed to have several different behaviors, in that the scission can occur at the base of the tubule or from the tip (Fig. 6A and movie S3). Alternatively, tubules can retract into a vesicle that is ejected to the cytosol (Fig. 6, A to E, and movies S3 and S4). The absence of SNX1, SNX3, and SNX27 at the tubule suggests a different sorting mechanism than that previously described (32) to recycle cargo such as CI-M6PR from endosomes to the TGN (fig. S7, G to I). Although JIP4-positive vesicles are motile in the cytosol, we often detected stationary vesicles in contact with other lysosomes (Fig. 6B). We could also identify moving vesicles that stop to interact with a lysosome transiently that are then released to move elsewhere (movie S5). Furthermore, using FIB-SEM, we were able to find a JIP4-positive vesicle contacting a lysosome (red arrowhead in Fig. 6C). The recipient lysosomes appear to be active, as the interactions occur at Magic Red CTSB–positive lysosomes for period of time up to 4 min (white arrowhead

in Fig. 6D and movie S6). Last, we occasionally observed a resolved tubule forming a vesicle that is then able to interact with other lysosomes (Fig. 6E and movie S4). Together, our data identify that LLOME-treated LYS forms JIP4-positive tubules to release vesicular structures that can then contact other lysosomes.

Our overall model is that LRRK2 is recruited to LYS that is not sufficiently damaged to trigger lysophagy. At the lysosomal membrane, LRRK2 is able to phosphorylate RAB35 and RAB10, leading to their retention in the membrane. This event is required to bring the motor adaptor protein JIP4 to the lysosomal membrane where it helps to form tubular structures along microtubules that can secondarily generate vesicles that can interact with other lysosomes (Fig. 6F). We call this newly described process LYsosomal Tubulation/sorting driven by LRRK2, or LYTL.

DISCUSSION

Although a genetic link between LRRK2 and PD was first reported in 2004 (1, 33), the role of this kinase in the cell remains uncertain. The localization of LRRK2 to intracellular membranes (34–36) and the observation that RAB GTPases are kinase substrates for LRRK2 (6, 7, 37) suggest that LRRK2 might be involved in vesicle-mediated transport (38). However, the major phenotype seen in LRRK2 KO animals or in animals treated with LRRK2 kinase inhibitors is accumulation of lysosomal damage (11, 22, 39). This suggests that a major role for endogenous LRRK2 is related to lysosomal function, but a specific mechanism that might explain this observation has not been identified to date. Here, we propose that mechanism is LYTL and that LRRK2 controls dynamic generation of vesicles from damaged lysosomes.

We speculate that LRRK2 may be recruited to lysosomes at a stage of membrane damage that is temporally before the presentation of Gal3 on the surface of the organelles but have not formally proven this conjecture at the present time. A deeper understanding of why LRRK2 is recruited to lysosomes, and what differentiates LRRK2 from Gal3 recruitment, will need to be addressed in the future. A notable feature of LYTL is the activation of LRRK2 kinase activity. This is reminiscent of activation at other membranes, including at the trans-Golgi network (TGN) (7, 40). However, activation of the TGN requires strong overexpression of RAB29, whereas LYTL requires only modest lysosomal membrane permeabilization, at levels less than those required to trigger lysophagy. Consequentially to activation, LRRK2 phosphorylates RAB35 and RAB10, leading to their retention in the lysosomal membrane, likely, in turn, due to diminished binding of p-RABs to GDI1/2 (15). At the same time, p-RABs are able to recruit JIP4 to the lysosomal surface, consistent with previous data showing enhanced binding of p-RABs to this motor adaptor protein (8). Previous literature suggests that phosphorylation-deficient RABs, including RAB8A (6) and RAB10 (16), retain their ability to interact with their respective guanine nucleotide exchange factors (GEFs), and we infer that is also likely to be true for RAB35. We therefore favor the hypothesis that the lack of ability of T72/73A versions of RAB10/RAB35 to be enriched on lysosomes is driven by diminished LRRK2-dependent phosphorylation rather than a lack of GEF-dependent activation. Our data suggest that RAB10 is the primary driver in the recruitment of JIP4; it is therefore possible that RAB35 plays a secondary role in bringing JIP4 to the lysosomal membrane and/or plays a different role once recruited by LRRK2. It is also plausible that the link between the RAB proteins and JIP4
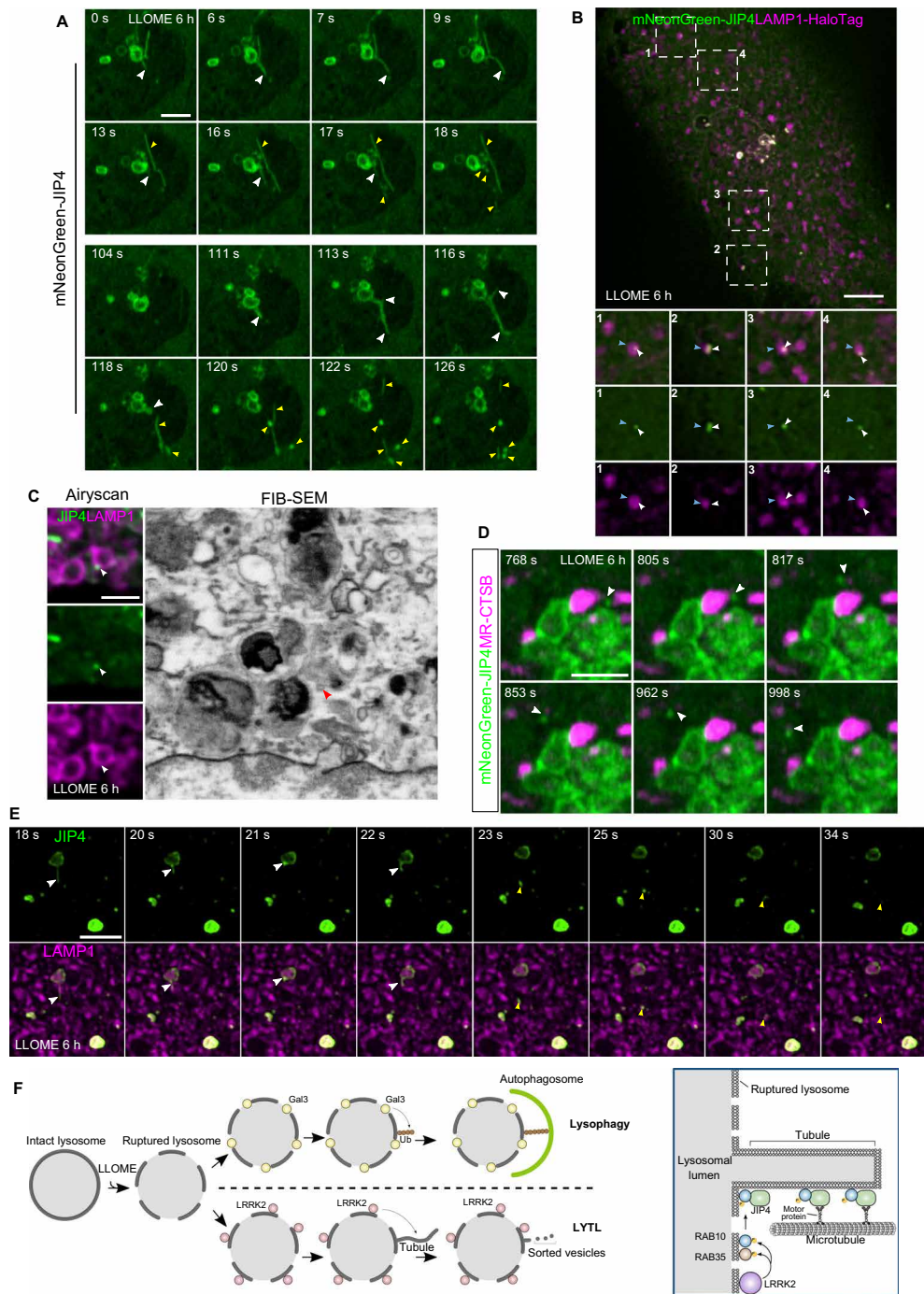
Fig. 6. JIP4-positive tubules are resolved in vesicular structures that contact with other lysosomes. (**A**) Time-lapse fast Airyscan confocal images of a LLOME-treated (6 hours) astrocyte expressing 3xflag-LRRK2-G2019S and mNeonGreen-JIP4 showing a group of JIP4-positive lysosomes for over 2 min, where the different tubular dynamics were under display (15 slices per frame were taken at 1 frame per second). (**B** and **C**) Astrocytes expressing 3xflag-LRRK2-G2019S, mNeonGreen-JIP4, and LAMP1-HaloTag and treated with LLOME (6 hours) were analyzed with a SoRa spinning disk super-resolution microscope. (B) A single frame of an astrocyte, where several JIP4-positive vesicles (white arrowhead) are in close proximity to other lysosomes (blue arrowhead). (C) Time-lapse confocal images of a resolved tubule that, after ejection to the cytosol, contacts other lysosomes (15 slices per frame, 1 frame per second). (**D**) FIB-SEM image of a JIP4-positive vesicle associated with a lysosome in a 3xflag-LRRK2-G2019S–transfected astrocyte after LLOME treatment (6 hours). Top panel shows the Airyscan image of a group of lysosomes (LAMP1) and a vesicle labeled with JIP4 (white arrow). Bottom panel shows the correlated EM image, with a red arrowhead pointing to the vesicle. (**E**) LLOME-treated astrocytes (6 hours) expressing 3xflag-LRRK2-G2019S and mNeonGreen-JIP4 and stained with Magic Red CTSB were analyzed with a fast Airyscan confocal microscope for almost 4 min, at 6.05 s per frame. (**F**) Schematic representation of our working model. White arrowhead marks a JIP4-positive vesicle associated with an active lysosome (red). White arrowheads indicate JIP4-positive lysosomal tubules, and yellow arrowheads show resolved tubules (vesicular structures and scissioned tubules) (A to C). Scale bars, 2 μm (D), 2.5 μm (A, C, and E), and 5 μm (B).

requires other steps or proteins beyond the phosphorylation by LRRK2. Thus, JIP4 acts as a RAB downstream interactor in the lysosomal membrane, similar to the role previously described for JIP4 in recycling endosomes (30).

Recently, Eguchi et al. (16) observed LRRK2 relocalization to LE/LYS in cells treated with chloroquine, a different lysosomotropic reagent that increases pH in lysosomes and late endosomes. Eguchi et al. proposed a scenario where LRRK2 promotes lysosomal exocytosis to release nondegraded cargo to the extracellular space. Our model is distinct in that JIP4-positive lysosomes failed to show a net movement toward the plasma membrane using live-cell imaging. The difference in lysosomal behavior may be related to the use of different cellular models (mouse primary astrocytes versus cancer cells) or the compound used to damage the lysosome (LLOME versus chloroquine). Exploration of the differences between different lysosomal damaging agents in different cell types may be mechanistically informative in future studies.

Sorting at other cellular compartments such as endosomes occurs through the formation of tubular structures that bud and extend from organelles. Tubular structures are then severed to produce vesicles that travel to the plasma membrane or the TGN (41). Our data show that JIP4 promotes the formation of tubular structures at the lysosome, which are to our knowledge described here for the first time, but may be similar to structures at other organelles including endosomes (31). It is likely that JIP4 mediates tubule dynamics by recruiting motor proteins (25), because we have demonstrated that tubule extension requires microtubules. JIP4-positive tubules undergo scission to generate smaller vesicular structures that travel through the cytosol and interact with other lysosomes and possibly other cellular organelles. Membrane contact sites have been shown to have different functions, such as the interchange of lipids, calcium, or other metabolites from one compartment to another (42). Neither the tubules nor the resolved material is positive for lysosomal membrane markers (LAMP1 or LIMP2), and the JIP4-positive tubules were resistant to paraformaldehyde (PFA) fixation. These observations argue against LYTL being involved in proto-lysosome formation through lysosomal reformation (LR), because LR tubules are amenable to PFA fixation (43) and positive for LAMP1 (44). LRRK2 has been associated (along with RAB2A) with the sorting of lysozyme from dense core vesicles (DCVs) in the gut (45). As astrocytes are considered a highly secretory cell in the central nervous system (46), LYTL could be used as an alternative sorting process beyond exosomes, DCVs, or secretory lysosomes, among others. Thus, the function of LYTL, including why lysosomes release membranous content and the overall effect of this sorting process in the cell, will require additional future investigations.

We view the activation of LRRK2 by lysosomal membrane permeabilization as an analogous process to the activation of another PD-associated kinase, PINK1, by mitochondrial damage (47). Specifically, one of the proposed functions of the PINK1/Parkin system during mitochondrial stress is the release of mitochondria-derived vesicles to lysosomes (48). These considerations may not directly suggest functional convergence of mitochondrial and lysosomal pathways but do indicate that there are multiple kinase-dependent events that can control function of organelles relevant to PD. However, indirectly, the ability of LRRK2 mutants to cause retention of RAB10 at the lysosomal membrane could prevent RAB10 from being recruited to depolarized mitochondria and, as a consequence, limit mitophagy (49).

Overall, we have identified a newly described cellular process that promotes lysosomal sorting material from lysosomes after induction of lysosomal membrane permeabilization. LYTL is controlled by LRRK2 kinase activity because the recruitment of all the downstream components is completely blocked by MLi-2. Conversely, the G2019S mutation in LRRK2 that is pathogenic for PD increases both the lysosomal localization of LRRK2 and JIP4 recruitment and tubulation. Considering the proposed centrality of lysosome biology in PD pathogenesis, it is possible that LYTL is involved in disease mechanisms. As increased lysosomal membrane damage has been associated with aging (50, 51), and aggregates or fibrils taken up by endocytosis can trigger lysosomal membrane permeabilization (52), it is possible that LYTL could be more active during aging and further enhanced in patients carrying LRRK2 pathogenic mutations, potentially contributing to neurodegeneration.

METHODS
Cell culture
All procedures with animals followed the guidelines approved by the Institutional Animal Care and Use Committee of the National Institute on Aging. Astrocyte cultures were prepared from C57BL/6J newborn (postnatal day 0) pups. Dissected mouse cortices were incubated in 1 ml/cortex Basal Medium Eagle (BME) (Sigma-Aldrich), containing 5 U of papain/(Worthington) for 30 min at 37°C. Five micrograms of deoxyribonuclease I was added to each cortex preparation, and brain tissue was dissociated into a cellular suspension that was washed twice with 10 volumes of BME and counted. Astrocyte cultures were plated in Dulbecco's modified Eagle's medium (DMEM) (Thermo Fisher Scientific), supplemented with 10% fetal bovine serum (FBS) (Lonza) into 75-cm^2 tissue culture flasks. For the preparation of purified astrocyte cultures, 7- to 10-day primary cultures were vigorously shaken to detach microglia and oligodendrocytes. Culture purity was assessed with GFAP for astrocytes, and OLIG2 and IBA1 to exclude oligodendrocytes and microglia. Cultures had >90% of astrocytes in all experiments. Astrocytes were used from passage 2 to passage 3.

HEK293FT cells were maintained in DMEM containing glucose (4.5 g/liter), 2 mM L-glutamine, and 10% FBS at 37°C in 5% CO$_2$. The HEK293T-inducible GFP-LRRK2-WT cell line was obtained from D. Alessi (University of Dundee), and expression was induced by addition of doxycycline (53). HEK293FT cells, HEK293T GFP-LRRK2 doxycycline-induced cells, and primary astrocytes were seeded on 12-mm coverslips precoated with Matrigel.

Reagents
LLOME (Sigma-Aldrich, L7393) was diluted in dimethyl sulfoxide (DMSO) and added at 1 mM for the indicated times. Nocodazole (Sigma-Aldrich, M1404) was diluted in DMSO and added at 10 μM 2 hours before fixation. Fixable Dextran–Alexa Fluor 555, 10 kDa (Thermo Fisher Scientific, D34679) was incubated for 6 hours (2.5 mg/ml). Cells were then washed three times with phosphate-buffered saline (PBS), and fresh medium was added to chase Dextran overnight (18 to 24 hours) before treating astrocytes with LLOME. MLi-2 (Tocris, 5756) was used at 1 μM, 90 min before LLOME addition. Magic Red CTSB was obtained from ImmunoChemistry Technologies (938) and incubated with cells at a dilution of 1:250 in medium for 30 min. Then, cells were washed three times with PBS before imaging. LysoTracker Red DND-99 (Thermo Fisher Scientific,

L7528) was added at 1 μM for 30 min before cells were washed three times with PBS and analyzed them using confocal microscopy. LAMP1-HaloTag–transfected cells were incubated with the JF646 peptide (Promega, GA1121) at 200 nM for 15 min, and cells were then washed three times and incubated with fresh medium before treated with LLOME.

Antibodies
The following primary antibodies were used: mouse anti-FLAG M2 [Sigma-Aldrich, F3165; 1:500 for immunocytochemistry (ICC) and 1:10,000 for western-blot (WB)], rabbit anti-JIP4 (Cell Signaling Technology; 5519, 1:1000 for WB and 1:100 for ICC), rat anti-LAMP1 [Developmental Studies Hybridoma Bank (DSHB), 1D4B; 1:100 for ICC], rat anti-LAMP2 (DSHB, 1:100 for ICC), mouse anti-LAMP2 (DSHB, H4B4; 1:100 for ICC), rat anti-FLAG (BioLegend, 637302; 1:100 for ICC), rabbit anti-RAB7A (Abcam, ab137029; 1:200 for ICC), rat anti-myc (Chromotek, 9e1-100; 1:500 for ICC), chicken anti-GFP (Aves Lab, GFP-1020; 1:500 to 1:1000 for ICC), mouse anti-GFP (Roche, 11814460001; 1:10,000 for WB), goat anti-CTSB (R&D Systems, AF965; 1:500 for ICC), mouse anti–α-tubulin (Cell Signaling Technology, 3873; 1:350 for ICC and 1:15,000 for WB), rabbit anti-RAB35 (Proteintech, 11329-2-AP; 1:100 for ICC and 1:1000 for WB), rabbit anti-RAB10 (Abcam, ab237703; 1:100 for ICC and 1:1000 for WB), rabbit anti-RAB10 (phospho-T73) (Abcam, ab241060; 1:100 for ICC and 1:1000 for WB), rabbit anti-LRRK2 (Abcam, ab133474; 1:1000 for WB), rabbit anti-LRRK2 (phospho-S1292) (Abcam, ab203181; 1:1000 for WB), rabbit anti-EEA1 (Cell Signaling Technology, 3288; 1:100 for ICC), mouse anti–β-actin (Sigma-Aldrich, A5441; 1:15,000 for WB), rabbit anti-LC3B (Cell Signaling Technology, 2775; 1:1000 for WB), and rabbit anti–cyclophilin B (Abcam, ab16045; 1:15,000 for WB).

For ICC, unless otherwise stated, the secondary antibodies were purchased from Thermo Fisher Scientific. The following secondary antibodies were used: donkey anti-mouse Alexa Fluor 568 (A10037, 1:500), donkey anti-rabbit Alexa Fluor 488 (A-21206, 1:500), donkey anti-mouse Alexa Fluor 568 (A-21202, 1:500), donkey anti-rat Alexa Fluor 488 (A-21208, 1:500), donkey anti-goat Alexa Fluor 488 (A-11055, 1:500), donkey anti-rabbit Alexa Fluor 568 (A10042, 1:500), donkey anti-mouse Alexa Fluor 647 (A-31571, 1:500), and goat anti-rat Alexa Fluor 647 (A-21247, 1:250 to 1:500). Donkey anti-chicken Alexa Fluor 488 (703-545-155, 1:500) and donkey anti-rat Alexa Fluor 405 (712-475-153, 1:100) were obtained from Jackson ImmunoResearch.

Cloning
Constructs for 3xflag-tagged LRRK2 WT/full length and domains, and GUS have been described previously (7, 54). JIP3, JIP4, and BICD2 Gateway PLUS shuttle clones were obtained from GeneCopoeia. BLOS1, MUTED, and STAM1 complementary DNA (cDNA) were obtained from Dharmacon. RAB35, RAB10, and APEX-NES cDNA were acquired from Addgene (Addgene, #49552, #49472, and #49386) (55–57). cDNAs were amplified with polymerase chain reaction (PCR) and cloned into pCR8/GW/TOPO vector (Thermo Fisher Scientific). Each was then subcloned into pDEST vectors using Gateway technology (Thermo Fisher Scientific). Full-length LRRK2 was subcloned into the pDEST-Emerald GFP and p3xflag-APEX2-DEST vectors; JIP3, STAM1, BICD2, BLOS1, and MUTED were subcloned into pDEST-53; JIP4 was also subcloned into pDEST-NeonGreen; RAB35 was subcloned into pDEST-53 and the pCMV-2xmyc-DEST vectors; and RAB10 was subcloned into pCMV-2xmyc-DEST plasmid.

2xmyc-RAB10-T73A and 2xmyc-RAB35-T72A were generated by directed mutagenesis from the WT vectors using the QuikChange Lightning Kit (Agilent). EGFP-RAB10 (Addgene, #49472) (56), EGFP-Gal3 (Addgene, #73080) (29), and LAMP1-RFP (Addgene, #1817) (58) were purchased from Addgene. The LAMP1-HaloTag construct was provided by the Bonifacino laboratory, and the LIMP2-myc vector was a gift from M. Schwake (59). All primers used for cloning are in table S5, and the expression constructs used in this study are summarized in table S4.

Transfection
Transient transfections of HEK293FT cells and astrocytes were performed using Lipofectamine 2000 and Stem reagents, respectively (Thermo Fisher Scientific). HEK293FT cells were transfected for 24 hours, and mouse primary astrocytes were transfected for 48 hours. For small interfering RNAs (siRNAs), cells were transfected with the SMARTpool ON-TARGET (Dharmacon) plus scramble or Rab35, Rab10, or Jip4 siRNAs using Lipofectamine RNAiMAX (Thermo Fisher Scientific) transfection reagent for astrocytes. Astrocytes were incubated with siRNA for a total of 4 days before fixation or lysis.

APEX2 reaction
HEK293FT cells were plated in 150-cm^2 flasks previously coated with Matrigel and transfected with the appropriate vectors. Twenty-four hours later, 500 μM biotin-phenol was preincubated with cells for 30 min at 37°C. H_2O_2 (1 mM) was added for 1 min while gently mixing, and the cells were subsequently washed twice with quenching buffer [tris-buffered saline (TBS) supplemented with 1 mM $CaCl_2$, 10 mM sodium ascorbate, 1 mM sodium azide, and 1 mM Trolox], once with PBS, and twice with quenching buffer for 1 min per wash. Cells were collected in 10 ml of quenching buffer and centrifuged at 3000g for 10 min. Cells were lysed in radioimmunoprecipitation assay (RIPA) buffer (Pierce) supplemented with 10 mM sodium ascorbate, 1 mM sodium azide, 1 mM Trolox, 1 mM dithiothreitol, and protease inhibitors (Roche Complete). Samples were briefly sonicated and pelleted at 10,000g for 10 min, and then equal amounts of proteins were applied to streptavidin magnetic beads (Thermo Fisher Scientific) and incubated for 1 hour at room temperature (RT) on a rotator. Cells were then washed sequentially with KCl (1 M), Na_2CO_3 (0.1 M), and urea (2 M) in 0.1 M tris buffer followed by two final washes with RIPA buffer. Beads were eluted by boiling in 45 μl of 2× protein loading buffer supplemented with 2 mM biotin and β-mercaptoethanol for 10 min. Protein lysates were loaded on an acrylamide gel and run for 1 hour at 150 V. The gel was then stained with GelCode Blue stain (Thermo Fisher Scientific) for 30 min and washed with dH_2O overnight.

Mass spectrometry analysis
Protein was quantified, and the lysates were mixed in a 1:1 ratio (light:heavy), with a final number of two to three replicates. Lysates were separated on a 4% to 20% polyacrylamide gel (Bio-Rad). Eight bands were cut from each replicate. Gel bands were reduced with tris(2-carboxyethyl)phosphine, alkylated with N-ethylmaleimide (NEM), and digested with trypsin. The system used for data acquisition is an Orbitrap Lumos mass spectrometer (Thermo Fisher Scientific) coupled with an UltiMate 3000 high-pressure liquid chromatography instrument (Thermo Fisher Scientific). Extracted peptides were desalted and then separated on an ES803 column (Thermo Fisher Scientific) using a gradient with mobile phase B (MP B) increasing from 5 to 27% over 60 min. The composition of MP A and MP B is

0.1% formic acid in 100% high-performance liquid chromatography (HPLC) acetonitrile. The liquid chromatography–tandem mass spectrometry (LC-MS/MS) data were acquired in data-dependent mode. The survey scan was performed in Orbitrap with the following parameters: mass range, 350 to 1500 mass/charge ratio (m/z); resolution, 120,000 at m/z 400; automatic gain control (AGC) target, 4×10^5 ions. The product scan was performed in ion trap with the following parameters: collision-induced dissociation on as many precursor ions as allowed in 3 s; isolation window, 1.6 Da. Database search and ratio calculation were performed using Proteome Discoverer 2.2 software. Conditions used in the database are listed below. Database: Sprot Human database; modifications: 13C(6) (R), 13C(6) (K), oxidation (M), NEM(C). Heavy/Light (H/L) ratios are calculated for each sample with (Fig. 4) or without (Fig. 1) normalization.

Phos-tag gels

HEK293FT cells were transfected with 3xflag-LRRK2 and GFP-RAB35 plasmids and, 24 hours later, treated with LLOME or DMSO for 2 hours. Cells were then lysed in 10× cell lysis buffer (Cell Signaling Technology) supplemented with EDTA-free protease inhibitor (Roche) and 1× Halt phosphatase inhibitor. Lysates were cleared by centrifugation at 20,000g. Phos-tag SDS–polyacrylamide gel electrophoresis (PAGE) was performed following the vendor's instructions (Wako). Briefly, gels for Phos-tag SDS-PAGE consisted of a stacking gel [4.5% acrylamide, 350 mM bis-tris/HCl, tetramethylethylenediamine (TEMED), and 0.05% ammonium persulfate (APS)] and a separating gel (12% acrylamide, 350 mM bis-tris/HCl, 50 μM Phos-tag solution, 100 μM ZnCl$_2$, TEMED, and 0.05% APS). Lysates were electrophoresed at 80 V for the stacking gel and at 150 V for the separating gel. After SDS-PAGE, the gels were washed twice (20 min each) with transfer buffer containing 10 mM EDTA. Gels were transferred to membranes by a semidry Trans-Blot Turbo transfer system (Bio-Rad).

Confocal microscopy

Confocal images were taken using a Zeiss LSM 880 microscope equipped with a 63× 1.4 numerical aperture (NA) objective. Super-resolution imaging was performed using the Airyscan mode. Raw data were processed using Airyscan processing in "autostrength" mode with Zen Black software version 2.3. Live-cell super-resolution imaging was performed in Fast Airyscan mode on an inverted Zeiss LSM 880 Fast Airyscan microscope equipped with a 63× 1.4 NA objective, and environmental chamber to maintain cells at 37°C with humidified 5% CO2 gas during imaging. Immersion oil for 37°C was used during imaging.

For spinning disk super-resolution microscopy, we used a W1-SoRa super-resolution spinning disk microscope (Nikon) with a 60× 1.49 NA oil immersion objective and a ×2.8 intermediate magnification (×168 combined), with an offset micro-lensed SoRa disk and environmental chamber to maintain cells at 37°C with humidified 5% CO2 gas during imaging. For deconvolution, we used 10 iterations of the Landweber algorithm. Images from two channels were acquired simultaneously using a Cairn twin-cam emission splitter and two Photometrics prime 95b sCMOS cameras, a 565LP DM, and appropriate emission cleanup filters. Unless otherwise stated, pictures are maximum intensity projection from Z stacks.

Tubular ratio measurements

Astrocytes were transfected with the 3xflag-LRRK2-G2019S plasmid and cotransfected or not with the GFP-JIP4 vector. After fixation

and staining, cells were imaged with a confocal microscope using the Airyscan module to enhance resolution. The tubular ratio in each cell was measured as follows: Ratio = #JIP4 + tubules/#JIP4 + lysosomes. A similar approach was used for endogenous RAB10. For each independent replicate, the ratio was normalized by the average value of the control group (i.e., DMSO, NTC, and MOCK). Data were generated from cells pooled across at least two independent experiments. Only cells with 10 or more JIP4 or RAB10-positive lysosomes per cell were imaged.

Coimmunoprecipitation

HEK293FT cells transfected with 3xflag-LRRK2, 2xmyc-RAB10, 2xmycRAB10-T73A, 2xmyc-RAB35, and 2xmyc-RAB35-T72A plasmids were lysed in IP buffer [20 mM tris-HCl (pH 7.5), 300 mM NaCl, 1 mM EDTA, 0.3% Triton X-100, 10% glycerol, 1× Halt phosphatase inhibitor cocktail (Thermo Fisher Scientific), and protease inhibitor cocktail (Roche)] for 30 min on ice. Lysates were centrifuged at 4°C for 10 min at 20,000g, and the supernatant was further cleared by incubation with EZview™ protein G agarose beads (Sigma-Aldrich) for 30 min at 4°C (only for FLAG IP). After agarose bead removal by centrifugation, lysates were incubated with anti-flag M2 agarose beads (Sigma-Aldrich) or myc-Trap agarose beads (Chromotek) for 1 hour at 4°C on a rotator. Beads were washed six times with IP wash buffer [20 mM tris-HCl (pH 7.5), 300 mM NaCl, 1 mM EDTA, 0.1% Triton X-100, 10% glycerol] and eluted in 1× kinase buffer (Cell Signaling Technology) containing 150 mM NaCl, 0.02% Triton X-100, and 3xflag peptide (150 ng/μl) (Sigma-Aldrich) by shaking for 30 min at 4°C (for FLAG IP) or by boiling samples in 2× loading buffer with β-mercaptoethanol for 5 min (for MYC IP).

Immunostaining

Primary cultures of astrocytes or HEK293FT cells were fixed with 4% PFA for 10 min, permeabilized with PBS/0.1% Triton X-100 for 10 min, and blocked with 5% donkey serum for 1 hour at RT. Primary antibodies were diluted in blocking buffer (1% donkey serum) and incubated overnight at 4°C. After three 5-min washes with PBS/0.1% Triton X-100, secondary fluorescently labeled antibodies were diluted in blocking buffer (1% donkey serum) and incubated for 1 hour at RT. Coverslips were washed twice with 1× PBS and an additional two times with dH$_2$O and mounted with ProLong Gold antifade reagent (Thermo Fisher Scientific).

SDS-PAGE and Western blotting

Proteins were resolved on 4 to 20% Criterion TGX precast gels (Bio-Rad) and transferred to membranes by a semi-dry Trans-Blot Turbo transfer system (Bio-Rad). The membranes were blocked with Odyssey Blocking Buffer (LI-COR, catalog no. 927-40000) and then incubated for 1 hour at RT or overnight at 4°C with the indicated primary antibody. The membranes were washed in TBS-Triton (TBS-T) (3 × 5 min) followed by incubation for 1 hour at RT with fluorescently conjugated goat anti-mouse, rat, or rabbit IRDye 680 or 800 antibodies (LI-COR). The blots were washed in TBST (3 × 5 min) and scanned on an Odyssey CLx (LI-COR). Quantitation of Western blots was performed using Image Studio (LI-COR).

Sample preparation for FIB-SEM

Following Airyscan microscopy, cells were fixed and processed largely as previously described (60) with small modifications. After dehydration, the MatTek glass coverslip was removed from the plastic using

propylene oxide. The removed glass coverslip was then rinsed in 100% ethanol followed by immersion in mixtures of Durcupan ACM and ethanol with the following ratios: 25:75 for 1.5 hours, 50:50 for 1.5 hours, 75:25 overnight. The sample was then immersed in 100% Durcupan ACM for 4 to 5 hours with replacement of fresh Durcupan every hour. The glass coverslip was then removed, and excess Durcupan was removed using filter paper. The coverslip was then placed in an oven at 60°C for 10 min, after which the sample was placed vertically in a 50-ml Falcon tube in folded filter papers and centrifuged for 15 min at 37°C and 750 relative centrifugal force (RCF). The glass coverslip was then placed in an oven at 60°C under vacuum and left to polymerize over 2 days. The sample was then sputter-coated with 50-nm gold and painted with silver paint, followed by drying under vacuum. The samples were imaged inside a Zeiss Crossbeam 540 FIB-SEM microscope. Platinum and carbon were deposited over the region of interest, and the run was set up and controlled by Atlas software (Fibics) SEM settings: 1.5 kV; 2.0 nA; milling probe: 300 pA. The slice thickness and the voxel size were set to 6 nm. The total volume acquired per tissue sample (XYZ) was 44.21 m × 4.22 m × 27.38 m.

Statistical analysis

Analyses based on cell counts were performed by an investigator blinded to treatment/transfection status. Statistical analysis for experiments with two treatment groups used Student's t tests with Welsh's correction for unequal variance. For more than two groups, we used one-way analysis of variance (ANOVA) or two-way ANOVA where there were two factors in the model. Tukey's post hoc test was used to determine statistical significance for individual comparisons in those cases where the underlying ANOVA was statistically significant and where all groups were compared; Dunnett's multiple comparison test was used where all groups were compared back to a single control group. Individual points in histograms represent the mean of each independent replicate (N). Unless otherwise stated, graphed data are presented as means ± SEM. Comparisons considered statistically significant are indicated: $*P < 0.05$; $**P < 0.01$; $***P < 0.001$; $****P < 0.0001$.

SUPPLEMENTARY MATERIALS

Supplementary material for this article is available at http://advances.sciencemag.org/cgi/content/full/6/46/eabb2454/DC1

View/request a protocol for this paper from *Bio-protocol*.

REFERENCES AND NOTES

1. C. Paisán-Ruíz, S. Jain, E. W. Evans, W. P. Gilks, J. Simón, M. van der Brug, A. López de Munain, S. Aparicio, A. M. Gil, N. Khan, J. Johnson, J. R. Martinez, D. Nicholl, I. Martí Carrera, A. S. Pena, R. de Silva, A. Lees, J. F. Martí-Massó, J. Pérez-Tur, N. W. Wood, A. B. Singleton, Cloning of the gene containing mutations that cause *PARK8*-linked Parkinson's disease. *Neuron* **44**, 595–600 (2004).
2. S. Lesage, A.-L. Leutenegger, P. Ibanez, S. Janin, E. Lohmann, A. Dürr, A. Brice; French Parkinson's Disease Genetics Study Group, *LRRK2* haplotype analyses in European and North African families with Parkinson disease: A common founder for the G2019S mutation dating from the 13th century. *Am. J. Hum. Genet.* **77**, 330–332 (2005).
3. D. Chang, M. A. Nalls, I. B. Hallgrímsdóttir, J. Hunkapiller, M. van der Brug, F. Cai; International Parkinson's Disease Genomics Consortium; 23andMe Research Team, G. A. Kerchner, G. Ayalon, B. Bingol, M. Sheng, D. Hinds, T. W. Behrens, A. B. Singleton, T. R. Bhangale, R. R. Graham, A meta-analysis of genome-wide association studies identifies 17 new Parkinson's disease risk loci. *Nat. Genet.* **49**, 1511–1516 (2017).
4. M. A. Nalls, C. Blauwendraat, C. L. Vallerga, K. Heilbron, S. Bandres-Ciga, D. Chang, M. Tan, D. A. Kia, A. J. Noyce, A. Xue, J. Bras, E. Young, R. von Coelln, J. Simón-Sánchez, C. Schulte, M. Sharma, L. Krohn, L. Pihlstrøm, A. Siitonen, H. Iwaki, H. Leonard, F. Faghri, J. R. Gibbs, D. G. Hernandez, S. W. Scholz, J. A. Botia, M. Martinez, J.-C. Corvol, S. Lesage, J. Jankovic, L. M. Shulman, M. Sutherland, P. Tienari, K. Majamaa, M. Toft, O. A. Andreassen, T. Bangale, A. Brice, J. Yang, Z. Gan-Or, T. Gasser, P. Heutink, J. M. Shulman, N. W. Wood, D. A. Hinds, J. A. Hardy, H. R. Morris, J. Gratten, P. M. Visscher, R. R. Graham, A. B. Singleton; 23andMe Research Team; System Genomics of Parkinson's Disease Consortium; International Parkinson's Disease Genomics Consortium, Identification of novel risk loci, causal insights, and heritable risk for Parkinson's disease: A meta-analysis of genome-wide association studies. *Lancet Neurol.* **18**, 1091–1102 (2019).
5. E. Greggio, S. Jain, A. Kingsbury, R. Bandopadhyay, P. Lewis, A. Kaganovich, M. P. van der Brug, A. Beilina, J. Blackinton, K. J. Thomas, R. Ahmad, D. W. Miller, S. Kesavapany, A. Singleton, A. Lees, R. J. Harvey, K. Harvey, M. R. Cookson, Kinase activity is required for the toxic effects of mutant *LRRK2*/dardarin. *Neurobiol. Dis.* **23**, 329–341 (2006).
6. M. Steger, F. Tonelli, G. Ito, P. Davies, M. Trost, M. Vetter, S. Wachter, E. Lorentzen, G. Duddy, S. Wilson, M. A. S. Baptista, B. K. Fiske, M. J. Fell, J. A. Morrow, A. D. Reith, D. R. Alessi, M. Mann, Phosphoproteomics reveals that Parkinson's disease kinase LRRK2 regulates a subset of Rab GTPases. *eLife* **5**, e12813 (2016).
7. A. Beilina, I. N. Rudenko, A. Kaganovich, L. Civiero, H. Chau, S. K. Kalia, L. V. Kalia, E. Lobbestael, R. Chia, K. Ndukwe, J. Ding, M. A. Nalls; International Parkinson's Disease Genomics Consortium; North American Brain Expression Consortium, M. Olszewski, D. N. Hauser, R. Kumaran, A. M. Lozano, V. Baekelandt, L. E. Greene, J.-M. Taymans, E. Greggio, M. R. Cookson, Unbiased screen for interactors of leucine-rich repeat kinase 2 supports a common pathway for sporadic and familial Parkinson disease. *Proc. Natl. Acad. Sci. U.S.A.* **111**, 2626–2631 (2014).
8. M. Steger, F. Diez, H. S. Dhekne, P. Lis, R. S. Nirujogi, O. Karayel, F. Tonelli, T. N. Martinez, E. Lorentzen, S. R. Pfeffer, D. R. Alessi, M. Mann, Systematic proteomic analysis of LRRK2-mediated Rab GTPase phosphorylation establishes a connection to ciliogenesis. *eLife* **6**, e31012 (2017).
9. A. Ramirez, A. Heimbach, J. Gründemann, B. Stiller, D. Hampshire, L. P. Cid, I. Goebel, A. F. Mubaidin, A.-L. Wriekat, J. Roeper, A. Al-Din, A. M. Hillmer, M. Karsak, B. Liss, C. G. Woods, M. I. Behrens, C. Kubisch, Hereditary parkinsonism with dementia is caused by mutations in *ATP13A2*, encoding a lysosomal type 5 P-type ATPase. *Nat. Genet.* **38**, 1184–1191 (2006).
10. A. D. Klein, J. R. Mazzulli, Is Parkinson's disease a lysosomal disorder? *Brain* **141**, 2255–2262 (2018).
11. Y. Tong, H. Yamaguchi, E. Giaime, S. Boyle, R. Kopan, R. J. Kelleher III, J. Shen, Loss of leucine-rich repeat kinase 2 causes impairment of protein degradation pathways, accumulation of α-synuclein, and apoptotic cell death in aged mice. *Proc. Natl. Acad. Sci. U.S.A.* **107**, 9879–9884 (2010).
12. A. G. Henry, S. Aghamohammadzadeh, H. Samaroo, Y. Chen, K. Mou, E. Needle, W. D. Hirst, Pathogenic LRRK2 mutations, through increased kinase activity, produce enlarged lysosomes with reduced degradative capacity and increase ATP13A2 expression. *Hum. Mol. Genet.* **24**, 6013–6028 (2015).
13. L. N. Hockey, B. S. Kilpatrick, E. R. Eden, Y. Lin-Moshier, G. C. Brailoiu, E. Brailoiu, C. E. Futter, A. H. Schapira, J. S. Marchant, S. Patel, Dysregulation of lysosomal morphology by pathogenic LRRK2 is corrected by TPC2 inhibition. *J. Cell Sci.* **128**, 232–238 (2015).
14. S. J. Orenstein, S.-H. Kuo, I. Tasset, E. Arias, H. Koga, I. Fernandez-Carasa, E. Cortes, L. S. Honig, W. Dauer, A. Consiglio, A. Raya, D. Sulzer, A. M. Cuervo, Interplay of LRRK2 with chaperone-mediated autophagy. *Nat. Neurosci.* **16**, 394–406 (2013).
15. R. C. Gomez, P. Wawro, P. Lis, D. R. Alessi, S. R. Pfeffer, Membrane association but not identity is required for LRRK2 activation and phosphorylation of Rab GTPases. *J. Cell Biol.* **218**, 4157–4170 (2019).
16. T. Eguchi, T. Kuwahara, M. Sakurai, T. Komori, T. Fujimoto, G. Ito, S.-I. Yoshimura, A. Harada, M. Fukuda, M. Koike, T. Iwatsubo, LRRK2 and its substrate Rab GTPases are sequentially targeted onto stressed lysosomes and maintain their homeostasis. *Proc. Natl. Acad. Sci. U.S.A.* **115**, E9115–E9124 (2018).
17. A. di Domenico, G. Carola, C. Calatayud, M. Pons-Espinal, J. P. Muñoz, Y. Richaud-Patin, I. Fernandez-Carasa, M. Gut, A. Faella, J. Parameswaran, J. Soriano, I. Ferrer, E. Tolosa, A. Zorzano, A. M. Cuervo, A. Raya, A. Consiglio, Patient-specific iPSC-derived astrocytes contribute to non-cell-autonomous neurodegeneration in Parkinson's disease. *Stem Cell Rep.* **12**, 213–229 (2019).
18. K. Stafa, A. Trancikova, P. J. Webber, J. Glauser, A. B. West, D. J. Moore, GTPase activity and neuronal toxicity of Parkinson's disease–Associated LRRK2 is regulated by ArfGAP1. *PLOS Genet.* **8**, e1002526 (2012).
19. A. Mamais, R. Chia, A. Beilina, D. N. Hauser, C. Hall, P. A. Lewis, M. R. Cookson, R. Bandopadhyay, Arsenite stress down-regulates phosphorylation and 14-3-3 binding of leucine-rich repeat kinase 2 (LRRK2), promoting self-association and cellular redistribution. *J. Biol. Chem.* **289**, 21386–21400 (2014).
20. X.-T. Cheng, Y.-X. Xie, B. Zhou, N. Huang, T. Farfel-Becker, Z.-H. Sheng, Characterization of LAMP1-labeled nondegradative lysosomal and endocytic compartments in neurons. *J. Cell Biol.* **217**, 3127–3139 (2018).
21. V. Hung, N. D. Udeshi, S. S. Lam, K. H. Loh, K. J. Cox, K. Pedram, S. A. Carr, A. Y. Ting, Spatially resolved proteomic mapping in living cells with the engineered peroxidase APEX2. *Nat. Protoc.* **11**, 456–475 (2016).

22. L. Pellegrini, D. N. Hauser, Y. Li, A. Mamais, A. Beilina, R. Kumaran, A. Wetzel, J. Nixon-Abell, G. Heaton, I. Rudenko, M. Alkaslasi, N. Ivanina, H. L. Melrose, M. R. Cookson, K. Harvey, Proteomic analysis reveals co-ordinated alterations in protein synthesis and degradation pathways in LRRK2 knockout mice. *Hum. Mol. Genet.* **27**, 3257–3271 (2018).

23. C. H. Hsu, D. Chan, B. Wolozin, LRRK2 and the stress response: Interaction with MKKs and JNK-interacting proteins. *Neurodegener Dis.* **7**, 68–75 (2010).

24. E.-J. Bae, D.-K. Kim, C. Kim, M. Mante, A. Adame, E. Rockenstein, A. Ulusoy, M. Klinkenberg, G. R. Jeong, J. R. Bae, C. Lee, H.-J. Lee, B.-D. Lee, D. A. Di Monte, E. Masliah, S.-J. Lee, LRRK2 kinase regulates α-synuclein propagation via RAB35 phosphorylation. *Nat. Commun.* **9**, 3465 (2018).

25. G. Montagnac, J.-B. Sibarita, S. Loubéry, L. Daviet, M. Romao, G. Raposo, P. Chavrier, ARF6 interacts with JIP4 to control a motor switch mechanism regulating endosome traffic in cytokinesis. *Curr. Biol.* **19**, 184–195 (2009).

26. T. Tanaka, M. Iino, K. Goto, Knockdown of Sec8 enhances the binding affinity of c-Jun N-terminal kinase (JNK)-interacting protein 4 for mitogen-activated protein kinase kinase 4 (MKK4) and suppresses the phosphorylation of MKK4, p38, and JNK, thereby inhibiting apoptosis. *FEBS J.* **281**, 5237–5250 (2014).

27. S. Aits, J. Kricker, B. Liu, A.-M. Ellegaard, S. Hämälistö, S. Tvingsholm, E. Corcelle-Termeau, S. Høgh, T. Farkas, A. Holm Jonassen, I. Gromova, M. Mortensen, M. Jäättelä, Sensitive detection of lysosomal membrane permeabilization by lysosomal galectin puncta assay. *Autophagy* **11**, 1408–1424 (2015).

28. D. L. Thiele, P. E. Lipsky, Mechanism of L-leucyl-L-leucine methyl ester-mediated killing of cytotoxic lymphocytes: Dependence on a lysosomal thiol protease, dipeptidyl peptidase I, that is enriched in these cells. *Proc. Natl. Acad. Sci. U.S.A.* **87**, 83–87 (1990).

29. I. Maejima, A. Takahashi, H. Omori, T. Kimura, Y. Takabatake, T. Saitoh, A. Yamamoto, M. Hamasaki, T. Noda, Y. Isaka, T. Yoshimori, Autophagy sequesters damaged lysosomes to control lysosomal biogenesis and kidney injury. *EMBO J.* **32**, 2336–2347 (2013).

30. H. Kobayashi, K. Etoh, N. Ohbayashi, M. Fukuda, Rab35 promotes the recruitment of Rab8, Rab13 and Rab36 to recycling endosomes through MICAL-L1 during neurite outgrowth. *Biol. Open* **3**, 803–814 (2014).

31. V. Marchesin, A. Castro-Castro, C. Lodillinsky, A. Castagnino, J. Cyrta, H. Bonsang-Kitzis, L. Fuhrmann, M. Irondelle, E. Infante, G. Montagnac, F. Reyal, A. Vincent-Salmon, P. Chavrier, ARF6-JIP3/4 regulate endosomal tubules for MT1-MMP exocytosis in cancer invasion. *J. Cell Biol.* **211**, 339–358 (2015).

32. P. J. Cullen, F. Steinberg, To degrade or not to degrade: Mechanisms and significance of endocytic recycling. *Nat. Rev. Mol. Cell Biol.* **19**, 679–696 (2018).

33. A. Zimprich, S. Biskup, P. Leitner, P. Lichtner, M. Farrer, S. Lincoln, J. Kachergus, M. Hulihan, R. J. Uitti, D. B. Calne, A. J. Stoessl, R. F. Pfeiffer, N. Patenge, I. C. Carbajal, P. Vieregge, F. Asmus, B. Müller-Myhsok, D. W. Dickson, T. Meitinger, T. M. Strom, Z. K. Wszolek, T. Gasser, Mutations in *LRRK2* cause autosomal-dominant parkinsonism with pleomorphic pathology. *Neuron* **44**, 601–607 (2004).

34. J. Alegre-Abarrategui, H. Christian, M. M. P. Lufino, R. Mutihac, L. L. Venda, O. Ansorge, R. Wade-Martins, LRRK2 regulates autophagic activity and localizes to specific membrane microdomains in a novel human genomic reporter cellular model. *Hum. Mol. Genet.* **18**, 4022–4034 (2009).

35. S. Biskup, D. J. Moore, F. Celsi, S. Higashi, A. B. West, S. A. Andrabi, K. Kurkinen, S.-W. Yu, J. M. Savitt, H. J. Waldvogel, R. L. M. Faull, P. C. Emson, R. Torp, O. P. Ottersen, T. M. Dawson, V. L. Dawson, Localization of LRRK2 to membranous and vesicular structures in mammalian brain. *Ann. Neurol.* **60**, 557–569 (2006).

36. Z. Berger, K. A. Smith, M. J. LaVoie, Membrane localization of LRRK2 is associated with increased formation of the highly active LRRK2 dimer and changes in its phosphorylation. *Biochemistry* **49**, 5511–5523 (2010).

37. D. A. MacLeod, H. Rhinn, T. Kuwahara, A. Zolin, G. Di Paolo, B. D. McCabe, K. S. Marder, L. S. Honig, L. N. Clark, S. A. Small, A. Abeliovich, *RAB7L1* interacts with *LRRK2* to modify intraneuronal protein sorting and Parkinson's disease risk. *Neuron* **77**, 425–439 (2013).

38. L. Bonet-Ponce, M. R. Cookson, The role of Rab GTPases in the pathobiology of Parkinson' disease. *Curr. Opin. Cell Biol.* **59**, 73–80 (2019).

39. Y. Tong, E. Giaime, H. Yamaguchi, T. Ichimura, Y. Liu, H. Si, H. Cai, J. V. Bonventre, J. Shen, Loss of leucine-rich repeat kinase 2 causes age-dependent bi-phasic alterations of the autophagy pathway. *Mol. Neurodegener.* **7**, 2 (2012).

40. E. Purlyte, H. S. Dhekne, A. R. Sarhan, R. Gomez, P. Lis, M. Wightman, T. N. Martinez, F. Tonelli, S. R. Pfeffer, D. R. Alessi, Rab29 activation of the Parkinson's disease-associated LRRK2 kinase. *EMBO J.* **38**, e101237 (2019).

41. K. E. McNally, P. J. Cullen, Endosomal retrieval of cargo: Retromer is not alone. *Trends Cell Biol.* **28**, 807–822 (2018).

42. W. A. Prinz, A. Toulmay, T. Balla, The functional universe of membrane contact sites. *Nat. Rev. Mol. Cell Biol.* **21**, 7–24 (2020).

43. S. Sridhar, B. Patel, D. Aphkhazava, F. Macian, L. Santambrogio, D. Shields, A. M. Cuervo, The lipid kinase PI4KIIIβ preserves lysosomal identity. *EMBO J.* **32**, 324–339 (2013).

44. L. Yu, C. K. McPhee, L. Zheng, G. A. Mardones, Y. Rong, J. Peng, N. Mi, Y. Zhao, Z. Liu, F. Wan, D. W. Hailey, V. Oorschot, J. Klumperman, E. H. Baehrecke, M. J. Lenardo, Termination of autophagy and reformation of lysosomes regulated by mTOR. *Nature* **465**, 942–946 (2010).

45. Q. Zhang, Y. Pan, R. Yan, B. Zeng, H. Wang, X. Zhang, W. Li, H. Wei, Z. Liu, Commensal bacteria direct selective cargo sorting to promote symbiosis. *Nat. Immunol.* **16**, 918–926 (2015).

46. A. Verkhratsky, M. Matteoli, V. Parpura, J.-P. Mothet, R. Zorec, Astrocytes as secretory cells of the central nervous system: Idiosyncrasies of vesicular secretion. *EMBO J.* **35**, 239–257 (2016).

47. S. Pickles, P. Vigié, R. J. Youle, Mitophagy and quality control mechanisms in mitochondrial maintenance. *Curr. Biol.* **28**, R170–R185 (2018).

48. G.-L. McLelland, V. Soubannier, C. X. Chen, H. M. McBride, E. A. Fon, Parkin and PINK1 function in a vesicular trafficking pathway regulating mitochondrial quality control. *EMBO J.* **33**, 282–295 (2014).

49. F. Wauters, T. Cornelissen, D. Imberechts, S. Martin, B. Koentjoro, C. Sue, P. Vangheluwe, W. Vandenberghe, *LRRK2* mutations impair depolarization-induced mitophagy through inhibition of mitochondrial accumulation of RAB10. *Autophagy* **16**, 203–222 (2020).

50. T. Kirkegaard, A. G. Roth, N. H. T. Petersen, A. K. Mahalka, O. D. Olsen, I. Moilanen, A. Zylicz, J. Knudsen, K. Sandhoff, C. Arenz, P. K. J. Kinnunen, J. Nylandsted, M. Jäättelä, Hsp70 stabilizes lysosomes and reverts Niemann–Pick disease–associated lysosomal pathology. *Nature* **463**, 549–553 (2010).

51. E. Gabandé-Rodríguez, A. Pérez-Cañamás, B. Soto-Huelin, D. N. Mitroi, S. Sánchez-Redondo, E. Martínez-Sáez, C. Venero, H. Peinado, M. D. Ledesma, Lipid-induced lysosomal damage after demyelination corrupts microglia protective function in lysosomal storage disorders. *EMBO J.* **38**, e99553 (2019).

52. C. Papadopoulos, H. Meyer, Detection and clearance of damaged lysosomes by the endo-lysosomal damage response and lysophagy. *Curr. Biol.* **27**, R1330–R1341 (2017).

53. R. J. Nichols, N. Dzamko, N. A. Morrice, D. G. Campbell, M. Deak, A. Ordureau, T. Macartney, Y. Tong, J. Shen, A. R. Prescott, D. R. Alessi, 14-3-3 binding to LRRK2 is disrupted by multiple Parkinson's disease-associated mutations and regulates cytoplasmic localization. *Biochem. J.* **430**, 393–404 (2010).

54. E. Greggio, I. Zambrano, A. Kaganovich, A. Beilina, J.-M. Taymans, V. Daniëls, P. Lewis, S. Jain, J. Ding, A. Syed, K. J. Thomas, V. Baekelandt, M. R. Cookson, The Parkinson disease-associated leucine-rich repeat kinase 2 (LRRK2) is a dimer that undergoes intramolecular autophosphorylation. *J. Biol. Chem.* **283**, 16906–16914 (2008).

55. B. Huang, A. Hubber, J. A. McDonough, C. R. Roy, M. A. Scidmore, J. A. Carlyon, The *Anaplasma phagocytophilum*-occupied vacuole selectively recruits Rab-GTPases that are predominantly associated with recycling endosomes. *Cell. Microbiol.* **12**, 1292–1307 (2010).

56. K. A. Rzomp, L. D. Scholtes, B. J. Briggs, G. R. Whittaker, M. A. Scidmore, Rab GTPases are recruited to chlamydial inclusions in both a species-dependent and species-independent manner. *Infect. Immun.* **71**, 5855–5870 (2003).

57. S. S. Lam, J. D. Martell, K. J. Kamer, T. J. Deerinck, M. H. Ellisman, V. K. Mootha, A. Y. Ting, Directed evolution of APEX2 for electron microscopy and proximity labeling. *Nat. Methods* **12**, 51–54 (2015).

58. N. M. Sherer, M. J. Lehmann, L. F. Jimenez-Soto, A. Ingmundson, S. M. Horner, G. Cicchetti, P. G. Allen, M. Pypaert, J. M. Cunningham, W. Mothes, Visualization of retroviral replication in living cells reveals budding into multivesicular bodies. *Traffic* **4**, 785–801 (2003).

59. K. S. Conrad, T.-W. Cheng, D. Ysselstein, S. Heybrock, L. R. Hoth, B. A. Chrunyk, C. W. am Ende, D. Krainc, M. Schwake, P. Saftig, S. Liu, X. Qiu, M. D. Ehlers, Lysosomal integral membrane protein-2 as a phospholipid receptor revealed by biophysical and cellular studies. *Nat. Commun.* **8**, 1908 (2017).

60. C. K. E. Bleck, Y. Kim, T. B. Willingham, B. Glancy, Subcellular connectomic analyses of energy networks in striated muscle. *Nat. Commun.* **9**, 5111 (2018).

Citation: L. Bonet-Ponce, A. Beilina, C. D. Williamson, E. Lindberg, J. H. Kluss, S. Saez-Atienzar, N. Landeck, R. Kumaran, A. Mamais, C. K. E. Bleck, Y. Li, M. R. Cookson, LRRK2 mediates tubulation and vesicle sorting from lysosomes. *Sci. Adv.* **6**, eabb2454 (2020).

Science Advances

LRRK2 mediates tubulation and vesicle sorting from lysosomes

Luis Bonet-PonceAlexandra BeilinaChad D. WilliamsonEric LindbergJillian H. KlussSara Saez-AtienzarNatalie LandeckRavindran KumaranAdamantios MamaisChristopher K. E. BleckYan LiMark R. Cookson

View the article online
https://www.science.org/doi/10.1126/sciadv.abb2454
Permissions
https://www.science.org/help/reprints-and-permissions

Use of this article is subject to the Terms of service

RESEARCH ARTICLE   **Open Access**

Preclinical modeling of chronic inhibition of the Parkinson's disease associated kinase LRRK2 reveals altered function of the endolysosomal system in vivo

Jillian H. Kluss[1,2], Melissa Conti Mazza[1], Yan Li[3], Claudia Manzoni[2,4], Patrick A. Lewis[2,5,6], Mark R. Cookson[1*] and Adamantios Mamais[7]

Abstract

The most common mutation in the Leucine-rich repeat kinase 2 gene (LRRK2), G2019S, causes familial Parkinson's Disease (PD) and renders the encoded protein kinase hyperactive. While targeting LRRK2 activity is currently being tested in clinical trials as a therapeutic avenue for PD, to date, the molecular effects of chronic LRRK2 inhibition have not yet been examined in vivo. We evaluated the utility of newly available phospho-antibodies for Rab substrates and LRRK2 autophosphorylation to examine the pharmacodynamic response to treatment with the potent and specific LRRK2 inhibitor, MLi-2, in brain and peripheral tissue in G2019S LRRK2 knock-in mice. We report higher sensitivity of LRRK2 autophosphorylation to MLi-2 treatment and slower recovery in washout conditions compared to Rab GTPases phosphorylation, and we identify pS106 Rab12 as a robust readout of downstream LRRK2 activity across tissues. The downstream effects of long-term chronic LRRK2 inhibition in vivo were evaluated in G2019S LRRK2 knock-in mice by phospho- and total proteomic analyses following an in-diet administration of MLi-2 for 10 weeks. We observed significant alterations in endolysosomal and trafficking pathways in the kidney that were sensitive to MLi-2 treatment and were validated biochemically. Furthermore, a subtle but distinct biochemical signature affecting mitochondrial proteins was observed in brain tissue in the same animals that, again, was reverted by kinase inhibition. Proteomic analysis in the lung did not detect any major pathway of dysregulation that would be indicative of pulmonary impairment. This is the first study to examine the molecular underpinnings of chronic LRRK2 inhibition in a preclinical in vivo PD model and highlights cellular processes that may be influenced by therapeutic strategies aimed at restoring LRRK2 physiological activity in PD patients.

Background

Mutations in *leucine-rich repeat kinase 2* (*LRRK2*) are a known genetic cause of familial Parkinson's disease (PD) [1–3];. Non-coding variation at the *LRRK2* locus has also been identified as a risk factor for sporadic PD, suggesting that both disease forms share common pathological mechanisms [4, 5]. The G2019S mutation, which lies within the kinase domain of LRRK2, is the most common mutation found in familial PD cases, as well as in 1–5% of apparently sporadic PD patients [6]. This mutation directly increases kinase activity while other mutations likely have convergent cellular effects, albeit through varying mechanisms [4]. Therefore, it is thought that targeting LRRK2 therapeutically may be advantageous in both familial and sporadic PD [7, 8].

* Correspondence: cookson@mail.nih.gov
[1]Cell Biology and Gene Expression Section, Laboratory of Neurogenetics, National Institute on Aging, National Institutes of Health, Bethesda, MD, USA
Full list of author information is available at the end of the article

A number of pharmacological tools that inhibit LRRK2 kinase activity in the CNS have been developed and characterized [9]. Some kinase inhibitors have been shown to reduce cytotoxicity associated with LRRK2 mutations in PD-relevant cell and animal models [10–12], supporting the hypothesis that LRRK2 inhibition may be efficacious for PD. One such LRRK2-specific inhibitor, MLi-2, has been found to be ~300x more selective for LRRK2 over other kinases and can readily cross the blood-brain barrier [13] demonstrating that it is possible to generate tool compounds that have clinical potential for therapeutic intervention in PD. However, as LRRK2 is expressed endogenously in many tissues and kinase inhibition is predicted to affect both mutant and wild-type LRRK2, whether such inhibitors would be safe to use clinically is uncertain. Preclinical studies have reported macroscopic changes in vivo that include morphological changes in lung from nonhuman primates, and kidney tissue from rats treated with specific LRRK2 inhibitors that are reversible after termination of treatment [14–16]. Importantly, some of these effects overlap with those seen in Lrrk2 knockout mice [17] demonstrating that they result from on-target effects of inhibitors on LRRK2 itself rather than resulting from inhibition of other kinases.

Here, we aimed to mimic a likely clinical use of LRRK2 inhibitor to understand the relationship between level of inhibition and effects on biochemistry of target tissues including brain and peripheral organs that express high levels of LRRK2. We first evaluated the utility of measuring autophosphorylation of LRRK2 vs downstream substrate Rab proteins as readouts of LRRK2 kinase activity in vivo across a series of acute and chronic dosing paradigms in kinase hyperactive G2019S LRRK2 knock-in mouse model. Secondly, we explore the molecular effects of long-term chronic LRRK2 inhibition by unbiased total and phospho-proteomics on brain, kidney, and lung tissue from G2019S LRRK2 mice following 60 mg/kg/day in-diet dosing of MLi-2 for 10 weeks. Based on these data, we report molecular pathways that are affected by chronic inhibition of LRRK2 in a clinically relevant paradigm. Importantly, we show that the effects of LRRK2 inhibition vary across tissues, which may be particularly relevant to selection of biomarkers for clinical trials where brain target engagement is inferred from peripheral tissue events.

Methods
Animals
All animal procedures were performed in accordance with a protocol approved by the Institutional Animal Care and Use Committee of the National Institute on Aging, NIH.

Wildtype, G2019S LRRK2 knock-in (KI), and LRRK2 knockout (KO) male and female mice raised on a C57Bl/6 background (3–8 months in age) were bred in-house on a 12-h day/night cycle for the following experiments. All mice were supplied with Rodent NIH-07 diet and water ad libitum.

Acute MLi-2 dosing
Dose response: 28 homozygous G2019S KI C57BL/6 J mice (5–8 months old) were randomized for treatment using the sample function in R, followed by matching for sex across groups. Mice were given an acute dose of vehicle [40% (w/v) Hydroxypropyl-β-Cyclodextran] or MLi-2 (at 1, 3, 10, 30, 60, or 90 mg/kg dissolved in vehicle) via oral gavage and euthanized 1 h after treatment. Based on our previous data on S1292 dephosphorylation in G2019S LRRK2 brain following acute MLi-2 treatment [18], $N = 4$ was used in this study for all acute MLi-2 experiments, as it was estimated at 90% power to detect a difference of effect size 6 at alpha = 0.05.

Time course: 28 homozygous G2019S KI C57BL/6 J mice (4–7 months old) were randomized for treatment using the sample function in R, followed by matching for sex across groups. Mice were given an acute dose of vehicle [40% (w/v) Hydroxypropyl-β-Cyclodextran] at time point zero, or MLi-2 (10 mg/kg dissolved in vehicle) via oral gavage and euthanized after time point 0.5, 1, 3, 12, 24, or 72 h post dose.

Chronic in-diet dosing
To determine the appropriate concentration of MLi-2 necessary to achieve S1292 phosphorylation levels that are comparable to the brain tissue levels in a wildtype animal, homozygous G2019S KI mice were given customized Rodent NIH-07 chow from Research Diets, either untreated or supplemented with various doses of MLi-2 (10, 30, or 60 mg/kg/day) for 10 days along with an untreated wildtype group, and S1292 phosphorylation signal was measured via Western blot ($N = 3$ mice were used per treatment group). Mice and chow were weighed daily to assess estimated doses of MLi-2 received each day. No difference was observed in food intake between mice receiving MLi-2 treated chow and mice receiving untreated chow. All mice were given chow and water ad libitum. After 10 days, mice were euthanized 2-3 h post start of their light cycle.

Ten day (short-term) and 10 week (long-term) chronic cohorts: Three-month old littermates from wildtype, homozygous G2019S KI, and homozygous LRRK2 KO litters were randomized into short-term (10 days) and long-term (10 weeks) chronic treatment groups: wildtype, G2019S KI, and LRRK2 KO groups received untreated chow, and a G2019S KI group received chow supplemented with 60 mg/kg of MLi-2 per day. Both

male and female mice were represented equally in all treatment groups ($N = 6$ mice were used per treatment group). All mice were given chow and water ad libitum. After 10 days, or 10 weeks, mice were euthanized 2-3 h post start of their light cycle.

Statistical analyses

Statistical analyses for each experiment can be found within each respective figure legend. Briefly, one-way ANOVA or two-way ANOVA with Tukey's post hoc test were used which were performed in GraphPad Prism v8.2.0 (GraphPad Software, San Diego, CA). If not otherwise stated, comparisons were considered statistically significant where $p < 0.05$. *, $p < 0.05$; **, $p < 0.01$; ***, $p < 0.001$; ****, $p < 0.0001$.

Immunoblotting

Tissues were homogenized at 20% w/v in 1x Cell Signaling Lysis Buffer (#9803S) with 1x protease and phosphatase inhibitors (Thermofisher; #1861279 and #78427, respectively) and left on ice for 30 min to lyse. Homogenates were spun at 20,000 g for 10 min at 4 degrees Celsius and pelleted debris were removed. Samples were supplemented with NuPage LDS sample buffer 4x (#NP0008), boiled for 5 min at 95 degrees Celsius and run on a Bio-Rad Criterion™ TGX™ polyacrylamide gel (#5671095) at 200 V for 37 min. Gels were transferred to nitrocellulose (#1704159) on a Bio-Rad Trans-Blot Turbo™ transfer system at 20 V for 10 min. A normalizer sample was added to the end of each blot to account for day-to-day variability in protein transfer and antibody incubation. This stock was prepared prior to beginning this study and single-use aliquots were prepared in loading buffer and stored at -80C until use to ensure no loss of phosphorylation nor protein degradation. The nitrocellulose was blocked for 1 h in 50% TBS (20 mM Tris, 0.5 M NaCl, pH 7.5), 50% Odyssey blocking buffer (Li-Cor; 927–40,000) and incubated overnight with primary antibodies in 50% TBS-T (20 mM Tris, 0.5 M NaCl, pH 7.5, 0.1% Tween 20), 50% Odyssey blocking buffer at 4 degrees Celsius. All antibody concentrations used in this study can be found in Table S1. Following 3×5 min washes with TBS-T, the nitrocellulose was incubated at RT with secondary antibodies for 1 h, washed 3×5 min and scanned at the Li-Cor platform.

All primary antibodies and working dilutions can be found in Table S1. Secondary antibodies were used at 1: 10,000 dilution: IRDyes 800CW Goat anti-Rabbit IgG (LiCor; #926–32,211) and 680RD Goat anti-Mouse IgG (LiCor; 926–68,070). All blots presented in each figure panel were derived from the same experiment and were processed in parallel. Raw densitometric signal was normalized to a common normalizer sample that was run on every blot.

Tissue preparation for proteomics and phosphoproteomics

One brain hemisphere, one half of a kidney, and one whole lung from each mouse in the short-term and long-term chronic experiments were processed and submitted for proteomics and phosphoproteomics analysis using TMT quantitation without and with TiO_2/iMAC enrichment. Briefly, tissues were homogenized in 15% w/v lysis buffer (0.5 mM HEPES, pH 7.4, 225 mM mannitol, 50 mM sucrose, 1 mM EDTA, 1x protease and phosphatase inhibitors (Thermofisher; #1861279 and #78427, respectively), and 2% CHAPS) followed by incubation on ice for 30 min, with periodic vortexing, to lyse. The homogenates were then spun down at 20,000 g at 4 degrees Celsius for 10 min to pellet cellular debris. A protein assay was performed on supernatants to determine protein concentration, and 270 µg of each sample were submitted for mass spectrometry. Additionally, 30 µg of each sample were pooled together to allow for normalization between runs during analysis.

Phosphoproteomics and bioinformatics analysis

Proteins were alkylated with NEM, digested with trypsin and labeled with TMTpro reagents. The brain and kidney samples were treated with the same method. Forty eight brain/kidney samples and 4 pooled samples were separated into 4 sets of TMT experiments. Each set contains 12 samples and one pooled sample. Twenty-four whole lung samples and 2 pooled samples were separated into 2 sets of TMT experiments. Each set contains 12 samples and one pooled sample. The pooled sample in each set was labeled with TMTpro-126 reagent, while the distribution and labeling of 12 samples were randomized (Data File S1). After the labeling and quenching, samples were combined together. 95% of the combined sample was used for phosphopeptide enrichment using TiO2 method followed by iMAC method. 5% of the combined sample was fractionated using Pierce high pH reverse phase cartridge, and 8 fractions were collected for each set. LC-MS/MS data acquisition were performed on a Thermo Scientific Orbitrap Lumos mass spectrometer which was coupled to a Thermo Scientific Ultimate 3000 HPLC. Peptides were separated on an ES802 nano-column over 136 min at a flow rate of 300 n/min. TMT MS2 method was used. Both MS1 and MS2 scans were performed in orbitrap. The resolution for MS1 and MS2 scans were 120 K and 50 K, respectively. Peptides were fragmented using the HCD method with collision energy fixed at 32%. The precursor isolation window is 1.5 Da.

Proteome Discoverer 2.4 was used for database search and TMT quantitation. Ratios of raw abundance values of each sample over the pooled sample were generated and analyzed in R using the limma package (version 4.0,

empirical Bayes method) [19]. Briefly, the proteomics datasets from four MS runs (or two for the lung samples) were combined and only hits that were detected in at least 4 out of 6 mice were kept, while the missing 1–2 values were imputed. These phospho-peptide and total protein datasets were merged and matched for accession number and the ratio of phospho/total abundance was generated for phosphopeptide significant hit detection. Principal component analysis was conducted for these datasets which revealed a modest batch effect that was corrected computationally. Statistical analyses were conducted, namely moderated t-tests between pairs were visualized as volcano plots [20], and z scores were calculated for heatmaps. Heatmaps were curated from statistically significant hits selected based on relevance to neurodegeneration and reported functions on cellular pathways affected in Parkinson's Disease. Proteins were considered significant hits with an adjusted *p*-value < 0.05, and for kidneys a fold change > 1.4. Functional enrichment analysis of the significant hits was performed using the R package gProfiler2 (precision cutoffs of adjusted *p*-values were < 1e-6 and < 1e-20 for kidney and brain hits, respectively, and term size < 1000 was kept [21]. All hits from the lungs did not return any significant terms within these parameters. Enrichment term networks were visualized using Cytoscape 3.7 [22].

Additionally, we generated a human interactome of LRRK2 and compared it with the significant hits found in kidney total and phospho- proteomics (Fig. S7) using the PINOT searching tool (http://www.reading.ac.uk/bioinf/PINOT/PINOT_form.html) which collates published, experimentally validated protein-protein interaction (PPI) data from 7 different databases (bhf-ucl, BioGRID, InnateDB, IntAct, MBInfo, MINT and UniProt), merged the annotations and performed quality control providing a final score indicative of reproducibility [23]. The PPIs of LRRK2 with a final score > 2 were kept as first layer interactors (i.e. reported in literature as able to directly bind to LRRK2). The first layer interactors of LRRK2 (220 proteins) were used as input in PINOT to download PPIs able to bind directly to the first layer (i.e. second layer interactors). The second layer interactors are proteins that are able to connect to LRRK2 via their direct connection with a protein within the first layer (Data File S2). Scripts were run in R (3.6.2) and networks were drawn using Cytoscape 3.5, mouse to human protein ID conversion was performed using g: Profiler [21].

Results

Relative sensitivity of LRRK2 autophosphorylation and Rab GTPase phosphorylation to MLi-2 inhibition in vivo

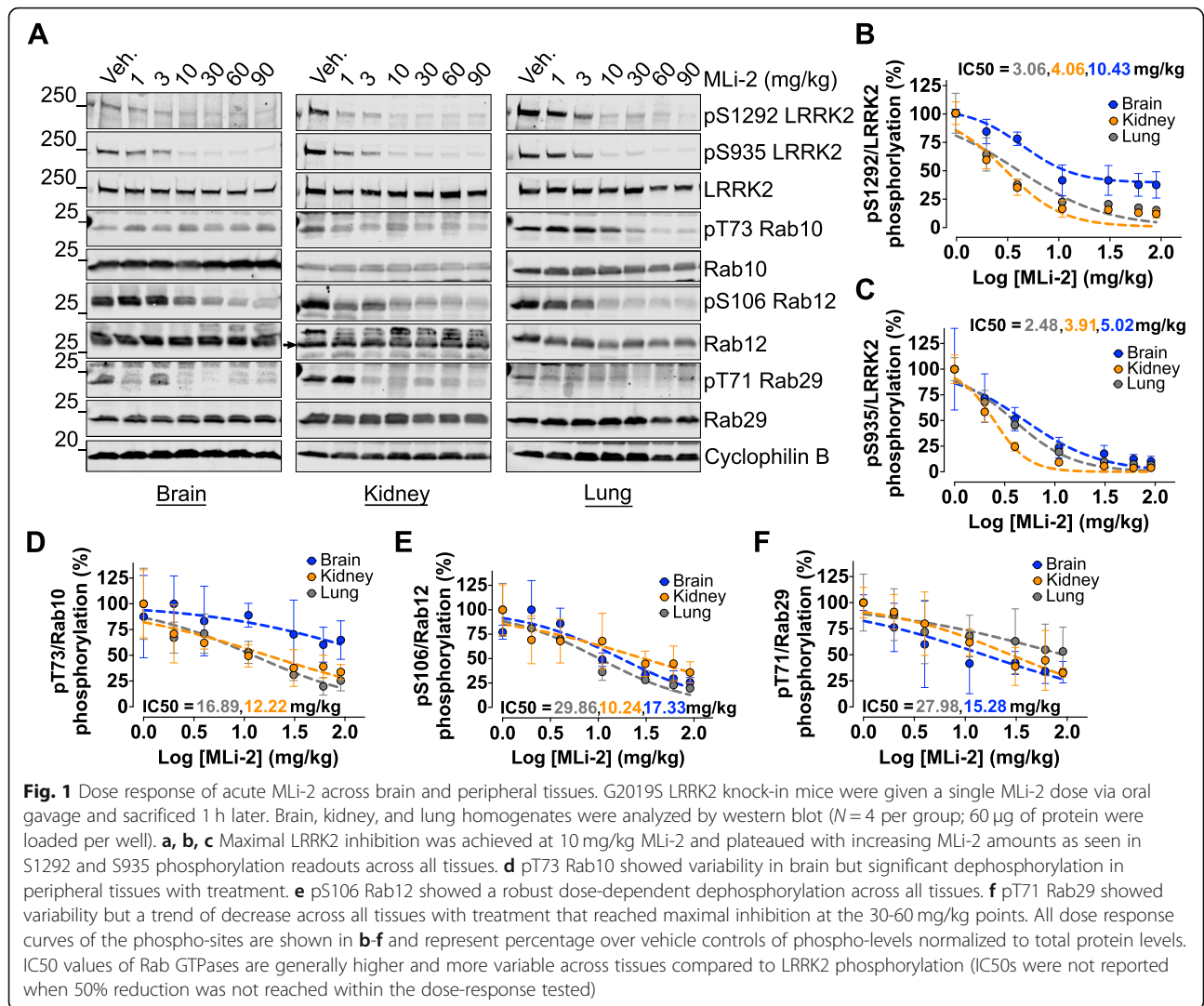Our aim in this series of studies was to mimic a likely clinical scenario where mutant LRRK2 is inhibited to levels similar to that seen with wild type protein, thus nullifying the potential toxic effects of enhanced pathogenic kinase activity. In order to be able to model this situation, we first needed to identify reliable markers of LRRK2 activity in vivo and understand the relationship between peripheral organ and brain target engagement. To this end, we compared the response of phosphorylation of LRRK2 itself and downstream Rab substrates to MLi-2 in vivo using two acute treatment paradigms.

First, we investigated the dose responsiveness of LRRK2 autophosphorylation and phosphorylation of Rab GTPases to acute kinase inhibition in vivo. G2019S KI mice were given an acute dose of MLi-2 at 1, 3, 10, 30, 60, or 90 mg/kg or vehicle via oral gavage and sacrificed 1 h post dose. We observed significant pS1292 dephosphorylation starting at the lowest dose of 1 mg/kg in kidney and lung (Fig. 1a, b). Maximal dephosphorylation was achieved in the brain, kidney and lung at 10 mg/kg for both pS1292 and pS935 (Fig. 1a, b, c). Maximal S1292 dephosphorylation in the brain did not exceed 60% signal decrease with increasing MLi-2 concentrations, suggesting that maximal inhibition was achieved. The S935 phospho-site had lower IC50 compared to pS1292 in the brain, suggesting that this marker is more sensitive to LRRK2 inhibition in vivo.

Phosphorylated Rab GTPases showed more variable responses to MLi-2 across tissues. The T73 Rab10 phospho-site responded significantly to MLi-2 treatment in peripheral tissues but not in the brain (Fig. 1a, d). Phospho- S106 Rab12 showed a robust response to MLi-2 in both brain and peripheral tissues with maximal dephosphorylation at 30-60 mg/kg (Fig. 1a, e; antibody validation experiments are shown in Figs. S2 and S3). The T71 Rab29 phospho-site responded with treatment in all tissues but with higher variability compared to Rab12, especially at lower doses (Fig. 1a, f). At 10 mg/kg, we saw ~ 50% decrease in Rab10, Rab12 and Rab29 phosphorylation in the periphery while higher doses retained ~ 30% residual phosphorylation signal. These results demonstrate that 10 mg/kg of MLi-2 is adequate to acutely inhibit LRRK2 autophosphorylation in brain and peripheral tissues. Based on these results, we selected a dose of 10 mg/kg MLi-2 for subsequent time course analyses and washout experiments.

Time course of acute MLi-2 administration reveals that phosphorylation of Rab GTPases recovers faster than LRRK2 phosphorylation

To further discriminate how LRRK2 and Rab phosphorylation events vary between brain and peripheral tissues, we compared time courses and recovery after washout of inhibitor application. An acute dose of MLi-2 at 10 mg/kg was administered via oral gavage to G2019S KI mice and sacrificed at 0.5, 1, 3, 12, 24, or 72 h post dose.
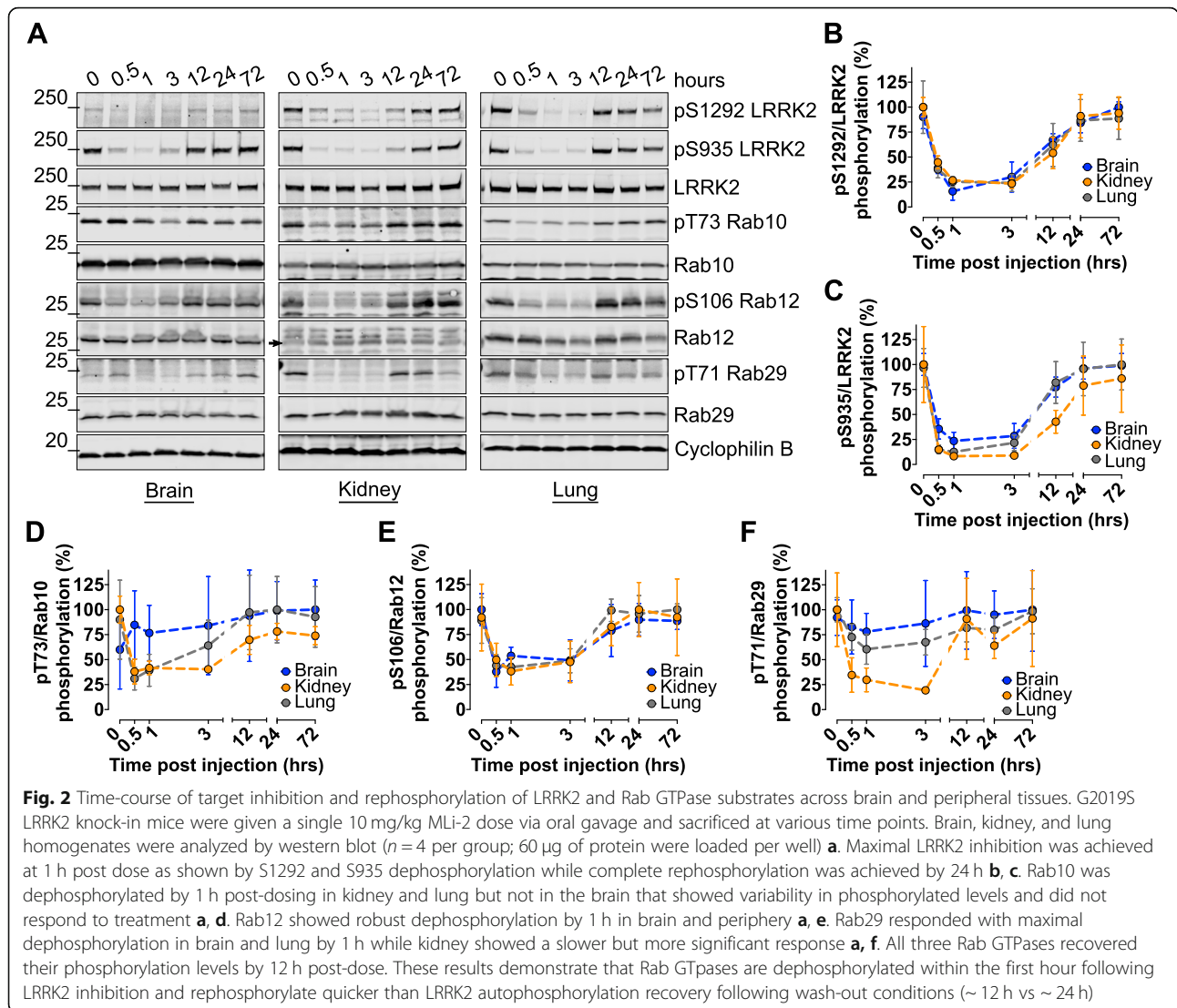
Fig. 1 Dose response of acute MLi-2 across brain and peripheral tissues. G2019S LRRK2 knock-in mice were given a single MLi-2 dose via oral gavage and sacrificed 1 h later. Brain, kidney, and lung homogenates were analyzed by western blot ($N = 4$ per group; 60 μg of protein were loaded per well). **a, b, c** Maximal LRRK2 inhibition was achieved at 10 mg/kg MLi-2 and plateaued with increasing MLi-2 amounts as seen in S1292 and S935 phosphorylation readouts across all tissues. **d** pT73 Rab10 showed variability in brain but significant dephosphorylation in peripheral tissues with treatment. **e** pS106 Rab12 showed a robust dose-dependent dephosphorylation across all tissues. **f** pT71 Rab29 showed variability but a trend of decrease across all tissues with treatment that reached maximal inhibition at the 30-60 mg/kg points. All dose response curves of the phospho-sites are shown in **b-f** and represent percentage over vehicle controls of phospho-levels normalized to total protein levels. IC50 values of Rab GTPases are generally higher and more variable across tissues compared to LRRK2 phosphorylation (IC50s were not reported when 50% reduction was not reached within the dose-response tested)

A time point of 0 h was included where animals were given an equivalent dose of vehicle and euthanized immediately thereafter to measure baseline phosphorylation.

Phospho- S1292 and S935 LRRK2 showed rapid dephosphorylation at 0.5 h, with maximal dephosphorylation achieved at 1 h post dose across all tissues (Fig. 2a - c). The dephosphorylation patterns of both phosphosites tightly correlated between brain, kidney, and lung tissues. Interestingly, maximal dephosphorylation for all pRabs was seen at 1 h in all tissues. However, these sites recovered more rapidly than pLRRK2 (~ 12 h versus 24 h; Fig. 2a, d - f). Measures of T73 Rab10 signal in brain tissue did not show MLi-2-dependent dephosphorylation compared to peripheral tissues (Fig. 2a, d). Dephosphorylation of T71 Rab29 was achieved in all three tissues to varying degrees, with kidneys showing the strongest response to MLi-2, reaching ~ 75% dephosphorylation compared to 20–30% seen in brain and lung tissue (Fig.

2a, f). pS106 Rab12 mimicked pLRRK2 most closely in that all tissues showed similar dephosphorylation patterns over time and reached a maximum of 60% dephosphorylation (Fig. 2a, e). It was also noted that Rab12 phosphorylation showed the least variability across mice compared to Rab10 and Rab29. These data suggest that Rab GTPases are dephosphorylated within the first hour after LRRK2 inhibition in a similar fashion to LRRK2 dephosphorylation, with Rab12 performing similarly to pLRRK2 in the brain and periphery. In contrast, the kinetics of Rab GTPase re-phosphorylation show a quicker recovery (~ 12 h) compared to LRRK2 (~ 24 h).

In-diet MLi-2 administration can diminish G2019S-dependent hyperphosphorylation to wild type levels

To evaluate the molecular effects of chronic LRRK2 inhibition, we first conducted a dose response experiment of MLi-2 in diet. With clinical relevance in mind, our aim was not to fully inactivate LRRK2, as inferred from
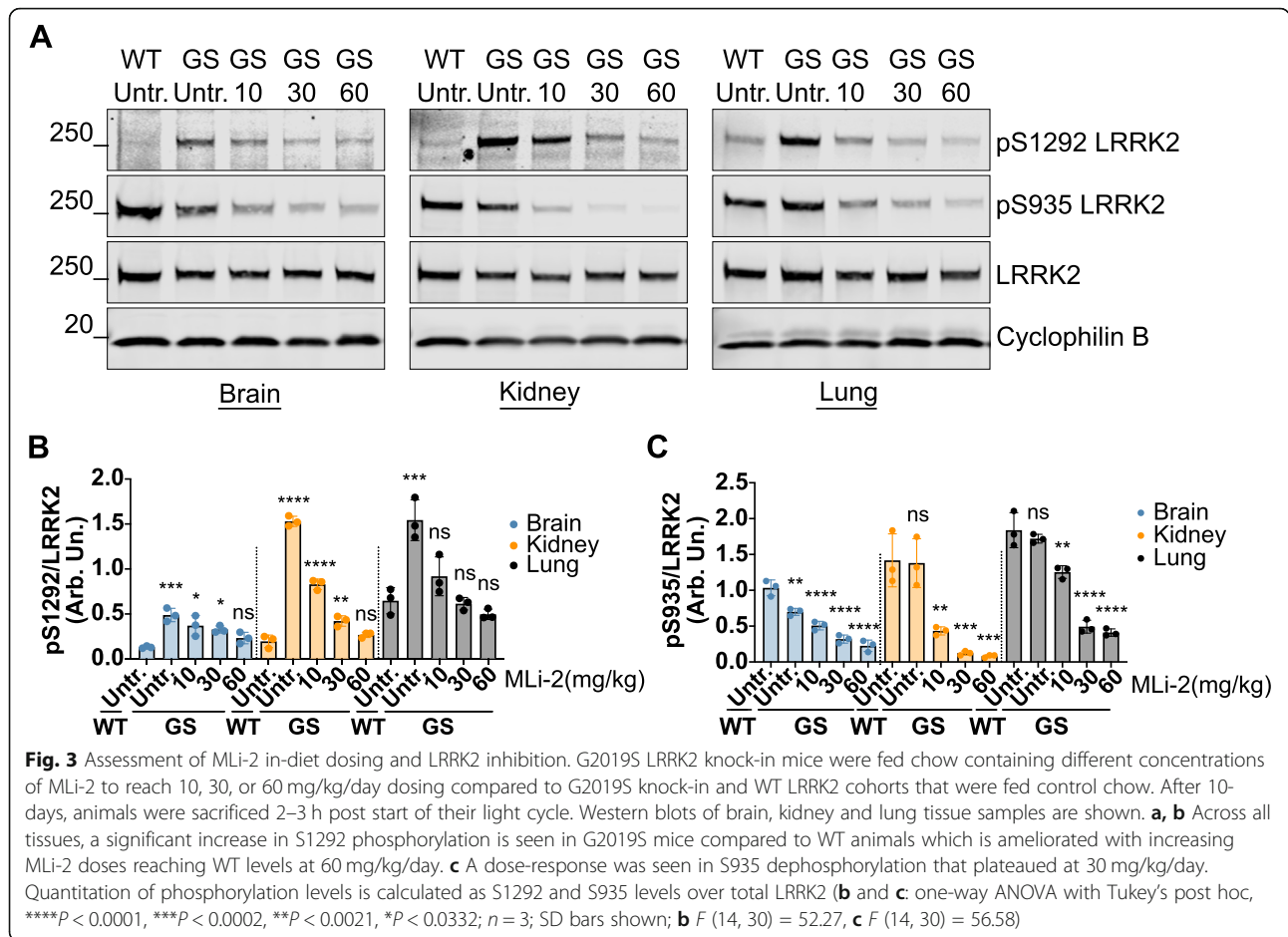
Fig. 2 Time-course of target inhibition and rephosphorylation of LRRK2 and Rab GTPase substrates across brain and peripheral tissues. G2019S LRRK2 knock-in mice were given a single 10 mg/kg MLi-2 dose via oral gavage and sacrificed at various time points. Brain, kidney, and lung homogenates were analyzed by western blot (*n* = 4 per group; 60 μg of protein were loaded per well) **a**. Maximal LRRK2 inhibition was achieved at 1 h post dose as shown by S1292 and S935 dephosphorylation while complete rephosphorylation was achieved by 24 h **b**, **c**. Rab10 was dephosphorylated by 1 h post-dosing in kidney and lung but not in the brain that showed variability in phosphorylation levels and did not respond to treatment **a**, **d**. Rab12 showed robust dephosphorylation by 1 h in brain and periphery **a**, **e**. Rab29 responded with maximal dephosphorylation in brain and lung by 1 h while kidney showed a slower but more significant response **a, f**. All three Rab GTPases recovered their phosphorylation levels by 12 h post-dose. These results demonstrate that Rab GTpases are dephosphorylated within the first hour following LRRK2 inhibition and rephosphorylate quicker than LRRK2 autophosphorylation recovery following wash-out conditions (~ 12 h vs ~ 24 h)

a complete dephosphorylation of S1292, but to ameliorate the hyperphosphorylation to a range observed in wildtype animals.

G2019S KI mice were fed a customized rodent chow supplemented with MLi-2 to achieve 10, 30, or 60 mg/kg/day dosing. For reference, we included wildtype and G2019S KI mice that were fed control chow for 10 days. In the treated animals, we observed that 60 mg/kg/day diminished S1292 phosphorylation to wildtype levels in brain and kidney, whereas a 10 mg/kg/day dose was sufficient to decrease phosphorylation to wildtype levels in lung tissue (Fig. 3a, b). This suggests some peripheral tissues with enrichment of LRRK2 may be more sensitive to drug-induced inhibition. Increasing doses of MLi-2 show a dose response in pS935 LRRK2 (Fig. 3a, c). These results confirm a dose of 60 mg/kg/day is sufficient to inhibit G2019S LRRK2 to wild type levels in vivo across tissues.

Chronic MLi-2 treatment in G2019S KI mice results in sustained LRRK2 and Rab12 dephosphorylation

To extend these results into a chronic timescale, G2019S KI mice were given customized chow supplemented with MLi-2 to reach a 60 mg/kg/day dose for 10 days or 10 weeks. Control groups of wildtype, G2019S KI, and LRRK2 KO mice receiving untreated chow were included for reference of baseline phosphorylation patterns. For the purpose of this experiment, we refer to the 10-day cohort as 'short-term' and the 10-week cohort as 'long-term' treatment groups. The schematic in Fig. 4a depicts the design of this experiment, in which brain, kidney, and lung tissues were collected and processed for Western blot analyses and additionally prepped for total and phospho-proteomics. Body weight and estimated food intake for each mouse was recorded daily to determine the daily dose of MLi-2 each mouse received (Fig. 4b - g). Both short- and long-term cohorts received
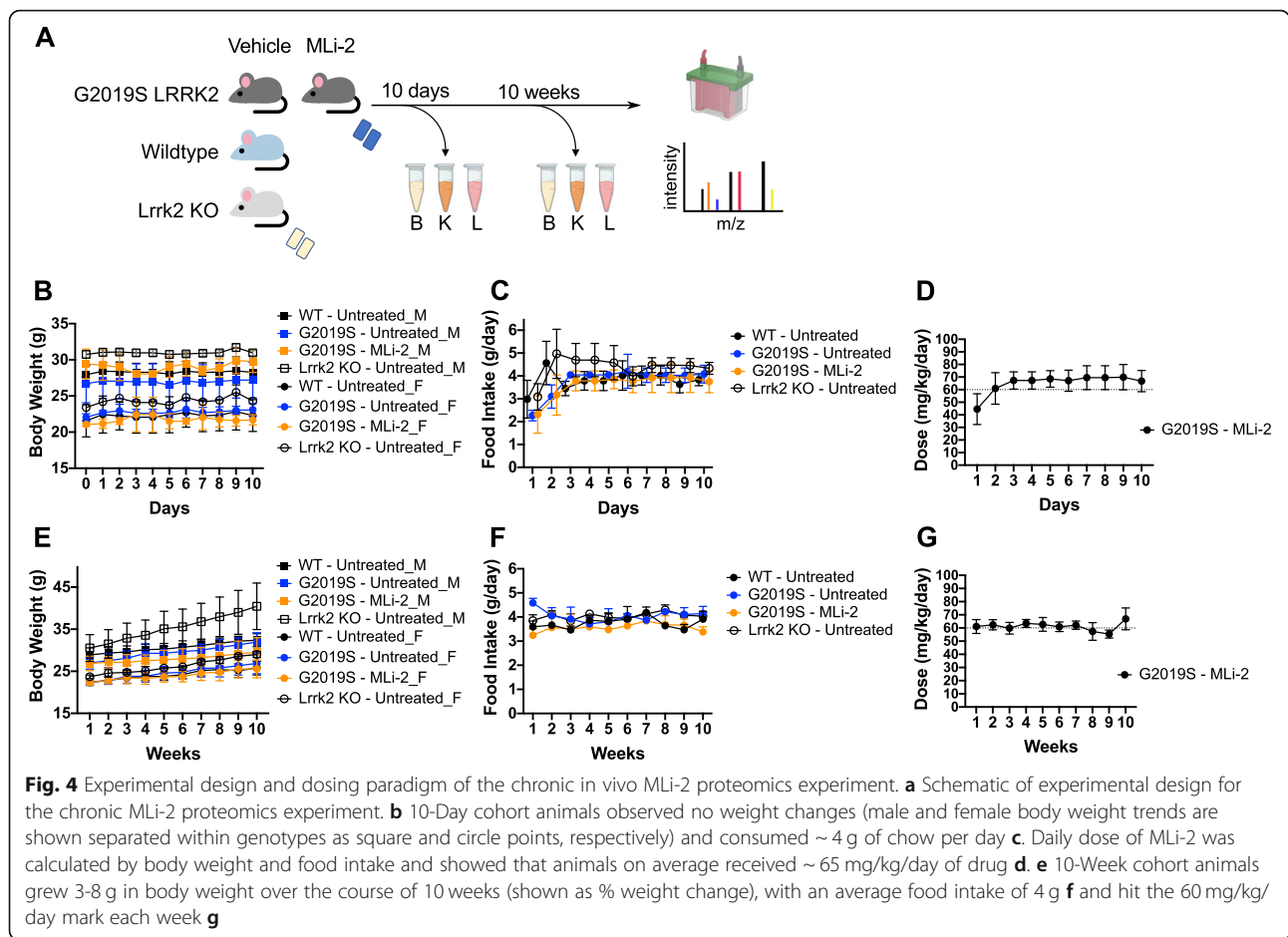
Fig. 3 Assessment of MLi-2 in-diet dosing and LRRK2 inhibition. G2019S LRRK2 knock-in mice were fed chow containing different concentrations of MLi-2 to reach 10, 30, or 60 mg/kg/day dosing compared to G2019S knock-in and WT LRRK2 cohorts that were fed control chow. After 10-days, animals were sacrificed 2–3 h post start of their light cycle. Western blots of brain, kidney and lung tissue samples are shown. **a, b** Across all tissues, a significant increase in S1292 phosphorylation is seen in G2019S mice compared to WT animals which is ameliorated with increasing MLi-2 doses reaching WT levels at 60 mg/kg/day. **c** A dose-response was seen in S935 dephosphorylation that plateaued at 30 mg/kg/day. Quantitation of phosphorylation levels is calculated as S1292 and S935 levels over total LRRK2 (**b** and **c**: one-way ANOVA with Tukey's post hoc, ****$P < 0.0001$, ***$P < 0.0002$, **$P < 0.0021$, *$P < 0.0332$; $n = 3$; SD bars shown; **b** $F_{(14, 30)} = 52.27$, **c** $F_{(14, 30)} = 56.58$)

the appropriate dose of MLi-2 and had comparable chow intake of ∼ 4 g, while weight increase was observed only in the 10-week cohort, particularly in the LRRK2 KO animals.

In both short-term and long-term cohorts, pS1292 levels of G2019S KI mice treated with MLi-2 were significantly decreased to levels comparable to wildtype mice (Fig. 5a - c). In the long-term cohort, mice treated with MLi-2 showed further dephosphorylation compared to wildtype levels in lung (Fig. 5c). S106 Rab12 showed significant dephosphorylation consistent throughout tissues, similar to the response of LRRK2 dephosphorylation (Fig. 5a, h - i), proving pRab12 is a reliable readout of LRRK2 activity and inhibition in this model. Additionally, phosphorylation of S935 LRRK2 was significantly reduced in all tissues compared to both G2019S and wildtype untreated animals in both cohorts as expected (Fig. 5a, d - e). In contrast, and similar to the tissue and dose-specific responses to acute inhibition, Rab10 and Rab29 did not respond consistently to LRRK2 inhibition in either 10-day or 10-week groups (Fig. S4 A-F). To test for covariates of Rab10 phosphorylation, we ran Pearson's correlation coefficient on all dosing

experiments in this study, testing for batch of tissue processing, gender, dose, age, treatment, and timepoints and found no contributing factor for the variation in phosphorylation (Fig. S4G). Furthermore, total LRRK2 levels in the 10-day MLi-2 cohort were comparable to their untreated G2019S counterparts in all tissues, whereas in the 10-week groups, there was a significant decrease in LRRK2 levels in kidney with treatment (Fig. 5a, f - g). This suggests chronic inactivation of LRRK2 leads to accelerated protein degradation, consistent with previous in vivo and in vitro studies using MLi-2 and other LRRK2 inhibitors [13, 24].

Unbiased proteomics reveal both therapeutic and dysregulatory effects in endolysosomal, trafficking, and mitochondrial pathways with chronic LRRK2 inhibition in mice

The above studies identified a chronic dosing regimen in which amelioration of the hyperphosphorylation of the S1292 autophosphorylation LRRK2 site and pS106 Rab12 in G2019S KI mice can be achieved to levels seen with wildtype LRRK2 at the endogenous level in vivo. We next used a series of proteomics approaches to

Fig. 4 Experimental design and dosing paradigm of the chronic in vivo MLi-2 proteomics experiment. **a** Schematic of experimental design for the chronic MLi-2 proteomics experiment. **b** 10-Day cohort animals observed no weight changes (male and female body weight trends are shown separated within genotypes as square and circle points, respectively) and consumed ~ 4 g of chow per day **c**. Daily dose of MLi-2 was calculated by body weight and food intake and showed that animals on average received ~ 65 mg/kg/day of drug **d**. **e** 10-Week cohort animals grew 3-8 g in body weight over the course of 10 weeks (shown as % weight change), with an average food intake of 4 g **f** and hit the 60 mg/kg/day mark each week **g**

determine, in an unbiased manner, what the consequences of this treatment might be to tissue proteome.

Proteomic analysis revealed 115 total proteins and 34 phospho-proteins that were differentially expressed in the kidney between chronic MLi-2-treated and untreated G2019S LRRK2 mice (false-discovery rate (FDR) adjusted $p < 0.05$; fold change (FC) > 1.4); (Fig. 6a, b). Among the top differentially abundant proteins, there was a strong enrichment for endolysosomal, trafficking and mitochondrial proteins (Fig. 6a, b). Multiple lysosomal proteins showed differential abundance, including cathepsin B (Ctsb), legumain (Lgmn), galactosidase beta 1 (Glb1), Lysosomal-associated membrane protein 1 (Lamp1), and N-acetylglucosamine-6-sulfatase (Gns). In addition, a number of proteins involved in vesicular trafficking, lipid metabolism, iron uptake and mitochondrial function were also significantly altered in kidneys of chronically treated animals. Hierarchical clustering of differential proteins in the G2019S MLi-2 treated group showed most similarity to the LRRK2 KO animals (Fig. 6c), suggesting that chronic inhibition of LRRK2 may mimic features of an absence of LRRK2 in the periphery. Among the significant phosphoprotein hits, additional

trafficking and mitochondrial proteins were identified, including sorting nexin 1 (pS188 Snx1) and vacuolar sorting protein 4b (pS102 Vps4b) (Fig. 6d). Analysis using Gene Ontology databases of significant hits from total and phospho-proteins showed enrichment of the endolysosomal system as well as mitochondrial membrane (Fig. 6e, f).

Additionally, we analyzed the human homologs of total and phospho-protein hits in silico to identify a LRRK2 protein-protein interactome using PINOT [23]. We converted the 115 total proteins and 34 phospho-proteins that were differentially expressed in the kidney between chronic MLi-2-treated and untreated G2019S LRRK2 mice to their human orthologues and identified 76 matches within the LRRK2 interactome. Five of the matching proteins (AHCYL1, EEF2, HSP90AA1, HSP90AB1 and RANBP2) were present in the first layer while 71 in the second layer of LRRK2 interactions. The difference between the average random result from 100, 000 simulated experiments (40 matches) and the real result (76 matches) was highly significant ($p = 2.78*10^{-11}$). The matching proteins were extracted from the LRRK2 interactome and their connectivity with LRRK2

Fig. 5 (See legend on next page.)

visualized (Fig. S7). This high degree of connectivity suggests that these proteins are in fact related to LRRK2 biology rather than an effect of MLi-2 treatment itself.

Proteomic analysis of brain tissue of 10-week MLi-2-treated mice revealed a number of mitochondrial proteins that showed statistically significant *p*-value (adjusted $p < 0.05$) compared to untreated G2019S KI controls, albeit with modest fold differences between treatment groups (Fig. 7a, b). These include Cytochrome C, NADH:Ubiquinone Oxidoreductase Subunit V3 (Nduvf3), the mitochondrial ATP synthase Atp5g1 and Voltage Dependent Anion Channel 2 (Vdac2) (Fig. 7a, b). Phospho-proteomics analysis revealed a decrease in S58 phosphorylation of the ion transporter Fxyd7 and increase in S109 phosphorylation of the PP2A inhibitor Ensa (Fig. 7b). Gene Ontology analyses revealed enrichment for proteins residing in different mitochondrial compartments as well synaptic proteins (Fig. 7c, d). These data suggest that even though the brain is more resilient in terms of potential endolysosomal defects that may be associated with LRRK2 inhibition, there are small changes in mitochondrial function resulting from chronic LRRK2 inhibition. Volcano plots comparing untreated groups of G2019S KI and wildtype mice showed that a number of proteins had the opposite trend to that seen in the chronic MLi-2 cohort (Fig. S5). For example, the transmembrane ion transporters Sfxn2 and Sfxn3, showed a modest upregulation in kidneys of G2019S LRRK2 compared to wildtype mice and this was rescued in the chronic MLi-2 G2019S LRRK2 cohort (Figs. S5A and Fig. 6a). For some mitochondrial proteins identified in our brain proteomics screen, Cytochrome C, Vdac1, Ndufs3, and Ndufv2 were downregulated in G2019S LRRK2 brain compared to wildtype and this was reversed in the chronic MLi-2 G2019S LRRK2 cohort (Figs. S5B and 7A). This suggests that treatment can significantly alter the expression of mitochondrial proteins in G2019S KI mice in a direction consistent with therapeutic potential.

Finally, 441 total proteins and 189 phosphopeptides were identified in whole lung homogenates as significant with an adjusted *p*-value of < 0.05, of which 14 phosphopeptides and 6 total proteins passed the fold change cutoff of 1.4x in the G2019S MLi-2 treated versus untreated mice (Fig. 7e-f). Of the significant proteins identified, we attempted to validated Myristoylated alanine-rich C-kinase substrate.

(Marcks) due to potential relevance to known LRRK2 pathways. Phosphorylation of Marcks within its ED domain localizes the protein to the plasma membrane of cells, as unphosphorylated protein is released into the cytosol and can bind GTP-bound Rab10 [25], a LRRK2 substrate. Marcks may also be relevant to lung inflammation [26, 27], where LRRK2 has also been implicated [28]. Marcks phosphorylated at S163 was significantly decreased in the MLi-2 treated group and was validated via Western blot (Fig. S6C-D). Additionally, Cyp1a1, a monooxygenase widely distributed via the bloodstream responsible for metabolizing various classes of drugs and carcinogens [29], was upregulated in the lungs of G2019S KI mice treated with MLi-2, which we also validated (Fig. S6C-D). Although these results confirm validity of the lung proteomics results, we did not recover any significant Gene Ontology categories, presumably due to the relative sparsity of significant changes in the lung proteome.

Validation of endolysosomal, trafficking, and mitochondrial proteins in chronically LRRK2 inhibited mice reveal both a rescue of mutant-driven effects and dysregulatory patterns in vivo

We next wanted to validate protein hits observed from our proteomics screens in kidney tissue. Through western blot analyses, we found two distinct patterns of effects, one we characterized as beneficial, based on a reverse in protein expression from G2019S KI animal levels back to wildtype levels and the other dysregulatory, based on a mimicking effect comparable to LRRK2 KO animals (Fig. 8a). In the former category, the non-glycosylated form of Lamp1, the ESCRT-0 protein Hgs, and the iron and serine mitochondrial transporter Sfxn3 were all shown to be significantly increased in protein levels in untreated G2019S KI mice compared to wildtype animals. These levels were ameliorated back to wildtype levels after MLi-2 treatment for 10 weeks (Fig. 8b). Conversely, the glycosylated form of Lamp1 and the lysosomal hydrolase Legumain were both significantly increased in the same animals, patterns of which have been previously characterized in LRRK2 KO animals, and is recapitulated here in our LRRK2 KO mice in this
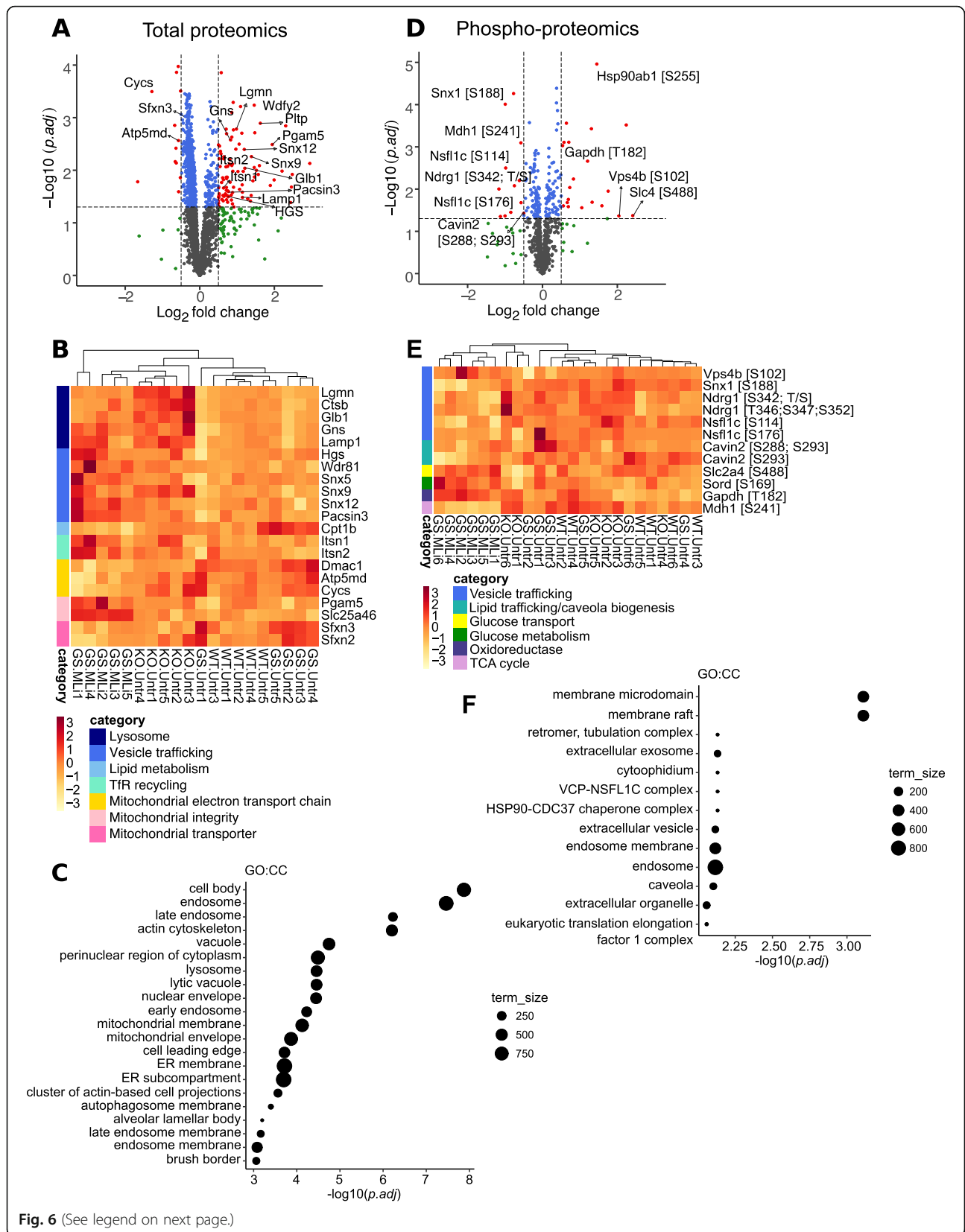
Fig. 6 (See legend on next page.)

(See figure on previous page.)

Fig. 6 Proteomic analysis of changes in kidney between G2019S LRRK2 MLi-2 and G2019S vehicle 10-week treated mouse cohorts. a Volcano plot showing changes in protein levels following chronic treatment, depicted as log2 fold changes (*x*-axis) versus the −log10 of adjusted *p*-values (*y*-axis) for each protein. A number of endolysosomal proteins were upregulated, including legumain and other lysosomal proteases in kidneys of G2019S LRRK2 KI mice that received chronic MLi-2 treatment for 10 weeks, compared to vehicle G2019S KI controls. **b** Heat maps of selected significant hits across the WT, G2019S KI and LRRK2 KO vehicle cohorts as well as the G2019S KI chronic MLi-2 cohort, highlighting proteins involved in vesicular trafficking, lipid metabolism, transferrin recycling and mitochondrial homeostasis. Z score is used for scaling. Using unsupervised hierarchical clustering we show that the G2019S MLi-2 and LRRK2 KO mice cluster together, suggesting that chronic LRRK2 inhibition mimics a LRRK2 KO effect in kidney. **c** Bubble plot showing GO:CC term enrichment in the significant total protein hits highlights enrichment for endolysosomal processes and compartments. **d** Volcano plot showing changes in phospho-proteins in G2019S MLi-2 treated vs G2019S untreated mice, highlighting dysregulation of proteins involved in trafficking, glucose transport and metabolism, and the TCA cycle **e**. **f** Bubble plot showing GO:CC term enrichment in the significant phospho-peptide hits highlights enrichment for endolysosomal processes as well as kidney-specific functional processes. Volcano plots key: grey = non-significant, blue = < 0.05 *p*-value, green = > 1.4x log fold change, red = < 0.05 p-value and > 1.4x log fold change

cohort [30]. In addition, we also discovered that the motor adaptor protein Jip4 was significantly reduced in LRRK2 KO mice, and this was also seen in G2019S KI mice treated with MLi-2 (Fig. 8c). Jip4 has recently been discovered, by our lab and others, to bind to LRRK2-dependent phosphorylated Rab8a, Rab10, and Rab35 and can be recruited to damaged lysosomal membranes [31, 32]. In the current study, all of these phenotypes are kidney-specific, as no significant difference of these proteins was observed in brain or lung tissues (Fig. S6 A-D). Additionally, these differences were not seen in mice that were treated with MLi-2 for only 10 days (Fig. S6 G-I), suggesting that chronic inhibition of LRRK2 is necessary to see these effects.

Discussion

In the present study, we have evaluated various markers of LRRK2 inhibition in vivo and demonstrated their utility across brain and peripheral tissues. In both acute and chronic treatment paradigms, we focused on a treatment paradigm that might reasonably mimic clinical applications where the hyperactive mutant of LRRK2, G2019S, expressed at the endogenous level is chronically depressed to that of wildtype animals. We performed proteomics to examine the molecular effects of chronic LRRK2 inhibition and identified changes to the endolysosomal, trafficking, and mitochondrial systems in kidneys at the total protein level as well as phosphorylation events. In addition, we noted a modest but statistically significant change in mitochondrial proteins, most notably enriched within the mitochondrial electron transport chain, in the brains of MLi-2 treated G2019S mice.

In our studies in mouse tissue, measuring LRRK2 phosphorylation, particularly the pS1292 autophosphorylation site, provides the most reliable marker of both G2019S-induced hyperactivity and MLi-2 dependent inhibition. Whether this can be extrapolated to human clinical samples is unclear as current tools have not yet allowed for robust detection of pS1292 LRRK2 in peripheral blood, although some studies have

demonstrated its efficacy in urinary and CSF exosomes [33, 34]. Using the commercially available pRab antibodies, we found that S106 Rab12 phosphorylation pattern resembled that of pS1292 LRRK2 most closely across experiments, in that G2019S KI mice displayed hyperphosphorylation that was ameliorated with MLi-2 treatment. This is in contrast to the hyperphosphorylation pattern of other Rab substrates, which have been demonstrated in mutations within the GTPase domain but not for G2019S [35, 36]. Thus, for G2019S-carriers and potentially other PD cases, detection of pRab12 has potential as a biomarker for LRRK2 activity and inhibition.

With regard to pRab10 and pRab29, we show that their levels do not correlate with MLi-2 treatment in vivo, particularly within the chronic in-diet treatment paradigm. We hypothesize a few reasons for this. Firstly, Vieweg et al. reported a PINK1-dependent S111 phospho-site conserved across multiple Rab substrates that can negatively regulate subsequent LRRK2-dependent phosphorylation by preventing Switch-II binding with its GEF, as demonstrated with pT72 Rab8a in vitro [37]. It is possible that Rab10 and Rab29 LRRK2-dependent phosphorylation could be regulated through a similar unknown mechanism and thus no change to basal levels of phosphorylation are observed with LRRK2 inhibition. Additionally, other unknown kinases that phosphorylate these Rabs on the same residue as LRRK2 and normally compete with LRRK2 for binding may be able to phosphorylate these proteins more readily under conditions of LRRK2 inhibition. Lastly, we recently reported differing localization patterns between pS106 Rab12 and pT73 Rab10 when artificially trapping LRRK2 to different cellular membranes. Independent of which membrane LRRK2 was directed to intracellularly, pRab12 was found to colocalize with LRRK2, whereas pRab10 was primarily detected at perinuclear lysosomes and Golgi after directing LRRK2 to these membranes [38]. This falls in line with the idea that a more complex mechanism surrounds the Rab10:LRRK2 interaction and
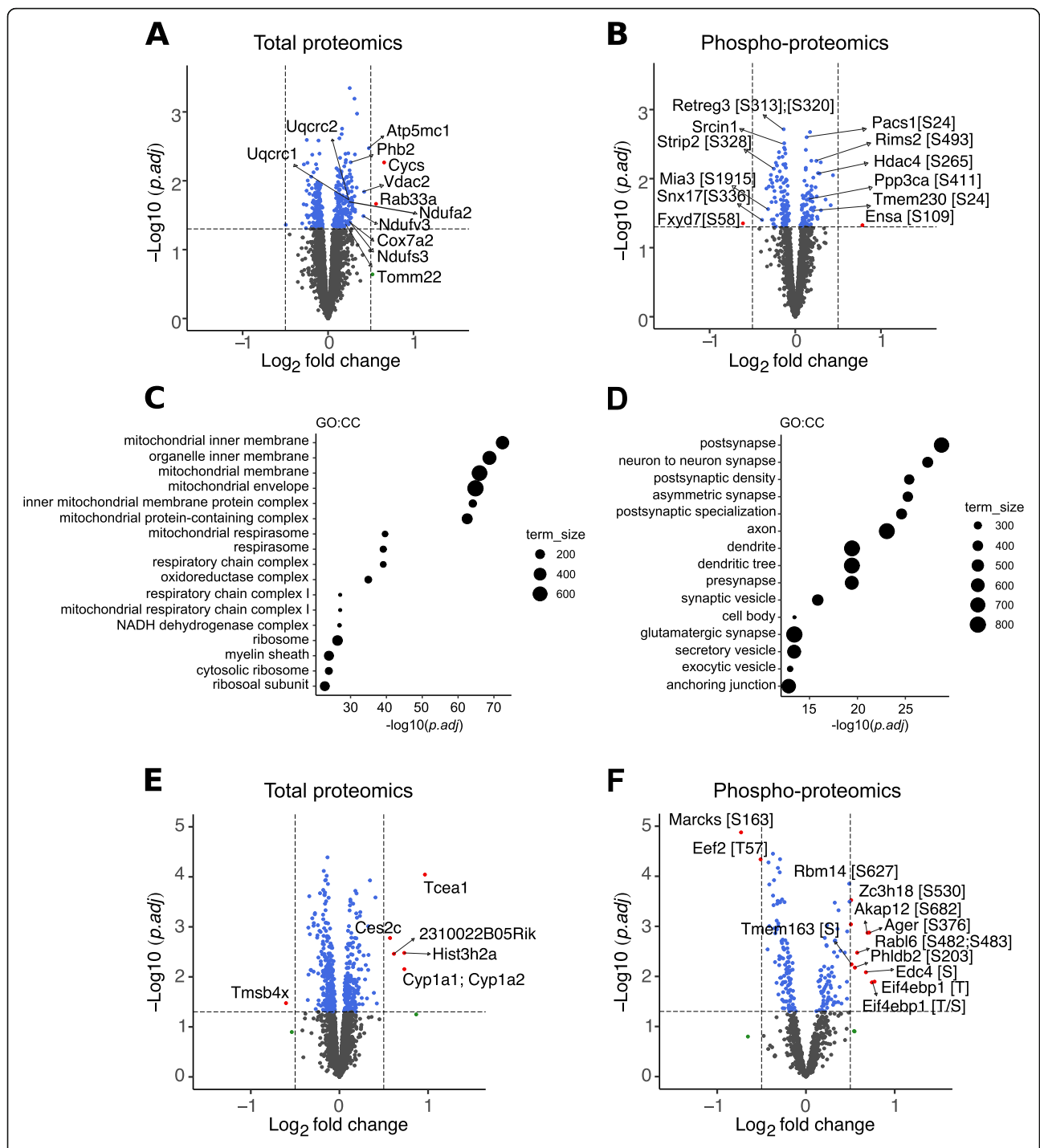
Fig. 7 Proteomic analysis of changes in brain and lung between G2019S LRRK2 MLi-2 and G2019S vehicle 10-week treated mouse cohorts. A volcano plot from total proteomics of whole brain tissue comparing the G2019S chronic MLi-2 cohort versus G2019S KI vehicle controls **a**. Modest upregulation was observed in mitochondrial proteins with treatment, specifically proteins of the electron transport chain **a**. Heatmap visualizes changes in phosphopeptides with treatment highlighted proteins involved in vesicular trafficking and postsynaptic regulation on a z score scale **b**. GO:CC term enrichment bubble plots were generated from the significant hits of the total and phospho-proteomics showing high enrichment for mitochondrial compartments, as well as proteins associated with postsynaptic function, respectively **c-d**. Volcano plots from total and phospho-proteomics of whole lung homogenates comparing treated versus untreated G2019S KI mice **e-f**. Volcano plots key: grey = non-significant, blue = < 0.05 *p*-value, green = > 1.4x log fold change, red = < 0.05 *p*-value and > 1.4x log fold change

Fig. 8 (See legend on next page.)

thus any influence LRRK2 has on Rab10 is more conditional compared to Rab12. These hypotheses could explain the lack of dephosphorylation of T73 Rab10 in the presence of MLi-2, and further exploration of other kinases and phosphatases that regulate Rab GTPase phosphorylation, such as PPM1H [39], will be necessary to elucidate the functional dynamics between Rab10 and LRRK2 across different organelles.

Using these two validated biomarkers, pS1292 LRRK2 and pS106 Rab12, a 60 mg/kg/day dosing of MLi-2 in G2019S KI mice via in-diet dosing for 10 days or 10 weeks was shown to be sufficient to revert the hyperactive mutation approximately to wild type levels. Such an approach could be helpful in identifying similar dosing regimens in humans. Importantly, we show that measurements in some peripheral tissues, particularly kidney, reflect events in the brain, the target organ for any PD clinical trial. However, we observed that after long-term chronic MLi-2 in-diet dosing, S1292 LRRK2 and S106 Rab12 phosphorylation was significantly lower than wildtype levels in lung. It is possible that lung tissue is more sensitive to LRRK2 inhibition than other tissues considered here and has also been suggested in a recent study investigating the toxicological and morphological effects of LRRK2 inhibition on nonhuman primate lungs, in which high doses of three structurally distinct LRRK2-specific inhibitors, including MLi-2, induced vacuolated cytoplasm in type II pneumocytes, however no pulmonary deficits were observed and the phenotype was quickly reversed after cessation of treatment [16]. These data were recently recapitulated in mice by Bryce and colleagues. In this study the authors treated wildtype mice with in-diet MLi-2 for six months and showed that the levels of prosurfactant protein C were increased early on in a 60 mg/kg/day dosing regimen and decreased back to control levels after 90 days [40]. These reports suggest that there is a lung-specific LRRK2-dependent mechanism that is affected by chronic LRRK2 inhibition. Based on these data, we probed our 10-day and 10-week treatment cohorts for proSP-C in lung tissue via Western blot. We found no changes at either timepoints in G2019S KI mice treated with MLi-2, although a slight but significant elevation of proSP-C was observed in the Lrrk2 KO animals (Fig. S6C-F). This would imply that the absence of LRRK2 has an effect of proSP-C levels and MLi-2 treatment would have a more dramatic effect on wildtype mouse lung tissue than in a G2019S KI. A 60 mg/kg-dosing inhibition on wildtype activity could potentially mimic LRRK2 deficiency and this is not recapitulated in our regimen where we aimed to lower G2019S LRRK2 activity to wildtype levels. Another important aspect to note is the potential limitation in detecting surfactant changes by western blot, due to their ~ 90% lipid/10% composition and further lipid analysis would be more informative in comparing wildtype and G2019S hyperactive kinase inhibition for possible differences. Overall, these data suggest that while LRRK2 inhibitors can be used to diminish hyperactive kinase to wild type levels of activity, there are tissue-specific differences in activity and stability of the protein that may be important to consider when using peripheral engagement to infer brain inhibition.

Unbiased proteomic screens revealed significant differences in endolysosomal, trafficking, and mitochondrial proteins in the kidneys of treated compared to untreated G2019S KI animals. We identified two subsets of proteins, those that suggest a therapeutic effect and those that are dysregulatory, with long-term chronic LRRK2 inhibition in vivo. Strikingly, all differential changes were specific to our 10-week treatment cohort compared to our 10-day cohort. This suggests that these molecular changes are specific to the length of LRRK2 inhibition. Thus, future preclinical efforts are needed that include long-term inhibitor treatment in order to understand what may happen in human disease. Proteins altered towards a therapeutic effect included non-glycosylated Lamp1, Hgs, and Sfxn3, whereas glycosylated Lamp1, leguman, and Jip4 showed likeness to LRRK2 KO expression levels. Based off of these proteins, we hypothesize a mechanism for the endolysosomal trafficking pathway in the context of both LRRK2 kinase hyperactivity and chronic inhibition, in which both dysfunctional LRRK2 kinase states converge on the same pathway through different means depicted in Fig. 8d.

In recent years, the role of LRRK2 at the lysosome has been a focus of research that explores how mutations in this gene cause disease. Multiple labs have now reported lysosomal dysfunction in both LRRK2 KO and G2019S mutant models, LRRK2 recruitment to lysosomes under stress as well as alpha-synuclein accumulation in Lrrk2 deficient models [10, 17, 32, 41]. We show here that increased non-glycosylated Lamp1 found in G2019S KI mice was ameliorated back to wildtype levels after 10-week MLi-2 treatment. Glycosylation of Lamp1 is an important feature in maintaining lysosomal stability and protein transport across its membrane [42]. Glycosylation is initiated in the rough endoplasmic reticulum and moves through the Golgi before reaching lysosomes. Thus, an increase in the non-glycosylated form suggests either that there has been an incomplete maturation of Lamp1 before reaching the lysosomes or an upregulation in Lamp1 translation due to increased lysophagy in the kidneys of G2019S KI mice. Premature lysophagy and redirection of proteins for degradation to the remaining active lysosomes may then overwhelm the system and lead to lysosomal stress. In contrast, an increase in glycosylated Lamp1 has been previously characterized in Lrrk2 KO mice and in the postmortem brains of sporadic PD patients [30, 43] and is shown here in G2019S KI mice treated with MLi-2 and LRRK2 KO mice. This suggests that there can be lysosomal buildup and protein accumulation in the absence of active LRRK2. Both alterations of Lamp1 suggest LRRK2 kinase activity plays a role in the integrity of lysosomes, and chronic inhibition of LRRK2 may restore healthy levels of the non-glycosylated form, while perpetuating a shift that mimics a loss of function effect in its glycosylated form. This suggests that treatment with LRRK2 kinase inhibitors may require careful consideration of both premature lysophagy and lysosomal protein accumulation.

In brain tissue, chronic MLi-2 treatment in G2019S KI mice showed a modest but significant upregulation of mitochondrial proteins compared to their untreated counterparts (Fig. 7a). Production of reactive oxygen species (ROS), mitochondrial elongation, decreased ATP production and mitochondrial DNA damage have been reported in G2019S PD patient-derived skin biopsies and G2019S-LRRK2 in vitro models [44–48]. In brain tissue, the majority of mitochondrial proteins found in our screens were associated with the respiratory chain Complex I and III. Further studies are needed in order to elucidate the effects of LRRK2 on the respiratory chain system. However, these results do not suggest a potential concern for LRRK2 kinase inhibition affecting mitochondrial function as in general they respond in the opposite direction of effect to the pathogenic G2019S mutation, i.e. are in the therapeutic direction. A limitation of this study is that whole brain homogenate was used for the proteomics analysis which may have limited our ability to determine regional- and cell type-dependent LRRK2 mechanisms. Further studies focused on regional and cell-specific parameters can shed a deeper mechanistic insight into the molecular consequences of LRRK2 inhibition in the brain.

Conclusion

The aim of the present study was twofold: to assess the suitability of new antibodies of known LRRK2 substrates as biomarkers for LRRK2 kinase inhibition and to evaluate what molecular effects are observed when LRRK2 is chronically inhibited. We found that pRab12 is a reliable readout of LRRK2 activity and inhibition, and that phosphorylation patterns seen in the periphery reflect events in the brain. Additionally, our study highlights the molecular effects of chronic inhibition that remain to be explored and warrant further investigation in the light of the ongoing clinical trials. What remains to be determined is which of these effects are truly protective or damaging, and how relevant they are to what happens in human disease.

As of yet, there continues to be a significant unmet medical need in the field of neurodegeneration for effective, long lasting treatments that either halt or slow disease progression. Existing drug treatments for PD target the symptoms of the disease rather than cause, and do not modify disease course. Clinical trials are currently underway to assess the safety and efficacy of LRRK2-specific kinase inhibition in PD patients [49]. In parallel with these trials, future work will need to elucidate the underlying disease mechanisms that cause PD and how LRRK2 mutations ultimately lead to neurodegeneration. Understanding the pathobiological role of LRRK2 kinase activity will greatly aid in the development and optimization of therapeutic strategies.

Supplementary Information

The online version contains supplementary material available at https://doi.org/10.1186/s13024-021-00441-8.

Additional file 1 Table S1: Table of antibody summary. All antibodies used in this study are listed with catalog numbers, and working concentrations used. IgG concentrations are supplied in brackets.

Additional file 2 S2. Characterization of pT73 Rab10 [MJF-R21 and MJF-R21–22-5] antibodies. (A, B) HEK293FT cells transiently expressing LRRK2 mutant constructs were analyzed for endogenous Rab10 phosphorylation [MJF-R21]. The LRRK2 genetic variants R1441G, Y1699C and I2020T invoked the highest increase in Rab10 phosphorylation compared to WT LRRK2, while the kinase-dead K1906M LRRK2 construct conferred a significantly lower pRab10 levels compared to WT. (C, D) HEK293FT cells transiently expressing LRRK2 genetic variants following Rab10 siRNA knock-down were probed for Rab10. Rab10 levels revealed successful knock-down of endogenous Rab10 compared to non-targeting controls. The pT73 Rab10 [MJF-R21] antibody detected a band at ~ 24 kDa, which was not detected in the Rab10 siRNA groups, suggesting specificity for Rab10. (E, F) In a similar experiment to (C), Rab10 expression was knocked-down in primary astrocytes from WT and homozygous G2019S LRRK2 knock-in mice. Rab10 knock-down was followed by a significant decrease in pT73 Rab10 signal using the MJF-R21 antibody (E, F). (G, H) Primary astrocytes treated with 1 μM of MLi-2 for 90 min showed that both pT73 Rab10 antibodies (MJF-R21 and MJF-R21–22-5) show significantly decreased levels of phosphorylation compared to control cells. Quantitation of phosphorylation levels in D and F are presented as raw pT73 intensity normalized to loading while B and H represent T73 phosphorylation signal over total Rab10 levels (B: one-way ANOVA with Tukey's post hoc, ****$P < 0.0001$, ***$P < 0.0002$, $n = 3$, $F_{(8, 18)} = 45.45$. D: two-way ANOVA with Sidak's multiple comparisons test; LRRK2 construct, $p < 0.0001$, $F_{(2, 12)} = 30.73$; siRNA, $p < 0.0001$, $F_{(1, 16)} = 550.0$, $n = 3$. F: two-way ANOVA with Sidak's multiple comparisons test; LRRK2 construct, $p = 0.7361$, $F_{(1, 8)} = 0.1218$; siRNA, $p < 0.0001$, $F_{(1, 8)} = 56.29$, $n = 3$. H: one-way ANOVA with Tukey's post hoc, ****$P < 0.0001$, $n = 3$; $F_{(3, 15)} = 160.3$). **S3**. Characterization of pS106 Rab12 [MJF-25-9] and pT71 Rab29 [MJF-R24–17-1] antibodies. (A) HEK293FT cells transiently expressing LRRK2 genetic variants following siRNA knock-down of Rab12 were analyzed for Rab12 phosphorylation. The pS106 Rab12 antibody showed a strong band at ~ 25 kDa with LRRK2 transfection, which was significantly decreased by Rab12 siRNA compared to non-targeting control (A, B). (C, D) HEK293FT cells transiently expressing LRRK2 mutant constructs were analyzed for endogenous pT71 Rab29. Endogenous Rab29 was found hyperphosphorylated in R1441C, R1441G, Y1699C, G2019S and I2020T LRRK2 expressing cells, compared to WT LRRK2. (E, F) siRNA Rab29 knockdown resulted in a significant decrease in pT71 Rab29 signal in HEK293FT cells over-expressing LRRK2 mutants compared to non-targeting controls. (G) The T71 Rab29 antibody tested did not detect a band in cells expressing the T71A Rab29 phospho-null variant while a strong band was observed in cells expressing WT Rab29 construct, in co-expression with LRRK2 constructs. (H) Lung tissue collected from Rab29 KO mice tissue showed no pT71 Rab29 signal, whereas G2019S Lrrk2 knock-in mice showed increase in Rab29 phosphorylation, compared to WT mice. Quantitation of phosphorylation levels is presented as S106 normalized to loading (cyclophilin B levels; in B), T71 over total Rab29 (in D) or normalized to loading (F). (B: two-way ANOVA with Sidak's multiple comparisons test; LRRK2 construct, $p = 0.0083$, $F_{(2, 12)} = 7.329$; siRNA, $p < 0.0001$, $F_{(1, 16)} = 367.8$, $n = 3$. D: one-way ANOVA with Tukey's post hoc, ****$P < 0.0001$, ***$P < 0.0002$, ** < 0.004, $F_{(8, 18)} = 528.0$, $n = 3$. F: two-way ANOVA with Sidak's multiple comparisons test; LRRK2 construct, $p < 0.0001$ $F_{(2, 12)} = 31.83$; siRNA, $p < 0.0001$, $F_{(1, 16)} = 191.1$, $n = 3$. Mean values with SD bars shown). **S4**. pT73 Rab10 and pT71 Rab29 phosphorylation following chronic MLi-2 treatment. Full blots from the 10-day and 10-week chronic studies are shown to account for animal-to-animal variability (A, B). pT73 Rab10 across tissues and treatment groups show large variability with no discernable trend after LRRK2 inhibition (C, E). Rab29 T71 phosphorylation levels do not respond to treatment across tissues and time points, with exception to brain tissue of the short-term cohort (D, F). (G) Pearson's correlation coefficients were conducted to test confounding variables within the acute and chronic paradigms of this study with regard to pT73 Rab10 variability, of which relationships with dose of MLi-2, length of experiment, age of mice, gender, and batch of tissue processing were not found. One-way ANOVA with

Tukey's post hoc; $n = 6$; ****$P < 0.0001$, ***$P < 0.0002$, **$P < 0.005$, *$P < 0.05$; (C) $F_{(11, 60)} = 28.56$, (D) $F_{(11, 60)} = 43.20$, (E) $F_{(11, 59)} = 24.70$, (F) $F_{(11, 60)} = 8.279$. **S5**. Proteomic analysis of changes in brain, kidney, and lung between untreated G2019S LRRK2 and wildtype mouse cohorts. Volcano plots depicting differences in levels of total proteins in kidney (A), brain (B), and lung (C) between untreated G2019S KI and wildtype mice. A number of proteins show subtle changes involved in iron transport and mitochondrial homeostasis are highlighted. Lung hits were not preferentially enriched for any particular cellular component. Volcano plots key: grey = non-significant, blue = < 0.05 p-value, green = > 1.4x log fold change, red = < 0.05 p-value and > 1.4x log fold change. **S6**. Kidney hits are tissue-specific with proteins identified in the 10-week cohort and do not show differential change in the 10-day cohort. Proteins identified in the kidney proteomics and validated via Western blot were also investigated in the brain and lung tissues of the 10-week cohort animals. We found that these proteins (Jip4, Lamp1, HGS/Vps27, Sfxn3 and legumain) were not statistically altered in the G2019S KI animals, neither MLi-2 treated nor untreated, in brain and lung (A-D). This implies a kidney-specific phenotype of these altered lysosomal and other membrane proteins. Additionally, we explored two of the mitochondrial proteins found in the brain total proteomics, Atp5mc1 and Cytochrome C. No difference was observed in G2019S MLi-2 treated mice compared to any other group (C-D). Additionally, proteins Cyp1a1 and pS163 Marcks identified in the lung proteomics were validated via Western blot analysis (C-D). Prosurfactant C was measured in both 10-week (C) and 10-day (E) cohorts in lung tissue of which Lrrk2 KO animals showed a significant elevation while G2019S KI animals receiving MLi-2 treatment were not affected in either cohort (C-F). Proteins identified as statistically significant in the 10-week cohort were also investigated in the 10-day cohort in order to determine if the effects observed occur after continued use of LRRK2 inhibitor long-term as opposed to more immediate effects (after 10 days). Western blot analysis confirmed that both therapeutic and dysregulatory effects were not observed in the 10-day cohort of treated animals (G-I). This suggests that the endolysosomal, trafficking, and mitochondrial changes we observed in our proteomics screen are effects of long-term treatment with MLi-2 in G2019S KI mice. Interestingly, the increase in protein expression in our untreated G2019S KI that was observed in our 10-week cohort, specifically non-glycosylated Lamp1, Hgs, and Sfxn3 was not seen in our 10-day cohort (H). Our current hypothesis is that these changes in protein expression are age-dependent in the context of the G2019S mutation in the mouse model, as the 10-week animals are double the age of the 10-day cohort at time of sacrifice. One-way ANOVA with Tukey's post hoc; $n = 6$; ****$P < 0.0001$, ***$P < 0.0002$, **$P < 0.005$, *$P < 0.05$; (B) Jip4: $F_{(3, 20)} = 0.8688$, glycosylated Lamp1: $F_{(3, 20)} = 0.4520$, HGS: $F_{(3, 20)} = 0.1410$, Legumain: $F_{(3, 20)} = 0.2312$, Atp5mc1: $F_{(3, 20)} = 1.953$, Sfxn3: $F_{(3, 20)} = 0.2285$, Cytochrome C: $F_{(3, 20)} = 1.698$, (D) Jip4: $F_{(3, 20)} = 1.772$, HGS: $F_{(3, 20)} = 0.1636$, Legumain: $F_{(3, 20)} = 0.1724$, Sfxn3: $F_{(3, 20)} = 1.156$, pS163 Marcks: $F_{(3, 20)} = 4.739$, Cyp1a1: $F_{(3, 20)} = 208.2$, ProSP-C: $F_{(3, 20)} = 4.495$, (F) ProSP-C: $F_{(3, 20)} = 4.185$, (H) non-glycosylated Lamp1: $F_{(3, 20)} = 2.802$, Hgs: $F_{(3, 20)} = 5.173$, Sfxn3: $F_{(3, 20)} = 3.002$, (I) glycosylated Lamp1: 4.702, Legumain: $F_{(3, 20)} = 4.409$, Jip4: $F_{(3, 20)} = 12.35$. **S7**. LRRK2 protein interactome from long-term chronic kidney proteomics. The 149 mouse kidney protein hits from chronically treated G2019S KI mice were converted to their human orthologues for LRRK2 interactome analyses using PINOT online tool. Seventy-six matches were identified within the LRRK2 interactome. Five of the matching proteins (AHCYL1, EEF2, HSP90AA1, HSP90AB1 and RANBP2) were present in the first layer while 71 in the second layer of LRRK2 interactions (one step from direct LRRK2 interactors). Two visualizations are shown: (A) highlights the proteins from total or phospho-proteomics runs, (B) depicts primary and secondary interactome layers.

Additional file 3:.

Additional file 4:.

Additional file 5:.

Author details
[1]Cell Biology and Gene Expression Section, Laboratory of Neurogenetics, National Institute on Aging, National Institutes of Health, Bethesda, MD, USA. [2]School of Pharmacy, University of Reading, Whiteknights Campus, Reading, UK. [3]Proteomic Core Facility, National Institute of Neurological Disorders and Stroke, Bethesda, MD, USA. [4]UCL School of Pharmacy, Brunswick Square, London, UK. [5]Royal Veterinary College, Royal College Street, London, UK. [6]Department of Neurodegenerative Diseases, UCL Queen Square Institute of Neurology, London, UK. [7]Department of Neuroscience, Center for Translational Research in Neurodegenerative Disease, Norman Fixel Institute for Neurological Diseases, University of Florida College of Medicine, Gainesville, Florida, USA.

References
1. Rudenko IN, Cookson MR. Heterogeneity of leucine-rich repeat kinase 2 mutations: genetics, mechanisms and therapeutic implications. Neurother J Am Soc Exp Neurother. 201;11(4):738–50.
2. Greggio E, Jain S, Kingsbury A, Bandopadhyay R, Lewis P, Kaganovich A, et al. Kinase activity is required for the toxic effects of mutant LRRK2/ dardarin. Neurobiol Dis. 2006;23(2):329–41.
3. West AB, Moore DJ, Choi C, Andrabi SA, Li X, Dikeman D, et al. Parkinson's disease-associated mutations in LRRK2 link enhanced GTP-binding and kinase activities to neuronal toxicity. Hum Mol Genet. 2007;16(2):223–32.
4. Cookson MR. The role of leucine-rich repeat kinase 2 (LRRK2) in Parkinson's disease. Nat Rev Neurosci. 2010;11(12):791–7.
5. Kluss JH, Mamais A, Cookson MR. LRRK2 links genetic and sporadic Parkinson's disease. Biochem Soc Trans. 2019;5:BST20180462.
6. Healy DG, Falchi M, O'Sullivan SS, Bonifati V, Durr A, Bressman S, et al. Phenotype, genotype, and worldwide genetic penetrance of LRRK2-associated Parkinson's disease: a case-control study. Lancet Neurol. 2008; 7(7):583–90.
7. Alessi DR, Sammler E. LRRK2 kinase in Parkinson's disease. Science. 2018; 360(6384):36–7.
8. West AB. Achieving neuroprotection with LRRK2 kinase inhibitors in Parkinson disease. Exp Neurol. 2017;298:236–45.
9. Estrada AA, Sweeney ZK. Chemical biology of Leucine-rich repeat kinase 2 (LRRK2) inhibitors. J Med Chem. 2015;58(17):6733–46.
10. Eguchi T, Kuwahara T, Sakurai M, Komori T, Fujimoto T, Ito G, et al. LRRK2 and its substrate Rab GTPases are sequentially targeted onto stressed lysosomes and maintain their homeostasis. Proc Natl Acad Sci U S A. 2018; 115(39):E9115–24.
11. Daher JPL, Abdelmotilib HA, Hu X, Volpicelli-Daley LA, Moehle MS, Faser KB, et al. LRRK2 Pharmacological Inhibition Abates α-Synuclein Induced Neurodegeneration. J Biol Chem. 2015:jbc.M115.660001.
12. Lee BD, Shin J-H, VanKampen J, Petrucelli L, West AB, Ko HS, et al. Inhibitors of leucine-rich repeat kinase-2 protect against models of Parkinson's disease. Nat Med. 2010;16(9):998–1000.
13. Fell MJ, Mirescu C, Basu K, Cheewatrakoolpong B, DeMong DE, Ellis JM, et al. MLi-2, a potent, selective, and centrally active compound for exploring the therapeutic potential and safety of LRRK2 kinase inhibition. J Pharmacol Exp Ther. 2015;355(3):397–409.
14. Fuji RN, Flagella M, Baca M, Baptista MAS, Brodbeck J, Chan BK, et al. Effect of selective LRRK2 kinase inhibition on nonhuman primate lung. Sci Transl Med. 2015;7(273):273ra15.
15. Andersen MA, Wegener KM, Larsen S, Badolo L, Smith GP, Jeggo R, et al. PFE-360-induced LRRK2 inhibition induces reversible, non-adverse renal changes in rats. Toxicology. 2018;395:15–22.
16. Baptista MAS, Merchant K, Barrett T, Bhargava S, Bryce DK, Ellis JM, et al. LRRK2 inhibitors induce reversible changes in nonhuman primate lungs without measurable pulmonary deficits. Sci Transl Med. 2020; 12(540). Available from: https://stm.sciencemag.org/content/12/540/eaav0820 [cited 2020 26 Apr]
17. Tong Y, Yamaguchi H, Giaime E, Boyle S, Kopan R, Kelleher RJ, et al. Loss of leucine-rich repeat kinase 2 causes impairment of protein degradation pathways, accumulation of α-synuclein, and apoptotic cell death in aged mice. Proc Natl Acad Sci. 2010;107(21):9879–84.
18. Kluss JH, Conti MM, Kaganovich A, Beilina A, Melrose HL, Cookson MR, et al. Detection of endogenous S1292 LRRK2 autophosphorylation in mouse tissue as a readout for kinase activity. Npj Park Dis. 2018;4(1):13.
19. Ritchie ME, Phipson B, Wu D, Hu Y, Law CW, Shi W, et al. Limma powers differential expression analyses for RNA-sequencing and microarray studies. Nucleic Acids Res. 2015;43(7):e47.
20. Blighe K, Rana S, Lewis M. EnhancedVolcano: Publication-ready volcano plots with enhanced colouring and labeling [Internet]. Bioconductor version: Release (3.11); 2020 [cited 2020 Jun 2]. Available from: https:// bioconductor.org/packages/EnhancedVolcano/
21. Reimand J, Kull M, Peterson H, Hansen J, Vilo J. g:Profiler—a web-based toolset for functional profiling of gene lists from large-scale experiments. Nucleic Acids Res. 2007; 35(Web Server issue):W193–W200.
22. Shannon P, Markiel A, Ozier O, Baliga NS, Wang JT, Ramage D, et al. Cytoscape: a software environment for integrated models of biomolecular interaction networks. Genome Res. 2003;13(11):2498–504.
23. Tomkins JE, Ferrari R, Vavouraki N, Hardy J, Lovering RC, Lewis PA, et al. PINOT: an intuitive resource for integrating protein-protein interactions. Cell Commun Signal. 2020;18(1):92.
24. Lobbestael E, Civiero L, De Wit T, Taymans J-M, Greggio E, Baekelandt V. Pharmacological LRRK2 kinase inhibition induces LRRK2 protein destabilization and proteasomal degradation. Sci Rep. 2016 23;6. Available from: https://www.ncbi.nlm.nih.gov/pmc/articles/PMC5034242/ [cited 2020 8 May]
25. Xu X-H, Deng C-Y, Liu Y, He M, Peng J, Wang T, et al. MARCKS regulates membrane targeting of Rab10 vesicles to promote axon development. Cell Res. 2014;24(5):576–94.
26. El Amri M, Fitzgerald U, Schlosser G. MARCKS and MARCKS-like proteins in development and regeneration. J Biomed Sci. 2018;25(1):43.
27. Sparvero LJ, Asafu-Adjei D, Kang R, Tang D, Amin N, Im J, et al. RAGE (receptor for advanced Glycation Endproducts), RAGE ligands, and their role in Cancer and inflammation. J Transl Med. 2009;7(1):17.
28. Wallings RL, Tansey MG. LRRK2 regulation of immune-pathways and inflammatory disease. Biochem Soc Trans. 2019;47(6):1581–95.
29. Lang D, Radtke M, Bairlein M. Highly variable expression of CYP1A1 in human liver and impact on pharmacokinetics of Riociguat and Granisetron in humans. Chem Res Toxicol. 2019;32(6):1115–22.
30. Pellegrini L, Hauser DN, Li Y, Mamais A, Beilina A, Kumaran R, et al. Proteomic analysis reveals co-ordinated alterations in protein synthesis and degradation pathways in LRRK2 knockout mice. Hum Mol Genet. 2018; 27(18):3257–71.
31. Waschbüsch D, Purlyte E, Pal P, McGrath E, Alessi DR, Khan AR. Structural Basis for Rab8a Recruitment of RILPL2 via LRRK2 Phosphorylation of Switch 2. Structure. 2020; 28(4):406–417.e6.
32. Bonet-Ponce L, Beilina A, Williamson CD, Lindberg E, Kluss JH, Saez-Atienzar S, et al. LRRK2 mediates tubulation and vesicle sorting from lysosomes. Sci Adv. 2020;6(46):eabb2454.
33. Fraser KB, Rawlins AB, Clark RG, Alcalay RN, Standaert DG, Liu N, et al. Ser(P)-1292 LRRK2 in urinary exosomes is elevated in idiopathic Parkinson's disease. Mov Disord. 2016;31(10):1543–50.
34. Wang S, West AB. Caught in the act: LRRK2 in exosomes. Biochem Soc Trans. 2019;47(2):663–70.

35. Lis P, Burel S, Steger M, Mann M, Brown F, Diez F, et al. Development of phospho-specific Rab protein antibodies to monitor in vivo activity of the LRRK2 Parkinson's disease kinase. Biochem J. 2018;475(1):1–22.

36. Purlyte E, Dhekne HS, Sarhan AR, Gomez R, Lis P, Wightman M, et al. Rab29 activation of the Parkinson's disease-associated LRRK2 kinase. EMBO J. 2018; 37:1–18.

37. Vieweg S, Mulholland K, Bräuning B, Kachariya N, Lai Y-C, Toth R, et al. PINK1-dependent phosphorylation of Serine111 within the SF3 motif of Rab GTPases impairs effector interactions and LRRK2-mediated phosphorylation at Threonine72. Biochem J. 2020;477(9):1651–68.

38. Kluss JH, Beilina A, Lewis PA, Cookson MR, Bonet-Ponce L. Membrane targeting activates Leucine-rich repeat kinase 2 with differential effects on downstream Rab activation. BioRxiv. 2020;12(01):406223.

39. Berndsen K, Lis P, Yeshaw WM, Wawro PS, Nirujogi RS, Wightman M, et al. PPM1H phosphatase counteracts LRRK2 signaling by selectively dephosphorylating Rab proteins. eLife [Internet]. [cited 2020 May 11];8. Available from: https://www.ncbi.nlm.nih.gov/pmc/articles/PMC6850886/

40. Bryce D, Ware CM, Woodhouse JD, Ciaccio PJ, Ellis JM, Hegde LG, et al. Characterization of the onset, progression, and reversibility of morphological changes in mouse lung following pharmacological inhibition of LRRK2 kinase activity. J Pharmacol Exp Ther [Internet]. 2021 1 [cited 2021 Feb 4]; Available from: https://jpet.aspetjournals.org/content/early/2021/01/28/jpet.120.000217

41. Herbst S, Campbell P, Harvey J, Bernard EM, Papayannopoulos V, Wood NW, et al. LRRK2 activation controls the repair of damaged endomembranes in macrophages. EMBO J. 2020;39(18):e104494.

42. Schwake M, Schröder B, Saftig P. Lysosomal membrane proteins and their central role in physiology. Traffic. 2013;14(7):739–48.

43. Mamais A, Raja M, Manzoni C, Dihanich S, Lees A, Moore D, et al. Divergent α-synuclein solubility and aggregation properties in G2019S LRRK2 Parkinson's disease brains with Lewy body pathology compared to idiopathic cases. Neurobiol Dis. 2013;58:183–90.

44. Sanders LH, Laganière J, Cooper O, Mak SK, Vu BJ, Huang YA, et al. LRRK2 mutations cause mitochondrial DNA damage in iPSC-derived neural cells from Parkinson's disease patients: reversal by gene correction. Neurobiol Dis. 2014;62:381–6.

45. Pereira C, Miguel Martins L, Saraiva L. LRRK2, but not pathogenic mutants, protects against H2O2 stress depending on mitochondrial function and endocytosis in a yeast model. Biochim Biophys Acta BBA. 2014;1840(6): 2025–31.

46. Howlett EH, Jensen N, Belmonte F, Zafar F, Hu X, Kluss J, et al. LRRK2 G2019S-induced mitochondrial DNA damage is LRRK2 kinase dependent and inhibition restores mtDNA integrity in Parkinson's disease. Hum Mol Genet. 2017;26(22):4340–51.

47. Mortiboys H, Johansen KK, Aasly JO, Bandmann O. Mitochondrial impairment in patients with Parkinson disease with the G2019S mutation in LRRK2. Neurology. 2010;75(22):2017–20.

48. Mamais A, Chia R, Beilina A, Hauser DN, Hall C, Lewis PA, et al. Arsenite stress down-regulates phosphorylation and 14-3-3 binding of leucine-rich repeat kinase 2 (LRRK2), promoting self-association and cellular redistribution. J Biol Chem. 2014;289(31):21386–400.

49. Inc DT. Denali Therapeutics Announces First Patient Dosed in Phase 1b Study of DNL151 for Parkinson's Disease and Launch of Its Engage Parkinson's Website [Internet]. GlobeNewswire News Room. 2019 [cited 2021 Mar 10]. Available from: http://www.globenewswire.com/newsrelease/2019/09/04/1910858/0/en/Denali-Therapeutics-Announces-First-Patient-Dosed-in-Phase-1b-Study-of-DNL151-for-Parkinson-s-Disease-and-Launch-of-Its-Engage-Parkinson-s-Website.html.

Publisher's Note

PLOS BIOLOGY
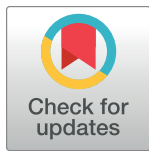
Mutations in LRRK2 linked to Parkinson disease sequester Rab8a to damaged lysosomes and regulate transferrin-mediated iron uptake in microglia

Adamantios Mamais[1,2], **Jillian H. Kluss**[1], **Luis Bonet-Ponce**[1], **Natalie Landeck**[1], **Rebekah G. Langston**[1], **Nathan Smith**[3], **Alexandra Beilina**[1], **Alice Kaganovich**[1], **Manik C. Ghosh**[4], **Laura Pellegrini**[5], **Ravindran Kumaran**[1], **Ioannis Papazoglou**[6], **George R. Heaton**[1], **Rina Bandopadhyay**[7], **Nunziata Maio**[4], **Changyoun Kim**[8], **Matthew J. LaVoie**[2], **David C. Gershlick**[9], **Mark R. Cookson**[1] *

1 Cell Biology and Gene Expression Section, National Institute on Aging, National Institutes of Health, Maryland, United States of America, **2** Department of Neurology, University of Florida, Gainesville, Florida, United States of America, **3** Department of Biochemistry and the Redox Biology Center, University of Nebraska, Lincoln, Nebraska, United States of America, **4** Molecular Medicine Branch, 'Eunice Kennedy Shriver' National Institute of Child Health and Human Development, Bethesda, Maryland, United States of America, **5** MRC Laboratory of Molecular Biology, Cambridge, United Kingdom, **6** National Institute of Diabetes and Digestive and Kidney Diseases, National Institutes of Health, Bethesda, Maryland, United States of America, **7** UCL Institute of Neurology and Reta Lila Weston Institute of Neurological Studies, University College London, London, United Kingdom, **8** Molecular Neuropathology Section, Laboratory of Neurogenetics, National Institute on Aging, National Institutes of Health, Bethesda, Maryland, United States of America, **9** Cambridge Institute for Medical Research, University of Cambridge, Cambridge, United Kingdom

* cookson@mail.nih.gov

Abstract

Mutations in leucine-rich repeat kinase 2 (LRRK2) cause autosomal dominant Parkinson disease (PD), while polymorphic LRRK2 variants are associated with sporadic PD. PD-linked mutations increase LRRK2 kinase activity and induce neurotoxicity in vitro and in vivo. The small GTPase Rab8a is a LRRK2 kinase substrate and is involved in receptor-mediated recycling and endocytic trafficking of transferrin, but the effect of PD-linked LRRK2 mutations on the function of Rab8a is poorly understood. Here, we show that gain-of-function mutations in LRRK2 induce sequestration of endogenous Rab8a to lysosomes in overexpression cell models, while pharmacological inhibition of LRRK2 kinase activity reverses this phenotype. Furthermore, we show that LRRK2 mutations drive association of endocytosed transferrin with Rab8a-positive lysosomes. LRRK2 has been nominated as an integral part of cellular responses downstream of proinflammatory signals and is activated in microglia in postmortem PD tissue. Here, we show that iPSC-derived microglia from patients carrying the most common LRRK2 mutation, G2019S, mistraffic transferrin to lysosomes proximal to the nucleus in proinflammatory conditions. Furthermore, G2019S knock-in mice show a significant increase in iron deposition in microglia following intrastriatal LPS injection compared to wild-type mice, accompanied by striatal accumulation of ferritin. Our data support a role of LRRK2 in modulating iron uptake and storage in response to proinflammatory stimuli in microglia.

Introduction

Missense mutations on the leucine-rich repeat kinase 2 (LRRK2) gene cause autosomal dominant Parkinson disease (PD), while common genetic variants identified by genome-wide association studies have been linked to idiopathic PD and inflammatory diseases [1–3]. LRRK2 is a multidomain enzyme, and PD-linked mutations are localized to its enzymatic domains, namely the kinase domain and Ras of complex proteins and C-terminal of ROC (ROC-COR) domains. LRRK2 has been linked to a number of cellular pathways including autophagy, lysosomal processing, inflammation, and vesicular trafficking [4]. LRRK2 is expressed in immune cells, and prior observations suggest a role of LRRK2 in microglial activation and an effect of PD-linked mutations on cytokine release and inflammation [5–7]. The kinase activity of LRRK2 is thought to drive disease pathology and thus is being targeted pharmacologically as a possible PD therapy [4].

A specific role of LRRK2 in vesicular trafficking has been nominated in recent years, and a number of studies have highlighted how downstream signaling pathways are affected by PD-linked mutations. LRRK2 can phosphorylate a subset of Rab GTPases, including Rab8a, Rab10, and Rab29, at a conserved motif, and this phosphorylation regulates Rab activity and association with effector molecules [8,9]. Rab GTPases control the spatiotemporal regulation of vesicle traffic and are involved in vesicle sorting, motility, and fusion [10]. Different Rab GTPases exhibit selectivity for different cellular compartments, thus conferring membrane identity that governs secretory and endocytic pathways [11]. For example, LRRK2 associates with Rab29, a Rab GTPase that is involved in vesicular transport and protein sorting [12,13] and a candidate risk gene for sporadic PD [14]. Rab29 can mediate recruitment of LRRK2 to the *trans*-Golgi network, inducing LRRK2 activity and membrane association at least under conditions of overexpression [12,15,16]. LRRK2 can phosphorylate Rab8a and Rab10, which may have downstream effects on the endolysosomal system. We, and others, have reported phosphorylation-dependent recruitment of Rab10 onto damaged lysosomes by LRRK2, in a process that orchestrates lysosomal homeostasis [17–19].

Rab8a is involved in a number of cellular functions including cell morphogenesis, neuronal differentiation, ciliogenesis, and membrane trafficking [20–22]. Rab8a regulates recycling of internalized receptors and membrane trafficking to the endocytic recycling compartment (ERC) [21,23]. Rab8a has been shown to interact directly with the transferrin receptor (TfR) and regulate polarized TfR recycling to cell protrusions [24] and transfer between cells through tunneling nanotubes [25]. Furthermore, Rab8a-depleted cells fail to deliver internalized TfR to the ERC [24]. Rab8a activity is controlled by its association with Rabin8, a guanine exchange factor [26]. Phosphorylation of Rab8a by LRRK2 inhibits its association with Rabin8 and thereby modulates Rab8a activity [8]. The G2019S LRRK2 mutation enhances Rab8a phosphorylation, mediating defects on EGFR recycling and endolysosomal transport [27]. Recently, mutations in LRRK2 were shown to mediate centrosomal deficits through Rab8a signaling [28–30], while ciliogenesis has been placed downstream of LRRK2 activity in different models [31].

Although these data indicate that Rab8a regulates exocytic and recycling membrane trafficking at the ERC, how phosphorylation of Rab8a affects downstream biology in PD-relevant cell types remains unclear. Here, we identify a novel role of LRRK2 in mediating Rab8a-dependent TfR recycling and show in vivo effects of LRRK2 mutation at the endogenous level on iron homeostasis in microglia. Expression of mutant LRRK2 induces sequestration of Rab8a to lysosomes and dysregulates transferrin recycling in a Rab8a-dependent manner. In induced pluripotent stem cell (iPSC)-derived microglia carrying the G2019S LRRK2 mutation, transferrin is mistrafficked to lysosomes in proinflammatory conditions, and this is accompanied

by subtle dysregulation of transferrin clearance compared to wild-type (WT) controls. Finally, we show that G2019S LRRK2 knock-in mice exhibit increased iron accumulation within microglia in the striatum in response to neuroinflammation compared to WT controls. These data support a role of LRRK2 in modulating normal iron uptake and storage in response to proinflammatory stimuli in microglia.

Results

Pathogenic mutant LRRK2 sequesters Rab8a to damaged lysosomes

In order to study endogenous Rab8a in cells, we first validated commercially available antibodies for western blotting and immunofluorescence employing small interfering RNA (siRNA)-mediated knock-down (S1 Fig). Using the validated antibody (Cell Signaling; D22D8; #6975), we examined the intracellular localization of Rab8a in the context of LRRK2 mutations. Endogenous Rab8a plays a part in receptor recycling and localizes in tubular recycling endosomes [21]. Consistent with such a function, in cells expressing WT LRRK2, Rab8a localized predominantly in tubular membranes not associated with Lamp2-positive lysosomes (Fig 1A). However, expression of R1441C or G2019S LRRK2 variants induced relocalization of endogenous Rab8a into enlarged perinuclear lysosomes (Fig 1A). Other pathogenic mutations, but not the kinase-dead variant K1906M, also induced relocalization of Rab8a (S2 Fig). The latter result suggested that the recruitment of Rab8a to lysosomes might be kinase dependent. To test this hypothesis, cells were treated with the LRRK2 kinase inhibitor MLi-2 for 1 hour prior to fixation and staining. LRRK2 kinase inhibition restored association of Rab8a with tubular recycling endosomes (Fig 1A). Our experiments show that around 60% of Rab8a staining colocalized with LRRK2 in cells expressing R1441C LRRK2 or G2019S LRRK2, and this was rescued back to WT LRRK2 levels (approximately 20%) by Mli-2 (Fig 1B). A parallel increase in colocalization was observed between Rab8a and Lamp2 in mutant LRRK2 expressing cells (Fig 1C). Recruitment of Rab8a by LRRK2 and colocalization with Lamp2 were rescued by MLi-2 treatment. Furthermore, we also quantified Rab8a recruitment by imaging Rab8a sequestration to large (>4 μm^2) cytoplasmic foci by high-content imaging (Cellomics, Thermo Fisher). We report a convergent phenotype for all PD-linked LRRK2 genetic variants with an increase in the fraction of cells that show a sequestered Rab8a phenotype while this was rescued by MLi-2 (S2B Fig). In our experiments, about 50% of cells expressing R1441C LRRK2 contained Rab8a-positive lysosomes, while this was true for about 30% of cells expressing G2019S LRRK2 and approximately 10% WT LRRK2 expressing cells (S2C Fig). To examine whether mutant LRRK2 and Rab8a are recruited to the lysosomal lumen or membrane, cells expressing G2019S LRRK2 were analyzed by superresolution microscopy (Airyscan), revealing a clear recruitment of both proteins to the membrane of Lamp1-positive lysosomes (Fig 1D).

Previous studies have reported recruitment of Rab8a to the perinuclear region in close proximity to centrosomes [29,30]; it is known that lysosomes are found in distinct perinuclear and peripheral pools and that the movement of lysosomes depends on microtubule-dependent transport and that the proportion of these 2 pools may differ between cancerous and nontransformed cells [32]. Furthermore, it is likely that permeabilization conditions used in fixed cell staining could cause rapid extraction of prenylated Rab GTPases from membranes that might bias which pool of Rab8a was readily imaged. To dissect lysosomal versus centrosomal pools of Rab8a in nontransformed cells, we compared standard immunocytochemistry protocols to live imaging of Rab8a in mouse primary astrocytes. G2019S LRRK2 was transiently expressed in primary mouse astrocytes, and endogenous Rab8a was stained along with Lamp1 (Fig 1E, left panel). For live imaging, transiently expressing a HaloTag pDEST G2019S LRRK2, visualized by JFX650 ligand, along with GFP-Rab8a and LAMP1-RFP were expressed and imaged
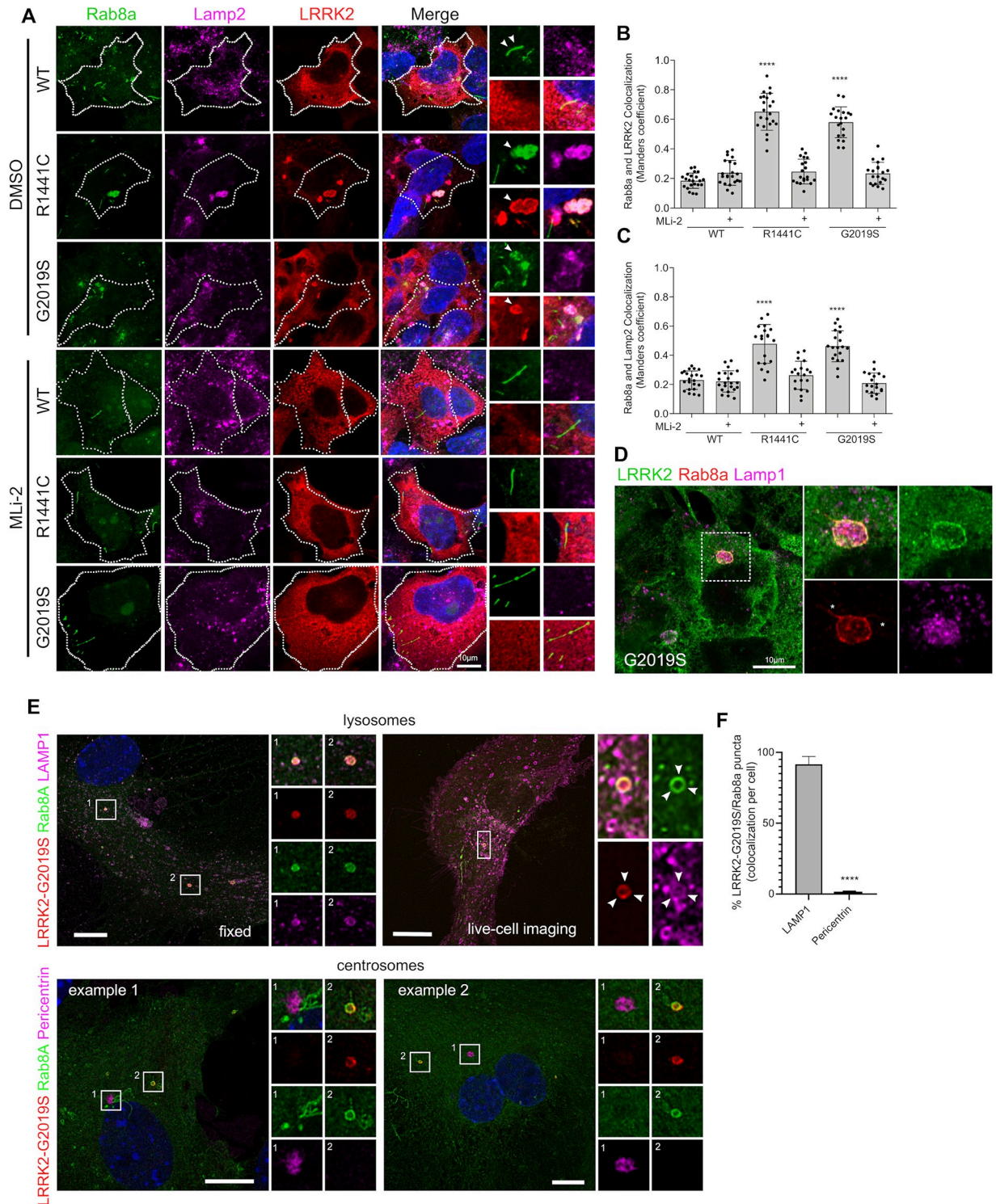
Fig 1. Pathogenic mutations of LRRK2 sequester endogenous Rab8a to lysosomes in a kinase-dependent manner. (A) Representative confocal images of HEK293T cells transiently expressing FLAG-tagged WT, R1441C, or G2019S LRRK2 constructs, stained for FLAG LRRK2, endogenous Rab8a, and endogenous Lamp2. Cells were treated with 1 μM MLi-2 for 1 hour or DMSO prior to staining, 24 hours posttransfection. (B, C) Quantification of Manders colocalization coefficient between Rab8a, LRRK2, and Lamp2 (B, C: $N > 20$ cells for each group across 2 independent experiments, $****P < 0.0001$, one-way ANOVA with Tukey post hoc test; B: F (5, 120) = 108.9; C: F (5, 120) = 35.85). (D) Superresolution confocal image of endogenous Rab8a and overexpressed G2019S LRRK2 localizing at the lysosomal membrane. (E) Mouse primary astrocytes were transfected with HaloTag-LRRK2(G2019S), GFP-Rab8a, and LAMP1-RFP (top panels). Cells were incubated

with JFX650 (100 nM) for 1 hour, washed, and imaged using a Nikon SoRa spinning disk microscope utilizing 3D Landweber deconvolution, 48 hours later. To analyze Rab8a localization to centrosomes, fixed cells were stained for pericentrin, following transient expression of G2019S LRRK2 and GFP-Rab8a. Images were taken with Airyscan (bottom panels). (F) Quantitation of the percentage of LRRK2/Rab8a puncta per cell that colocalizes with either LAMP1 or Pericentrin ($N > 19$ cells for each condition from 2 independent experiments; unpaired t test; $P < 0.0001$). The underlying data can be found in S1 Data. LRRK2, leucine-rich repeat kinase 2; WT, wild-type.

https://doi.org/10.1371/journal.pbio.3001480.g001

(Fig 1E, right panel). In these experiments, fixed and live Rab8a imaging identically showed sequestration of Rab8a to the lysosomal membrane. In these nontransformed cells transiently expressing G2019S LRRK2, we did not detect Rab8a staining at the centrosome using pericentrin as a marker (Fig 1E and 1F). However, in HEK293T cells expressing G2019S LRRK2, we detected recruitment of endogenous Rab8a to the perinuclear region in close proximity to centrosomes (pericentrin staining), and this was partially rescued by nocodazole treatment (S3A and S3B Fig). Additionally, we found that approximately 50% of total Rab8a colocalizes with Lamp2 in the presence of G2019S LRRK2, and this is decreased to approximately 30% after treatment with nocodazole (S3C and S3D Fig). These data are in accordance with previous studies [17,30] and suggest that there are likely at least 2 pools of Rab8a in the presence of mutant LRRK2, one bound to the centrosome, and the other to lysosome-related structures.

Previous studies have shown that LRRK2 can localize in enlarged lysosomes along with Rab GTPases [17]. Furthermore, we have shown that LRRK2 can be recruited to damaged lysosomes that have low degradative capacity [18]. To further extend our previous findings in the context of Rab8a recruitment by LRRK2, we evaluated whether LRRK2-positive lysosomes were deficient in Cathepsin D. While LRRK2 mutations induced an increase in colocalization with Lamp2, minimal colocalization with Cathepsin D was detected in WT or pathogenic LRRK2 (Fig 2B), a finding also supported by superresolution imaging (Fig 2C). This result suggested that Rab8a was recruited specifically to damaged lysosomes. To further test this hypothesis, we treated cells with the lysosomal destabilizing agent LLOMe that interacts with the lysosomal membrane and luminal hydrolases. We found that LLOMe induced recruitment of WT LRRK2 to the membrane of enlarged lysosomes as previously shown [18] (Fig 2D). Endogenous Rab8a was also recruited to the lysosomal membrane in WT LRRK2 cells after treatment with LLOMe (Fig 2E). Furthermore, the cytosolic scaffolding protein JIP4 was also recruited to the same structure suggesting mistrafficking of factors involved in vesicle-mediated transport (Fig 2F). These data suggest that Rab8a is recruited to damaged lysosomes by mutant LRRK2 in a kinase-dependent manner.

LRRK2-mediated T72 Rab8a phosphorylation blocks interaction with Rabin8 but not MICAL-L1

The above data suggest that Rab8a can move from its normal location at the ERC to the lysosome after expression of LRRK2 mutations. Given that all LRRK2 mutations are proposed to increase Rab phosphorylation, at T72 for Rab8a [8], we reasoned that the mechanism of relocalization might be related to this phosphorylation event. The pT72 Rab8a antibody that was available during this study was not specific to Rab8a and cross-reacted with Rab3A, Rab10, Rab35, and Rab43, which have a high degree of sequence conservation (for datasheet, refer to ab230260; Abcam). Therefore, using a tagged version of Rab8a, we found that exogenous expression of R1441C, Y1699C, G2019S, or I2020T LRRK2 induced a significant increase in Rab8a phosphorylation at T72 compared to WT or the kinase-dead variant K1906M, and this was blocked by MLi-2 treatment (Fig 3A and 3B).

Having established that Rab8a phosphorylation at T72 is increased by all pathogenic LRRK2 mutations, we next investigated how this affects interactions with known Rab8a
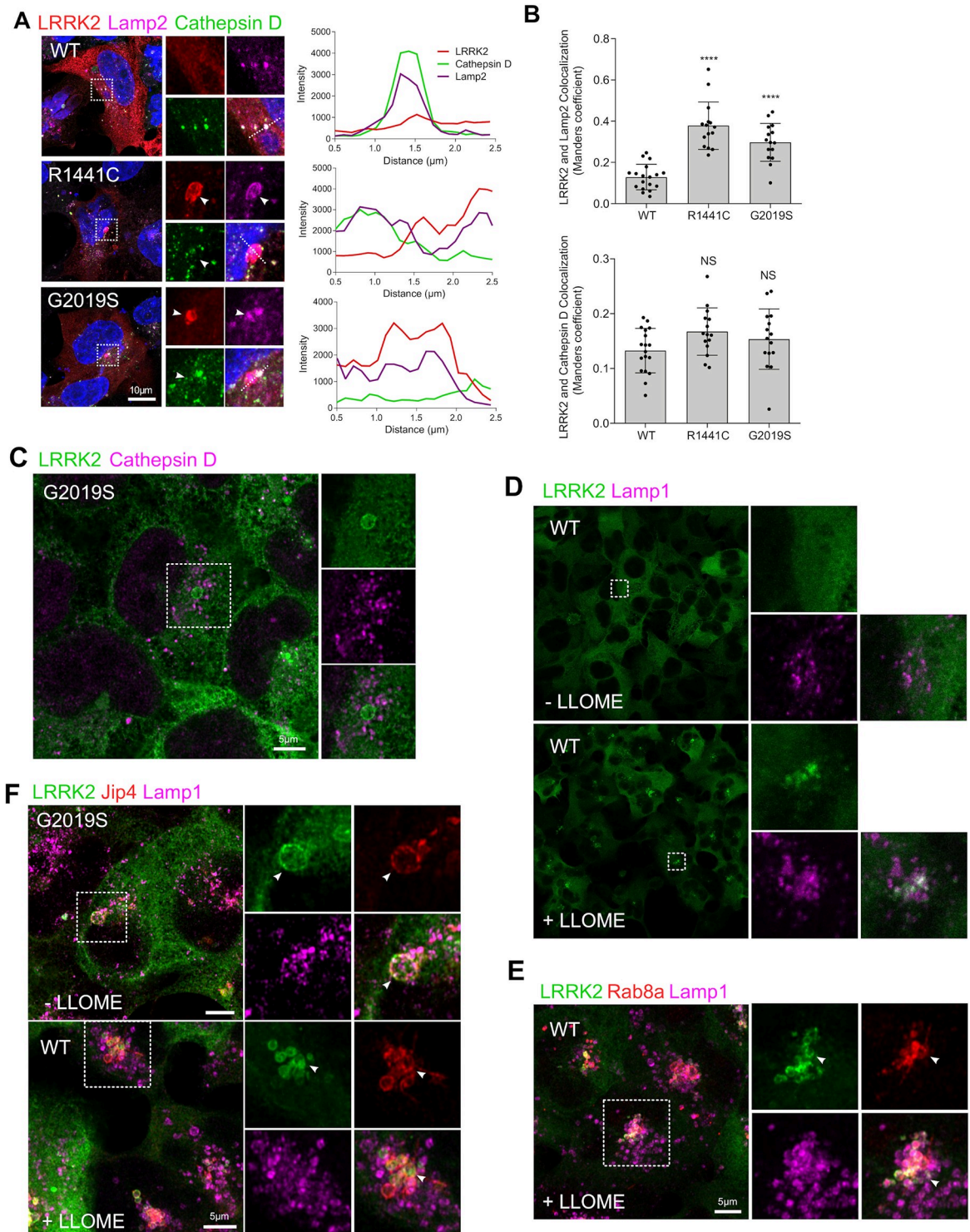
Fig 2. LRRK2 and Rab8a are recruited to the membrane of damaged lysosomes. (A) HEK293T cells transiently expressing FLAG-tagged WT, R1441C, or G2019S LRRK2 for 24 hours were stained for FLAG LRRK2, Lamp2, and Cathepsin D and analyzed by confocal microscopy. Staining intensity profiles were generated on sections indicated by the dotted lines. (B, C) Manders colocalization coefficient of LRRK2 versus Lamp2 or Cathepsin D staining ($N > 20$ cells per group across 2 independent experiments, ****$P < 0.0001$, one-way ANOVA with Tukey post hoc; Lamp2: F (5, 57) = 41.73; Cathepsin D: *NS*). (C) Superresolution image of HEK293T cells stably expressing GFP G2019S LRRK2 costained for Cathepsin D. HEK293T cells stably expressing GFP WT LRRK2 were treated with 1 mM LLOMe for 4 hours and stained for endogenous Lamp1 (D) and Rab8a (E). (F) GFP WT and G2019S expressing cells were treated with LLOMe as in

(E) and stained for Jip4 and Lamp1 prior to imaging by superresolution microscopy. The underlying data can be found in S1 Data. LRRK2, leucine-rich repeat kinase 2; WT, wild-type.

https://doi.org/10.1371/journal.pbio.3001480.g002

partners. We focused on the known activating GEF, Rabin8, and MICAL-L1, which is an established Rab8a-interacting partner [23] that localizes in tubular endosomes and is essential for efficient endocytic trafficking from the ERC to the plasma membrane [21]. Modeling the interaction between Rab8a and Rabin8, we predicted that the Threonine at position 72 on Rab8a resides 2.8 to 3.9 Å away from the neighboring Glutamate (E192) on Rabin8 (Fig 3C). Addition of a phosphate group on T72 will likely hinder the interaction with the negatively charged Glutamate, therefore destabilizing Rab8a–Rabin8 interaction. This prediction is consistent with work by Steger and colleagues who demonstrated biochemically that phosphorylation of Rab8a by LRRK2 can limit its activation by Rabin8 [8]. Threonine 72 of Rab8a is closest to a Phenylalanine (F647) on MICAL-L1 at a 6.7 to 8.4 Å distance, suggesting that phosphorylation at this site will not affect this interaction. To validate this prediction biochemically, we performed co-immunoprecipitation experiments by coexpressing Rab8a with WT, kinase-hyperactive I2020T, and kinase-dead K1906M LRRK2 in cells. In these conditions Rab8a was T72 hyperphosphorylated by I2020T LRRK2, and this modification did not hinder association with endogenous MICAL-L1 (Fig 3D). To investigate the retention of this association in the context of Rab8a recruitment to lysosomes, we stained for Rab8a and MICAL-L1 in cells expressing LRRK2. Cells expressing WT LRRK2 showed colocalization of Rab8a with MICAL-L1 in tubular membranes, while I2020T LRRK2 expression resulted in the recruitment of both proteins to LRRK2-positive structures consistent with the lysosomal phenotype described above (Fig 3E). This was also recapitulated by R1441C and G2019S LRRK2 that recruited endogenous MICAL-L1 and induced association of this trafficking protein with lysosomes (S4 Fig). Our data suggest that mutant LRRK2 can phosphorylate Rab8a inducing recruitment of both Rab8a and MICAL-L1 away from the ERC.

Mutant LRRK2 sequesters Rab8a leading to transferrin mistrafficking and accumulation of intracellular iron

Given the above data showing that LRRK2 phosphorylation prevents binding of Rab8a to its effectors and redirects Rab8a and MICAL-L1 away from the ERC, we speculated that these events would then lead to a defect in Rab8a-mediated recycling. To evaluate this hypothesis, we examined the recycling of the transferrin receptor 1 (TfR), which is known to depend on Rab8a function [24]. Cells expressing LRRK2 genetic variants were stained for endogenous TfR and analyzed. TfR localized in distinct cytoplasmic vesicles in cells expressing WT LRRK2, whereas LRRK2 pathogenic mutants showed a clustered TfR localization that associated with LRRK2. The distribution of TfR vesicles in LRRK2-expressing cells was analyzed in Imaris (Bitplane, Zürich, Switzerland) where vesicles were rendered to spots throughout z-stack 3D reconstructed images and distances between them were measured (Fig 4A, right-hand panels). TfR vesicles were significantly more clustered in cells expressing LRRK2 mutants compared to WT LRRK2 expressing cells (Fig 4B and 4C). To test whether the coalescent TfR staining that we observe with mutant LRRK2 associates with lysosomes, we analyzed the fraction of TfR colocalizing with the late endosome/lysosome marker Lamp2 (S5 Fig). We found a significant increase in colocalization between TfR and Lamp2 in cells expressing R1441C (approximately 50% of whole-cell TfR staining) and G2019S LRRK2 (approximately 40%) compared to WT LRRK2 expressing cells (S5A and S3B Fig). Our data are consistent with prior reports of perinuclear localization of TfR in cells expressing kinase hyperactive mutant LRRK2 [31]. Our
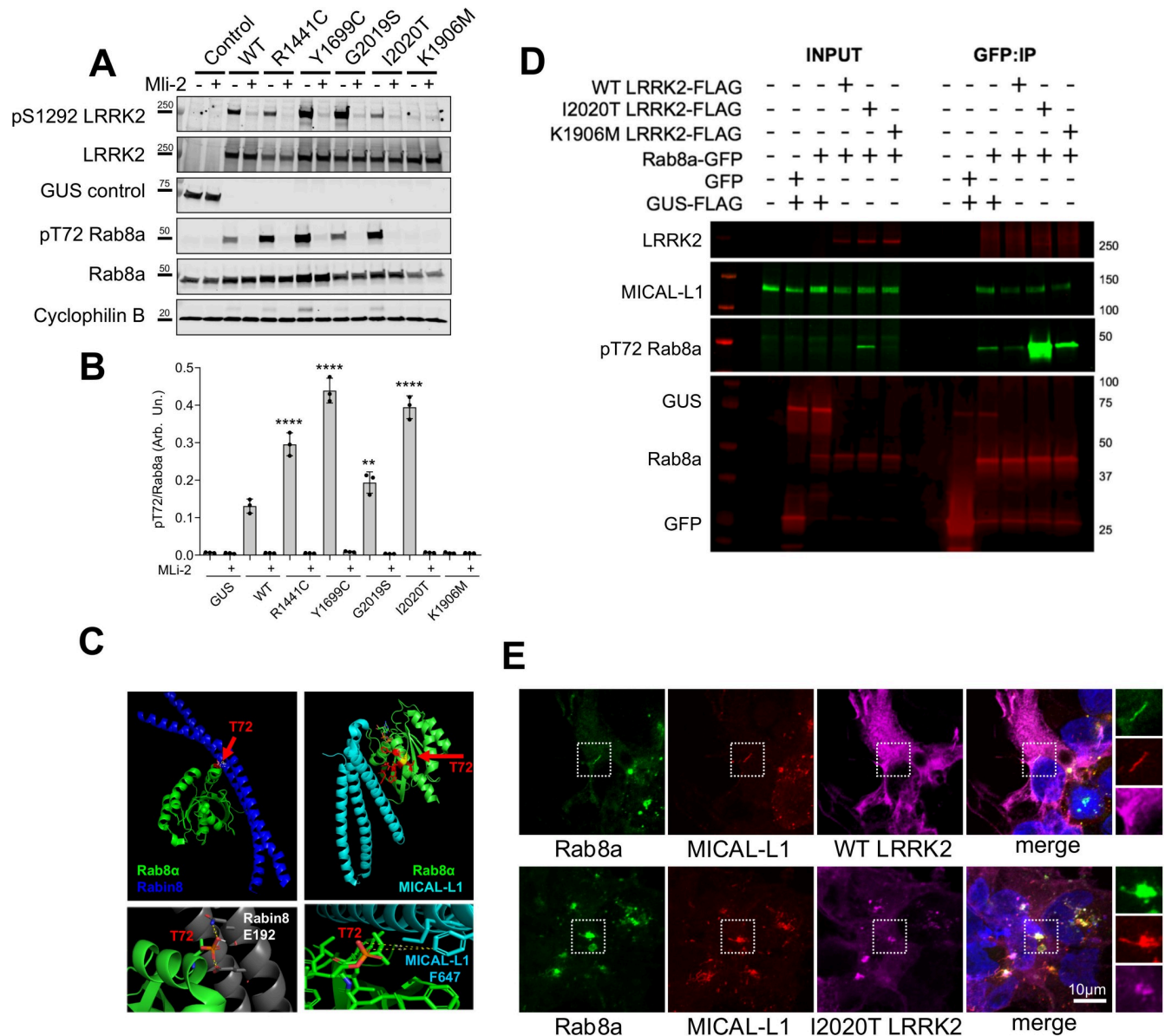
Fig 3. Rab8a phosphorylation retains interaction with MICAL-L1 that is corecruited in mutant LRRK2 expressing cells. (A) HEK293T cells expressing control (GUS), FLAG WT, or mutant LRRK2 variants were treated with MLi-2 prior to lysis and analysis by western blotting for pS1292 and total LRRK2, as well as pT72 and total Rab8a. (B) Quantification of pT72 Rab8a levels normalized to total Rab8a (B, two-way ANOVA; $N = 3$ independent experiments; treatment: $P < 0.0001$, F (1, 28) = 1473, genotype: $P < 0.0001$, F (6, 28) = 157.1). (C) Structural modeling of T72 phosphorylation on Rab8a in association with Rabin8 or MICAL-L1. T72 is between 2.8–9.9 Å from the closest glutamate on Rabin8 and 6.7–8.4 Å from the closest phenylalanine on MICAL-L1. (D) HEK293T cells expressing FLAG WT, I2020T, or K1906M LRRK2 along with GFP Rab8a, GFP control, or FLAG-GUS control were lysed and proteins immunoprecipitated using GFP beads. Co-immunoprecipitated proteins were analyzed by western blotting probed for MICAL-L1 as well as pT72 and total Rab8a. (E) Cells expressing FLAG WT or I2020T LRRK2 were stained for endogenous Rab8a and MICAL-L1 and analyzed by confocal microscopy. The underlying data can be found in S1 Data. LRRK2, leucine-rich repeat kinase 2; WT, wild-type.

https://doi.org/10.1371/journal.pbio.3001480.g003

data suggest that TfR is recruited to damaged lysosomes by mutant LRRK2. To further test this hypothesis, we treated cells with LLOMe and analyzed intracellular localization by Airyscan (S5C Fig). We observe TfR recruitment in LRRK2-positive and Rab8a-positive membranes consistent with damaged lysosomes as previously described [18].
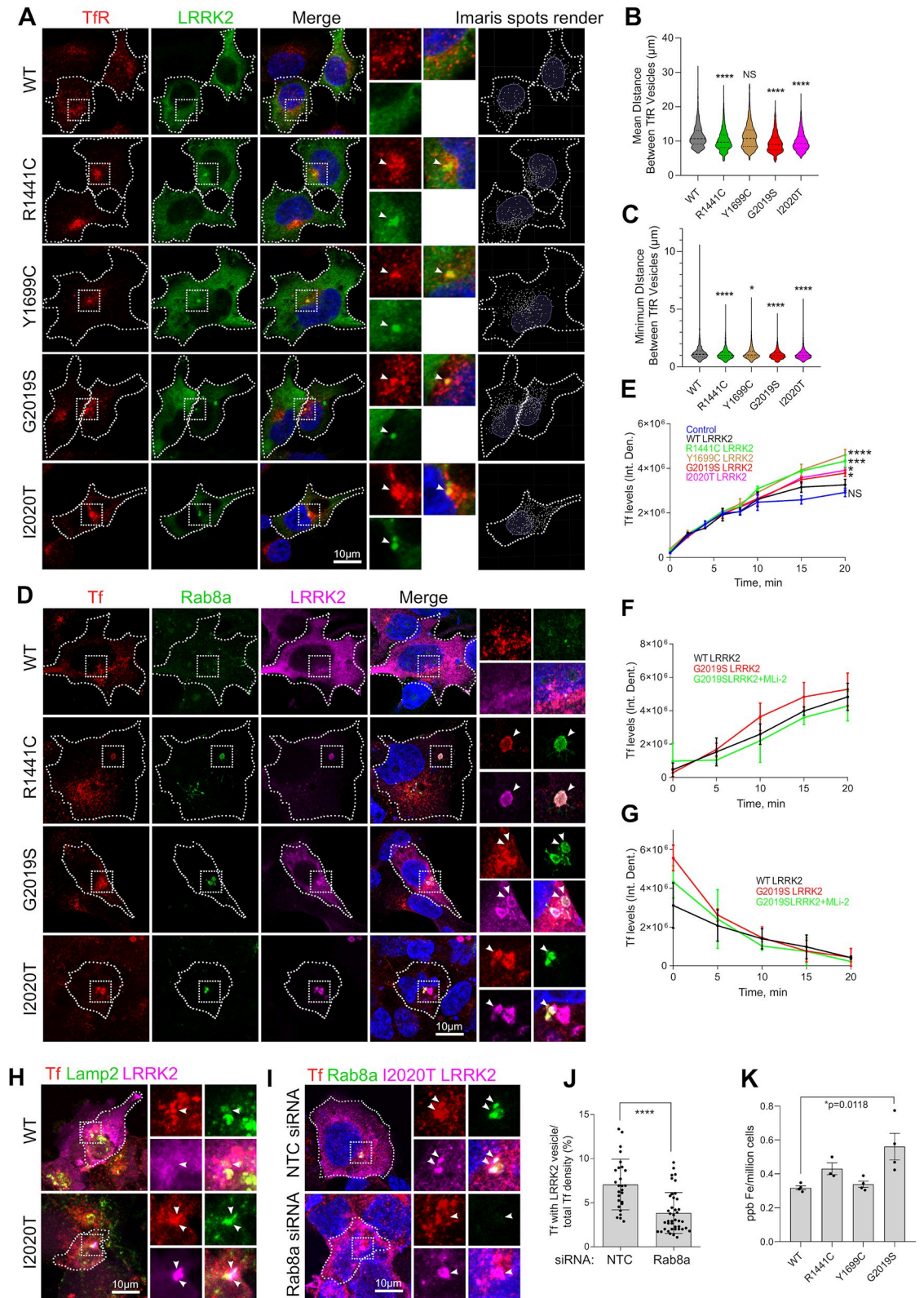
Fig 4. Mutant LRRK2 sequesters TfR and dysregulates transferrin recycling. (A) HEK293T cells exogenously expressing WT and mutant LRRK2 constructs were stained for TfR and visualized by superresolution microscopy. TfR vesicles were analyzed using the Imaris Spot Detection module, and the mean and minimum distances between spots were plotted (B, C). ($N > 2,000$ vesicles were

counted in at least 20 cells per construct from 2 independent experiments, $^*P < 0.05$, $^{****}P < 0.0001$, one-way ANOVA with Tukey post hoc, B: $F_{(4, 13334)} = 46.14$, C: $F_{(4, 13336)} = 194.1$). (D) HEK293FT cells expressing LRRK2 genetic variants were incubated with Alexa Fluor 568–conjugated transferrin, fixed at 20 minutes of incubation and stained for endogenous Rab8a and FLAG LRRK2 (D). (E) Uptake of Alexa Fluor 568–conjugated transferrin was monitored by high-content imaging, and transferrin levels per cell were plotted at different time points (E: T = 20 minutes, $N = 3$ technical replicates per construct (>800 cells/well) one-way ANOVA, Tukey post hoc, $^*P < 0.05$, $^{***}P = 0.0005$, $^{****}P < 0.0001$). (F) HEK293T cells exogenously expressing FLAG WT or G2019S LRRK2 constructs were incubated in DMEM supplemented with 1 μM MLi-2 or DMSO for 45 minutes prior to addition of Alexa Fluor 568–conjugated transferrin in the same media, and high-content imaging was used to monitor Tf uptake at different time points (F: $N = 3$ technical replicates per construct (>800 cells/well), two-way ANOVA, genotype: $P < 0.05$, $F_{(2,30)} = 3.575$; Time: $P < 0.0001$, $F_{(4, 30)} = 44.96$). (G) Cells were treated with MLi-2 as in (F), and incubated with Alexa Fluor–conjugated transferrin for 30 minutes, prior to changing to fresh media containing MLi-2 and monitoring transferrin release by high-content imaging (G; at T10: $N = 3$ technical replicates per construct (>800 cells/well), one-way ANOVA, Tukey post hoc, $P < 0.05$, $F_{(2, 30)} = 3.575$). (H) HEK293T cells transiently expressing WT or I2020T LRRK2 were stained for Tf, Lamp2, and LRRK2 (FLAG) and analyzed by confocal microscopy. (I, J) Cells were transfected with Rab8a siRNA or scrambled sequence constructs (control) and 24 hours later were transfected with I2020T LRRK2 that was expressed overnight, before fixation and staining for Tf, Rab8a, and LRRK2 (FLAG). ($N = 27$ cells for NTC siRNA, $N = 41$ cells for Rab8a siRNA imaged across 2 independent experiments, two-tailed Mann–Whitney U test, $^{****}P < 0.0001$). Intracellular iron levels were analyzed by ICP-MS in cells stably expressing GFP WT or mutant LRRK2 constructs (K) ($N = 4$ confluent plates of cells per construct, two-way ANOVA with Tukey post hoc, $^*P = 0.018$, $F_{(3, 11)} = 6.225$). [SD bars are shown]. The underlying data can be found in S1 Data. ICP-MS, inductively coupled plasma mass spectrometry; LRRK2, leucine-rich repeat kinase 2; siRNA, small interfering RNA; TfR, transferrin receptor; WT, wild-type.

https://doi.org/10.1371/journal.pbio.3001480.g004

The observed altered TfR intracellular distribution in cells transiently expressing mutant LRRK2 prompted us to test whether LRRK2 functionally affected Rab8a-dependent Tf recycling. Cells expressing WT or mutant LRRK2 were preloaded with Alexa Fluor 568-Tf and visualized at T10 minutes of recycling in fresh media. Mutant LRRK2 expressing cells exhibited association of Tf with enlarged vesicles that were labeled with LRRK2 and Rab8a (Fig 4D). Tf vesicles were clustered in G2019S LRRK2 expressing cells compared to WT LRRK2, while this was rescued by treatment with MLi-2 prior to Tf loading (S5D Fig). In Tf uptake time course experiments, LRRK2 mutant expressing cells plateaued at higher Tf levels compared to WT at T15 to T20 minutes as monitored by high-throughput imaging, pointing to Tf accumulation driven by dysregulated recycling (Fig 4E). The modest increase in net transferrin levels detected in G2019S LRRK2 expressing cells was partly reversed in cells treated with MLi-2 (Fig 4F). We further evaluated a possible impairment of Tf recycling employing pulse-chase experiments to monitor Tf clearance. Tf recycling assays revealed higher initial transferrin levels at T0 following 45 minutes of loading in G2019S LRRK2 expressing cells compared to WT, while this difference was not evident at later time points (Fig 4G). In parallel experiments, we detected no significant difference in the total levels or surface-bound levels of TfR in cells expressing G2019S LRRK2 and WT LRRK2 (S5E Fig). These data cumulatively suggest a subtle dysregulation of transferrin clearance driven by transient expression of mutant LRRK2.

The intracellular localization of internalized Tf in the context of LRRK2 mutations was explored further. In cells overexpressing I2020T LRRK2, we observed partial colocalization of internalized Tf with Lamp2 (Fig 4H), suggesting that excess Tf may associate with lysosomes. To test whether this phenotype was Rab8a dependent, the localization of internalized Tf in I2020T LRRK2 expressing cells was investigated following Rab8a siRNA knock-down. Knockdown of Rab8a decreased the proportion of Tf that colocalized with mutant LRRK2 relative to total internalized Tf (Fig 4I and 4J). Lastly, inductively coupled plasma mass spectrometry (ICP-MS) analysis revealed elevated iron levels in cells stably expressing G2019S LRRK2 compared to WT LRRK2, while the pathogenic R1441C and Y1699C mutants do not show detectable alterations in iron levels, at least as measured by ICP-MS (Fig 4K). Collectively, these data suggest subtle dysregulation of Tf-mediated iron uptake and iron homeostasis by LRRK2 mutations as a consequence of altered Rab8a localization away from the ERC and toward lysosomes.

Endolysosomal and iron-binding gene expression in microglia is modulated by inflammation, in vitro and in vivo

LRRK2 is expressed in microglia and has been linked to inflammation, cytokine release, and phagocytosis. Our data presented here show that LRRK2 associates with lysosomes and that LRRK2 mutations dysregulate Tf-dependent iron uptake mechanisms. Glial cells are known to be iron rich, and microglia activation state is integrally linked to brain iron content [33]. Proinflammatory stimuli are known to induce uptake of extracellular iron by microglia, and, conversely, the iron status of their environment can modulate their activation. Given the role of LRRK2 in inflammation, we asked whether endolysosomal processes and iron homeostasis might converge in proinflammatory conditions. We addressed this hypothesis using 2 genome-scale approaches. First, we mined our previously described RNA-Seq dataset [34] of primary microglia treated with lipopolysaccharide (LPS) or preformed α-synuclein fibrils in culture (Fig 5A). Analysis of the shared hits between the 2 treatments using gene ontology revealed enrichment for endosomal and lysosomal pathways (Fig 5B and 5C). Unsupervised hierarchical clustering of differential gene expression separated the controls from the 2 treatment groups (Fig 5D). These data demonstrate that genes involved in the endolysosomal system are consistently regulated by inflammatory stimuli.

We next asked whether the same regulation could be confirmed in vivo. Either WT or Lrrk2 knockout (KO) mice were given a single intrastriatal injection of LPS or vehicle control and 3 days later adult microglia were isolated using CD11b microbeads (Fig 5E). Between 3,000 and 5,000 cells were recovered from each of the 4 groups and analyzed using single-cell RNA-Seq (scRNA-Seq). We identified 5 distinct clusters of cells based on transcriptome similarity that represent resting microglia and 4 activation states (Fig 5F), with PBS-injected animals exhibiting predominantly resting microglia whereas the LPS-injected animals spanned the range of activation states (Fig 5G). Notably, we did not see strong differences between genotypes other than the KO animals tended to have fewer activated microglia, suggesting that Lrrk2 influences how microglia respond to proinflammatory stimuli [35]. Gene ontology showed enrichment for lysosomal and endocytic membrane processes (Fig 5H). These analyses identified genes involved in iron storage and uptake (FTH1; ferritin heavy chain), vesicular transport (SNAP23), acidification of vesicles (ATP6V1G1), and the late endosomal pathway (Rab7) (Fig 5I). These data demonstrate that processes of vesicular trafficking and iron homeostasis are modulated in a synchronized manner by inflammation. Given the importance of iron uptake in microglia activation, we hypothesized that LRRK2 may play a role in trafficking of TfR and that PD-linked mutations may affect iron uptake and accumulation in inflammatory conditions. Thus, we next sought to examine the effect of LRRK2 mutations on Tf recycling and iron uptake in proinflammatory conditions.

G2019S LRRK2 induces transferrin mislocalization and association with lysosomes in iPSC-derived microglia

To examine whether endogenous LRRK2 mutations might influence Tf-mediated iron uptake as modulated by neuroinflammation, iPSC-derived microglia from G2019S carriers were examined in resting and proinflammatory conditions, and Tf localization was assessed by superresolution microscopy (characterization of iPSC-derived microglia is shown in S6 Fig). Endogenous Tf showed partial colocalization with lysosomes in control conditions that was significantly decreased following LPS treatment, reflecting induction of iron uptake and recycling close to the plasma membrane, in WT cells. In contrast, the G2019S LRRK2 cells retained association of Tf with lysosomes following LPS treatment (Fig 6A and 6B). After 3D rendering (Fig 6A, right-hand panels; S1–S4 Movies for Imaris processing), Tf vesicle size and proximity
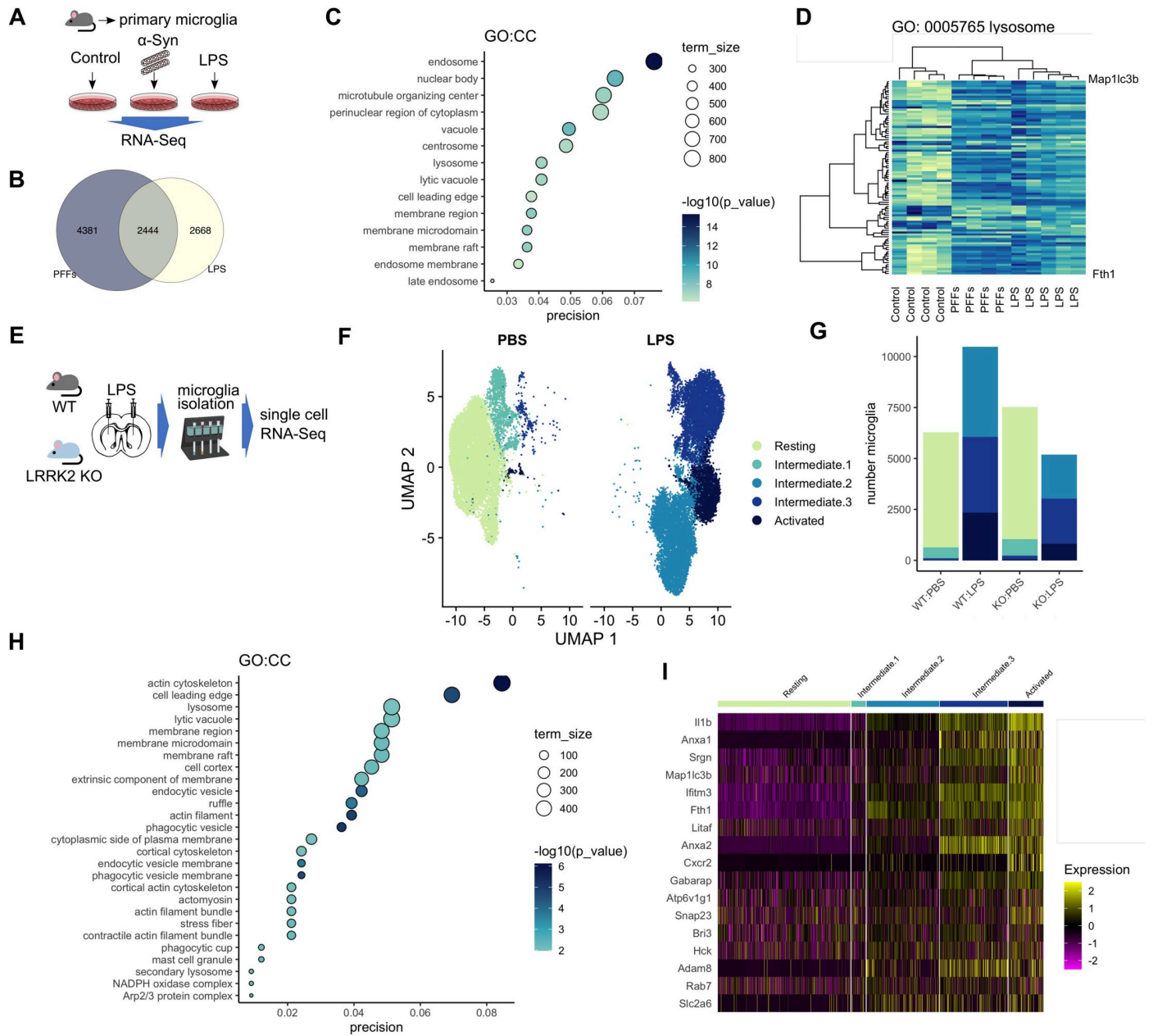
Fig 5. Neuroinflammation remodels endolysosomal gene expression in microglia, in vitro and in vivo. (A) Outline of RNA-Seq experiment: Primary mouse microglia cultures were incubated with LPS or α-synuclein fibrils, and transcriptomic profiles were analyzed by RNA-Seq. (B) Common and distinct hits were detected between the LPS and PFF-treated groups. (C) Bubble plot showing GO:CC term enrichment in the shared hits from LPS and PFF-treated primary microglia highlights enrichment for endolysosomal processes. (D) Unsupervised hierarchical clustering shows that the treated groups cluster together suggesting common transcriptomic profiles. (E) Schematic of the in vivo experiment where LPS striatal injections were administered to WT and LRRK2 KO mice, followed by microglia isolation and single-cell RNA-Seq. (F) UMAP plot showing separation of the retrieved microglia in distinct groups of activation states. (G) Microglia from LPS-injected animals spanned the activation states, while PBS-injected animals gave predominantly resting microglia. (H) Lysosomal and endocytic mechanisms as well as cytoskeletal pathways are enriched in the cumulative data. (I) Heatmap showing clustering of microglia in distinct activation states highlighting increase in lysosomal and iron-related gene expression by inflammation. The underlying data have been deposited in NCBI's GEO [75] and are accessible through GEO accession numbers GSE186483 and GSE186559. GEO, Gene Expression Omnibus; KO, knockout; LRRK2, leucine-rich repeat kinase 2; LPS, lipopolysaccharide; PFF, preformed fibril; scRNA-Seq, single-cell RNA-Seq; WT, wild-type.
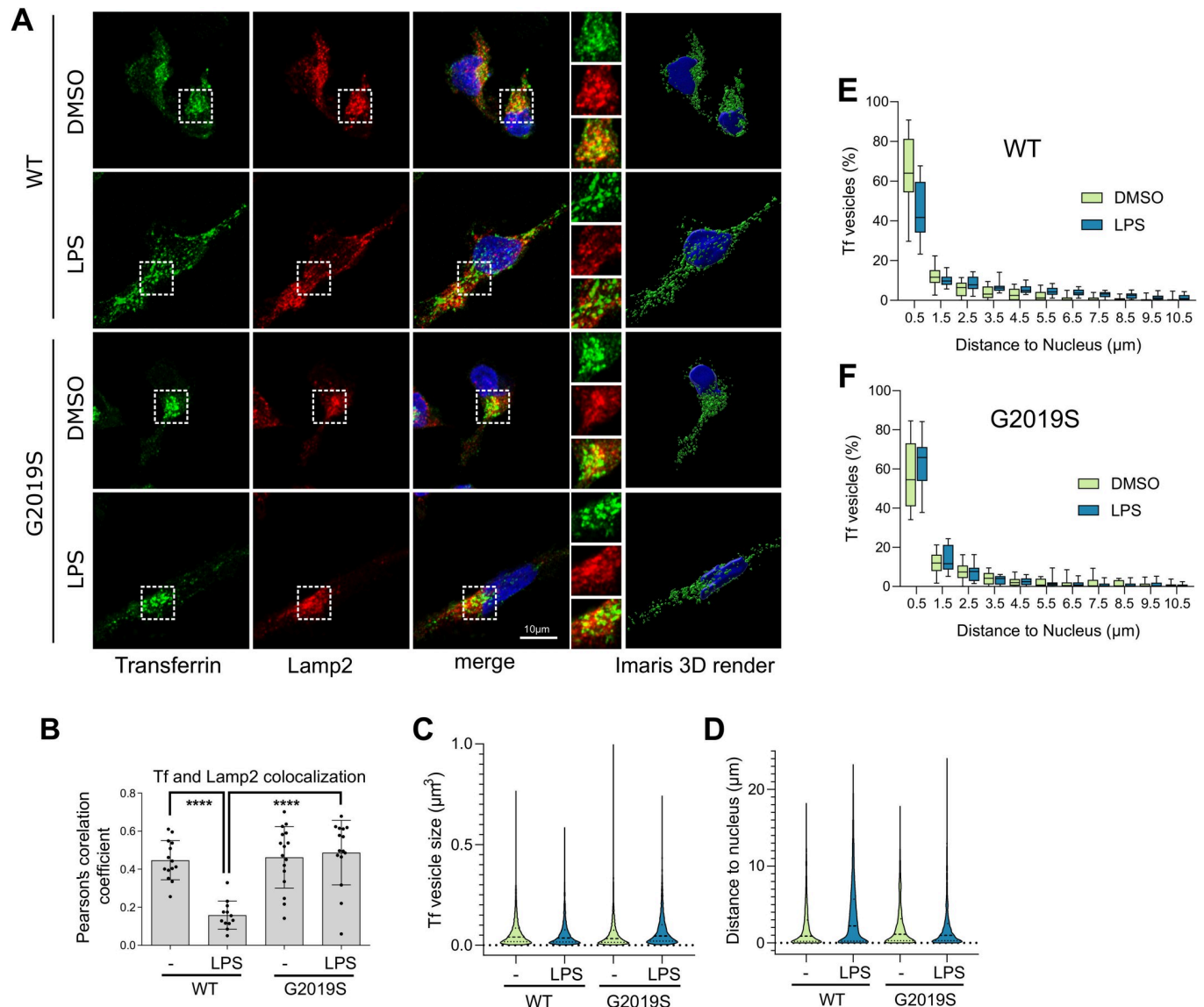
Fig 6. G2019S LRRK2 modulates Tf recycling in iPSC-derived human microglia. (A) iPSC-derived human microglia from WT or G2019S LRRK2 carriers were treated with LPS, and the localization of endogenous Tf and Lamp2 was analyzed by superresolution microscopy and the Imaris Surface render module (A). Partial colocalization between Tf and Lamp2 was observed in control that was significantly decreased with LPS treatment in WT cells but not in G2019S LRRK2 cells that retained lysosomal association of Tf (B) ($N > 12$ cells per group from 2 differentiations, one-way ANOVA Tukey post hoc, ****$P < 0.0001$, F (3,53) = 16.16). G2019S LRRK2 iPSC microglia exhibited larger Tf vesicles compared to WT while LPS treatment induced a decrease in average vesicle size in both cohorts (C) (minimum 3,000 vesicles were counted from 16 cells per group from 2 differentiations, two-way ANOVA, genotype: $P < 0.0001$, F(1,17753) = 16.38, treatment: $P < 0.0001$, F(1,17753) = 20.57). LPS treatment induced an increase in the average distance of Tf vesicles from the nucleus in WT cells but that was not significant in G2019S LRRK2 cells (D) (minimum 3,000 vesicles were counted from 16 cells per group from 2 differentiations, two-way ANOVA, genotype: $P < 0.0001$, F(1,14735) = 104.9, treatment: $P < 0.0001$, F (1, 14735) = 105.0). The frequency distributions of Tf vesicle proximity to the nucleus were plotted in E and F. The percentage of Tf vesicles proximal to the nucleus was significantly decreased with LPS treatment in WT but not G2019S LRRK2 cells (E, F) (E: bin at 0.5 μm, two-tailed Student t test; Mann–Whitney U post hoc; **$P = 0.0022$; F: bin at 0.5 μm, two-tailed Student t test; Mann–Whitney U post hoc; NS). The underlying data can be found in S1 Data. iPSC, induced pluripotent stem cell; LPS, lipopolysaccharide; LRRK2, leucine-rich repeat kinase 2; Tf, transferrin; WT, wild-type.

to the nucleus were measured (Fig 6C and 6D). The G2019S LRRK2 cells showed significantly larger Tf vesicles that were sequestered closer to the nucleus compared to WT cells (Fig 6C and 6D). Additionally, in resting conditions, around 50% to 60% of Tf vesicles were concentrated near the juxtanuclear region, positioned within 1.5 μm from the nuclear membrane, in

both WT and G2019 LRRK2 cells. Upon activation by LPS, WT LRRK2 cells exhibited a more dispersed Tf localization throughout the cytoplasm with a lower fraction of vesicles close to the perinuclear recycling compartment (approximately 40% within 1.5 μm), while in contrast, G2019S LRRK2 cells showed an increase in proximity to the nucleus (Fig 5E and 5F). These data suggest that in G2019S LRRK2 cells, Tf was retained in the perinuclear recycling compartment region associated with lysosomes, under proinflammatory conditions. To characterize the dynamics of Tf trafficking in this model, we assayed Tf uptake and recycling by high-content imaging of cells in resting or proinflammatory conditions. Tf uptake levels per cell showed variability in our cultures, and no significant difference between conditions or genotype was observed (S7A and S7B Fig). While cell-to-cell variability was also noted in pulse-chase experiments, we detected a modest increase in Tf in G2019S LRRK2 cells under LPS treatment and a subtle effect of slower recycling compared to the other groups (S7C and S7D Fig). Our data support a model whereby endogenous LRRK2 mutations dysregulate recycling mechanisms and redirect Tf receptors to lysosomes under inflammatory conditions in microglia, predicting impairment of iron homeostasis. We next tested whether we could support this hypothesis in vivo using the G2019S LRRK2 knock-in mouse model that expresses this mutation in the appropriate endogenous context.

G2019S LRRK2 induces iron and ferritin accumulation in inflammatory microglia in vivo

To examine the effect of LRRK2 mutations on iron accumulation in inflammation, we again used intrastriatal LPS injections on age-matched WT, Lrrk2 KO, and G2019S knock-in mice. Perls staining was used to visualize iron deposition in sections that spanned the striatum and substantia nigra (SN) 72 hours after injection (Fig 7A). The G2019S LRRK2 knock-in mice showed a marked increase in iron deposition in the striatum compared to WT and Lrrk2 KO mice as analyzed by densitometry (Fig 7B and 7C). Higher-magnification images revealed that the Perls stained cells had a microglial morphology, in line with our in vitro data that suggest dyshomeostasis of iron regulation mechanisms in inflammatory microglia (Fig 7D).

Additional sections from the same animals were stained for FTH1 and Tf. Accumulation of ferritin was observed in G2019S LRRK2 mice compared to WT and LRRK2 KO mice, with patterns similar to that seen with iron deposition (Fig 8A and 8B) while Tf was not significantly altered in the knock-in model (Fig 8C). To characterize further the type of cells that accumulate ferritin, sections were costained for Iba1 and analyzed by imaging (Fig 8D). Iba1-positive microglia were positive for ferritin in both WT and G2019S LRRK2 LPS-treated cohorts. About 50% of ferritin-positive cells were Iba1 positive in both groups (Fig 8E). Combined with the enhanced overall intensity of ferritin staining, we infer that these results are not due to increased numbers of Iba1-positive microglia but rather due to increased ferritin expression per cell. These data suggest that microglia, potentially among other cell types, accumulate ferritin in the striatum upon LPS-induced inflammation and drive ferritin-bound iron accumulation in G2019S LRRK2 knock-in mice compared to WT mice.

Discussion

In this study, we show that PD-linked LRRK2 mutations have a convergent phenotype of Rab8a mislocalization away from the ERC and recruitment to damaged lysosomes that is distinct from WT protein. This relocalization is associated with dysregulation of Rab8a-mediated transferrin recycling both in heterologous cell lines and in human iPSC-derived microglia from PD patients with LRRK2 mutations following inflammatory stimulus (Fig 9 for model schematic). Furthermore, we show that in G2019S LRRK2 knock-in mice, LPS-induced
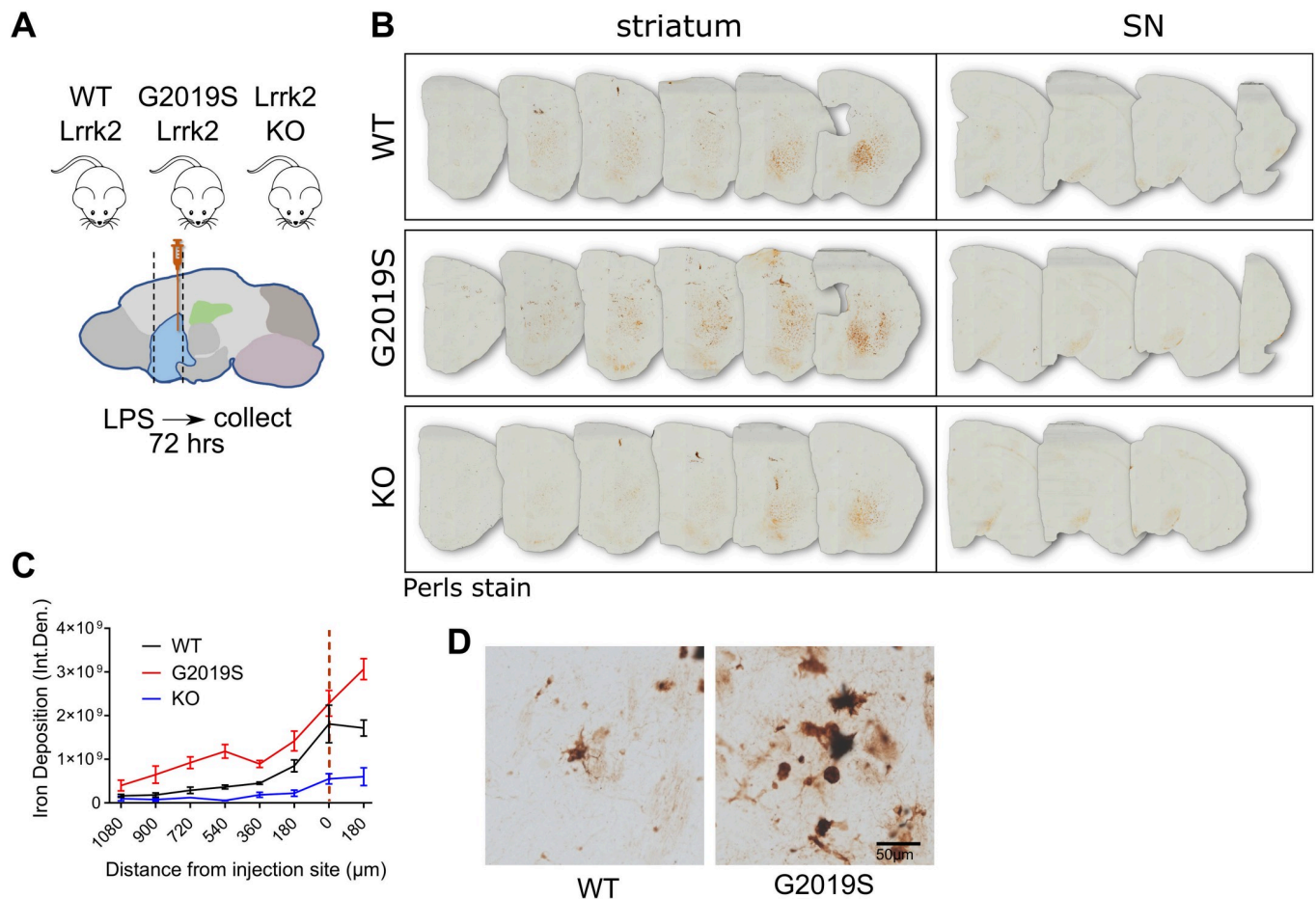
Fig 7. G2019S LRRK2 induces iron accumulation in inflammatory microglia in vivo. (A) Schematic of experimental design: WT, G2019S knock-in, and Lrrk2 KO mice were administered intrastriatal injections of LPS, and 72 hours later, brains were collected and stained by Perls stain. (B, C) G2019S LRRK2 knock-in mice exhibited significantly higher iron deposition in the striatum proximal to the injection site compared to WT and Lrrk2 KO, while minimal signal was detected in the SN in all groups ($N = 4$ WT mice, 4 G2019S and 2 Lrrk2 KO; two-way ANOVA, Tukey post hoc, Genotype: $^{***}P = 0.0007$, F (2, 7) = 24.70, Distance from injection site: $^{****}P < 0.0001$, F (7, 49) = 32.28). High-magnification images revealed iron deposition in inflammatory microglia (D). [SEM bars are shown]. The underlying data can be found in S1 Data. KO, knockout; LPS, lipopolysaccharide; LRRK2, leucine-rich repeat kinase 2; SN, substantia nigra; WT, wild-type.

inflammation in the striatum results in higher iron accumulation in microglia and increased ferritin staining in vivo. These results suggest that LRRK2 plays a role in iron homeostasis response in neuroinflammation, driven, at least in part, by altered endolysosomal functions.

Transferrin-mediated uptake is the main route of iron delivery to most cell types. Extracellular transferrin binds ferric iron (Fe^{3+}) and is internalized by TfR through clathrin-mediated endocytosis. TfR is trafficked through early endosomes and can either be rapidly recycled back to the membrane or associate with the ERC in a slower recycling step. In the acidic lumen of endolysosomes, ferric iron (Fe^{3+}) is reduced to ferrous iron (Fe^{2+}), which mediates its release from Tf and the export to the cytosol through DMT1, where iron is subsequently delivered to different subcellular components. Lysosomal pH regulates iron release and impaired lysosomal acidification has been reported to trigger iron deficiency and inflammation in vivo as well as mitochondrial defects [36,37]. As LRRK2 mutations have been reported to alter the autophagic lysosomal pathway in carriers [38,39], as well as to perturb lysosomal acidification in knock-in mouse models [40], it is plausible that LRRK2 mutations affect Tf-mediated iron uptake by
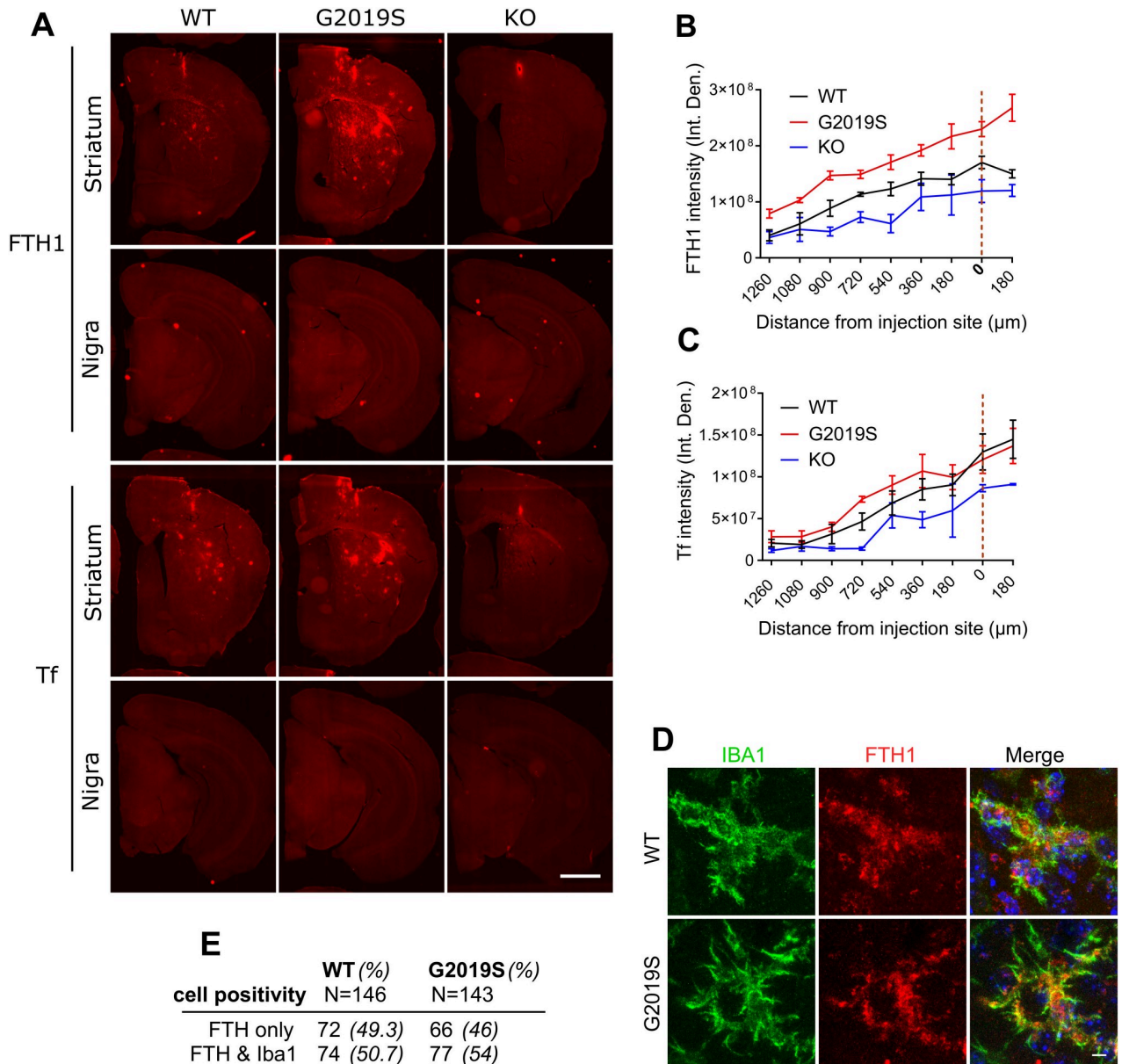
Fig 8. Inflammation induces ferritin accumulation in microglia in G2019S LRRK2 knock-in mice. FTH and Tf were stained and visualized in collected brains, 72 hours after post-intrastriatal injections of LPS. G2019S LRRK2 mice exhibited higher levels of FTH across the striatum compared to WT and Lrrk2 KO mice while Tf was not altered significantly in the knock-in (A, B, C) (N = 4 WT mice, 4 G2019S and 2 Lrrk2 KO; B: two-way ANOVA, Tukey post hoc, Genotype: $**P$ = 0.0017, F (2, 7) = 18.27, Distance from injection site: $****P < 0.0001$, F (8, 56) = 50.25; C: two-way ANOVA, Tukey post hoc, Genotype: P = 0.1040, F (2, 7) = 3.182, Distance from injection site: $****P < 0.0001$, F (8, 56) = 29.17). Microglia are positive for FTH in both WT and G2019S LRRK2 cohorts (D). Similar percentages of FTH-positive microglia were observed between the WT and G2019S LRRK2 groups (E). [SEM bars are shown]. The underlying data can be found in S1 Data. FTH, ferritin heavy chain; KO, knockout; LPS, lipopolysaccharide; LRRK2, leucine-rich repeat kinase 2; Tf, transferrin; WT, wild-type.

modulating lysosomal acidification. Furthermore, other studies have reported enlarged and damaged lysosomes in the context of LRRK2 mutations, consistent with our data [41,42]. In our experiments, we observe sequestration of TfR and accumulation to lysosomes driven by mutant LRRK2, while no significant difference was found on total or membrane-bound TfR levels in these cells or in G2019S knock-in mice that exhibited iron deposition and ferritin up-

Fig 9. A model of the recruitment of Rab8a to lysosomes and dysregulation of transferrin recycling by mutant LRRK2. Following clathrin-mediated endocytosis, TfR can undergo (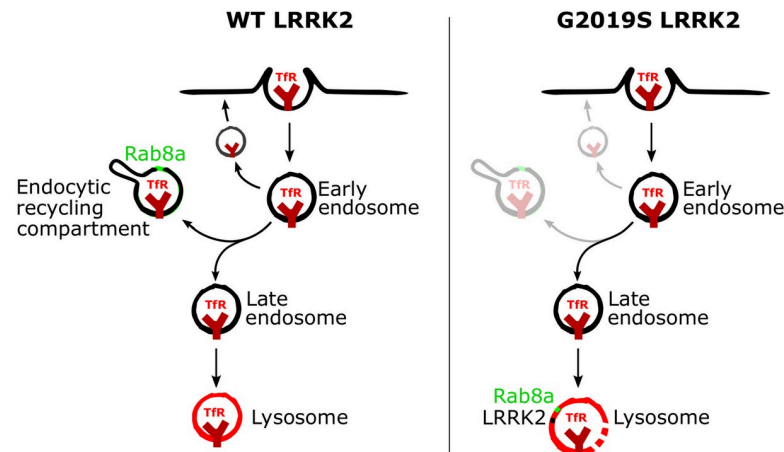a) rapid recycling close to the membrane; (b) slower recycling via the ERC; or (c) targeting to lysosomes. Rab8a mediates recycling of TfR via the ERC, and hyperphosphorylation of Rab8a by mutant LRRK2 induces sequestration to damaged lysosomes and dysregulation of Rab8a-mediated trafficking. ERC, endocytic recycling compartment; LRRK2, leucine-rich repeat kinase 2; TfR, transferrin receptor; WT, wild-type.

https://doi.org/10.1371/journal.pbio.3001480.g009

regulation following LPS administration. Consistent with these observations, TfR levels are not being found to be increased in PD or in mouse models of the disease [43,44], suggesting that the regulation of transferrin recycling through the endolysosomal system rather than over-all levels contribute to iron dyshomeostasis. While our data support the notion that pathogenic LRRK2 causes sequestration of TfR and accumulation in degradation-deficient lysosomes, it remains possible that the identity of this vesicular compartment is not lysosomal but endoso-mal in nature, as a significant portion of Lamp1 can reportedly colocalize with early endo-somes in neurons [45]. LRRK2 deficiency also reportedly impairs recycling of TfR and is required to maintain the lysosomal degradative capacity of endocytic and autophagic cargo [46]. The LRRK2 G2019S mutation can affect Rab8a-mediated receptor recycling and endoly-sosomal transport [29]. We have previously reported that LRRK2 mutations can impair cla-thrin-mediated endocytosis in cell models, which governs internalization of different receptors including TfR [47].

We have recently shown that chronic pharmacological LRRK2 inhibition in G2019S Lrrk2 knock-in mice induces dysregulation of endolysosomal processes and subtle changes in mito-chondrial homeostasis factors, further establishing a link between LRRK2 kinase activity and trafficking pathways that can control iron homeostasis [48]. Our data support an effect of LRRK2 mutations in dysregulating trafficking of internalized transferrin, promoting associa-tion with lysosomes. Additionally, we observe concomitant up-regulation of net intracellular iron in cells expressing G2019S LRRK2. It is important to note that in the ICP-MS experiment, we extracted and assayed whole-cell iron and thus cannot infer which cellular organelles are responsible for the observed up-regulation in G2019S LRRK2 expressing cells. It is known that lysosomes are physiological stores of Fe(II) and that lysosomal impairment or dysregulation of their ability to acidify leads to perturbations in iron homeostasis, and so we hypothesize that LRRK2 mutations may dysregulate the dynamics of TfR transport to lysosomes and the integ-rity of the target lysosomal membranes, thus affecting lysosomal iron stores. This hypothesis warrants further investigation in the context of iron dysregulation in disease.

Iron deposition in the brain is a feature of PD and other neurodegenerative diseases. Imag-ing and biochemical methods have confirmed iron accumulation in the SN of PD patients

correlating with severity of motor symptoms [49–52]. Iron deposition can be detected by transcranial sonography in postmortem brains from PD patients, which correlates with increased ferritin levels and loss of neuromelanin content as assessed biochemically [53]. Studies on animal models have also supported a role of iron in nigral neurodegeneration in PD. In a model of acute MPTP intoxication in mice, dopaminergic cell loss correlated with iron accumulation and increase in lipoperoxidation coinciding with up-regulation of the divalent metal transporter DMT1 [54]. Furthermore, iron chelators can rescue dopaminergic neuron loss and behavioral effects caused by intracerebroventricular administration of 6-hydroxydopamine in rats [55]. In the case of LRRK2, higher nigral iron deposition has been reported in LRRK2 mutation carriers compared to idiopathic patients, while also the same trend has been highlighted in Parkin mutation carriers [56]. Pink1 and Parkin have been linked to degradation of mitochondrial iron importers [57,58] while iron overload can induce a Pink1/Parkin-mediated mitophagic response [59]. These data identify convergent pathways that regulate iron homeostasis and that may be involved in PD pathogenesis in patients.

Our data reflect altered iron handling in microglia in G2019S knock-in versus WT LRRK2 mice, but how this relates to the reported increase in iron in dopaminergic neurons, as relevant for PD pathogenesis, remains unclear. Studies have reported a cooperative effect of neuroinflammation and iron accumulation. Microglial activation by LPS induces secretion of IL-1β and TNF-α that in turn activate iron regulatory proteins in dopaminergic neurons inducing iron overload and neurotoxicity [60]. In these experiments, the iron status of microglia exacerbated proinflammatory cytokine release and neuronal degeneration. Furthermore, in mixed-culture models, microglia play a pivotal role in iron-elicited dopaminergic neurotoxicity via increase in cytokine production [61]. The iron storage protein ferritin is reportedly decreased in the SN of PD patients compared to controls [49]. Increased iron deposition together with lower ferritin levels could indicate increase in intracellular labile iron pools that constitute chelatable redox-active iron damaging to cells. Transgenic mice overexpressing human ferritin protein in dopaminergic SN neurons do not exhibit increases in reactive oxygen species or SN neuron loss following systemic administration of MPTP [62]. In G2019S LRRK2 knock-in mice, we observe an increase in ferritin that may represent a compensatory event to limit neurotoxicity, as a result of dysregulated Tf recycling and iron accumulation.

Iron overload in the brain can activate glial cells and promote the release of inflammatory and neurotrophic factors that control iron homeostasis in dopaminergic neurons. Increased iron in neurons can be toxic through production of hydroxyl radicals via Fenton chemistry, responsible for oxidation of lipids, proteins, and DNA. LRRK2 is modulated by oxidative stress in cells and PD-linked mutations compromise mitochondrial integrity [28,63,64]. Recent studies have demonstrated direct delivery of iron from Tf-endosomes to mitochondria via "kiss-and-run" events while highlighting how these events sustain mitochondrial biogenesis [65]. Dysregulation of iron storage or uptake by LRRK2 in microglia may in turn affect cytokine production and neuronal survival, as well as have a feedback effect on LRRK2 activity in the brain.

We have not yet established whether the observed effects of LRRK2 on iron homeostasis and transferrin recycling are damaging in the context of disease. This is due to the limitations of the available knock-in animal models that they do not present with baseline neurodegeneration. As a consequence of this, it remains uncertain whether iron modulation is a promising therapeutic avenue in the context of LRRK2 mutation carriers. Iron chelators have proven promising in neurodegeneration with brain iron accumulation disorders [66], but iron chelation therapy did not improve motor-UPDRS scores and quality of life significantly [67]. In recent years, LRRK2 has been nominated to play roles in a number of cellular processes ranging from inflammation, autophagy, and endolysosomal pathways to mitochondrial

homeostasis, processes that may also be cell type specific. Given the role that iron dyshomeostasis seems to play in basal ganglia diseases, a combination therapy of iron chelation along with inhibition of LRRK2 could present a viable strategy.

Our data suggest an effect of LRRK2 mutations on Rab8a function, driven by increased kinase activity, which may drive a dysfunction of iron uptake mechanisms in response to inflammatory stimuli in resident microglia. Deciphering the protein trafficking pathways around LRRK2 will help us understand the mechanistic underpinnings of neurodegeneration and the biological implications of blocking LRRK2 kinase in the clinic, while highlighting signaling avenues that can be targeted as therapeutic means.

Materials and methods

Cell culture, treatments, and constructs

HEK293FT cells (Thermo Scientific) were cultured in DMEM supplemented with 10% FBS and maintained at 37˚C, 5% CO2. HEK293T cell lines stably expressing different GFP LRRK2 variants were grown and cultured as described previously [68]. HEK293FT cells were transfected using Lipofectamine 2000 using standard procedures. For siRNAs transfection, cells were transfected with the SMARTpool ON-TARGETplus or scrambled siRNA control (Dharmacon) using the DharmaFECT reagent, according to the manufacturer's instructions. The 3×FLAG-tagged construct of LRRK2 in pCHMWS plasmid was a gift from Dr. J. M. Taymans (KU Leuven, Belgium). LLOMe treatment was at 1 mM for 4 hours, prior to fixation and staining. Nocodazole treatment was at 200 nM for 2 hours.

Live imaging

Mouse primary astrocytes were transiently transfected with HaloTag-LRRK2(G2019S), GFP-Rab8a, and LAMP1-RFP using lipofectamine reagents. Cells were incubated with the JFX650 ligand (100 nM) for 1 hour, washed, and imaged using a Nikon SoRa spinning disk microscope utilizing 3D Landweber deconvolution, 48 hours later.

Structure modeling

Heterodimeric complexes (Rab8a and Rabin8) and (Rab8a and Mical-L1) were modeled in PyMol (PDB: 4LHY and 5SZH, respectively) [69–71]. Insertion of the phosphate at T72 was modeled, and resulting distances were measured using the tools available (PyMOL version 2.0).

Animal procedures

C57BL/6J mice were housed in standardized conditions at 2 to 5 animals per cage and with ad libitum access to food and water on a 12-hour light–dark cycle. The protocols used here are approved by the Institutional Animal Care and Use Committee of National Institute on Aging, NIH (protocol ID: 463-LNG-2021). The NIA IRP maintains an assurance with the Office of Laboratory Animal Welfare (OLAW) via the Office of Animal Care and Use (OACU) of the NIH. The NIA IRP complies with standards of the Guide for the Care and Use of Laboratory Animals, NRC, 2011, and the PHS Policy on Humane Care and Use of Laboratory Animals, USDHHS, NIH, OLAW, 2015 for all animals, as well as the Animal Welfare Act, USDA, regulations and USDA Animal Care Policies for USDA's Animal Welfare Act, USDA, APHIS.

Stereotaxic surgery

One-year-old WT, LRRK2 KO, or LRRK2 G2019S mice were kept under anesthesia using 1% to 2% isoflurane. Mice were placed into a stereotaxic frame, an incision was made above the midline, and the skull was exposed using cotton tips. At anteroposterior +0.2 mm, mediolateral +/−2.0 mm from bregma (bilateral injection), a hole was drilled into the skull. A pulled glass capillary (blunt) attached to a 5-μl Hamilton glass syringe was used for injecting either 1 μl of either PBS or 5 mg/ml LPS solution (5 μg) per hemisphere. The capillary was lowered to dorsoventral −3.2 mm from bregma into the dorsal striatum. The solution was delivered at a rate of 0.1 μl per 10 seconds. After the injection, the capillary was held in place for 2 minutes, retracted 0.1 μm, and another 1 minute was waited before it was slowly withdrawn from the brain. The head wound was closed using surgical staples. Ketoprofen solution at 5 mg/kg was administered subcutaneously as analgesic treatment for the following 3 days.

Histology

Animals were killed 3 days after surgery. Mice were deeply anesthetized using an IP injection of 200 μl of 10% ketamine. The thoracic cavity was opened to expose the heart. The whole body was perfused with 10 ml of 0.9% NaCl (2 minutes). Brains were removed, the left hemisphere was used for WB analysis, while the right hemisphere was fixed in 4% PFA for 48 hours. After 2 days, fixed hemispheres were transferred to 30% sucrose solution for cryoprotection. The brains were cut into 30 μm thick coronal sections—6 series—and stored in antifreeze solution (0.5 M phosphate buffer, 30% glycerol, 30% ethylene glycol) at −20˚C until further processed.

Immunohistochemistry

Sections were washed with PBS and incubated for 30 minutes in blocking buffer (10% Normal Donkey Serum (NDS), 1% BSA, 0.3% Triton in PBS). Afterwards, primary antibodies rabbit anti-FTH1 (D1D4; 4393S, Cell Signaling) and goat anti-Iba1 (Abcam, ab5076) were used at 1:500 and incubated overnight at 4˚C in 1% NDS, 1% BSA, 0.3% Triton in PBS. Next day, sections were washed 3× for 10 minutes each with PBS and incubated with Alexa Fluorophore (568 or 647)-conjugated secondary antibodies for 1 hour at room temperature (RT). After 3 washes with PBS, sections were mounted on glass slides, coverslipped using Prolong Gold Antifade mounting media (Invitrogen), and imaged using a Zeiss LSM 880 confocal microscope equipped with Plan-Apochromat 63X/1.4 numerical aperture oil-objective (Carl Zeiss AG). Sections were further imaged using an Olympus VS120 (Olympus, Center Valley, Pennsylvania) slide scanner microscope.

Perls blue staining

Sections were washed in ddH2O 3× for 10 minutes each. Afterwards, sections were incubated in a 1:1 mix of 4% potassium ferrocyanide (Sigma-Aldrich P3289-100G) and 4% HCl. After 30 minutes, brain slices were washed 3× for 10 minutes with PBS and quenched using 10% Methanol + 3% H2O2 diluted in PBS for 1 hour. Sections were then rinsed again using PBS and incubated in 3,3′-Diaminobenzidine and H2O2 according to instructions (SIGMAFAST D4418-50SET, Sigma-Aldrich). Then, slices were washed with PBS 3× for 10 minutes, mounted on SuperFrost Plus slides (Fisher Scientific), dried overnight and dehydrated using 70% Ethanol, 95% Ethanol, 100% Ethanol followed by Xylene and DPX mounting media (Sigma, 06522), and analyzed on ImageJ for signal intensity of selected ROIs.

ICP-MS

Total iron concentrations in the samples were measured by ICP-MS (Agilent model 7900). For each sample, 200 μL of concentrated trace-metal-grade nitric acid (Fisher) was added to 25 μL or 100 μL of sample taken in a 15-mL Falcon tube. Tubes were sealed with electrical tape to prevent evaporation, taken inside a 1-L glass beaker, and then placed at 90°C oven. After overnight digestion, each sample was diluted to a total volume of 4 mL with deionized water and then analyzed by ICP-MS.

iPSC differentiation

iPSC lines were derived from reprogrammed peripheral mononuclear blood cells (PBMCs) collected from participants of the Parkinson Progression Marker Initiative (PPMI). Differentiation of iPSC to microglia was accomplished via a hematopoietic stem cell intermediate stage according to published protocols [72,73]. Mature iPSC-derived microglia were characterized by western blot and ICC for Iba1 expression (S6 Fig). The lines used were PPMI 3448 (WT) and PPMI 51782 (G2019S LRRK2 carrier). LPS activation was done in differentiation media at 100 ng/ml for 16 hours prior to fixation and staining. Activation by LPS treatment was verified by WB of pNFKb, p38, and imaging of Iba1 staining (S5 Fig).

Co-immunoprecipitation

HEK-293T were transfected with 3×FLAG-Rab8a variants and 3xFLAG-GUS (Fig 3D) or 3xFLAG LRRK2 variants and GFP-Rab8a (Fig 3E), using Lipofectamine 2000 as per the manufacturer's instructions. After 24 hours, cells were lysed in buffer containing 20 mM Tris/HCl (pH 7.4), 137 mM NaCl, 3 mM KCl, 10% (v/v) glycerol, 1 mM EDTA, and 0.3% Triton X-100 supplemented with protease inhibitors and phosphatase inhibitors (Roche Applied Science). Lysates were centrifuged at $21,000 \times g$, 4°C for 10 minutes, and the supernatants were analyzed for protein concentration (Pierce). About 5 μg of total protein from each supernatant was analyzed by SDS-PAGE for expression of the proteins in question. For FLAG immunoprecipitations, 3 mg of each sample was precleared with EZview protein G beads (Sigma-Aldrich) for 0.5 hours at 4°C, and, subsequently, FLAG M2 beads were incubated with the lysates for 2 hours at 4°C to IP target constructs. FLAG-tagged proteins were eluted in 1× kinase buffer (Cell Signaling), containing 150 mM NaCl, 0.02% Triton, and 150 ng/μl of 3xFLAG peptide (Sigma-Aldrich) by shaking for 30 minutes at 4°C. For GFP IPs, Chromotek-GFP-Trap-agarose resin (Allele Biotech) was incubated with lysates for 2 hours at 4°C. The beads were washed 4 times with buffer containing 20 mM Tris/HCl (pH 7.4), 137 mM NaCl, 3 mM KCl, and 0.1% Triton X-100. The washed beads were boiled for 6 minutes in 4× NuPAGE loading buffer (Invitrogen) supplemented with 1.4 M β-mercaptoethanol and analyzed by western blot.

Cell surface biotinylation

Cells stably expressing GFP WT or G2019S LRRK2 were surface biotinylated, lysed, and surface proteins were enriched by avidin-conjugated agarose following the manufacturer's protocol (Pierce kit, A44390). Surface enriched proteins were analyzed by western blot.

Western blot

Standard western blot protocols were used with the following antibodies: anti-LRRK2 (ab133474; Abcam), anti-Rab8a (6975, Cell Signaling), anti-MICAL-L1 (H00085377, Abnova),

GDI1/2 (716300, Thermo Scientific), Rabin8 (12321-1-AP, Protein Tech), FLAG (F1804, Sigma-Aldrich).

RNA isolation and RNA-Seq

For Fig 5A–5D, RNA was isolated from primary microglia and analyzed by bulk RNA sequencing following methods published in [34]. For Fig 5E–5I, mice were administered striatal LPS injections and killed 3 days later. Collected brain hemispheres were dissociated using the Adult Brain Dissociation kit (Miltenyi Biotec), and brain microglia cells were isolated using CD11b microbeads and MACS sorting columns (Miltenyi Biotec). Single-cell suspensions were subjected to scRNA-seq at the National Cancer Institute Single-Cell Analysis Core Facility, Bethesda, Maryland, and followed the 10xGenomics pipeline. Data were analyzed using the R package Seurat (version 3, PMIDS: 26000488; PMID: 29608179) as described in [34].

Immunocytochemistry

HEK293fT cells were seeded at 0.1×10^6 cells/well on 12 mm coverslips precoated with poly-D-lysine (Millicell EZ slide, Millipore) and cultured as described above. Cells were fixed in 4% (w/v) formaldehyde/PBS for 15 minutes, permeabilized in 0.2% Triton X-100/PBS for 10 minutes at RT, blocked in 5% (v/v) FBS in PBS, and incubated with primary antibodies in 1% (v/v) FBS/PBS for 3 hours. Following 3 washes in PBS, the cells were incubated for 1 hour with secondary antibodies (Alexa Fluor 488, 568, 647-conjugated; ThermoFisher). After 3 PBS washes, the coverslips were mounted, and the cells were analyzed by confocal microscopy (Zeiss LSM 880 and Airyscan superresolution microscopy). For high-content imaging, where Rab8a translocation was quantified, cells were plated in 96-well plates, precoated with matrigel, transfected with LRRK2 mutants, and processed following 24 hours of expression. Cells were treated with DMSO or 1 μM MLi-2 for 1 hour prior to fixation and staining with the corresponding antibodies. Cells were visualized with the ThermoFisher Cellomics ArrayScan using the HCS Studio platform and the SpotDetector v4 bioassay protocol. A minimum of 800 cells were imaged per well from a total of 6 wells per construct and condition, and Rab8a localization was analyzed. The ezColocalization ImageJ plugin was used for analysis of the Manders overlap coefficient [74]. Analysis of Rab8a presence near the centrosome was performed as in [30], where the percentage of Rab8a staining that resides within a 2.2-μm diameter circular ROI enclosing centrosomal staining, versus whole-cell Rab8a staining, was calculated. The antibodies used were Rab8a (Cell Signaling Technology; #6975), TfR1 (Abcam; ab84036), Ferritin Heavy Chain (Thermo Fisher; PA5-27500), transferrin (Abcam; ab82411), MICAL-L1 (Novus; H00085377-B01P), Cathepsin D (Calbiochem; 219361), Lamp1 (DSHB; 1D4B), and Lamp2 (DSHB; H4B4).

Imaris analysis

Following superresolution microscopy, the Imaris platform (Bitplane, Zürich, Switzerland) was used to analyze the localization of TfR and Tf in different experiments. In Fig 4A, the Imaris Spots Detection module was used to identify TfR vesicles throughout z planes in the 3D volume, and the distance between them was calculated. In Fig 6, superresolution (Airyscan) z-stack images of iPSC-derived microglia were processed through the Imaris Surface Contour module to render Tf and nuclear staining to surfaces and measure the distance of Tf vesicles from the nucleus edge (3D rendering process outlined in S1–S4 Movies).

Transferrin uptake and recycling assay

Cells that were plated and transfected on 12 mm poly-D-lysine coated coverslips were processed following 24 hours of expression. Initially, cells were incubated in prewarmed DMEM for 45 minutes. Alexa 568 fluorophore–conjugated transferrin (T23365, ThermoFisher) was added to the media at 20 μg/ml final concentration, and cells were incubated for 20 minutes. Following one quick wash in prewarmed media, cells were incubated with prewarmed DMEM, 10% (v/v) FBS media for 10 minutes and fixed and stained as detailed above. For the uptake assay, cells were plated on matrigel-coated 96-well plates (15,000 cells/well), transiently transfected and processed 24 hours posttransfection. Cells were incubated in DMEM for 45 minutes, and subsequently equal volume of DMEM media containing Alexa 568–conjugated transferrin was added to the wells to achieve 20 μg/ml final transferrin concentration. Transferrin was added at different time intervals, and the plate was washed in cold PBS and fixed at 20 minutes of total uptake, achieving 0, 2, 4, 6, 8, 10, 15, and 20 minutes of uptake time points. A similar setup was followed for recycling assays whereby cells were loaded with Tf-568 in DMEM for 30 minutes, washed once in DMEM, and then incubated in DMEM/10% FBS media for the different time points of recycling, followed by a quick wash in cold PBS and fixation. Similar paradigms were followed in Tf uptake/recycling assays in iPSC-derived microglia, using DMEM/F12 media plus supplements as per differentiation protocols.

Statistical analysis

Statistical tests used are noted in figure legends of representative graphs. Briefly, one-way ANOVA or two-way ANOVA with Tukey post hoc test and two-tailed unpaired Student t test with Mann–Whitney U post hoc test were used. All statistical analyses were performed using GraphPad Prism 7 (GraphPad Software, San Diego, California).

Supporting information

S1 Fig. Validation of Rab8a antibodies for endogenous detection. (A, B) The rabbit anti-Rab8A antibody by Cell Signaling (D22D8; #6975) and rabbit anti-Rab8a (#ab188574) antibody were tested in ICC and western blotting against Rab8a siRNA treated Hek293T cells. The Cell Signaling (#6975) antibody validated against knock-down for detection of endogenous Rab8a and was used throughout this study. ICC, immunocytochemistry; siRNA, small interfering RNA.
(TIF)

S2 Fig. LRRK2 genetic variants sequester endogenous Rab8a to lysosomes in a kinase-dependent manner. (A) HEK293T cells transiently expressing WT or mutant LRRK2 constructs were treated with MLi-2 or DMSO for 1 hour prior to fixation and staining for Rab8a, Lamp2, and LRRK2 (FLAG). Rab8a was sequestered to Lamp2-positive lysosomes in cells expressing R1441C, Y1699C, G2019S, or I2020T LRRK2, but not the kinase-dead K1906M LRRK2 or transfection control (GUS). MLi-2 treatment rescues this phenotype. (B) High-content imaging (Cellomics) was used to quantitate the percentage of cells exhibiting sequestered Rab8a (>4 μm^2 Rab8a foci, >800 cells imaged per well, 4 wells per condition). Higher Rab8a sequestration was observed in cells expressing R1441C, Y1699C, G2019S, and I2020T LRRK2 compared to WT LRRK2, while this is ameliorated by MLi-2. (C) The percentage of cells that exhibited Rab8a-positive lysosomes was significantly increased in cells expressing R1441C LRRK2 or G2019S LRRK2 compared to WT LRRK2 expressing cells (a minimum of 200 cells were counted per group across $N = 4$ different experiments, one-way ANOVA Tukey post hoc, ***$P < 0.001$, *$P < 0.05$, F (2, 9) = 17.03). The underlying data can be found in S1 Data.

LRRK2, leucine-rich repeat kinase 2; WT, wild-type.
(TIF)

S3 Fig. Association of Rab8a with centrosomes and lysosomes in HEK293T cells expressing G2019S LRRK2. (A) HEK293T cells transiently expressing FLAG G2019S LRRK2 were treated with nocodazole (200 nM) or DMSO for 2 hours and stained for FLAG G2019S LRRK2, endogenous Rab8a, and pericentrin. (B) Quantification of the percentage of Rab8a staining that resides within a 2.2-μm diameter circular ROI enclosing centrosomal staining versus whole-cell Rab8a staining (B: $^{**}P < 0.01$, $N > 19$ cells per group from 2 independent experiments, two-tailed Student t test, Mann–Whitney U). (C) Cells were treated as in (A) and stained for FLAG G2019S LRRK2, endogenous Rab8a, and endogenous Lamp2. (D) Quantification of Manders colocalization coefficient between Rab8a and lamp2 staining (D: $^{**}P < 0.01$, $N > 14$ cells per group from 2 independent experiments, two-tailed Student t test, Mann–Whitney U). The underlying data can be found in S1 Data. LRRK2, leucine-rich repeat kinase 2; ROI, region of interest.
(TIF)

S4 Fig. Endogenous MICAL-L1 is recruited by mutant LRRK2 to lysosomes. (A) HEK293T cells transiently expressing WT or mutant LRRK2 were stained for MICAL-L1, LRRK2 (FLAG), and Lamp2 and analyzed by confocal microscopy. The Manders overlap coefficient between MICAL-L1 and LRRK2, or MICAL-L1 and Lamp2 were calculated in ImageJ. (B,C: $N > 10$ cells per group collected in 1 experiment; one-way ANOVA Tukey post hoc, $^{***}P < 0.001$, $^{**}P < 0.01$, $^{*}P < 0.05$, B: F (2, 30) = 13.66, C: F (2, 31) = 11.40). The underlying data can be found in S1 Data. LRRK2, leucine-rich repeat kinase 2; WT, wild-type.
(TIF)

S5 Fig. Mutant LRRK2 induces mistrafficking of TfR. (A) HEK293T cells transiently expressing WT or mutant LRRK2 constructs were stained for endogenous TfR and Lamp2 and visualized by confocal microscopy. Colocalization between TfR and Lamp2 was analyzed in ImageJ. (A, B) ($N > 19$ cells per group collected in 2 independent experiment, $^{****}P < 0.0001$, one-way ANOVA with Tukey post hoc; F (2, 42) = 30.92). (C) Cells stably expressing WT LRRK2 were treated with LLOMe for 2 hours and stained. LLOMe treatment induced the sequestration of Rab8a to LRRK2-positive vesicles with partial recruitment of TfR. (D) HEK293T cells transiently expressing WT or G2019S LRRK2 were treated with MLI-2, loaded with Alexa Fluor 568-Tf and visualized at T10 minutes of recycling in fresh media containing MLi-2. The mean distance between Tf vesicles was calculated in Imaris ($N > 2,500$ vesicles were counted in at least 20 cells per construct from 2 independent experiments, $^{****}P < 0.0001$, one-way ANOVA with Tukey post hoc, F (2, 7932) = 560.1). (E) Cells stably expressing GFP WT or G2019S LRRK2 were surface biotinylated and surface proteins were enriched by avidin-conjugated agarose before western blotting for TfR ($N = 2$ experimental replicates). The underlying data can be found in S1 Data. LRRK2, leucine-rich repeat kinase 2; TfR, transferrin receptor; WT, wild-type.
(TIF)

S6 Fig. Characterization of iPSC-derived microglia. (A) Immunoblot analysis of iPSC-derived microglia following treatment with 100 ng/mL LPS. (B, C) Quantification of indicated phospho-proteins normalized against total protein and loading control b-actin in treated vs. untreated cells (technical $N = 3$, unpaired t test, $P < 0.01$). (D) Iba1 staining of DMS and LPS treated microglia from WT and G2019S cell lines. (E) Cell size of iPSC-derived microglia under DMSO or LPS treatment was measured in ImageJ ($N > 19$ cells counted in 2 differentiations). The underlying data can be found in S1 Data. iPSC, induced pluripotent stem cell; LPS,

lipopolysaccharide; WT, wild-type.
(TIF)

S7 Fig. Tf recycling in iPSC-derived microglia. iPSC-derived human microglia from WT or
G2019S LRRK2 carriers were treated with LPS, and high-content imaging was used to monitor
the uptake of Alexa Fluor 568–conjugated Tf (A, B) or recycling following Tf preloading in
pulse-chase experiments (C, D). (N = 5 technical replicates of >50 counted cells, two-way
ANOVA; B: time point: $P < 0.0001$, F (4, 80) = 155.1, genotype: NS; D: time point: $P < 0.0001$,
F (4, 80) = 115.2, genotype: $P < 0.05$, F (3, 80) = 3.664). The underlying data can be found in
S1 Data. iPSC, induced pluripotent stem cell; LPS, lipopolysaccharide; LRRK2, leucine-rich
repeat kinase 2; Tf, transferrin; WT, wild-type.
(TIF)

S8 Fig. Uncropped western blots of figures. (A) Panel of Fig 3A: HEK293T cells expressing
control (GUS), FLAG WT, or mutant LRRK2 variants were treated with MLi-2 prior to lysis
and analysis by western blotting for pS1292 and total LRRK2, as well as pT72 and total Rab8a.
(B) Panel of Fig 3D: HEK293T cells expressing FLAG WT, I2020T, or K1906M LRRK2 along
with GFP Rab8a, GFP control, or FLAG-GUS control were lysed and proteins immunoprecipi-
tated using GFP beads. Co-immunoprecipitated proteins were analyzed by western blotting
probed for MICAL-L1 as well as pT72 and total Rab8a. (C) Panel of S5E Fig: Cells stably
expressing GFP WT or G2019S LRRK2 were surface biotinylated, and surface proteins were
enriched by avidin-conjugated agarose before western blotting for TfR. (D) Panel of S6A Fig:
Immunoblot analysis of iPSC-derived microglia following treatment with 100 ng/mL LPS. (E)
Panel of S1 Fig: western blot validation of Rab8a antibodies for endogenous detection. iPSC,
induced pluripotent stem cell; LPS, lipopolysaccharide; LRRK2, leucine-rich repeat kinase 2;
TfR, transferrin receptor; WT, wild-type.
(TIF)

**S1 Data. Individual numerical values that underlie the summary data displayed in the fol-
lowing figure panels: Figs 1B, 1C, 1F, 2B, 3B, 4B, 4D–4G, 4J, 4K, 6B–6F, 7C, 8B, 8C, S2B,
S2C, S3B, S3D, S4B, S4C, S5B, S5D, S5E, S6B, S6C, S6E, S7B and S7D.**
(XLSX)

**S1 Movie. Imaris 3D surface rendering of endogenous transferrin and Lamp2 staining in
WT LRRK2 iPSC-derived microglia.** iPSC, induced pluripotent stem cell; LRRK2, leucine-
rich repeat kinase 2; WT, wild-type.
(MP4)

**S2 Movie. Imaris 3D surface rendering of endogenous transferrin and Lamp2 staining in
WT LRRK2 iPSC-derived microglia treated with 100 ng/ml LPS for 16 hours.** iPSC,
induced pluripotent stem cell; LPS, lipopolysaccharide; LRRK2, leucine-rich repeat kinase 2;
WT, wild-type.
(MP4)

**S3 Movie. Imaris 3D surface rendering of endogenous transferrin and Lamp2 staining in
G2019S LRRK2 iPSC-derived microglia.** iPSC, induced pluripotent stem cell; LRRK2, leu-
cine-rich repeat kinase 2.
(MP4)

**S4 Movie. Imaris 3D surface rendering of endogenous transferrin and Lamp2 staining in
G2019S LRRK2 iPSC-derived microglia treated with 100 ng/ml LPS for 16 hours.** iPSC,

induced pluripotent stem cell; LPS, lipopolysaccharide; LRRK2, leucine-rich repeat kinase 2. (MP4)

Acknowledgments

Author Contributions

Conceptualization: Adamantios Mamais, Ravindran Kumaran, Changyoun Kim, Mark R. Cookson.

Data curation: Luis Bonet-Ponce, Nathan Smith, Alexandra Beilina, Alice Kaganovich, Manik C. Ghosh, Rina Bandopadhyay, David C. Gershlick, Mark R. Cookson.

Formal analysis: Adamantios Mamais, Jillian H. Kluss, Luis Bonet-Ponce, Natalie Landeck, Rebekah G. Langston, Nathan Smith, Alexandra Beilina, Alice Kaganovich, Manik C. Ghosh, Laura Pellegrini, Ravindran Kumaran, Ioannis Papazoglou, George R. Heaton, Nunziata Maio.

Funding acquisition: Mark R. Cookson.

Investigation: Adamantios Mamais, Jillian H. Kluss, Natalie Landeck, Rebekah G. Langston, Alexandra Beilina, Laura Pellegrini, Nunziata Maio, Changyoun Kim, David C. Gershlick.

Methodology: Adamantios Mamais, Changyoun Kim.

Project administration: Mark R. Cookson.

Resources: Matthew J. LaVoie.

Supervision: Matthew J. LaVoie, Mark R. Cookson.

Writing – original draft: Adamantios Mamais, Mark R. Cookson.

Writing – review & editing: Mark R. Cookson.

References

1. Barrett JC, Hansoul S, Nicolae DL, Cho JH, Duerr RH, Rioux JD, et al. Genome-wide association defines more than 30 distinct susceptibility loci for Crohn's disease. Nat Genet. 2008 Aug; 40(8):955–62. https://doi.org/10.1038/ng.175 PMID: 18587394

2. Paisán-Ruíz C, Jain S, Evans EW, Gilks WP, Simón J, van der Brug M, et al. Cloning of the gene containing mutations that cause PARK8-linked Parkinson's disease. Neuron. 2004 Nov 18; 44(4):595–600. https://doi.org/10.1016/j.neuron.2004.10.023 PMID: 15541308

3. Zimprich A, Biskup S, Leitner P, Lichtner P, Farrer M, Lincoln S, et al. Mutations in LRRK2 Cause Autosomal-Dominant Parkinsonism with Pleomorphic Pathology. Neuron. 2004 Nov 18; 44(4):601–7. https://doi.org/10.1016/j.neuron.2004.11.005 PMID: 15541309

4. Kluss JH, Mamais A, Cookson MR. LRRK2 links genetic and sporadic Parkinson's disease. Biochem Soc Trans. 2019 Apr 30; 47(2):651–61. https://doi.org/10.1042/BST20180462 PMID: 30837320

5. Cook DA, Kannarkat GT, Cintron AF, Butkovich LM, Fraser KB, Chang J, et al. LRRK2 levels in immune cells are increased in Parkinson's disease. NPJ Parkinsons Dis. 2017 Mar 28; 3(1):1–12. https://doi.org/10.1038/s41531-017-0010-8 PMID: 28649611

6. Gillardon F, Schmid R, Draheim H. Parkinson's disease-linked leucine-rich repeat kinase 2(R1441G) mutation increases proinflammatory cytokine release from activated primary microglial cells and

resultant neurotoxicity. Neuroscience. 2012 Apr 19; 208:41–8. https://doi.org/10.1016/j.neuroscience.2012.02.001 PMID: 22342962

7. Moehle MS, Webber PJ, Tse T, Sukar N, Standaert DG, DeSilva TM, et al. LRRK2 Inhibition Attenuates Microglial Inflammatory Responses. J Neurosci. 2012 Feb 1; 32(5):1602–11. https://doi.org/10.1523/JNEUROSCI.5601-11.2012 PMID: 22302802

8. Steger M, Tonelli F, Ito G, Davies P, Trost M, Vetter M, et al. Phosphoproteomics reveals that Parkinson's disease kinase LRRK2 regulates a subset of Rab GTPases. eLife. 2016 Jan 29 [cited 2016 Apr 28]; 5. Available from: http://elifesciences.org/lookup/doi/10.7554/eLife.12813. PMID: 26824392

9. Thirstrup K, Dächsel JC, Oppermann FS, Williamson DS, Smith GP, Fog K, et al. Selective LRRK2 kinase inhibition reduces phosphorylation of endogenous Rab10 and Rab12 in human peripheral mononuclear blood cells. Sci Rep. 2017 Aug 31; 7(1):10300. https://doi.org/10.1038/s41598-017-10501-z PMID: 28860483

10. Stenmark H. Rab GTPases as coordinators of vesicle traffic. Nat Rev Mol Cell Biol. 2009 Aug; 10(8):513–25. https://doi.org/10.1038/nrm2728 PMID: 19603039

11. Pfeffer SR. Rab GTPase regulation of membrane identity. Curr Opin Cell Biol. 2013 Aug; 25(4):414–9. https://doi.org/10.1016/j.ceb.2013.04.002 PMID: 23639309

12. Beilina A, Rudenko IN, Kaganovich A, Civiero L, Chau H, Kalia SK, et al. Unbiased screen for interactors of leucine-rich repeat kinase 2 supports a common pathway for sporadic and familial Parkinson disease. Proc Natl Acad Sci U S A. 2014 Feb 18; 111(7):2626–31. https://doi.org/10.1073/pnas.1318306111 PMID: 24510904

13. MacLeod DA, Rhinn H, Kuwahara T, Zolin A, Di Paolo G, McCabe BD, et al. RAB7L1 interacts with LRRK2 to modify intraneuronal protein sorting and Parkinson's disease risk. Neuron. 2013 Feb 6; 77(3):425–39. https://doi.org/10.1016/j.neuron.2012.11.033 PMID: 23395371

14. Nalls MA, Pankratz N, Lill CM, Do CB, Hernandez DG, Saad M, et al. Large-scale meta-analysis of genome-wide association data identifies six new risk loci for Parkinson's disease. Nat Genet. 2014 Sep; 46(9):989–93. https://doi.org/10.1038/ng.3043 PMID: 25064009

15. Liu Z, Bryant N, Kumaran R, Beilina A, Abeliovich A, Cookson MR, et al. LRRK2 phosphorylates membrane-bound Rabs and is activated by GTP-bound Rab7L1 to promote recruitment to the trans-Golgi network. Hum Mol Genet. 2018; 27(2):385–95. https://doi.org/10.1093/hmg/ddx410 PMID: 29177506

16. Purlyte E, Dhekne HS, Sarhan AR, Gomez R, Lis P, Wightman M, et al. Rab29 activation of the Parkinson's disease-associated LRRK2 kinase. EMBO J. 2018 Jan 4; 37(1):1–18. https://doi.org/10.15252/embj.201798099 PMID: 29212815

17. Eguchi T, Kuwahara T, Sakurai M, Komori T, Fujimoto T, Ito G, et al. LRRK2 and its substrate Rab GTPases are sequentially targeted onto stressed lysosomes and maintain their homeostasis. Proc Natl Acad Sci U S A 2018 Sep 25; 115(39):E9115–24. https://doi.org/10.1073/pnas.1812196115 PMID: 30209220

18. Bonet-Ponce L, Beilina A, Williamson CD, Lindberg E, Kluss JH, Saez-Atienzar S, et al. LRRK2 mediates tubulation and vesicle sorting from lysosomes. Sci Adv. 2020 Nov 1; 6(46):eabb2454. https://doi.org/10.1126/sciadv.abb2454 PMID: 33177079

19. Herbst S, Campbell P, Harvey J, Bernard EM, Papayannopoulos V, Wood NW, et al. LRRK2 activation controls the repair of damaged endomembranes in macrophages. EMBO J. 2020 Sep 15; 39(18): e104494. https://doi.org/10.15252/embj.2020104494 PMID: 32643832

20. Peränen J. Rab8 GTPase as a regulator of cell shape. Cytoskeleton. 2011; 68(10):527–39. https://doi.org/10.1002/cm.20529 PMID: 21850707

21. Sharma M, Giridharan SSP, Rahajeng J, Naslavsky N, Caplan S. MICAL-L1 links EHD1 to tubular recycling endosomes and regulates receptor recycling. Mol Biol Cell. 2009 Dec; 20(24):5181–94. https://doi.org/10.1091/mbc.e09-06-0535 PMID: 19864458

22. Yoshimura S-I, Egerer J, Fuchs E, Haas AK, Barr FA. Functional dissection of Rab GTPases involved in primary cilium formation. J Cell Biol. 2007 Jul 30; 178(3):363–9. https://doi.org/10.1083/jcb.200703047 PMID: 17646400

23. Kobayashi H, Etoh K, Ohbayashi N, Fukuda M. Rab35 promotes the recruitment of Rab8, Rab13 and Rab36 to recycling endosomes through MICAL-L1 during neurite outgrowth. Biology Open. 2014 Sep 15; 3(9):803–14. https://doi.org/10.1242/bio.20148771 PMID: 25086062

24. Hattula K, Furuhjelm J, Tikkanen J, Tanhuanpaa K, Laakkonen P, Peranen J. Characterization of the Rab8-specific membrane traffic route linked to protrusion formation. J Cell Sci. 2006 Nov 14; 119(23):4866–77. https://doi.org/10.1242/jcs.03275 PMID: 17105768

25. Burtey A, Wagner M, Hodneland E, Skaftnesmo KO, Schoelermann J, Mondragon IR, et al. Intercellular transfer of transferrin receptor by a contact-, Rab8-dependent mechanism involving tunneling nanotubes. FASEB J. 2015 Jul 28; 29(11):4695–712. https://doi.org/10.1096/fj.14-268615 PMID: 26220176

26. Wang J, Ren J, Wu B, Feng S, Cai G, Tuluc F, et al. Activation of Rab8 guanine nucleotide exchange factor Rabin8 by ERK1/2 in response to EGF signaling. PNAS. 2015 Jan 6; 112(1):148–53. https://doi.org/10.1073/pnas.1412089112 PMID: 25535387

27. Rivero-Ríos P, Romo-Lozano M, Madero-Pérez J, Thomas AP, Biosa A, Greggio E, et al. The G2019S variant of leucine-rich repeat kinase 2 (LRRK2) alters endolysosomal trafficking by impairing the function of the GTPase RAB8A. J Biol Chem. 2019 Mar 29; 294(13):4738–58. https://doi.org/10.1074/jbc.RA118.005008 PMID: 30709905

28. Mamais A, Chia R, Beilina A, Hauser DN, Hall C, Lewis PA, et al. Arsenite Stress Downregulates Phosphorylation and 14-3-3 Binding of Leucine-rich Repeat Kinase 2 (LRRK2) Promoting Self-Association and Cellular Redistribution. J Biol Chem. 2014 Jun 18:jbc.M113.528463.

29. Fernández B, Lara Ordóñez AJ, Fdez E, Mutez E, Comptdaer T, Leghay C, et al. Centrosomal cohesion deficits as cellular biomarker in lymphoblastoid cell lines from LRRK2 Parkinson's disease patients. Biochem J. 2019 Oct 15; 476(19):2797–813. https://doi.org/10.1042/BCJ20190315 PMID: 31527116

30. Madero-Pérez J, Fdez E, Fernández B, Lara Ordóñez AJ, Blanca Ramírez M, Gómez-Suaga P, et al. Parkinson disease-associated mutations in LRRK2 cause centrosomal defects via Rab8a phosphorylation. Mol Neurodegener. 2018 Jan 23; 13 (1):3. https://doi.org/10.1186/s13024-018-0235-y PMID: 29357897

31. Dhekne HS, Yanatori I, Gomez RC, Tonelli F, Diez F, Schüle B, et al. A pathway for Parkinson's Disease LRRK2 kinase to block primary cilia and Sonic hedgehog signaling in the brain. Burd CG, Malhotra V, editors. Elife. 2018 Nov 6; 7:e40202.

32. Pu J, Guardia CM, Keren-Kaplan T, Bonifacino JS. Mechanisms and functions of lysosome positioning. J Cell Sci 2016 Dec 1; 129(23):4329–39. https://doi.org/10.1242/jcs.196287 PMID: 27799357

33. Nnah IC, Wessling-Resnick M. Brain Iron Homeostasis: A Focus on Microglial Iron. Pharmaceuticals (Basel). 2018 Nov 23 [cited 2020 Jul 12]; 11(4). Available from: https://www.ncbi.nlm.nih.gov/pmc/articles/PMC6316365/. https://doi.org/10.3390/ph11040129 PMID: 30477086

34. Russo I, Kaganovich A, Ding J, Landeck N, Mamais A, Varanita T, et al. Transcriptome analysis of LRRK2 knock-out microglia cells reveals alterations of inflammatory- and oxidative stress-related pathways upon treatment with α-synuclein fibrils. Neurobiol Dis. 2019; 129:67–78. https://doi.org/10.1016/j.nbd.2019.05.012 PMID: 31102768

35. Wallings RL, Tansey MG. LRRK2 regulation of immune-pathways and inflammatory disease. Biochem Soc Trans. 2019 Dec 20; 47(6):1581–95. https://doi.org/10.1042/BST20180463 PMID: 31769472

36. Yambire KF, Rostosky C, Watanabe T, Pacheu-Grau D, Torres-Odio S, Sanchez-Guerrero A, et al. Impaired lysosomal acidification triggers iron deficiency and inflammation in vivo. Pfeffer SR, McPherson PS, editors. Elife. 2019 Dec 3; 8:e51031. https://doi.org/10.7554/eLife.51031 PMID: 31793879

37. Miles AL, Burr SP, Grice GL, Nathan JA. The vacuolar-ATPase complex and assembly factors, TMEM199 and CCDC115, control HIF1α prolyl hydroxylation by regulating cellular iron levels. Chacinska A, editor. Elife. 2017 Mar 15; 6:e22693. https://doi.org/10.7554/eLife.22693 PMID: 28296633

38. Mamais A, Manzoni C, Nazish I, Arber C, Sonustun B, Wray S, et al. Analysis of macroautophagy related proteins in G2019S LRRK2 Parkinson's disease brains with Lewy body pathology. Brain Res. 2018 Dec 15; 1701:75–84. https://doi.org/10.1016/j.brainres.2018.07.023 PMID: 30055128

39. Manzoni C, Mamais A, Dihanich S, McGoldrick P, Devine MJ, Zerle J, et al. Pathogenic Parkinson's disease mutations across the functional domains of LRRK2 alter the autophagic/lysosomal response to starvation. Biochem Biophys Res Commun. 2013 Nov 29; 441(4):862–6. https://doi.org/10.1016/j.bbrc.2013.10.159 PMID: 24211199

40. Schapansky J, Khasnavis S, DeAndrade MP, Nardozzi JD, Falkson SR, Boyd JD, et al. Familial knockin mutation of LRRK2 causes lysosomal dysfunction and accumulation of endogenous insoluble α-synuclein in neurons. Neurobiol Dis. 2018 Mar; 111:26–35. https://doi.org/10.1016/j.nbd.2017.12.005 PMID: 29246723

41. Hockey LN, Kilpatrick BS, Eden ER, Lin-Moshier Y, Brailoiu GC, Brailoiu E, et al. Dysregulation of lysosomal morphology by pathogenic LRRK2 is corrected by TPC2 inhibition. J Cell Sci. 2015 Jan 15; 128 (2):232–8. https://doi.org/10.1242/jcs.164152 PMID: 25416817

42. Henry AG, Aghamohammadzadeh S, Samaroo H, Chen Y, Mou K, Needle E, et al. Pathogenic LRRK2 mutations, through increased kinase activity, produce enlarged lysosomes with reduced degradative capacity and increase ATP13A2 expression. Hum Mol Genet. 2015 Nov 1; 24(21):6013–28. https://doi.org/10.1093/hmg/ddv314 PMID: 26251043

43. Faucheux BA, Hauw J-J, Agid Y, Hirsch EC. The density of [125I]-transferrin binding sites on perikarya of melanized neurons of the substantia nigra is decreased in Parkinson's disease. Brain Res. 1997 Feb 21; 749(1):170–4. https://doi.org/10.1016/s0006-8993(96)01412-6 PMID: 9070646

44. He Y, Lee T, Leong SK. Time course of dopaminergic cell death and changes in iron, ferritin and transferrin levels in the rat substantia nigra after 6-hydroxydopamine (6-OHDA) lesioning. Free Radic Res. 1999 Aug; 31(2):103–12. https://doi.org/10.1080/10715769900301611 PMID: 10490239

45. Cheng X-T, Xie Y-X, Zhou B, Huang N, Farfel-Becker T, Sheng Z-H. Characterization of LAMP1-labeled nondegradative lysosomal and endocytic compartments in neurons. J Cell Biol. 2018 Sep 3; 217(9):3127–39. https://doi.org/10.1083/jcb.201711083 PMID: 29695488

46. Lanning NJ, VanOpstall C, Goodall ML, MacKeigan JP, Looyenga BD. LRRK2 deficiency impairs trans-Golgi to lysosome trafficking and endocytic cargo degradation in human renal proximal tubule epithelial cells. Am J Physiol Renal Physiol. 2018; 315(5):F1465–77. https://doi.org/10.1152/ajprenal.00009.2018 PMID: 30089035

47. Heaton GR, Landeck N, Mamais A, Nalls MA, Nixon-Abell J, Kumaran R, et al. Sequential screening nominates the Parkinson's disease associated kinase LRRK2 as a regulator of Clathrin-mediated endocytosis. Neurobiol Dis. 2020 May17; 141:104948. https://doi.org/10.1016/j.nbd.2020.104948 PMID: 32434048

48. Kluss JH, Mazza MC, Li Y, Manzoni C, Lewis PA, Cookson MR, et al. Preclinical modeling of chronic inhibition of the Parkinson's disease associated kinase LRRK2 reveals altered function of the endolysosomal system in vivo. Mol Neurodegener. 2021 Mar 19; 16(1):17. https://doi.org/10.1186/s13024-021-00441-8 PMID: 33741046

49. Dexter DT, Carayon A, Vidailhet M, Ruberg M, Agid F, Agid Y, et al. Decreased Ferritin Levels in Brain in Parkinson's Disease. J Neurochem. 1990; 55 (1):16–20. https://doi.org/10.1111/j.1471-4159.1990.tb08814.x PMID: 2355217

50. Guan X, Xuan M, Gu Q, Huang P, Liu C, Wang N, et al. Regionally progressive accumulation of iron in Parkinson's disease as measured by quantitative susceptibility mapping. NMR Biomed. 2017 Apr; 30 (4). https://doi.org/10.1002/nbm.3489 PMID: 26853890

51. Langkammer C, Pirpamer L, Seiler S, Deistung A, Schweser F, Franthal S, et al. Quantitative Susceptibility Mapping in Parkinson's Disease. PLoS ONE. 2016; 11 (9):e0162460. https://doi.org/10.1371/journal.pone.0162460 PMID: 27598250

52. Sofic E, Paulus W, Jellinger K, Riederer P, Youdim MB. Selective increase of iron in substantia nigra zona compacta of parkinsonian brains. J Neurochem. 1991 Mar; 56(3):978–82. https://doi.org/10.1111/j.1471-4159.1991.tb02017.x PMID: 1704426

53. Zecca L, Berg D, Arzberger T, Ruprecht P, Rausch WD, Musicco M, et al. In vivo detection of iron and neuromelanin by transcranial sonography: a new approach for early detection of substantia nigra damage. Mov Disord. 2005 Oct; 20(10):1278–85. https://doi.org/10.1002/mds.20550 PMID: 15986424

54. Salazar J, Mena N, Hunot S, Prigent A, Alvarez-Fischer D, Arredondo M, et al. Divalent metal transporter 1 (DMT1) contributes to neurodegeneration in animal models of Parkinson's disease. Proc Natl Acad Sci U S A. 2008 Nov 25; 105(47):18578–83. https://doi.org/10.1073/pnas.0804373105 PMID: 19011085

55. Youdim MBH, Stephenson G, Shachar DB. Ironing Iron Out in Parkinson's Disease and Other Neurodegenerative Diseases with Iron Chelators: A Lesson from 6-Hydroxydopamine and Iron Chelators, Desferal and VK-28. Ann N Y Acad Sci. 2004; 1012(1):306–25. https://doi.org/10.1196/annals.1306.025 PMID: 15105275

56. Pyatigorskaya N, Sharman M, Corvol J-C, Valabregue R, Yahia-Cherif L, Poupon F, et al. High nigral iron deposition in LRRK2 and Parkin mutation carriers using R2* relaxometry. Mov Disord. 2015; 30 (8):1077–84. https://doi.org/10.1002/mds.26218 PMID: 26011561

57. Kang R, Xie Y, Zeh HJ, Klionsky DJ, Tang D. Mitochondrial quality control mediated by PINK1 and PRKN: links to iron metabolism and tumor immunity. Autophagy. 2019; 15(1):172–3. https://doi.org/10.1080/15548627.2018.1526611 PMID: 30252570

58. Li C, Zhang Y, Cheng X, Yuan H, Zhu S, Liu J, et al. PINK1 and PARK2 Suppress Pancreatic Tumorigenesis through Control of Mitochondrial Iron-Mediated Immunometabolism. Dev Cell. 2018; 46 (4):441–455.e8. https://doi.org/10.1016/j.devcel.2018.07.012 PMID: 30100261

59. Zhang L, Hou L, Liu Z, Huang S, Meng Z, Liang L. A mitophagic response to iron overload-induced oxidative damage associated with the PINK1/Parkin pathway in pancreatic beta cells. J Trace Elem Med Biol. 2020 Jul 1; 60:126493. https://doi.org/10.1016/j.jtemb.2020.126493 PMID: 32179427

60. Wang J, Song N, Jiang H, Wang J, Xie J. Pro-inflammatory cytokines modulate iron regulatory protein 1 expression and iron transportation through reactive oxygen/nitrogen species production in ventral mesencephalic neurons. Biochim Biophys Acta. 2013 May; 1832(5):618–25. https://doi.org/10.1016/j.bbadis.2013.01.021 PMID: 23376588

61. Zhang W, Yan Z, Gao J, Sun L, Huang X, Liu Z, et al. Role and Mechanism of Microglial Activation in Iron-Induced Selective and Progressive Dopaminergic Neurodegeneration. Mol Neurobiol. 2014 Jun; 49(3):1153–65. https://doi.org/10.1007/s12035-013-8586-4 PMID: 24277523

62. Kaur D, Yantiri F, Rajagopalan S, Kumar J, Mo JQ, Boonplueang R, et al. Genetic or Pharmacological Iron Chelation Prevents MPTP-Induced Neurotoxicity In Vivo: A Novel Therapy for Parkinson's Disease. Neuron. 2003 Mar 27; 37(6):899–909. https://doi.org/10.1016/s0896-6273(03)00126-0 PMID: 12670420

63. Mortiboys H, Johansen KK, Aasly JO, Bandmann O. Mitochondrial impairment in patients with Parkinson disease with the G2019S mutation in LRRK2. Neurology. 2010 Nov 30; 75(22):2017–20. https://doi.org/10.1212/WNL.0b013e3181ff9685 PMID: 21115957

64. Di Maio R, Hoffman EK, Rocha EM, Keeney MT, Sanders LH, De Miranda BR, et al. LRRK2 activation in idiopathic Parkinson's disease. Sci Transl Med. 2018; 10(451). https://doi.org/10.1126/scitranslmed.aar5429 PMID: 30045977

65. Das A, Nag S, Mason AB, Barroso MM. Endosome–mitochondria interactions are modulated by iron release from transferrin. J Cell Biol. 2016 Sep 26; 214 (7):831–45. https://doi.org/10.1083/jcb.201602069 PMID: 27646275

66. Klopstock T, Tricta F, Neumayr L, Karin I, Zorzi G, Fradette C, et al. Safety and efficacy of deferiprone for pantothenate kinase-associated neurodegeneration: a randomised, double-blind, controlled trial and an open-label extension study. Lancet Neurol. 2019 Jul 1; 18(7):631–42. https://doi.org/10.1016/S1474-4422(19)30142-5 PMID: 31202468

67. Martin-Bastida A, Ward RJ, Newbould R, Piccini P, Sharp D, Kabba C, et al. Brain iron chelation by deferiprone in a phase 2 randomised double-blinded placebo controlled clinical trial in Parkinson's disease. Sci Rep. 2017 Dec [cited 2019 Jun 7]; 7(1). Available from: http://www.nature.com/articles/s41598-017-01402-2

68. Nichols RJ, Dzamko N, Morrice NA, Campbell DG, Deak M, Ordureau A, et al. 14-3-3 binding to LRRK2 is disrupted by multiple Parkinson's disease-associated mutations and regulates cytoplasmic localization. Biochem J. 2010 Sep 15; 430(3):393–404. https://doi.org/10.1042/BJ20100483 PMID: 20642453

69. Berman HM, Westbrook J, Feng Z, Gilliland G, Bhat TN, Weissig H, et al. The Protein Data Bank. Nucleic Acids Res. 2000 Jan 1; 28(1):235–42. https://doi.org/10.1093/nar/28.1.235 PMID: 10592235

70. Guo Z, Hou X, Goody RS, Itzen A. Intermediates in the guanine nucleotide exchange reaction of Rab8 protein catalyzed by guanine nucleotide exchange factors Rabin8 and GRAB. J Biol Chem. 2013 Nov 8; 288(45):32466–74. https://doi.org/10.1074/jbc.M113.498329 PMID: 24072714

71. Rai A, Oprisko A, Campos J, Fu Y, Friese T, Itzen A, et al. bMERB domains are bivalent Rab8 family effectors evolved by gene duplication. Elife. 2016; 23:5. https://doi.org/10.7554/eLife.18675 PMID: 27552051

72. Abud EM, Ramirez RN, Martinez ES, Healy LM, Nguyen CHH, Newman SA, et al. iPSC-Derived Human Microglia-like Cells to Study Neurological Diseases. Neuron. 2017 Apr 19; 94(2):278–293.e9. https://doi.org/10.1016/j.neuron.2017.03.042 PMID: 28426964

73. McQuade A, Coburn M, Tu CH, Hasselmann J, Davtyan H, Blurton-Jones M. Development and validation of a simplified method to generate human microglia from pluripotent stem cells. Mol Neurodegener. 2018; 13(1):67. https://doi.org/10.1186/s13024-018-0297-x PMID: 30577865

74. Stauffer W, Sheng H, Lim HN. EzColocalization: An ImageJ plugin for visualizing and measuring colocalization in cells and organisms. Sci Rep. 2018 Oct 25; 8(1):15764. https://doi.org/10.1038/s41598-018-33592-8 PMID: 30361629

75. Edgar R, Domrachev M, Lash AE. Gene Expression Omnibus: NCBI gene expression and hybridization array data repository. Nucleic Acids Res. 2002 Jan 1; 30(1):207–10. https://doi.org/10.1093/nar/30.1.207 PMID: 11752295

Directing LRRK2 to membranes of the endolysosomal pathway triggers RAB phosphorylation and JIP4 recruitment

Jillian H. Kluss [a,b,1], Luis Bonet-Ponce [a,1], Patrick A. Lewis [b,c,d], Mark R. Cookson [a,*]

[a] *Cell Biology and Gene Expression Section, Laboratory of Neurogenetics, National Institute on Aging, National Institutes of Health, Bethesda, MD 20892-3707, USA*
[b] *School of Pharmacy, University of Reading, Whiteknights, Reading, UK*
[c] *Royal Veterinary College, Royal College Street, London, UK*
[d] *UCL Queen Square Institute of Neurology, Queen Square, London, UK*

ARTICLE INFO

Keywords:
LRRK2
Parkinson's disease
Endolysosomal membranes

ABSTRACT

Coding mutations in the *Leucine-rich repeat kinase 2* (*LRRK2*) gene, which are associated with dominantly inherited Parkinson's disease (PD), lead to an increased activity of the encoded LRRK2 protein kinase. As such, kinase inhibitors are being considered as therapeutic agents for PD. It is therefore of interest to understand the mechanism(s) by which LRRK2 is activated during cellular signaling. Lysosomal membrane damage represents one way of activating LRRK2 and leads to phosphorylation of downstream RAB substrates and recruitment of the motor adaptor JIP4. However, it is unclear whether the activation of LRRK2 would be seen at other membranes of the endolysosomal system, where LRRK2 has also shown to be localized, or whether these signaling events can be induced without membrane damage. Here, we use a rapamycin-dependent oligomerization system to direct LRRK2 to various endomembranes including the Golgi apparatus, lysosomes, the plasma membrane, recycling, early, and late endosomes. Irrespective of membrane location, the recruitment of LRRK2 to membranes results in local accumulation of phosphorylated RAB10, RAB12, and JIP4. We also show that endogenous RAB29, previously nominated as an activator of LRRK2 based on overexpression, is not required for activation of LRRK2 at the Golgi nor lysosome. We therefore conclude that LRRK2 signaling to RAB10, RAB12, and JIP4 can be activated once LRRK2 is accumulated at any cellular organelle along the endolysosomal pathway.

1. Introduction

Multiple pathogenic mutations in the *Leucine-rich repeat kinase 2* (*LRRK2*) have been documented in families with ascertained autosomal dominant inheritance of Parkinson's disease (PD) (Funayama et al., 2005; Paisán-Ruíz et al., 2004; Zimprich et al., 2004). Additionally, due to incomplete age-dependent penetrance of *LRRK2* alleles, mutations are also associated with apparently sporadic PD (Gilks et al., 2005; Iwaki et al., 2020; Lee et al., 2017). Finally, non-coding variants in the promoter region of *LRRK2* are also risk factors for sporadic PD (Nalls et al., 2019). Thus, the genomic region encompassing *LRRK2* contains multiple types of genetic risk covering a range of identified modes of inheritance

(Singleton and Hardy, 2011).

Because familial cases with LRRK2 mutations show clinical presentations that are indistinguishable from sporadic PD (Kumari and Tan, 2009, p. 2), it is reasonable to infer that the different types of LRRK2 variants work through common mechanisms. The most promising explanatory event uncovered to date is an increase in LRRK2 kinase activity, mediated either directly by mutation in the LRRK2 kinase domain or by decreased GTP hydrolysis, which is encoded by the adjacent Ras of complex proteins (ROC) and C-terminal of ROC (COR) bidomain (Cookson, 2010). All known pathogenic mutations identified to date increase either LRRK2 autophosphorylation at residue S1292 (Sheng et al., 2012) or on downstream Ras-associated binding proteins

---

(RABs), including RAB10 and RAB12 (Steger et al., 2016). Non-coding variants likely influence disease risk by virtue of higher *LRRK2* gene expression, being an example of an expression quantitative trait locus (eQTL) (Ryan et al., 2017). An important corollary of these observations is that inhibition of LRRK2 might be clinically beneficial for inherited and, by extension, sporadic PD (Kluss et al., 2019; West, 2014).

Protein kinases are typically subject to regulation by multiple mechanisms within cellular signaling pathways, allowing for control of activity appropriate to internal or external cues. LRRK2 has been shown to be regulated in multiple cellular contexts. Inflammatory cell activation, which has been implicated in PD, has been shown to regulate LRRK2 phosphorylation, dimer formation and recruitment to intracellular membranes (Berger et al., 2010). We and others have also shown that lysosomal damage is sufficient to recruit LRRK2 to these organelles (Bonet-Ponce et al., 2020; Eguchi et al., 2018), which may be relevant to inflammatory signaling as exposure to specific intracellular pathogens can result in disruption of lysosomes (Herbst et al., 2020). Subsequent to lysosomal recruitment, LRRK2 phosphorylates RAB10 and RAB35 that are then able to recruit JNK-interacting protein 4 (JIP4), a motor adaptor protein, resulting in tubulation and sorting of lysosomal membranes, a process we termed LYTL (Bonet-Ponce et al., 2020). A related process may occur in neurons where pRAB10 can also recruit JIP4 to alter transport of autophagosomes along microtubules (Boecker et al., 2021).

Additionally, LRRK2 may be activated by interaction with RAB29, itself a candidate risk gene for sporadic PD (Nalls et al., 2019). Several groups have shown that overexpression of RAB29 can lead to LRRK2 recruitment to the Golgi apparatus (Beilina et al., 2020; Beilina et al., 2014) with downstream activation of RAB10 (Fujimoto et al., 2018; Liu et al., 2018; Purlyte et al., 2018). Of note, RAB29 overexpression has been reported to cause alteration of Golgi structure (Fujimoto et al., 2018), implying potential damage to this organelle. Interestingly, directing RAB29 to the mitochondrial membrane is also sufficient to activate LRRK2 signaling, suggesting that membrane identity is not important in LRRK2 activation pathways (Gomez et al., 2019). Additionally, whether RAB29 regulates LRRK2 in a physiological context has been questioned as knockout of RAB29 does not lower LRRK2-dependent phosphorylation of RAB10 in vivo (Kalogeropulou et al., 2020).

Here, we revisit the question of whether LRRK2 can be activated at particular membranes compared to others along the endolysosomal pathway, as well as whether membrane damage is necessary to activate LRRK2 once at the membrane. To do this, we utilized the rapamycin-binding domain from the 12 kDa FK506 binding protein (FKBP), which we fused to the N-terminus of LRRK2, and the FKBP-rapamycin-binding (FRB) domain of mTOR fused to six different membrane resident proteins (Liberles et al., 1997; Robinson et al., 2010). In the presence of rapamycin, the FKBP and FRB domains will dimerize, thus trapping LRRK2 to a specific membrane. In this manner, we recruited LRRK2 to the Golgi, lysosomes, recycling endosomes, early endosomes, late endosomes and plasma membrane. In each case we found evidence for accumulation of pRAB10 and pRAB12 and recruitment of JIP4 to the directed membrane in the absence of membrane damaging agents. Further, we confirmed that RAB29 is not required for LRRK2 activation at the Golgi nor lysosome by using an siRNA knockdown of endogenous RAB29, thus implying that the overexpression of RAB29 influences LRRK2 localization but the physical interaction is not needed for LRRK2 kinase activity at the membrane. The results underscore that LRRK2 can be activated at multiple *endo*-membranous compartments in cells and that this is sufficient to initiate downstream LRRK2 signaling.

2. Methods

2.1. Cell culture

HEK293FT cells were maintained in DMEM containing 4.5 g/l

glucose, 2 mM L-glutamine, 5% Pen/Strep and 10% FBS at 37 °C in 5% CO_2. For immunocytochemistry experiments, cells were seeded on 12 mm coverslips (Corning, #354087). For Western blot experiments, cells were plated in 24-well plates. For all experiments, Matrigel coating (Corning, #354230) was used when seeding cells.

2.2. Reagents and treatments

For all experiments, rapamycin (Cayman Chemicals, cat #13346) was added at 200 nM in ethanol for 15 min before fixing or lysing cells for downstream analyses. Addition of MLi-2 (Tocris, cat #5756) was used at 1 μM in DMSO, 90 min prior to rapamycin treatment.

2.3. Cloning

FKBP sequence was tagged to 3xFLAG-pDEST and mScarlet-pDEST vectors using IN-FUSION HD cloning technology (Clontech, Takara, cat #638920). LRRK2-WT, LRRK2-R1441C, LRRK2-Y1669C, LRRK2-K1906M and LRRK2-G2019S, previously cloned into pCR™8/GW/TOPO™ vector (ThermoFisher, cat #250020), were transferred into the 3xFLAG-FKBP-pDEST and mScarlet-FKBP-pDEST plasmids using Gateway technology (ThermoFisher, cat #11791043). CFP-FRB-LAMP1 vector (Willett et al., 2017) was a gift from Rosa Puertollano (NIH). EHD1-FRB-GFP was kindly provided by Tsukasa Okiyoneda (Kwansei Gakuin University). iRFP-FRB-RAB5, iRFP-FRB-RAB7, and PM-FRB-CFP plasmids (Addgene plasmid #51612, #51613, and #67517) (Hammond et al., 2014; Varnai et al., 2006) were gifts from Tamas Balla (NIH). FRB-ECFP-Giantin was provided by Dorus Gadella (Addgene plasmid #67903) (van Unen et al., 2015).

2.4. Transfection and siRNA knockdown

Transient transfections of HEK293FT cells were performed using Lipofectamine 2000 in Gibco's Opti-MEM (ThermoFisher, cat #31985088). HEK293FT cells were transfected followed by a 24-h incubation period prior to any treatments, fixation, or lysis. The following concentrations were used for each construct: 0.4 μg for LRRK2, CFP-FRB-Giantin, and iRFP-FRB-RAB7, 0.25 μg for GFP-FRB-EHD1, CFP-FRB-LAMP1, and iRFP-FRB-RAB5, and 0.05 μg for CFP-FRB-PMTS. For endogenous RAB29 knockdown experiments, cells were treated with either non-targeting control siRNA or human RAB29 siRNA (40 nM working concentration) together with Lipofectamine RNAiMAX (ThermoFisher, cat #13778075) in Gibco's Opti-MEM and incubated for 24 h prior to starting the transfection protocol. We chose a 24-h incubation period as prior experiments suggest that this is sufficient time for robust protein expression in HEK293FT cells and, similarly, siRNA will result in efficient knockdown, at least for proteins with shorter half-lives, without inducing cellular toxicity.

2.5. Antibodies

The following primary antibodies were used: mouse anti-FLAG M2 (Sigma-Aldrich, cat #F3165, 1:500 for ICC and 1:10,000 for WB), mouse anti-LAMP1 (DSHB, cat #H4B3, 1:100 for ICC), rat anti-FLAG (Biolegend, cat #637302, 1:100 for ICC), chicken anti-GFP (AvesLab, GFP-1020, 1:1000 for ICC), mouse anti-GFP (Roche, cat #11814460001, 1:10,000 for WB), sheep anti-TGN46 (Biorad, cat #AHP500GT, 1:500 for ICC), rabbit anti-Rab8a (Cell Signaling Technology, cat #6975, 1:500 for ICC), rabbit anti-EEA1 (Cell Signaling Technology, cat #3288, 1:100 for ICC), rabbit anti-Lamtor4 (Cell Signaling Technology, cat#12284, 1:200 for ICC), rabbit anti-RAB10 (Abcam, cat #ab237703, 1:2000 for WB), rabbit anti-RAB10 (phospho-T73) (Abcam, cat #ab23026, 1:300 for ICC and 1:2000 for WB), rabbit anti-RAB12 (Proteintech, cat #18843–1-AP, 1:1000 for WB), rabbit anti-RAB12 (phospho-S106) (Abcam, cat #ab256487, 1:100 for ICC and 1:2000 for WB), rabbit anti-RAB29 (Abcam, cat #ab256526, 1:2000 for WB), rabbit anti-

LRRK2 (Abcam, cat #ab133474, 1:2000 for WB), rabbit anti-LRRK2 (phospho S1292) (Abcam, cat #ab203181, 1:2000 for WB), rabbit anti-cyclophilin B (Abcam, cat #ab16045, 1:2000 for WB), rabbit anti-JIP4 (Cell Signaling Technology, cat#5519, 1:100 for ICC), rabbit anti-LC3B (Cell Signaling Technology, cat#3868, 1:2000 for WB), mouse anti-p62 (Abcam, cat#ab280086, 1:2000 for WB). For staining of the plasma membrane, Phalloidin was used at 1:20 concentration to visualize F-actin (ThermoFisher, cat #A30107).

For ICC, unless otherwise stated, the secondary antibodies were purchased from ThermoFisher. The following secondary antibodies were used: donkey anti-mouse Alexa-Fluor 568 (cat #A10037, 1:500), donkey anti-rabbit Alexa-Fluor 488 (cat #A-21206, 1:500), donkey anti-mouse Alexa-Fluor 568 (cat #A-21202, 1:500), donkey anti-rat Alexa-Fluor 488 (cat #A-21208, 1:500), donkey anti-goat Alexa-Fluor 488 (cat #A-11055, 1:500), donkey anti-rabbit Alexa-Fluor 568 (cat #A10042, 1:500), donkey anti-mouse Alexa-Fluor 647 (cat #A-31571, 1:500), goat anti-rat Alexa-Fluor 647 (cat #A-21247, 1:250–1:500). Donkey anti-chicken Alexa-Fluor 405 (cat #703–475-155, 1:300) was obtained from Jackson ImmunoResearch.

For WB, all secondary antibodies were used at 1:10,000 dilution: IRDyes 800CW Goat anti-Rabbit IgG (Licor, cat #926–32,211) and 680RD Goat anti-Mouse IgG (Licor, cat #926–68,070).

2.6. Confocal microscopy

Confocal images were taken using a Zeiss LSM 880 microscope equipped with a 63×1.4 NA objective. Super-resolution imaging was performed using the Airyscan mode. Raw data were processed using Airycan processing in 'auto strength' mode with Zen Black software version 2.3. Only low plasmid expression cells without obvious over-expression artifacts were imaged. For measuring colocalization, Fiji plugin JACoP was used in which Mander's correlation corrected for threshold was used to quantify LRRK2:pRAB colocalization. Colocalized maps were made using the Colocalization Finder plugin in Fiji. For measuring signal intensity, integrated density of each cell was measured using Fiji without thresholding (ImageJ, NIH).

2.7. Immunostaining

HEK293FT cells were fixed with 4% PFA for 10 mins, permeabilized with PBS/ 0.1% Triton for 10 mins and blocked with 5% Donkey Serum (Sigma, cat #D9663) for 1 h at RT. Primary antibodies were diluted in blocking buffer (1% Donkey Serum) and incubated overnight at 4 °C. After three 5 min washes with PBS/ 0.1% Triton, secondary fluorescently labeled antibodies were diluted in blocking buffer (1% Donkey Serum) and incubated for 1 h at RT. Coverslips were washed two times with $1 \times$ PBS and an additional $2 \times$ with dH_2O, and mounted with Pro-Long® Gold antifade reagent (ThermoFisher, cat #P10144).

2.8. SDS PAGE and Western Blotting

Proteins were resolved on 4–20% Criterion TGX precast gels (Biorad, cat #5671095) and transferred to nitrocellulose membranes (Biorad, cat #170415) by semi-dry trans-Blot Turbo transfer system (Biorad). The membranes were blocked with Odyssey Blocking Buffer (Licor, cat #927–40,000) and then incubated for 1 h at RT or overnight at 4 °C with the indicated primary antibody. Membranes were simultaneously probed antibodies against a loading reference protein, Cyclophilin B, to allow for accurate relative quantification and ensure equal loading between samples. The membranes were washed in TBST (3×5 min) followed by incubation for 1 h at RT with fluorescently conjugated secondary antibodies as stated above (Licor). The blots were washed in TBST (3×5 min) and scanned on an ODYSSEY® CLx (Licor). Quantitation of western blots was performed using Image Studio (Licor). All blots presented in each figure panel were derived from the same experiment and were processed in parallel.

2.9. Statistical analysis

Analyses based on cell counts were performed by an investigator blinded to treatment/transfection status. Unpaired student's *t*-tests were used in experiments with two comparable groups, one-way ANOVAs were used for experiments with more than two groups, and two-way ANOVAs were used for experiments where there were two factors in the model. Tukey's *post-hoc* tests were used to determine statistical significance for individual comparisons in those cases where the underlying ANOVA was statistically significant and where all groups' means were compared to every other mean. Unless otherwise stated, graphed data are presented as means $\pm$ SD. Comparisons were considered statistically significant where $p < 0.05$. $*p < 0.05$; $**p < 0.01$; $***p < 0.001$; $****p < 0.0001$.

3. Results

3.1. Trapping LRRK2 to Golgi or lysosomal membranes results in enhanced kinase activity

To establish whether membrane targeting is sufficient to activate LRRK2, we generated a series of FRB traps with fluorescence fusion proteins targeting the lysosome using LAMP1 (Fig. 1A); the Golgi using Giantin (Fig. 1F); recycling endosomes using EHD1 (Fig. 1K); early endosomes using Rab5 (Fig. 1P); late endosomes using RAB7 (Fig. 1U); and the plasma membrane using a plasma membrane-targeting sequence (PMTS) from GAP43 (MLCCMRRTKQVEKNDDQKI) (Fig. 1Z). Co-transfection of each of these plasmids with 3xFlag-FKBP-LRRK2 resulted in diffuse cytosolic LRRK2 staining as expected, however, after a 15 min incubation of 200 nM rapamycin, LRRK2 was relocalized to intracellular structures labeled with the trap construct. These signals also colocalized with appropriate endogenous markers of each organelle (Fig. 1). Live imaging of cells expressing either RE-trap or lyso-trap constructs together with a mScarlet-FKBP-LRRK2 construct show this dimerization in real time, with both traps being able to colocalize LRRK2 in a matter of seconds following the addition of rapamycin (Supplementary Fig. 1). Thus, the system employed here is sufficient to rapidly induce partial recruitment of LRRK2 to specified membranes. Importantly, treatment with rapamycin at such a low concentration for 15 min does not induce autophagy in HEK293FT cells (Supplementary Fig. 2A-C).

Having established these tools, we next examined whether recruitment to these membranes was sufficient to increase LRRK2 kinase activity as measured by three molecular readouts: autophosphorylation of LRRK2 at site S1292, pT73 RAB10 and pS106 RAB12. Constructs were transfected into HEK293FT cells and treated with rapamycin in order to evaluate phosphorylation events via Western blot. In each case, the addition of rapamycin resulted in statistically significant increases in S1292 LRRK2 autophosphorylation (Fig. 1B,C; G,H; L, M; Q, R; V,W; a,b) pT73 RAB10 (Fig. 1B,D; G,I; L, N; Q, S; V,X; a,c) and pS106 RAB12 (Fig. 1B,D; G,J; L,O; Q, T; V,Y; a,d) compared to untreated controls. Additionally, treatment of cells with MLi-2 decreased LRRK2 autophosphorylation, RAB10 and RAB12 phosphorylation below baseline levels, demonstrating that the changes in RAB phosphorylation are LRRK2 kinase-dependent. Thus, translocation of LRRK2 to intracellular membranes is sufficient to increase kinase activity and influence RAB substrate phosphorylation, irrespective of membrane identity.

Importantly, rapamycin-treated cells that were transfected with LRRK2 alone did not increase S1292 LRRK2, T73 RAB, nor S106 RAB12 phosphorylation, confirming that LRRK2 kinase activation is dependent on membrane presence and is not a byproduct of the treatment itself (Supplementary Fig. 2D-G). We also conducted a control experiment in which we transfected cells with 3xFLAG-FKBP-LRRK2 and a plasmid containing the FRB domain without any membrane-targeting protein. Under these conditions, cells treated with rapamycin did not have any effect on LRRK2 autophosphorylation nor RAB10 and RAB12
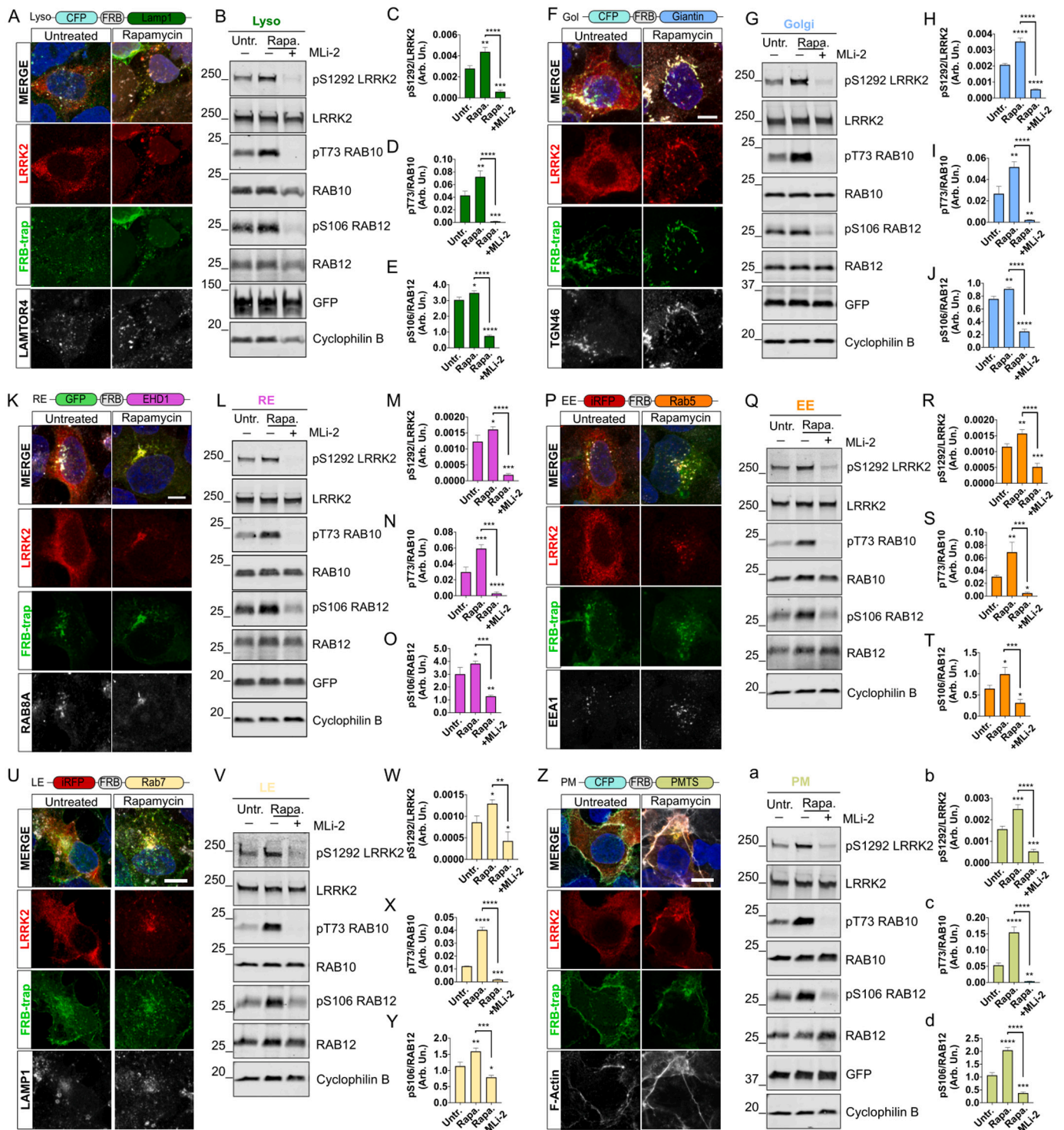
Fig. 1. Recruitment of LRRK2 to multiple intracellular membranes results in activation of LRRK2 kinase activity. Cells were transfected with lysosome (A-E), Golgi (F-J), recycling endosome (K—O), early endosome (P-T), late endosome (U—Y) and plasma membrane (Z-d) traps (green) along with FKBP-tagged LRRK2 (red). All trap construct designs are illustrated above each image respectively. Untreated cells were used as negative controls while rapamycin treatment in the absence or presence of MLi-2 were used for recruitment and kinase inhibition of LRRK2 respectively. Endogenous markers for each targeted membrane are shown in grey. Scale bar = 10 μm. Evaluation of pS1292 LRRK2, pRAB10 and pRAB12 are included via Western blot for each trap (B-E, G-J, L-O, Q-T, V—Y, a-d). (C-E, H-J, M-O, R-T, W—Y, b-d): one-way ANOVA with Tukey's post hoc, ****$p < 0.0001$, ***$p < 0.001$, **$p < 0.01$, *$p < 0.05$, $n = 3$; SD bars shown; (C) $F_{(2,6)} = 116.4$, (D) $F_{(2,6)} = 81.12$, (E) $F_{(2,6)} = 376.3$, (H) $F_{(2,6)} = 323.0$, (I) $F_{(2,6)} = 75.25$, (J) $F_{(2,6)} = 306.8$, (M) $F_{(2,6)} = 104.6$, (N) $F_{(2,6)} = 110.5$, (O) $F_{(2,6)} = 48.55$, (R) $F_{(2,6)} = 69.67$, (S) $F_{(2,6)} = 36.89$, (T) $F_{(2,6)} = 26.02$, (W) $F_{(2,6)} = 22.40$, (X) $F_{(2,6)} = 691.5$, (Y) $F_{(2,6)} = 48.89$, (b) $F_{(2,6)} = 119.8$, (c) $F_{(2,6)} = 154.4$, (d) $F_{(2,6)} = 277.7$. (For interpretation of the references to colour in this figure legend, the reader is referred to the web version of this article.)

phosphorylation, suggesting that it is indeed the presence of a membrane that is critical to heighten LRRK2 kinase activity and is not affected by the binding of LRRK2 to the FRB domain alone (Supplementary Fig. 2H-K).

We next evaluated whether the addition of hyperactive LRRK2 mutations in the ROC (R1441C), COR (Y1699C) and kinase (G2019S) domains of LRRK2 would produce greater activation of LRRK2 signaling than wildtype protein in the context of FKBP-FRB dimerization. We also included a hypothesis testing kinase dead LRRK2 mutant, K1906M, as a negative control. Using the lyso-trap (Fig. 2A), we found that the addition of rapamycin caused a robust increase in pS1292 LRRK2 normalized to total LRRK2 levels which was blocked by MLi-2 (Fig. 2B). Phosphorylation of RAB10 relative to total RAB10 was also increased by rapamycin to similar magnitudes across mutations, with baseline levels being most affected by the R1441C and Y1699C mutations as expected (Fig. 2C). This phosphorylation was significantly reduced with MLi-2 treatment (Fig. 2C). Finally, increased phosphorylation of RAB12 relative to total RAB12 was also noted with wildtype LRRK2 after rapamycin treatment, but not with mutant LRRK2 (Fig. 2D). In all cases, the kinase dead K1906M LRRK2 did not support pRAB10 or pRAB12 activation, demonstrating that these effects on RAB phosphorylation were LRRK2 kinase-dependent.

Similar patterns of LRRK2 activation and RAB phosphorylation were seen using the Golgi-trap construct (Fig. 2E), with the strongest effects on pS1292 LRRK2 found with the G2019S mutation (Fig. 2F) whereas R1441C and Y1699C mutations contributed to the strongest effect on RAB10 phosphorylation (Fig. 2G). Interestingly, increases in pRAB12 were also only observed in rapamycin-treated cells transfected with wildtype LRRK2, with only mild increases observed in the mutant LRRK2 conditions (Fig. 2H). In all cases, inhibition of LRRK2 using MLi-2 or by substitution with the K1906M variant, resulted in minimal activity. These results collectively show either membrane is sufficient in activating LRRK2 kinase, however, divergent patterns of RABs phosphorylation emerge within the context of LRRK2 mutants.

3.2. Phosphorylated RAB proteins accumulate at intracellular membranes via trapped LRRK2

RAB proteins are localized to a variety of intracellular membranes with generally distinct and restricted distributions for each RAB (Homma et al., 2021). Of the two RAB proteins evaluated here, RAB10 has been localized to early endosomes and the endocytic recycling compartment (Babbey et al., 2006; Etoh and Fukuda, 2019; Liu et al., 2013; Štimac et al., 2021) while RAB12 has been found in a variety of vesicular compartments related to endosome function (Efergan et al., 2016; Iida et al., 2005; Matsui et al., 2011; Rydell et al., 2014). As neither RAB is prominently localized to lysosomes or Golgi, we next evaluated the localization of pRABs following the translocation of LRRK2 to these membranes via immunocytochemistry.

As expected, the addition of rapamycin resulted in the redistribution of LRRK2 from diffuse cytosolic expression to structures resembling lysosomes with lyso-trap (Fig. 3A) or Golgi with Golgi-trap (Fig. 3B). In conditions where the lyso-trap was used, pRAB12 staining showed broad colocalization with LRRK2 at lysosomes while pRAB10 was most clearly seen on perinuclear lysosomes after treatment with rapamycin and treatment with MLi-2 diminished the staining of both pRABs. (Fig. 3A). When LRRK2 was directed to the Golgi, pRAB12 was also detected at this organelle, as was pRAB10 although the latter showed only partial localized staining (Fig. 2B). To quantify these effects, we used Mander's coefficient for colocalization between LRRK2 and each pRAB when LRRK2 was translocated to lysosomes (Fig. 3C) and Golgi (Fig. 3D). When comparing between membranes, each pRAB showed similar levels of colocalization with LRRK2, while pRAB12 showed the most colocalization with LRRK2 compared to pRAB10 (Fig. 3E). This finding reinforces the idea that pRAB accumulation consequential to LRRK2 activation is unaffected by membrane identity.

Similarly, relocalizing LRRK2 to perinuclear structures morphologically reminiscent of recycling endosomes resulted in strong staining of pRAB10 and pRAB12 that was blocked by MLi-2 (Fig. 4A). Treatment with rapamycin in the presence of E*E*-trap expression resulted in relocalization of LRRK2 to early endosomes where pRAB10 and pRAB12 levels were also observed (Fig. 4B). Mander's correlation coefficient showed strong colocalization between LRRK2 and pRABs at both early and recycling endosomes (Fig. 4C-F). Thus, LRRK2 can phosphorylate RABs at multiple membranes along the endolysosomal pathway, however, differences in the distribution of pRABs may be visible depending on which membrane LRRK2 is accumulated at.

3.3. JIP4 can be recruited to multiple cellular membranes dependent on LRRK2 kinase activity

Prior studies have suggested that the motor adaptor protein JIP4 can be recruited by phosphorylated RABs to either lysosomes (Bonet-Ponce et al., 2020) or autophagosomes (Boecker et al., 2021) in different cell types. We therefore wanted to test whether LRRK2 could also promote JIP4 recruitment when placed at a variety of membranes within the cell. We found that endogenous JIP4 could be recruited to LRRK2-positive structures using either lyso-trap (Fig. 5A-B), Golgi-trap (Fig. 5C-D), EE-trap (Fig. 5 E-F), or RE-trap (Supplementary Fig. 3A-B). Trap-dependent recruitment of JIP4 was blocked by treatment with MLi-2, consistent with dependence of JIP4 recruitment on RAB phosphorylation. Thus, membrane identity is equally unimportant for JIP4 recruitment once pRABs accumulate at a given membrane.

3.4. RAB29 is not necessary for LRRK2 activation at the lysosome

Although prior data using knockout cells suggests that endogenous RAB29 is not required for LRRK2 activity (Kalogeropoulou et al., 2020), it is striking that both LRRK2 and RAB29 knockout mice exhibit prominent lysosomal abnormalities (Kuwahara et al., 2016). Additionally, RAB29 has been characterized as a resident Golgi protein, with overexpression studies showing colocalization to TGN46, GM130 and other known Golgi markers (Beilina et al., 2014; Wang et al., 2014). We therefore examined the potential role of RAB29 in the activation of LRRK2 trapped at the Golgi membrane by knocking down endogenous RAB29 (Fig. 6A), recognising that this would not be possible using approaches to drive LRRK2 to membranes using RAB29 overexpression or RAB9 fusion proteins. Despite the efficient knockdown of RAB29 in which 70–80% of endogenous protein was lost (Fig. 6A, E), we saw no difference in pS1292 LRRK2 between siRNA against RAB29 versus non-targeting control under basal or rapamycin-induced trapping of LRRK2 to the Golgi via Western blot (Fig. 6B). Similar negative results were seen with both pRAB10 (Fig. 6C) and pRAB12 (Fig. 6D). Immunocytochemistry confirmed these results, as no difference in LRRK2 localization was seen in groups transfected with RAB29 compared to NTC siRNA (F). These experiments demonstrate that RAB29 is not required for the activation of LRRK2 in the context of controlled recruitment to the Golgi. Additionally, we evaluated LRRK2 in the proximity of the lysosomal membrane using lyso-trap after RAB29 siRNA knockdown. Similarly, we saw no impairment nor increase in the ability of LRRK2 to translocate to the lysosome following rapamycin treatment, nor was its distribution affected under conditions without rapamycin (Supplementary 3C). More importantly, T73 RAB10 staining in RAB29 siRNA knockdown cells still colocalized to LRRK2 when LRRK2 was translocated to the lysosomal membrane (Supplementary 3C). This suggests that in the absence of RAB29, LRRK2 activation at lysosomes is unaffected and is thus able to phosphorylate RAB10.

4. Discussion

Understanding the mechanisms by which LRRK2 activity is controlled is fundamentally important for discerning the role of this
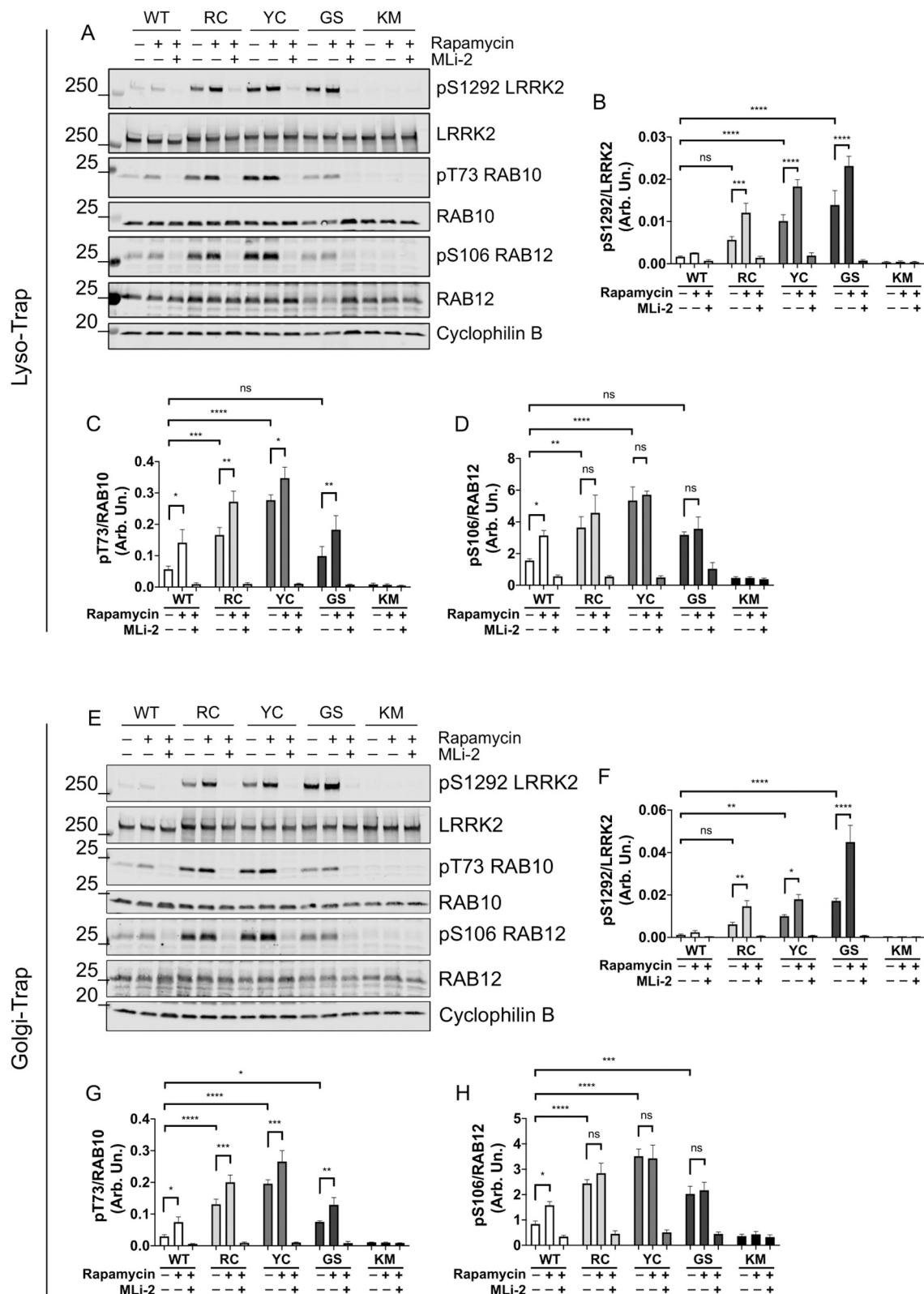
Fig. 2. LRRK2 and RAB10 phosphorylation patterns show additive effects of LRRK2 membrane recruitment and pathogenic mutations. The lyso-trap (A) or Golgi-trap (E) were co-transfected with either WT, R1441C, Y1669C, G2019S, or K1906M LRRK2(-FKBP-3xFlag or mScarlet) varieties and Western blots were run, probing for pS1292 LRRK2, pT73 RAB10, and pS106 RAB12 (B—D, F—H). (B—D, F—H): two-way ANOVA with Tukey's *post-hoc* test, $n = 3$ independent experiments; SD bars shown; (B) treatment, $p < 0.0001$, $F_{(2,30)} = 208.2$; genotype, $p < 0.0001$, $F_{(4, 30)} = 130.8$, (C) treatment, $p < 0.0001$, $F_{(2, 30)} = 200.5$; genotype, $p < 0.0001$, $F_{(4, 30)} = 95.63$, (D) treatment, $p < 0.0001$, $F_{(2, 30)} = 97.52$; genotype, $p < 0.0001$, $F_{(4, 30)} = 45.79$, (E) treatment, $p < 0.0001$, $F_{(2, 30)} = 177.0$; genotype, $p < 0.0001$, $F_{(4, 30)} = 121.5$, (F) treatment, $p < 0.0001$, $F_{(2, 30)} = 310.7$; genotype, $p < 0.0001$, $F_{(4, 30)} = 156.0$, (G) treatment, $p < 0.0001$, $F_{(2, 30)} = 210.1$; genotype, $p < 0.0001$, $F_{(4, 30)} = 117.9$.
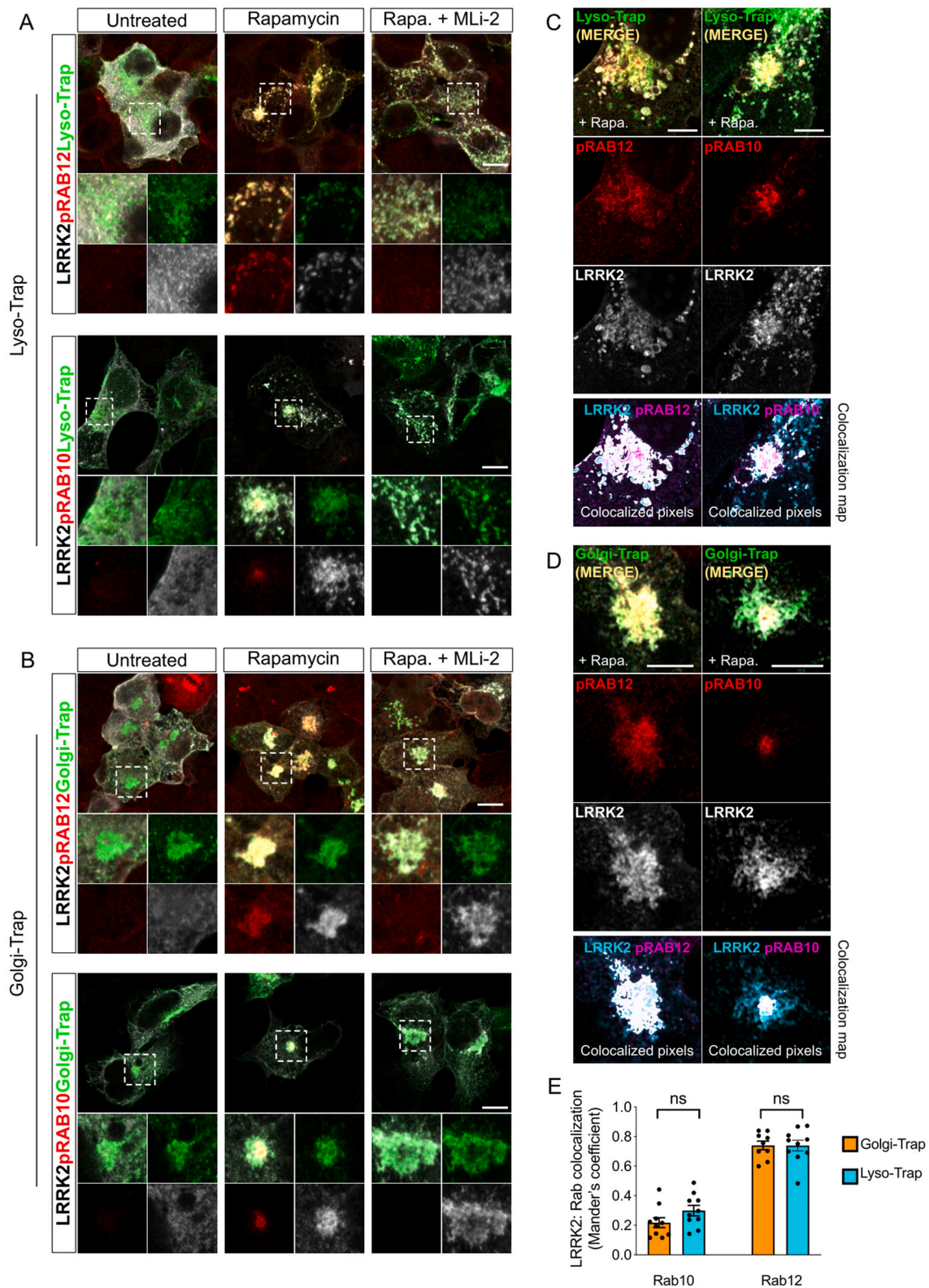
Fig. 3. pT73 RAB10 and pS106 RAB12 are phosphorylated by LRRK2 at the lysosome and Golgi. Utilizing the FRB-FKBP system, representative confocal microscopy images show colocalization of LRRK2 and its RAB substrates at membranes. Using the lyso-trap (A) or the Golgi-trap (B), both pS106 RAB12 and pT73 RAB10 (red) were stained with LRRK2 (grey) and colocalization was measured using airyscan images (C-E) Colocalized pixels are shown for clarity of colocalization. Scale bar = 10 μm (A, B); 5 μm (C, D). E: Quantification of LRRK2:RAB colocalization coefficient from $n = 9$–10 cells for Golgi-trap (orange) and Lyso-trap (cyan) for pRAB10 (left) and pRAB12 (right). One-way ANOVA with Tukey's post hoc analyses: $F(3,35) = 68.18$. Error bars show SEM, ns = not significant. (For interpretation of the references to colour in this figure legend, the reader is referred to the web version of this article.)
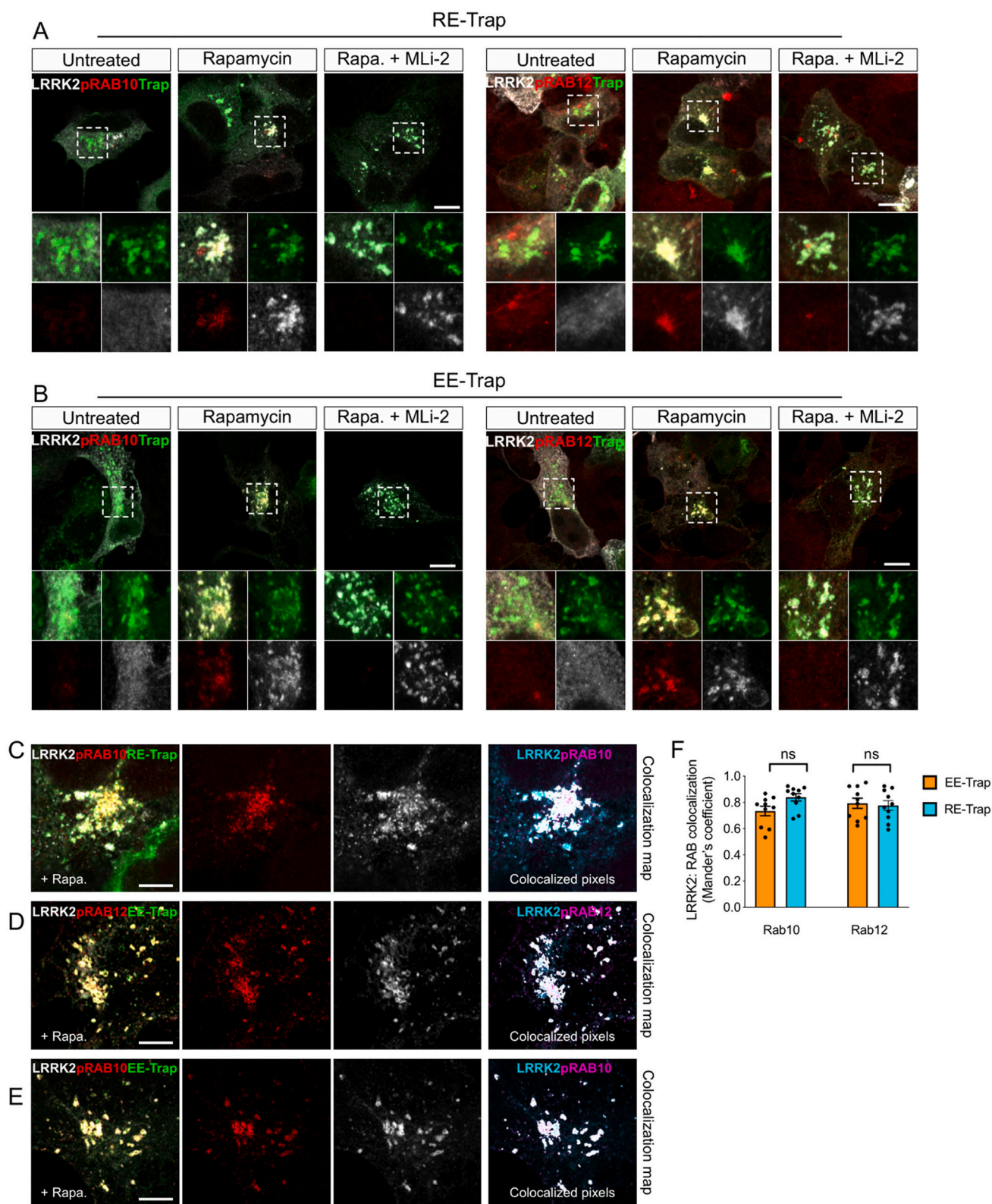
Fig. 4. Colocalization of LRRK2 with pT73 RAB10 and pS106 RAB12 at the early and recycling endosomal membranes. Utilizing the FRB-FKBP system, representative confocal microscopy images show colocalization of LRRK2 and its RAB substrates at the early and recycling endosomal membranes. (A) Using the RE-trap or EE-trap (green), colocalization of pS106 RAB12 and pT73 RAB10 (red) with LRRK2 (grey) were observed when treated with and without rapamycin, and MLi-2 treatment (A-B). Colocalization between LRRK2 and pRABs were measured using airyscan images (C—F). Scale bar = 10 μm (A, B); 5 μm (C-E). F: Quantification of LRRK2:pRAB colocalization coefficient from $n = 10$ cells for EE-trap (orange) and RE-trap (cyan) for pRAB10 (left) and pRAB12 (right). One-way ANOVA with Tukey's post hoc analyses: $F(3,36) = 1.511$. Error bars show SEM, ns = not significant. (For interpretation of the references to colour in this figure legend, the reader is referred to the web version of this article.)
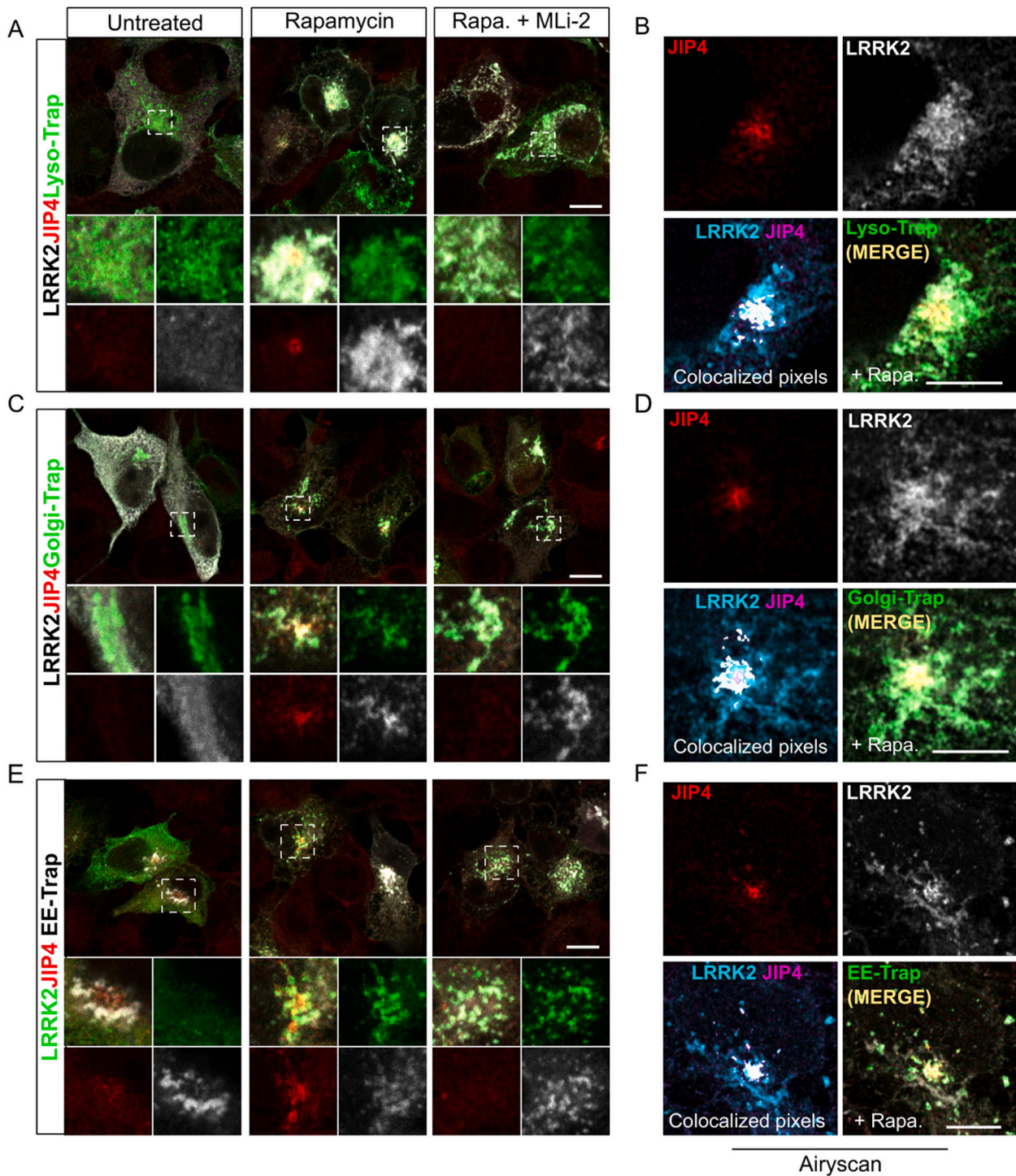
Fig. 5. Recruitment of JIP4 is observed after trapping LRRK2 to the lysosome, Golgi or early endosomes. To investigate whether any events downstream of RAB10 are observed in this trap system, we stained for JIP4 after trapping LRRK2 to the lysosomal (A,B) Golgi (C,D) and early endosome (E,F) membranes under conditions with or without rapamycin or MLi-2 treatments. Airyscan images and colocalization pixels are shown in (B,D,F) for each trap. Scale bar = 10 μm (A, B); 5 μm (C—D). Scale bar = 10 μm (A,C,E); 5 μm (B,D,F).

protein in PD and has strong implications for the clinical application of LRRK2 kinase inhibitors. In the current study, we evaluated whether direction to a variety of endomembranes is sufficient to result in LRRK2 activation, even in the absence of membrane damage. We show that recruitment of LRRK2 to various membranes results in the accumulation of pRABs and recruitment of the effector protein JIP4, regardless of the membrane targeted.

Several prior studies have supported the concept that LRRK2

activation requires membrane targeting, but in the context of either immune signaling and/or membrane damage (Berger et al., 2010; Bonet-Ponce et al., 2020; Eguchi et al., 2018; Herbst et al., 2020). Our study adds to this body of knowledge, showing that once LRRK2 is at any membrane, kinase activation is enhanced, presumably via self-interaction as seen in vitro (Civiero et al., 2012; Greggio et al., 2008; Klein et al., 2009). Our data indicate that membrane damage is not specifically required for LRRK2 activation. Furthermore, all membranes
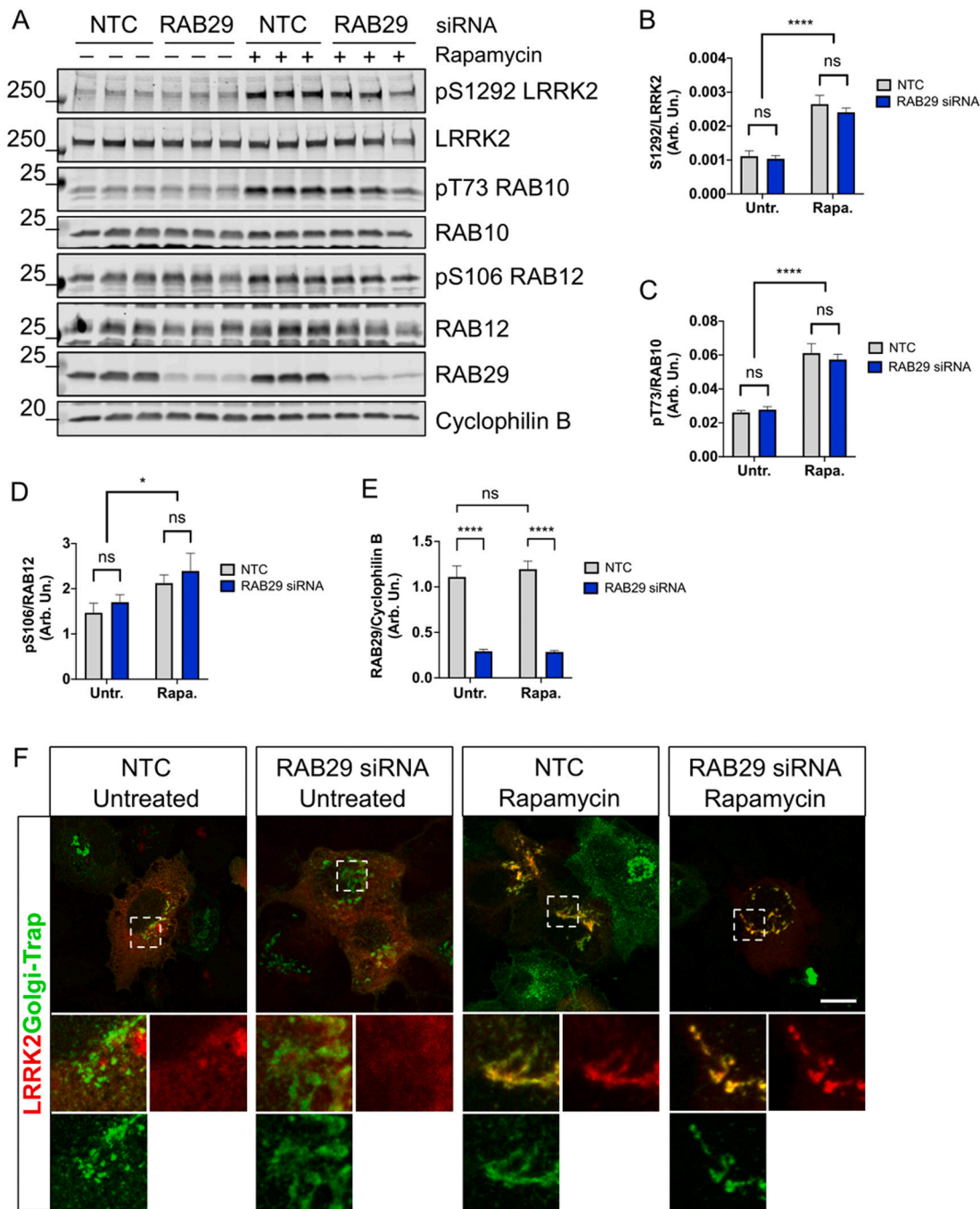
Fig. 6. Knockdown of endogenous RAB29 does not affect LRRK2 activation at the Golgi or lysosomal membranes. Following a 24 h incubation of siRNA RAB29 or non-targeting control, HEK293FT cells were transfected with 3xFlag-FKBP-LRRK2 and Golgi-trap. Cells were then treated with rapamycin for 15 min before lysing and pS1292 LRRK2, pT73 RAB10, and pS106 RAB12 levels were evaluated via Western blot (A-D). RAB29 knockdown efficiency was measured via total levels of endogenous protein (E). (B-E): two-way ANOVA with Tukey's multiple comparisons test, $n = 3$; SD bars shown; (B) treatment, $p < 0.0001$, $F(1, 8) = 214.9$; siRNA, $p = 0.1536$, $F(1, 8) = 2.485$, (C) treatment, $p < 0.0001$, $F(1, 8) = 267.3$; siRNA, $p = 0.6008$, $F(1, 8) = 0.2967$, (D) treatment, $p < 0.0019$, $F(1, 8) = 20.69$; siRNA, $p = 0.1269$, $F(1, 8) = 2.901$, (E) treatment, $p = 0.3936$, $F(1, 8) = 0.8127$; siRNA, $p < 0.0001$, $F(1, 8) = 381.9$.

were equally suitable for activating LRRK2, implying that there are no specific membrane resident proteins involved in LRRK2 activation. Overall, our data are consistent with a model where membrane recruitment is sufficient for LRRK2 activation, although this needs to be tested in future studies. It should be noted that such a model does not exclude that membrane damage and recruitment may both independently contribute to LRRK2 activation.

Interestingly, we also found that once mutant LRRK2 is directed to lysosome or Golgi membranes, phosphorylation of RAB12 is unaffected compared to the robust accumulation of pRAB10. Previous studies have shown that mutant LRRK2 is more prone to accumulate at membranes compared to wildtype protein (Berger et al., 2010; Mamais et al., 2021) and we observed that pRAB12 more strongly colocalized with mutant LRRK2 at membranes compared to pRAB10. Thus, one possible explanation for the minimal effect of membrane-bound mutant LRRK2 on pRAB12 is that mutant LRRK2 is present at membranes prior to induced recruitment. More extensive studies will be needed in order to elucidate differences between mutant LRRK2-dependent RAB phosphorylation.

Prior work has shown that a mitochondrial-targeting sequence fused to the N-terminus of RAB29 is sufficient to direct LRRK2 to mitochondria, increasing its activity and subsequent RAB10 phosphorylation. However, in vivo data from RAB29 knockout mice and in vitro data from RAB29 knockout cells showed no difference in LRRK2 kinase measurements (Gomez et al., 2019; Kalogeropoulou et al., 2020). Here, we have confirmed, using the orthogonal approach of siRNA rather than knockout, that RAB29 is not necessary for the activation of LRRK2, as RAB29 deficient cells showed the same magnitude of LRRK2 activation as control cells using LRRK2, RAB10, and RAB12 phosphorylation readouts at both Golgi and lysosomal membranes. Therefore, and in agreement with other recent data, we infer that RAB29 is not an endogenous activator of LRRK2. However, both LRRK2 and RAB29 knockout mice have similar lysosomal phenotypes, suggesting that there is an unresolved pathway relationship between LRRK2 and RAB29 which should be evaluated in future studies.

Collectively, the current results further establish that LRRK2 can be activated by association with multiple endomembranes, resulting in phosphorylation of RABs that then accumulate at local membranes and can recruit effector proteins including JIP4. Additional studies are required to further delineate how LRRK2 becomes activated at endomembranes in cells under pathological conditions.

Supplementary data to this article can be found online at https://doi.org/10.1016/j.nbd.2022.105769.

Author contributions

Conceptualization, L.B-P., M.R.C., J.H.K.; Methodology, L.B-P., J.H. K.; Formal Analysis, J.H.K., L.B-P.; Investigation, J.H.K., L.B-P.; Writing, M.R.C., J.H.K., L.B-P.; Supervision, M.R.C., P.A.L.; Funding, M.R.C., P.A. L.

Declaration of Competing Interest

The authors have no competing interests related to this work.

Acknowledgements

References

Babbey, C.M., Ahktar, N., Wang, E., Chen, C.C.-H., Grant, B.D., Dunn, K.W., 2006. Rab10 regulates membrane transport through early endosomes of polarized Madin-Darby canine kidney cells. Mol. Biol. Cell 17, 3156–3175. https://doi.org/10.1091/mbc.e05-08-0799.

Beilina, A., Rudenko, I.N., Kaganovich, A., Civiero, L., Chau, H., Kalia, S.K., Kalia, L.V., Lobbestael, E., Chia, R., Ndukwe, K., Ding, J., Nalls, M., Olszewski, M., Hauser, D.N., Kumaran, R., Lozano, A.M., Baekelandt, V., Greene, L.E., Taymans, J.-M., Greggio, E., Cookson, M.R., 2014. Unbiased screen for interactors of leucine-rich repeat kinase 2 supports a common pathway for sporadic and familial Parkinson disease. Proc. Natl. Acad. Sci. U. S. A. 111, 2626–2631. https://doi.org/10.1073/pnas.1318306111.

Beilina, A., Bonet-Ponce, L., Kumaran, R., Kordich, J.J., Ishida, M., Mamais, A., Kaganovich, A., Saez-Atienzar, S., Gershlick, D.C., Roosen, D.A., Pellegrini, L., Malkov, V., Fell, M.J., Harvey, K., Bonifacino, J.S., Moore, D.J., Cookson, M.R., 2020. The Parkinson's disease protein LRRK2 interacts with the GARP complex to promote retrograde transport to the trans-Golgi network. Cell Rep. 31, 107614 https://doi.org/10.1016/j.celrep.2020.107614.

Berger, Z., Smith, K.A., Lavoie, M.J., 2010. Membrane localization of LRRK2 is associated with increased formation of the highly active LRRK2 dimer and changes in its phosphorylation. Biochemistry 49, 5511–5523. https://doi.org/10.1021/bi100157u.

Boecker, C.A., Goldsmith, J., Dou, D., Cajka, G.G., Holzbaur, E.L.F., 2021. Increased LRRK2 kinase activity alters neuronal autophagy by disrupting the axonal transport of autophagosomes. Curr. Biol. CB 31, 2140–2154.e6. https://doi.org/10.1016/j.cub.2021.02.061.

Bonet-Ponce, L., Beilina, A., Williamson, C.D., Lindberg, E., Kluss, J.H., Saez-Atienzar, S., Landeck, N., Kumaran, R., Mamais, A., Bleck, C.K.E., Li, Y., Cookson, M.R., 2020.

LRRK2 mediates tubulation and vesicle sorting from lysosomes. Sci. Adv. 6 https://doi.org/10.1126/sciadv.abb2454.

Civiero, L., Vancraenenbroeck, R., Belluzzi, E., Beilina, A., Lobbestael, E., Reyniers, L., Gao, F., Micetic, I., De Maeyer, M., Bubacco, L., Baekelandt, V., Cookson, M.R., Greggio, E., Taymans, J.-M., 2012. Biochemical characterization of highly purified leucine-rich repeat kinases 1 and 2 demonstrates formation of homodimers. PLoS One 7, e43472. https://doi.org/10.1371/journal.pone.0043472.

Cookson, M.R., 2010. The role of leucine-rich repeat kinase 2 (LRRK2) in Parkinson's disease. Nat. Rev. Neurosci. 11, 791–797. https://doi.org/10.1038/nrn2935.

Efergan, A., Azouz, N.P., Klein, O., Noguchi, K., Rothenberg, M.E., Fukuda, M., Sagi-Eisenberg, R., 2016. Rab12 regulates retrograde transport of mast cell secretory granules by interacting with the RILP-dynein complex. J. Immunol. Baltim. Md 1950 (196), 1091–1101. https://doi.org/10.4049/jimmunol.1500731.

Eguchi, T., Kuwahara, T., Sakurai, M., Komori, T., Fujimoto, T., Ito, G., Yoshimura, S.-I., Harada, A., Fukuda, M., Koike, M., Iwatsubo, T., 2018. LRRK2 and its substrate Rab GTPases are sequentially targeted onto stressed lysosomes and maintain their homeostasis. Proc. Natl. Acad. Sci. U. S. A. 115, E9115–E9124. https://doi.org/10.1073/pnas.1812196115.

Etoh, K., Fukuda, M., 2019. Rab10 regulates tubular endosome formation through KIF13A and KIF13B motors. J. Cell Sci. 132, jcs226977. https://doi.org/10.1242/jcs.226977.

Fujimoto, T., Kuwahara, T., Eguchi, T., Sakurai, M., Komori, T., Iwatsubo, T., 2018. Parkinson's disease-associated mutant LRRK2 phosphorylates Rab7L1 and modifies trans-Golgi morphology. Biochem. Biophys. Res. Commun. 495, 1708–1715. https://doi.org/10.1016/j.bbrc.2017.12.024.

Funayama, M., Hasegawa, K., Ohta, E., Kawashima, N., Komiyama, M., Kowa, H., Tsuji, S., Obata, F., 2005. An LRRK2 mutation as a cause for the parkinsonism in the original PARK8 family. Ann. Neurol. 57, 918–921. https://doi.org/10.1002/ana.20484.

Gilks, W.P., Abou-Sleiman, P.M., Gandhi, S., Jain, S., Singleton, A., Lees, A.J., Shaw, K., Bhatia, K.P., Bonifati, V., Quinn, N.P., Lynch, J., Healy, D.G., Holton, J.L., Revesz, T., Wood, N.W., 2005. A common LRRK2 mutation in idiopathic Parkinson's disease. Lancet 365, 415–416. https://doi.org/10.1016/S0140-6736(05)17830-1.

Gomez, R.C., Wawro, P., Lis, P., Alessi, D.R., Pfeffer, S.R., 2019. Membrane association but not identity is required for LRRK2 activation and phosphorylation of Rab GTPases. J. Cell Biol. 218, 4157–4170. https://doi.org/10.1083/jcb.201902184.

Greggio, E., Zambrano, I., Kaganovich, A., Beilina, A., Taymans, J.-M., Daniëls, V., Lewis, P., Jain, S., Ding, J., Syed, A., Thomas, K.J., Baekelandt, V., Cookson, M.R., 2008. The Parkinson disease-associated leucine-rich repeat kinase 2 (LRRK2) is a dimer that undergoes intramolecular autophosphorylation. J. Biol. Chem. 283, 16906–16914. https://doi.org/10.1074/jbc.M708718200.

Hammond, G.R.V., Machner, M.P., Balla, T., 2014. A novel probe for phosphatidylinositol 4-phosphate reveals multiple pools beyond the Golgi. J. Cell Biol. 205, 113–126. https://doi.org/10.1083/jcb.201312072.

Herbst, S., Campbell, P., Harvey, J., Bernard, E.M., Papayannopoulos, V., Wood, N.W., Morris, H.R., Gutierrez, M.G., 2020. LRRK2 activation controls the repair of damaged endomembranes in macrophages. EMBO J. e104494 https://doi.org/10.15252/embj.2020104494.

Homma, Y., Hiragi, S., Fukuda, M., 2021. Rab family of small GTPases: an updated view on their regulation and functions. FEBS J. 288, 36–55. https://doi.org/10.1111/febs.15453.

Iida, H., Noda, M., Kaneko, T., Doiguchi, M., Mōri, T., 2005. Identification of rab12 as a vesicle-associated small GTPase highly expressed in Sertoli cells of rat testis. Mol. Reprod. Dev. 71, 178–185. https://doi.org/10.1002/mrd.20294.

Iwaki, H., Blauwendraat, C., Makarious, M.B., Bandres-Ciga, S., Leonard, H.L., Gibbs, J. R., Hernandez, D.G., Scholz, S.W., Faghri, F., Nalls, M.A., Singleton, A.B., 2020. Penetrance of Parkinson's disease in LRRK2 p.G2019S carriers is modified by a polygenic risk score. Mov. Disord. Off. J. Mov. Disord. Soc. https://doi.org/10.1002/mds.27974.

Kalogeropoulou, A.F., Freemantle, J.B., Lis, P., Vides, E.G., Polinski, N.K., Alessi, D.R., 2020. Endogenous Rab29 does not impact basal or stimulated LRRK2 pathway activity. Biochem. J. 477, 4397–4423. https://doi.org/10.1042/BCJ20200458.

Klein, C.L., Rovelli, G., Springer, W., Schall, C., Gasser, T., Kahle, P.J., 2009. Homo- and heterodimerization of ROCO kinases: LRRK2 kinase inhibition by the LRRK2 ROCO fragment. J. Neurochem. 111, 703–715. https://doi.org/10.1111/j.1471-4159.2009.06358.x.

Kluss, J.H., Mamais, A., Cookson, M.R., 2019. LRRK2 links genetic and sporadic Parkinson's disease. Biochem. Soc. Trans. BST20180462 https://doi.org/10.1042/BST20180462.

Kumari, U., Tan, E.K., 2009. LRRK2 in Parkinson's disease: genetic and clinical studies from patients. FEBS J. 276, 6455–6463. https://doi.org/10.1111/j.1742-4658.2009.07344.x.

Kuwahara, Tomoki, Inoue, Keiichi, D'Agati, V.D., Fujimoto, T., Eguchi, T., Saha, Shamol, Wolozin, Benjamin, Iwatsubo, Takeshi, Abeliovich, A., Paisan-Ruiz, C., Zimprich, A., Satake, W., Simon-Sanchez, J., Zhang, F.R., Umeno, J., Lewis, P.A., Manzoni, C., Greenman, C., Hassin-Baer, S., MacLeod, D.A., Pihlstrom, L., Bultema, J.J., Pietro, S. M.D., Ma, J., Plesken, H., Treisman, J.E., Edelman-Novemsky, I., Ren, M., Hermann, G.J., Grill, B., MacLeod, D., Plowey, E.D., Cherra, S.J., Liu, Y.J., Chu, C.T., Parisiadou, L., Chan, D., Citro, A., Cordy, J.M., Shen, G.C., Wolozin, B., Beilina, A., Tong, Y., Herzig, M.C., Hinkle, K.M., Tong, Y., Fuji, R.N., Newell-Litwa, K., Seong, E., Burmeister, M., Faundez, V., Dell'Angelica, E.C., Wolozin, B., Gabel, C., Ferree, A., Guillily, M., Ebata, A., Kuwahara, T., Sakaguchi-Nakashima, A., Meir, J.Y., Jin, Y., Matsumoto, K., Hisamoto, N., Currie, E., Dell'Angelica, E.C., Shotelersuk, V., Aguilar, R.C., Gahl, W.A., Bonifacino, J.S., Peden, A.A., Shotelersuk, V., Dell'Angelica, E.C., Hartnell, L., Bonifacino, J.S., Gahl, W.A., Zhen, L., Swank, R.T., Reddington, M., Howlett, O., Novak, E.K., Seong, E., Biskup, S., Steger, M.,

Dell'Angelica, E.C., Ooi, C.E., Bonifacino, J.S., Faundez, V.V., Kelly, R.B., Azevedo, C., Burton, A., Ruiz-Mateos, E., Marsh, M., Saiardi, A., Martin, I., West, A. B., Smith, W.W., Guttentag, S.H., Brenner, S., Saha, S., Kuwahara, T., Tonegawa, R., Ito, G., Mitani, S., Iwatsubo, T., Ito, G., Inoue, K., Inoue, K., 2016. LRRK2 and RAB7L1 coordinately regulate axonal morphology and lysosome integrity in diverse cellular contexts. Sci. Rep. 6, 29945. https://doi.org/10.1038/srep29945.

Lee, A.J., Wang, Y., Alcalay, R.N., Mejia-Santana, H., Saunders-Pullman, R., Bressman, S., Corvol, J.-C., Brice, A., Lesage, S., Mangone, G., Tolosa, E., Pont-Sunyer, C., Vilas, D., Schüle, B., Kausar, F., Foroud, T., Berg, D., Brockmann, K., Goldwurm, S., Siri, C., Asselta, R., Ruiz-Martinez, J., Mondragón, E., Marras, C., Ghate, T., Giladi, N., Mirelman, A., Marder, K., for the Michael J. Fox LRRK2 Cohort Consortium, 2017. Penetrance estimate of *LRRK2* p.G2019S mutation in individuals of non-Ashkenazi Jewish ancestry: *LRRK2* mutation in non-Ashkenazi Jewish ancestry. Mov. Disord. 32, 1432–1438. https://doi.org/10.1002/mds.27059.

Liberles, S.D., Diver, S.T., Austin, D.J., Schreiber, S.L., 1997. Inducible gene expression and protein translocation using nontoxic ligands identified by a mammalian three-hybrid screen. Proc. Natl. Acad. Sci. U. S. A. 94, 7825–7830. https://doi.org/10.1073/pnas.94.15.7825.

Liu, Y., Xu, X.-H., Chen, Q., Wang, T., Deng, C.-Y., Song, B.-L., Du, J.-L., Luo, Z.-G., 2013. Myosin Vb controls biogenesis of post-Golgi Rab10 carriers during axon development. Nat. Commun. 4, 2005. https://doi.org/10.1038/ncomms3005.

Liu, Z., Bryant, N., Kumaran, R., Beilina, A., Abeliovich, A., Cookson, M.R., West, A.B., 2018. LRRK2 phosphorylates membrane-bound Rabs and is activated by GTP-bound Rab7L1 to promote recruitment to the trans-Golgi network. Hum. Mol. Genet. 27, 385–395. https://doi.org/10.1093/hmg/ddx410.

Mamais, A., Kluss, J.H., Bonet-Ponce, L., Landeck, N., Langston, R.G., Smith, N., Beilina, A., Kaganovich, A., Ghosh, M.C., Pellegrini, L., Kumaran, R., Papazoglou, I., Heaton, G.R., Bandopadhyay, R., Maio, N., Kim, C., LaVoie, M.J., Gershlick, D.C., Cookson, M.R., 2021. Mutations in LRRK2 linked to Parkinson disease sequester Rab8a to damaged lysosomes and regulate transferrin-mediated iron uptake in microglia. PLoS Biol. 19, e3001480 https://doi.org/10.1371/journal.pbio.3001480.

Matsui, T., Itoh, T., Fukuda, M., 2011. Small GTPase Rab12 regulates constitutive degradation of transferrin receptor. Traffic Cph. Den. 12, 1432–1443. https://doi.org/10.1111/j.1600-0854.2011.01240.x.

Nalls, M.A., Blauwendraat, C., Vallerga, C.L., Heilbron, K., Bandres-Ciga, S., Chang, D., Tan, M., Kia, D.A., Noyce, A.J., Xue, A., Bras, J., Young, E., von Coelln, R., Simón-Sánchez, J., Schulte, C., Sharma, M., Krohn, L., Pihlstrøm, L., Siitonen, A., Iwaki, H., Leonard, H., Faghri, F., Gibbs, J.R., Hernandez, D.G., Scholz, S.W., Botia, J.A., Martinez, M., Corvol, J.-C., Lesage, S., Jankovic, J., Shulman, L.M., Sutherland, M., Tienari, P., Majamaa, K., Toft, M., Andreassen, O.A., Bangale, T., Brice, A., Yang, J., Gan-Or, Z., Gasser, T., Heutink, P., Shulman, J.M., Wood, N.W., Hinds, D.A., Hardy, J.A., Morris, H.R., Gratten, J., Visscher, P.M., Graham, R.R., Singleton, A.B., 23andMe Research Team, System Genomics of Parkinson's Disease Consortium, International Parkinson's Disease Genomics Consortium, 2019. Identification of novel risk loci, causal insights, and heritable risk for Parkinson's disease: a meta-analysis of genome-wide association studies. Lancet Neurol. 18, 1091–1102. https://doi.org/10.1016/S1474-4422(19)30320-5.

Paisán-Ruíz, C., Jain, S., Evans, E.W., Gilks, W.P., Simón, J., van der Brug, M., López de Munain, A., Aparicio, S., Gil, A.M., Khan, N., Johnson, J., Martinez, J.R., Nicholl, D., Carrera, I.M., Pena, A.S., de Silva, R., Lees, A., Martí-Massó, J.F., Pérez-Tur, J., Wood, N.W., Singleton, A.B., 2004. Cloning of the gene containing mutations that cause PARK8-linked Parkinson's disease. Neuron 44, 595–600. https://doi.org/10.1016/j.neuron.2004.10.023.

Purlyte, E., Dhekne, H.S., Sarhan, A.R., Gomez, R., Lis, P., Wightman, M., Martinez, T.N., Tonelli, F., Pfeffer, S.R., Alessi, D.R., 2018. Rab29 activation of the Parkinson's disease-associated LRRK2 kinase. EMBO J. 37, 1–18. https://doi.org/10.15252/embj.201798099.

Robinson, M.S., Sahlender, D.A., Foster, S.D., 2010. Rapid inactivation of proteins by rapamycin-induced rerouting to mitochondria. Dev. Cell 18, 324–331. https://doi.org/10.1016/j.devcel.2009.12.015.

Ryan, K.J., White, C.C., Patel, K., Xu, J., Olah, M., Replogle, J.M., Frangieh, M., Cimpean, M., Winn, P., McHenry, A., Kaskow, B.J., Chan, G., Cuerdon, N., Bennett, D.A., Boyd, J.D., Imitola, J., Elyaman, W., De Jager, P.L., Bradshaw, E.M., 2017. A human microglia-like cellular model for assessing the effects of neurodegenerative disease gene variants. Sci. Transl. Med. 9 https://doi.org/10.1126/scitranslmed.aai7635.

Rydell, G.E., Renard, H.-F., Garcia-Castillo, M.-D., Dingli, F., Loew, D., Lamaze, C., Römer, W., Johannes, L., 2014. Rab12 localizes to Shiga toxin-induced plasma membrane invaginations and controls toxin transport. Traffic Cph. Den. 15, 772–787. https://doi.org/10.1111/tra.12173.

Sheng, Z., Zhang, S., Bustos, D., Kleinheinz, T., Le Pichon, C.E., Dominguez, S.L., Solanoy, H.O., Drummond, J., Zhang, X., Ding, X., Cai, F., Song, Q., Li, X., Yue, Z., van der Brug, M.P., Burdick, D.J., Gunzner-Toste, J., Chen, H., Liu, X., Estrada, A.A., Sweeney, Z.K., Scearce-Levie, K., Moffat, J.G., Kirkpatrick, D.S., Zhu, H., 2012. Ser1292 autophosphorylation is an indicator of LRRK2 kinase activity and contributes to the cellular effects of PD mutations. Sci. Transl. Med. 4, 164ra161. https://doi.org/10.1126/scitranslmed.3004485.

Singleton, A., Hardy, J., 2011. A generalizable hypothesis for the genetic architecture of disease: pleomorphic risk loci. Hum. Mol. Genet. 20, R158–R162. https://doi.org/10.1093/hmg/ddr358.

Steger, M., Tonelli, F., Ito, G., Davies, P., Trost, M., Vetter, M., Wachter, S., Lorentzen, E., Duddy, G., Wilson, S., Baptista, M.A., Fiske, B.K., Fell, M.J., Morrow, J.A., Reith, A. D., Alessi, D.R., Mann, M., 2016. Phosphoproteomics reveals that Parkinson's disease kinase LRRK2 regulates a subset of Rab GTPases. eLife 5. https://doi.org/10.7554/eLife.12813.

Štimac, I., Jug Vučko, N., Blagojević Zagorac, G., Marcelić, M., Mahmutefendić Lučin, H., Lučin, P., 2021. Dynamin inhibitors prevent the establishment of the cytomegalovirus assembly compartment in the early phase of infection. Life Basel Switz. 11, 876. https://doi.org/10.3390/life11090876.

van Unen, J., Reinhard, N.R., Yin, T., Wu, Y.I., Postma, M., Gadella, T.W.J., Goedhart, J., 2015. Plasma membrane restricted RhoGEF activity is sufficient for RhoA-mediated actin polymerization. Sci. Rep. 5, 14693. https://doi.org/10.1038/srep14693.

Varnai, P., Thyagarajan, B., Rohacs, T., Balla, T., 2006. Rapidly inducible changes in phosphatidylinositol 4,5-bisphosphate levels influence multiple regulatory functions of the lipid in intact living cells. J. Cell Biol. 175, 377–382. https://doi.org/10.1083/jcb.200607116.

Wang, S., Ma, Z., Xu, X., Wang, Z., Sun, L., Zhou, Y., Lin, X., Hong, W., Wang, T., 2014. A role of Rab29 in the integrity of the trans-Golgi network and retrograde trafficking of Mannose-6-phosphate receptor. PLoS One 9, e96242. https://doi.org/10.1371/journal.pone.0096242.

West, A.B., 2014. Ten years and counting: moving leucine-rich repeat kinase 2 inhibitors to the clinic. Mov. Disord. Off. J. Mov. Disord. Soc. https://doi.org/10.1002/mds.26075.

Willett, R., Martina, J.A., Zewe, J.P., Wills, R., Hammond, G.R.V., Puertollano, R., 2017. TFEB regulates lysosomal positioning by modulating TMEM55B expression and JIP4 recruitment to lysosomes. Nat. Commun. 8 (1), 1580.

Zimprich, A., Biskup, S., Leitner, P., Lichtner, P., Farrer, M., Lincoln, S., Kachergus, J., Hulihan, M., Uitti, R.J., Calne, D.B., Stoessl, A.J., Pfeiffer, R.F., Patenge, N., Carbajal, I.C., Vieregge, P., Asmus, F., Müller-Myhsok, B., Dickson, D.W., Meitinger, T., Strom, T.M., Wszolek, Z.K., Gasser, T., 2004. Mutations in LRRK2 cause autosomal-dominant parkinsonism with pleomorphic pathology. Neuron 44, 601–607. https://doi.org/10.1016/j.neuron.2004.11.005.

Taylor & Francis
Taylor & Francis Group

REVIEW

🔓 OPEN ACCESS ⟳ Check for updates

Leucine-rich repeat kinase 2 (LRRK2): an update on the potential therapeutic target for Parkinson's disease

Jillian H. Kluss ⓘ[a,b], Patrick A. Lewis ⓘ[a,c,d] and Elisa Greggio ⓘ[e,f]

aSchool of Pharmacy, University of Reading, Whiteknights, Reading, UK; bCell Biology and Gene Expression Section, National Institute on Aging, National Institutes of Health, Bethesda, Maryland, USA; cDepartment of Neurodegenerative Disease, UCL Queen Square Institute of Neurology, London, UK; dDepartment of Comparative Biomedical Sciences, Royal Veterinary College, London, UK; eDepartment of Biology, University of Padova, Padova, Italy; fCentro Studi per la Neurodegenerazione (CESNE), University of Padova, Padova, Italy

ABSTRACT

Mutations in Leucine-rich repeat kinase 2 (LRRK2) are a risk factor for and a cause of sporadic and familial Parkinson's disease (PD), respectively. These mutations are some of the most common genetic contributors to PD and render the kinase hyperactive. Increasingly within the past decade, there has been substantial effort investigating LRRK2 as a target for therapeutics in preclinical studies, and currently, small-molecule inhibitors and antisense oligonucleotides are being assessed in clinical trials as therapies to reduce the toxic hyperactivity of its kinase and/or reduce total levels of the protein in healthy individuals and people with PD.

Areas covered: In this review, we will provide an update on the current status of drugs and other technologies that have emerged in recent years and provide an overview of their efficacy in ameliorating LRRK2 kinase activity and overall safety in animal models and humans.

Expert opinion: The growth of both target discovery and innovative drug design has sparked a lot of excitement for the future of how we treat Parkinson's disease. Given the immense focus on LRRK2 as a therapeutic target, it is expected within the next decade to determine its therapeutic properties, or lack thereof, for PD.

1. Introduction

Parkinson's disease (PD) is a progressive neurodegenerative disorder affecting voluntary movement with cardinal features being bradykinesia, muscle rigidity, and resting tremor and most often including a slew of other non-motor symptoms including depression, constipation, hyposmia, postural instability, and insomnia [1]. A definitive diagnosis of PD is confirmed by loss of dopaminergic neurons within the substantia nigra pars compacta of the brain as well as the protein and lipid inclusions known as Lewy bodies observed through autopsy. Thus, a prehumous diagnosis relies on clinical observation of the presence of the cardinal features [2,3]. Additionally, a series of supportive data from motor and cognitive tests, and, in some cases dopamine transporter (DAT) positron emission tomography scans, can also be used to exclude other diseases or disorders. One such test is the observation of a positive response, or lack thereof, to a dopamine replacement therapy such as levodopa [1]. Levodopa, a soluble precursor of dopamine, helps to increase dopamine levels in the brain and diminish bradykinesia and rigidity. However, levodopa-induced motor complications will occur such as dyskinesias after a few years of continued use that impede daily activities and reduce patient quality of life [4]. Other medications that may be prescribed in the early stages of disease in order to prolong the onset of levodopa-

induced complications are those curbing dopamine metabolism such as monoamine oxidase type b (MAO-B) inhibitors or medications that bypass dopamine by stimulating dopamine receptors directly such as dopamine agonists [4,5]. While useful in curtailing some of the symptoms of PD, currently there are no medications available that aid in slowing or stopping the progression of the disease.

Two decades ago, linkage analysis helped to identify coding variants in *Leucine-rich repeat kinase 2* (LRRK2) as a genetic cause of PD [6,7], and since then extensive genetic analyses and genome-wide association studies have confirmed mutations in *LRRK2* as one of the most common causes of PD, with non-coding variants associated with enhanced lifetime risk of developing idiopathic PD [8–10]. More recently, it has become clear that non-coding variants at the *LRRK2* locus are associated with the rate of progression of the primary tauopathy Progressive Supranuclear Palsy (PSP) [11]. PD-associated mutations in LRRK2 produce a toxic hyperactive kinase, as observed in *in vitro* and *in vivo* models utilizing a LRRK2 autophosphorylation site at serine 1292, a indirect but kinase conformation-dependent phosphorylation site at serine 935, and a subset of small Rab GTPase substrates [12–16]. LRRK2 activity has been associated with a variety of organellar membranes, demonstrating the protein's wide influence on many pathways including the endolysosomal system, autophagy, ciliogenesis,

CONTACT Jillian H. Kluss ✉ jillian.kluss@nih.gov; j.kluss@pgr.reading.ac.uk 🖳 Cell Biology and Gene Expression Section, Laboratory of Neurogenetics, National Institute on Aging, NIH, 35 Convent Drive, Room 1A–107, Bethesda, MD 20892–3707, USA

trans-Golgi integrity, vesicle sorting, and mitochondrial integrity, presumably via its interactions with Rab proteins and other as of yet unidentified substrates [17–28]. Therefore, inhibiting hyperactive LRRK2 is potentially beneficial in altering PD pathogenesis.

A complex protein with both GTPase and kinase domains, LRRK2 is conceptually a strong candidate for the development of targeted therapeutics. Currently, many structurally distinct small-molecule LRRK2 kinase inhibitors are commercially available for experimental purposes and one inhibitor is soon to start phase II of clinical trials. In this review, we will give an update on efforts to employ LRRK2 kinase inhibitors, the potential difficulties of targeting LRRK2 systemically based on the results of preclinical studies, and alternative methods currently being explored to lower LRRK2 kinase activity as a therapy for PD.

2. Type I and type II LRRK2 kinase inhibitors

Since the development of the first small-molecule kinase inhibitor used as an alternative to chemotherapy in cancer patients in 2001, the use of kinase inhibitors as a targeted treatment in a variety of diseases and illnesses have skyrocketed, with currently over 50 kinase inhibitors approved by the US Food and Drug Administration (FDA) available on the market [29,30]. Similarly, LRRK2 kinase inhibitors have gained a large focus as a potential treatment for PD. Years before the initial announcements of a LRRK2 clinical trial, commercially available LRRK2 kinase inhibitors were and continue to be a vital tool in basic biology research. Most LRRK2 kinase inhibitors are orthosteric, thus belonging to the type I class of inhibitors and bind to the ATP-binding pocket of LRRK2 with an 'in' orientation of the DYG activation loop (Figure 1), and range widely in structure and potency. Currently, the most used are the third-generation, structurally distinct, and brain penetrant molecules MLi-2 [31], PF-06685360 (PFE-360), and GNE-7915 for basic research purposes [32]. Each have been observed to strongly inhibit LRRK2 kinase activity via significant decreases in autophosphorylation at S1292 LRRK2 as well as dephosphorylation of downstream Rab substrates in varying models *in vitro* and *in vivo* [13,31–36]. Interestingly, a cluster of phosphorylation sites near the N-terminus of LRRK2, S910/S935/S955/S973 were found to promote 14-3-3 binding to the monomeric form of LRRK2 and are also dephosphorylated after acute and chronic administration of ATP-competitive inhibitors [37,38]. Thus, this cluster of phosphorylation sites have played an important role as readouts for LRRK2 inhibition, although indirect, as direct autophosphorylation readouts can be challenging to detect robustly due to low stoichiometry in some tissues, CSF, and blood [31,39,40].

Alternatively, type II kinase inhibitors, classified as binding to the ATP-binding pocket with an 'out' orientation of the activation loop (Figure 1), such as GZD-824, Rebastinib and Ponatinib, all of which were developed to counteract resistance against the popular drug for chronic myelogenous leukemia, imatinib, have also been found to target LRRK2 kinase activity [43–45]. When compared to the type I molecule MLi-2, all three type II drugs similarly were able to dephosphorylate downstream Rabs such as Rab10 and Rab12 at sites T73 and S105, respectively, in mouse embryonic fibroblasts [45]. Interestingly, type II inhibitors do not dephosphorylate residues S910/S935/S955/S973, however, require upwards of ~30-300x higher concentration compared to type I inhibitors in *in vitro* kinase assays utilizing wild-type LRRK2 [45]. Interestingly, when comparing the potency of type II inhibitors between wildtype and G2019S LRRK2 mutant proteins in a kinase assay using the synthetic LRRK2 substrate Nictide [46], Tasegian and colleagues observed that all three drugs had a lower potency when inhibiting mutant G2019S LRRK2, and this was recapitulated when measuring Rab10 dephosphorylation in both G2019S and R1441C LRRK2 knock-in MEFs [45]. This phenomenon was also observed by Kelly et al. when using the type I inhibitor MLi-2 in rats expressing human G2019S LRRK2 [36]. This suggests that the G2019S mutation may be more resilient to kinase inhibition, regardless of the conformation of LRRK2, although earlier data on the previous generation orthosteric inhibitor LRRK2-IN-1 reported higher sensitivity in G2019S LRRK2 cells compared to wild-type cells, suggesting that this may be drug-specific rather than class-specific [47].

To combat this G2019S resilience, a recent study introduced the synthesis of another indazole-based type I LRRK2 inhibitor with 2000-fold selectivity to G2019S LRRK2 compared to wild-type LRRK2 [48]. This inhibitor, named Compound 38, has also been shown to cross the blood–brain barrier, a first for G2019S-specific molecules, and provides a promising alternative specific for patients carrying the G2019S mutation. An additional compound, EB-42168, is reported to be 100x more selective for G2019S LRRK2 and been shown to ameliorate its hyperactive effects while sparing wild-type LRRK2 in peripheral blood mononuclear cells taken from G2019S-positive PD patients [49]. Thus, the creation of molecules with selective affinity to G2019S LRRK2 may be helpful when considering the drug efficacy of targeting hyperactive kinase specifically in G2019S-positive PD patients.

With regards to molecule affinity, Ponatinib, GZD-824, and Rebastinib have been found to inhibit 14–40 other kinases identified in a small drug screen of 140 different kinases [45], whereas type I compounds such as MLi-2 and Compound 38 are highly selective for LRRK2 [31]. As of yet, there are no
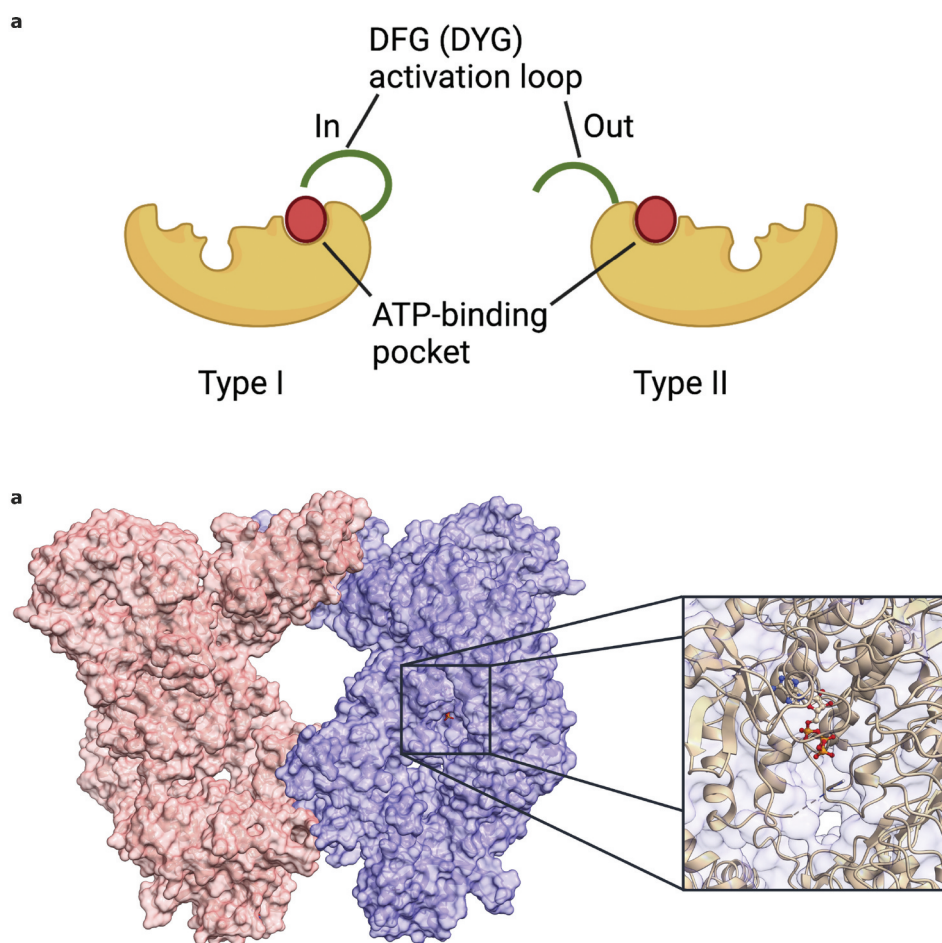
Figure 1. Structural differences between type I and II small molecule kinase inhibitors.

A generic enzyme (yellow) is shown depicting the difference in structural conformation of the DFG/DYG motif (green) when bound to type I and II class kinase inhibitors (red), respectively (A). Dimeric structure for the LRRK2 complex, showing the active site of the kinase with ATP bound (B). Image derived from PDB 7LHT [41] using UCSF chimera [42].

LRRK2-specific type II inhibitors that have been developed. Based on these data, type I inhibitor drugs would seem the better fit when considering chemical compounds for therapeutic use at this time. However, as both classes render LRRK2 in different structural conformations, with type I inhibitor binding favoring a closed, active conformation, which has been associated with microtubule interaction [50–52], and type II binding favoring an open, inactive conformation, both classes hold equal purpose in the continuing efforts to understand the relationship between LRRK2 structure, activity, and its downstream consequences.

2.1. Ongoing clinical trials using kinase inhibitors

Currently, there is one ongoing clinical trial using an orally administered, type I small molecule LRRK2 kinase inhibitor made by Denali Therapeutics (clinicaltrials.gov ID: NCT04056689). This compound, denoted as DNL151, and later BIIB122/DNL151 after a partnership between Denali and Biogen was announced mid-2020, was reported to have met all goals in phase 1 of the trial, in which 184 healthy individuals received a range of doses for up to 28 days. These goals included on-target engagement utilizing phosphorylation sites S935 LRRK2 (greater than or equal to 80%

dephosphorylation) and T73 Rab10 (up to 50% dephosphorylation) as readouts in whole blood and PBMCs, respectively [53]. In addition, this trial reported a dose-dependent reduction in 22:6-bis[monoacylglycerol] phosphate (BMP) in urine, a lysosomal lipid and marker of lysosomal function. Phase 1b completed in late 2020 reported similar results and included 36 patients with Parkinson's disease [53]. So far, BIIB122/DNL151 has been well tolerated with minimal adverse events, namely nausea and headaches, which were quickly reversed after cessation of the drug [53]. Development of late-stage clinical trials using BIIB122/DNL151 are currently ongoing.

3. Complications of systemic employment of LRRK2 kinase inhibitors: what preclinical studies tell us

Some of the most successful kinase inhibitors on the market today are those that have systemic targets as on-target effects are easily achieved via oral administration, for example, Janus kinase inhibitors (JAKs) in the treatment for rheumatoid arthritis. What can be particularly challenging for any drug delivered systemically (i.e. oral, intravenous, or intramuscular administration) for neurodegenerative diseases is to design a molecule that can cross the blood–brain barrier, as well as have limited peripheral side effects with chronic use.

Since the generation of third wave LRRK2 inhibitor molecules, a few preclinical studies have been conducted across various animal models to gain insight into the efficacy and safety of targeting LRRK2 kinase chronically. Here, we will provide an update on the effects of type I kinase inhibitors at the molecular and tissue levels across mice, rats, and cynomolgus monkeys.

3.1. Molecular effects of acute and chronic LRRK2 inhibition

Recent studies have shown both consistent results as well as discrepancies between animal species treated with LRRK2 kinase inhibitors. First, several studies in mice and cynomolgus monkeys have shown that total LRRK2 levels in lung and kidney tissues diminish with type I inhibitors GNE-7915, GNE-0877, PFE-360, and MLi-2 within 7 days of daily PO dosing [38,39,54], as had been previously suggested by in vitro and kinase-dead knock-in mice studies [55–57]. However, one of these studies suggests that decreased levels are readily restored in peripheral tissues with cessation of treatment, as was observed in mice dosed PO with 120 mg/kg of MLi-2, the dose needed to achieve maximal dephosphorylation of S935, after a seven-day washout period [54]. This loss of total LRRK2 was not observed in rats in the same peripheral tissues, however total levels in brain tissue showed a dose-dependent decrease using in-diet dosing of PFE-360 [36]. Taken together, these data suggest that kinase activity may play a role in the stability of the protein, and thus dosing may need to be carefully monitored when considering LRRK2 kinase inhibitor use in PD patients.

Moreover, wild-type mice given a 60 mg/kg daily in-diet dose of MLi-2 for 6 months showed increased levels of pro-surfactant protein C (proSP-C) in lungs, with an observed peak at 28 days, followed by a gradual decrease back to levels comparable to control groups [54]. This suggests that surfactant trafficking can adapt to chronic high levels of LRRK2 inhibition. Further investigation showed that surfactant secretion is not affected by LRRK2 kinase inhibition across species as measured by surfactant D and A levels in bronchoalveolar lavage fluid [38,39,54]. These studies, executed in wild-type animals, show relatively modest effects on lung tissue after high doses of MLi-2. Interestingly, in G2019S LRRK2 knock-in mice given a 60 mg/kg/day in-diet dose of MLi-2 for 2.5 months showed no difference in proSP-C levels at both 10 days of dosing and at endpoint compared to untreated wildtype animals, suggesting that inhibition of hyperactive LRRK2 kinase does not develop the same molecular effects in lung tissue as wild-type LRRK2 [33]. This is an important distinction, as patients carrying mutant LRRK2 may then have less of a risk in developing secondary lung effects when drugs target hyperactive LRRK2 compared to those without a LRRK2 mutation.

Additionally, in-diet MLi-2 dosing of G2019S LRRK2 knock-in mice at 60 mg/kg/day was sufficient to lower hyperactive LRRK2 back to wild-type levels of activity, as concluded by comparable levels of S1292 autophosphorylation, at both 10 day and 10-week timepoints [33]. Interestingly, phospho- and total proteomic analyses of kidney tissue showed significant changes in endolysosomal proteins comparative to LRRK2 knockout animals [33,58]. This suggests that LRRK2 inhibition can mimic some loss-of-function (LOF) effects in the endolysosomal system in peripheral tissues, as these proteins remained unaffected in the brain tissue of these animals. However, modest changes in proteins of mitochondrial integrity were observed in brain tissue, such that treated G2019S LRRK2 knock-in animals resembled wildtype animals, suggesting that G2019S LRRK2 mutant animals have slight mitochondrial defects that are ameliorated with chronic LRRK2 inhibition [33].

What remains to be shown is whether any of these molecular effects are translatable to humans. Studies have shown that people with LRRK2 haploinsufficiency have reduced levels of total LRRK2 protein; however, there have been conflicting reports on whether reduced levels are associated with phenotypes or disease states in these individuals, with one claiming an increased risk for lung adenocarcinoma [59–61]. The caveat here is that chronic LRRK2 inhibition is not the same as LOF variants. In the former, the body must alter its normal mechanisms to account for reduced LRRK2 kinase activity, whereas the latter already developed mechanisms to cope with lower LRRK2 levels in utero. Lower LRRK2 protein levels may also not produce the same effects as lower kinase activity. Thus, it will be imperative to monitor the effects of LRRK2 kinase inhibitors as it relates to normal protein function.

3.2. Morphological changes in peripheral tissues

The most prominent morphological effects observed in vivo following LRRK2 kinase inhibitor treatments over a period of time have been an increase of vacuolation in lung type-II pneumocytes across wildtype mice and cynomolgus monkeys [39,54]. This returned to normal levels after a 1-week washout period. Studies using GNE-7915, GNE-0877, PFE-360, and MLi-2 all reported this vacuolation, suggesting that this is a result of on-target effects [31,38,39,54,62]; however, pulmonary function was also shown to be unaffected in monkeys receiving a 50 mg/kg PO MLi-2 daily dose for 28 days [39]. One potential concern here is that vacuolation has not been reported to regulate with continued treatment use. Thus, if translatable to humans, this phenotype may have the potential to harbor long-term adverse effects in PD patients using a LRRK2 inhibitor treatment.

Additionally, rats given 7.5 mg/kg of PFE-360 BID for 10 weeks showed hyperpigmentation of the kidneys, a phenotype seen in LRRK2 KO rats and mice [58,63]. It is worth noting that this was not observed in the treatments of mice nor monkeys, suggesting this is a species-specific phenotype [33,38,39,54]. Overall, it is currently unknown whether any lung or kidney complications will arise in humans, and thus careful monitoring of these organs will be critical in current and future clinical trials testing the efficacy of LRRK2 kinase inhibitors.

4. Alternative approaches to reduce LRRK2 kinase activity

Aside from type I and II kinase inhibitors, additional approaches have been suggested and are currently in

development. Here, we will briefly highlight some of these approaches as alternative therapies targeting LRRK2 kinase activity.

4.1. Antisense oligonucleotides

In recent years, there has been much excitement centered around the practicality and potential therapeutic use of anti-sense oligonucleotides (ASOs) in neurodegenerative diseases. This synthetic technology is aimed at reducing mutant or pathogenic proteins by marking the target's mRNA for degra-dation, or at producing more functional proteins via modula-tion of the splicing of RNA. The most successful use of an ASO in the neurodegenerative space has been for Spinal Muscular Atrophy (SMA), in which large deletions or LOF mutations found in the *SMN1* gene result in terminal disease [64]. The ASO nusinersen, approved by the FDA in 2016, works to modulate the splicing of the homologue gene *SMN2* such that full-length SMN transcripts are increased two-to six-fold and thereby increase its wild-type protein [65]. Patients who have received this treatment in clinical trials reported no serious adverse effects and observed significant improvements in motor function, survival rate, and independence from per-manent ventilation [65]. This is a huge milestone in the treat-ment for SMA that sparked hope for many other neurodegenerative diseases targeting mutant proteins and LOF alleles. Clinical trials evaluating the therapeutic efficacy of ASOs for Huntington's, Alzheimer's, Amyotrophic Lateral Sclerosis (ALS), and Parkinson's diseases are currently under-way, with varying degrees of success [66–70].

In August 2019, a phase 1 clinical trial using an ASO desig-nated BIIB094, to target LRRK2 through intrathecal administra-tion began, with the primary and secondary outcomes measuring safety/tolerability and pharmacokinetics in the blood of people with and without LRRK2 mutations (NCT03976349). The aim of reducing LRRK2 mRNA is to reduce the synthesis of LRRK2 protein in order to ameliorate the toxic effects of gain-of-function mutations in patients with LRRK2 mutations and reduce kinase activity in patients without LRRK2 mutations. Phase 1 is expected to conclude in 2023.

A preclinical study in mice showed that ASOs were able to successfully reduce LRRK2 mRNA in the brain, leaving periph-eral tissues unaffected and thus potentially bypassing the peripheral toxicity observed in models using small-molecule inhibitors [71]. However, clinical relevant efficacy in the reduc-tion of total LRRK2 protein has yet to be determined in humans, i.e. slowing, stopping, or reversing the progression of the disease. As LRRK2 haploinsufficiency is not associated with human diseases [59,60], this approach is predicted to be safe long term.

4.2. LRRK2 GTPase modulators

Both LRRK2 GTPase and kinase domains interact and depend on one another for proper functioning at the cytosol and organellar membranes. In fact, common mutations found within the GTPase domain have been shown to alter the affinity of GTP and decrease GTP hydrolysis, affecting LRRK2 localization and kinase activity [14,72–78]. Recently, two

studies revealed that the Roc GTPase domain exists in a dynamic dimer-monomer equilibrium, and that the R1441C/G/H mutations alter this equilibrium [79,80]. Therefore, modulating its GTPase activity may impart thera-peutic benefits by allosterically reducing kinase activity.

Two GTP-binding inhibitors, Compound 68 and FX2149, have been shown to decrease LRRK2 kinase activity, utilizing kinase assays *in vitro* as well as measuring a reduction in S935 phosphorylation *in vivo* [75,81–83]. Moreover, an increase in LRRK2 ubiquitination was observed after GTP-binding inhibitor treatment in the brains of mice receiving two doses of 10 mg/kg FX2149 intraperitoneally for 3 days [82]. This suggests GTP-binding inhibition may reduce total levels of LRRK2 similarly to kinase inhibitors. With longer treatment time points, it will be interesting to determine whether similar peripheral effects on kidneys and lungs of animals occur as observed in those treated with kinase inhibitors.

Additionally, recent studies suggest a role of LRRK2 in inflammatory response mechanisms across various PD models and PD patients [84–87]. Interestingly, LRRK2-dependent inflammatory effects, such as TNF-alpha secretion, have been shown to be reduced in human lymphoblasts treated with Compound 68 prior to incubation with LPS for up to 4 hours *in vitro*, suggesting that the GTPase domain is critical in reg-ulating inflammatory stimuli, and thus GTPase modulation may have protective effects against neuroinflammation that is often observed in PD pathology [83]. Alternatively, methods to increase the GTP hydrolysis of LRRK2, especially when deal-ing with mutations in the ROC-COR domains, should also be considered when developing GTPase modulators for therapeutics.

4.3. Nanobodies

Nanobodies, small single-domain antigen-binding fragments originating from camelid heavy chain-only antibodies, have recently made their way into clinical trials as potential ther-apeutics in autoimmune disorders and cancer with one, capla-cizumab, receiving approval from the European Medicines Agency (EMA) and the FDA for treatment of patients with thrombotic thrombocytopenic purpura [88–90]. Nanobodies have strong affinity for their targets and can act as antago-nists, agonists, allosteric inhibitors or activators. Additionally, nanobody affinities are conformation-specific. Taken together, nanobodies provide high modulability and versatility, with the therapeutic potential to target many wide-ranging disorders and diseases.

LRRK2-targeting nanobodies have recently been developed by Singh et al. to determine their binding capabilities and potential therapeutic properties [91]. They reported the gen-eration of 10 distinct nanobodies that show a strong affinity for both over-expressed human and endogenous mouse LRRK2 as detected with immunoprecipitation assays *in vitro*. Interestingly, some nanobodies worked to allosterically inhibit or activate LRRK2 kinase, depending on their affinity for GDP-, GTP-bound or unbound LRRK2, as measured by *in vitro* kinase assays with LRRK2-specific AQT0615 peptide substrate, as well as Western blot analyses of pS1292 LRRK2 and pT73 Rab10 in HEK293FT cells over-expressing G2019S LRRK2 [91]. Overall,

nanobodies provide a promising and exciting alternative avenue for LRRK2 kinase modulation. As the generation of nanobodies targeting LRRK2 is brand new, it will be important for future studies to test the safety and efficacy of these tools *in vivo*, as well as the evaluation of their capacity to cross the blood–brain barrier.

5. Conclusion

The current development of such a wide array of tools targeting LRRK2 has indeed provided much hope for the field of PD therapeutics. We are now within the liminal space determining this target's efficacy to either revert, halt, or slow disease progression. As we await the outcomes of kinase inhibitor and ASO trial studies, we can reflect on the significant genetic and mechanistic gains the field has made which has provided a clearly defined target, with a stratified population and obvious routes to modulating activity of LRRK2. There is also evidence for the potential to generalize this target to other patients should it be successful in the genetically defined population.

6. Expert opinion

LRRK2 is a large protein, encompassing a GTPase and kinase catalytic core, flanked by WD40, ankyrin, and leucine-rich repeat protein–protein interaction and stabilization domains. Most disease-causing mutations have been identified within the enzymatic domains and all of which contribute to the hyperactivity of its kinase function [92–94]. Thus far, ATP-competitive kinase inhibitors have been the most focused avenue as a therapeutic intervention in reducing LRRK2 kinase activity; however, other tools such as ASOs, GTPase modulators, and nanobodies pose interesting and creative alternatives that are worth investigation (Figure 2). An important perspective to consider, aside from the clinical relevant

efficacy of any of these therapeutic tools, is of their logistical merit as a long-term therapy for patients, i.e. cost of treatment, ease of administration, and potential adverse side effects. Small molecules as well as nanobodies are highly stable, low molecular weight compounds. Additionally, they are cheap to produce and thus can keep costs relatively low for patients [95,96]. Alternatively, ASOs cost more to produce and require large volumes of hazardous materials and energy [97]. A single intrathecal injection of the SMA ASO nusinersen costs $125,000 USD, creating a huge wealth gap between families that can and cannot afford life-saving treatment [98]. Therefore, in terms of patient accessibility, cheaper alternative drugs would be much more inclusive for the majority, however, considering the economies of scale for a common disease such as PD may allow for cheaper costs for ASO treatments. Additionally, orally administered small-molecule drugs also lend themselves to patient accessibility, as patients and caretakers would not need to schedule in-person visits every few months for intrathecal injection, not to mention is much more comfortable, without risk of developing adverse effects at the sight of insertion such as tenderness, bruising or infection. In contrast, intrathecal administration of ASOs allows for little to no risk of peripheral side effects as observed with kinase inhibitors in preclinical models.

The ongoing clinical trials for LRRK2 kinase inhibitors and ASOs will, over the coming years, clarify whether targeting LRRK2 will be therapeutically advantageous in PD, opening up the possibility for treatment to be patient stratified based on mutation, risk status, and/or drug toleration [99]. In addition to those with specific LRRK2 mutations, studies have shown that enhanced LRRK2 kinase activity can also be found in patients with idiopathic PD and therefore suggest that LRRK2-modifying treatments may be useful to a broader scope of PD patients rather than mutation carriers only [100,101]. Aside from PD, recent advances in PSP genetics have identified a lead single-nucleotide polymorphism (SNP)
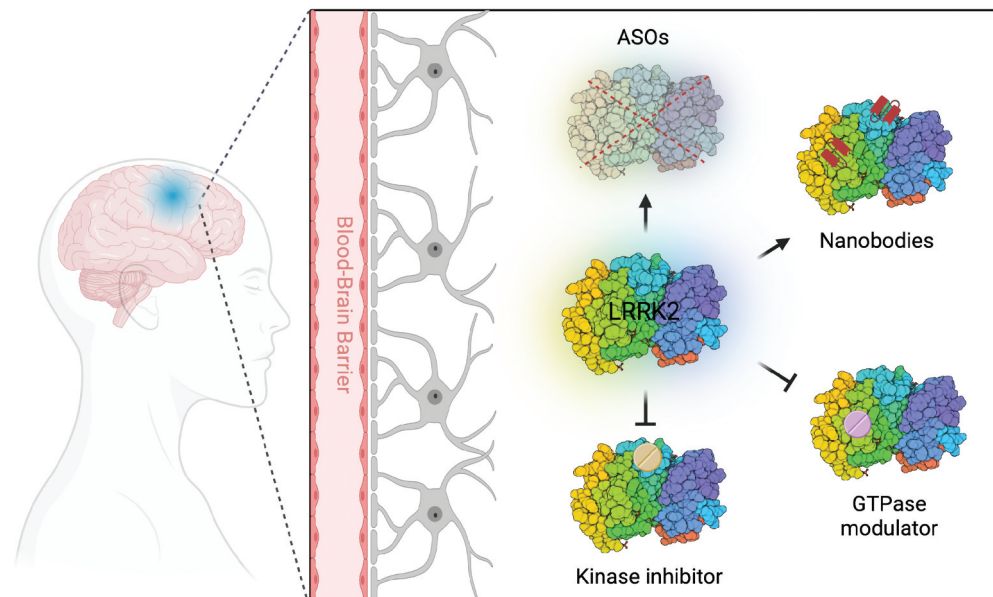

Figure 2. Schematic of potential LRRK2-targeting treatments. This schematic was created in Biorender, utilizing the PDB Builder feature for the LRRK2 structure (ID: 5U6l).

that regulates LRRK2 expression as a factor for survival outcome in people with PSP [11]. Therefore, intervention with therapies targeting LRRK2 could potentially serve as an umbrella therapy, benefiting those with PSP as well. In addition to PSP, some case studies have reported a potential link between LRRK2 and multiple-system atrophy (MSA), whereas others have reported no association [102–105]. Therefore, it will require additional investigation in order to confirm a true mechanistic link between LRRK2 and MSA.

For nearly the last six decades, the treatment of PD has been centered on dopamine replacement therapies, as progress in the development of disease-modifying treatments for PD has been limited. Thus, it is a particularly exciting time for PD therapeutics, with multiple clinical trials underway for mechanistically targeted therapies, i.e. LRRK2, GBA and alpha-synuclein [106]. However, there is still a long way to go in the development of disease-modifying treatments for PD. In comparison, there have been over 200 clinical trials to date to assess treatments for Alzheimer's disease (AD), of which 99% have failed to be efficacious, most probably due to the complexity of the disease and its aging component that most disease models lack [107]. This has both positive and negative implications for PD. The failures of AD clinical trials highlight what hurdles may be on the horizon for PD and give us the opportunity to prepare for them. Realistically however, it would not come as a surprise if PD clinical trials mirror a similar path, as PD is just as complex, and the most commonly used models still lack an aging component. It is just the beginning for PD therapeutics; however, the path to effective treatments is now more hopeful than at any other time in the past half century.

Funding

Declaration of interest

The authors have no relevant affiliations or financial involvement with any organization or entity with a financial interest in or financial conflict with the subject matter or materials discussed in the manuscript. This includes employment, consultancies, honoraria, stock ownership or options, expert testimony, grants or patents received or pending, or royalties.

Reviewer disclosures

Peer reviewers on this manuscript have no relevant financial or other relationships to disclose

ORCID

Jillian H. Kluss http://orcid.org/0000-0002-6262-6661
Patrick A. Lewis http://orcid.org/0000-0003-4537-0489
Elisa Greggio http://orcid.org/0000-0002-8172-3598

References

Papers of special note have been highlighted as either of interest (•) or of considerable interest (••) to readers.

1. Jankovic J. Parkinson's disease: clinical features and diagnosis. J Neurol Neurosurg Psychiatry. 2008 Apr;79(4):368–376.
2. Postuma RB, Berg D, Stern M, et al. MDS clinical diagnostic criteria for Parkinson's disease. Mov Disord. 2015;30(12):1591–1601.
3. Hughes AJ, Daniel SE, Kilford L, et al. Accuracy of clinical diagnosis of idiopathic Parkinson's disease: a clinico-pathological study of 100 cases. J Neurol Neurosurg Psychiatry. 1992 Mar;55(3):181–184.
4. Schapira AHV. Present and future drug treatment for Parkinson's disease. J Neurol Neurosurg Psychiatry. 2005 Nov 1;76 (11):1472–1478.
5. Nemade D, Subramanian T, Shivkumar V. An update on medical and surgical treatments of Parkinson's disease. Aging Dis. 2021 Jul 1;12(4):1021–1035.
6. Paisán-Ruíz C, Jain S, Evans EW, et al. Cloning of the gene containing mutations that cause PARK8-linked Parkinson's disease. Neuron. 2004 Nov 18;44(4):595–600.
7. Zimprich A, Müller-Myhsok B, Farrer M, et al. The PARK8 locus in autosomal dominant Parkinsonism: confirmation of linkage and further delineation of the disease-containing interval. Am J Hum Genet. 2004 Jan;74(1):11–19.
8. Satake W, Nakabayashi Y, Mizuta I, et al. Genome-wide association study identifies common variants at four loci as genetic risk factors for Parkinson's disease. Nat Genet. 2009 Dec;41(12):1303–1307.
9. Simón-Sánchez J, Schulte C, Bras JM, et al. Genome-wide association study reveals genetic risk underlying Parkinson's disease. Nat Genet. 2009 Dec;41(12):1308–1312.
10. Nalls MA, Blauwendraat C, Vallerga CL, et al. Identification of novel risk loci, causal insights, and heritable risk for Parkinson's disease: a meta-analysis of genome-wide association studies. Lancet Neurol. 2019 Dec 1;18(12):1091–1102.
11. Jabbari E, Koga S, Valentino RR, et al. Genetic determinants of survival in progressive supranuclear palsy: a genome-wide association study. Lancet Neurol. 2021 Feb 1;20(2):107–116.
12. Sheng Z, Zhang S, Bustos D, et al. Ser1292 autophosphorylation is an indicator of LRRK2 kinase activity and contributes to the cellular effects of PD mutations. Sci Transl Med. 2012 Dec 12;4 (164):164ra161–164ra161.
13. Kluss JH, Conti MM, Kaganovich A, et al. Detection of endogenous S1292 LRRK2 autophosphorylation in mouse tissue as a readout for kinase activity. Npj Park Dis. 2018 Apr 19;4(1):13.
14. West AB, Moore DJ, Choi C, et al. Parkinson's disease-associated mutations in LRRK2 link enhanced GTP-binding and kinase activities to neuronal toxicity. Hum Mol Genet. 2007 Jan 15;16 (2):223–232.
15. Steger M, Tonelli F, Ito G, et al. Phosphoproteomics reveals that Parkinson's disease kinase LRRK2 regulates a subset of Rab GTPases. eLife. 2016 Jan 29;5. DOI:10.7554/eLife.12813.
16. Greggio E, Jain S, Kingsbury A, et al. Kinase activity is required for the toxic effects of mutant LRRK2/dardarin. Neurobiol Dis. 2006 Aug 1;23(2):329–341.
17. Greggio E, Zambrano I, Kaganovich A, et al. The Parkinson disease-associated leucine-rich repeat kinase 2 (LRRK2) is a dimer that undergoes intramolecular autophosphorylation. J Biol Chem. 2008 Jun 13;283(24):16906–16914.
18. Manzoni C, Mamais A, Dihanich S, et al. Inhibition of LRRK2 kinase activity stimulates macroautophagy. Biochim Biophys Acta BBA - Mol Cell Res. 2013 Dec 1;1833(12):2900–2910.
19. Bonet-Ponce L, Beilina A, Williamson CD, et al. LRRK2 mediates tubulation and vesicle sorting from lysosomes. Sci Adv. 2020 Nov 1;6(46):eabb2454.
20. Liu Z, Bryant N, Kumaran R, et al. LRRK2 phosphorylates membrane-bound Rabs and is activated by GTP-bound Rab7L1 to promote recruitment to the trans-Golgi network. Hum Mol Genet. 2018 15;27(2):385–395.
21. Purlyte E, Dhekne HS, Sarhan AR, et al. Rab29 activation of the Parkinson's disease-associated LRRK2 kinase. EMBO J. 2019 Jan 15;38(2):e101237.
22. Steger M, Diez F, Dhekne HS, et al. Systematic proteomic analysis of LRRK2-mediated Rab GTPase phosphorylation establishes

a connection to ciliogenesis. eLife. 2017 10;6. DOI:10.7554/eLife.31012.

23. Herbst S, Campbell P, Harvey J, et al. LRRK2 activation controls the repair of damaged endomembranes in macrophages. EMBO J. 2020 Sep 15;39(18):e104494.

24. Beilina A, Bonet-Ponce L, Kumaran R, et al. The Parkinson's disease protein LRRK2 interacts with the GARP complex to promote retrograde transport to the trans-golgi network. Cell Rep. 2020 May 5;31 (5):107614.

25. Bonello F, Hassoun SM, Mouton-Liger F, et al. LRRK2 impairs PINK1/ Parkin-dependent mitophagy via its kinase activity: pathologic insights into Parkinson's disease. Hum Mol Genet [Internet]. 28 (10):1645–1660. [cited 2019 Feb 4]; Available from: https://academic.oup.com/hmg/advance-article/doi/10.1093/hmg/ddz004/5281397

26. Korecka JA, Thomas R, Christensen DP, et al. Mitochondrial clearance and maturation of autophagosomes are compromised in LRRK2 G2019S familial Parkinson's disease patient fibroblasts. Hum Mol Genet. 2019 Oct 1;28(19):3232–3243.

27. Dhekne HS, Yanatori I, Vides EG, et al. LRRK2-phosphorylated Rab10 sequesters Myosin Va with RILPL2 during ciliogenesis blockade. Life Sci Alliance [Internet]. 2021 May 1;4(5). [cited 2022 Jan 9]; Available from: https://www.life-science-alliance.org/content/4/5/e202101050

28. Kluss JH , Bonet-Ponce L, Lewis, PA, et al. Directing LRRK2 to membranes of the endolysosomal pathway triggers RAB phosphorylation and JIP4 recruitment. Neurobiology of disease.2022 May;170:0969–9961.

29. Jeon J, Sparreboom A, Baker S. Kinase inhibitors: the reality behind the success. Clin Pharmacol Ther. 2017 Nov;102(5):726–730.

30. Roskoski R. Properties of FDA-approved small molecule protein kinase inhibitors: a 2020 update. Pharmacol Res. 2020 Feb;152:104609.

31. Fell MJ, Mirescu C, Basu K, et al. MLi-2, a potent, selective, and centrally active compound for exploring the therapeutic potential and safety of LRRK2 kinase inhibition. J Pharmacol Exp Ther. 2015 Dec;355(3):397–409.
•• This is the first in-depth in vivo dosing study using MLi-2.

32. Estrada AA, Liu X, Baker-Glenn C, et al. Discovery of highly potent, selective, and brain-penetrable leucine-rich repeat kinase 2 (LRRK2) small molecule inhibitors. J Med Chem. 2012 Nov 26;55 (22):9416–9433.

33. Kluss JH, Mazza MC, Li Y, et al. Preclinical modeling of chronic inhibition of the Parkinson's disease associated kinase LRRK2 reveals altered function of the endolysosomal system in vivo. Mol Neurodegener. 2021 Mar 19;16(1):17.
• This is the first study to employ chronic in vivo dosing of MLi-2 to G2019S KI mice to ameliorate hyperactive LRRK2 levels back to wildtype levels. This study includes total and phospho-proteomic analyses of brain and peripheral tissues known to be affected by LRRK2 inhibitors.

34. Wang S, Kelly K, Brotchie JM, et al. Exosome markers of LRRK2 kinase inhibition. NPJ Park Dis. 2020 Nov 13;6(1):32.

35. Ito G, Katsemonova K, Tonelli F, et al. Phos-tag analysis of Rab10 phosphorylation by LRRK2: a powerful assay for assessing kinase function and inhibitors. Biochem J. 2016 01;473(17):2671–2685.

36. Kelly K, Wang S, Boddu R, et al. The G2019S mutation in LRRK2 imparts resiliency to kinase inhibition. Exp Neurol. 2018 Nov 1;309:1–13.

37. Nichols RJ, Dzamko N, Morrice NA, et al. 14-3-3 binding to LRRK2 is disrupted by multiple Parkinson's disease-associated mutations and regulates cytoplasmic localization. Biochem J. 2010 Sep 15;430(3):393–404.

38. Fuji RN, Flagella M, Baca M, et al. Effect of selective LRRK2 kinase inhibition on nonhuman primate lung. Sci Transl Med. 2015 Feb 4;7 (273):273ra15.
•• This study compares three structurally distinct LRRK2-specific type I inhibitors in non-human primates. An in-depth characterization of pulmonary function is included.

39. Baptista MAS, Merchant K, Barrett T, et al. LRRK2 inhibitors induce reversible changes in nonhuman primate lungs without measurable pulmonary deficits. Sci Transl Med [Internet]. 2020 Apr 22;12 (540). [cited 2020 Apr 26]; Available from: https://stm.sciencemag.org/content/12/540/eaav0820

40. Dzamko N, Deak M, Hentati F, et al. Inhibition of LRRK2 kinase activity leads to dephosphorylation of Ser910/Ser935, disruption of 14-3-3 binding and altered cytoplasmic localization. Biochem J. 2010 Aug 27;430(3):405–413.

41. Myasnikov A, Zhu H, Hixson P, et al. Structural analysis of the full-length human LRRK2. Cell. 2021 Jun 24;184(13):3519–3527.e10.

42. Pettersen EF, Goddard TD, Huang CC, et al. UCSF Chimera–a visualization system for exploratory research and analysis. J Comput Chem. 2004 Oct;25(13):1605–1612.

43. Liu M, Bender SA, Cuny GD, et al. Type II kinase inhibitors show an unexpected inhibition mode against Parkinson's disease-linked LRRK2 mutant G2019S. Biochemistry. 2013 Mar 12;52 (10):1725–1736.

44. O'Hare T, Shakespeare WC, Zhu X, et al. AP24534, a Pan-BCR-ABL inhibitor for chronic myeloid leukemia, potently inhibits the T315I mutant and overcomes mutation-based resistance. Cancer Cell. 2009 Nov 3;16(5):401–412.

45. Tasegian A, Singh F, Ganley IG, et al. Impact of type II LRRK2 inhibitors on signaling and mitophagy. Biochem J. 2021 Oct 6;478 (19):3555–3573.

46. Nichols RJ, Dzamko N, Hutti JE, et al. Substrate specificity and inhibitors of LRRK2, a protein kinase mutated in Parkinson's disease. Biochem J. 2009 Oct 23;424(1):47–60.

47. Deng X, Dzamko N, Prescott A, et al. Characterization of a selective inhibitor of the Parkinson's disease kinase LRRK2. Nat Chem Biol. 2011 Apr;7(4):203–205.

48. Leśniak RK, Nichols RJ, Schonemann M, et al. Discovery of G2019S-Selective leucine rich repeat protein kinase 2 inhibitors with in vivo efficacy. Eur J Med Chem. 2022 Feb 5;229:114080.

49. Bright JM, Carlisle HJ, Toda AMA, et al. Differential inhibition of LRRK2 in Parkinson's disease patient blood by a G2019S selective LRRK2 inhibitor. Mov Disord. 2021;36(6):1362–1371.

50. Deniston CK, Salogiannis J, Mathea S, et al. Structure of LRRK2 in Parkinson's disease and model for microtubule interaction. Nature. 2020 Dec;588(7837):344–349.

51. Watanabe R, Buschauer R, Böhning J, et al. The in situ structure of Parkinson's disease-linked LRRK2. Cell. 2020 Sep 17;182(6):1508–1518.e16.

52. Schmidt SH, Weng JH, Aoto PC, et al. Conformation and dynamics of the kinase domain drive subcellular location and activation of LRRK2. Proc Natl Acad Sci U S A. 2021 Jun 8;118(23):e2100844118.

53. Press Release [Internet]. Denali. [cited 2021 Nov 30]. Available from: https://www.denalitherapeutics.com/investors/press-release
•• The most recent update on results of the Phase I trials of DNL151/BIIB122.

54. Bryce D, Ware CM, Woodhouse JD, et al. Characterization of the onset, progression, and reversibility of morphological changes in mouse lung following pharmacological inhibition of LRRK2 kinase activity. J Pharmacol Exp Ther [Internet]. 2021 Jan 1;377(1):11–19. [cited 2021 Feb 4]; Available from: https://jpet.aspetjournals.org/content/early/2021/01/28/jpet.120.000217
• In line with studies in non-human primates, this study confirms morphological changes to lung type II pneumocytes in wildtype mice treated with LRRK2 kinase inhibitors.

55. Lobbestael E, Civiero L, De Wit T, et al. Pharmacological LRRK2 kinase inhibition induces LRRK2 protein destabilization and proteasomal degradation. Sci Rep [Internet]. 2016 Sep 23;6. [cited 2020 May 8]; Available from: https://www.ncbi.nlm.nih.gov/pmc/articles/PMC5034242/

56. Zhao J, Molitor TP, Langston JW, et al. LRRK2 dephosphorylation increases its ubiquitination. Biochem J. 2015 Jul 1;469(Pt 1):107–120.

57. Herzig MC, Kolly C, Persohn E, et al. LRRK2 protein levels are determined by kinase function and are crucial for kidney and

lung homeostasis in mice. Hum Mol Genet. 2011 Nov 1;20 (21):4209–4223.

58. Pellegrini L, Hauser DN, Li Y, et al. Proteomic analysis reveals co-ordinated alterations in protein synthesis and degradation pathways in LRRK2 knockout mice. Hum Mol Genet. 2018 15;27(18):3257–3271.

59. Blauwendraat C, Reed X, Kia DA, et al. Frequency of loss of function variants in LRRK2 in Parkinson disease. JAMA Neurol. 2018 Nov 1;75 (11):1416–1422.

60. Whiffin N, Armean IM, Kleinman A, et al. The effect of LRRK2 loss-of-function variants in humans. Nat Med. 2020 Jun;26(6):869–877.

61. Lebovitz C, Wretham N, Osooly M, et al. Loss of Parkinson's susceptibility gene LRRK2 promotes carcinogen-induced lung tumorigenesis. Sci Rep. 2021 Jan 22;11(1):2097.

62. Scott JD, DeMong DE, Greshock TJ, et al. Discovery of a 3-(4-Pyrimidinyl) Indazole (MLi-2), an orally available and selective leucine-rich repeat kinase 2 (LRRK2) inhibitor that reduces brain kinase activity. J Med Chem. 2017 Apr 13;60(7):2983–2992.

63. Andersen MA, Wegener KM, Larsen S, et al. PFE-360-induced LRRK2 inhibition induces reversible, non-adverse renal changes in rats. Toxicology. 2018 15;395:15–22.

64. Lunn MR, Wang CH. Spinal muscular atrophy. Lancet Lond Engl. 2008 Jun 21;371(9630):2120–2133.

65. Wurster CD, Ludolph AC. Nusinersen for spinal muscular atrophy. Ther Adv Neurol Disord. 2018 Mar 13;11:1756285618754459.

66. Kingwell K. Double setback for ASO trials in huntington disease. Nat Rev Drug Discov. 2021 May 19;20(6):412–413.

67. Miller T, Cudkowicz M, Shaw PJ, et al. Phase 1–2 trial of antisense oligonucleotide tofersen for SOD1 ALS. N Engl J Med. 2020 Jul 9;383(2):109–119.

68. Grabowska-Pyrzewicz W, Want A, Leszek J, et al. Antisense oligonucleotides for Alzheimer's disease therapy: from the mRNA to miRNA paradigm. EBioMedicine [Internet]. 2021 Dec 1;74. [cited 2022 Jan 5]; Available from: https://www.thelancet.com/journals/ebiom/article/PIIS2352-3964(21)00485-0/fulltext#seccesectitle0003

69. Cole TA, Zhao H, Collier TJ, et al. α-Synuclein antisense oligonucleotides as a disease-modifying therapy for Parkinson's disease. JCI Insight. 2021;6(5):e135633.

70. Kingwell K. Zeroing in on neurodegenerative α-synuclein. Nat Rev Drug Discov. 2017 Jun 1;16(6):371–373.

71. Zhao HT, John N, Delic V, et al. LRRK2 antisense oligonucleotides ameliorate α-synuclein inclusion formation in a Parkinson's disease mouse model. Mol Ther Nucleic Acids. 2017 Sep 15;8:508–519.

72. Lewis PA, Greggio E, Beilina A, et al. The R1441C mutation of LRRK2 disrupts GTP hydrolysis. Biochem Biophys Res Commun. 2007 Jun 8;357(3):668–671.

73. Li C, Ting Z, Qin X, et al. The prevalence of LRRK2 Gly2385Arg variant in Chinese han population with Parkinson's disease. Mov Disord Off J Mov Disord Soc. 2007 Dec;22(16):2439–2443.

74. Xiong Y, Coombes CE, Kilaru A, et al. GTPase activity plays a key role in the pathobiology of LRRK2. PLOS Genet. 2010 Apr 8;6(4): e1000902.

75. Liao J, Wu CX, Burlak C, et al. Parkinson disease-associated mutation R1441H in LRRK2 prolongs the "active state" of its GTPase domain. Proc Natl Acad Sci U S A. 2014 Mar 18;111(11):4055–4060.

76. Soliman A, Cankara FN, Kortholt A. Allosteric inhibition of LRRK2, where are we now. Biochem Soc Trans. 2020 Oct 20;48(5):2185–2194.

77. Blanca Ramírez M, Ordóñez AJL, Fdez E, et al. GTP binding regulates cellular localization of Parkinson's disease-associated LRRK2. Hum Mol Genet. 2017 Jul 15;26(14):2747–2767.

78. Biosa A, Trancikova A, Civiero L, et al. GTPase activity regulates kinase activity and cellular phenotypes of Parkinson's disease-associated LRRK2. Hum Mol Genet. 2013 Mar 15;22(6):1140–1156.

79. Wu CX, Liao J, Park Y, et al. Parkinson's disease-associated mutations in the GTPase domain of LRRK2 impair its nucleotide-dependent conformational dynamics. J Biol Chem. 2019 Apr 12;294(15):5907–5913.

80. Huang X, Wu C, Park Y, et al. The Parkinson's disease–associated mutation N1437H impairs conformational dynamics in the G domain of LRRK2. FASEB J. 2019 Apr;33(4):4814–4823.

81. Li T, He X, Thomas JM, et al. A novel GTP-Binding inhibitor, FX2149, Attenuates LRRK2 toxicity in Parkinson's disease models. PLoS ONE. 2015 Mar 27;10(3):e0122461.
• This study characterizes a LRRK2 GTP-binding inhibitor in vitro.

82. Thomas JM, Wang X, Guo G, et al. GTP-binding inhibitors increase LRRK2-linked ubiquitination and Lewy body-like inclusions. J Cell Physiol. 2020;235(10):7309–7320.

83. Li T, Ning B, Kong L, et al. A LRRK2 GTP binding inhibitor, 68, reduces LPS-induced signaling events and TNF-α release in human lymphoblasts. Cells. 2021 Feb 23;10(2):480.

84. Dzamko NL. LRRK2 and the immune system. Adv Neurobiol. 2017;14:123–143.

85. Brockmann K, Apel A, Schulte C, et al. Inflammatory profile in LRRK2-associated prodromal and clinical PD. J Neuroinflammation. 2016 May 24;13(1):122.

86. Wallings RL, Tansey MG. LRRK2 regulation of immune-pathways and inflammatory disease. Biochem Soc Trans. 2019 Dec 20;47 (6):1581–1595.

87. Kluss JH, Mamais A, Cookson MR. LRRK2 links genetic and sporadic Parkinson's disease. Biochem Soc Trans. 2019 Apr 30;47(2):651–661.

88. Jovčevska I, Muyldermans S. The therapeutic potential of nanobodies. BioDrugs Clin Immunother Biopharm Gene Ther. 2020 Feb;34(1):11–26.

89. Fernandes JC. Therapeutic application of antibody fragments in autoimmune diseases: current state and prospects. Drug Discov Today. 2018 Dec;23(12):1996–2002.

90. Scully M, Cataland SR, Peyvandi F, et al. Caplacizumab treatment for acquired thrombotic thrombocytopenic purpura. N Engl J Med [Internet]. 2019 Jan 9;380(4):335–346. [cited 2022 Jan 9]; Available from: https://www.nejm.org/doi/10.1056/NEJMoa1806311

91. Singh RK, Soliman A, Guaitoli G, et al. Nanobodies as allosteric modulators of Parkinson's disease–associated LRRK2. Proc Natl Acad Sci. 2022 Mar;119(9):e2112712119.
• This study describes the development and characterization of the first LRRK2-targeting nanobodies.

92. Berwick DC, Heaton GR, Azeggagh S, et al. LRRK2 biology from structure to dysfunction: research progresses, but the themes remain the same. Mol Neurodegener. 2019 Dec 21;14(1):49.

93. Greggio E, Cookson MR. Leucine-rich repeat kinase 2 mutations and Parkinson's disease: three questions. ASN NEURO. 2009 Apr 14;1(1):e00002.

94. Cookson MR. The role of leucine-rich repeat kinase 2 (LRRK2) in Parkinson's disease. Nat Rev Neurosci. 2010 Dec;11(12):791–797.

95. Makurvet FD. Biologics vs. small molecules: drug costs and patient access. Med Drug Discov. 2021 Mar 1;9:100075.

96. Muyldermans S. A guide to: generation and design of nanobodies. FEBS J. 2021;288(7):2084–2102.

97. Andrews BI, Antia FD, Brueggemeier SB, et al. Sustainability challenges and opportunities in oligonucleotide manufacturing. J Org Chem. 2021 Jan 1;86(1):49–61.

98. Jalali A, Rothwell E, Botkin JR, et al. Cost-Effectiveness of nusinersen and universal newborn screening for spinal muscular atrophy. J Pediatr. 2020 Dec 1;227:274–280.e2.

99. Bandres-Ciga S, Diez-Fairen M, Kim JJ, et al. Genetics of Parkinson disease: an introspection of its journey towards precision medicine. Neurobiol Dis. 2020 Apr;137:104782.

100. Di Maio R, Hoffman EK, Rocha EM, et al. LRRK2 activation in idiopathic Parkinson's disease. Sci Transl Med. 2018 Jul 25;10(451): eaar5429.

101. Rocha EM, Keeney MT, Maio RD, et al. LRRK2 and idiopathic Parkinson's disease. Trends Neurosci. 2022 Mar 1;45(3):224–236.

102. Heckman MG, Schottlaender L, Soto-Ortolaza AI, et al. LRRK2 exonic variants and risk of multiple system atrophy. Neurology. 2014 Dec 9;83(24):2256–2261.

103. Riboldi GM, Palma J, Cortes E, et al. Early-onset pathologically proven multiple system atrophy with LRRK2 G2019S mutation. Mov Disord. 2019 Jul;34(7):1080–1082.

104. Ozelius LJ, Foroud T, May S, et al. G2019S mutation in the leucine-rich repeat kinase 2 gene is not associated with multiple system atrophy. Mov Disord. 2007;22(4):546–549.

105. Katzeff JS, Phan K, Purushothuman S, et al. Cross-examining candidate genes implicated in multiple system atrophy. Acta Neuropathol Commun. 2019 Jul 24;7(1):117.

106. McFarthing K, Rafaloff G, Baptista MAS, et al. Parkinson's disease drug therapies in the clinical trial pipeline: 2021 update. J Park Dis. 2021;11(3):891–903.

107. Yiannopoulou KG, Anastasiou AI, Zachariou V, et al. Reasons for failed trials of disease-modifying treatments for alzheimer disease and their contribution in recent research. Biomedicines. 2019 Dec 9;7(4):97.

 • **This comprehensive review provides an in-depth discussion on the reasons why clinical trials for Alzheimer's disease therapies have failed. This is particularly important, as it foreshadows what may be in store for those pursuing drug trial success in Parkinson's disease.**